ANALYSIS OF WIND INDUCED OSCILLATIONS IN CABLE STAYED BRIDGES

A THESIS

Submitted in fulfilment of the
requirements for the award of the degree
of
DOCTOR OF PHILOSOPHY
in
CIVIL ENGINEERING

By

LAKSHMY PARAMESWARAN

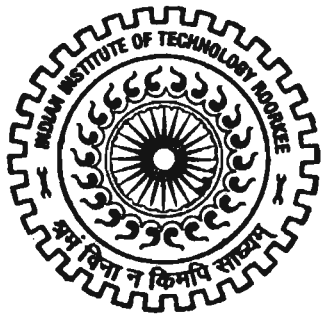

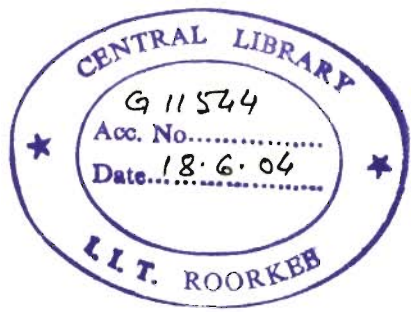

DEPARTMENT OF CIVIL ENGINEERING
INDIAN INSTITUTE OF TECHNOLOGY ROORKEE
ROORKEE–247 667 (INDIA)

JANUARY, 2002

INDIAN INSTITUTE OF TECHNOLOGY ROORKEE

CANDIDATE'S DECLARATION

I hereby certify that the work which is being presented in the thesis entitled "**ANALYSIS OF WIND INDUCED OSCILLATIONS IN CABLE STAYED BRIDGES**" in fulfilment of the requirement for the award of the Degree of Doctor of Philosophy and submitted in the Department of Civil Engineering of the Institute is an authentic record of my own work carried out during a period from July 1994 to January 2002 under the supervision of **Dr. D. N. Trikha** and **Dr. P. N. Godbole**, Professors of Civil Engineering.

The matter presented in this thesis has not been submitted by me for the award of any other degree in this or any other Institute/University.

Lakshmy.N

(LAKSHMY PARAMESWARAN)

This is to certify that the above statement made by the candidate is correct to the best of our knowledge.

Date : 23-01-2002

(Dr. D. N. TRIKHA)
Former Director
SERC, Ghaziabad
Professor of Civil Engg.
UPM, Malaysia

(Dr. P. N. GODBOLE)
Professor (Retd.)
Department of Civil Engg.
IIT, Roorkee–247667
India

The Ph.D. Viva-Voce examination of LAKSHMY PARAMESWARAN, Research Scholar, has been held on 21/1/2002

Signature of Supervisors

2.7.02

Signature of H.O.D.

Signature of Examiner

ABSTRACT

The analysis of cable stayed bridges to estimate the dynamic response due to wind loading is an imperative requirement in the design criteria, as they are relatively lightweight, flexible and lightly damped structures. The research in the area of bridge aerodynamics marked a beginning in this direction after the collapse of Tacoma Narrows Bridge in 1940s. The last two decades witnessed a lot of progress in wind tunnel testing techniques, analytical assessment and development of software to evaluate wind induced response. These advancements in the state-of-the-art, applied to the design, helped in the design of long span cable stayed bridges such as Normandy Bridge in France (main span 856m) and Tatara Bridge in Japan (main span 890m).

The wind induced oscillatory phenomena can be grouped into limited amplitude oscillations such as buffeting, vortex excitation, etc. and divergent amplitude oscillations such as flutter and galloping. This dissertation is devoted to buffeting as well as flutter analysis of long span cable stayed bridges, as the former affects the safety and serviceability states whereas the latter may become critical in design.

Some of the problems in the area of buffeting and flutter analysis of long span cable stayed bridges are identified after a detailed literature review. As these bridges are geometrically nonlinear structures, any attempt to simplify the analysis may lead to inaccurate prediction of responses. Also, usage of assumed modal structural damping in the aerodynamic analysis of these bridges might not reflect their actual behaviour under the action of wind. Therefore, there is a need to apply reliable analytical methods for evaluation of modal structural damping for rational wind analysis.

Type of deck supports at towers and abutments such as fixed, movable, floating and elastic supports play an important role in design of cable stayed bridges. However, their influence on aerodynamic behaviour is not reported so far.

Frequency domain buffeting analysis, even though computationally efficient, is not capable of handling nonlinearities in the system. The other option to conduct

aeroelastic model investigations of long span bridges, may demand larger size wind tunnels, or compel to make a compromise on modelling of wind and structure, which may lead to inaccurate prediction of responses under wind. Further, modelling of the bridge deck supports for wind tunnel investigations of aeroelastic models is not an easy task. The limitations of conventional methods can be overcome by performing buffeting analysis using time domain.

With longer span lengths, the possibility of occurrence of coupled flutter, especially combined lateral and torsional modes, needs to be investigated. As innovations in the design of cable stayed bridges are still in progress, new generation cable stayed bridges with improved and elegant designs are likely to be constructed in the near future. To realize these innovative long span bridges, there is a need to develop realistic analytical procedures to understand the complex wind induced oscillatory problems.

After considering the state-of-the-art analytical procedures in bridge aerodynamics, a comprehensive approach for buffeting and flutter analysis of long span cable stayed bridges is developed. The steps include (i) nonlinear static analysis under dead load accounting for geometric nonlinearities, (ii) vibration analysis using dead load deformed geometry (iii) evaluation of energy based modal structural damping (iv) digital simulation of wind velocity field (v) time domain buffeting analysis using generated buffeting forces and (vi) flutter analysis.

In this thesis, the above methodology has been used to study the effect of (i) terrain roughness, (ii) mean wind speed and (iii) bridge deck supports at towers and abutments, on the aerodynamic response of cable stayed bridges. The steps involved are described below.

Nonlinear Static and Vibration Analysis: The nonlinear static analysis of cable stayed bridges is performed after idealizing these bridges as a three-dimensional space system and the deformed geometry is obtained under dead loads and initial cable tension. After modifying the initial geometry, the vibration analysis is carried out using Lanczos iteration procedure and the frequencies and mode shapes are determined.

Using the modal ordinates and element and geometric stiffness matrices of the deck, tower and cable elements, the modal strain energy and potential energy contribution of these components is computed. Using the energy loss factors corresponding to the materials of these bridge components, the total energy dissipated is computed. The modal structural damping is evaluated as ratio of total energy dissipated to potential energy. Software routine ENDAMP has been developed for evaluation of energy based modal structural damping.

Digital Simulation of Wind: For the time domain buffeting analysis, the wind field along the span of bridge is generated using the spectral representation method using the Kaimal spectrum and Panofsky-McCormick spectrum for longitudinal and vertical velocity fluctuations respectively. The method essentially consists of representing the components of random process/velocity fluctuations as sum of cosine functions with random frequencies and phase angles corresponding to the target cross-spectral density matrix. Computer software WINGEN has been developed for generation of spatially correlated wind velocity field along the span of bridge.

Time Domain Buffeting Analysis: The buffeting forces in the lateral, vertical and rotational directions required for performing time domain analysis are first generated by modified quasi-steady approach using the simulated wind fluctuations, steady state force coefficients and their derivatives as well as aerodynamic admittance functions. These forces are generated at a time step of 0.25 seconds, and a total duration of 512 seconds was chosen after a sensitivity analysis. The net modal damping required for buffeting analysis is obtained by summing up the modal structural and aerodynamic dampings. The aerodynamic damping in vertical, lateral and rotational directions are evaluated using the expressions, which matched well with aerodynamic damping measured in wind tunnel studies (Irwin, 1977). The buffeting analysis is performed by time integration of equations of motion in modal co-ordinates using Wilson-θ method.

Flutter Analysis: The formulation for equations of motion for flutter analysis are derived along with methodology for two-dimensional and three-dimensional flutter analyses. The possibility of occurrence of coupled lateral and torsional motion is examined.

Numerical Analysis of Bridges: After duly validating the procedures for buffeting and flutter analysis as presented above, their applications are illustrated with numerical analyses of four cable stayed bridges – two each with three spans and the other two with five spans. The three span bridges are composite structures with steel deck and concrete A-shaped towers with total span length of 627.8m (Bridge # 1) and 1255.8m (Bridge # 2). The five span bridges included are : the existing steel bridge, the Luling Bridge in USA with a span of 836.6m (Bridge # 3), and a concrete bridge, the Yamuna Bridge with a total span of 610m (Bridge # 4), under construction in India.

The nonlinear static and vibration analyses of the bridges are performed first. The modal structural damping is theoretically evaluated. The time domain buffeting analysis has been performed for (i) terrain categories TC-1 to TC-4 with surface roughness parameter 0.005m, 0.03m, 0.3m and 1.0m (ii) mean wind speed in the range of 30 to 60m/sec, at steps of 10m/sec and (iii) type of deck supports (DST-1 to DST-6). After performing the time domain buffeting analysis, the results are compared with the mean wind response. The gust response factor – ratio of peak to mean static response – has been evaluated to quantify the amplification in response due to buffeting. Based on gust response factor, the best type of deck supports suitable for aerodynamic design of cable stayed bridges has been selected. The effect of buffeting on forces in cables, deck, tower as well as on the reactions at tower base and deck supports at towers and abutments has been quantified by comparing the results of buffeting analysis with static response of the bridges under mean wind.

Flutter analysis of these bridges is carried out to observe the effect of bridge vibration in higher modes, effect of angle of attack, influence of deck supports on occurrence of flutter, and, prediction of flutter due to coupling of lateral and torsional motions.

The main findings of this study are summarized as follows:

1. Improvement in state-of-the-art wind analysis is achieved by adoption of theoretically evaluated modal structural damping for wind analysis, time domain approach for buffeting analysis and prediction of critical flutter speed

for coupled lateral and torsional modes in long span cable stayed bridges. Detailed studies are carried out to observe the effect of type of deck supports on aerodynamic behaviour of cable stayed bridges.

2. The time domain approach used in this study to compute buffeting response of cable stayed bridges, serves as an alternate tool to aeroelastic wind tunnel testing which is time consuming and expensive.

3. Buffeting response increases nonlinearly with mean wind speed. The major contribution to buffeting response in vertical direction is by the first and second symmetrical vertical bending modes. The number of modes to be included for buffeting analysis of long span flexible bridges depends on the type of bridge deck supports and could be decided on the basis of vibration characteristics. Buffeting induced forces in outer cables, deck member near tower as well as the vertical reaction at deck supports at abutments or near cable anchorages are significantly high in comparison to forces induced by mean wind.

4. Nonlinear static response of cable stayed bridge is dependent on the type of deck supports. The mode type and order in which the bridge gets excited varies with type of deck supports.

5. Energy based evaluation of damping serves as an efficient analytical tool to assess the modal structural damping for the analysis and design of cable stayed bridges under random wind forces.

6. The effect of bridge vibration in higher modes on criteria for onset of flutter is to reduce the critical wind speed in long span cable stayed bridges. The angle of attack of wind plays an important role in flutter analysis, as the critical wind speed for occurrence of flutter significantly decreases with increase in angle of attack (positive). Therefore, it is necessary to determine the flutter derivatives at various wind angles and perform flutter analysis at different angles of attack of wind for a rational wind design.

ACKNOWLEDGEMENT

The research work presented in this thesis was completed under the joint supervision of Dr. D. N. Trikha, (Former Director, SERC, Ghaziabad) and Dr. P. N. Godbole, both Professors of Civil Engineering. I take this opportunity to express my profound gratitude to them for their invaluable guidance, continuous encouragement, suggestions and discussions at various stages of work. I am highly indebted to them for motivating me to take up this pursuit along with my busy official schedules, and providing me moral support throughout this work.

I am extremely grateful to Dr. Krishen Kumar, Professor of Civil Engineering and Co-ordinator, Wind Engineering Centre, IIT Roorkee, for providing me computational facilities, technical guidance throughout and moral support without which this work could not have been completed in time.

I am thankful to Dr. Prem Krishna and Dr. D. K. Paul for timely suggestions and encouragement.

I take this opportunity to express my deep sense of gratitude to Director General, Council of Scientific and Industrial Research, for sanctioning me study leave for a period of one year and five months to complete my residential requirement as well as this work.

I am grateful to Prof. P. K. Sikdar, Director, and Sri M. V. Bhaskara Rao, Head Bridge Engineering Division, Central Road Research Institute, New Delhi, for support and encouragement, especially during the last phase of work.

I express my sincere thanks to Dr. S. P. Sharma, Dr. M. G. Tamhankar and Sri S. K. Agarwal for persuading me to work in the area of Bridge Aerodynamics, especially in the initial stages. Sincere thanks are due to Sri M. S. Kapla and Dr. Ram Kumar for their support and help. I take this opportunity to thank my colleagues at Structural Engineering Research Centre Ghaziabad, for providing me support to conduct wind tunnel studies on tall structures and long span bridges.

I take this opportunity to express my sincere gratitude to eminent professors Late Prof. Robert H. Scanlan, Prof. N. P. Jones, Prof. G.N.V. Rao and Prof. V.G. Pandarinathan for imparting me the basic knowledge in Bridge Aerodynamics, Wind Engineering, Structural Dynamics and Finite Element Methods.

I express my sincere thanks to Mr. Sandeep Jain for preparing illustrations used in the thesis.

The author expresses deep sense of gratitude to all her family members.

I am extremely grateful to my parents-in-law, Smt J. Swaranmbal and Sri P. Narayana Iyer, for their encouragement and continuous support and help throughout the course of this work, without which it could not have been completed.

I am grateful to my loving parents Smt Rajam Swamy and Sri R. Narayana Swamy, brother Sankar and sister Radhika for their affection, continuous encouragement, moral support and help.

I am extremely thankful to my beloved husband Parameswaran and little daughter, Swarna for their affection, inspiration during the course of this work and for immense patience displayed during the last stages of this work.

I am grateful to God for bringing this day in my life.

(LAKSHMY PARAMESWARAN)

CONTENTS

Title			Page No.
Candidate's Declaration			*i*
Abstract			*iii*
Acknowledgement			*ix*
List of Figures			*xvii*
List of Tables			*xxv*
Nomenclature			*xxix*
Chapter 1 :	**INTRODUCTION**		1
	1.1	General	1
	1.2	Basic Concepts of Bridge Aerodynamics	3
		1.2.1 Static Wind Effects	4
		1.2.2 Dynamic Wind Effects	7
		1.2.3 Overview of Methodology	11
	1.3	Problem Identification and Objective of the Study	13
	1.4	Plan of Study	14
	1.5	Organization of the Thesis	15
Chapter 2 :	**LITERATURE REVIEW**		17
	2.1	Introduction	17
	2.2	Historical Evolution and Developments	17
	2.3	Basic Design Concepts	22
	2.4	Static Behavior and Methods for Analysis	31
	2.5	Dynamic Behavior and Methods for Analysis	33
		2.5.1 Modal Structural Damping	37
	2.6	Buffeting Analysis	44
		2.6.1 Frequency Domain Analysis	44
		2.6.2 Time Domain Analysis	49
		2.6.3 Methods for Buffeting Response Control	52

2.7 Unsteady Aerodynamics and Flutter Analysis 53
2.7.1 Determination of Unsteady Forces 54
2.7.1.1 Experimental techniques 54
2.7.1.2 Computational fluid dynamics techniques 56
2.7.2 Two-Dimensional Flutter Analysis 57
2.7.3 Three-Dimensional Flutter Analysis 59
2.7.4 Flutter Stabilization 60
2.8 Critical Review of Literature 64

Chapter 3 : NONLINEAR STATIC AND VIBRATION ANALYSIS 67
3.1 Introduction 67
3.2 The Cable Stayed Bridge Defined 67
3.2.1 Structural Idealization 68
3.2.1.1 Cable element 69
3.2.1.2 Three-dimensional beam element for tower/deck members 71
3.2.1.3 Rotation transformation matrix 75
3.3 Nonlinear Static Analysis 76
3.4 Free Vibration Analysis 77
3.4.1 Lanczos Iteration Method 78
3.5 Energy Based Evaluation of Modal Structural Damping 82
3.6 Numerical Analysis 87
3.6.1 Details of Bridges 87
3.6.2 Modelling of Bridges 98
3.6.3 Nonlinear Static Analysis 100
3.6.4 Frequencies and Mode Shapes 108
3.6.5 Modal Structural Damping 117
3.7 Summary 126

Chapter 4 : DIGITAL SIMULATION OF STOCHASTIC WIND VELOCITY FIELD 127
4.1 Introduction 127

4.2 Wind Defined 127
4.2.1 Mean Wind 130
4.2.2 Turbulent Wind 131
4.2.2.1 Turbulence intensity 133
4.2.2.2 Turbulent length scale 134
4.2.2.3 Power spectral density functions 136
4.2.2.4 Cross-spectral density / Coherence 137
4.2.2.5 Autocorrelation function 138
4.2.2.6 Cross-correlation function 139
4.2.2.7 Probability density function and peak factor 139
4.3 Simulation of Gaussian Process – Previous Methods 141
4.4 Present Method 145
4.4.1 Spectral Representation Method –Theoretical Background 146
4.4.2 Application of Explicit Form for Cholesky's Decomposition in Spectral Representation Method 149
4.4.3 Simulation Procedure 152
4.5 Details of Software 155
4.6 Validation of Software 160
4.7 Summary 166

Chapter 5 : TIME DOMAIN BUFFETING ANALYSIS **167**
5.1 Introduction 167
5.2 Aerodynamic Forces 167
5.2.1 Buffeting Forces 169
5.2.1.1 Steady-state Force Coefficients 170
5.2.1.2 Aerodynamic admittance function 171
5.2.2 Aeroelastic Forces 173
5.2.3 Rationalised Buffeting Forces 174
5.2.4 Refined Model for Aerodynamic Forces 176
5.2.4 Details of Software 178
5.3 Modal Damping 179
5.4 Time Domain Analysis 182

5.4.1 Application of Wilson-θ Method for Solution of Equations of Motion in Normal Coordinates 184
5.4.2 Time Domain Procedure for Buffeting Response 187
5.4.3 Validation of Time Domain Analysis 189
5.5 Summary 189

Chapter 6 : BUFFETING ANALYSIS OF THREE SPAN CABLE STAYED BRIDGES **191**

6. 1 Introduction 191
6.2 Data for Buffeting Analysis 191
6.2.1 Wind Data 191
6.2.2 Steady-state Force Coefficients 193
6.2.3 Modal Damping 193
6.3 Mean Wind Responses 197
6.4 Buffeting Analysis 200
6.4.1 Buffeting Forces 200
6.4.2 Buffeting Response 201
6.4.2.1 Validation of time domain approach 201
6.4.2.2 Sensitivity analysis 202
6.4.3 Effect of Mean Wind Speed 205
6.4.4 Effect of Terrain Roughness 224
6.4.5 Effect of Type of Deck Supports 233
6.5 Summary 239

Chapter 7 : BUFFETING ANALYSIS OF FIVE SPAN CABLE STAYED BRIDGES **241**

7.1 Introduction 241
7.2 Data for Buffeting Analysis 241
7.2.1 Wind Data 241
7.2.2 Steady-state Force Coefficients 243
7.2.3 Modal Damping 244
7.3 Mean Wind Responses 247
7.4 Buffeting Analysis 247

7.4.1 Buffeting Forces 248
7.4.2 Buffeting Response 248
7.4.3 Effect of Mean Wind Speed 249
7.4.4 Effect of Terrain Roughness 270
7.5 Summary 273

Chapter 8 : FLUTTER ANALYSIS 277
8.1 Introduction 277
8.2 Theoretical Formulation for Flutter 277
8.2.1 Flutter Derivatives 281
8.2.1.1 Airfoil and flat plate derivatives 285
8.2.1.2 Experimentally Determined Flutter Derivatives for Bridge #3 286
8.2.3 Lateral Flutter Derivatives 292
8.3 Two-dimensional Flutter Analysis 292
8.3.1 Solution of Flutter Equations – Deck Subjected to Vertical and Torsional Motions 293
8.3.2 Solution of Flutter Equations –Deck Subjected to Lateral and Torsional Motions 295
8.4 Three-dimensional Flutter Analysis 298
8.4.1 Equations of Motion 298
8.4.2 Flutter Equation of the System 299
8.4.2.1 Aerodynamic Matrices 300
8.4.3 Quadratic Eigenvalue Problem 301
8.4.4 Linearised Eigenvalue Problem 302
8.4.5 Computational Procedure 303
8.5 Details of Software 304
8.5.1 Validation of Software 305
8.6 Numerical Analysis for Flutter 310
8.6.1 Effect of Bridge Vibration in Higher Modes 311
8.6.2 Effect of Angle of Attack 316

8.6.3 Flutter Criteria for Onset of Coupled Lateral and Torsional Motions 318
8.6.4 Effect of Type of Deck Supports 318
8.7 Summary 322

Chapter 9 : CONCLUSIONS AND SCOPE FOR FUTURE RESEARCH 325
9.1 Overview 325
9.2 Conclusions 327
9.2.1 Buffeting Response 327
9.2.1.1 Effect of mean wind speed 328
9.2.1.2 Effect of terrain roughness 328
9.2.2 Flutter Analysis 329
9.2.2.1 Effect of bridge deck vibration in higher modes 329
9.2.2.2 Effect of angle of attack 329
9.2.3 Effect of Support Type for Bridge Deck in Static, Dynamic and Aerodynamic Behaviour of Three Span Bridges 329
9.3 Advancements 330
9.4 Scope for Future Research 331

APPENDIX-I 333
APPENDIX-II 337
APPENDIX-III 339

REFERENCES 345

LIST OF FIGURES

Fig. No.	Description	Page No.
1.1	Wind Effects on Long Span Cable Stayed Bridges	4
1.2	Aerodynamic Forces and Moment	6
2.1	Examples of Different Support Types for Deck in Three Span Cable Stayed Bridges	28
2.2	Relationship between Average Modal Damping and Main Span Length in Three Span Cable Stayed Bridges	40
2.3	Modal Damping and Dynamic Strain Vs Sag to Span Ratio for Inclined Stay Cables	43
3.1	Idealization of Cable Stayed Bridge as a Three-Dimensional Space Structure	68
3.2	Cable Element in Local Co-ordinate System	70
3.3	Three-Dimensional Beam Element in Local Co-ordinate System	72
3.4	Three-Dimensional Beam Element with Co-ordinate Systems	76
3.5	Flow Diagram for Evaluation of Energy Based Damping in Cable Stayed Bridges	86
3.6	Details of Bridge # 1 with Total Span of 627.8 m	88
3.7	Details of Bridge # 2 with Total Span of 1255.8 m	91
3.8	Details of Bridge # 3 with Total Span of 836.6 m	93
3.9	Details of Bridge # 4 with Total Span of 610 m	96
3.10	Three-Dimensional Modelling of Bridge # 1 and Bridge #2	99
3.11	Three-Dimensional Modelling of Bridge # 3	99
3.12	Three-Dimensional Modelling of Bridge # 4	99
3.13	Nonlinear Static Analysis of Bridge # 3 under Dead Load and Initial Cable Tensions	101
3.14	Nonlinear Static Response (Deck Deflection) of Three Span Bridges under Dead Load – Variation with Types of Deck Support	103

3.15	Nonlinear Static Analysis of Bridge # 1 under Dead Load and Initial Cable Tensions	104
3.16	Nonlinear Static Analysis of Bridge # 2 under Dead Load and Initial Cable Tensions	105
3.17	Comparison of Frequencies of Three Span Bridges	109
3.18	Effect of Support Types for Bridge Deck on Frequencies of Three Span Cable Stayed Bridges	109
3.19	Vibration Modes for Bridge # 1 with Type of Deck Support DST-2	110
3.20	Vibration Modes for Bridge # 2 with Type of Deck Support DST-6	111
3.21	Comparison of Frequencies of Bridge # 3 with Three Types of Bridge Deck Cross-Sections	112
3.22	Vibration Modes for Bridge # 3	113
3.23	Vibration Modes for Bridge # 4	114
3.24	Distribution of Modal Strain Energy in Components of Bridge # 1 with Different Types of Deck Support	118
3.25	Distribution of Modal Strain Energy in Components of Bridge # 2 with Different Types of Deck Support	119
3.26	Distribution of Modal Strain Energy in Components of Five Span Cable Stayed Bridges	124
4.1	Turbulent Wind Velocity Field	129
4.2	Mean Wind Profile with Variation in Terrain Roughness	132
4.3	Variation of Longitudinal (I_u) and Vertical (I_w) Turbulence Intensities with Height – Effect of Terrain Roughness	135
4.4	Probability Density Function	140
4.5	Schematic Diagram for WINGEN-Digital Simulation of Stochastic Wind Field	155
4.6	Jiangyin Bridge with Main Span of 1385 m	161
4.7	Spectral Density Functions for Simulated Wind Field of Jiangyin Bridge	163
4.8	Correlation Functions for Simulated Wind Field for Jiangyin Bridge	164

4.9	Digitally Simulated Turbulent Wind Field for Jiangyin Bridge	165
5.1	(a) Lumped Aerodynamic Forces; (b) Degrees of Freedom of Element	168
5.2	The Relationship between Relative Velocity U_r and Effective Angle of Attack α_e.	177
5.3	Schematic Diagram Illustrating the Time Domain Buffeting Analysis	188
6.1	Aerodynamic Damping in Vertical Bending Modes for Bridge # 1	195
6.2	Aerodynamic Damping in Torsional Modes for Bridge # 1	195
6.3	Aerodynamic Damping in Vertical Bending Modes for Bridge # 2	196
6.4	Aerodynamic Damping in Torsional Modes for Bridge # 2	196
6.5	Comparison of Vertical Buffeting Response at Midspan of Bridge # 1 – Time Domain Vs Frequency Domain Approach	203
6.6	Peak Vertical Buffeting Response for Bridge # 1 – Variation with Number of Modes	203
6.7	Time Domain Analysis for Vertical Buffeting Response in Bridge # 1 at U(30) = 34.3 m/sec for TC-1	207
6.8	Responses in Bridge # 1 for Terrain Category TC-1 – Variation with Mean Wind Speed	208
6.9	Absolute Maximum Axial Forces in Cables of Bridge # 1 – Variation with Mean Wind Speed	210
6.10	Absolute Maximum Axial Force in Towers of Bridge # 1 – Variation with Mean Wind Speed	211
6.11	Deck Axial Force Diagram for Bridge # 1	212
6.12	Absolute Maximum Deck Axial Force and Reactions at Deck Supports in Bridge # 1 – Variation with Mean Wind Speed	213
6.13	Deck Vertical Shear Force Diagram for Bridge # 1 at Wind Speed U(30) = 34.3 m/sec for TC-1	214
6.14	Deck Bending Moment Diagram for Bridge # 1 at Wind Speed U(30) = 34.3 m/sec for TC-1	215

6.15	Time Domain Analysis for Buffeting Response in Torsion for Bridge # 1	216
6.16	Time Domain Analysis for Vertical Buffeting Response in Bridge # 2 at U(45) = 43.2 m/sec for TC-2	218
6.17	Responses in Bridge # 2 for Terrain Category TC-2 - Variation with Mean Wind Speed	219
6.18	Absolute Maximum Axial Forces in Cables of Bridge # 2 – Variation with Mean Wind Speed	220
6.19	Absolute Maximum Axial Force in Towers of Bridge # 2 - Variation with Mean Wind Speed	221
6.20	Deck Axial Force Diagram for Bridge # 2	222
6.21	Absolute Maximum Axial Force in Deck and Reactions at Deck Supports in Bridge # 2 – Variation with Mean Wind Speed	223
6.22	Deck Vertical Shear Force Diagram for Bridge # 2 at Wind Speed U(45) = 43.2 m/sec for TC-2	225
6.23	Deck Bending Moment Diagram for Bridge # 2 at Wind Speed U(45) = 43.2 m/sec for TC-2	226
6.24	Time Domain Analysis for Buffeting Response in Lateral Direction for Bridge # 2	227
6.25	Time Domain Analysis for Buffeting Response in Torsion for Bridge # 2	228
6.26	Wind Induced Response of Bridge # 1 – Effect of Terrain Roughness	230
6.27	Spatial Distribution of Gust Response Factor for Bridge # 1 – Effect of Terrain Roughness	230
6.28	Effect of Terrain Roughness on Buffeting Induced Absolute Maximum Axial Force in Components of Bridge # 1	231
6.29	Wind Induced Response of Bridge # 2 – Variation with Terrain Roughness	232
6.30	Spatial Distribution of Gust Response Factor for Bridge # 2 – Effect of Terrain Roughness	234

6.31	Effect of Terrain Roughness on Buffeting Induced Absolute Maximum Axial Force in Components of Bridge # 2	235
6.32	Spatial Distribution of Gust Response Factors for Bridge # 1 – Variation with Support Types for Bridge Deck	238
6.33	Spatial Distribution of Gust Response Factors for Bridge # 2 – Variation with Support Types for Bridge Deck	238
7.1	Aerodynamic Damping in Vertical Bending Modes for Bridge # 3	245
7.2	Aerodynamic Damping in Torsional Modes for Bridge # 3	245
7.3	Aerodynamic Damping in Vertical Bending Modes for Bridge # 4	246
7.4	Aerodynamic Damping in Torsional Modes for Bridge # 4	246
7.5	Time Domain Analysis for Vertical Buffeting Response in Bridge # 3 at U(34) = 43.2 m/sec for TC-3	250
7.6	Responses in Bridge # 3 for Terrain Category TC-3 – Variation with Mean Wind Speed	251
7.7	Forces in Cables of Bridge # 3 – Variation with Mean Wind Speed	253
7.8	Absolute Maximum Axial Force in Towers of Bridge # 3 – Variation with Mean Wind Speed	254
7.9	Deck Axial Force Diagram for Bridge # 3	255
7.10	Absolute Maximum Axial Force in Deck and Reactions at Deck Supports in Bridge # 3 – Variation with Mean Wind Speed	256
7.11	Deck Vertical Shear Force Diagram for Bridge # 3 at Wind Speed U(34) = 43.2 m/sec for TC-3	257
7.12	Deck Bending Moment Diagram for Bridge # 3 at Wind Speed U(34) = 43.2 m/sec for TC-3	258
7.13	Time Domain Analysis for Buffeting Response in Lateral Direction for Bridge # 3	260
7.14	Time Domain Analysis for Buffeting Response in Torsion for Bridge # 3	261
7.15	Time Domain Analysis for Vertical Buffeting Response in Bridge # 4 at U(27) = 45.2 m/sec for TC-1	262

7.16	Responses in Bridge # 4 for Terrain Category TC-1 – Variation with Mean Wind Speed	263
7.17	Absolute Maximum Axial Force in Cables of Bridge # 4 – Variation with Mean Wind Speed	264
7.18	Absolute Maximum Axial Force in Towers of Bridge # 4 – Variation with Mean Wind Speed	266
7.19	Deck Axial Force Diagram for Bridge # 4	267
7.20	Absolute Maximum Axial Force in Deck and Reactions at Deck Supports in Bridge # 4 – Variation with Mean Wind Speed	268
7.21	Time Domain Analysis for Buffeting Response in Torsion for Bridge # 4	269
7.22	Wind Induced Response of Bridge # 3 - Effect of Terrain Roughness	271
7.23	Spatial Distribution of Gust Response Factor for Bridge # 3 - Effect of Terrain Roughness	271
7.24	Effect of Terrain Roughness on Buffeting Induced Absolute Maximum Axial Force in Components of Bridge # 3	272
7.25	Wind Induced Response of Bridge # 4 – Effect of Terrain Roughness	274
7.26	Spatial Distribution of Gust Response Factor for Bridge # 4 – Effect of Terrain Roughness	274
7.27	Effect of Terrain Roughness on Buffeting Induced Absolute Maximum Axial Force in Components of Bridge # 4	275
8.1	Spring Suspended Bridge Deck Model with Three Degrees of Freedom	278
8.2	Flutter Derivatives for a Typical Trapezoidal Box Section	283
8.3	Flutter Derivatives for a Typical Streamlined Box Section	284
8.4	Flutter Derivatives for Thin Airfoil and Flat Plate	287
8.5	Comparison of Deck Section Configurations for Bridge #3	288
8.6	Flutter Derivatives for Deck Section C-2 of Bridge #3	289
8.7	Flutter Derivatives for Deck Section C-2C of Bridge #3	290
8.8	Flutter Derivatives for Deck Section C-1B of Bridge #3	291

8.9	Flutter Derivatives for Lions' Gate Bridge (Renovated Deck Cross-Section)	307
8.10	Determination of Incipient Stage for Flutter for Lions' Gate Bridge	309
8.11	Determination of Incipient Stage for Flutter for Vasco da Gama Bridge	309
8.12	Determination of Incipient Stage for Flutter of Bridge #1 – Effect of Bridge Deck Vibration in Higher Modes	313
8.13	Determination of Incipient Stage for Flutter of Bridge # 2 – Effect of Bridge Deck Vibration in Higher Modes	314
8.14	Determination of Incipient Stage for Flutter of Bridge #4 (1^{st} Symmetric Vertical and Torsional Modes)	315
8.15	Determination of Incipient Stage for Flutter of Bridge # 3 with Deck Configuration C-1B at Various Angles of Attack	317
8.16	Determination of Incipient Stage for Coupled Lateral and Torsional Flutter of Bridge #2 (1^{st} Symmetric Vertical and Torsional Modes)	319
8.17	Determination of Incipient Stage for Flutter of Bridge #1 – Effect of Type of Deck Supports (1^{st} Symmetric Vertical and Torsional Modes)	320
8.18	Determination of Incipient Stage for Flutter of Bridge #2 – Effect of Type of Deck Supports (1^{st} Symmetric Vertical and Torsional Modes)	321
A-1.1	Axial Forces and End Moments for a Beam Element	333

LIST OF TABLES

Table No.	Description	Page No.
1.1	World's Long Span Cable Stayed Bridges	2
2.1	Measured Modal Structural Damping of Ikuchi Bridge	39
2.2	Modal Structural Damping of Tsurumi Tsubasa Bridge	41
2.3	Modal Damping of Normandy and Vasco da Gama Bridge	42
2.4	Summary of Damping Ratio for Cables	42
3.1(a)	Structural Properties for Bridge # 1	89
3.1(b)	Details of Cables for Bridge # 1	89
3.2(a)	Structural Properties for Bridge # 2	90
3.2(b)	Details of Cables for Bridge # 2	92
3.3(a)	Structural Properties of Bridge Deck for Bridge #3	94
3.3(b)	Structural Properties of Towers for Bridge #3	94
3.3(c)	Details of Cables for Bridge #3	95
3.4(a)	Structural Properties of Deck and Towers for Bridge #4	97
3.4(b)	Details of Cables for Bridge #4	97
3.5	Comparison of Nonlinear Static Response for Bridge # 3	100
3.6	Nonlinear Static Response for Bridge # 4	102
3.7	Nonlinear Static Response for Bridge # 1 with Different Support Types for Bridge Deck	106
3.8	Nonlinear Static Response for Bridge # 2 with Different Support Types for Bridge Deck	107
3.9	Vibration Characteristics of Bridge # 1 with Different Support Types for Bridge Deck	115
3.10	Vibration Characteristics of Bridge # 2 with Different Support Types for Bridge Deck	116
3.11(a)	Modal Structural Damping for Bridge # 1 with Deck Support Types DST-1 and DST-2	121

3.11(b)	Modal Structural Damping for Bridge # 1 with Deck Support Types DST-3 and DST-4	121
3.11(c)	Modal Structural Damping for Bridge # 1 with Deck Support Types DST-5 and DST-6	122
3.12(a)	Modal Structural Damping for Bridge # 2 with Deck Support Types DST-1 and DST-2	122
3.12(b)	Modal Structural Damping for Bridge # 2 with Deck Support Types DST-3 and DST-4	123
3.12(c)	Modal Structural Damping for Bridge # 2 with Deck Support Types DST-5 and DST-6	123
3.13(a)	Modal Structural Damping for Bridge # 3 with Deck Configuration C-1B	125
3.13(b)	Modal Structural Damping for Bridge # 4	125
4.1	Surface Roughness Parameters and Surface Drag Coefficient	131
4.2	Values of β for Various Roughness Lengths	133
5.1	Steady-state Force Coefficients for Some of the Cable Bridges	172
6.1	Net Modal Damping for Bridge #1 – Variation with Mean Wind (Support Type for Bridge Deck - DST-2)	197
6.2	Static Response for Bridge #1 due to Dead Load and Mean Wind Forces - Effect of Support Types for Bridge Deck (Mean Wind Speed U(30)=45.8m/sec for Terrain Category TC-1)	198
6.3	Axial Force in Cables of Bridge #1 due to Dead Load and Mean Wind Forces - Effect of Support Types for Bridge Deck (Mean Wind Speed U(30)=45.8m/sec for Terrain Category TC-1)	198
6.4	Static Response for Bridge #2 due to Dead Load and Mean Wind Forces - Effect of Support Types for Bridge Deck (Mean Wind Speed U(45)=43.20m/sec for Terrain Category TC-2)	199
6.5	Axial Force in Cables of Bridge #2 due to Dead Load and Mean Wind Forces - Effect of Support Types for Bridge Deck (Mean Wind Speed U(45)=43.20m/sec for Terrain Category TC-2)	199
6.6	Peak Buffeting Response with Number of Modes for Bridge#1	204

6.7	Peak Buffeting Response for Bridge # 1 – Effect of Support Types for Bridge Deck (Mean Wind Speed U(30)=45.8m/sec for Terrain Category TC-1)	236
6.8	Absolute Maximum Axial Force in Cables of Bridge #1 due to Buffeting – Effect of Support Types for Bridge Deck	236
6.9	Peak Buffeting Response for Bridge # 2 – Effect of Support Types for Bridge Deck (Mean Wind Speed U(45) = 43.2 m/sec for Terrain Category TC-2)	237
6.10	Absolute Maximum Axial Force in Cables of Bridge #2 due to Buffeting - Effect of Support Types for Bridge Deck (Mean Wind Speed U(45) = 43.2 m/sec for Terrain Category TC-2)	237
8.1	Inertia and Frequency Parameters for the Renewed Lions' Gate Deck Section	308
8.2	Inertia and Frequency Parameters for Vaso da Gama Bridge Deck Section	308
8.3	Critical Flutter Speed for Bridge #3 with Different Deck Configuration-Effect of Angles of Attack of Approaching Wind	316

NOMENCLATURE

The principal symbols used in the text are listed below. All symbols, including those listed here, are defined at appropriate places in the text, usually at the time of first occurrence. Occasionally, the same symbol may be used to represent more than one parameter, but the meaning should be quite unambiguous when read in context.

A	Exposed surface area to wind
A	Cross- sectional area of member
A_c	Cross-section area of cable
B	Reference along-wind dimension
C_L	Lift coefficient
C_D	Drag coefficient
C_{Dc}	Drag coefficient of cable
C_M	Moment coefficient
C_p	Non dimensional pressure coefficient
d	Reference dimension of cross-section
d_c	Diameter of cable
E	Member material modulus of elasticity
E_{eq}	Equivalent modulus
E_c	Cable material effective modulus
$(E_P)_i^n$	Modal potential energy for i^{th} element for n^{th} mode
$(E_{ST})_i^n$	Modal strain energy
$(E_G)_i^n$	Modal potential energy due to work done by the initial stress due to modal strain.
f	Vortex shedding frequency
F_L	Lift force
F_D	Drag force
F_M	Aerodynamic moment

G	Member material shear modulus
H_i^*, P_i^*, A_i^*	Flutter derivatives and functions of K for the deck cross-section in vertical, lateral and torsional directions, respectively (i=1,6)
i,k	Unit vectors in horizontal and vertical directions, respectively
I	Mass moment of inertia of deck per unit length
I_y and I_z	Moments of inertia of the cross-section about the local principal y and z axes, respectively
I_x	Torsional moment of inertia of the cross- section
k	Von Karman's constant
J_0, J_1, Y_0, Y_1	Bessel functions of the first and second kind respectively.
K	Reduced frequency
$[K]$	System stiffness matrix
L	Member length
L_{hc}	Projected length of cable
L_{ae}, D_{ae}, M_{ae}	Unsteady aerodynamic or self-excited forces in vertical, lateral and torsional degrees of freedom respectively.
m_c	Linear mass of cable per unit length
M	Mass per unit deck length,
$[M]$	Diagonal mass matrix (assuming no mass coupling)
n_h, n_α, and n_p	Natural frequencies of bridge in vertical, torsional and lateral directions.
p	Local pressure at some point on the structure
p_o	Pressure in undisturbed flow far upwind
$\dot{p}, \dot{h}$ and $\dot{\alpha}$	Velocities of the bridge at time 't' with respect to the transverse, vertical and rotational directions respectively
q	Dynamic pressure at some reference point
q_i	i^{th} generalized coordinate
$\dot{q}_i$	i^{th} generalized velocity
Q_i	i^{th} generalized force
T	Kinetic energy
T_c	Cable tension

T_n	Period of vibration of cable for n^{th} mode
u	Horizontal displacement of point A
u_*	Friction velocity
U	Strain energy
U	Wind speed in m/sec
U (10)	Mean wind velocity at 10m above ground level
w	Vertical displacement of point A
w_c	Weight per unit length of the cable
z_o	Surface roughness factor
z	Height above mean ground surface

Greek Symbols

α	Rotation angle of bridge at time 't'
α_w	Angle of incidence of wind
$\{\phi\}$	Normalized mode shapes (eigenvectors)
κ	Surface drag coefficient
λ	Eigenvalues
ρ	Air density
ω_n	Circular frequency of cable for n^{th} mode
$\omega_h, \omega_p, \omega_\alpha$	Circular natural frequencies for vertical, lateral and torsional degrees of freedom respectively
ξ_h, ξ_p, ξ_α	Ratio of damping to critical damping for vertical, lateral and torsional degrees of freedom respectively.

Chapter 1
INTRODUCTION

1.1 GENERAL

The analysis of cable stayed bridges to estimate the dynamic response due to wind loading is an imperative requirement in the design criteria, as they are relatively lightweight, flexible and lightly damped large span structures. The research in the area of bridge aerodynamics marked a beginning in this direction after the collapse of Tacoma Narrows Bridge in 1940s. The last two decades witnessed lot of progress in wind tunnel testing techniques, analytical assessment and development of software to evaluate wind induced response. These advancements in the state–of–the art, applied to the design, helped in achieving cable stayed bridges of about 900m main span as in the case of Normandy Bridge in France (main span of 856m) and Tatara Bridge in Japan (main span of 890m). Thus cable stayed bridges have successfully taken over the region of span in which once suspension bridges dominated, as can be seen from Table 1.1. There are two major structural advantages for achieving success in design of longer spans of cable stayed bridges. Firstly, since a number of compact cables can be self – anchored in a cable stayed bridge, massive–scale anchorage is not necessary as in a conventional suspension bridge. Secondly, the diagonally tensioned cables in a cable stayed bridge have greater rigidity and are less deflective than those of a suspension bridge, leading to cost reductions. In addition to structural advantages, varieties of structural forms for pylon and cable system are aesthetically attractive.

Based on a detailed study on alternate design of Great Belt Crossing by Peterson *et al* (1991), it is reported that cable stayed system is economical when the span is less than 1200m. However, some later studies by Fujino and Nagai (1994 a, b) indicate that the main span of a cable stayed bridge can reach to even 1400m without

Table 1.1 : World's Long Span Cable Stayed Bridges

No.	Name of Bridge	Country	Year	Mainspan L (m)	Width B (m)	Depth d (m)	Deck
1	Tatara	Japan	1999	890	27.4	2.7	Steel + PC
2	Normandy	France	1995	856	21.2	3.0	Composite + PC
3	Nanjing Yangtze II	China	U.C	628			Steel
4	Qing Zhou	China	U.C	605			Steel
5	Yangpu	China	1993	602	32.5	2.6	Composite
6	Xupu	China	1997	590			Composite
7	Meiko Central	Japan	1993	590	37.5	3.5	Steel
8	Skarnsundet	Norway	1991	530	13.0	2.15	PC
9	Tsurumi	Japan	1995	510	38.0	4.0	Steel
10	Ikuchi	Japan	1991	490	24.1	2.48	Steel + PC
11	Oresund	Denmark/ Sweden	2000	490	24.7	6.25	Steel Truss
12	East Kobe	Japan	1994	485	17.0	9.0	Steel Truss
13	Ting Kau	Hong Kong	1998	475			Steel
14	Seohae	Korea	2000	470			
15	Alex Frazer	Canada	1986	465	28.0	2.265	Composite
16	Yokohama	Japan	1989	460	40.2	12.0	Steel Truss
17	2nd Hooghly	India	1989	457	35.0	2.25	Composite
18	2nd Severn	U.K.	1996	456	34.0		Composite
19	Rama IX	Thailand	1987	450	32.5	3.58	Steel
20	Queen Elizabeth II	U.K.	1991	450	22.0	2.0	Composite
21	Luna	Spain	1983	440	22.5	2.30	Concrete
22	Helgeland	Norway	1991	425	11.95	1.20	Concrete
23	Nanpu	China	1991	423	30.35	2.1	Composite
24	Hitsuishijima/ Iwakurojima	Japan	1988	420	27.5	13.9	Steel Truss
25	Vasco da Gama	Portugal	1999	420	30.9	2.62	Steel
26	Meiko-East	Japan		410			Steel
27	Meiko-West	Japan	1985	405			Steel
28	Saint Nazaire	France	1975	404	14.8	3.2	Steel

losing its competitiveness. The alternate design of Messina straits crossing, which was done in 1982 for a span of 1800m, carrying railroad plus highway, proved the constructability and safety as reported by Leonhardt and Zellner (1990). As the innovations in the design of cable stayed bridges is still in progress, new generation of cable stayed bridges that are more efficient and elegant, is expected to be constructed during this century as predicted by Ito *et al* (1990) and Gimsing (1996).

Realization of such long spans is inevitably accompanied by great difficulties particularly in wind resistant design. Aerodynamic investigations on long span bridges is primarily assessed by wind tunnel testing, in which section–model test has more frequently and historically been used for reasons of simplicity and relative cost. Wind tunnel testing with an aeroelastic full model is alternatively used for the purpose of final verification, aiming at the investigation on three-dimensional, atmospheric turbulence and multimode effects.

On the other hand, recently analytical assessment in wind resistant design of long span bridges is becoming popular and seems to have taken a significant role in design process, reflecting the long-time accumulation of research in bridge aerodynamics and rapid advancement in computer technology. Hence to realize these super span bridges, it is essential to develop realistic analytical procedures to understand the complex wind induced oscillatory problems and wind resistant design.

The basic concepts of bridge aerodynamics and review of previous studies related to static, dynamic and aerodynamic analysis of cable stayed bridges is presented before giving the details of objectives and scope of study.

1.2 BASIC CONCEPTS OF BRIDGE AERODYNAMICS

The wind effects on long span cable bridges can be classified as in Fig. 1.1. The static and dynamic wind effects as well as the methodology for estimation of wind induced response and wind resistant design are given in the following sections.

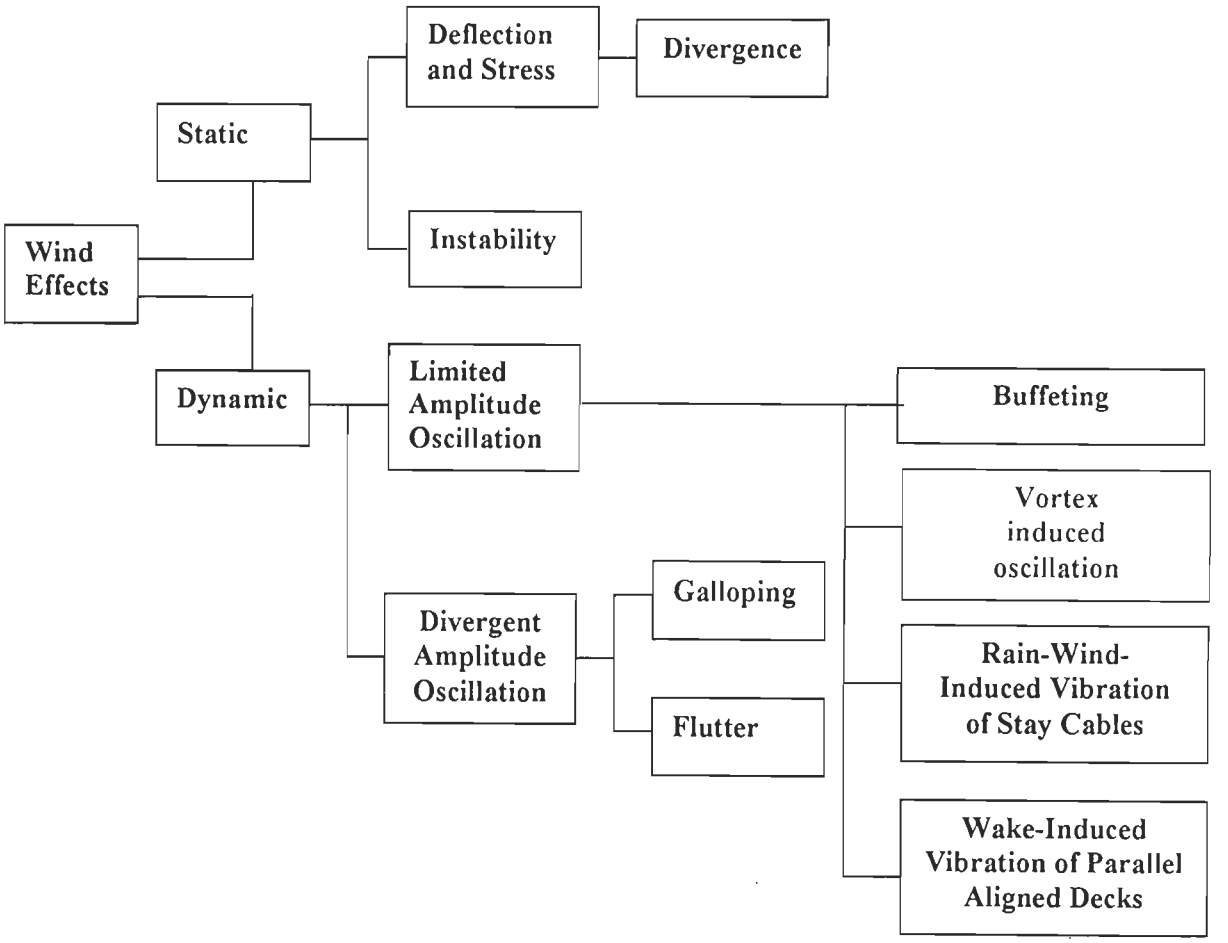

Fig. 1.1 : Wind Effects on Long Span Cable Stayed Bridges

1.2.1 Static Wind Effects

When the wind flows past a bridge deck or other component, it gives rise to pressures in the upstream, downstream and upper and lower surfaces of the deck. It is usual to non-dimensionalise all pressures with respect to the mean dynamic pressure at some reference point where the flow is undisturbed by the presence of the structure. Non-dimensional pressure coefficients are thus defined as,

$$C_p = \frac{p - p_o}{q} \tag{1.1}$$

where,

C_p = non dimensional pressure coefficient

p = local pressure at some point on the structure

p_o = pressure in undisturbed flow far upwind

q = dynamic pressure at some reference point

The pressures developed around the structure generate wind forces. The resultant wind force acting on the structure is usually resolved into two components, one parallel and the other normal to the direction of wind flow. These forces are termed as drag or along-wind force, and the lift or across-wind force, respectively. The unsymmetrical pressure distribution around the bridge deck section produces aerodynamic moment. The aerodynamic moment with respect to some arbitrary point is equal to the product of the aerodynamic force and its lever arm distance with respect to that point. As illustrated in Fig. 1.2 the static wind forces acting on the deck are,

$$F_L(\alpha_\omega) = qAC_L(\alpha_\omega) \tag{1.2}$$

$$F_D(\alpha_\omega) = qAC_D(\alpha_\omega) \tag{1.3}$$

$$F_M(\alpha_\omega) = qABC_M(\alpha_\omega) \tag{1.4}$$

where,

F_L = lift force

F_D = drag force

F_M = aerodynamic moment

q = dynamic pressure

A = exposed surface area

B = reference along-wind dimension

C_L = lift coefficient

C_D = drag coefficient

C_M = moment coefficient and

α_w = angle of incidence of wind

The non-dimensional drag, lift and moment coefficients are generally determined through wind tunnel investigations for bridge decks, tower sections and cables. These coefficients are generally functions of angle of incidence α_w, defined as angle between the oncoming wind and the plane of bridge deck.

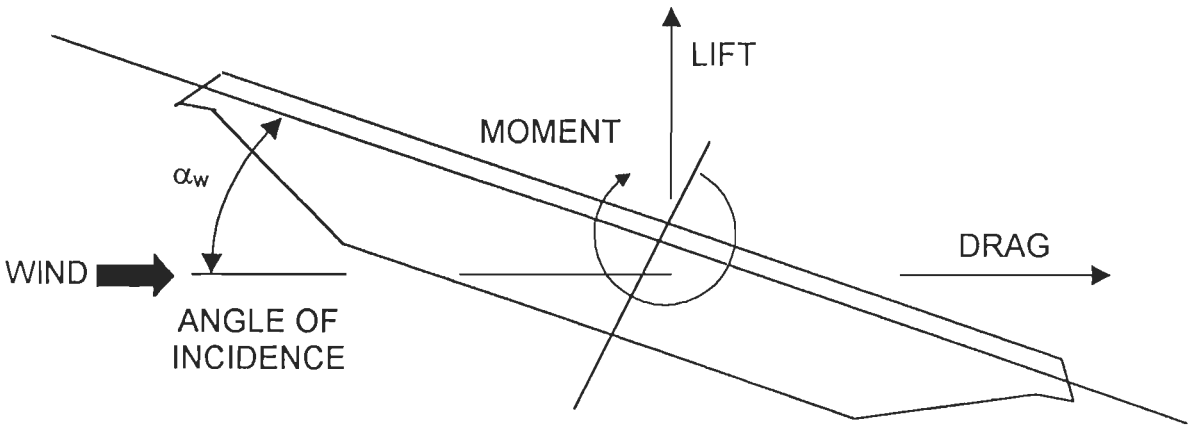

Fig. 1.2 : Aerodynamic Forces and Moment

The three components of the wind load are used in the three–dimensional nonlinear analysis of cable stayed bridges. Further, with longer spans, the wind load from the cables becomes larger than the wind load which directly acts on the deck. Therefore it is essential to include the wind loads on all structural components for the three-dimensional analysis, which demands steady-state coefficients for deck, tower and cables.

Divergence

Divergence is analogous to static buckling and is thus an instability condition. As discussed earlier, wind flow across a bridge deck produces static aerodynamic moment (Eq. 1.4) related to square of velocity and an accompanying torsional rotation. The bridge deck has certain torsional rigidity depending on the modulus of rigidity, torsional constant and the support conditions. For low wind velocities, bridge deck's capacity to resist torsion will be greater than the aerodynamic moment. At some critical wind velocity, the aerodynamic moment equals the torsional strength of deck. The deck becomes unstable in torsion, hence divergence. In long span cable suspended bridges with typically high torsional resistance, other instabilities usually occur before the onset of divergence and the wind velocity divergence is very high. Analytical solution for divergence may be found given in Scanlan (1981), Simiu and Scanlan (1996).

1.2.2 Dynamic Wind Effects

The dynamic wind effects which cause oscillations of limited amplitude in bridges are described first and subsequently the divergent oscillatory phenomena has been explained in the following sections:

Buffeting

Buffeting is defined as the forced random response to fluctuations in the wind, either produced by natural turbulence or upwind obstructions. As the natural wind is not steady but turbulent in character, wind fluctuations in vertical and longitudinal or along-wind directions are random in space and thus the wind pressure along a bridge is random in time and space. Depending on the spectral distribution of pressure vectors, certain modes of vibration of a bridge may selectively get excited. In fact, these wind induced buffeting oscillations are related not only to the wind characteristics, but also to the shape of cross-section of the bridge deck, fluid–structure interaction and signature buffeting, i.e., due to separated flow as in the case of bluff bridge sections.

Even though, buffeting response does not lead to catastrophic failures, with record breaking lengths of modern cable stayed bridges, it drastically enhances the design wind loads acting on the bridge. Further, its importance has greatly increased due to possibility of occurrence of fatigue damage of structural components and connections, instability of vehicles traveling on the bridge deck and discomfort to pedestrians. During the design stage, there is a need to ascertain whether the buffeting response would be harmful to bridge over its lifetime from either user comfort or fatigue consideration and to control those parameters that counteract buffeting.

Vortex Induced Oscillations

Vortex induced oscillations are caused by the periodic across-wind forces arising from the shedding of vortices alternatively in the wake, from upper and lower surfaces of the bridge deck over one or more limited ranges of wind speed. The

frequency of shedding of complementary pairs of vortices is expressed in non-dimensional form by the Strouhal number 'S', which is typical for any particular geometrical shape of deck.

$$S = fd/U \tag{1.5}$$

f = vortex shedding frequency

d = reference dimension of cross-section

U = wind speed

The range of wind speed over which the frequency of excitation comes close enough to a natural frequency of the bridge, resonant across-wind oscillations in isolated vertical bending mode occur. Since the across-wind forces are not necessarily at the center of twist of bridge deck, alternating aerodynamic moments are also generated, which, in turn produces large steady-state torsional oscillations when the vortex shedding frequency coincides with one of the torsional frequencies of the bridge. Usually, the response is said to "lock-in" to a natural mode and is not catastrophic. Vortex induced oscillations in bridges are usually discomforting to humans and may cause accelerated fatigue damage.

The Strouhal number for various bluff bodies is typically in the range 0.1 to 0.3. For no vortex induced oscillation to take place, the critical wind speed for vortex excitation U_c should be greater than the design wind speed at the site.

Generally, for a cable stayed bridge, the critical wind speed for vortex excitation is much lower than the design wind speed at site and it is necessary to control the amplitude of vibration by suitable means. Geometrical design features of cross–section which help in narrowing the width of wake are found to reduce the strength of vortex excitation and thus the amplitude of oscillation. Such features are usage of shallow sections, perforations in deck, soffit plates to close the space between the main girders, attachment of tapered fairings to side faces, use of deflection vanes, flaps and by avoiding high solidity fittings near the edge of deck.

Studies on vortex induced oscillations of cable bridges; analytical models and design procedures can be found in Wardlaw (1968), Gade (1974), Scanlan (1975), Scanlan (1981), Milne (1981), Ehshan (1988) and Nagao *et al* (1999).

Rain-Wind-Induced Oscillations of Stay Cables

Rain-wind-induced oscillations of stay cables is caused by the formation of water rivulets on the cable surface, the axial flow in the wake of the cable, and, the two-dimensional Karman vortex shedding as a result of which oscillations of long stay cables occur in the across-wind direction.

The studies on rain induced vibrations, its mechanism, and remedial measures can be found in Hikami and Shirashi (1988), Matsumato *et al* (1988,1992, 1994), Kobayashi *et al* (1994), Ruscheweyh (1999).

Wake Induced Vibration of Parallel Aligned Decks

Wake induced vibrations of decks occur, when there are parallel aligned bridge decks close to each other and the separated flow in the wake of one bridge deck influences the oscillations of the other deck, i.e., the oscillatory responses get magnified. Aerodynamic response of parallel aligned decks has been reported in Scanlan and Jones (1990).

The phenomena explained above are limited amplitude oscillations and are not catastrophic. These may, however, may lead to fatigue problems, whereas the galloping and flutter are self-excited oscillations, i.e., the motion of structure itself produces the forcing mechanism responsible for the large amplitude or divergent oscillations.

Galloping

Galloping describes the large–amplitude divergent response of flexible structures with non- circular cross-sections. It is caused by the effective angle of attack due to vertical or torsional motion of the structure. When the energy fed into the

oscillating structure is larger than the energy dissipated by damping, the structure gallops. It is mainly dependent on the quasi-steady behaviour of the structure. A negative slope in the plot of static lift or torsional moment coefficient versus angle of attack usually indicates the tendency for galloping. It can be identified with Den Hertog criterion, which states that there is a destabilizing aerodynamic zone when the following criterion is satisfied.

$$\frac{dC_L}{d\alpha_\omega} + C_D < 0 \tag{1.6}$$

It has been found that the rectangular cross-sections with width to depth ratio less than five are prone to galloping. With possible exception of pedestrian and pipeline bridges, highway bridges are not susceptible to galloping because of their slenderness. However, it is important to consider galloping in the design of towers, particularly during erection before the cables and decks are installed.

Flutter

Flutter oscillation originates from the mutual interaction of elastic, inertial and damping and self-excited aerodynamic forces. Recalling from elementary dynamics that a damping force is proportional to the structure's velocity, it is possible for the forces to add, rather than to dissipate, energy if velocity dependent components of the wind forces are generated 180 degrees out-of-phase with the structure's damping forces. Under such conditions, the bridges oscillate in a divergent or destructive manner at some critical wind speed. Flutter can be classified as damping driven flutter and stiffness driven flutter.

Damping driven flutter is a single degree of freedom oscillation in vertical or torsional direction, often observed in bridge deck sections with bluff cross–section and is identified by the wind speed that produces enough negative aerodynamic damping to offset the bridge's own structural damping.

Stiffness driven or classical flutter is characterized by the coupling of vertical bending and torsional or lateral bending and torsional modes as in long span bridges with streamlined cross-sections. This kind of flutter occurs when the frequencies in still air of vertical and torsional modes ω_h and ω_α or of lateral and torsional modes ω_p and ω_α are close to each other. The aerodynamic forces try to increase either vertical stiffness or lateral stiffness and reduce the torsional stiffness and these modes try to couple. The tendency of modal coupling can be examined mathematically using the mode shapes.

During the design stage, checking the susceptibility for flutter essentially consists of analysing the bridge to determine the lowest wind speed that indicates the incipient stage of flutter. To eliminate the possibility of occurrence, the critical wind speed for flutter U_{fc} should be much higher than the design wind velocity at the bridge location.

The present study concerns itself only with buffeting and flutter analyses of long span cable stayed bridges. An overview of methodology for determining the wind induced response and evaluating the aerodynamic design is given in the following section.

1.2.3 Overview of Methodology

The methodology for the estimation of wind induced oscillatory responses (Jones *et al*, 1998) and wind resistant design of cable stayed bridges consists of following steps:

- Measurement of a comprehensive set of aerodynamic and aeroelastic parameters for the bridge deck cross-section using a suitably scaled section model. These parameters include
  - The aerodynamic force coefficients C_D, C_L and C_M at a number of angles of attack. This enables the estimation of the derivatives of force coefficients with respect to angle of attack which is needed for buffeting analysis.

- The flutter derivatives H_1^* - H_6^*, A_1^* - A_6^*, P_1^* - P_6^* (measurement of all the eighteen is now routinely possible), at several positive and negative angles of attack (as the critical flutter condition is commonly found to occur at a non–zero angle of attack) Sarkar *et al* (1992,1994), Singh *et al* (1995,1996).

- Carrying out a finite element dynamic analysis for the bridge under consideration. This analysis is expected to provide a comprehensive set of eigen values and eigen vectors of the structure.
- Making use of an analytical framework and associated computational aids, synthesize the above aerodynamic and aeroelastic parameters and structural vibration characteristics such as frequencies, mode shapes and modal damping (generally assumed) along with wind environment descriptions. Thus predict the response due to buffeting and identify the incipient stage of flutter (Jain *et al* 1995,1996).
- If the estimated buffeting response and the critical flutter speed are within the permissible limits, the design is acceptable. If not, the aerodynamic behaviour of the bridge can be improved (i) by adding geometrical features such as flaps, fairings, splitter plates, etc., (ii) by making structural modifications such as adjusting mass distribution and increasing stiffness or (iii) by employing mechanical means such as passive or active dampers.
- Check the effectiveness of modifications by aeroelastic model testing in case of aerodynamic modifications. Use analytical methods for checking the effectiveness of structural and mechanical modifications before accepting the design.

1.3 PROBLEM IDENTIFICATION AND OBJECTIVE OF THE STUDY

The static, dynamic and aerodynamic analysis of long span cable stayed bridges is a complex problem. As these bridges are geometrically nonlinear, any attempt to simplify the analysis may lead to inaccurate prediction of responses. For instance, nonlinearities due to sag in cable, axial-flexural interaction of deck and tower members, and the overall large displacements due to high flexibility, affect the accuracy of static and dynamic analyses. Further, usage of assumed modal structural damping for subsequent flutter and buffeting analysis may not reflect the actual behavior of the bridge. Frequency domain buffeting analysis, even though computationally efficient, is not capable in handling the nonlinearities in the aerodynamic forces. With longer span lengths, the possibility of occurrence of coupled flutter, especially lateral and torsional modes, needs to be addressed. Also, uncoupled aerodynamic response is not justified since aerodynamic forces are always generated simultaneously and are coupled. Finally, the support type for bridge deck at the towers and abutments such as fixed, movable, floating or elastically supported can have a significant influence on the aerodynamic behaviour of the three span cable stayed bridge and needs to be investigated.

After considering the state-of–the-art of analytical procedures in bridge aerodynamics, a comprehensive approach for buffeting and flutter analysis of long span cable stayed bridges is developed. The systematic approach includes: (i) performing a non linear static analysis under dead load condition accounting for nonlinearities due to cable sag, axial – flexural interaction in deck and tower members and large displacements, (ii) vibration analysis using the dead load deformed geometry, (iii) estimation of modal structural damping by energy dissipation method, (iv) time domain buffeting analysis in which the digital simulation of wind is achieved through spectral representation method, and (v) flutter analysis of cable stayed bridge.

1.4 PLAN OF STUDY

The comprehensive procedure for analysis of wind-induced oscillations in cable stayed bridges is achieved by

(i) Use of dead load deformed state, obtained by the nonlinear static analysis under dead load and initial tension, for vibration and aerodynamic analysis.

(ii) Use of theoretically estimated modal structural damping based on energy dissipation for aerodynamic and aeroelastic analysis.

(iii) Digital generation of wind velocity along the span of bridge deck using spectral representation method, including the spanwise correlation effects employing coherence function.

(iv) Performing buffeting analysis using time domain approach on three dimensional finite element model of a cable stayed bridge rather than on bridge deck alone.

(v) Flutter analysis to identify the incipient flutter state when the bridge deck is subjected to either vertical and torsional motions or lateral and torsional motions.

In this thesis, the above methodology has been adopted for buffeting and flutter analysis of four cable stayed bridges, two with three spans and the other two with five spans. Time domain buffeting analysis of three span composite bridges, Bridge #1 with total span of 627.8m, Bridge#2 with total span of 1255.8m and five span bridges, Bridge#3 –an existing steel bridge with total span of 836.6m and Bridge #4 - a concrete bridge with total span of 610m, have been performed to examine the effect of (i) increase in mean wind speed and (ii) terrain roughness on buffeting responses. Further, analyses of three span bridges (Bridge#1 and Bridge#2) have also been carried out to observe the effect of support types for bridge deck at towers and abutments on static, dynamic and aerodynamic behaviour.

Flutter analysis of three span bridges (Bridge #1 and Bridge #2) and five span bridge (Bridge #4) has been performed to study the effect of bridge vibration in higher modes on critical flutter speed. Bridge #3 has been analysed to observe the effect of angle of attack on critical flutter speed. Further, Bridge #2 has been analysed to predict the criteria for onset of flutter when the deck is subjected to lateral and torsional motions. Also, the effect of type of deck supports at towers and abutments on flutter tendencies of three span bridges has been examined.

1.5 ORGANIZATION OF THE THESIS

This dissertation consists of nine chapters, which are organized as follows:

A literature review on historical developments of cable stayed bridges, basic design concepts, static and dynamic behavior, developments in static and dynamic analysis with emphasis on measurement of modal structural damping, advancements in buffeting and flutter analysis and aerodynamic design aspects are presented in Chapter 2.

Chapter 3 describes the structural idealization of cable stayed bridges and formulations for nonlinear static and vibration analysis using matrix approach. The methodology for estimation of modal structural damping by energy dissipation method is given along with the details of software developed. The nonlinear static and vibration analyses of three span bridges - Bridge #1, Bridge#2 and five span bridges - Bridge #3 and Bridge#4 have been illustrated. Analysis has been performed to examine the effect of support types for bridge deck at towers and abutments on static and vibration characteristics of three span cable stayed bridges. Also, the theoretically estimated modal structural damping for all the four bridges has been given.

Modelling of wind is no less important than the structural modelling for the analysis of wind induced oscillations. The statistical parameters necessary for wind simulation along the span of a long bridge are described in detail. A review of previous methods used for digital simulation of Gaussian wind velocity field has been presented. Chapter 4 also explains the methodology for digital simulation of wind velocity field along the span of the bridge using spectral representation method along with the details

of software developed and its validation.

Chapter 5 illustrates the formulations for buffeting analysis of cable stayed bridges using time domain approach. The buffeting forces along the span of the bridge have been computed using the digitally simulated longitudinal and vertical wind velocity fluctuations. The important parameters necessary for buffeting analysis such as steady-state force coefficients, aerodynamic admittance functions and aerodynamic damping for bridge decks have been described. The procedure for time domain analysis is presented with the solution techniques.

Chapter 6 presents the time domain buffeting analysis of three span composite bridges namely Bridge #1 and Bridge#2. The validation of time domain approach is illustrated for Bridge #1, by comparing the results obtained by frequency domain method. Sensitivity analysis is also performed to find out the effect of time duration of buffeting forces, number of modes and modal damping on the buffeting response. Further, the observations on effect of (i) variation in mean wind speed (ii) terrain roughness and (iii) support types for bridge deck at towers and abutments on the buffeting responses of three span bridges have been presented. The buffeting induced forces for deck; towers, cables and deck supports have also been quantified for rational wind design.

In Chapter 7, the time domain buffeting analyses of five span cable stayed bridges denoted as Bridge #3 and Bridge#4 have been presented. The effect of (i) variation in mean wind speed and (ii) terrain roughness on buffeting responses of these bridges have been examined.

Chapter 8 describes the methodology for two-dimensional flutter analysis, when the bridge deck is subjected to either vertical and torsional or lateral and torsional motions. The formulation for three-dimensional flutter analysis is also outlined. Validation of flutter analysis has been illustrated with examples of two cable bridges. Also the numerical flutter analyses of three span and five span cable stayed bridges have been presented.

Chapter 9 offers conclusions and suggestions for future studies.

Chapter 2
LITERATURE REVIEW

2.1 INTRODUCTION

The present chapter aims to establish a current understanding of the buffeting and flutter analysis of cable stayed bridges. The advancement in the static, dynamic and aerodynamic analysis is reviewed in detail. Developments of methods for stabilizing wind induced oscillations in cable stayed bridges due to buffeting and flutter are also discussed.

Historical evolution of cable stayed bridges and their progress towards longer spans are presented. The basic design concepts of cable stayed bridges to achieve wind resistant design are also given to provide the necessary background for the problem needing complex analysis.

2.2 HISTORICAL EVOLUTION AND DEVELOPMENTS

It is nature of engineering to identify a problem and find a solution, sometimes after a catastrophic failure has occurred. Loscher evolved the concept of cable stayed bridge long way back in 1784, with a bridge consisting of timber stays attached to a timber tower. Later, in 1821, Poyet suggested the use of steel bar stays suspended from towers. Another version of the cable stayed bridge was suggested by Hatley, in 1840 by using chain stays in parallel configuration In Gischlard-Arnodin Cable Bridge, cables were used in radial configuration. But the failure of the cable stayed bridges built during 1818-1824 due to wind induced oscillations and overloading, helped suspension bridges to gain popularity.

Many suspension bridges built during this period also suffered severe damages or destruction under the action of wind. At the time of these failures, no analytical

methods for wind response prediction or wind resistant design were available. In United States, the collapse of a suspension bridge over the Ohio River, West Virginia, in 1854, marked the beginning of realizing the significance of aerodynamic instability. Other notable wind induced failures in U.S. were those of Niagara- Lewiston Bridge in 1864, and the Niagara-Clifton Bridge in 1889. The failure of the Wheeling Bridge greatly influenced the bridge designers, most notably John Roebling, designer of Brooklyn Bridge in New York, who later proposed cable stays to supplement the suspension cable system for stability.

In the area of bridge engineering, the period of early twentieth century to World War II was an exciting period with design and construction of important suspension bridges. The most impressive bridges built were the Manhattan Bridge, 1909; George Washington Bridge, 1931; San Francisco- Oakland Bay Bridge and Golden Gate Bridge, in the late 1930's. All these bridge designs were benefited from improvements in the static analysis. Steinman (1934) provided a state-of-the-art account of suspension bridge theory as of 1934. At that time, no reliable methods existed for dynamic analysis of suspension bridges. Most investigations of bridge dynamics were limited to live load effects as discussed by Timoshenko (1927) and Inglis (1934).

In 1938, Dischinger rediscovered cable stayed bridges, while attempting to design a 2460ft span suspension bridge. Cable stayed bridges emerged as popular and cost-effective alternative to suspension bridges only after World War II. The first modern cable- stayed bridge; Stromsund Bridge (183m) in Sweden was opened to traffic in 1956. The cable system of this bridge consisted of just two pairs of cables radiating from the top of the tower.

The first cable stayed bridge constructed in Germany was Theodor Heuss Bridge (260m, 1957). In this design, two box girders were suspended by two sets of parallel-placed cables tensioned from the tower in a harp pattern. Subsequently, many bridges were constructed with technical innovations in design. Examples are Severins

Bridge (302m, 1959)- two box girders suspended with two sets of cables in harp pattern from a A-shaped tower, Bonn-Nord Bridge (280m, 1967) with multi cable system with radially tensioned cables from a single tower. The bending moment in the bridge deck is drastically reduced with multi cable system as it offers continuous supports to the deck along the span.

Knie Bridge with asymmetric span (319m, 1969) was constructed with a total span of over 600m, and with two independent towers of height 114m. The Duisburg-Neuenkamp Bridge (350m, 1970) was provided with a box girder deck with long cantilever part of road supported by struts. In the asymmetric Kurt Schumacher Bridge (287m, 1972), prestressed concrete girders were used in the relatively short side spans together with rocker piers. Also it employed the Hi-Am anchor for the first time.

In Kohlbrand Bridge (325m, 1974), a floating system was adopted with the deck suspended by cables even at the towers thereby reducing the bending moment at the supports. Dampers for the cables were introduced in this bridge to reduce the wind generated vibrations.

The Dusseldorf Flehe Bridge (368m, 1979) is a composite cable stayed bridge having a wide orthotropic steel deck with long cantilevers for main span, prestressed concrete girders in side spans and with inverted Y-shaped concrete towers. Thus within two decades many innovations were introduced in the design of cable stayed bridges in Germany and subsequently many bridges were built in other countries - examples are Rande Bridge in Spain (400m, 1977), Brazo Bridge in Argentina (330m, 1978) and Tjorn Bridge in Sweden (366m, 1982). These bridges are composite bridges i.e. towers made of concrete and the deck made of steel in order to make them lighter and thereby allowing the spans to be longer. In a composite bridge, concrete is often used in towers, which are subjected to maximum compressive forces. This method has been naturally practiced in countries not prone to frequent earthquakes, with an intention to minimize the cost of construction. The most notable example of composite cable stayed bridge is

the Normandy Bridge in France (856m, 1995) having concrete towers, steel deck for main span and prestressed concrete girder for side spans.

The main span of cable stayed bridges crossed the mark of 400m, with the construction of Saint Nazaire Bridge in France (404m, 1975). The bridge consisted of stream lined box girder deck section and two torsion-resistant parallel–placed cables.

Concrete bridges were also built with extended spans- Brotonne Bridge (320m, 1977) in France, Pasco- Kennewick Bridge in USA (299m, 1978) followed by Luna Bridge in Spain (440m, 1984).

The usage of composite deck became popular in 1980's with a reinforced concrete slab placed on two–I girders, so called edge girders, at each edge of the slab to withstand axial compression. To make this type of deck construction feasible, cross beams were placed between the I-girders at close intervals of about 5m and high strength precast concrete was used for the slab, which was prestressed by making use of an axial force introduced by the stay cables. Existing examples of bridges with composite decks are Alex Fraser Bridge in Canada (465m, 1986), Quincy Bridge in USA (274m, 1987), 2nd Hooghly Bridge in India (457m, 1988) and Weirton-Steubenville Bridge in USA (250m, 1990). Another bridge having similar type of deck is Kessock Bridge in U K (240m, 1982), which suffered from wind-induced vibrations.

In the United States, bridge decks supported with two edge girders got innovated with the use of concrete edge girders. Most important examples are Dame Point Bridge (396m, 1989) and the Talmadge Memorial Bridge (335m,1991).

In Japan, the construction of cable stayed bridge started in 1970s. Steel has been extensively used for cables stayed bridges as these structures are built on soft soils and have to withstand severe earthquakes. Also availability of high strength steel in Japan at reasonable price helped its wide application in bridge construction.

Most of the bridges have steel decks consisting of single or twin boxes with orthotropic single decks for highway bridges and trusses for double deck bridges

carrying both railway and highway or two levels of highway. The problem of vortex excitation had been found in the deck of Onomichi Bridge (215m, 1968) and Ishkari-Kako Bridge (160m, 1972). Rigorous wind tunnel investigations were conducted to study the effect on different deck cross-sections fitted with fairings, flaps, and vanes. The cross-sections were selected based on wind tunnel tests for bridges such as Toyasato Bridge (216m, 1970), Kamome Bridge (250m, 1975), Suehiro Bridge (240m, 1975) and Rokko Bridge (220m, 1970) .The Meiko–West Bridge (405m, 1985) and Katshushika Bridge (220m, 1987) are examples of bridges having fairing modified box section as deck. The Tempozan Bridge (350m, 1990) is provided with a unique shallow and wide hexagonal box with splitter plates for deck.

When the ratio of side span to center span is small, it is advantageous to use a steel girder in the main span and continuously extended concrete deck in side spans as in the Ikuchi Bridge (490m, 1991). In towers, as they are mainly subjected to compressive stress, it is advantageous to use reinforced concrete structure embedded in steel.

Innovations in geometric shapes of towers to achieve aerodynamic design are quite evident in bridges namely Katsushika Harp Bridge (220m,1987) - tower with corner deflectors, Sugawara-Shirokita Bridge-central slits in tower cross-section and East Kobe Bridge (485m, 1994)-tower with corner cuts.

To alleviate the wind- induced oscillatory problems of tower, Tuned Mass Dampers (TMD) are installed in Sakitama, Meiko–West (405m, 1985) and Yokohama Bay Bridge (460m, 1989).

In the Rokko Bridge, usage of cables having hexagonal cross-section resulted in severe vibrations caused by wind. Connecting the cables with wires solved this problem. Cross-ties between cables were also fitted in Meiko–West, Hitsuishi and Iwakuro Bridges (420m, 1988). To minimize the wind induced vibration the application of oil dampers is utilized in Aratsu Bridge (185m, 1988) in Japan besides Brotonne Bridge in France and Sunshine Skyway Bridge in USA (366m, 1987).

On contrary to Japan, concrete and composite cable stayed bridges are popular in China. Remarkable increase in span lengths can be seen with the construction of Nanpu Bridge (423m, 1992) and Yangpu Bridge (602m, 1993).

In short, rapid development can be seen in cable stayed bridges all over the world due to aesthetics, efficient utilization of structural material, greater stiffness in comparison to suspension bridges, efficient and fast mode of construction, much smaller size of cables and relatively small size of substructure. With the number of existing cable stayed bridges touching almost 500, longer and innovative spans could be expected in the future.

2.3 BASIC DESIGN CONCEPTS

Cable stayed bridge presents a space system consisting of stiffening girders supporting the bridge deck, inclined cables in tension, which run from the tower top down to the anchor points at the bridge deck and the towers in compression. Based on the transverse layout of cables in space, they are classified as single, double or triple plane system. On the basis of longitudinal layout of cables, they are classified as radiating, fan, harp and asymmetric lay out.

The basic design of cable stayed bridges depends on (i) cross-section of bridge deck (ii) ratio between main span to side span (iii) shape and stiffness of towers (iv) layout of stay cables (v) spacing of stay cables (vi) cable anchorages and (vii) support types for bridge deck at towers and abutments.

Cross-section of Bridge Deck

The span of bridge, number of lanes of traffic, transverse layout of cables and aerodynamic stability govern the design of bridge deck cross-section. Commonly used cross-sections are rectangular solid slab, deck supported with twin or multiple I-girders, single rectangular or trapezoidal box girder, twin rectangular or trapezoidal box girder and truss supported deck.

For highway bridges with single plane cable system, single box girder has become a standard solution. For highway bridges with double plane system, depending on the span and width of bridge, the selection can be made as follows. For spans upto 200m with deck width in the range of 15 to 20m, simple solid concrete slab without edge beams is the best solution. For wider decks between 20 and 25m, and spans in the range of 200m to 500m, T or I-beam supported deck with cross beams is more economical. All steel girder with orthotropic deck is preferable for deck width greater than 25m and spans above 500m as the dead load gets reduced. For very long spans between 500m and 1500m, shallow box sections with wind nose or fairing is preferred as the fairings help to reduce the wind loads and increase aerodynamic stability.

The increase of torsional stiffness of deck is effective in increasing the critical wind speed for flutter, which often governs the design of long span bridges. Deck consisting of either streamlined box section or the section with openings such as a latticed truss would meet these requirements.

In addition to the consideration on basic cross-sectional shape of the deck, usage of various aerodynamic appendages has been incorporated in design, when substantial change of the basic cross-sectional shape is not allowed for design reasons. These aerodynamic appendages are known as wake stabilizers, which prevent interaction of entrainment layers and affect flow separation or reattachment of the separated shear layers. Examples are fairings, splitter plates, flaps and corner deflectors. Sometimes, intermittent arrangement of these appendages is effective because of the reduction in spanwise correlation of aerodynamic forces. However, when the appendages are contemplated, attention must be paid on the trade-off possibility of increasing cross- wind turbulence and spoiling the appearance of bridge.

According to Leonhardht and Zellner (1991) for concrete bridges with double plane cable system, there is no danger against wind induced oscillation for a deck with fairing if B> 10d or B>L/30. For steel bridges with lightweight deck and spans above

400m, it is preferable to have B> L/25 or use a deck with fairing for aerodynamic design.

Ratio of Main Span to Side Span

For a normal three span bridge, the ratio between the side span to main span significantly influences the stress change in the side span and force in the back stay cables. The main design aspect has to be to keep the stresses in backstay cables below the fatigue strength of these cables at anchorage. For highway bridges the ratio of side span to main span can be about 0.42. For steel bridges it is in the range of 0.3-0.42 and for composite decks about 0.4. When the ratio of side span to main span is small, the use of steel deck in the main span and continuously extended concrete deck in the side spans provides an economic design.

Shape and Stiffness of Tower

The selection of type of tower depends on the cable geometry and site soil conditions. The tower may consist of a single cantilever member for single plane cable system, two cantilever towers, and portal frame and A- shaped towers for double plane cable system. The shape of the towers is decisive from aesthetic view and their design should always be refined, choosing good proportions and tapering of shafts. The general ratio of height of tower to main span is 1:6 to 1:2.5. The concrete tower offers an economical solution with slip form construction; steel and reinforced concrete with embedded steel are the other alternatives. .

For very long span bridges located in zones of high winds, A- shaped tower is the ideal solution for wind stability. The upper level and deck level struts connecting the tower legs further help to improve the resistance in torsion.

Cable Layout

The lay out of stay cables influences the structural performance, method of erection as well as economy. The dynamic behaviour of cable stayed bridges is

governed by transverse layout of stay cables. For example, bridges with single plane cable system will have low torsional natural frequencies and low torsional damping. Bridges with double plane cable system provide high degree of resistance to torsional oscillations with high natural frequencies as well as damping in torsional mode. The damping of cable stayed bridge is influenced by the longitudinal layout of cables such as radiating, fan, harp or asymmetric lay out. While deciding the longitudinal layout of cables for a bridge, it is also necessary to consider the type of deck supports at towers and abutments.

Cable Spacing

The spacing of stay cables depends on the type of material used for bridge deck as well as the method of erection. A few cables result in large cable forces, which in turn results in massive complicated anchorages and heavily reinforced bridge deck system. However, with multiple stay cable system, the anchorages get simplified and permit the use of shallower girder depth. For a concrete deck, the stay spacing is of the order 5m to 10m, for composite deck in the range 10m to 15m and for steel deck it is usually in the range of 15 to 25m.

The damping of a cable stayed bridge increases with multiple cable system, thereby reducing the wind induced oscillations.

Cable Anchorages

The cable anchorages must allow adjustment of length of cable at one end. They should be designed such that the replacement of a damaged cable is possible without interrupting the traffic. Bending stresses in wires or stands at the socket due to change of sag or due to oscillations must be prevented. The dampers to prevent cable vibrations should be installed at some distance from the anchors. Generally, a cable anchorage consists of a steel pipe encased in the concrete or welded to the steel edge girder with a correct angle of inclination. The steel pipe of cable anchor at deck extends about 1.2m

above the road level to protect the cable against aberrant vehicles. At its upper end there is a thick soft neoprene pad, which stops flexural movement of cable and helps to damp oscillations. Length adjustment of cable is often done at tower anchor. At the tower, cable should be anchored at each side separately and easily accessible. Eccentricities must be kept small to avoid torsion in tower head.

Tamhankar (1976) discussed the design of cables and their anchorages in cable stayed bridges.

More details on these design aspects of cable stayed bridges are available in Podolony (1976), Troitsky (1988), Walther (1988) and Gimsing (1996).

Support Types for Bridge Deck at Towers and Abutments

The deck support types at towers and abutments play a dominant role in cable stayed bridges as they fulfill functions such as (i) to transfer force from various parts of superstructure components or from superstructure to substructure (ii) permit longitudinal or transverse movement or rotation of one part with respect to the other (iii) allowing free movements in some directions but restraining movements in certain specified directions. These connections are generally established through bearings of suitable type to support the deck at towers/abutments. Selection of bearings is based on the type of material of bridge deck, whether the deck is straight or curved in plan, seismic performance and maintenance requirements of bearings. Stresses due to temperature and possible movement in the expansion joints also need to be considered while selecting the deck support conditions.

The connections/bearings are designed for the maximum load to be transferred and for maximum movements or rotations to be permitted. Lee (1986, 1994) has illustrated the developments and design details of different types of bridge bearings.

The connection between the deck and tower in a cable stayed bridge can be broadly classified as (i) rigid connection (ii) floating/swinging and (iii) elastically

supported. They are illustrated in guidelines for the design of cable stayed bridges ASCE (1992) and in Ito (1992). Various combination of fixed, moveable, elastically fixed, unsupported or rigidly connected with towers, as shown in Fig. 2.1, are possible. A fixed connection between deck and tower/abutment is achieved through rocker bearing, a movable connection through roller/pot bearing and an elastic connection through elastic links, springs or elastomeric bearings, etc. The advantages and limitations of three types of connections of bridge deck with towers, viz; rigid, floating and elastic are examined in the following sections.

The deck can be rigidly connected to both towers as in Fig. 2.1(a) or only at one tower as in Fig. 2.1(b) or to one abutment as in Fig. 2.1(c). In case large clearance height for the bridge deck is required, it is often provided with fixed hinges at both flexible towers as in Fig. 2.1(a). Temperature stresses can be released owing to the flexibility of towers, and both tower piers can sustain seismic reactions. Some difficulties may arise, however, in giving the towers both flexibility to absorb deformation of the girder due to temperature change and the stiffness to cope up with seismic effects. For bridges with medium or short span lengths, deck connections as in Fig. 2.1 (b) or (c) have been widely used because temperature effects are released and the seismic force applied to the substructure is small. With increasing span length, design and construction of the pier fixed to deck becomes difficult and supporting condition as in Fig. 2.1(c) is preferred over Fig. 2.1(b).

The rigid connections between the deck and tower will result in reduced movements under service loading conditions (i.e., dead loads and live loads) and will attract higher seismic forces during earthquake. Even though construction problems are limited with this type of connection, geometric control during erection has to be taken very seriously, as there exists little chance of correction later. Some of the existing examples using rigid connection/support for the deck are Coatzacoalcos Bridge in Mexico-concrete bridge with total span of 622m, Sunshine Skyway Bridge in USA-precast concrete structure with total span of 695m, and Evripos bridge in Greece-concrete bridge with total span of 395m as mentioned by Virlogeux (1991).

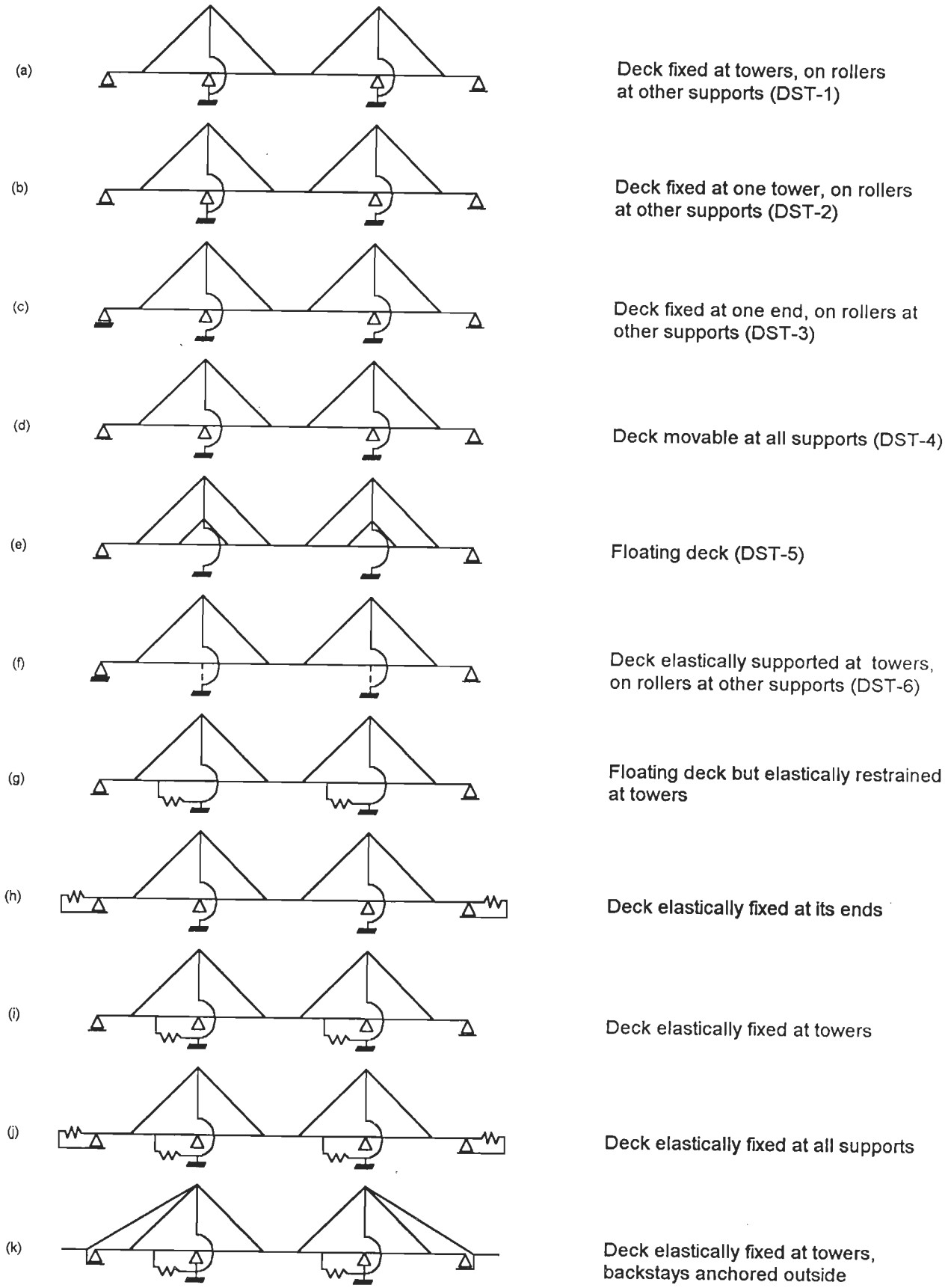

Fig. 2.1 : Examples of Different Support Types for Deck in Three Span Cable Stayed Bridges

An example of a bridge rigidly connected at both the abutments is the Barrios de Luna Bridge in Spain - concrete bridge with total span of 644m, with no connection between deck and tower. However, to allow for thermal deformations, an expansion joint has been placed at the middle of the central span again stated by Virlogeux (1991).

If the deck is supported freely both at the towers and abutments, as in Fig. 2.1(e), the induced seismic force will be kept to a minimum but the bridge may be very flexible under service loading conditions. Proper attention should be paid to the excessive displacement of the deck and likely possibility of instability of towers. An existing example is Glebe Island Bridge in Australia, concrete deck with total span of 779m, having no longitudinal restraint within the cable stayed section, as described by Tang (1998).

The unique feature of Higashi-Kobe Bridge in Japan, truss-supported deck with a total span of 885m, is the connection of deck with towers and piers in such a way that the deck is movable in longitudinal direction. This supporting method helped to lengthen the fundamental period of the bridge to a relatively longer duration. However, to reduce the displacements of the bridge, harp type cable arrangement has been incorporated in the design instead of the frequently used fan type arrangement as explained by Yamada *et al* (1991).

Vertical cables have been used to swing the deck at towers and damping devices have been installed at end piers in the East Kobe Bridge in Japan (Ito, 1991) with a double deck truss (for highway & railway) and main span of 485m length. A harp type cable arrangement was chosen to reduce the longitudinal displacement of the floating deck.

Another example for cable stayed bridge with floating deck is the Akkar Bridge in Sikkim, India – a concrete bridge with total span of 154m. The deck is completely suspended by cables and the problem of steep cables close to the tower top was

overcome by expanding the tower top as explained by Schlaich (1991). In the Second Hooghly Bridge in India, with a total span of 823m, modified elastomeric bearings are provided at floating deck ends as described by Ghosh (1992).

By providing connections that permit longitudinal movement as well as devices at the tower deck connections, as in Fig. 2.1(f)-(k), to absorb large seismic energy as well as to reduce the resonance amplitudes, the drawbacks of the types of deck supports such as fixed, movable, floating as in Fig. 2.1(a)-(e), can be reduced. The different types of such connections are rubber-lead block bearings, elastic links, spring shoes and elastomeric bearings.

Some of the existing bridges are, Brotonne Bridge in France- concrete cable stayed bridge with main span of 320m in which the deck is supported at the pier, and the towers through a ring of neoprene bearings, which can transfer bending moments as well as permit the longitudinal movements of the deck as mentioned by Virlogeux (1991).

The Quincy Bridge in USA, with composite deck and total span of 542m is provided with tied down links at the deck ends and vertical and transverse (elastomeric bearing) supports for connection between the deck and tower, stated by Wilson *et al* (1991). Longitudinal bearing has been provided for connection of deck with one of the towers only.

Maeda *et al* (1991) used short tension links to sling the girder from tower, with rocker type bearing on piers, on the Yokohoma bay Bridge in Japan with steel double deck and a total span of 860m. Large springs, as in Fig. 2.1(h), were fitted to the rocker bearings at each end of the pier of Hitsuishi/ Iwakuro bridges in Japan with total span of 790m to control longitudinal restraint stiffness as explained by Ito (1991). On Meiko- Nishi Bridge and some other bridges in Japan, deck was elastically restrained by attaching horizontal cables between the girder and tower. Endo *et al* (1991) mentioned that the overall elastic bucking stability is achieved in Tatara Bridge in

Japan with orthotropic steel deck and a total span of 1480m, by fixing the deck elastically to the towers, as in Fig.2.1 (i).

The proposed Yamuna Bridge at Allahabad, India, a concrete cable stayed bridge with total span of 610m has been designed by Veje *et al* (1999) using elastomeric bearings to achieve the elastic connection between deck and tower.

2.4 STATIC BEHAVIOR AND METHODS FOR ANALYSIS

A cable stayed bridge is a statically indeterminate structure in which the bridge deck behaves as a continuous beam supported elastically at the points of cable attachment.

The components of cable stayed bridges are made of mainly steel, composite and concrete. Steel, always used for the cables and sometimes for deck and tower, exhibits linear load-deformation behaviour, below the material's elastic limit. Composite materials, used sometimes for bridge deck and concrete used in deck and tower, exhibit nonlinear load–deformation behaviour, but are practically linear for low service load levels. In general, the cable stayed bridge materials behave in a linear elastic manner. Yet, the bridge's overall load–deformation relationship is nonlinear.

The nonlinearity results from three distinct effects - the nonlinear axial force versus elongation relationship for the inclined cables due to sag caused under its own weight; nonlinear axial-flexural interaction for the bending members, which occurs due to simultaneous action of large bending moments and axial forces in the deck and tower; and large displacements, which occur due to structure's high flexibility.

For smaller spans, it may be appropriate to analyse by assuming it as a linear elastic system. However, with longer span lengths, nonlinear static analysis under dead load has become essential for evaluating stresses and deformations induced by vehicular and environmental loads. The advancements in the static analysis of cable stayed bridge are discussed in the following section.

Smith (1968 a, b) presented a linear analysis method for single-plane cable stayed bridges and later extended to double plane bridges using a mixed force-displacement formulation, in which cable and tower forces are chosen as redundants in a flexibility approach. Tang (1971, 1972) presented application of transfer matrix method for analysis of cable stayed bridges. Troitsky and Lazar (1972) used the flexibility method to perform a linear analysis by idealizing as a plane frame structure, to obtain envelopes of bending moment, axial force, and shear force. Lazar and Troitsky (1972) extended the work to include initial tension in the cables. Cheung and Kajita (1973) employed a two-step method for linear analysis of cable stayed bridges, in which compatibility equations were written for the deformations at the junctions of towers and cables with deck, and the deck was modelled with a 12-noded shell element in a finite element analysis. Fleming (1979) and Loganathan *et al* (1980) extended Lazar's work to include the effects of initial cable tension, automatic dead load analysis, and member loads in addition to joint loads, by idealizing the cable stayed bridge as two- dimensional plane frame. Shiu (1983) extended to three-dimensional analysis with single box girder decks with warping torsion effects included, but limited the cable arrangement to a single plane.

Lazar (1972) performed a nonlinear analysis of cable stayed bridges based on the stiffness method. The bridge was modelled as a two-dimensional structure, with external loads being applied at the joints only. Based on initial geometry and external loading, the deformations were computed. Then the unbalanced forces and moments at all joints were applied as loads on the deformed geometry of the structure and the changes in the deformations were calculated. These steps were repeated iteratively at each load increment until the balanced forces and moments became negligibly small. Before the load was increased, the stiffness matrix was updated based on the most deformed configuration of the structure.

Namini (1989) extended Lazar's stiffness formulation for three-dimensional

analysis, incorporating cable tension, automatic inclusion of dead load, member–oriented loading and global-oriented joint loading. The deck and tower were modelled with a space frame element allowing for axial flexural interaction. The cables were modelled with an axial rod element, whose nonlinearity is reflected by the use of an equivalent modulus of elasticity.

Nazmy and Abdel-Ghaffar (1990) presented nonlinear static analysis of three-dimensional long span cable stayed bridges under effect of their own dead weight and a set of initial tensions. A computer program that uses a tangent stiffness iterative-incremental procedure is described to perform nonlinear static analysis. All sources of geometric nonlinearity, such as cable sag, axial force–bending moment interaction and change of bridge geometry due to large displacements are included in the analysis.

In an attempt towards further sophistication in analytical assessment in wind resistant design of long span bridges in Japan, Katsuchi *et al* (1998) have indicated about the three-dimensional nonlinear analysis under wind loading rather than gravity loading as an initial step towards dynamic and flutter analysis as the deformed state of bridge under wind and gravity loading are different. However, more studies on this aspect are necessary.

2.5 DYNAMIC BEHAVIOR AND METHODS FOR ANALYSIS

The dynamic behaviour of cable stayed bridges invoke great interest as the influence of moving loads, seismic and wind forces on these structures are mainly dependent on these characteristics.

The long span cable stayed bridges have four prominent types of vibration namely longitudinal-oscillation along the span; bending - oscillation vertical to span; sway - oscillation transverse to span; and torsion - rotation about deck's elastic axis. Of these, bending, sway and torsional oscillations are important in cable stayed bridges under the action of wind.

Wyatt (1991) presented the fundamental and parametric studies on the dynamic behaviour of cable stayed bridges. The vertical oscillation of bridge deck depends on the stiffness in vertical direction of stay cables and mass of structure. The stiffness of stay system mainly depends on main span length, ratio of side span to main span length, ratio of tower height above bridge deck level to main span length and area of stay cables. The torsional frequency depends on the torsional stiffness of the bridge deck- e.g. box girder and for bridge deck weak in torsion, on differential vertical motion of stays. The tower is effective in torsion only if the tower shafts are tied with cross beams. The resistance to lateral bending mode is offered by deck only.

The dynamic behaviour of cable stayed bridges is governed to a large extent on how the cable, tower and deck are interconnected. For example, cables arranged in a single plane and connected to deck along the centerline provide no resistance to torsional rigidity. Such bridges have low torsional natural frequencies and low torsional damping. On the contrary, cables arranged in two planes and connected to the deck along the edges provide high degree of resistance to torsional oscillations. This arrangement enhances the natural frequencies as well as damping in torsional mode. For example, A-shaped towers with inclined cables provide higher resistance to torsional oscillations than with a H-shaped tower with double plane cable arrangement. Long span cable stayed bridges tend to have very closely spaced natural frequencies and significant structural coupling of flexural and torsional modes of vibration due to separation of mass center and stiffness center of deck. Also the dynamic behaviour of a cable-stayed bridge after completion is appreciably different from that of bridge during construction stages.

An important aspect regarding dynamic behaviour of cable stayed bridge is that the divergent vibration amplitudes can be limited by the system damping caused by the interference of many cables, i.e., damping increases with increasing vibration amplitudes and resistance to dynamic instability increases with multiple cables. Also,

the dynamic behaviour of cable stayed bridges may involve a single member or the entire structure. The local behaviour pertains to dynamic properties associated with one component of the bridge. For example, the cables may be excited into violent oscillations due to resonance or wake galloping.

The advancements in the dynamic analysis of cable stayed bridges are presented in the following section.

Kajita and Cheung (1973) extracted the natural modes of vibration for cable stayed bridges by dynamic analysis using lumped mass formulation. Tang (1971), Morris (1974) and Isyumov *et al* (1977) all determined the lowest natural modes from a linear- elastic lumped mass formulation while the latter also considered the coupling between the torsional and sway modes caused by the vertical eccentricity between the center of gravity and the elastic axis.

Fleming and Egeseli (1980) presented 2-D mathematical model, to evaluate the dynamic response of cable stayed bridges subjected to wind, seismic and traffic loads. They brought out the effect of damping on response of bridge and stressed the need for further investigations to determine the realistic values for damping. They also stressed the need for three-dimensional analysis to capture the behaviour of long span cable stayed bridge with complex geometry for towers, two planes of cables, etc.

Sethia *et al* (1987) compared analytical and test values of natural frequencies of a cable stayed bridge, but obtained the experimental natural frequencies by vibrating a model, which was designed to satisfy only static scaling laws.

Namini (1989) presented dynamic analysis using both lumped as well as consistent mass formulation using subspace iteration.

Abdel-Ghaffar and Khalifa (1991) presented the dynamic behaviour of cable stayed bridge when the vibration characteristics of stay cables are taken into consideration by discretizing each cable into multiple elements.

Wilson and Gravelle (1991) presented a detailed description of development of

a linear elastic finite element model for dynamic analysis of Quincy Bay View Bridge with a total span of 542m. The translation of structural data into a form useful for formulation of a 3-D finite element model is illustrated for the bridge including evaluation of translational and rotational mass and stiffness for deck, modelling of towers, cables and bearings and consideration for accurate geometric representation between FEM model and full scale structure. Wilson and Liu (1991) compared the modal behaviour predicted by finite element model with field measured ambient vibration properties of Quincy Bridge. An extensive programme of full-scale ambient vibration tests was conducted with a microcomputer based system to collect and analyse the ambient vibration data. A total of 25 modal frequencies and associated mode shapes in the frequency range of 0-2Hz and estimation of damping ratios were obtained from field studies. They observed occurrence of mainly closely spaced modal frequencies and spatially complicated mode shapes. Most tower modes were found to be interacting with deck modes, implying a considerable interaction between the deck and tower structure.

Muria-Vila *et al* (1991) explained the field-monitoring program conducted on Tampico cable stayed Bridge in Mexico with a total span of 876.8m with main span length of 360m. The bridge was subjected to free vibration by quick release of 200KN weight attached to the bridge deck at mid point of the center of span. Servo accelerometers were arranged in different set ups either vertically or laterally to measure vibration characteristics. Ambient vibration conditions were produced by traffic and wind. Fundamental periods, mode shapes and damping were estimated by different methods using the ambient vibration studies as well as pull back tests of the bridge.

Wei (1993), presented the following formulae for the first bending frequency (f_h) and torsional frequency (f_t) in terms of span (L) for double tower steel cable stayed bridges based on data of twenty existing bridges in the world.

$$f_h = 98.0748/L^{0.95}, f_t = 184/L^{0.9} \quad (2.1)$$

Bruno and Leonardi (1998) presented a parametric analysis of the natural periods of fan shaped long span cable stayed bridges with A-type and H-type towers. The study has been carried out using a continuous mathematical model and a finite element model of a bridge.

2.5.1 Modal Structural Damping

For cable stayed bridges, the modal structural damping is one of the important indispensable parameter for checking the dynamic safety of the structure, but usually assumed empirically without theoretical considerations, while the dynamic behaviour of the cable stayed bridge may change depending on the assumed value.

Significant developments in the method of evaluation of structural damping as well as vibration control of long span cable stayed bridges using damping devices have been taken place in the last decade.

Experimental studies on the models of cable stayed bridges and field measurements have helped in estimating the damping values of cable stayed bridges. Most popular methods for estimating damping from experimental data are the half power bandwidth method in frequency domain and logarithmic decrement method in time domain. The first method is more popular in full-scale measurements and the latter in model studies.

Jones and Spartz (1990) addressed the quantitative assessment of mechanical damping for long span cable bridges based on ambient wind and motion data. They attempted to separate and estimate the mechanical and aerodynamic damping of a prototype bridge structure and compared the results with values traditionally used in design.

Narita and Yokoyama (1991) presented a summarized account of damping capacity and measures against wind action in cable stayed bridges in Japan based on

field measurements of 22 bridges.

In Japan, as per the Wind Resistant Design Manual for Highway Bridges (1991), the reference values of structural damping, expressed as logarithmic decrement for wind resistant design of cable stayed bridges with truss and box girder supported deck are taken as 0.03 and 0.02 respectively

Muria –Vila *et al* (1991) during the field instrumentation studies on Tampico Bridge in Mexico noticed drastic differences in damping values estimated by three different methods namely, logarithmic decrement, half power point bandwidth of auto spectral peak and method based on power spectral density function as suggested by Kawasumi and Shima (1965). They stressed the need for research in methods for estimation of structural damping. Further, for this bridge, with inverted Y-shaped towers, the measured damping values in torsion are lower than the damping in vertical direction. The same trend is observed from the field instrumentation studies of Saint Nazaire Bridge in France with inverted Y-shaped towers.

Theoretical estimate of modal damping by energy dissipation method has been discussed by Kawashima *et al* (1991, 1993) and investigated its validity through a comparison with free–oscillation test on bridge model. Dependence of the damping ratio on oscillation amplitude and cable arrangement is observed.

Garevski and Severn (1993) described the damping and response measurement on a small-scale model of Jindo Bridge in South Korea with a total span of 484m. Hammer, sinusoidal and random signal tests have been performed to determine the dynamic characteristics of the model built to satisfy dynamic scaling laws. They studied the influence of stay cable vibration on damping. It was found that the damping characteristics of model varied with excitation amplitude. However, the stay vibration did not affect significantly the vibration amplitude of the deck.

A database of modal damping of 29 cable stayed bridges in Japan has been presented and its mode dependency discussed in detail by Yamaguchi and Ito (1995).

The vibration modes of cable stayed bridges considered in the wind resistant design are girder dominant modes, which are generally coupled with the tower motion or cable motion. Since the damping characteristics of each component may differ from one another, the modal damping of cable stayed bridges can be strongly related to the coupling characteristics, which are different for different modes. The modal damping therefore has a poor correlation with natural frequency. As the modal damping is dependent on the coupling characteristics of mode shapes, it increases linearly with cable damping. The modal damping of bridge can be smaller, if the cable damping is lower than the damping of girder itself. The average modal damping decreases with increase in span length. Further, the structural damping depends on the longitudinal layout of cables and type of bridge deck, i.e., more for truss type deck as shown in Fig. 2.2. It increases with oscillatory amplitude. For theoretical estimation of structural damping, energy based method has been discussed. They also stressed the need for research on theoretical discussions and quantitative estimation of modal damping so as to make wind resistant design of cable stayed bridges more rational.

For Ikuchi Bridge in Japan, a complex multi cable stayed bridge with steel deck for central span and prestressed concrete girder for side spans of 150m each, with steel A-shaped towers, structural damping values were measured using forced vibrations created by a large size exciter. The measured structural damping in torsional mode is greater than that in the vertical mode as seen from Table 2.1.

Table 2.1 : Measured Modal Structural Damping of Ikuchi Bridge

Mode No.	Frequency (Hz)	Mode Type	Modal Damping Ratio (ξ_s)	Logarithmic Decrement (δ_s)
1	0.342	V-S1	0.0028	0.018
2	0.450	V-AS1	0.0030	0.020
3	0.613	V-S2	0.0049	0.031
4	0.733	T-S1	0.0060	0.038
5	1.074	T-AS1	0.0033	0.021

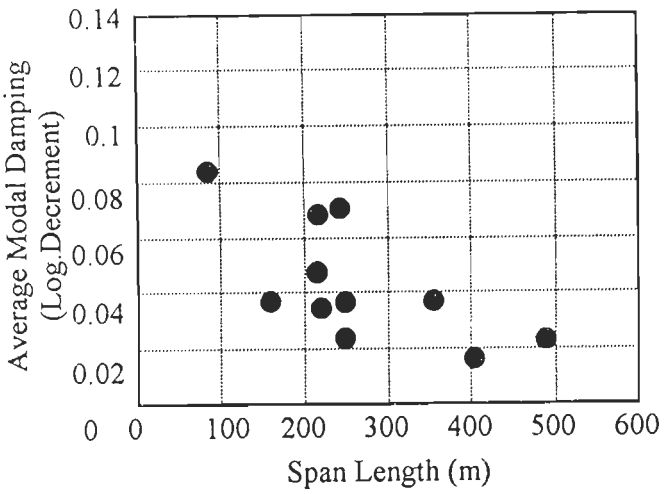

(i) Vertical bending mode

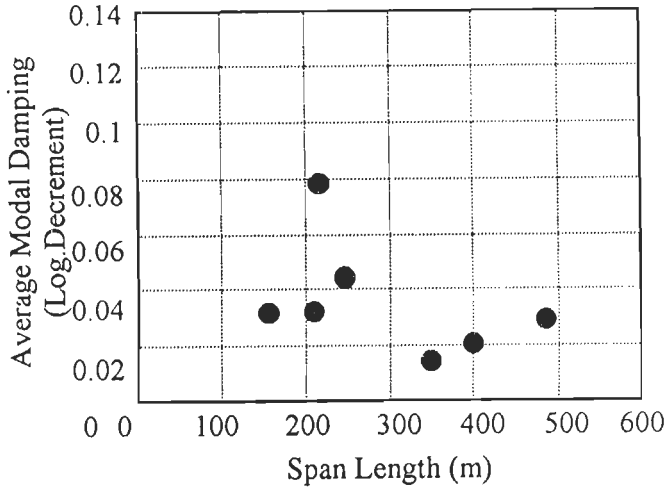

(ii) Torsional mode

(a) For cable stayed bridges with truss girder

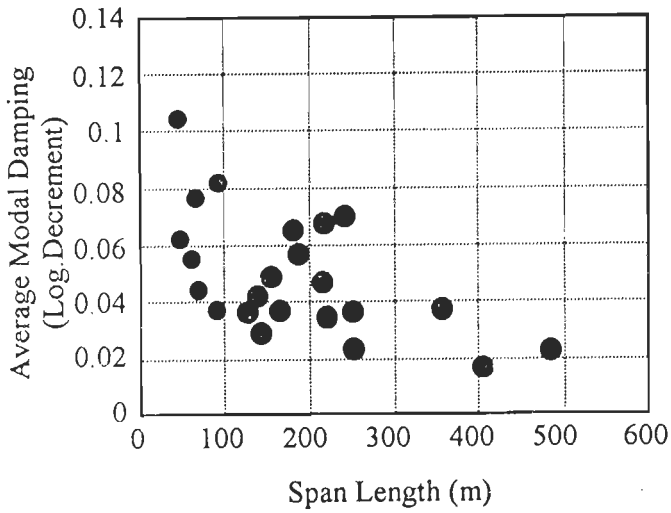

(i) Vertical bending mode

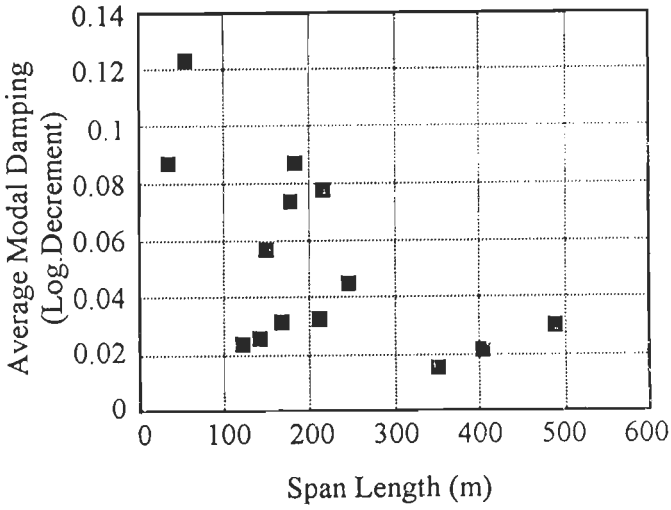

(ii) Torsional mode

(b) For cable stayed bridges with box girder

Fig. 2.2 : Relationship between Average Modal Damping and Main Span Length in Three Span Cable Stayed Bridges

Takano *et al* (1998) reported the field measured modal damping values for Tsurumi Tusaba Bridge in Japan with total span of 1020m, single plane bridge with streamlined steel box girder supported deck. The field studies are conducted by free vibration tests (oscillation of bridge induced by gigantic exciters) and summary of modal damping values are tabulated in Table 2.2.

Table 2.2 : Modal Structural Damping of Tsurumi Tsubasa Bridge

Mode No.	Frequency (Hz)	Mode Type	Modal Damping Ratio (ξ_s)	Logarithmic Decrement (δ_s)
1	0.213	V-S1	0.0110	0.07
2	0.293	V-AS1	0.0063	0.04
3	0.544	T-S1	0.0110	0.07
4	0.517	V-S2	0.0159	0.10
5	0.598	V-AS2	0.0063	0.04

Delaunay *et al* (1999) in an attempt to validate the wind design studies for long span bridges through field instrumentation studies have measured modal structural damping of Normandy Bridge and Vasco da Gama Bridge through forced vibrations. It is interesting to note that the Normandy Bridge is provided with Tuned Mass Damper to suppress sway motion.

Vasco da Gama Bridge with main span 420m and 203m side span each has a 30.9m wide deck- supported by two prestressed concrete longitudinal girders with transverse steel I-beams and H-shaped towers. The connection between the deck and tower is through hysteric damping system, which consists of two sets of cantilever steel beams, which acts as a damper in longitudinal and transverse direction. The measured modal damping values are given in Table 2.3.

Table 2.3 : Modal Damping of Normandy and Vasco da Gama Bridge

Mode No.	Mode Type	Normandy Bridge			Vasco de Gama Bridge		
		Freq. (Hz)	ξ_s	δ_s	Freq. (Hz)	ξ_s	δ_s
1	L-1	0.171	0.006	0.037	0.293	0.011	0.0690
2	V-1	0.232	0.003	0.018	0.336	0.003	0.0180
3	V-2	0.293	0.002	0.012	0.458	0.0028	0.0170
4	V-3	0.388	0.002	0.012	0.650	0.005	0.0314
5	V-4	0.727	0.0043	0.027	0.47	0.0027	0.0160

With the main span of bridges reaching 890m as in Tatara Bridge, the cable length also increases to 500m. These long inclined cables in tension are prone to wind, wind-rain-induced vibration and wake galloping. Recently, cable vibrations have received the attention of researchers as some cables broke in Saint Nazaire Bridge in France and Zarate Brazo Bridge in Argentina due to fatigue induced cable vibration as reported by Virlogeux (1998). He reported the measured damping ratio for cables of seven existing bridges with different type of cables, a summary of which is given in Table 2.4.

Table 2.4 : Summary of Damping Ratio for Cables

No.	Name of Bridge	Type of Cables	Damping ratio
1	Saint Nazaire	Lock -coil cables	0.001
2	Seyssel	Lock-coil cables	0.0005
3	Brotonne	Parallel strands	0.0001
4	Second Severn	Parallel strands	0.001-0.006
5	Vasco da Gama	Parallel strands	0.0013
6	Erasmus	Parallel strands	0.002
7	Iroise	Parallel strands	0.0014

In addition to structural damping the aerodynamic damping needs to be accounted for while designing systems to alleviate wind induced oscillations of stay cables. The aerodynamic damping ratio for n^{th} mode when the cable moves in the direction of wind and transverse to the wind is expressed as:

$$\xi_a = \frac{\rho U d_c C_{Dc}}{2 m_c \omega_n} \quad \text{in the direction of wind} \tag{2.2}$$

$$\xi_a = \frac{\rho U d_c C_{Dc}}{4 m_c \omega_n} \quad \text{in transverse direction} \tag{2.3}$$

Where ρ is the air density, U –the wind speed in m/sec, d_c- diameter of cable, C_{Dc} is the drag coefficient of cable with a value of about 0.7, m_c is the linear mass of cable per unit length and ω_n is the circular frequency of cable for n^{th} mode. The period of vibration of cable for n^{th} mode T_n is given in terms of length L_c, m_c and cable tension T_c as:

$$T_n = \frac{2L_c}{n}\sqrt{\frac{m_c}{T_c}} \tag{2.4}$$

Damping values in cables are dependent on sag to length ratio and frequency. Yamaguchi and Fujino (1998) reported modal damping expressed as logarithmic decrement for 30° inclined cables as close to 0.01 based on experimental studies as evident from Fig. 2.3.

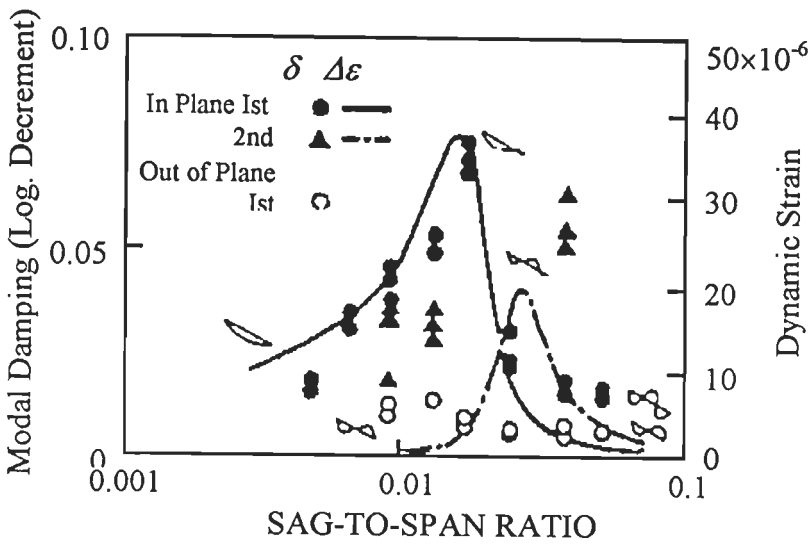

Fig. 2.3 : Modal Damping and Dynamic Strain Vs Sag to Span Ratio for Inclined Stay Cables (Yamaguchi and Fujino, 1987)

Oil dampers, connecting the cables with wires and tuned mass dampers help in increasing the damping values. It is evident from Rokko Ohashi, Hitsuishi, Jima Iwaguro and Yabuko Ohashi in Japan; the damping increased much without any relation to the number of wires. On the other hand application of oil dampers to increase the damping capacity is seen in Aratsu, Sakitama, Brotonne, Kohlbrand and Sunshine Skyway Bridges. Structural damping expressed as logarithmic decrement of 0.02 is enough to suppress rain-wind-induced vibration and 0.05 to suppress wake galloping of cables. These values give reference to design a damper.

2.6 BUFFETING ANALYSIS

Buffeting is the random response of a structure due to turbulence present in the approaching flow and signature or self-induced turbulence. It gets further complicated with bluff bridge deck sections, as the approach flow turbulence and bridge signature turbulence interact with motion of bridge and change the random forces acting on the deck considerably. Even though the buffeting response does not generally lead to catastrophic failures, it is important from serviceability considerations as well as fatigue of structural materials. Also, long span flexible cable stayed bridges are vulnerable to turbulent wind during construction stages.

The buffeting response analysis is predominantly in frequency domain mainly due to its computational efficiency, particularly handling the unsteady aerodynamic forces that are functions of frequency.

2.6.1 Frequency Domain Analysis

The pioneering work in frequency domain buffeting analysis has been done by Davenport (1961, 1962). He applied the statistical concept of stationary time series and random vibration theory to buffeting analysis of long span bridges. Also introduced aerodynamic admittance function and joint acceptance function in consideration of temporal and spatial distributions of aerodynamic forces along the bridge deck.

Irwin (1977) described a theoretical model, an extension of Davenport's method by including the coupled torsional and lateral motion. Application of evaluation of buffeting response in vertical, torsional and lateral directions of cable supported bridges is demonstrated by comparing the theoretically obtained results with aeroelastic model studies for Lions' Gate Bridge.

Scanlan and Gade (1977) extended their research results for flutter stability to buffeting response. They believed that the aeroelastic forces (self-excited forces) would affect the buffeting response of bridge deck and hence suggested considering aerodynamic forces due to wind turbulence and aeroelastic forces due to motion of bridge deck in buffeting analysis. With the aeroelastic forces considered, both aeroelastic stiffness and damping in flexural and torsional vibrations were included in the analysis by means of flutter derivatives.

Narita and Sato (1981) described a method for calculating the vertical buffeting response of cable stayed bridge. A comparison is made between the theoretical results and the field measurements of buffeting response for Suehiro Bridge. Also proposed simplified formulae for estimating the vertical buffeting response, i.e., the standard deviation of vertical buffeting response (σ_h) at the main span of long span bridge whose symmetrical vertical bending mode dominates in buffeting is approximately estimated as

$$\sigma_h(L/2) = Const.\frac{dC_L}{d\alpha_w} I_w U^2 B^{\frac{1}{2}} f_h^{-2} L^{-\frac{1}{3}} (mg)^{-1} \qquad (2.5)$$

The constant value is in the range 3 to 6, σ_h in m, U in m/sec, B in meter, f_h in Hz, L in meters and mg in N/m.

Scanlan (1978b, 1981), with the help of analytical means in frequency domain illustrated the buffeting of flexible bridges in the presence of self-excited or aeroelastic forces, considering the complex three-dimensional vibration modes of bridges. Formulas were given for multimodal response estimation of expected buffeting

excursions in vertical and torsional directions for long span bridges.

The buffeting theories as proposed by Davenport and Scanlan are a combination of numerical, experimental and analytical approaches. Finite element techniques are usually adopted to determine the natural frequencies and mode shapes of cable stayed bridges. The wind tunnel tests on bridge deck section models provide flutter derivatives and aerodynamic coefficients. By idealizing the bridge deck as a continuous beam, they determined buffeting response of each mode and then superimposed the results using square root of sum of squares of modal responses. However, the coupling between the modes is ignored in the buffeting analysis by them.

As the natural frequencies of various modes of vibration of cable stayed bridges are closely spaced as well as coupled, contribution from multi modes and inter-modes of vibration are to be included while estimating the buffeting response of deck. To consider the multimode buffeting response, Lin and Yang (1983) proposed a general linear theory for computation of cross-spectra of deck response for turbulent wind using a continuous beam model.

Scanlan and Jones (1990) presented analytical methods to frequency domain utilizing the experimental flutter derivatives for self-excited forces, including the three dimensional complexities of vibrating cable stayed bridges. They have illustrated that the buffeting induced response of a twin deck structure under construction is about 1.5 times higher than the buffeting response of completed bridge. The analytical results compared favorably with wind tunnel results.

Scanlan (1993) highlighted the extreme vulnerability of cable stayed bridges to turbulent skew winds during the construction stages. An analytical method in frequency domain has been presented which takes into account the effect of skew winds upon the exposed cantilever deck. An example of bridge under construction, using the flat plate flutter derivatives suitably modified for aspect ratio corrections, is presented. The study indicated that the buffeting response is sensitive to effective lift and other coefficients

under along and across wind flow as well as turbulent characteristics of wind.

Qu and Xiang (1993) presented a three-dimensional analysis in frequency domain for estimation of buffeting response of a long span suspension bridge. The method includes the aerodynamic coupling between modes.

Chen *et al* (1993) developed a technique for measuring the swaying aerodynamic derivatives, in order to predict the swaying buffeting response. They presented a method for accurate buffeting response estimation based on Scanlan's buffeting theory, by incorporating the aerodynamic admittance function. For practical applications, a simplified response spectrum method for evaluation of buffeting response is also given based on a detailed parametric analysis. They reported a close agreement of computed buffeting responses in vertical, lateral and torsional directions by accurate as well as simplified methods for Yangpu Bridge.

Tanaka *et al* (1995) presented with experimental evidences that the buffeting response of cable stayed bridge at their erection stages could be greater under wind with skew angles rather than a wind coming normal to the bridge axis. Based on the studies it was concluded that even though the mean response of bridge deck generally follows the cosine rule, the dynamic buffeting response does not follow the cosine rule and some times even increases with yaw angle.

Jain *et al* (1995,1996) based on the state of the art described by Scanlan and Jones (1990) considered both multimode and inter-mode buffeting responses using the continuous beam model and random vibration based mode superposition approach. They demonstrated the significance of intermode response through the comparison with the Scanlan's mode-by-mode method. Their study indicated that the bluff nature of the bridge deck cross–section assists in suppressing any significant aerodynamic and aeroelastic coupling that might have provided unfavourable results.

Field measurements of cable stayed bridges have indicated that the accuracy of buffeting response prediction can rather be poor, unless the input parameters, such as

aerodynamic admittance, coherence decay laws, turbulent spectral densities and steady aerodynamic force coefficients are known with great confidence. Thus, to obtain more reliable results, Kiviluoma (1998) has used a multimode approach in frequency domain in which the aerodynamic coupling due to self-excited aerodynamic forces is considered including the aerodynamic damping effects of cables, towers and other secondary structures. The bridge is idealized as a detailed three-dimensional model rather than a conventional straight beam and analysis performed for user given turbulence models, aerodynamic admittance function and coherence functions.

Xu *et al* (1998) presented a new algorithm in frequency domain with pseudo excitation method for buffeting analysis. In this method, the aeroelastic forces described as functions of flutter derivatives and motion of bridge deck as given in Jain (1996) are first converted into nodal forces to form aeroelastic damping and stiffness matrices. Aerodynamic buffeting forces are converted into nodal forces to obtain the element loading vectors. Equation of motion is assembled and converted into frequency domain, the spectral matrix of buffeting response is formed and pseudo-excitation method is developed to determine the buffeting response of bridge. The advantages of the algorithm are (i) to readily handle complex bridge decks with significant varying structural properties along the deck (ii) to make use of the finite element model of the bridge developed for eigen value analysis and (iii) to include intermode and multimode contributions of buffeting response of bridge deck.

Xu (1999) applied the psuedo-excitation approach to Tsing Ma suspension Bridge in Hong Kong to examine the effects of coupling of multimodes and intermodes of vibration on deck response and to investigate the buffeting response of whole bridge. The analytical results were compared with wind tunnel tests. The results show that effects of multimode responses are larger than the single mode responses in the vertical and torsional motions of deck. Significant intermode responses may exist between the vibration modes of similar shapes. The buffeting of towers and main cables does affect the lateral vibration of bridge deck.

Gu *et al* (1999) described the concept of buffeting based selection of the cross-section of long span cable suspended bridges during the preliminary design, which is in practice in China. Comparative buffeting factors were defined and relevant formulas were derived based on the buffeting analysis method based on the methodology given by Scanlan and Gade (1977).

Kimura *et al* (1999) studied analytically the lateral sway buffeting of cable stayed bridges at its erection stage in yawed wind. By simplifying the bridge deck as a cantilevered beam, a formulation was presented for the lateral response prediction in the yawed wind. The effects of wind yaw angle were incorporated by considering the change in the temporal wind direction caused by the lateral fluctuating wind velocity component and the dependence of the normal force distribution on the wind yaw angle. The assumption of normal force distribution and the aerodynamic damping with different wind yaw angle were found to affect the predicted buffeting response considerably. They stressed the need to study the effect of construction equipments located near the free end of bridge on aerodynamic characteristics of the deck during erection of bridge. They also stressed the need for inclusion of aerodynamic forces on cables and towers for more accurate prediction of buffeting response.

Frequency domain analysis, even though popular due to its computational efficiency, is not capable to consider the nonlinear behaviour of cable stayed bridge and non linear dependence of aerodynamic force coefficients on the angle of attack. Further, linear analysis is not valid in the ultimate limit zone. Therefore time domain analysis has emerged as an efficient tool to overcome the limitations of frequency domain analysis. The developments in this area are discussed below.

2.6.2 Time Domain Analysis

Diana (1986) has presented a time domain approach for estimating the buffeting response of long span suspension bridges.

Svensson *et al* (1992) discussed nonlinear time domain analysis for estimation of the buffeting response of Helgeland Bridge and Great Belt and Eastern Bridge. In frequency domain the nonlinear behaviour of cable stayed bridges and nonlinear dependence of aerodynamic force coefficients upon the angle of attack of wind are not considered, which are decisive for large span bridges. To arrive at an economical design, the authors have used nonlinear time domain approach to examine the actual behaviour of structure in the ultimate limit zone.

Kovacs *et al* (1992) brought out the advantages of nonlinear time domain analysis for the aerodynamic design of a long, very slender cable stayed bridge subjected to extreme wind speeds and high turbulence intensities. The analysis has been carried out for the service state as well as ultimate limit state through mathematical modelling of turbulent wind in space and time. For wind simulation, the turbulence spectra by Von Karman has been used. A mathematical model has been used to digitally simulate the turbulent part of the momentary wind velocity. Aerodynamic force coefficients of the deck cross-section are adopted from the wind tunnel results of static section model tests. For ultimate limit state, nonlinear stress strain relations and force interactions are considered. They pointed out the necessity of research in the area of coherence properties of strong winds.

Santos *et al* (1993) and Miyata *et al* (1995) presented an analytical investigation on three-dimensional buffeting response of a very long suspension bridge to gusty wind by a time domain approach. A multidimensional ARMA model based on the specified correlation is used to simulate the fluctuating wind velocities along the bridge axis. Based on the quasi-steady formulation, the aerodynamic forces include the aerodynamic coupling of three-dimensional vibration as well as the nonlinear aerodynamic forces and damping. The analytical results of Akashi Kaikyo Bridge show that the buffeting response of the long span bridge exhibits the instantaneous coupled three-dimensional random vibration about the mean deformed configuration.

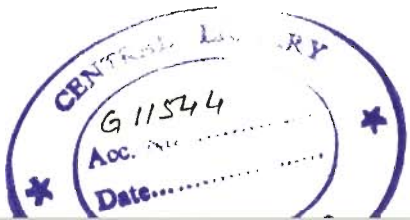

Borri *et al* (1995) have presented a computational model for the time domain simulation of stochastic response of long span suspension bridges under turbulent wind. A multidimensional wind velocity field generated by a multi-correlated autoregressive process (AR) of higher order represents the turbulent boundary layer flow. The cross-coherence of an-isotropic homogeneous turbulence is also dealt with. The buffeting forces are obtained following a fully nonlinear quasi-stationary approach assuming micro-scales of turbulence in the deck height, where interaction forces are evaluated from a relative flow around the bridge deck.

Li and He (1995) presented a method to predict the buffeting response of long span bridges based on statistical theory.

Xiang *et al* (1995) have proposed a linear time domain method, for buffeting analysis of Shantou Bay Suspension Bridge. The buffeting forces are simulated as multicorrelated random processes, and self-excited forces are expressed according to unit impulse function. The turbulent wind has been generated by the method given by Kovacs (1992). For longitudinal turbulence, spectra given by Simiu, and for vertical component, Panofsky - McCormick spectrum have been used.

Niemann and Hoffer (1995) discussed in detail the various nonlinear effects in buffeting problem of wind sensitive structures including long span flexible bridges.

Chen *et al* (2000) presented a time domain approach for predicting the coupled flutter and buffeting response of a long span suspension bridge. The frequency dependent unsteady aerodynamic forces are represented by the convolution integrals involving aerodynamic impulse functions and structural motions or wind fluctuations. The aerodynamic impulse functions are derived from experimentally measured flutter derivatives, aerodynamic admittance functions and spanwise coherence of aerodynamic forces using rational function approximations. A significant feature of the proposed approach is that the frequency characteristics of unsteady aerodynamic forces and the

nonlinearities of both aerodynamic and structural origins can be modelled in the buffeting response analysis. For a 2000m suspension bridge, both flutter and buffeting responses had been analysed and are compared with frequency domain approach. The coupling introduced by the effect of the coupled self-excited forces and unsteady characteristics of buffeting forces are also investigated. For the time domain analysis, the multi-dimensional multivariate wind velocity time histories with prescribed spectral characteristics, i.e., Von Karman spectra, along the bridge axis were generated using the autoregressive scheme for 120sec at an interval of 0.1sec. The coherence functions between u and w components are neglected and between different u components or w components are included in the analysis.

2.6.3 Methods for Buffeting Response Control

As understood from the buffeting analysis, response of bridge deck to fluctuating wind depends on the steady state drag (C_D), lift (C_L) and moment (C_M) coefficients as well as the derivatives of lift ($dC_L/d\alpha_w$) and moment coefficients ($dC_M/d\alpha_w$) with respect to angle of attack of wind. Selection of a cross-section for bridge deck such that these aerodynamic design parameters and their derivatives are minimum, could lead to lower buffeting response.

Also, the buffeting response is a function of frequency of vibration as well as damping. By increasing the modal structural damping, the buffeting response can be controlled. Gu *et al* (1993) proposed use of Tuned Mass Dampers for controlling vertical buffeting response. As a further advancement, Gu *et al* (1999) have proposed a multiple level–type of TMD system for the control of buffeting response of Yangpu cable stayed bridge. The control efficiency of MTMD is sensitive to its frequency characteristics rather than the damping ratio. The advantage of the MTMD is that it requires less space for installation as compared to the traditional hanging type of TMD.

2.7 UNSTEADY AERODYNAMICS AND FLUTTER ANALYSIS

The developments in bridge aerodynamics are attributed to early research in aircraft aerodynamics. An analytical expression of aerodynamic lift force on a harmonically oscillating flat plate was first given by Birnbaum in 1922 as an application of Prandtl's theory of bound vortices. Through the following decade, the analysis of unsteady aerodynamic forces on an oscillating two-dimensional plate attracted significant interests of aerodynamicists such as Wagner, Glauert, Kussner, Duncan and Collar but the most complete solution to this problem was presented by Theodorsen (1935).

After the collapse of original Tacoma Narrows Bridge, Bleich tried to analyse the incident as flutter by applying the Theodorsen's aerodynamic formulation to the bridge and found that the critical flutter speed thus calculated was considerably higher than that wind speed at which Tacoma Narrows collapsed. It was obvious that the airfoil flutter derivatives were not applicable to aerodynamically bluff section such as this bridge.

Bleich tried to overcome this defect by modifying the Theodorsen's expression by considering an additional lift force term corresponding to the effect of vortex formation from leading edge of the deck but was not very successful. Pugsley commented at this point that the experimentally determined flutter derivatives rather than Theodorsen's may be of help in future. He was right. Ironically, the use of stream lined shallow box girder as suspension bridge stiffening girder has become quite popular, inspired by its success in both Severn and Lillebaelt crossings in late 1960s. For these cases, the flow separation is much less than in the bluff deck cross-section similar to Tacoma Narrows Bridge and Bleich's original calculation with Theodorsen's functions can actually yield a reasonably good approximation.

Determination of unsteady aerodynamic forces, a key parameter in flutter analysis, is discussed in the following section.

2.7.1 Determination of Unsteady Forces

The unsteady aerodynamic forces acting on a bridge deck, expressed in terms of flutter derivatives are generally extracted experimentally through wind tunnel tests on section models by either forced oscillation or free oscillation method. Recently, efforts to evaluate them through computational fluid dynamics techniques are in progress. In the following section, advancements in determination of unsteady forces have been discussed.

2.7.1.1 Experimental techniques

In the absence of any analytical means to determine unsteady aerodynamic forces for stalled wings, where flow separation is involved, an extensive experimental evaluation of these forces was attempted since 1930s. There are basically two ways to do it. One is to make a direct measurement of aerodynamic force components by dynamometers, strain gauges and so on when the body is given a specific motion, and another is to calculate the force indirectly from the induced motion of the body. The same principles have been applied to airfoils as well as bridge deck sections.

Forsching (1958) applied the direct method for the measurement of unsteady aerodynamic forces on various prisms but Ukeguchi *et al* (1966) were probably the first to apply it to bridge deck section. Rigid bridge deck models were mechanically driven into simple harmonic motion with a range of specific frequency and amplitude in two-dimensional air stream and the reactions at model supports were detected. Halfman extensively applied this method in 1952 to airfoil aerodynamics.

Miyata *et al* (1975) have analysed the wind induced aeroelastic oscillations of long span bridge deck structures on the basis of unsteady aerodynamic forces measured by forced oscillation method, considering the nonlinear characteristics of forces with amplitude of oscillation.

Jacobsen (1995) presented a system identification method for extraction of motion induced wind forces in terms of flutter derivatives from the buffeting response for a suspension bridge box girder deck. The system identification method, covariance block Hankel matrix decomposing method (CBHM-method) is valid for a linear dynamic system driven by white noise. The motion-induced forces are also determined from the pressure recordings around the bridge section model in forced vibrations.

As opposed to direct measurement, the indirect measurement of aerodynamic forces by detecting the induced response of models in wind flow generally requires less-complicated experimental set-ups but more careful conditioning of them. Application of this method in bridge aerodynamics was initiated by Scanlan *et al* (1968,1969 1971) and has been widely practised all over the world.

Scanlan and Tomko (1971) examined the fairly close parallelism in form between the problems of aerodynamic instability of bridge decks and flutter of airfoils. Further, they examined the validity of free oscillation tests for extraction of aerodynamic flutter derivatives. They also presented the aerodynamic flutter derivatives for seven actual and hypothetical bridge deck sections obtained by free oscillation technique under laminar flow condition, at zero angle of attack.

Sarkar *et al* (1992) have described the development of system identification procedure designed to estimate all the 8 flutter derivatives (H_1^* - H_4^* & A_1^* - A_4^*) simultaneously.

Naresh Kumar *et al* (1995) evaluated the aerodynamic stability of a cable stayed bridge having composite I-girder deck, under smooth and grid generated turbulent flow, with the help of flutter derivatives obtained by free oscillation method.

Singh *et al* (1995, 1996) have described a 3-DOF-suspension system developed to extract all the eighteen flutter derivatives. The flutter derivatives associated with sway are illustrated for a streamlined and bluff deck section. Experimental results are compared to pseudo-static approximation and their significance in the estimation of

flutter speed discussed.

Some attempts have been made to investigate the effect of turbulence by Scanlan and Lin (1978), Tanaka and Davenport (1979) and nonlinearity on flutter derivatives by Morimitsu *et al* (1973).

2.7.1.2 Computational fluid dynamics techniques

Larsen and Walther (1997) have simulated the two-dimensional viscous incompressible flow past bridge girder cross sections using CFD technique, Discrete Vortex Method (DVM). The flow around stationary cross sections as well as cross-sections undergoing bending and torsional motions are investigated for assessment of drag coefficient, Strouhal Number and aerodynamic derivatives for application in aeroelastic analysis. For four bridges with bluff deck cross-section, good to excellent agreement with wind tunnel test results is demonstrated for analyses of wind loading, flutter wind speed and vortex induced response.

Enevoldsen *et al* (1999) reported the computational wind simulations around cable supported bridges using a CFD code based on large eddy simulation (LES), a FEM code for calculating the structural deflection and a coupler tying the two codes together. For closed box girder cross-sections, the non- dimensional static and motion induced force coefficients were determined using these codes and found to be reasonably in good agreement with the wind tunnel results. Similar approach has been used by Selvam and Bosch (1999) in finite element modelling of flow around bridges.

Numerical modelling of vortex induced oscillations and flutter of bridge sections using finite elements on stationary and moving two–dimensional grids, with the intention of developing aerodynamic cross-sections in design phase, have been reported by Frandsen and McRobie (1999).

2.7.2 Two-Dimensional Flutter Analysis

After obtaining the unsteady aerodynamic forces acting on a bridge deck in terms of flutter derivatives, it is necessary to identify the incipient stage for flutter by computing the critical flutter speed. The most traditional way is to perform the 2D-flutter analysis, which is an application of strip theory. In this analysis, interaction between the wind and bridge deck at a two-dimensional section perpendicular to the longitudinal axis of the bridge is considered. Consequently, any three-dimensional effects along the longitudinal axis of structure are assumed to be negligible. The flutter analysis is based on the assumption that the deck is performing a simple harmonic motion in vertical bending and torsion simultaneously with same frequency and small amplitudes.

The 2D-flutter analysis in frequency and time domain methods are discussed in the following sections.

Frequency Domain

Scanlan (1978a, 1981) described in detail flutter analysis in frequency domain. Scanlan (1986) explained a methodology for quantitatively interpreting the modes, which are likely to participate in flutter. Scanlan (1988) discussed on bridge flutter and buffeting build–up by high velocity turbulent wind beyond the critical wind velocity for stability. For the bridges with bluff deck sections, the flutter condition is identified with the help of negative aerodynamic damping in a critical torsion mode, as identified by the corresponding flutter derivatives of bridge deck section. The build–up time of oscillations depends on the value of aerodynamic damping that develops over the structure and duration time of high-velocity wind gust.

Scanlan (1993) presented an integrated version of aeroelastic theory applicable to long flexible bluff bodies such as suspended – span bridges. Illustrated is a useful frequency domain model into which the observed experimental results can be incorporated and used in the aerodynamic design of bridges.

Kobayashi *et al* (1993) studied the effect of turbulence on torsional flutter of a bluff bridge deck. It was observed that for a shallow plate girder supported deck, the torsional flutter is suppressed by an upstream gust.

Pfeil and Batista (1995) presented a finite element modal formulation to deal with cable stayed bridges under laminar flow. In this numerical model aeroelastic forces are described as functions of the experimentally obtained flutter derivatives, and coupling among various vibration modes are also considered.

Lakshmy (1995) presented flutter analysis of a cable stayed bridge by using experimentally determined eight flutter derivatives in vertical and torsional direction.

Scanlan (1999) explained a method for estimating the skew wind speeds for bridge flutter, based on the conceptual view of how skew wind may attack a uniform, horizontally deployed structure. A modified form of cosine rule has been given based on the experimental analysis of wind-normal condition and its associated key flutter derivatives, particularly the one linked to bridge deck torsional instability. Clearly, skew winds will, in general, require higher velocities in order to elicit the same flutter condition.

Time Domain

Scanlan *et al* (1974, 1984) were the first to work on solving the flutter problem entirely in time domain, introducing the indicial functions which were earlier used in aeronautical field. Bucher and Lin (1988) investigated the effect of randomly fluctuating wind on stochastic stability of suspension bridges. Bartoli *et al* (1995) studied the bridge deck aeroelastic behavoiur under turbulent wind by means of analysis of stochastic characteristics of response using Ito's stochastic differential calculus. Diana *et al* (1995) presented a time domain model, based on the equivalent oscillator extended Kalman Filter, capable to reproduce the nonlinearity between aerodynamic forces and displacements of deck, including vortex shedding phenomena and aerodynamic coefficients dependence on the reduced velocity.

2.7.3 Three-Dimensional Flutter Analysis

Application of flutter analysis by idealizing the cable bridge as a three-dimensional structure has a relatively short history. The calculation can be performed in two different ways: one to apply unsteady aerodynamic forces, either in frequency domain or in time domain, directly to a 3-D finite element model of the structure known as direct method; another to consider the structural response separately in various vibration modes and assemble them using mode superposition method.

Miyata and Yamada (1990) formulated the direct method leading to a complex eigen value problem by use of aerodynamic flutter derivatives in frequency domain. The method has a straightforward philosophy but drawbacks are that it requires large computer capacity and solving of complex eigenvalue problem tends to be time consuming. For the mode superposition method, on the other hand, researchers have employed several techniques. Agar (1989, 1991) developed modal techniques to solve linearized quadratic eigen equations. As an extension of p-k method, which has been used in the field of aircraft industry, Namini *et al* (1992) presented a more general numerical procedure called p-k-F method to determine pre and post flutter solution to modal equations. Further to these, Lin and Yang (1983), Jones and Scanlan (1990) Tanaka *et al* (1992), Jain (1996) and so on directly utilized the determinant search method to calculate the complex eigenvalues in general terms of impedance matrix.

Mendes and Semiao (1999) discussed the use of Double QR method for complex eigenvalue problem for flutter analysis of long span cable stayed bridges.

Cai *et al* (1999, 2000) have studied the effect of turbulence on aerodynamic instability, using random parametric excitation analysis based on flutter derivatives using a finite element formulation. In this method, the flutter derivatives measured in a laminar flow are used. However, the random turbulence effects of wind on self-excited forces have been introduced with mean wind velocity U + u (t), turbulent component of longitudinal velocity fluctuations in the flutter equations, i.e., due to random nature of

turbulent wind, the equations of motion have random stiffness terms that are associated with displacement, random damping terms that are associated with displacement velocity.

Chen *et al* (2000) investigated the effects of aerodynamic coupling among the modes of vibration on the flutter and buffeting response of long span bridges.

Tau *et al* (2000) presented a numerical analysis procedure for 3-D flutter analysis of bridges based on the spline finite-strip method. A significant advantage of his formulation is that the effect of spatial distribution of aerodynamic forces on the bridge deck structure can be taken into account by distributing the aerodynamic forces over the cross section of bridge deck. The flutter problem has been solved through p-k-F method, i.e., the critical flutter wind velocity and pre-flutter response of the bridge has been determined through iteration of flutter determinant. The numerical analysis has been applied to a 423m long span cable stayed bridge to illustrate the reliability and accuracy of the proposed method.

Ge and Tanaka (2000) presented multimode and full-mode flutter analysis of cable- supported bridges.

2.7.4 Flutter Stabilization

(i) Aerodynamic means with geometric modifications, (ii) structural means by improving the natural frequency, i.e., improving structural stiffness distribution along the bridge deck, mass distribution or (iii) improvement in structural damping by passive or active control are efficient methods in achieving flutter stability as can be seen from the summary of studies given below.

Between the two world wars, the concept of mass-balancing was developed to prevent flutter. This was simply a means for artificially providing mass to align shear center and the center of gravity, which would decouple the flutter equations inertially and increase flutter performance.

Most studies conducted after the collapse of Tacoma Narrows concluded that flutter resistance could be greatly increased by separation of vertical and torsional modes, high torsional rigidity for deck, the use of cable stays and streamlined bridge deck cross-sections. These new features were incorporated into the new Tacoma Narrows Bridge. For example, a lateral bracing system enhanced the torsional strength, an open–slotted deck tested in wind tunnel enhanced the aerodynamic stability and heavy damping systems attenuated the oscillatory amplitude of bridge.

Engineers successfully strengthened some of the existing bridges. Well known examples are Bronx-Whitestone Bridge and Golden Gate Bridge, in which cable stays and lower lateral bracing of the deck were added to increase the overall bridge torsional rigidity.

Steinman (1947) illustrated that the aerodynamic instability in long span bridges may be reduced, and in some cases eliminated, through the use of proper combination of slots (openings on the bridge deck floor) and fins (lateral projections). Since the lateral or central slots eliminate vertical instability and outside fins reduce or eliminate torsional instability, a combination of the above two in suitable proportions has been found to yield cure for both vertical and torsional instability.

Tanaka and Ito (1969) have discussed the characteristics of the aerodynamic forces in self- excited oscillation of bridge deck sections such as box, H, Π and flat plate with or without slots. The study indicated that the critical velocity of classical type section is augmented by the installation of open grating in the deck. Further, it is better to locate the open grating as outer as possible in the section with area of opening more than 30% of the deck area.

Krishna Swamy *et al* (1971) discussed the wind tunnel studies on proposed cable stayed bridge across river Ganga for examining its aerodynamic stability.

Ito and Nakamura (1982) discussed in detail the various means such as geometric, structural and mechanical to improve the aerodynamic stability of bridge decks.

Nagao *et al* (1993), studied the mechanism of improvements of aerodynamic behaviour of box girder bridges with triangular fairings with the help of wind tunnel experiments for aerodynamic responses, unsteady pressure distribution and flow visualization in forced oscillation conditions. The improvement in the aerodynamic stability is achieved by controlling the unsteady aerodynamic forces, i.e., by promoting the reattachment of the separated flow with the help of triangular fairings. However, the shape of fairings needs to be carefully selected such that they do not increase the vortex-induced response.

Jones *et al* (1993), studied the effect of section model details on flutter derivatives with the help of wind tunnel testing of a streamlined bridge deck section with railing modelled to maintain reasonable similitude, impermeable railing and without railing. Their study indicated that with the impermeable railing the bridge deck became unstable, i.e., it showed single degree of freedom flutter in torsion, whereas, the other two configurations remained stable. Flutter derivatives H_2^* and A_4^* seem to be very sensitive to small model details of the deck. The study concluded that, since railings are required to guard the traffic, it should be made permeable for better stability.

Matsumato *et al* (1995) have clarified the flutter mechanism and its stabilization of 2D rectangular and 2D elliptical section to develop high performance against flutter instability. The stabilizing effects are caused by the double inner circulatory flows or the double separation bubbles on each side surface created using the central barrier, i.e., the presence of central barrier increased the flutter stability by decreasing the value of A_2^* (K).

Larsen (1995) has discussed the torsional instability during the erection stage of long span suspension bridge and method of controlling the flutter by provision of eccentric ballast.

Miyata *et al* (1995) explained that improvement in aerodynamic stability of super long span bridges could be achieved by controlling the stiffness distribution along the span of bridge deck, i.e., by flutter mode shape control.

Fujino *et al* (1995) proposed active control techniques for flutter suppression. They computed the unsteady aerodynamic forces acting on a bridge deck by rational function approximation (RFA). Utilizing RFA, and by applying the optimal control theory, it was concluded that the stabilizing forces for flutter suppression are obtained by active control of pitch of two additional control surfaces attached below the deck.

Gu *et al* (1998) have studied theoretically and experimentally, the method of increasing the critical flutter wind speed of long- span bridges by using tuned mass dampers. The Routh - Hurwitz stability criterion is used to study the aerodynamic instability of the bridge based on the characteristic equation of the bridge with TMD. The method has been confirmed with the wind tunnel test on section model of Tiger Gate Bridge, a suspension bridge with steel box and center span 888m.

Matsumato *et al* (2000) discussed the aerodynamic stability behaviour of bridge decks with two edge girders of three different shapes. The study indicated that the square shape edge girder has better flutter characteristics. Also studied is the influence of location of edge I-girder on flutter stability. Higher flutter onset velocity is expected, when the I-girders are installed inward. In comparison with the thin plate, stiffened girder and thin box sections, the bridge deck with two edge girders, have poorer flutter characteristics. However, the torsional frequencies of multi-cable stayed bridges with two edge girders are about 0.5Hz for the long span cable stayed bridge with main span of about 600m. This fact can make long cable stayed bridges with deck consisting of two edge girders stable against flutter. They have discussed the flutter stabilization of bridge decks of super long span bridges. The isolated three-box girder deck of the Messina Strait Bridge is stable with flutter onset velocity of 90m/sec, on account of lower magnitude of flutter derivatives, or reduced unsteady forces to excite the flutter

instability. This is mainly because of the provision for air gaps among three box girders and suitable edge modification of bridge deck. Also their studies indicated that the cross-sections of bridge deck such as the rectangular shape with a vertical central barrier, elliptical, triangular or modified rhombus have stable flutter characteristics than thin plate, by controlling the unsteady pressure distribution on the deck surface under heaving or torsional motion by the secondary flow separation. For future long span bridges, the bridge decks with two flow separation points on their surface and with separated two box girders provide stable solutions against flutter.

2.8 CRITICAL REVIEW OF LITERATURE

In the previous sections, the genesis and developments in cable stayed bridge technology, basic aerodynamic design concepts, methods for static, dynamic, aerodynamic and aeroelastic analyses as well as methods for stabilizing the bridge against buffeting and flutter are discussed in detail. The critical remarks on review of literature is presented below to identify the area for research:

- Cable stayed bridge technology is advancing towards very long spans.
- Great advancements have taken place in the last decade in an attempt to develop realistic analytical procedures to understand the complex wind induced oscillatory problems. More work in this direction is further needed to achieve wind resistant design so that the super span bridges could be realized.
- Even though, in the guidelines on cable stayed bridge design, the various types of supports for bridge deck at towers and abutments have been reported, influence of these deck supports on static, dynamic and aerodynamic behaviour of cable stayed bridges is not fully understood.
- An important parameter usually assumed in aerodynamic analysis is the structural damping, which can strongly influence the aerodynamic behaviour of bridge. Reliable theoretical methods to evaluate the modal structural damping and its

application in analyses of long span bridges for wind forces are required for rational design. Modal structural damping would also serve as a benchmark for the design of vibration controlling devices such as dampers, etc.

- More attention needs to be diverted in understanding the turbulent nature of wind, its quantification and application in wind resistant design of long span cable stayed bridges.
- Frequency domain buffeting analysis, even though popular due to computational efficiency is not capable of considering the nonlinear behaviour of cable stayed bridges. It is evident that much less is available in the literature on buffeting analysis of cable stayed bridges by time domain method. Therefore, more efforts are necessary to develop time domain analysis of long span cable stayed bridges as 'Numerical Wind Tunnel Test', an alternative to wind tunnel investigations using aeroelastic models.
- The aerodynamic design parameters of components of a cable stayed bridge, particularly the deck system should be evaluated by wind tunnel investigations or CFD techniques.
- Research on application of computational fluid dynamics techniques to simulate wind flow around bridge decks would help in quick determination of aerodynamic and aeroelastic parameters as well as in the development of bridge deck sections suitable for super spans.
- The dynamic and aerodynamic behaviour of long span cable stayed bridges at different construction stages needs to be investigated.
- In medium span cable stayed bridges with bluff bridge deck cross-sections, stability against single degree of freedom flutter in torsion is a major issue. However, for very long span bridges, with streamlined decks the occurrence of coupled flutter in vertical bending and torsion as well as lateral bending and torsion needs to be checked. Determination of lateral flutter derivatives and software for three-

dimensional finite element based flutter analysis are essential for complex aeroelastic analysis.

- With very long span bridges, the inclined stay lengths are becoming longer so that cable vibration and its control need to be given due attention.
- Development of ideal geometric shapes for deck, tower, cables as well as parapets, railings and wind screens, to achieve wind resistant design of super span cable stayed bridges is another remaining challenging area.
- The use of vibration control devices to suppress wind induced oscillations in cable stayed bridges is gaining popularity. Efforts are necessary to develop efficient and economical control devices for long span bridges.

Chapter 3

NONLINEAR STATIC AND VIBRATION ANALYSIS

3.1 INTRODUCTION

In this chapter, structural idealization of cable stayed bridges and formulations for nonlinear static and vibration analysis are presented using matrix approach.

The theory for evaluation of energy based modal structural damping is discussed. The methodology and details of software developed for estimation of modal structural damping in major components of cable stayed bridge such as deck, towers and cables are given.

The procedures for nonlinear static and vibration analyses as well as energy based evaluation of modal structural damping explained in this chapter are also applied and illustrated with numerical examples of three span and five span cable stayed bridges.

3.2 THE CABLE STAYED BRIDGE DEFINED

In the present study, three span composite bridges as well as five span cable stayed bridges are considered. The components of these bridges are as follows:

(i) Deck – In the composite and steel bridges, deck consists of orthotropic plate supported by two longitudinal box girders connected with transverse cross-girders. In the concrete bridge, the deck consists of slab supported by two longitudinal solid edge girders connected with transverse cross girders.

(ii) Towers - A- shaped towers in steel bridge, A-shaped towers made of concrete in composite bridges and H-shaped towers in concrete bridge.

(iii) Cables - Cables are arranged in double plane configuration in all these bridges.

(iv) Piers and abutments.

(v) Deck supports at towers and abutments like fixed, movable or elastic supports by means of bearings, elastic links, etc.

3.2.1 Structural Idealization

As the cable stayed bridges included in this study consist of decks supported by two longitudinal box or solid girders connected with transverse cross girders, the deck is idealized using two rows of longitudinal beam elements connected with cross beam elements.

Cables are idealized using cable elements and the girder/tower members using three-dimensional beam elements. The idealization of a cable-stayed bridge as a three-dimensional space structure is illustrated in Fig. 3.1.

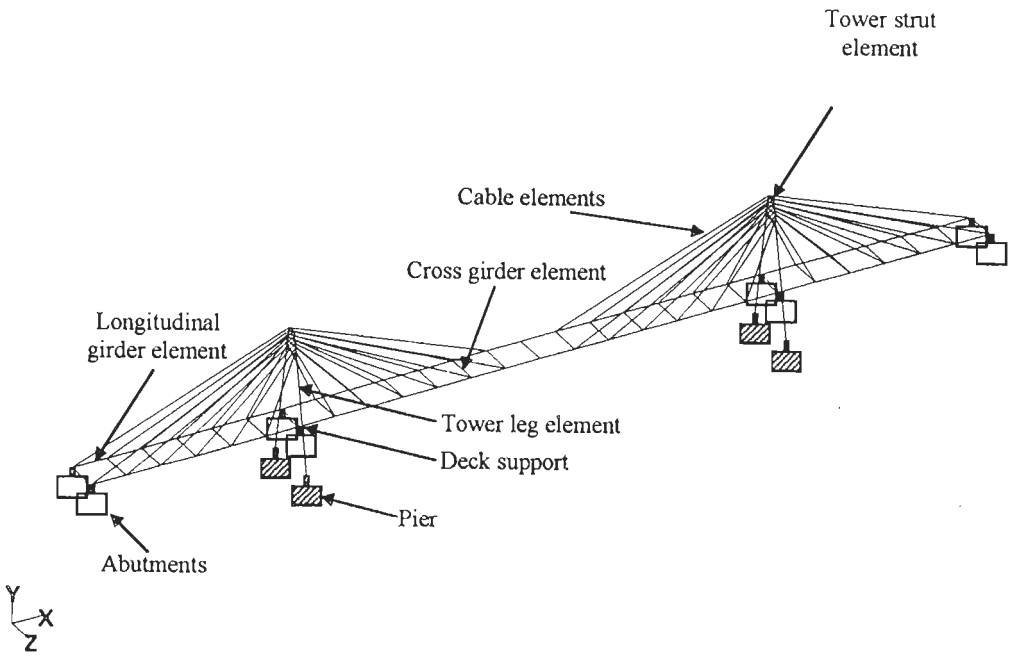

Fig. 3.1 : Idealization of Cable Stayed Bridge as a Three-Dimensional Space Structure

The major structural elements of a cable stayed bridges are:

(i) Cable elements: The long cables spanning between the towers and deck are capable of resisting axial tension only.

(ii) Deck elements: The longitudinal and transverse deck girder members have bending stiffness in vertical and lateral directions and are capable of resisting torsional moments.

(iii) Tower Elements: Each tower, though a plane frame, is represented by three-dimensional beam elements and is fully fixed against movements at its base.

3.2.1.1 Cable element

Cable element is regarded as a member capable of resisting axial tension only, as they have very small bending stiffness. In three-dimensional analysis, the cable element is composed of two nodes that have a total of six degrees of freedom as shown in Fig. 3.2. For a cable element the displacement vector {u} can be written as

$$\{u\} = [\, u_i \; v_i \; w_i \; u_j \; v_j \; w_j \,]^T \tag{3.1}$$

The nonlinear behaviour of the individual cables in a cable stayed bridge results from sag phenomenon. The axial stiffness of the cable element is affected by the cable sag, which is influenced by the tension in the cable. When the cable tension increases, the sag decreases and apparent axial stiffness increases. An equivalent straight chord member with an equivalent modulus of elasticity that combines both effects of material and geometric deformations is used to account for this variation in the cable axial stiffness.

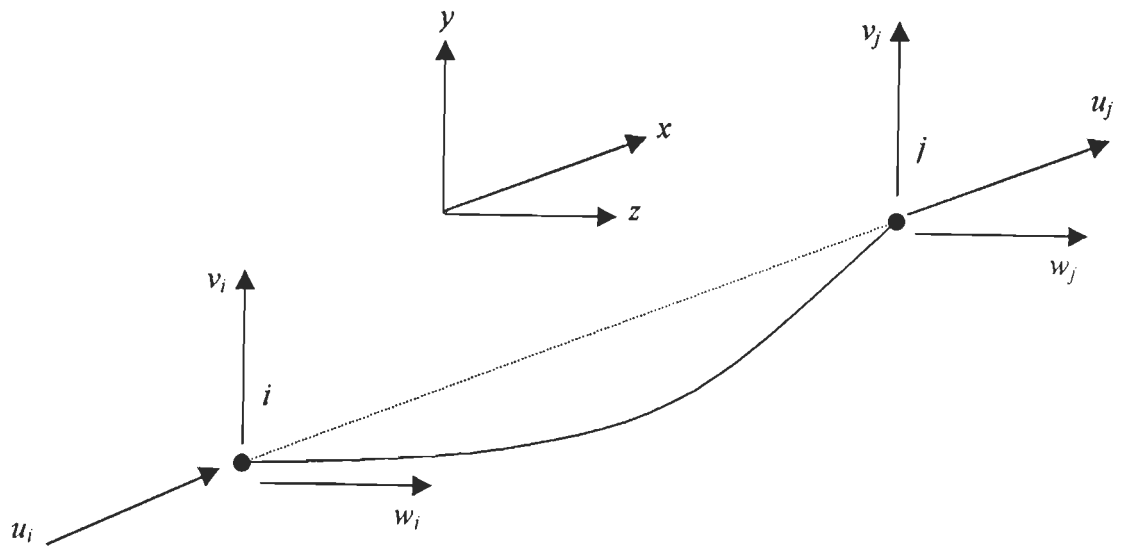

Fig. 3.2 : Cable Element in Local Co-ordinate System

The concept of equivalent cable modulus of elasticity first introduced by Ernst (1965) and later verified by several other investigators is given by:

$$E_{eq} = \frac{E_c}{1 + \left[\frac{(w_c L_{hc})^2 A_c E_c}{12 T_c^3} \right]} \tag{3.2}$$

Where E_{eq} = equivalent modulus

E_c = cable material effective modulus

L_{hc} = projected length of cable

w_c = weight per unit length of the cable

A_c = cross-section area of cable

T_c = cable tension

The element stiffness matrix for the cable is given by

$$|k_E|_c = \frac{A_c E_{eq}}{L_c} \begin{bmatrix} 1 & 0 & 0 & -1 & 0 & 0 \\ 0 & 0 & 0 & 0 & 0 & 0 \\ 0 & 0 & 0 & 0 & 0 & 0 \\ -1 & 0 & 0 & 1 & 0 & 0 \\ 0 & 0 & 0 & 0 & 0 & 0 \\ 0 & 0 & 0 & 0 & 0 & 0 \end{bmatrix} \tag{3.3}$$

The tangent stiffness of a cable stay of chord length L_c and cross sectional area A_c, when subjected to an axial tension T_c, is equal to that of a truss element of equal length and cross-sectional area and with an equivalent modulus given by Eq. 3.2, and subjected to axial tension T_c. There are different approaches for computing the tangent stiffness matrix of that truss element using large deflection theory (Baron and Venkatesan, 1971 and Przemieniecki, 1968). All of these approaches lead to the same result, which is simply given by:

$$[k_T]_c = [k_E]_c + [k_G]_c \tag{3.4}$$

Where $[k_T]_c$ is the element tangent stiffness matrix in local coordinates, $[k_E]_c$ is the elastic stiffness matrix obtained from Eq. 3.3 and $[k_G]_c$ is geometric stiffness matrix of truss element and is given by:

$$[k_G]_c = \frac{T_c}{L_c} \begin{bmatrix} 0 & 0 & 0 & 0 & 0 & 0 \\ 0 & 1 & 0 & 0 & -1 & 0 \\ 0 & 0 & 1 & 0 & 0 & -1 \\ 0 & 0 & 0 & 0 & 0 & 0 \\ 0 & -1 & 0 & 0 & 1 & 0 \\ 0 & 0 & -1 & 0 & 0 & 1 \end{bmatrix} \tag{3.5}$$

3.2.1.2 Three-dimensional beam element for tower/deck members

In the three-dimensional modelling, the beam element used to idealize tower/deck members has 12 degrees of freedom as in Fig. 3.3. For a three-dimensional beam element, the displacement vector {u} can be written as:

$$\{u\} = [\, u_i \; v_i \; w_i \; \theta_{xi} \; \theta_{yi} \; \theta_{zi} \; u_j \;\; v_j \; w_j \;\; \theta_{xj} \; \theta_{yj} \; \theta_{zj} \,]^T \tag{3.6}$$

The large deformation that occurs in the tower and girder elements of a cable stayed bridge under the combined effect of large bending moments and high axial forces produce a strong coupling between axial and flexural stiffness in these members. The coupling can be considered in the refined nonlinear analysis by introducing the concept of stability functions as given in Weaver and Gere (1980).

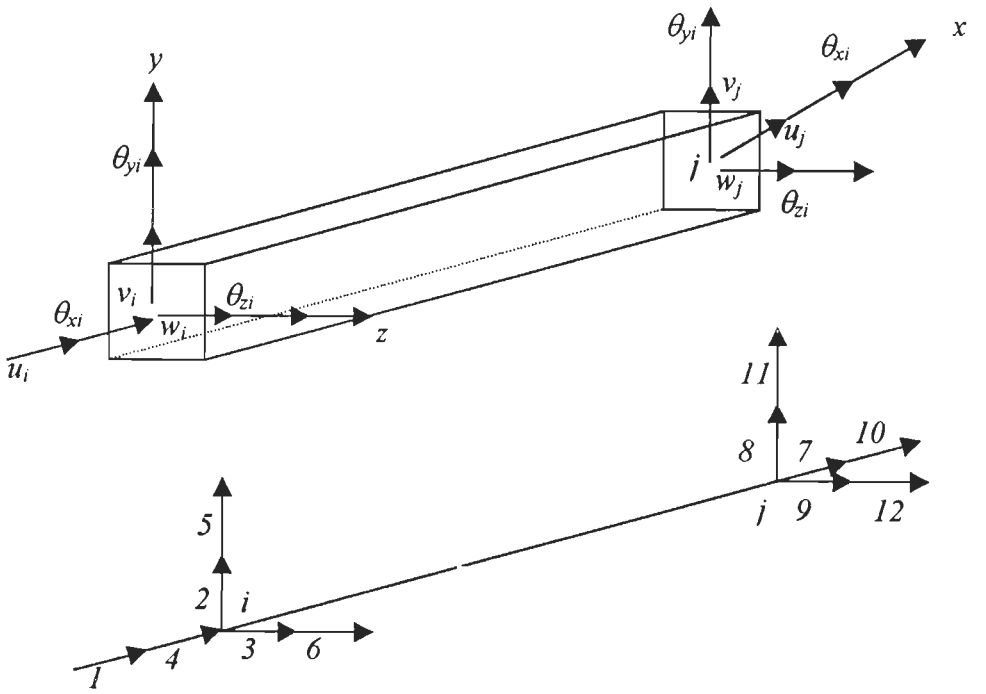

Fig. 3.3 : Three-Dimensional Beam Element in Local Co-ordinate System

These functions are multiplication factors used to modify both bending and axial stiffness of the member. The secant stiffness matrix for a three-dimensional beam–column element is given by :

$$[k_E]_b = \begin{bmatrix}
\left(\frac{EA}{L}\right)S5 & & & & & & & & & & & & \\
0 & \left(\frac{12EI_z}{L^3}\right)S1_z & & & & & & & & & & & \\
0 & 0 & \left(\frac{12EI_y}{L^3}\right)S1_Y & & & & & & & & & & \\
0 & 0 & 0 & \left(\frac{GI_X}{L}\right) & & & & & & & & & \\
0 & 0 & \left(-\frac{6EI_Y}{L^2}\right)S2_y & 0 & \left(\frac{4EI_y}{L}\right)S3_y & & & & & & & & \\
0 & \left(\frac{6EI_z}{L^2}\right)S2_z & 0 & 0 & 0 & \left(\frac{4EI_z}{L}\right)S3_z & & & & & & & \\
\left(-\frac{EA}{L}\right)S5 & 0 & 0 & 0 & 0 & 0 & \left(\frac{EA}{L}\right)S5 & & & & & & \\
0 & \left(-\frac{12EI_z}{L^3}\right)S1_z & 0 & 0 & 0 & \left(-\frac{6EI_z}{L^2}\right)S2_z & 0 & \left(\frac{12EI_z}{L^3}\right)S1_z & & & & & \\
0 & 0 & \left(-\frac{12EI_y}{L^3}\right)S1_y & 0 & \left(\frac{6EI_y}{L^2}\right)S2_y & 0 & 0 & 0 & \left(\frac{12EI_y}{L^3}\right)S1_y & & & & \\
0 & 0 & 0 & \left(-\frac{GI_x}{L}\right) & 0 & 0 & 0 & 0 & 0 & \left(\frac{GI_x}{L}\right) & & & \\
0 & 0 & \left(-\frac{6EI_y}{L^2}\right)S2_y & 0 & \left(\frac{2EI_z}{L}\right)S4_y & 0 & 0 & 0 & \left(\frac{6EI_y}{L^2}\right)S2_y & 0 & \left(\frac{4EI_y}{L}\right)S3_y & & \\
0 & \left(\frac{6EI_z}{L^2}\right)S2_z & 0 & 0 & 0 & \left(\frac{2EI_z}{L}\right)S4_z & 0 & \left(-\frac{6EI_z}{L^2}\right)S2_z & 0 & 0 & 0 & \left(\frac{4EI_z}{L}\right)S3_z
\end{bmatrix} \qquad (3.7)$$

sym

Where E is the member material modulus of elasticity, A is the cross- sectional area, L is the member length, I_y and I_z are the moments of inertia of the cross-section about the local principal y and z axes, respectively, I_x is the torsional moment of inertia of the cross- section, G is the member material shear modulus, and the S's are the stability functions, $S1_y$ through $S4_y$ modify the bending stiffness of the member about the local y axis, while $S1_z$ through $S4_z$ modify the bending stiffness about the local z axis and $S5$ modifies the axial stiffness. The stability functions as available in Nazmy *et al* (1990) are given in Appendix – I.

The stiffness matrix of a beam -column element as given by Eq. 3.7 is in fact the secant stiffness matrix. The tangent stiffness matrix of such element can be obtained using large deflection theory and nonlinear strain-displacement relationships discussed by Oran (1973) to give:

$$[k_T]_b = [k_E]_b + [k_G]_b \tag{3.8}$$

Where $[k_T]_b$ is the beam element tangent stiffness matrix in its local coordinates, $[k_E]_b$ is the elastic stiffness matrix as given by Eq. 3.7, and $[k_G]_b$ is the geometric stiffness matrix of beam element. For a 3-D beam element, it is given by:

$$[k_G]_b = \frac{P}{L}\begin{bmatrix}
0 & & & & & & & & & & & \\
0 & \frac{6}{5} & & & & & & & & & & \\
0 & 0 & \frac{6}{5} & & & & & & & & & \\
0 & 0 & 0 & 0 & & & & & & & & \\
0 & 0 & -\frac{L}{10} & 0 & \frac{2}{15}L^2 & & & & & & & \\
0 & \frac{L}{10} & 0 & 0 & 0 & \frac{2}{15}L^2 & & & & & & \\
0 & 0 & 0 & 0 & 0 & 0 & 0 & & & & & \\
0 & -\frac{6}{5} & 0 & 0 & 0 & -\frac{L}{10} & 0 & \frac{6}{5} & & & & \\
0 & 0 & -\frac{6}{5} & 0 & \frac{L}{10} & 0 & 0 & 0 & \frac{6}{5} & & & \\
0 & 0 & 0 & 0 & 0 & 0 & 0 & 0 & 0 & 0 & & \\
0 & 0 & -\frac{L}{10} & 0 & -\frac{L^2}{30} & 0 & 0 & 0 & \frac{L}{10} & 0 & \frac{2}{15}L^2 & \\
0 & \frac{L}{10} & 0 & 0 & 0 & -\frac{L^2}{30} & 0 & \frac{-L}{10} & 0 & 0 & 0 & \frac{2}{15}L^2
\end{bmatrix} \tag{3.9}$$

Where P is the axial force in the member and L is the length of member.

3.2.1.3 Rotation transformation matrix

The element matrices defined in local co-ordinate system are to be transformed to global co-ordinate system before assembly to get the global matrices. The transformation of components of force or displacement vectors is achieved by using the rotation transformation matrix as follows:

$$\{\bar{u}\} = [T]\{u\} \tag{3.10}$$

$$\{\bar{F}\} = [T]\{F\} \tag{3.11}$$

The transformation matrix $[T]$ is a [12 x 12] matrix given by:

$$[T] = \begin{bmatrix} R & 0 & 0 & 0 \\ 0 & R & 0 & 0 \\ 0 & 0 & R & 0 \\ 0 & 0 & 0 & R \end{bmatrix} \tag{3.12}$$

where rotation matrix $[R]$ is a [3x3] matrix and depends on the rotation of member axes. For a space frame element as shown in Fig. 3.4, it is given as follows :

$$[\mathrm{R}] = \begin{bmatrix} l_x & m_x & n_x \\ -m_x/D & l_x/D & 0 \\ -l_x n_x/D & -m_x n_x/D & D \end{bmatrix} \tag{3.13}$$

where $l_x = (x_j - x_i)/L$; $m_x = (y_j - y_i)/L$; $n_x = (z_j - z_i)/L$ $D = \sqrt{l_x^2 + m_x^2}$,

(x_i, y_i, z_i) and (x_j, y_j, z_j) are the co-ordinates of first and second nodes of element respectively and L is the length of member.

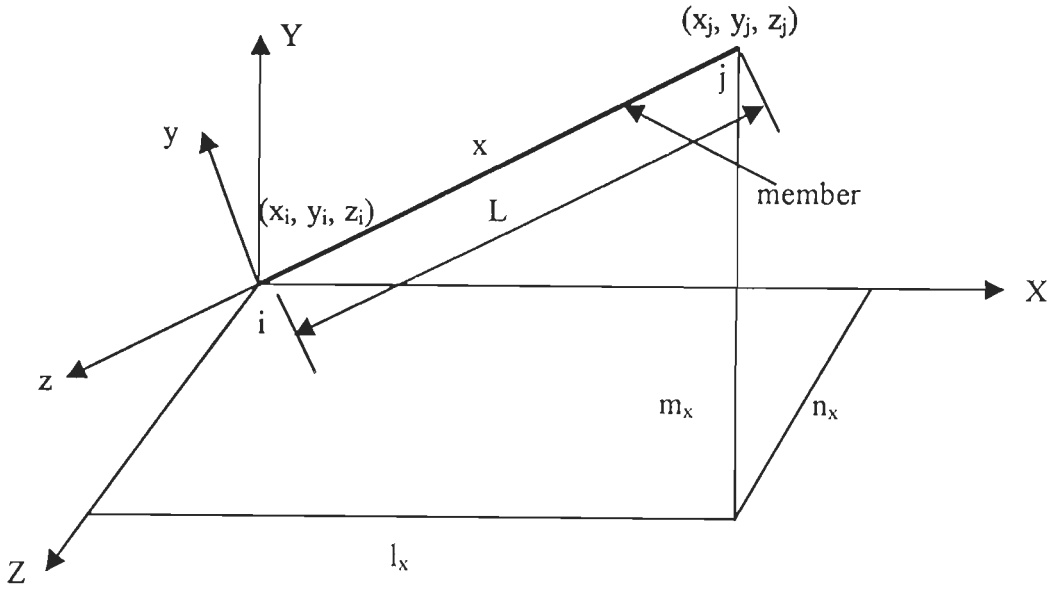

Fig. 3.4 : Three-Dimensional Beam Element with Co-ordinate Systems

3.3 NONLINEAR STATIC ANALYSIS

Nonlinear static analysis of cable stayed bridges has been performed using an algorithm which incorporates correction for both element geometric stiffness as well as for secondary loading. The nonlinear analysis algorithm consists of the following steps:

(i) First, primary displacements are calculated for the applied loading.

(ii) Stiffness corrections are applied on element stiffness matrices based on observed displacements. New global stiffness matrix is assembled based on revised element stiffness matrices

(iii) Load vectors are revised to include the secondary effects due to primary displacements

(iv) The new set of equations are solved to generate the new displacements.

(v) Member forces and support reactions are calculated for these new displacements.

(vi) The nonlinear analysis algorithm allows the user to go through the multiple iterations of the above procedure.

In an iterative scheme, it is necessary to establish the convergence criteria, to ensure sufficient accuracy for termination of computational procedure. The member

end forces are evaluated by performing a convergence check on the joint displacement. In each step, the displacements are compared with those of previous iterations in order to check whether the convergence is attained.

In the present study, the number of iterations is specified as 20 and the convergence criteria is established by setting a norm for displacement changes between the successive iterations.

In the nonlinear analysis, also the divergence tolerance limit '*dt*' could be specified. If the displacement computed on any iteration exceeds '*dt*', the solution is diverging and the iterative process is terminated. The default value for 'dt' is the span of bridge divided by 120.

In the present study, the nonlinear static analysis of the cable stayed bridges has been performed using the available STAAD-PRO (2001) software.

3.4 FREE VIBRATION ANALYSIS

Any structural model, which consists of stiffness matrix and 'n' mass degrees of freedom, contains 'n' normal modes of vibration. Each normal mode occurs at a specific frequency of vibration known as natural frequency or eigenvalue. At these frequencies, the structure oscillates from positive to negative about mean position and the nodal displacements are known as the mode shape or eigenvector.

The process of calculating the system eigenvalues and eigenvectors is known as modal extraction and is performed by solving the equations :

$$\omega^2 [M] \{\phi\} - [K] \{\phi\} = 0 \qquad (3.14)$$

where

$[M]$ = diagonal mass matrix (assuming no mass coupling)

ω = natural circular frequencies (eigenvalues)

$\{\phi\}$= normalized mode shapes (eigenvectors)

The broad classification of methods available for solution of the eigen problem is : transformation methods, iterative methods and determinant search method. Examples of transformation methods are Jacobi, Householder and QR methods. The

iterative methods include direct vector iteration – power method, vector iteration with shifts- inverse iteration, subspace iteration and Lanczos iteration methods.

The selection of numerical method in a specific case depends on the nature of the problem, which affects the size of the matrices involved and their properties such as symmetry, positive definiteness, bandedness and sparsity. Suitability of solution procedure also depends on the type of solution desired, for example, whether all the mode shapes and frequencies are required or only a few needs to be found, or whether the few modes to be found are those at the lowest or highest frequencies.

The vibration analysis could be performed using available STAAD-PRO software either by subspace iteration or STARDYNE advanced analysis – Lanczos method as well as HQR-II GUYAN method. The Lanczos algorithm is very effective in determination of eigenvalues and eigenvectors of a large symmetric matrix. In the present study, the natural frequencies and mode shapes of the cable stayed bridges have been obtained using Lanczos iteration method and its details are presented in the following section.

3.4.1 Lanczos Iteration Method

Lanczos iteration method has great potential in partial eigen solutions, i.e., first few eigenvalues of large banded symmetric matrices. The standard eigenvalue problem is given by

$$[A]\{q\} = \lambda\{q\} \tag{3.15}$$

The method essentially consists of evaluation of Lanczos transformation matrix $[X]$ consisting of a series of mutually orthogonal vectors $[\{x_1\}, \{x_2\}, \ldots\ldots \{x_N\}]$ such that

$$[X]^T [X] = [I] \tag{3.16}$$

The transformation is expressed as $[X]^T [A][X] = [\hat{T}]$ or $[A][X] = [X][\hat{T}]$, where $[A]$ is the matrix to be tridiagonalized using $[X]$ and $[\hat{T}]$ is the tridiagonal matrix so that both $[A]$ and $[\hat{T}]$ have the same eigenvalues.

Premultiplying both sides of Eq. 3.15 by $[X]^T$ and using orthogonality

relationship $[X][X]^T = [X]^T [X] = [\ I\ ]$ results in

$$[X]^T [A][X][X]^T \{q\} = \lambda [X]^T \{q\} \quad \text{or} \tag{3.17}$$

$$[\hat{T}]\{\tilde{q}\} = \lambda \{\tilde{q}\} \tag{3.18}$$

where $\{\tilde{q}\} = [X]^T \{q\}$

The eigenvalues of triadiagonal matrix can be evaluated using any of the standard matrix LR or QR method. Even though theoretically Lanczos vectors $[\{x_1\}, \{x_2\},\ldots\ldots\{x_N\}]$ are mutually orthogonal to each other, because of round-off errors during computations, orthogonality relationship breaks down when vectors are sufficiently separated from each other. For large systems, this source of error makes Lanczos method unstable. It is therefore necessary to re-orthogonalize a newly determined Lanczos vector by sweeping off any contribution from the vectors determined previously. Purification is carried out by Gram-Schmidt process. Denoting the purified vector by $\bar{x}_j$, we have

$$\bar{x}_j = x_j - \sum_{k=1}^{j-1} (\bar{x}_k^T x_j)\, \bar{x}_k \tag{3.19}$$

The application of Lanczos method for vibration analysis, i.e., solution of linearized eigenvalue problem is achieved by converting the problem to a standard symmetric form as discussed below.

The standard eigenvalue problem is given as

$$[K]\{\phi\} = \lambda [M]\{\phi\} \quad \text{and} \tag{3.20}$$

$$[K]^{-1}[M]\{\phi\} = \frac{1}{\lambda}\{\phi\} \tag{3.21}$$

where $[K]$ and $[M]$ are the system stiffness and mass matrices, λ represents the eigenvalues and $\{\phi\}$ is the eigenvector.

The linearized eigenvalue problem is converted into symmetric form as given by :

$$[M]\{\phi\} = \lambda [L_K][L_K]^T \{\phi\} \tag{3.22}$$

or $$[L_K]^{-1}[M][L_K^T]^{-1}[L_K]^T\{\phi\} = \lambda[L_K]^T\{\phi\} \tag{3.23}$$

$$[\bar{D}]\{\bar{\phi}\} = \gamma\{\bar{\phi}\} \tag{3.24}$$

in which $[K] = [L_K]\,[L_K]^T$ represents the factorization of $[K]$ into a lower triangular matrix and its transpose,

$$[\bar{D}] = [L_K]^{-1}[M][L_K^T]^{-1} \text{ and } \{\bar{\phi}\} = [L_K]^T\{\phi\}.$$

During Lanczos iterations, $[\bar{D}]$ in Eq. 3.24 plays the same role as [A] in standard form of iteration as described earlier by Eq. 3.15.

Alternatively, the need for transformation of linearized eigen problem into standard symmetric form could be avoided by selecting the Lanczos vector orthonormal with respect to mass matrix such that

$$[X]^T[M][X] = 1 \tag{3.25}$$

By premultiplying Eq. 3.21 by $[X]^T[M]$, we get

$$[X]^T[M][K]^{-1}[M][X]\{\bar{\phi}\} = \frac{1}{\lambda}[X]^T[M][X]\{\bar{\phi}\} \tag{3.26}$$

or $$[\hat{T}]\{\bar{\phi}\} = \frac{1}{\lambda}\{\bar{\phi}\} \tag{3.27}$$

where $$\{\phi\} = [X]\{\bar{\phi}\},\quad [X]^T[M][K]^{-1}[M][X] = [\hat{T}] \tag{3.28}$$

or because $$[X]^T[M] = [X]^{-1} \tag{3.29}$$

$$[K]^{-1}[M][X] = [X][\hat{T}] \tag{3.30}$$

The method of determining Lanczos transformation matrix $[X] = [\{x_1\},\{x_2\},\ldots\{x_N\}]$ is possible if we express Eq. 3.30 as

$$[K]^{-1}[M][\{x_1\},\{x_2\},\ldots,\{x_N\}] = [\{x_1\},\{x_2\},\ldots,\{x_N\}]\begin{bmatrix} \alpha_1 & \beta_2 & 0 & \ldots & 0 & 0 & 0 \\ \beta_2 & \alpha_2 & \beta_3 & \ldots & 0 & 0 & 0 \\ \ldots & \ldots & \ldots & \ldots & \ldots & \ldots & \ldots \\ 0 & 0 & 0 & \ldots & \beta_{N-1} & \alpha_{N-1} & \beta_N \\ 0 & 0 & 0 & \ldots & 0 & \beta_N & \alpha_N \end{bmatrix} \tag{3.31}$$

Expansion of Eq. 3.31 gives the following:

$$
\begin{aligned}
&[K]^{-1}[M]\{x_1\} = \alpha_1\{x_1\} + \beta_2\{x_2\} \\
&[K]^{-1}[M]\{x_2\} = \beta_2\{x_1\} + \alpha_2\{x_2\} + \beta_3\{x_3\} \\
&\cdots\cdots \quad \cdots\cdots \\
&[K]^{-1}[M]\{x_j\} = \beta_j\{x_{j-1}\} + \alpha_j\{x_j\} + \beta_{j+1}\{x_{j+1}\} \\
&\cdots \quad \cdots \\
&[K]^{-1}[M]\{x_N\} = \beta_N\{x_{N-1}\} + \alpha_N\{x_N\}
\end{aligned}
\tag{3.32}
$$

The process of finding Lanczos vectors begins with an arbitrary selection of $\{\tilde{x}_1\}$, where $\{\tilde{x}_1\} = \beta_1\{x_1\}$. The unknown parameter β_1 and hence $\{x_1\}$ is determined by considering that vector $\{x_1\}$ should be orthonormal.

To begin the iteration process, an arbitrary vector $\tilde{x}_1$ is selected and normalized with respect to mass matrix so that

$$\{x_1\}^T[M]\{x_1\} = 1.$$

Thus $$\beta_1^2 = \{\tilde{x}_1\}^T[M]\{\tilde{x}_1\}$$

$$\{x_1\} = \frac{\{\tilde{x}_1\}}{\beta_1} \tag{3.33}$$

Now premultiplying the first of Eq. 3.32 by $\{x_1\}^T[M]$ and selecting $\alpha_1 = \{x_1\}^T[M][K]^{-1}[M]\{x_1\}$, we get $\{x_1\}^T[M]\{x_2\} = 0$. The first of Eqs. 3.32 then gives

$$
\begin{aligned}
\{\tilde{x}_2\} &= \beta_2\{x_2\} \\
&= [K]^{-1}[M]\{x_1\} - \alpha_1\{x_1\}
\end{aligned}
\tag{3.34}
$$

$$\beta_2^2 = \{\tilde{x}_2\}^T[M]\{\tilde{x}_2\}$$

$$\{x_2\} = \frac{\{\tilde{x}_2\}}{\beta_2}$$

The complete iteration process is easily deduced as

$$\beta_j^2 = \{\tilde{x}_j\}^T [M]\{\tilde{x}_j\}$$

$$\{x_j\} = \frac{\{\tilde{x}_j\}}{\beta_j} \tag{3.35}$$

$$[K]\{\bar{x}_{j+1}\} = [M]\{x_j\}$$

$$\{\alpha_j\} = \{x_j\}^T [M]\{\bar{x}_{j+1}\}$$

$$\{\tilde{x}_{j+1}\} = \{\bar{x}_{j+1}\} - \beta_j\{x_{j-1}\} - \alpha_j\{x_j\}$$

Thus the Lanczos iteration vectors constituting the transformation matrix are obtained. Considerable amount of research has gone into Lanczos iteration method. More details are available in Humar (1990), Parlett *et al* (1979) and Scott (1981).

3.5 ENERGY BASED EVALUATION OF MODAL STRUCTURAL DAMPING

The damping ratio of a mode of vibration is proportional to the energy dissipation. There are various factors causing energy dissipation in a cable stayed bridge. It is generally due to material nonlinearity, friction at movable bearings, energy dissipation from foundation to ground and friction with air. Predominant factors contributing to modal damping ratio in a cable stayed bridge vary with structural types, however an important step in estimation of damping ratio is to evaluate the total energy dissipation. As the energy dissipation capability of the components such as cables, deck and towers are different it is necessary to evaluate the energy dissipation of each structural component. Once the energy dissipation in each type of structural component is determined, the total energy dissipation in the whole structural system can be obtained by summing up the energy dissipation in each structural component. Similarly, the total potential energy of the whole system is obtained by summing up the potential energy of each component. The modal damping ratio corresponding to n^{th} mode is defined as the ratio of dissipated energy per cycle, E_D, to the potential energy per one cycle, E_P as given by Clough and Penzien (1993).

$$\xi^n = \frac{(E_D)^n_{bridge}}{4\pi(E_P)^n_{bridge}} \tag{3.36}$$

Based on the method discussed by Kawashima *et al* (1993) and Yamaguchi and Ito (1995), the step-by-step procedure for evaluation of energy based modal damping is given below:

(i) Discretize the cable stayed bridge into deck, tower and cable elements. Let 'nd', 'nt' and 'nc' represents the number of deck, tower and cable elements respectively in a cable stayed bridge.

(ii) Perform nonlinear static analysis under dead load and initial tensions of cables.

(iii) For the dead load deformed geometry of bridge, perform free vibration analysis to determine 'n' natural frequencies and mode shapes.

(iv) Compute the strain energy $(E_{ST})_i^n$ for i^{th} element for n^{th} mode using element stiffness matrices given by Eq. 3.3 for cable and Eq. 3.7 for deck and tower elements as well as the mode shapes $\{\phi^n\}$ corresponding to n^{th} mode obtained by vibration analysis, using the following equation:

$$(E_{ST})_i^n = \frac{1}{2}\{\Phi_i^n\}^T [k_e]\{\Phi_i^n\} \tag{3.37}$$

(v) Sum up the strain energies of deck elements, tower elements and cable elements and by using the respective energy loss factors of corresponding materials, i.e., η_{deck}, η_{tower} and η_{cable} to work out the energy dissipation of these components for n^{th} mode:

$$(E_D)_{deck}^n = 2\pi\eta_{deck}\sum_{i=1}^{nd}(E_{ST})_{deck}^n \tag{3.38}$$

$$(E_D)_{tower}^n = 2\pi\eta_{tower}\sum_{i=1}^{nt}(E_{ST})_{tower}^n \tag{3.39}$$

$$(E_D)_{cable}^n = 2\pi\eta_{cable}\sum_{i=1}^{nc}(E_{ST})_{cable}^n \tag{3.40}$$

(vi) Compute the total energy dissipated in the structure by summing up the energy dissipated by different components.

$$(E_D)_{bridge}^n = (E_D)_{deck}^n + (E_D)_{tower}^n + (E_D)_{cable}^n \tag{3.41}$$

(vii) Compute the modal potential energy of cable stayed bridge by summing up the contribution of deck, tower and cable elements. The modal potential energy $(E_P)_i^n$ for ith element for nth mode consists of two parts, i.e., modal strain energy $(E_{ST})_i^n$ as well as the modal potential energy $(E_G)_i^n$ due to work done by the initial stress due to modal strain. It should be noted that the modal potential energy due to initial stress is the potential energy corresponding to geometric stiffness caused by the axial force in each bridge component.

$$(E_P)_i^n = (E_{ST})_i^n + (E_G)_i^n \tag{3.42}$$

$$\text{Where } (E_G)_i^n = \frac{1}{2}\{\Phi_i^n\}^T [k_G]_i^T \{\Phi_n^i\} \tag{3.43}$$

$$(E_P)_{bridge}^n = (E_P)_{deck}^n + (E_P)_{tower}^n + (E_P)_{cable}^n \tag{3.44}$$

Equations 3.5 and 3.9 give the element geometric stiffness matrices for cable and deck/tower elements respectively. $(E_{ST})_i^n$ for bridge components are calculated using Eq. 3.37.

(viii) The modal structural damping ratio is computed using Eq. 3.36.

To implement the above procedure, a main program ENDAMP with three subroutines has been developed which uses the outputs from nonlinear static analysis as well free vibration analysis. The overall flow diagram of 'ENDAMP' – evaluation of energy based modal structural damping in cable stayed bridges – is illustrated in Fig. 3.5. The input requirement for ENDAMP includes – structural properties and axial forces in members, member nodal coordinates and member modal coordinates. The software ENDAMP calls subroutines MDGIR, MDTOW and MDCAB which are used to compute the strain and potential energies of the deck elements, tower elements and cable elements respectively for a particular mode of vibration.

The input requirement for MDGIR includes the mode number for which damping is being estimated, total number of deck elements, i.e., sum of longitudinal and transverse deck girders, Young's modulus of elasticity, shear modulus and energy

loss factor for deck material, cross-sectional area of girder elements, length of girder elements based on dead load deformed geometry, area moments of inertia I_y and I_z, torsion constant I_x, and the modal ordinates at nodes of deck elements in the local co-ordinate system.

The input for MDTOW are – mode number for which damping is being evaluated, total number of tower elements (sum of vertical leg members, cross member at deck level and upper level struts for A or H-shaped towers), Young's modulus of elasticity, shear modulus and energy loss factor for tower material, area of tower elements, length of tower elements based in dead load deformed geometry obtained by nonlinear static analysis, area moments of inertia I_y, I_z, torsion constant I_x, and the modal ordinates of the tower member nodes in the local co-ordinate system. The modal ordinates obtained from the vibration analysis are transformed into local co-ordinate system using the transformation matrix given by Eq. 3.13.

For the routine MDCAB, the input requirements are – mode number for which the damping is being estimated, number of cables, Young's modulus of elasticity, energy loss factor for cable elements, geometrical co-ordinates at cable nodes based on dead load deformed state, area, weight per unit length and tension in each cable as well as the modal ordinates in the global co-ordinate system. In the program, the modal ordinates are converted into local co-ordinate system using the transformation matrix as given by Eq. 3.13.

The energy loss factors for the materials of deck, tower and cables are obtained from experiments. Typical values for concrete and steel are given in Lazan (1968) and Blevins (1990). In the present study the energy loss factor for steel deck members are taken as 0.0026 and for concrete tower members as 0.024. For cables the value has been appropriately chosen depending on the type of cable, i.e., for locked-coil or parallel wire strands as discussed in Section 2.5.1.

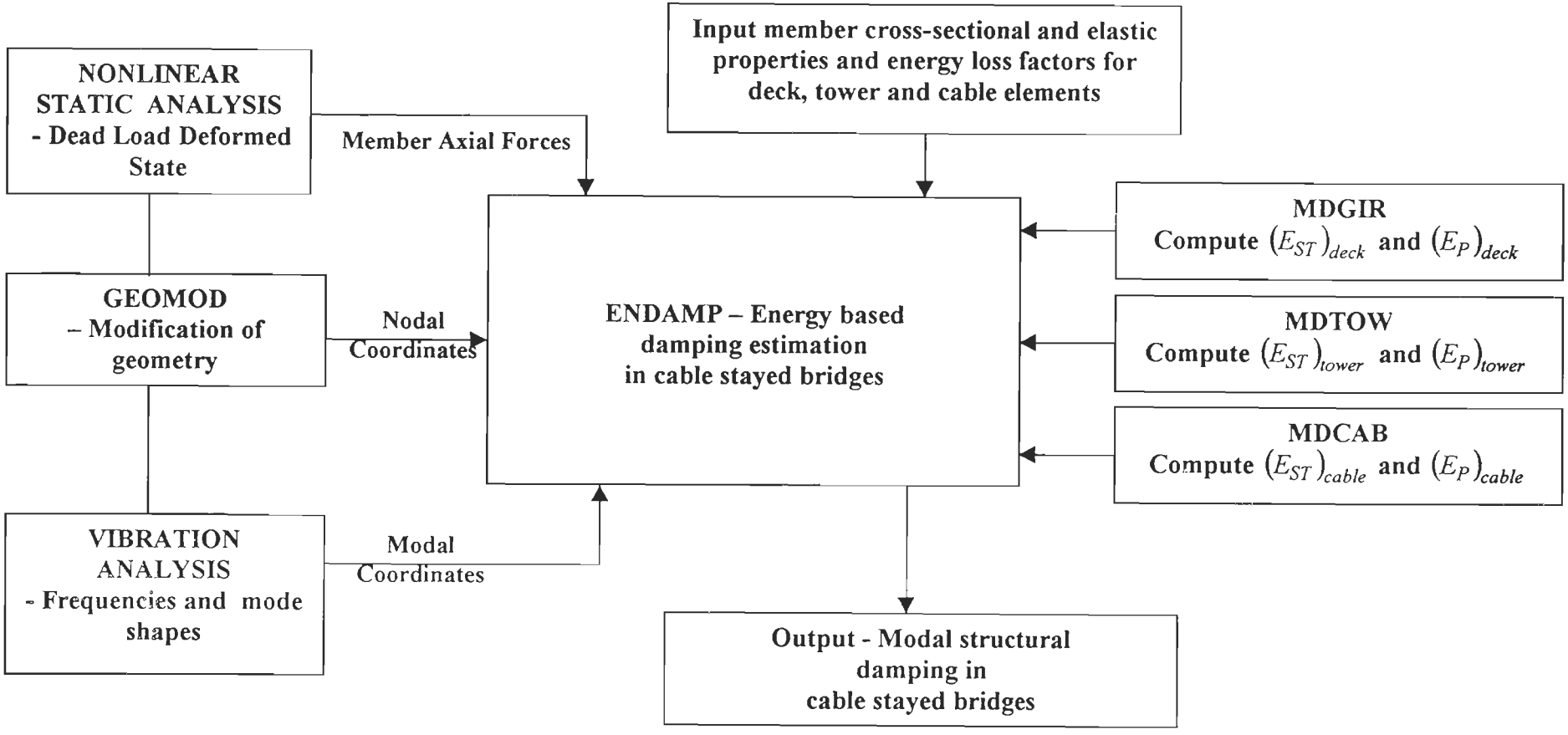

Fig. 3.5 : Flow Diagram for Evaluation of Energy Based Damping in Cable Stayed Bridges

3.6 NUMERICAL ANALYSIS

This section deals with the nonlinear static and vibration analysis of four cable stayed bridges – two bridges with three spans (Bridge #1 and Bridge#2) and other two with five spans (Bridge#3 and Bridge#4). The nonlinear static analysis has been performed to obtain the deformed geometry of these bridges under dead loads and initial cable tensions. Further, vibration analysis has been performed to obtain natural frequencies and mod shapes. The results of static and vibration analyses – nodal displacements and modal coordinates have been subsequently used for evaluation of modal structural damping, based on energy dissipated in deck, towers and cables of these bridges.

The three span bridges – Bridge#1 and Bridge#2 have been analysed to study the effect of support types for bridge deck at towers and abutments on static and vibration characteristics.

Also, the structural details and three-dimensional modelling of these bridges have been discussed.

3.6.1 Details of Bridges

Bridge #1

Bridge #1 taken for the present study is a 627.8m long, four-lane cable stayed bridge. It is a composite structure, with span length similar to Talmadge Memorial Bridge in USA. The bridge has main span of 335.2m with two side spans of 146.3m each. The cables are arranged in double-plane fan configuration with 12 cables in each plane connected to each tower. The bridge has a steel deck and two numbers of A–shaped towers made of concrete. Figure 3.6 shows the longitudinal profile, plan view and tower details of the bridge. The cross-sectional properties of bridge components as reported by Nazmy and Abdel Ghaffar (1990) are given in Table 3.1(a). The area and initial tension for various cable groups are given in Table 3.1(b)

Bridge#2

Bridge #2 taken for the present study is a long span bridge having a total span of 1255.8m with four-lane carriage way. The bridge has main span of 670.6m and two side spans of 292.6m each. The cables are arranged in double-plane fan configuration with 12 cables in each plane connected to each tower. The bridge has a steel deck and two numbers of A-shaped towers made of concrete. Figure 3.7 shows the longitudinal profile, plan view and tower details of the bridge. The cross-sectional properties of bridge components as reported by Nazmy and Abdel Ghaffar (1990) are given in Tables 3.2(a) and 3.2(b).

Table 3.2(a) : Structural Properties for Bridge # 2

Member Description	Area (m^2)	Torsional Constant I_X ($_m^4$)	Moment of Inertia (m^4)	
			Transverse Bending	Vertical Bending
Girder (steel)	0.696	0.10357	107.88	0.647
Cross beams in Deck (steel)	0.139	0.01295	5.1785	0.0518
Tower leg below Deck level (concrete)	18.58	129.46	215.77	215.77
Tower leg above Deck Level (concrete)	13.00	34.52	86.30	43.15
Upper Tower Struts (concrete)	6.503	1.295	7.767	1.294
Deck Level Strut (concrete)	7.7432	1.726	8.630	1.726
Tower Deck Links (steel) Horizontal Links Vertical Links	 0.2787 0.2787	 8.635e-6 8.635e-6	 8.635e-6 0.05176	 8.635e-6 8.635e-6

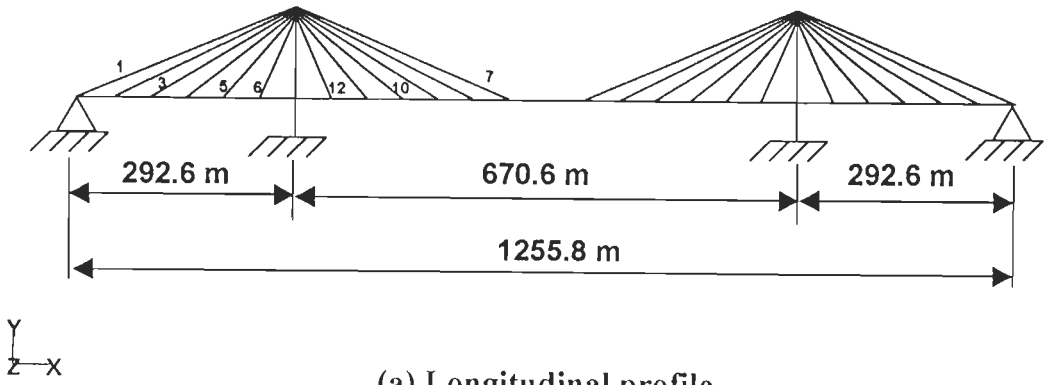

(a) Longitudinal profile

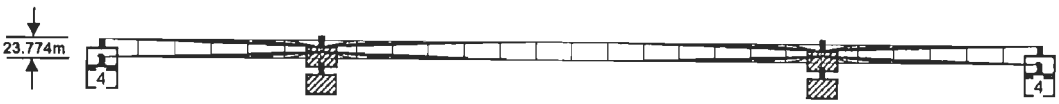

(b) Plan view

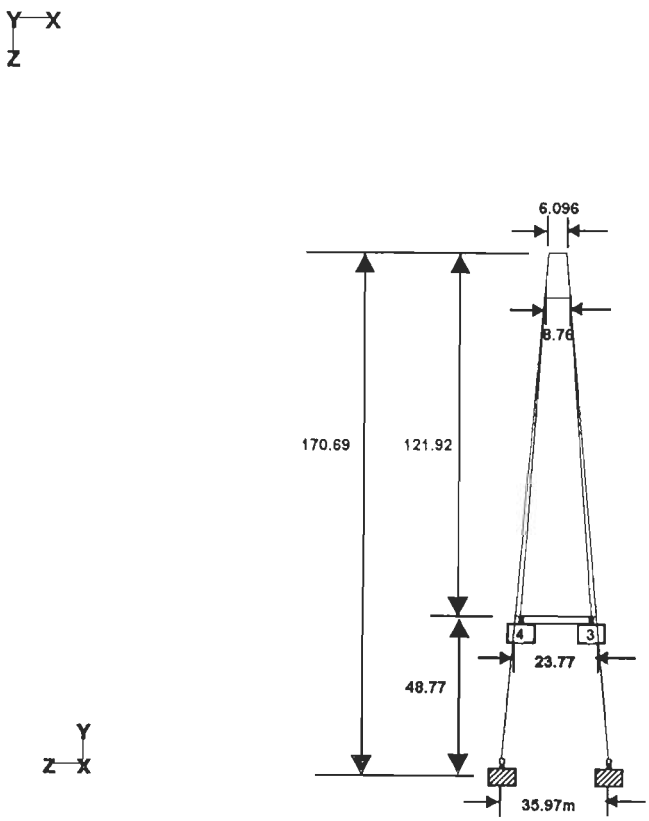

(c) Tower details

Fig. 3.7 : Details of Bridge # 2 with Total Span of 1255.8 m

Table 3.2(b): Details of Cables for Bridge # 2

Cable Group	Cable Numbers	Area (m^2)	Initial Cable Tension (kN)
C1	1,24,25,48	0.0399	19151
C2	2, 11, 14, 23, 26, 35, 38, 47	0.0250	12025
C3	3, 10, 15, 22, 27, 34, 39, 46	0.0220	10911
C4	4, 9, 16, 21, 28, 33, 40, 45	0.0195	9353
C5	5, 8, 17, 20, 29, 32, 41, 44	0.0160	7750
C6	6, 7, 18, 19, 30, 31, 42, 43	0.0123	5923
C7	12, 13, 36, 37	0.0422	20265

Bridge # 3- Luling Bridge

Bridge #3 taken for the present study is the Luling Bridge having a span of 836.6m with four traffic lanes. It is situated on Interstate 310 (formerly, I-410) and spans the Mississippi River between the towns of Luling and Destrehan in Louisiana. The total span of the bridge is divided into five spans consisting of 372.5m long center span between the towers; two anchor spans of 154.8m and 150.9m each and two 79.2m long approach spans. The cables are arranged in a double–plane fan configuration with 12 cables in each plane. Figure 3.8 shows the longitudinal profile, plan view and tower details of the bridge.

The selection of bridge deck cross-section of Luling Bridge was made after conducting a series of wind tunnel studies. The prototype bridge deck cross-section designated by C-1B (Table 3.3(a)) was chosen for the final design of the Luling Bridge because it exhibited efficient static and dynamic behaviour while maintaining flutter stability. The good flutter performance resulted mainly from the smooth wind flow over the tapered railing and welded fascia plate.

The structural properties pertinent to bridge deck, tower and cables of Luling Bridge (Namini, 1989) are given in Table 3.3.

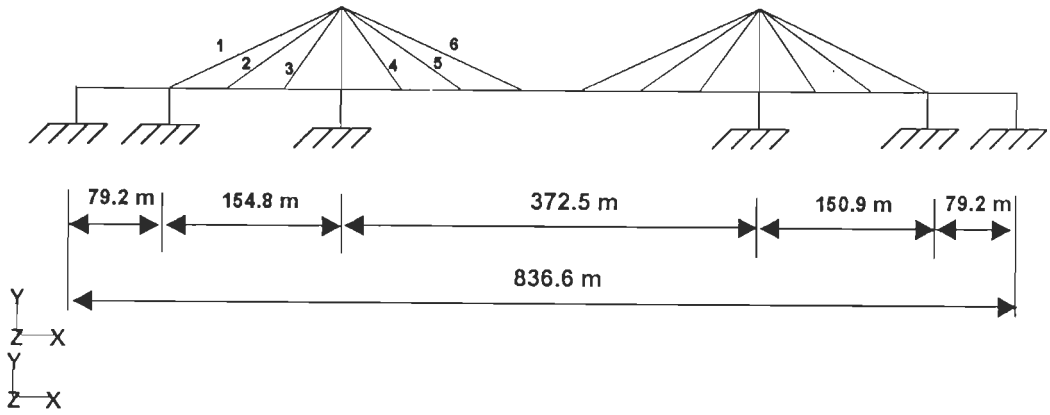

(a) Longitudinal profile

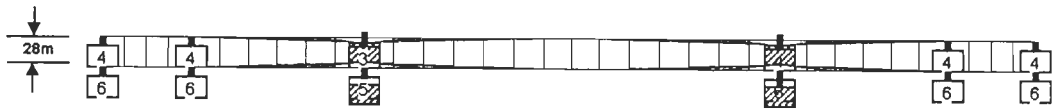

(b) Plan view

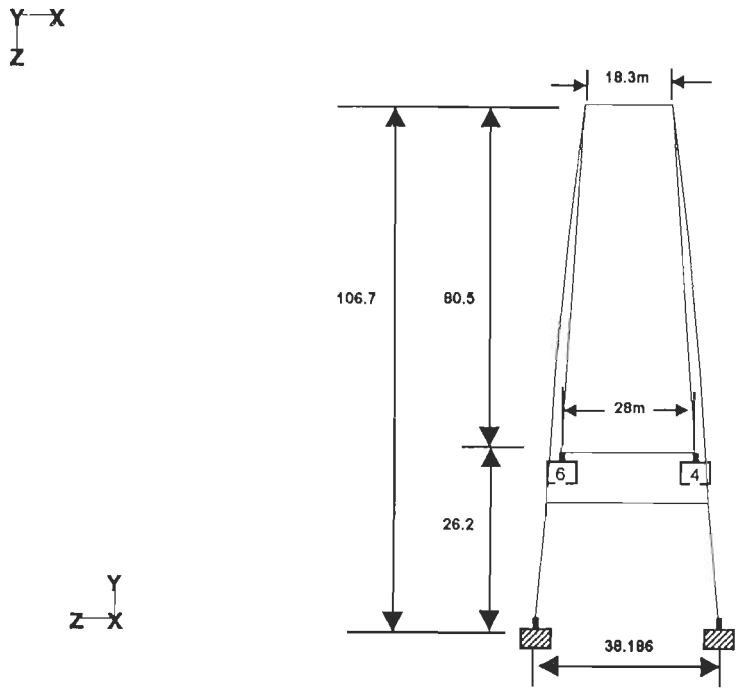

(c) Tower details

Fig. 3.8 : Details of Bridge # 3 with Total Span of 836.6 m

Table 3.3(a) : Structural Properties of Bridge Deck for Bridge #3

Identification	C-1B	C-2	C-2C
Weight (kN/m)	176.90	218.7	234.9
Vertical Distance of Centre of Gravity From Base of Section	2.847	3.343	3.249
Cross –sectional Area (m^2)	1.106	1.279	1.479
Moment of inertia in Vertical Bending (m^4)	3.10	3.48	3.74
Moment of Inertia in Transverse Bending (m^4)	41.94	61.37	61.37
Torsion Constant (m^4)	2.63	3.25	3.25

Table 3.3(b) : Structural Properties of Towers for Bridge #3

Identification	Quantity
Tower base Cross-sectional area(m^2)	1.099
Vertical and Transverse moment of Inertia at Tower Base (m^4)	7.066
Torsion Constant at Tower Base (m^4)	4.504
Tower Top Cross- sectional area (m^2)	0.455
Vertical and Transverse Moment of Inertia (m^4)	1.143
Torsion Constant at Tower Base (m^4)	1.181
Cross-Sectional Area of Lower Strut (m^4)	0.505
Vertical and Transverse moment of Inertia of Lower Strut (m^4)	0.694
Torsion Constant of Lower strut (m^4)	2.462
Cross- sectional Area of Upper strut (m^4)	0.681
Vertical and Transverse Moment of Inertia of Upper Strut (m^4)	2.154
Torsion Constant of Upper Strut (m^4)	7.118

Table 3.3(c) : Details of Cables for Bridge #3

Identification	Area (m^2)
Cables 1 and 12	0.0343
Cables 2 and 11	0.0134
Cables 3 and 10	0.0134
Cables 4 and 9	0.0130
Cables 5 and 8	0.0267
Cables 6 and 7	0.0194

Bridge #4 – Yamuna Bridge

The cable stayed bridge over river Yamuna at Allahabad in Uttar Pradesh, India, is designed with largest bridge span in concrete with four-lane carriageway. The cable stayed module of the project consists of total bridge length of 610m in five spans, with main span of 260m, two anchor spans of 115m each and two approach spans of 60m each and cables stayed from two towers on well foundations in deep channel of the river. The longitudinal profile, plan view and tower details of the bridge are illustrated in Fig. 3.9 (Veje *et al*, 1999). The deck consists of simple prestressed concrete π beam section with low beam depth. The twin leg tower, with a total height of 90m holds the key to the bridge aesthetics. The distance between the centers of tower legs at base is limited by well dimension of 13.0m. At the lower cross beam level at height 27.0m this widens to 30.0m. The distance between the tower leg centers reduces to 18.2m at upper cross-beam level at a height of 75.0m above well top and continues so for another 15.0m The tower legs have a solid hexagonal section 4.0m wide and deep. The tower upper part has a solid rectangular section 2.2m wide and thickness varying from 2.5m to 4.0m. The lower cross beams are 4.0m wide and deep and have a wall thickness of 0.8m.

The stay arrangement consists of locked-coil cables in fan pattern, with total number of 104 cables with their diameters varying from 76mm to 116mm. The structural properties of deck, tower as well as geometric size and stay forces in cables are given in Table 3.4.

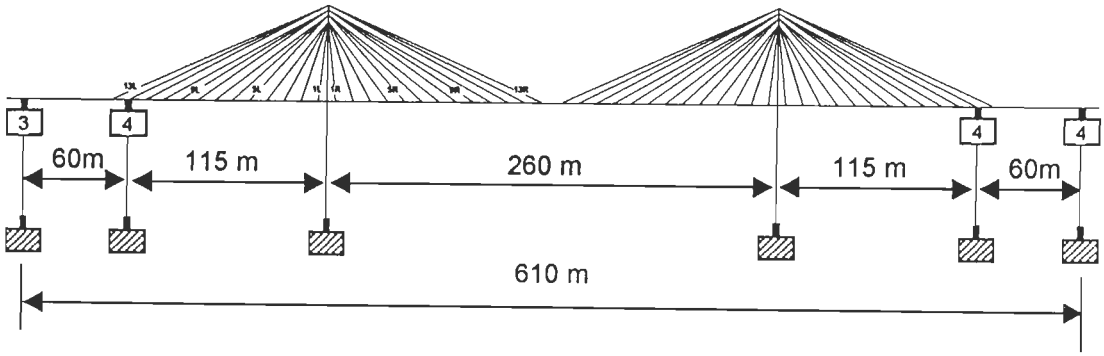

(a) Longitudinal profile

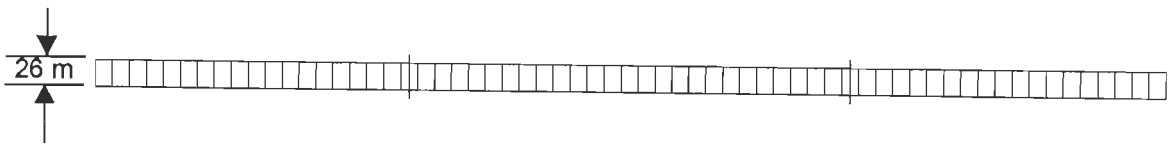

(b) Plan view

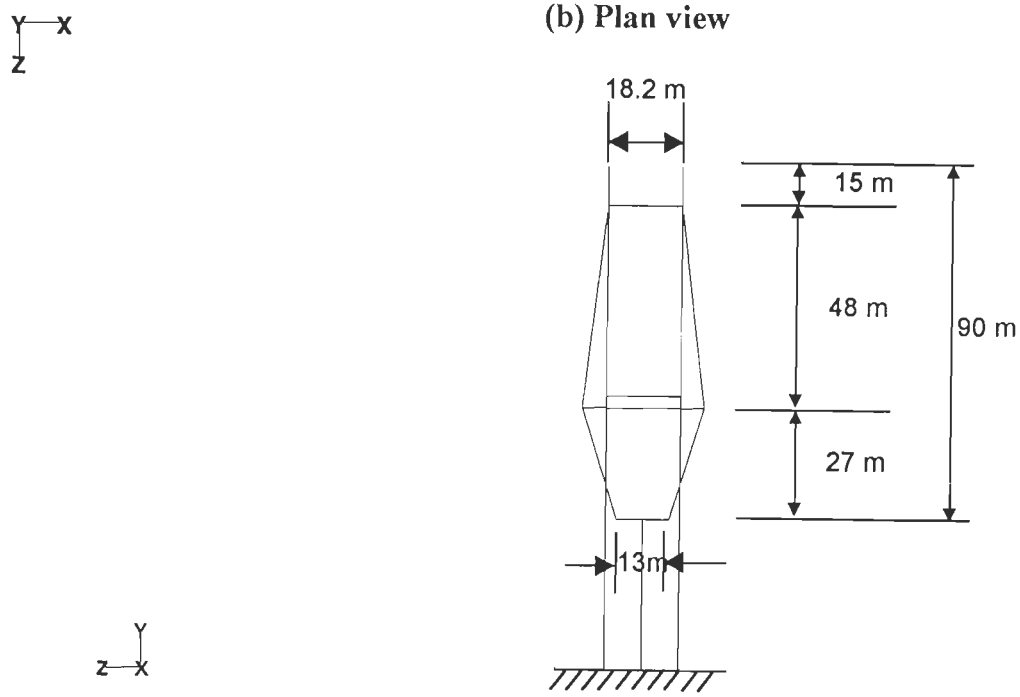

(c) Tower details

Fig. 3.9 : Details of Bridge # 4 with Total Span of 610 m

Table 3.4(a) : Structural Properties of Deck and Towers for Bridge #4

Member Description	Area (m^2)	Torsional Constant I_X (m^4)	Moment of Inertia (m^4)	
			Transverse Bending	Vertical Bending
Girder (concrete) Mainspan and Anchor Span Approach Span	 4.7 7.9	 0.475 2.40	 222.968 489.70	 0.473 7.49
Cross beams in Deck (concrete) Main Span and Anchor Span Approach span	 3.5 9.268	 0.09 3.175	 $1x10^6$ $1x10^6$	 0.45 10.8
Tower leg below Deck level (concrete)	12.63	30.865	17.65	15.21
Tower leg above Deck Level (concrete)	7.15	6.61	6.293	2.887
Upper Tower Struts (concrete)	8.0	7.296	2.667	10.67
Deck Level Strut (concrete)	10.24	27.41	18.57	18.57

Table 3.4(b) : Details of Cables for Bridge #4

Cable Stay	Diameter (mm)	Cable Forces (kN)
1	76	1890
2	76	1837
3	78	1971
4	81	2153
5	85	2370
6	89	2630
7	92	2882
8	96	3141
9	100	3405
10	103	3669
11	107	3935
12	110	4164
13	113	4427

3.6.2 Modelling of Bridges

Three Span Bridges

For three span bridges, Bridge #1 and Bridge #2 analyses have been performed to study the effect of support types for bridge deck on static and vibration characteristics of bridges. In this study, the following support types for bridge deck (as shown in Fig. 2.1) are included :

(a) Deck fixed at tower piers, on rollers at girder ends (DST-1)

(b) Deck fixed at one tower pier, on rollers at other supports (DST-2)

(c) Deck fixed at one end of girder, on rollers at other supports (DST-3)

(d) Deck movable on all supports (DST-4)

(e) Floating deck (DST-5)

(f) Deck elastically connected at towers through links (DST-6)

These bridges are modelled with 48 cable elements, 42 tower elements and 79 deck elements, i.e., with a total of 169 elements as in Fig. 3.10 for deck supports DST-1 to DST-5. With elastic supports (DST-6) for deck at towers, the elastic links are also appropriately included in the modelling and the total number of elements becomes 185.

The tower consisted of main tower leg elements as well as upper strut elements and deck level strut element. The deck consisted of box girder, diaphragm and cross beam elements. The deck is modelled with two longitudinal rows of beam elements, with one row per box girder. Each cable corresponds to one element.

Five Span Bridges

The Bridge #3 is modelled with 103 deck elements, 20 tower elements and 24 cable elements with a total of 147 elements as in Fig. 3.11 The bridge deck is idealized as two longitudinal trapezoidal girders connected with cross beam members. The tower consisted of main vertical leg members along with lower and upper strut members. In this study, the bridge deck is assumed to be fixed at one tower and on rollers at all other supports.

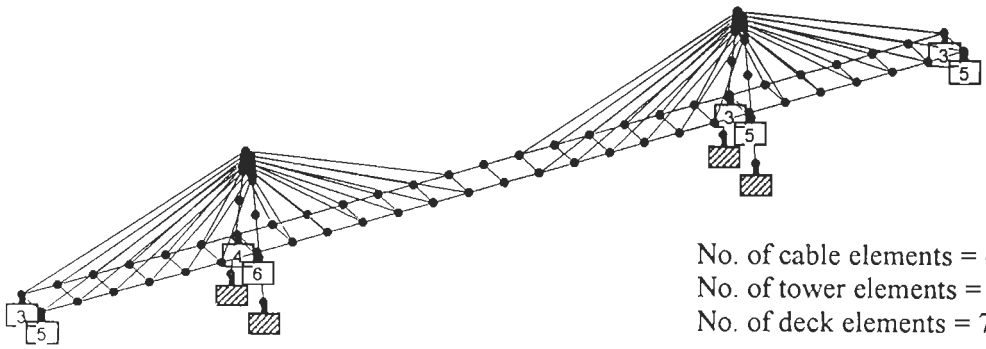

Fig. 3.10 : Three-Dimensional Modelling of Bridge # 1 and Bridge #2

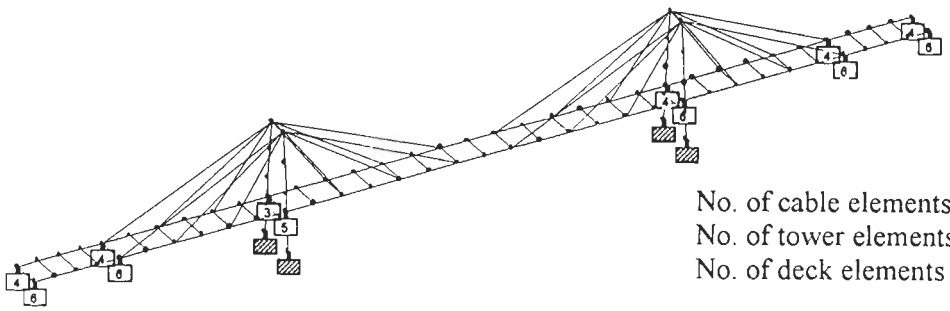

Fig. 3.11 : Three-Dimensional Modelling of Bridge # 3

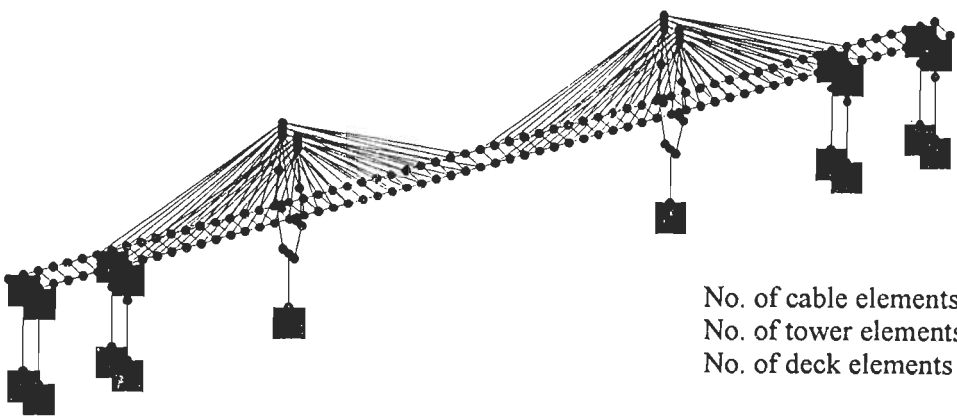

Fig. 3.12 : Three-Dimensional Modelling of Bridge # 4

The modelling of Bridge #4 as shown in Fig. 3.12 consists of 196 deck elements, 60 elements for towers and piers and 104 cable elements with a total of 360 elements. The bridge deck is idealized as two longitudinal rectangular solid girders connected with cross beam members. The H-shaped tower consisted of main vertical leg members along with lower and upper strut members. In this study, the deck is assumed to be fixed at one end and on rollers at all other supports.

3.6.3 Nonlinear Static Analysis

To validate the nonlinear static analysis, an example of five span bridge – Bridge #3 has been chosen. For Bridge #3, the nonlinear static response under dead load and initial cable tensions obtained in the present study are in good agreement with the results reported earlier by Namini (1989) as shown in Table 3.5. The closeness of the results validate the formulations for nonlinear static analysis presented in Section 3.3. The deck axial force, vertical shear and bending moment diagrams under dead loads are shown in Fig. 3.13.

Table 3.5 : Comparison of Nonlinear Static Response for Bridge # 3

Description	Present Study	Namini (1989)
Mid Span Vertical Deflection (m)	0.541	0.571
Tower Tip Longitudinal Deflection (m)	0.1091	0.1001
Axial Force in Deck at Tower-Deck Junction (kN)	21924	21770
Vertical Shear Force in Deck at Tower-Deck Junction (kN)	3060	3068
Cable-1 Axial Force (kN)	14840	14360
Cable-2 Axial Force (kN)	6440	6569
Cable-5 Axial Force (kN)	12670	12581

The summary of results of nonlinear static analysis for the other five span bridge, Bridge #4 is given in Table 3.6.

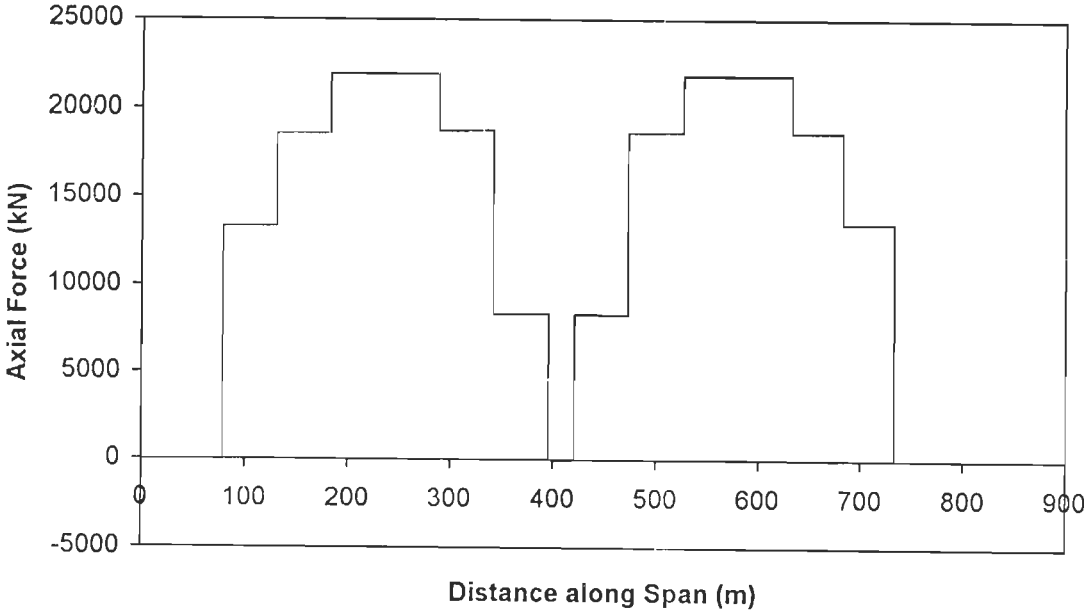

(a) Deck axial force diagram

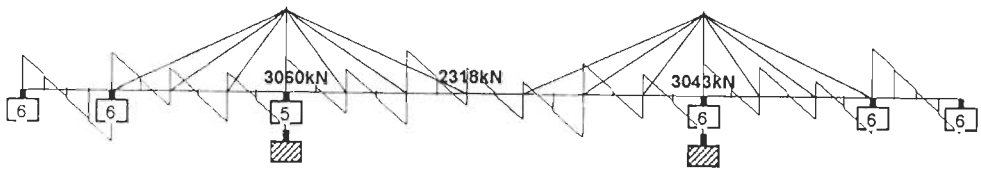

(b) Deck vertical shear force diagram

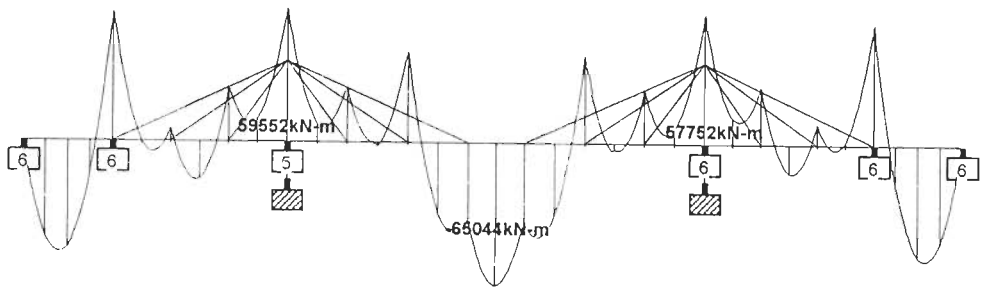

(c) Deck bending moment diagram

Fig. 3.13 : Nonlinear Static Analysis of Bridge # 3 under Dead Load and Initial Cable Tensions

Table 3.6 : Nonlinear Static Response for Bridge # 4

Description	Present Study
Mid Span Vertical Deflection (m)	0.2016
Tower Tip Longitudinal Deflection (m)	0.0623
Axial Force in Deck at Tower-Deck Junction (kN)	20106
Vertical Shear Force in Deck at Tower-Deck Junction (kN)	652
Cable-1 Axial Force (kN)	3780
Cable-2 Axial Force (kN)	3308
Cable-5 Axial Force (kN)	2561

The nonlinear static analysis for the three span bridges under dead load and initial cable tensions has been performed for six types of deck support conditions as mentioned in Section 3.6.2. Table 3.7 and Table 3.8 summarize the selected results of the static analysis for Bridge #1 and Bridge # 2 respectively. The responses of bridge deck under dead loads and initial cable tensions are shown in Fig. 3.14 for deck supports DST-1 to DST-6. The variation in axial force, shear force and bending moments in the deck due to dead loads calculated in the present study is shown in Figs 3.15 and 3.16 for Bridge #1 and Bridge#2 respectively.

From the results of three span cable stayed bridges, Bridge #1 and Bridge #2, it is clear that the deformation of a typical three span bridge under dead load and initial cable tensions depends on the support type for bridge deck at towers and abutments. The deck deflection is lowest when the deck is fixed at towers (DST-1) and maximum when the deck is floating (DST-5). By suitable design of elastic supports the deck deflection can be controlled.

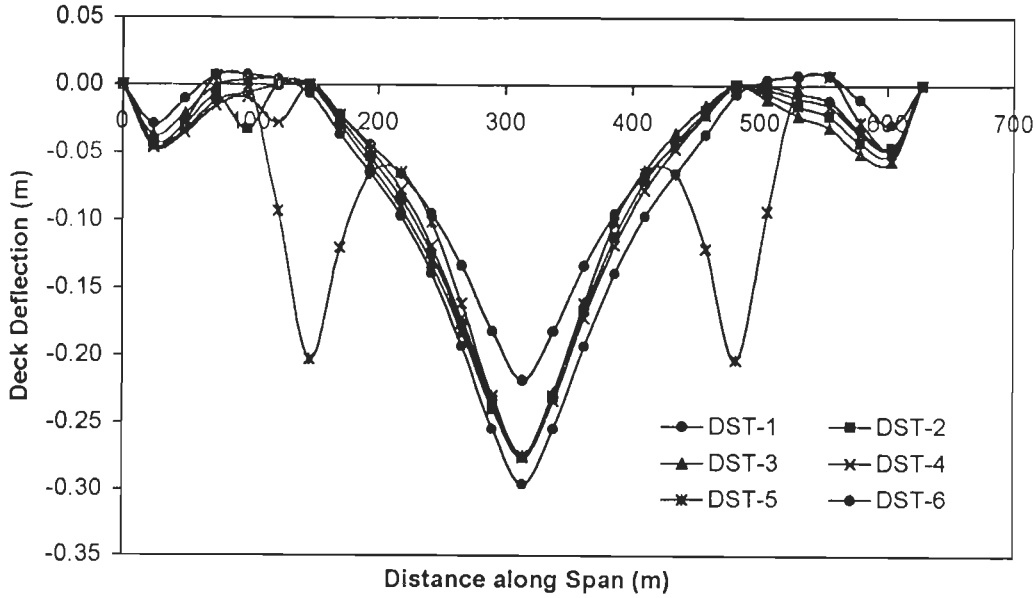

(a) Bridge # 1

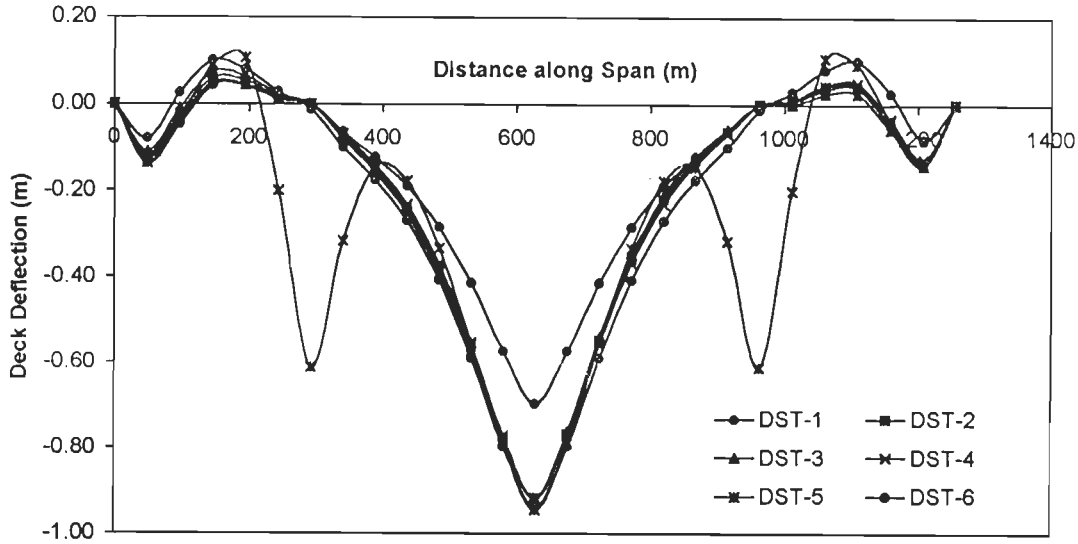

(b) Bridge # 2

DST-1 : Deck fixed at towers, on rollers at other supports
DST-2 : Deck fixed at one tower, on rollers at other supports
DST-3 : Deck fixed at one end, on rollers at other supports
DST-4 : Deck movable at all supports
DST-5 : Floating deck
DST-6 : Deck elastically supported at towers, on rollers at other supports

Fig. 3.14 : Nonlinear Static Response (Deck Deflection) of Three Span Bridges under Dead Load – Variation with Types of Deck Support

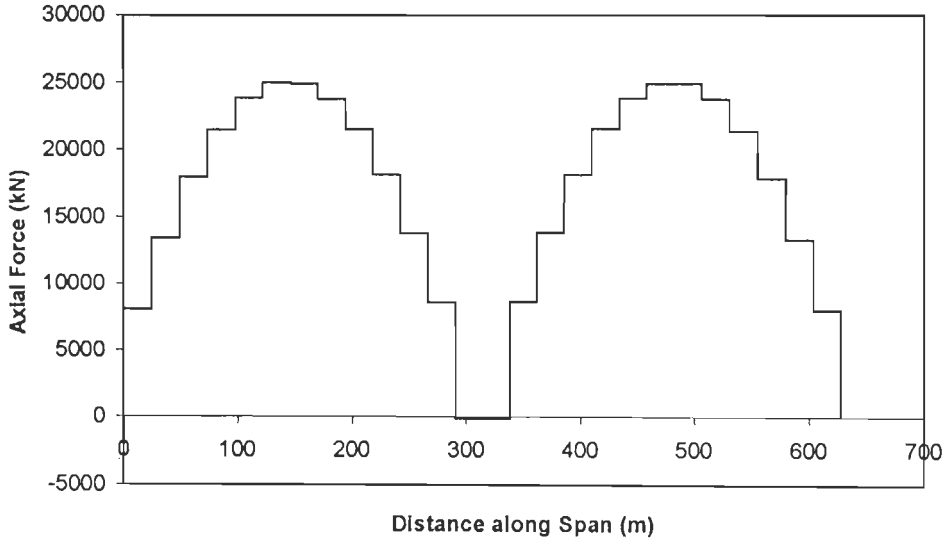

(a) Deck axial force diagram

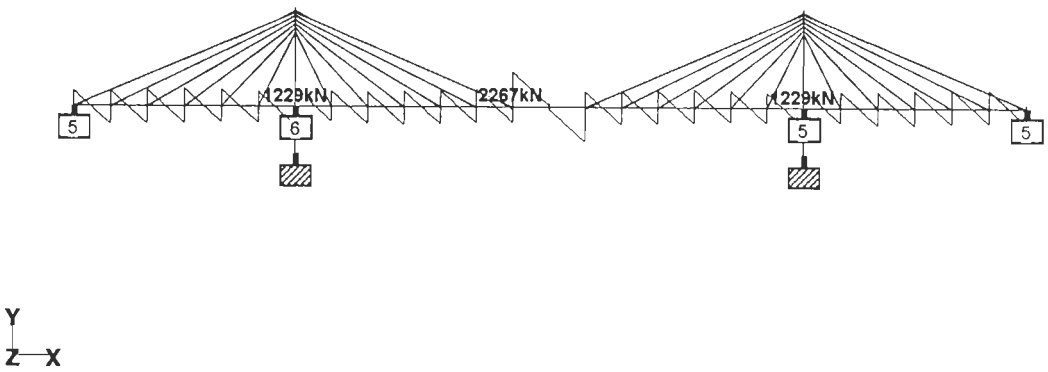

(b) Deck vertical shear force diagram

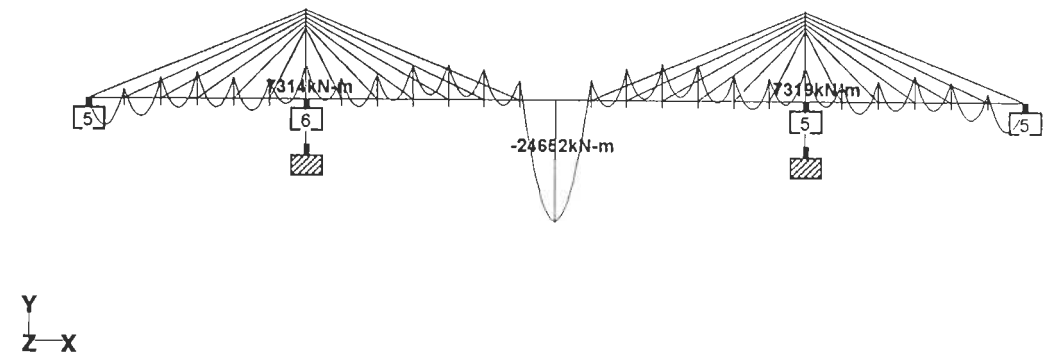

(c) Deck bending moment diagram

Fig. 3.15 : Nonlinear Static Analysis of Bridge # 1 under Dead Load and Initial Cable Tensions

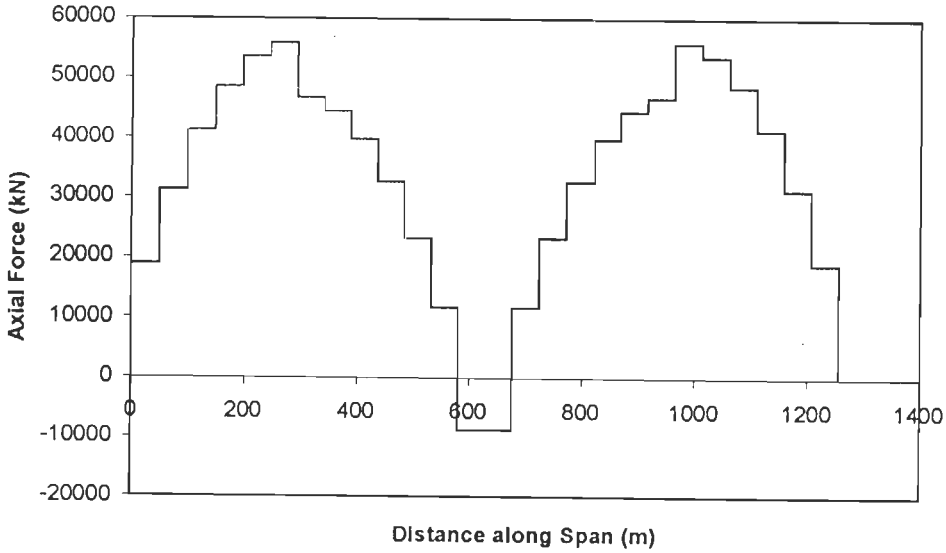

(a) Deck axial force diagram

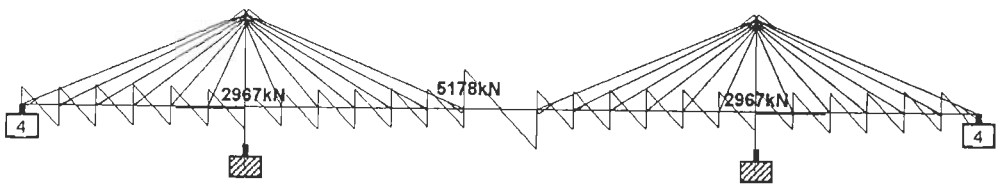

(b) Deck vertical shear force diagram

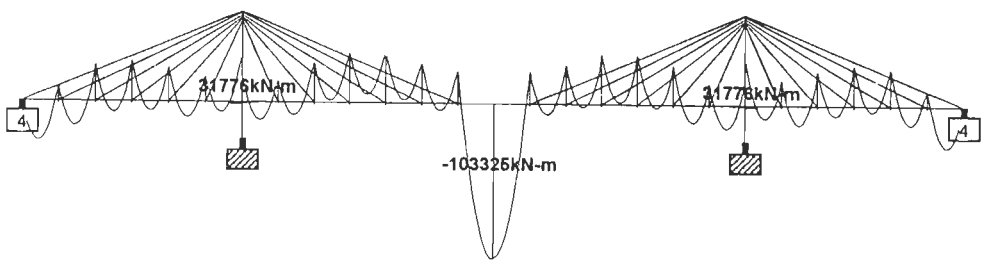

(c) Deck bending moment diagram

Fig. 3.16 : Nonlinear Static Analysis of Bridge # 2 under Dead Load and Initial Cable Tensions

Table 3.7 : Nonlinear Static Response for Bridge # 1 with Different Support Types for Bridge Deck

DESCRIPTIONS	SUPPORT TYPES FOR BRIDGE DECK					
	DST-1	DST-2	DST-3	DST-4	DST-5	DST-6
Mid-span Vertical Deflection (m)	0.2177	0.2755	0.2751	0.2757	0.2739	0.2957
Maximum side span (Left) Vertical Deflection (m)	0.03285	0.02871	0.02707	0.03542	0.02645	0.01055
Maximum side span (Right) Vertical Deflection (m)	0.03285	0.04212	0.05004	0.03542	0.02645	0.01055
Tower Tip Longitudinal Deflection (m) (Left Tower)	0.03855	0.04111	0.01478	0.0634	0.06507	0.07204
Tower Tip Longitudinal Deflection (m)(Right Tower)	0.03855	0.08554	0.1114	0.06340	0.06507	0.07204
Axial Force in Deck at Tower-Deck Junction (kN)	24965	25016	24834	24967	25328	25217
Vertical Shear Force in Deck at Tower-Deck Junction (kN)	1222	1229	1229	1228	73.74	1223
Bending Moment in Deck at Tower-Deck Junction (kN-m)	7197	7344	7312	7371	20263	7174
Axial Force in Cables (kN)						
Cable-1	8802	8853	8895	8819	8826	9059
Cable-2	5958	5971	5983	5961	5959	6026
Cable-3	5245	5244	5241	5245	5172	5237
Cable-4	4408	4404	4397	4409	4161	4379
Cable-5	3428	3425	3421	3429	3261	3406
Cable-6	2632	2625	2627	2623	4289	2645
Cable-7	9557	9567	9557	9576	9493	9563

Table 3.8 : Nonlinear Static Response for Bridge # 2 with Different Support Types for Bridge Deck

DESCRIPTIONS	SUPPORT TYPES FOR BRIDGE DECK					
	DST-1	DST-2	DST-3	DST-4	DST-5	DST-6
Mid-span Vertical Deflection (m)	0.6951	0.9182	0.9174	0.9186	0.9441	0.9389
Maximum Side Span (Left) Vertical Deflection (m)	0.1373	0.1179	0.1089	0.1253	0.1367	0.1003
Maximum Side Span (Right) Deflection(m) (Right)	0.1373	0.1329	0.1416	0.1253	0.1367	0.1003
Tower Tip Longitudinal Deflection (m)(Left)	0.1313	0.1456	0.0636	0.2163	0.1658	0.2288
Tower Tip Longitudinal Deflection (m)(Right)	0.1313	0.0736	0.3679	0.2163	0.1658	0.2288
Axial Force in Deck at Tower- Deck Junction (kN)	55080	55354	55124	55296	55820	55839
Vertical Shear Force in Deck at Tower-Deck Junction (kN)	2934	2950	2953	2948	1017	2967
Bending Moment in Deck at Tower-Deck Junction (kN-m)	31105	31529	31458	31601	98105	31775
Axial Force in Cables (kN)						
Cable-1	20001	20281	20349	20226	20204	20801
Cable-2	13637	13696	13710	13682	13749	13807
Cable-3	12002	11981	11974	11986	11996	11942
Cable-4	9469	9445	9436	9455	8910	9393
Cable-5	7594	7590	7584	7597	6545	7556
Cable-6	5788	5780	5781	5779	9761	5787
Cable-7	22406	22615	22600	22630	22620	22530

To conclude this section on the nonlinear static analysis, it is evident that the response of the cable stayed bridges under dead loads and initial cable tensions have been accurately modelled in the present study.

3.6.4 Frequencies and Mode Shapes

The free vibration analysis is performed for the deformed configuration of bridge under dead loads and initial cable tensions and the frequencies and mode shapes for the first thirty modes are determined. Comparison of frequency values obtained in the present study with that reported by Abdel Ghaffar and Khalifa (1991) as shown in Fig. 3.17 for Bridge #1 and Bridge#2 which indicates good agreement of results.

The frequencies of the twenty-five modes with vibration pattern are given for different support types for bridge deck at towers and abutments are shown in Tables 3.9 and 3.10 for Bridge #1 and Bridge#2 respectively. The variation in frequencies of first 30 modes for these three span cable stayed bridges with different deck supports are illustrated in Fig.3.18. The results indicate that the type of vibration mode which gets excited depends on the support type for bridge deck at towers and abutments.

On the basis of total span of the bridge, the support type DST-2 for Bridge #1 and DST-6 for Bridge #2 have been chosen for parametric studies on buffeting analysis in Chapter 6. Hence, for this deck support type the mode shapes corresponding to the first 12 modes of vibration are illustrated in Figs. 3.19 for Bridge #1 and in Fig. 3.20 for Bridge#2.

From the results on vibration characteristics of three span cable stayed bridges, it is observed that the vibration pattern, and hence the expected response to dynamic loads is dependent on the support type for bridge deck at towers and abutments. Effect of support type becomes more prominent with increase in span length of the bridge. With long span bridges, the tower becomes flexible and the lateral motion of tower in both symmetric and asymmetric oscillations is found to be significant in Bridge #2, 3 and 4.

Comparison of frequencies of Bridge#3, with three different cross-sectional properties of deck C-1B, C-2 and C-2C, given in Table 3.3(a) are shown in Fig. 3.21.

For five span bridges, the pattern of first twelve modes of vibration for Bridge#3 is shown in Fig. 3.22 and for Bridge#4 in Fig. 3.23.

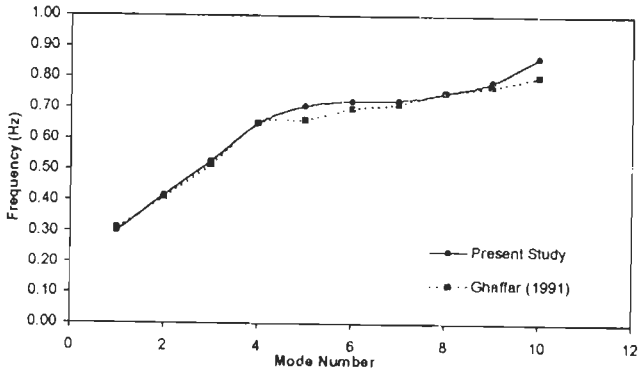

(a) Bridge # 1

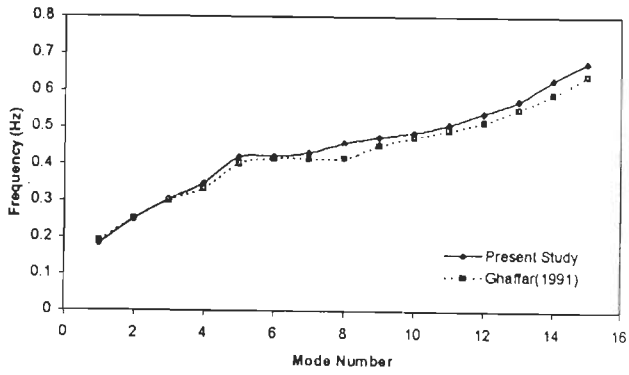

(b) Bridge # 2

Fig. 3.17 : Comparison of Frequencies of Three Span Bridges

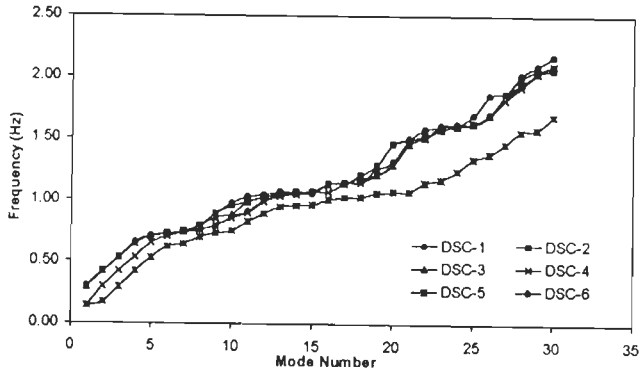

(a) Bridge # 1

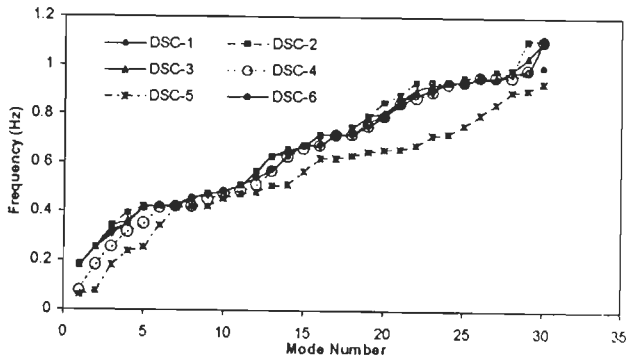

(b) Bridge # 2

DST-1 : Deck fixed at towers, on rollers at other supports
DST-2 : Deck fixed at one tower, on rollers at other supports
DST-3 : Deck fixed at one end, on rollers at other supports
DST-4 : Deck movable at all supports
DST-5 : Floating deck
DST-6 : Deck elastically supported at towers, on rollers at other supports

Fig. 3.18 : Effect of Support Types for Bridge Deck on Frequencies of Three Span Cable Stayed Bridges

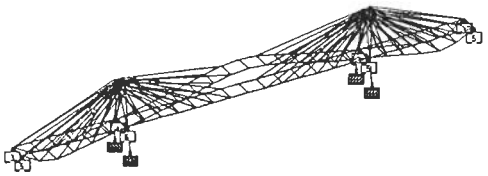

(a) Mode # 1 Frequency = 0.291 Hz

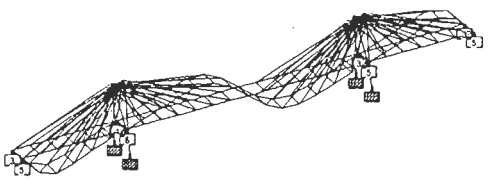

(b) Mode # 2 Frequency = 0.415 Hz

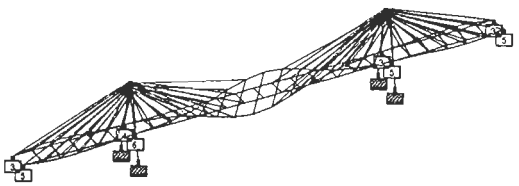

(c) Mode # 3 Frequency = 0.525 Hz

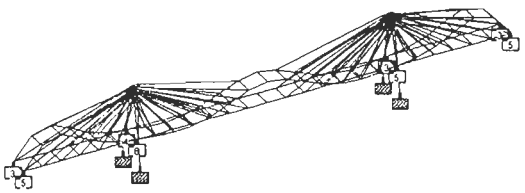

(d) Mode # 4 Frequency = 0.640 Hz

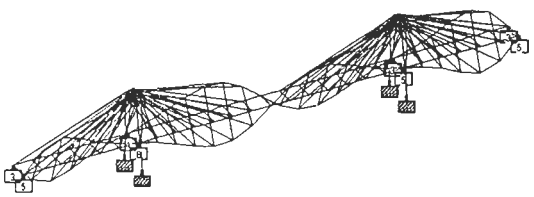

(e) Mode # 5 Frequency = 0.692 Hz

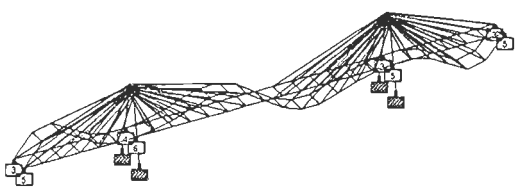

(f) Mode # 6 Frequency = 0.727 Hz

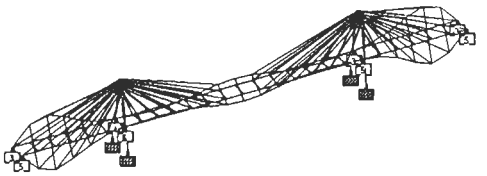

(g) Mode # 7 Frequency = 0.746 Hz

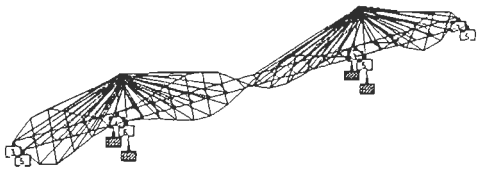

(h) Mode # 8 Frequency = 0.790 Hz

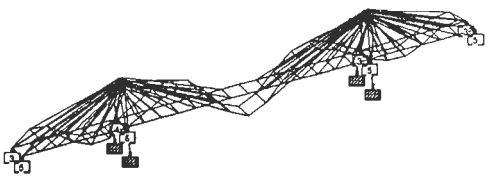

(i) Mode # 9 Frequency = 0.890 Hz

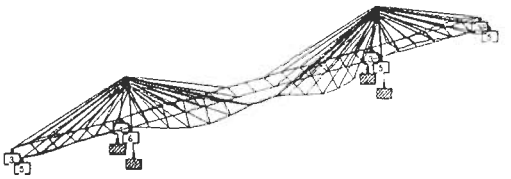

(j) Mode # 10 Frequency = 0.952 Hz

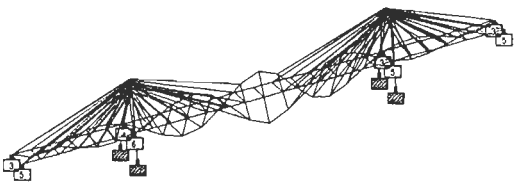

(k) Mode # 10 Frequency = 0.988 Hz

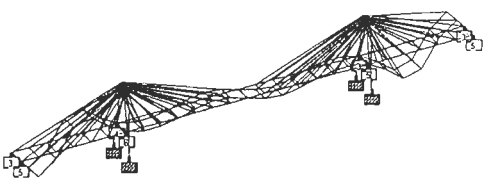

(l) Mode # 12 Frequency = 1.027 Hz

Fig. 3.19 : Vibration Modes for Bridge # 1 with Type of Deck Support DST-2 (DST-2 : Deck fixed at one tower, on rollers at other supports)

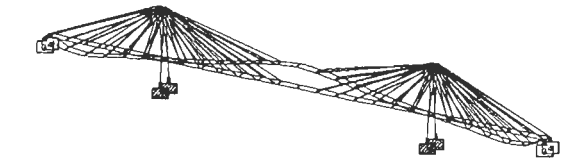

(a) Mode # 1 Frequency = 0.183 Hz

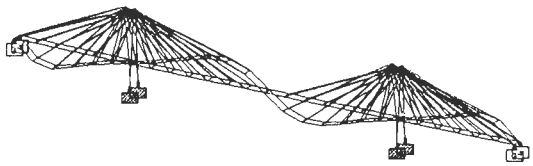

(b) Mode # 2 Frequency = 0.251 Hz

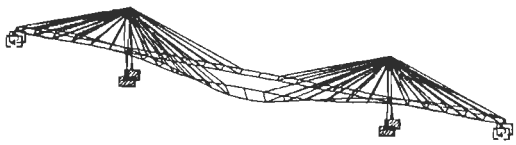

(c) Mode # 3 Frequency = 0.303 Hz

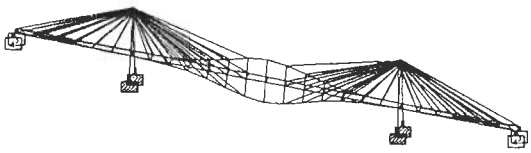

(d) Mode # 4 Frequency = 0.349 Hz

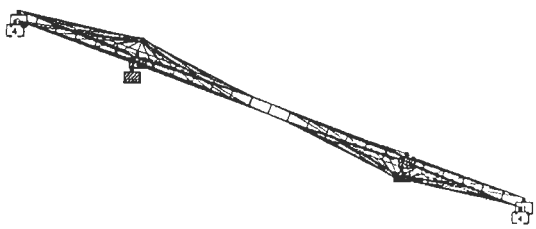

(e) Mode # 5 (Plan view) Frequency = 0.420 Hz

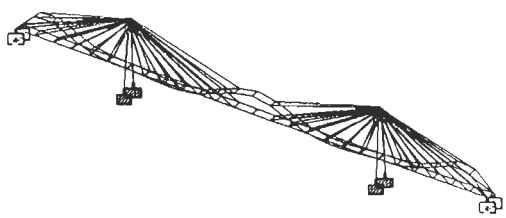

(f) Mode # 6 Frequency = 0.422 Hz

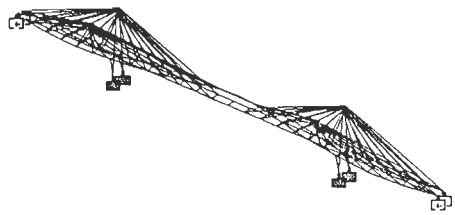

(g) Mode # 7 Frequency = 0.432 Hz

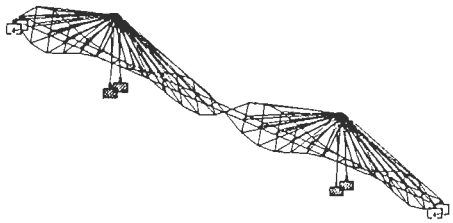

(h) Mode # 8 Frequency = 0.458 Hz

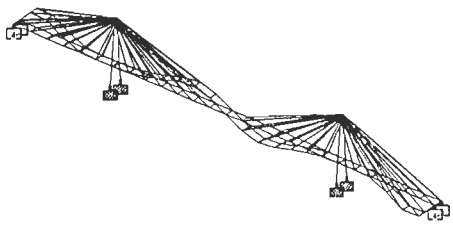

(i) Mode # 9 Frequency = 0.474 Hz

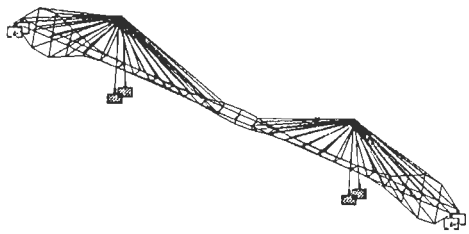

(j) Mode # 10 Frequency = 0.487 Hz

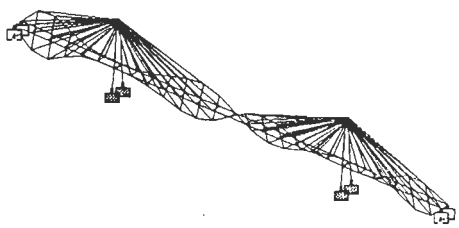

(k) Mode # 10 Frequency = 0.509 Hz

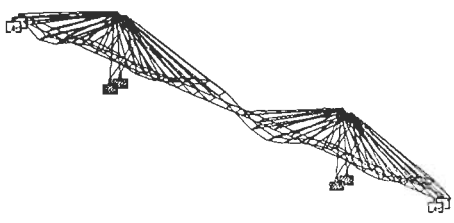

(l) Mode # 12 Frequency = 0.539 Hz

Fig. 3.20 : Vibration Modes for Bridge # 2 with Type of Deck Support DST-6
(DST-6 : Deck elastically supported at towers, on rollers at other supports)

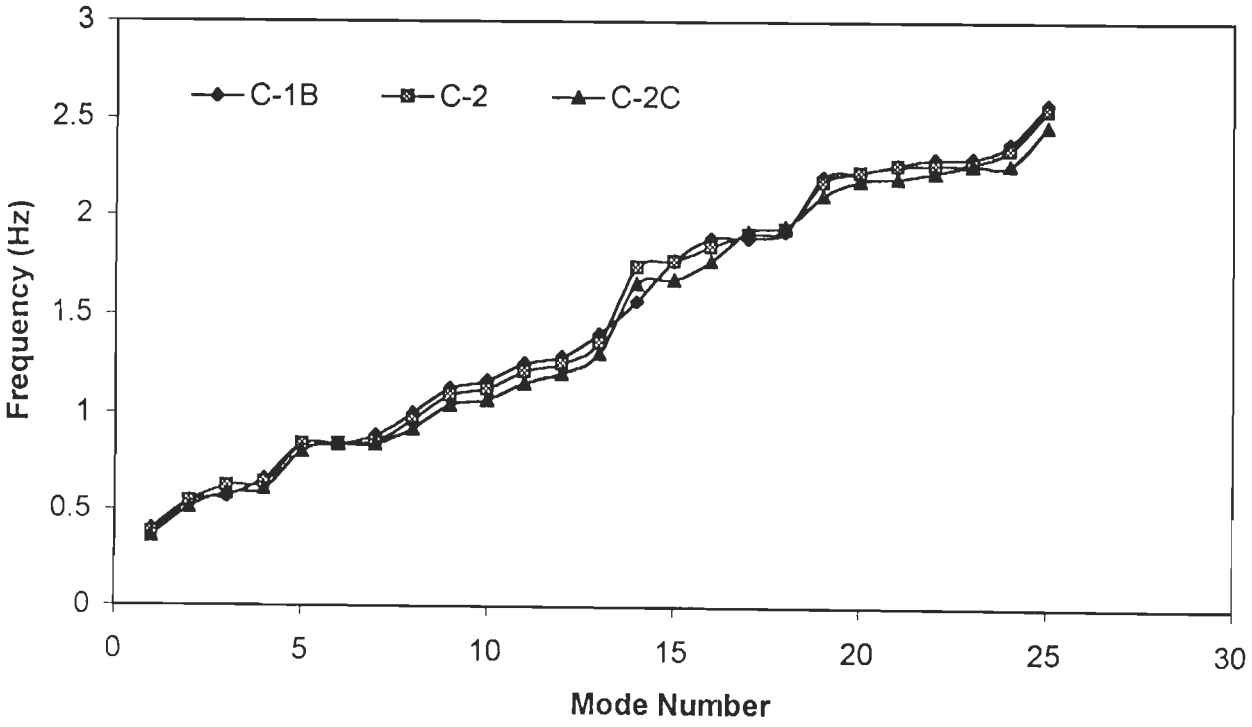

Fig. 3.21 : Comparison of Frequencies of Bridge # 3 with Three Types of Bridge Deck Cross-Sections

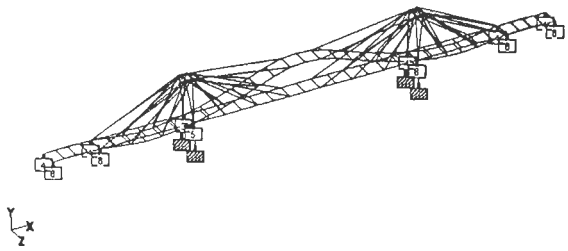

(a) Mode # 1 Frequency = 0.398 Hz

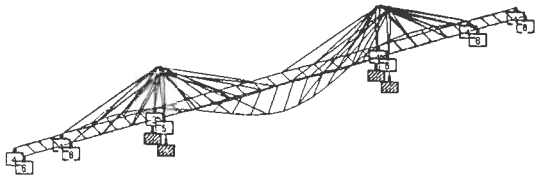

(b) Mode # 2 Frequency = 0.547 Hz

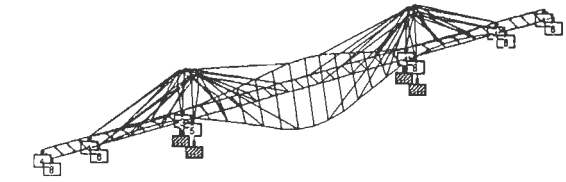

(c) Mode # 3 Frequency = 0.570 Hz

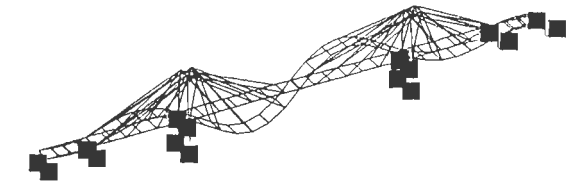

(d) Mode # 4 Frequency = 0.667 Hz

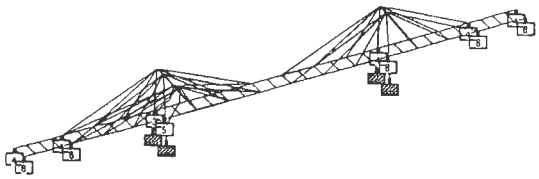

(e) Mode # 5 Frequency = 0.841 Hz

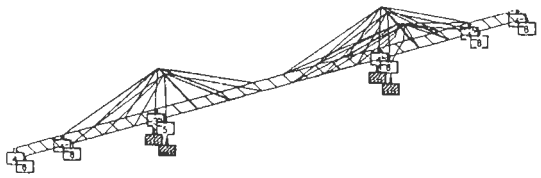

(f) Mode # 6 Frequency = 0.842 Hz

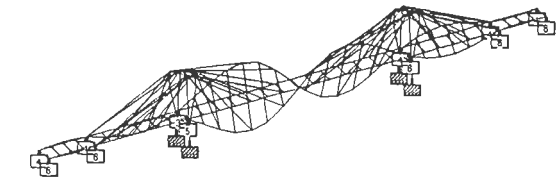

(g) Mode # 7 Frequency = 0.887 Hz

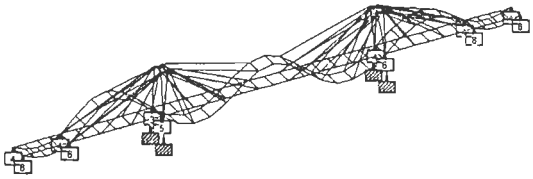

(h) Mode # 8 Frequency = 0.998 Hz

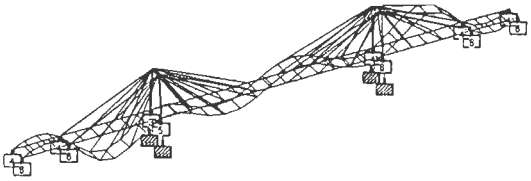

(i) Mode # 9 Frequency = 1.125 Hz

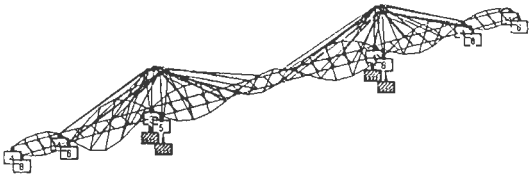

(j) Mode # 10 Frequency = 1.165 Hz

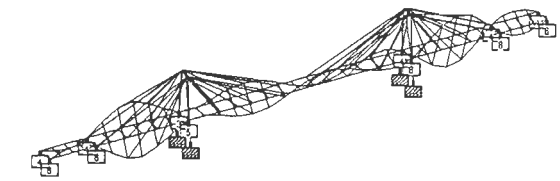

(k) Mode # 10 Frequency = 1.252 Hz

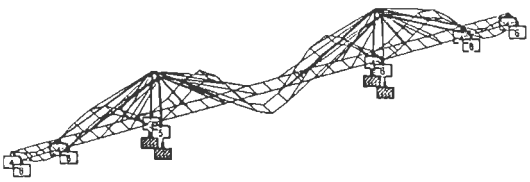

(l) Mode # 12 Frequency = 1.287 Hz

Fig. 3.22 : Vibration Modes for Bridge # 3

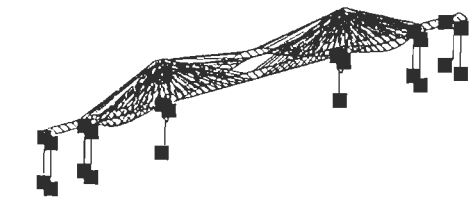

(a) Mode # 1 Frequency = 0.402 Hz

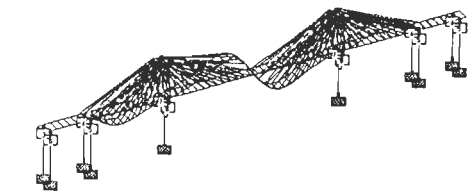

(b) Mode # 2 Frequency = 0.517 Hz

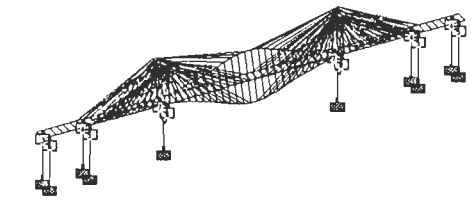

(c) Mode # 3 Frequency = 0.521 Hz

(d) Mode # 4 (Plan view) Frequency = 0.565 Hz

(e) Mode # 5 (Plan view) Frequency = 0.566 Hz

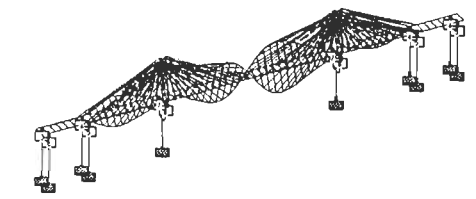

(f) Mode # 6 Frequency = 0.585 Hz

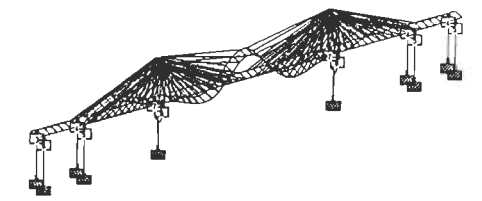

(g) Mode # 7 Frequency = 0.717 Hz

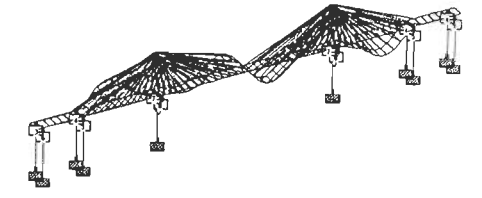

(h) Mode # 8 Frequency = 0.819 Hz

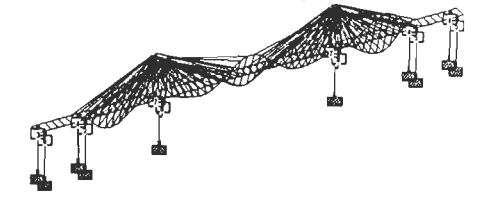

(i) Mode # 9 Frequency = 0.916 Hz

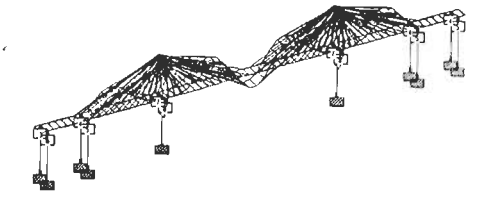

(j) Mode # 10 Frequency = 0.974 Hz

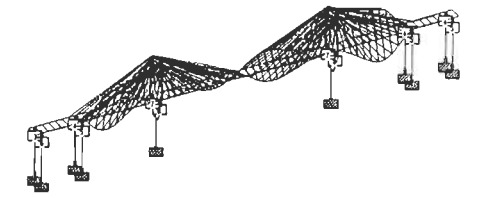

(k) Mode # 10 Frequency = 0.983 Hz

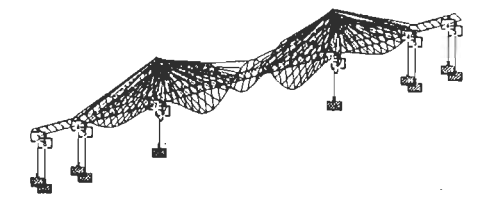

(l) Mode # 12 Frequency = 1.022 Hz

Fig. 3.23 : Vibration Modes for Bridge # 4

Table 3.9: Vibration Characteristics of Bridge # 1 with Different Support Types for Bridge Deck

Mode No.	DST-1		DST-2		DST-3		DST-4		DST-5		DST-6	
	Freq. (Hz)	Mode Type	Freq. (Hz)	Mode Type	Freq. (Hz)	Mode Type	Freq. (Hz)	Mode Type	Freq. (Hz)	Mode Type	Freq. (Hz)	Mode Type
1	0.292	V-S1	0.291	V-S1	0.291	V-S1	0.139	LONG	0.139	LONG	0.301	V-S1
2	0.415	VAS1	0.415	VAS1	0.414	VAS1	0.295	V-S1	0.173	L-S1	0.417	VAS1
3	0.525	T-S1	0.525	T-S1	0.524	T-S1	0.421	VAS1	0.291	V-S1	0.527	T-S1
4	0.647	V-S2	0.640	V-S2	0.639	V-S2	0.530	T-S1	0.417	VAS1	0.651	V-S2
5	0.692	TAS1	0.692	TAS1	0.692	TAS1	0.647	V-S2	0.527	T-S1	0.707	TAS1
6	0.727	VAS2	0.727	VAS2	0.726	VAS2	0.695	TAS1	0.618	LAS1	0.725	L-S1
7	0.746	T-S2	0.746	T-S2	0.747	T-S2	0.732	VAS2	0.640	V-S2	0.727	VAS2
8	0.790	TAS2	0.790	TAS2	0.790	TAS2	0.751	T-S2	0.693	TAS1	0.751	T-S2
9	0.890	V-S3	0.890	V-S3	0.855	L-S1	0.795	TAS2	0.727	VAS2	0.787	TAS2
10	0.979	T-S3	0.952	L-S1	0.889	V-S3	0.848	L-S1	0.748	T-S2	0.864	LONG
11	1.027	VAS3	0.988	T-S3	0.982	T-S3	0.895	V-S3	0.823	TAS2	0.910	V-S3
12	1.047	V-S4	1.027	VAS3	1.027	VAS3	0.986	T-S3	0.889	V-S3	0.996	T-S3
13	1.071	TOW	1.046	V-S4	1.046	V-S4	1.031	VAS3	0.947	T-S3	1.037	TOW
14	1.071	TOW	1.071	TOW	1.071	TOW	1.050	V-S4	0.959	VAS3	1.050	V-S4
15	1.078	LS1	1.071	TOW	1.071	TOW	1.071	TOW	0.965	V-S4	1.054	VAS3
16	1.135	TAS3	1.134	TAS3	1.134	TAS4	1.071	TOW	1.008	TAS3	1.139	TOW
17	1.143	T-S4	1.142	T-S4	1.142	T-S4	1.137	TAS3	1.026	T-S4	1.143	TAS3
18	1.208	VAS4	1.208	VAS4	1.182	LONG	1.145	T-S4	1.028	VAS4	1.153	T-S4
19	1.288	TAS4	1.288	TAS4	1.209	VAS4	1.211	VAS4	1.059	V-S5	1.256	VAS4
20	1.458	V-S5	1.457	V-S5	1.287	TAS5	1.290	TAS4	1.071	TOW	1.314	TAS4
21	1.504	VAS5	1.490	VAS5	1.458	V-S5	1.460	V-S5	1.071	TOW	1.490	V-S5
22	1.579	T-S5	1.529	VAS6	1.507	VAS5	1.508	VAS5	1.143	TAS4	1.516	VAS5
23	1.603	V-S6	1.578	T-S5	1.578	T-S5	1.580	T-S5	1.171	T-S5	1.611	T-S5
24	1.623	TAS5	1.604	V-S6	1.603	V-S6	1.604	V-S6	1.238	VAS5	1.621	V-S6
25	1.690	T-S6	1.622	TAS5	1.622	TAS6	1.624	TAS5	1.338	TAS5	1.628	TAS5

LONG – longitudinal; L – lateral; V – vertical bending; T – torsional; TOW– tower vibration; S – symmetric; AS - asymmetric

Table 3.10 : Vibration Characteristics of Bridge # 2 with Different Support Types for Bridge Deck

Mode No.	DST-1		DST-2		DST-3		DST-4		DST-5		DST-6	
	Freq. (Hz)	Mode Type	Freq. (Hz)	Mode Type	Freq. (Hz)	Mode Type	Freq. (Hz)	Mode Type	Freq. (Hz)	Mode Type	Freq. (Hz)	Mode Type
1	0.182	V-S1	0.181	V-S1	0.181	V-S1	0.077	LONG	0.061	L-S1	0.183	V-S1
2	0.253	VAS1	0.253	VAS1	0.253	VAS1	0.181	V-S1	0.077	LONG	0.251	VAS1
3	0.341	T-S1	0.335	T-S1	0.319	L-S1	0.253	VAS1	0.181	V-S1	0.303	L-S1
4	0.394	L-S1	0.363	L-S1	0.350	T-S1	0.316	L-S1	0.237	LAS1	0.349	T-S1
5	0.421	V-S2	0.415	V-S2	0.413	V-S2	0.349	T-S1	0.253	VAS1	0.420	TOW
6	0.422	TOW	0.422	TOW	0.422	TOW	0.416	V-S2	0.343	T-S1	0.422	V-S2
7	0.422	TOW	0.422	TOW	0.422	TOW	0.422	TOW	0.416	V-S2	0.432	TOW
8	0.453	TAS1	0.453	TAS1	0.453	TAS1	0.422	TOW	0.422	TOW	0.458	TAS1
9	0.474	VAS2	0.474	VAS2	0.473	VAS2	0..453	TAS1	0.422	TOW	0.474	VAS2
10	0.486	T-S2	0.486	T-S2	0.486	T-S2	0.474	VAS2	0.454	TAS1	0.487	T-S2
11	0.511	TAS2	0.510	TAS2	0.511	TAS2	0.486	T-S2	0.474	VAS2	0.509	TAS2
12	0.568	V-S3	0.568	V-S3	0.564	V-S3	0.511	TAS2	0.481	T-S2	0.539	LONG
13	0.627	T-S3	0.627	T-S3	0.627	T-S3	0.568	V-S3	0.509	L-S3	0.573	V-S3
14	0.657	VAS3	0.655	VAS3	0.646	VAS3	0.627	T-S3	0.513	TAS2	0.630	T-S3
15	0.674	V-S4	0.673	V-S4	0.671	V-S4	0.659	VAS3	0.568	V-S3	0.676	V-S4
16	0.716	TAS3	0.716	TAS3	0.676	V-S5	0.673	V-S4	0.621	VAS3	0.676	VAS3
17	0.720	T-S4	0.720	T-S4	0.716	TAS3	0.716	TAS3	0.621	V-S4	0.718	TAS3
18	0.750	VAS4	0.746	VAS4	0.720	T-S4	0.720	T-S4	0.633	T-S3	0.721	T-S4
19	0.793	TAS4	0.792	TAS4	0.755	VAS4	0.750	VAS4	0.649	TAS3	0.771	VAS4
20	0.850	V-S5	0.811	LONG	0.792	TAS4	0.792	TAS4	0.657	T-S4	0.797	TAS4
21	0.881	VAS5	0.859	V-S5	0.852	V-S6	0.845	LONG	0.660	VAS4	0.839	LAS2
22	0.932	V-S6	0.903	VAS5	0.885	LAS2	0.869	LAS2	0.675	V-S5	0.877	V-S5
23	0.933	T-S5	0.920	LAS2	0.896	VAS5	0.892	VAS5	0.716	TAS4	0.905	VAS5
24	0.935	VAS6	0.933	T-S5	0.931	V-S7	0.924	V-S5	0.723	T-S4	0.929	L-S3
25	0.952	TAS5	0.933	V-S6	0.933	T-S5	0.933	T-S5	0.757	VAS5	0.936	TAS5

LONG – longitudinal; L – lateral; V – vertical bending; T – torsional; TOW– tower vibration; S – symmetric; AS - asymmetric

3.6.5 Modal Structural Damping

The modal structural damping is theoretically computed using the formulations for energy based evaluation, as described in Section 3.5. The contribution to the modal strain energy by bridge components is different in various modes for Bridge #1 and Bridge #2 are indicated in Fig. 3.24 and Fig. 3.25 respectively. The energy loss factor for components made of steel and concrete has been taken as 2.6e-3 and 0.024 respectively based on the details given in Lazan (1968) and Blevins (1990). Assuming the stays of the Bridge #1 as parallel wire strands, the energy loss factor is assumed as 5.2×10^{-3} on the basis of summary of damping ratios given in Table 2.4. The modal structural damping thus estimated for Bridge #1 and Bridge #2 by energy dissipation method for the first ten modes is given in Tables 3.11 and 3.12 for six different support types for bridge deck DST-1 to DST-6.

To study the influence of cable type on modal structural damping of Bridge #1, the values are computed by considering the stays as locked-coil cables, with energy loss factor assumed as 0.0026, based on the average damping ratios given in Table 2.4. By comparing the modal structural damping values thus computed with the results in Tables 3.11, it is found that (i) the modal damping in vertical bending mode is sensitive to the type of stays used in the bridge; by using parallel wire type cables, an increase in the modal structural damping in the first symmetrical mode to the tune of 25% to 30% is achieved over the value obtained with locked–coil stays, (ii) the increase in the torsional damping is by about 5% only, and (iii) the structural damping in the lateral and longitudinal modes is not changed with cable type.

From Tables 3.11 and 3.12, it is clear that the modal structural damping in the torsional mode is higher than the damping in the vertical mode of vibration. A similar trend in the values of modal structural damping can be noticed from Table 2.1 for Ikuchi Bridge. The increase in modal damping in the torsional mode can be attributed to the strain energy contribution of the cross girder members of the deck system and the

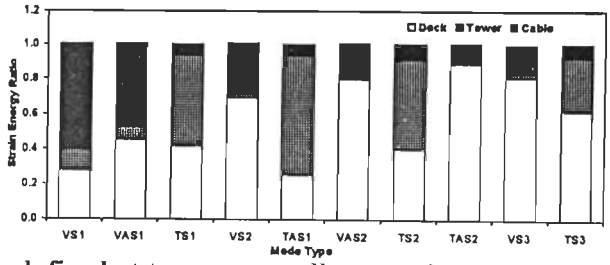

(a) Deck fixed at towers, on rollers at other supports (DST-1)

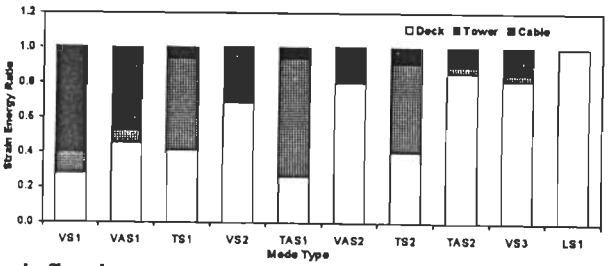

(b) Deck fixed at one tower, on rollers at other supports (DST-2)

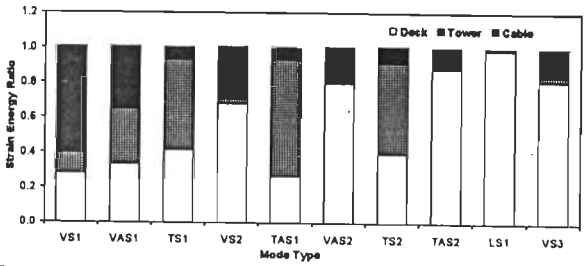

(c) Deck fixed at one end, on rollers at other supports (DST-3)

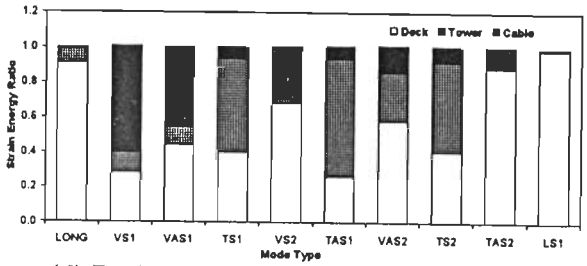

(d) Deck movable at all supports (DST-4)

LONG	– longitudinal
L	– lateral
V	– vertical bending
T	– torsional
S	– symmetric
AS	- asymmetric

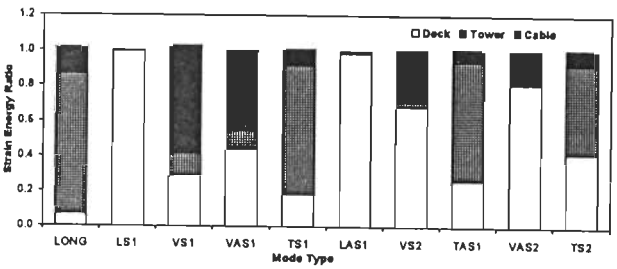

(e) Floating deck (DST-5)

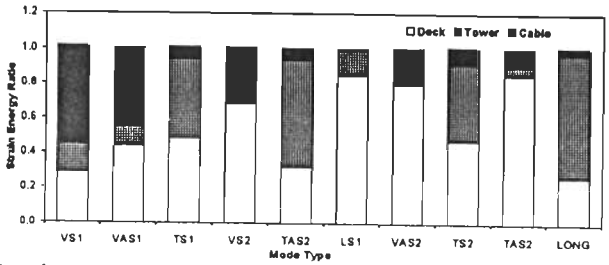

(f) Deck elastically supported at towers, on rollers at other supports (DST-6)

Fig. 3.24 : Distribution of Modal Strain Energy in Components of Bridge # 1 with Different Types of Deck Support

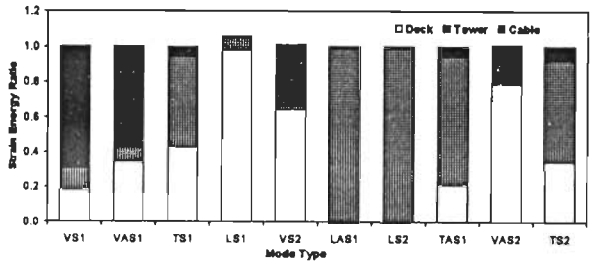

(a) Deck fixed at towers, on rollers at other supports (DST-1)

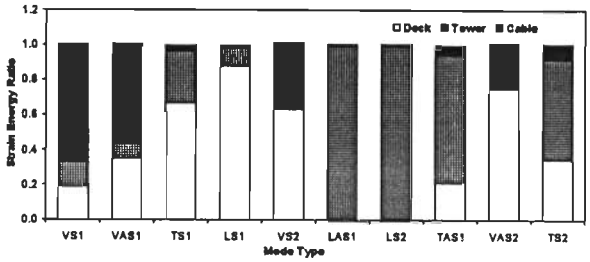

(b) Deck fixed at one tower, on rollers at other supports (DST-2)

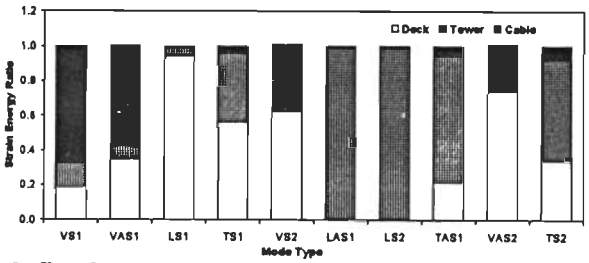

(c) Deck fixed at one end, on rollers at other supports (DST-3)

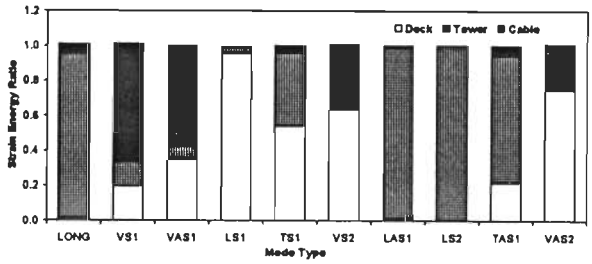

(d) Deck movable at all supports (DST-4)

LONG	– longitudinal
L	– lateral
V	– vertical bending
T	– torsional
TOW	– tower vibration
S	– symmetric
AS	- asymmetric

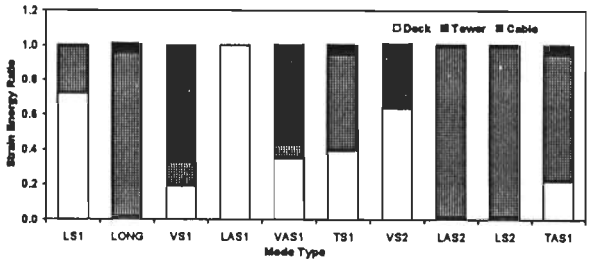

(e) Floating deck (DST-5)

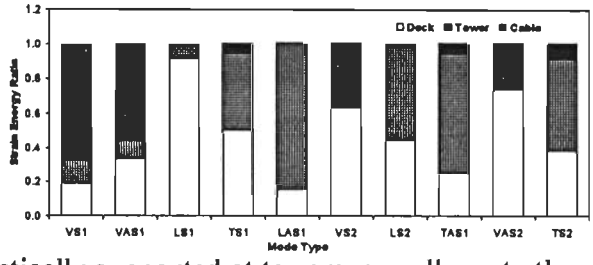

(f) Deck elastically supported at towers, on rollers at other supports (DST-6)

Fig. 3.25 : Distribution of Modal Strain Energy in Components of Bridge # 2 with Different Types of Deck Support

lower and upper strut members of the A-shaped towers. With different support types for bridge deck at towers and abutments in three span cable stayed bridges, the order of mode type which gets excited is changed. From Table 3.11 and 3.12, it is clear that the modal structural damping for a particular type of vibrating mode also varies with support type for bridge deck. It is observed that for bridge width elastically supported deck (DST-6) has slightly higher structural damping in vertical bending mode.

The modal strain energy distribution of selected number of modes for the five span bridges is shown in Fig 3.26. The estimated modal structural damping for Bridge #3 and Bridge #4 are given in Table 3.13.

From the results of these four bridges on modal structural damping, the following observations are made:

Damping in the 1st vertical symmetric mode (V-S1) is mainly due to energy dissipation in the cables. Hence it depends on the type of cable – more for bridge with parallel wire strands than with locked-coil strands. With higher vertical bending modes, the contribution to damping from cables reduces. The damping in the 1st vertical asymmetric mode (V-AS1) is sensitive to the type of deck support.

The contribution to modal damping by components of bridge such as deck, cables and tower are different in different modes. This causes modal dependency of structural damping. The damping in the longitudinal mode is mainly due to energy dissipation in towers. The damping in longitudinal mode is much higher than the damping in vertical, lateral and torsional modes of vibrations. In a lateral mode, with prominent deck or tower vibrations, the damping is due to energy dissipation in the respective component.

In both the three span cable stayed bridges with A-shaped towers, it is seen that the damping in the 1st torsional symmetric mode (T-S1) is higher than in the 1st vertical symmetric mode (V-S1) of vibration. This is due to the major contribution to strain energy by cross beam members in the deck and in the A-shaped towers.

Table 3.11(a): Modal Structural Damping for Bridge # 1 with Deck Support Types DST-1 and DST-2

(η_{cable}=5.2e-3,η_{deck}=2.6e-3,η_{tower} =2.4e-2)

Mode No.	DST-1				DST-2			
	Freq. (Hz)	Mode Type	Damping Ratio (ξ_s)	Logarithmic Decrement (δ_s)	Freq. (Hz)	Mode Type	Damping Ratio (ξ_s)	Logarithmic Decrement (δ_s)
1	0.292	V-S1	0.0033	0.0208	0.291	V-S1	0.00335	0.02100
2	0.415	VAS1	0.0027	0.0170	0.415	V-AS1	0.00270	0.01690
3	0.525	T-S1	0.0069	0.0435	0.525	T-S1	0.00696	0.04370
4	0.647	V-S2	0.0019	0.0122	0.640	V-S2	0.00194	0.01218
5	0.692	T-AS1	0.0086	0.0540	0.692	T-AS1	0.00853	0.05350
6	0.727	V-AS2	0.0016	0.0102	0.727	V-AS2	0.00162	0.01010
7	0.746	T-S2	0.0068	0.0428	0.746	T-S2	0.00665	0.04180
8	0.790	T-AS2	0.0015	0.0097	0.790	T-AS2	0.00189	0.01190
9	0.890	V-S3	0.0018	0.0114	0.890	V-S3	0.00183	0.01150
10	0.979	T-S3	0.0047	0.0293	0.952	L-S1	0.00259	0.01620

Table 3.11(b): Modal Structural Damping for Bridge # 1 with Deck Support Types DST-3 and DST-4

(η_{cable} =5.2e-3, η_{deck} =2.6e-3, η_{tower}= 2.4e-2)

Mode No.	DST-3				DST-4			
	Freq. (Hz)	Mode Type	Damping Ratio (ξ_s)	Logarithmic Decrement (δ_s)	Freq. (Hz)	Mode Type	Damping Ratio (ξ_s)	Logarithmic Decrement (δ_s)
1	0.291	V-S1	0.00335	0.02100	0.139	LONG	0.00211	0.01319
2	0.414	V-AS1	0.005110	0.03210	0.295	V-S1	0.00333	0.02090
3	0.524	T-S1	0.00690	0.04350	0.421	V-AS1	0.00296	0.01850
4	0.639	V-S2	0.00197	0.012370	0.530	T-S1	0.00707	0.04444
5	0.692	T-AS1	0.00854	0.05360	0.647	V-S2	0.00194	0.01220
6	0.726	V-AS2	0.00161	0.01011	0.695	T-AS1	0.00858	0.05390
7	0.747	T-S2	0.00689	0.04320	0.732	V-AS2	0.00442	0.02770
8	0.790	T-AS2	0.00155	0.00972	0.751	T-S2	0.00685	0.04303
9	0.855	L-S1	0.00137	0.00863	0.795	T-AS2	0.00156	0.00980
10	0.889	V-S3	0.00184	0.01156	0.848	L-S1	0.00140	0.00879

LONG – longitudinal; L – lateral; V – vertical bending; T – torsional; TOW– tower vibration; S – symmetric; AS - asymmetric

Table 3.11(c): Modal Structural Damping for Bridge # 1 with Deck Support Types DST-5 and DST-6

(η_{cable} = 5.2e-3, η_{deck}= 2.6e-3, η_{tower} =2.4e-2)

Mode No.	DST-5				DST-6			
	Freq. (Hz)	Mode Type	Damping Ratio (ξ_s)	Logarithmic Decrement (δ_s)	Freq. (Hz)	Mode Type	Damping Ratio (ξ_s)	Logarithmic Decrement (δ_s)
1	0.139	LONG	0.0100	0.06280	0.301	V-S1	0.0037	0.02320
2	0.173	L-S1	0.00259	0.01620	0.417	V-AS1	0.00307	0.01930
3	0.291	V-S1	0.00339	0.02130	0.527	T-S1	0.0062	0.03890
4	0.417	V-AS1	0.00297	0.01860	0.651	V-S2	0.00192	0.01200
5	0.527	T-S1	0.00940	0.05900	0.707	T-AS1	0.00786	0.04940
6	0.618	LAS1	0.00135	0.00850	0.725	L-S1	0.00291	0.01820
7	0.640	V-S2	0.00193	0.01210	0.727	V-AS2	0.00165	0.01030
8	0.693	T-AS1	0.00850	0.05370	0.751	T-S2	0.00608	0.03820
9	0.727	V-AS2	0.00155	0.00970	0.787	T-AS2	0.00194	0.01218
10	0.748	T-S2	0.00670	0.04200	0.864	LONG	0.00880	0.05520

Table 3.12(a): Modal Structural Damping for Bridge # 2 with Deck Support Types DST-1 and DST-2

(η_{cable} =2.6e-3,η_{deck} =2.6e-3,η_{tower}= 2.4e-2)

Mode No.	DST-1				DST-2			
	Freq. (Hz)	Mode Type	Damping Ratio (ξ_s)	Logarithmic Decrement (δ_s)	Freq. (Hz)	Mode Type	Damping Ratio (ξ_s)	Logarithmic Decrement (δ_s)
1	0.182	V-S1	0.00267	0.01680	0.181	V-S1	0.00273	0.01720
2	0..253	V-AS1	0.00209	0.01316	0.253	V-AS1	0.00218	0.01376
3	0.341	T-S1	0.00676	0.04252	0.335	T-S1	0.0044	0.02820
4	0.394	L-S1	0.00149	0.00939	0.363	L-S1	0.00823	0.01570
5	0.421	V-S2	0.00152	0.00955	0.415	V-S2	0.00151	0.00950
6	0.422	TOW	0.01183	0.07432	0.422	TOW	0.01184	0.07440
7	0.422	TOW	0.01184	0.07440	0.422	TOW	0.01187	0.07460
8	0.453	T-AS1	0.00906	0.05694	0.453	T-AS1	0.00905	0.05690
9	0.474	V-AS2	0.00135	0.00851	0.474	V-AS2	0.00136	0.00854
10	0.486	T-S2	0.00747	0.04694	0.486	T-S2	0.00746	0.04690

LONG – longitudinal; L – lateral; V – vertical bending; T – torsional; TOW– tower vibration; S – symmetric; AS - asymmetric

Table 3.12(b): Modal Structural Damping for Bridge # 2 with Deck Support Types DST-3 and DST-4

(η_{cable} =2.6e-3, η_{deck} =2.6e-3, η_{tower}= 2.4e-2)

Mode No.	DST-3				DST-4			
	Freq. (Hz)	Mode Type	Damping Ratio (ξ_s)	Logarithmic Decrement (δ_s)	Freq. (Hz)	Mode Type	Damping Ratio (ξ_s)	Logarithmic Decrement (δ_s)
1	0.181	V-S1	0.00278	0.01746	0.077	LONG	0.0113	0.07110
2	0.253	VAS1	0.00213	0.01338	0.181	V-S1	0.00273	0.01720
3	0.319	L-S1	0.00185	0.0116	0.253	V-AS1	0.00210	0.01320
4	0.350	T-S1	0.00544	0.0342	0..316	L-S1	0.00172	0.01080
5	0.413	V-S2	0.00156	0.0098	0.349	T-S1	0.00571	0.03590
6	0.422	TOW	0.01184	0.07439	0.416	V-S2	0.00150	0.00944
7	0.422	TOW	0.01188	0.07463	0.422	TOW	0.01183	0.07430
8	0.453	T-AS1	0.00906	0.0569	0.422	TOW	0.01187	0.07460
9	0.473	V-AS2	0.00132	0.00827	0.453	T-AS1	0.00904	0.05680
10	0.486	T-S2	0.00750	0.04714	0.474	V-AS2	0.00136	0.00856

Table 3.12(c): Modal Structural Damping for Bridge # 2 with Deck Support Types DST-5 and DST-6

(η_{cable} =2.6e-3, η_{deck} =2.6e-3, η_{tower}= 2.4e-2)

Mode No.	DST-5				DST-6			
	Freq. (Hz)	Mode Type	Damping Ratio (ξ_s)	Logarithmic Decrement (δ_s)	Freq. (Hz)	Mode Type	Damping Ratio (ξ_s)	Logarithmic Decrement (δ_s)
1	0.061	L-S1	0.00425	0.02670	0.183	V-S1	0.00273	0.0172
2	0.079	LONG	0.0113	0.07113	0.251	V-AS1	0.00248	0.01532
3	0.181	V-S1	0.00274	0.01723	0.303	L-S1	0.00212	0.0133
4	0.237	L-AS1	0.0013	0.00818	0.349	T-S1	0.0060	0.0377
5	0.253	V-AS1	0.00212	0.0133	0.420	L-AS1	0.0103	0.065
6	0.343	T-S1	0.00714	0.04488	0.422	V-S2	0.0013	0.0082
7	0.416	V-S2	0.00149	0.00942	0.432	L-S2	0.00067	0.0042
8	0.422	TOW	0.01185	0.07448	0.458	T-AS1	0.00175	0.0110
9	0.422	TOW	0.0118	0.07414	0.474	V-AS2	0.00161	0.0101
10	0.454	T-AS1	0.00905	0.05689	0.487	T-S2	0.00131	0.0082

LONG – longitudinal; L – lateral; V – vertical bending; T – torsional; TOW– tower vibration; S – symmetric; AS - asymmetric

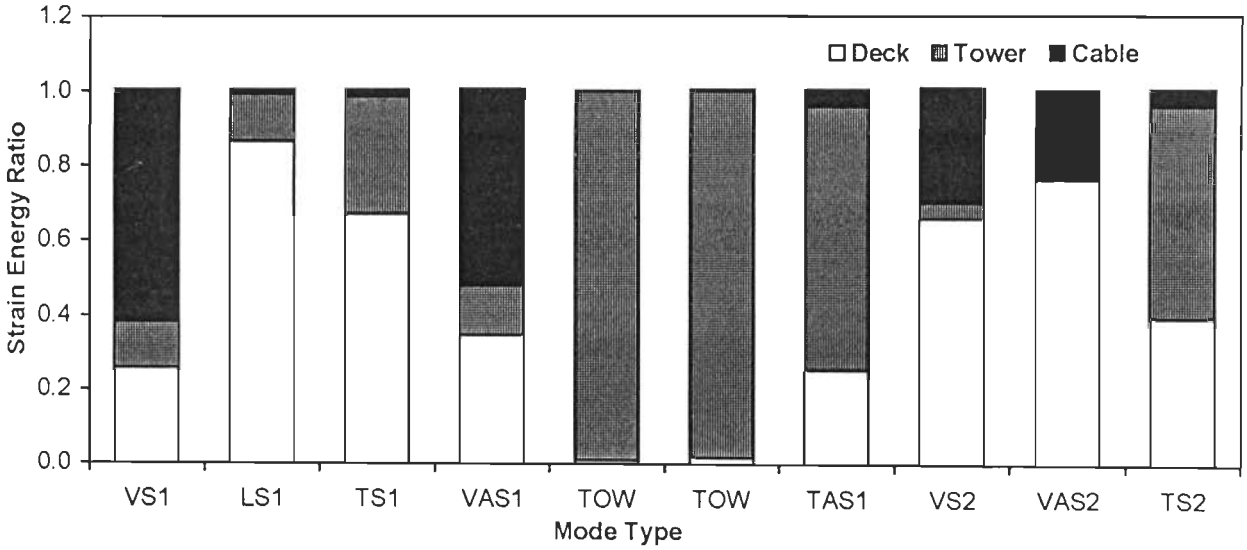

(a) For Bridge # 3

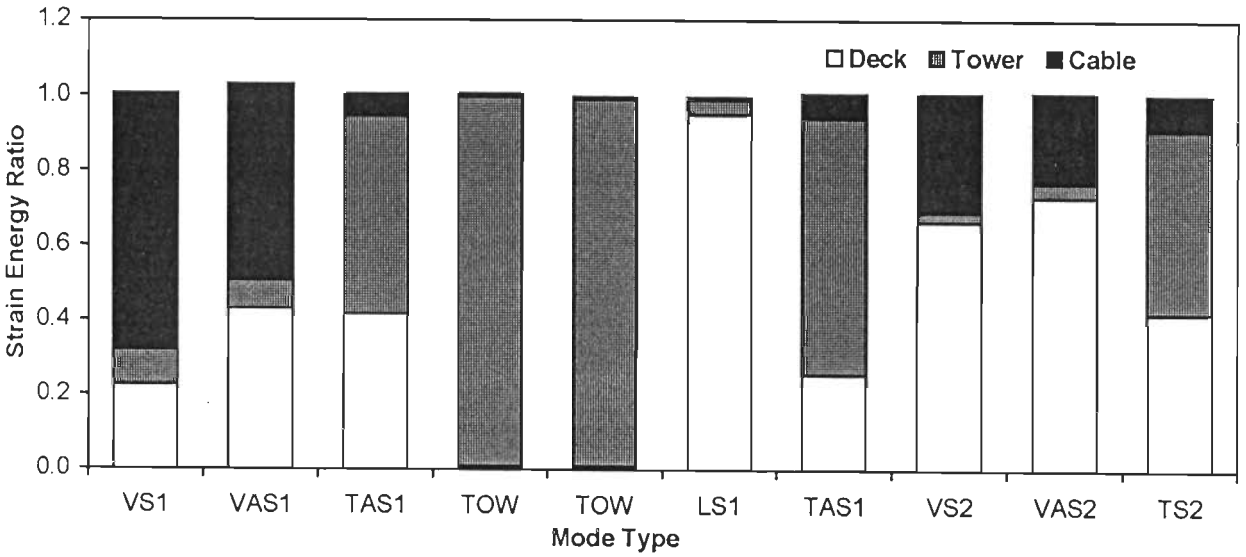

(b) For Bridge # 4

L	– lateral
V	– vertical bending
T	– torsional
S	– symmetric
AS	- asymmetric

Fig. 3.26 : Distribution of Modal Strain Energy in Components of Five Span Cable Stayed Bridges

Table 3.13(a): Modal Structural Damping for Bridge # 3 with Deck Configuration C-1B

(η_{cable}=5.2e-3, η_{deck}=2.6e-3, η_{tower} =2.6e-3)

Mode No.	Freq. (Hz)	Mode Type	Damping Ratio (ξ_s)	Logarithmic Decrement (δ_s)
1	0.398	V-S1	0.00200	0.0132
2	0.547	L-S1	0.00131	0.0083
3	0.570	T-S1	0.00133	0.0083
4	0.667	V-AS1	0.00199	0.0125
5	0.840	TOW	0.00122	0.0080
6	0.841	TOW	0.00130	0.0080
7	0.887	T-AS1	0.00136	0.0085
8	0.998	V-S2	0.00170	0.0106
9	1.125	V-AS2	0.00160	0.0101
10	1.65	T-S2	0.00136	0.0086

Table 3.13(b): Modal Structural Damping for Bridge # 4

(η_{cable}=2.6e-3, η_{deck}=2.4e-2, η_{tower} =2.4e-2)

Mode No.	Freq. (Hz)	Mode Type	Damping Ratio (ξ_s)	Logarithmic Decrement (δ_s)
1	0.402	V-S1	0.00470	0.0296
2	0.517	V-AS1	0.00674	0.0423
3	0.521	T-S1	0.01140	0.0716
4	0.565	TOW	0.01190	0.0752
5	0.566	TOW	0.01190	0.0747
6	0.585	L-S1	0.01190	0.0748
7	0.717	T-AS1	0.01130	0.0714
8	0.819	V-S2	0.00870	0.0540
9	0.916	V-AS2	0.00950	0.0590
10	0.974	T-S2	0.01100	0.0690

L – lateral; V – vertical bending; T – torsional; TOW– tower vibration; S – symmetric; AS - asymmetric

3.7 SUMMARY

This chapter is devoted to the nonlinear static and vibration analysis of cable stayed bridges – the first step towards the analysis for wind induced oscillations. The evaluation of modal structural damping based on the energy dissipated by each type of structural component has been explained along with the working details of the software. The numerical analysis of three span and five span bridges are also presented. Validation of results of the nonlinear static analysis and vibration analysis of cable stayed bridges is also illustrated. The modal structural damping for all the four bridges has been theoretically evaluated on the basis of energy dissipated by deck, cables and towers. Based on the numerical analyses of four bridges included in this study, following conclusions are drawn on static and dynamic behaviour of cable stayed bridges.

(i) Nonlinear static response of three span cable stayed bridges is dependent on support type for bridge deck at towers and abutments.

(ii) The mode type, which gets excited during vibration of three span cable stayed bridges, is changed with type of support for bridge deck at towers and abutments.

(iii) The modal strain energy distribution is different in various modes of vibration and this causes mode dependency of structural damping in these bridges. However, modal structural damping of a particular mode type, varies with change in type of support for bridge deck.

(iv) With five supports along the span, stiffness of the bridge increases. Thus the natural frequencies of a five span cable stayed bridge are higher in comparison to a three span cable stayed bridge of similar span length.

Chapter 4

DIGITAL SIMULATION OF STOCHASTIC WIND VELOCITY FIELD

4.1 INTRODUCTION

This chapter describes the digital simulation of stochastic wind velocity field used in the analysis of wind induced oscillations in long span cable stayed bridges. The mean wind profile and other important statistical parameters used to describe the turbulent wind field are explained. An overview of numerical techniques used in the past, for generation of turbulent wind, as a Gaussian process, is also presented.

In this study, simulation of wind velocity field along the bridge span length has been achieved through spectral representation or wave superposition method. Theoretical background, simulation procedure, development and validation of computer software for generation of wind velocity field by spectral representation are described in detail.

The use of digitally simulated wind for evaluation of instantaneous buffeting forces acting on bridge deck are explained in Chapter 5. Further, the application of simulated buffeting forces in time domain analysis is illustrated with numerical examples of three span and five span cable stayed bridges in Chapters 6 and 7 respectively.

4.2 WIND DEFINED

Wind is defined as motion of air, created by the differential heating of atmosphere producing pressure gradients, which are subsequently modified by the rotation of earth. As wind flows over the ground surface, atmospheric boundary layer (ABL) is formed, in which the wind speed decreases to near zero at the earth's surface

from a maximum value at the top of ABL. The reduction in wind velocity near the surface is due to the frictional drag of the surface and the drag of all bodies protruding into the flow such as trees, mountains and buildings and other structures. These retarding forces are transmitted through the layers by shear forces and by the exchange of momentum due to vertical movement of air. The process of momentum exchange between the layers is the mechanism leading to the formation and decay of eddies termed as turbulence. The resulting mixing of air produces, along all three orthogonal axes, fluctuations in wind speed, commonly called as gusts. The turbulent wind velocity field thus generated is depicted in Fig. 4.1.

The flow is moving with a mean wind velocity U(z) along the x-axis and u(t), v(t) and w(t) are the instantaneous longitudinal, lateral and vertical components of fluctuating velocities respectively. The mean of any gust component is zero since there is only mean motion in x-direction. The wind velocity at any point in space is thus a vector quantity, which has a magnitude and direction and both change rapidly with time. Thus the vector quantity has a magnitude given by:

$$\left[\{U+u(t)\}^2+v^2(t)+w^2(t)\right]^{1/2} \tag{4.1}$$

The three gust components u(t), v(t) and w(t) at a given point are random functions of time(t) and also vary in space as in Fig. 4.1. However, there is some correlation between the measurements of a gust component taken at different times and also between gust components measured at two points in space. The correlation decreases as the time lag or separation distance between the measurements increases.

For ground-mounted structures the properties of the longitudinal component of gust are most important but the lateral component does contribute to lateral forces. However, vertical component of gust is very important in the context of lift forces on bridge decks.

Mean and turbulent components of wind velocity are described in the following sections.

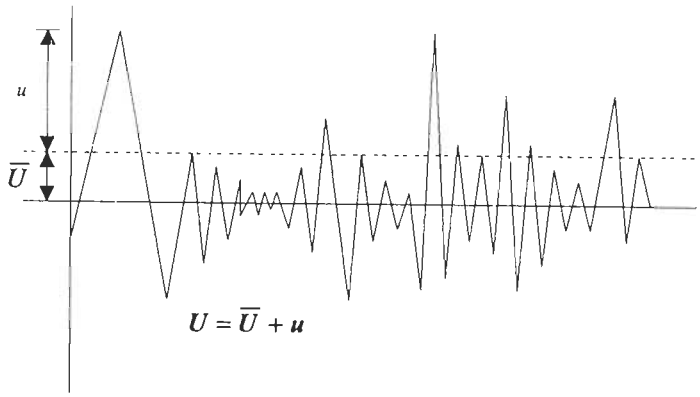

(a) Variation with time

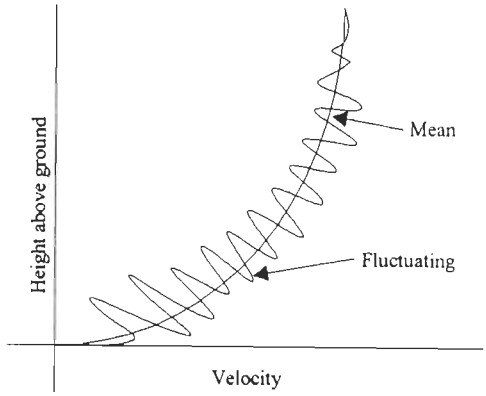

(b) Variation with height

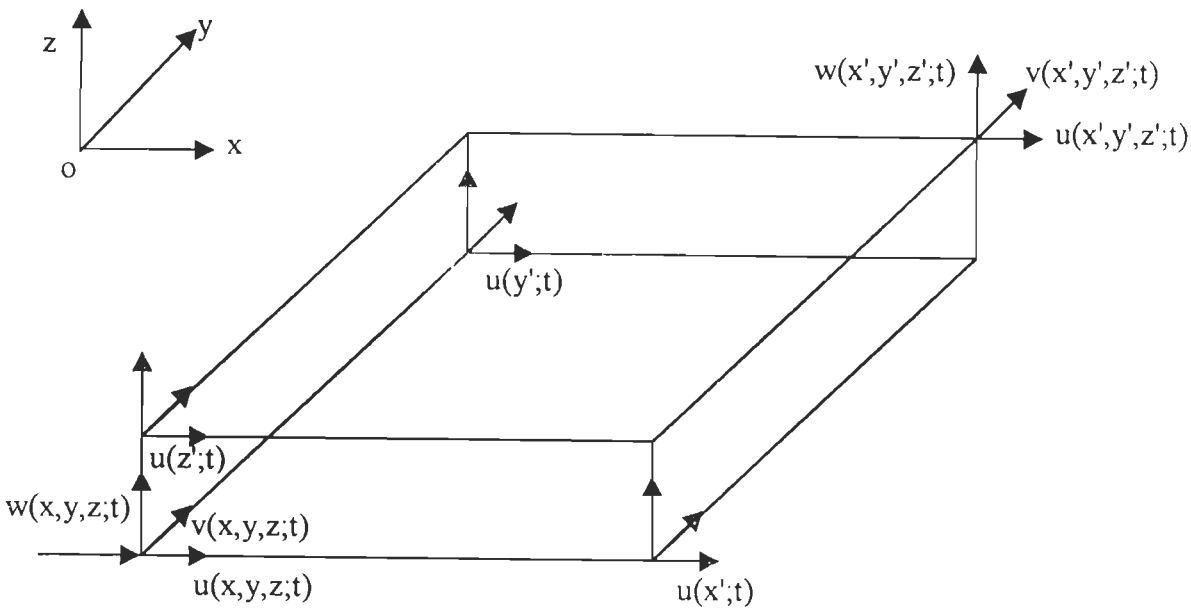

(c) Variation with space

Fig. 4.1 : Turbulent Wind Velocity Field

4.2.1 Mean Wind

The mean wind velocity is defined as the wind velocity averaged over a time T and expressed as

$$U(z) = \frac{1}{T}\int_0^T U(z,t) \tag{4.2}$$

Mean wind velocity is taken as the velocity averaged over a period of one hour at full scale. The averaging time of one hour has been selected as it gives stable averages and also it is the basis for the meteorological data.

The mean wind velocity varies with height above ground as well as terrain roughness and expressed mathematically using the power law or logarithmic law. Power law is generally used in the simulation of wind profile in wind tunnel investigations. However, meteorologists regard the logarithmic law as a superior representation of strong wind profiles in the lower atmosphere. In the present study logarithmic law as discussed by Simiu (1973) has been used for description of the mean wind profile, which is given below:

$$U(z) = \frac{1}{k} u_* \ln\left[\frac{z}{z_0}\right] \tag{4.3}$$

where, $u_* = \dfrac{U(10)}{2.5 ln(10/z_0)}$ (4.4)

u_* = friction velocity

U (10) = mean wind velocity at 10m above ground level

z_o = surface roughness factor (see Table 4.1)

z = height above mean ground surface

k = Von Karman's constant ≈ 0.4 or obtained from Eq. 4.5

$$\kappa = \left[\frac{k}{ln(10/z_0)}\right]^2 \tag{4.5}$$

in which κ, the surface drag coefficient, is given in Table 4.1.

It may be noted that in Table 4.1, the values of surface roughness parameters given for sparsely and densely built up suburbs as well as for centers of large cities are based on the assumption that the values of zero plane displacement are zero as stated in Simiu and Scanlan (1996). If this assumption is not satisfied, the values of surface roughness parameters along with the corresponding zero plane displacement values are to be taken from ESDU 85020.

Table 4.1 Surface Roughness Parameters and Surface Drag Coefficient

Type of Surface	z_0 (m)	$10^3 \kappa$
Sand	0.0001-0.001	1.2-1.9
Snow Surface	0.001-0.006	1.9-2.9
Mown Grass	0.001-0.01	1.9-3.4
Low grass, Steppe	0.01-0.04	3.4-5.2
Fallow field	0.02-0.03	4.1-4.7
High Grass	0.04-0.1	5.2-7.6
Palmetto	0.1-0.3	7.6-13.0
Pine Forest	0.9-1.0	28.0-30.0
Sparsely built-up Suburbs	0.2-0.4	10.5-15.4
Densely built –up suburbs, towns	0.8-1.20	25.1-35.6
Centers of large cities	2.0-3.0	61.8-110.4

As the design in speed of cable stayed bridges are generally in the range of 30 m/sec to 60 m/sec, in the present study, the values of mean wind speed are taken as 30,40,50 and 60m/sec at 10 m level corresponding to a terrain roughness z_0 equal to 0.005m. The mean wind profile for different terrain categories TC-1, TC-2, TC-3 and TC-4 with ground surface roughness parameters z_0 equal to 0.005m, 0.03m, 0.3m and 1.0m respectively are illustrated in Fig. 4.2.

4.2.2 Turbulent Wind

As discussed earlier, turbulence in wind originates from the action of the shear stresses at ground level due to surface roughness and ground obstructions, which are transmitted upwards through the atmosphere leading to formation and decay of eddies.

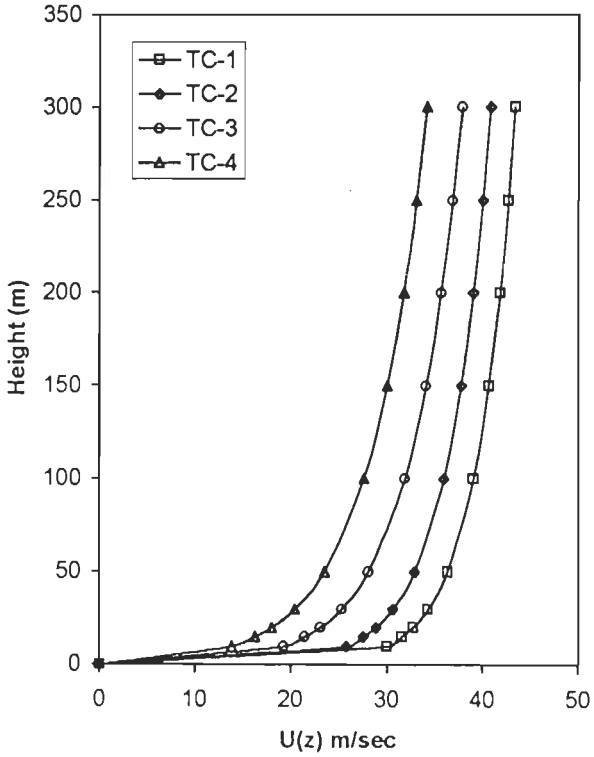

(a) U(10)=30m/sec

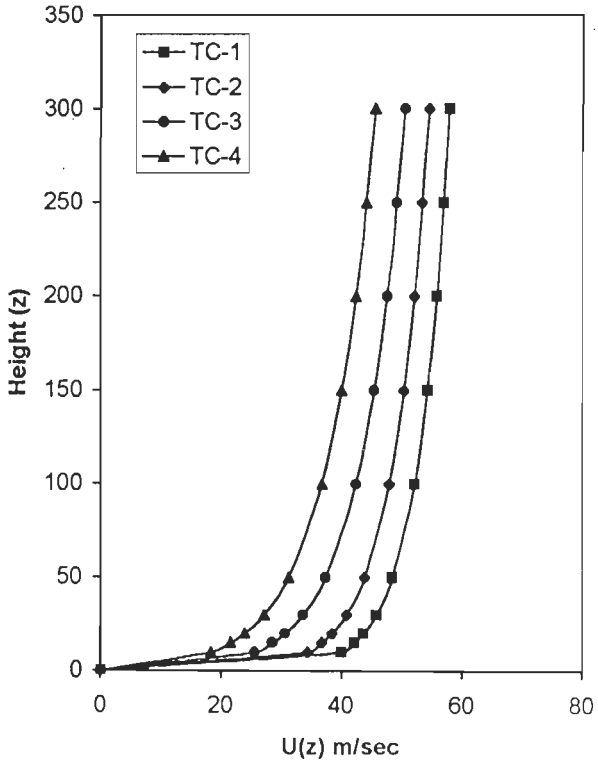

(b) U(10)=40m/sec

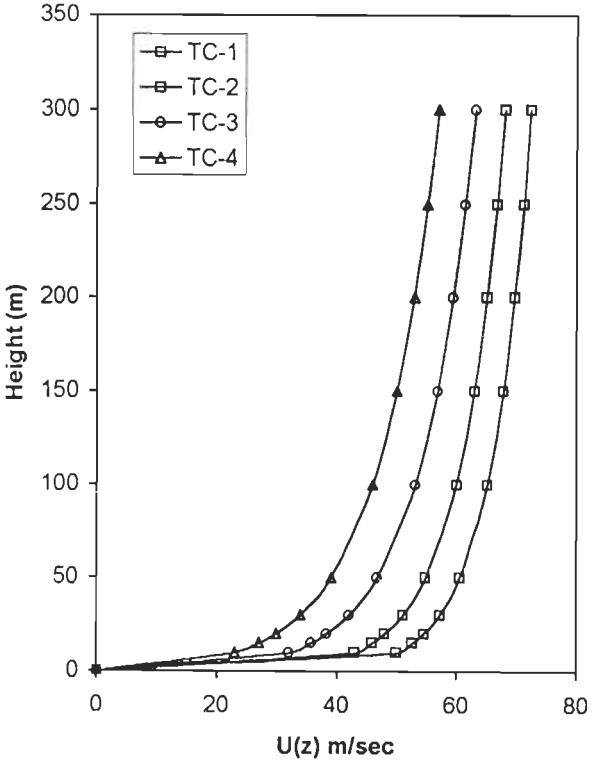

(c) U(10)=50m/sec

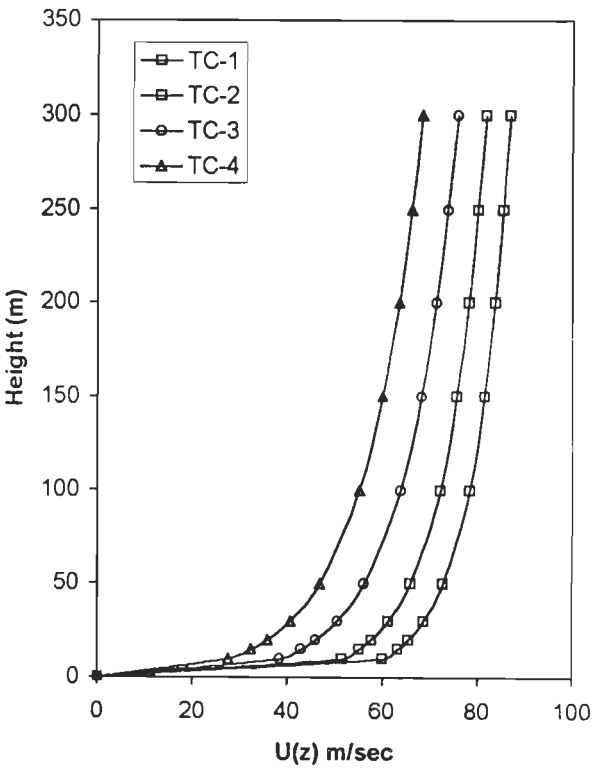

(d) U(10)=60m/sec

Fig. 4.2 : Mean Wind Profile with Variation in Terrain Roughness

The need for considering the turbulence nature of atmosphere, for estimation of wind effects on long span bridges, arises due to following reasons -(i) the points of separation and reattachment of flow are affected by the turbulence in the approaching flow and consequently the wake characteristics as well as the steady-state force coefficients and (ii) because of the fluctuating wind velocities, in addition to the quasi-static forces, the flexible bridge is subjected to dynamic or unsteady forces, when immersed in a turbulent flow. These unsteady forces gain importance as they are responsible for wind induced oscillations.

As the atmospheric turbulence is changing continuously with time and space, it is necessary to describe its properties in statistical terms. These statistical parameters are based on amplitude, time and frequency scales of fluctuations and are defined in the following sections

4.2.2.1 Turbulence intensity

The longitudinal turbulence intensity is defined as the ratio of standard deviation of along wind fluctuating components of wind to mean wind speed at the same height. It is a non-dimensional quantity given as follows:

$$I_u = \sigma_u / U_z \quad \text{for u –component} \tag{4.6}$$

$$I_v = \sigma_v / U_z \quad \text{for v – component} \tag{4.7}$$

$$I_w = \sigma_w / U_z \quad \text{for w – component} \tag{4.8}$$

$$\sigma_u = \sqrt{\beta u_*^2} \tag{4.9}$$

The values of β for different terrains are given in Table 4-2.

Table 4.2 : Values of β for Various Roughness Lengths

z_0 (m)	0.005	0.07	0.30	1.00	2.50
β	6.50	6.00	5.25	4.85	4.00

The turbulence intensities in the lateral and vertical directions can be expressed in terms of turbulence intensity in the longitudinal direction. It has been understood from numerous model boundary layers that the three turbulence intensities tend to become equal, as they approach zero at gradient height. Near the ground the three intensities tend to stay in fixed proportions of I_v/I_u=0.68 and I_w/I_u =0.45, which has been confirmed by field measurements in ABL. For intermediate heights, at least over the height of 300m the value of I_v (z) and I_w(z) are estimated using the following expressions given by Teunissen (1980) :

$$I_v = I_u\left[1 - 0.32\left(1 - \left(z - z_d\right)/z_g\right)^2\right] \tag{4.10}$$

$$I_w = I_u\left[1 - 0.55\left(1 - \left(z - z_d\right)/z_g\right)^2\right] \tag{4.11}$$

where z_g is the gradient height, estimated as 275m, 300m, 375m and 410m corresponding to the surface roughness z_0 = 0.005m, 0.03m, 0.3m and 1.0m, using the formulae given in Simiu and Scanlan (1996) and z_d is zero plane displacement.

As discussed earlier, the longitudinal and vertical turbulence intensities are important for estimating the bridge response. The variation of I_u and I_w with height for terrain roughness categories TC-1, TC-2, TC-3 and TC-4 with surface roughness parameter z_0 equal to 0.005m, 0.03m, 0.3m and 1.0m respectively, estimated using Eqs. 4.6, 4.10 and 4.11, are shown in Fig. 4.3.

4.2.2.2 Turbulent length scale

The length scales of turbulence are a comparative measure of average size of a gust in appropriate direction and are important scaling factors in determining how rapidly the gust properties vary in time and space. The main parameters that determine the turbulent length scale are, height above the ground, terrain roughness and the mean wind speed There are nine integral scales of turbulence corresponding to three dimensions of eddies associated with the longitudinal, transverse and vertical components of fluctuating velocity, u, v and w. They are obtained by integrating the

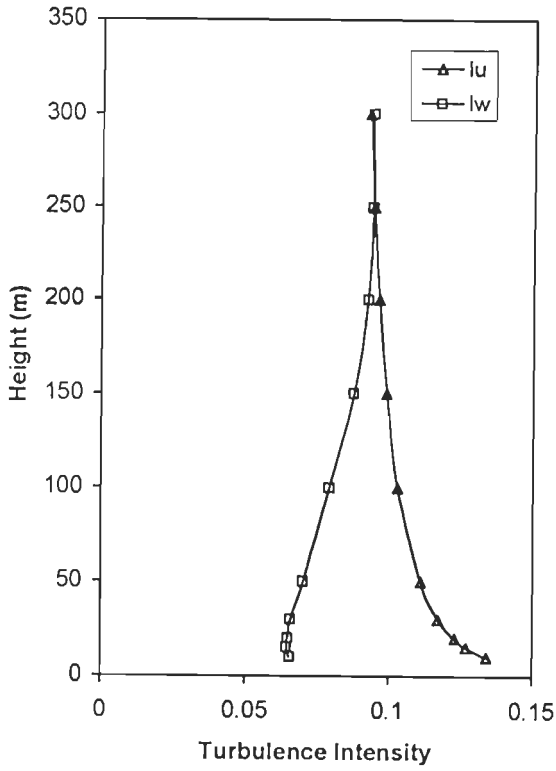

(a) z_o = 0.005m

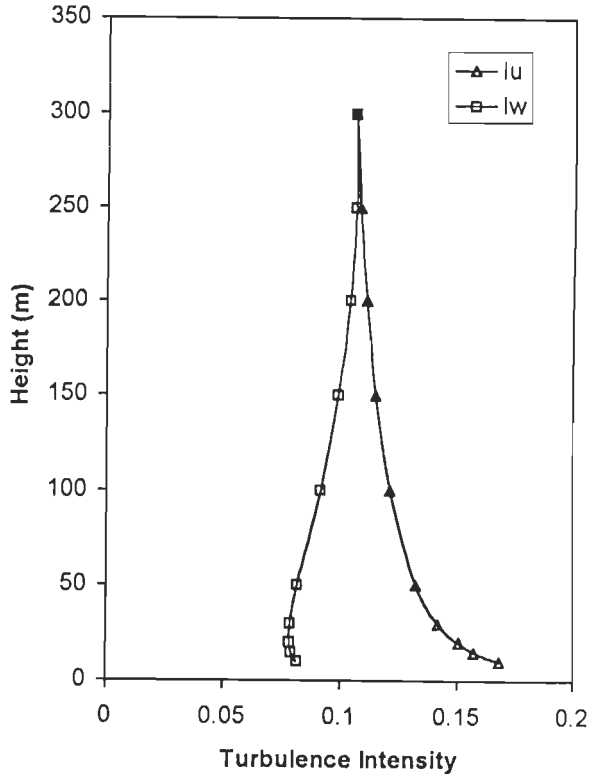

(b) z_o = 0.03m

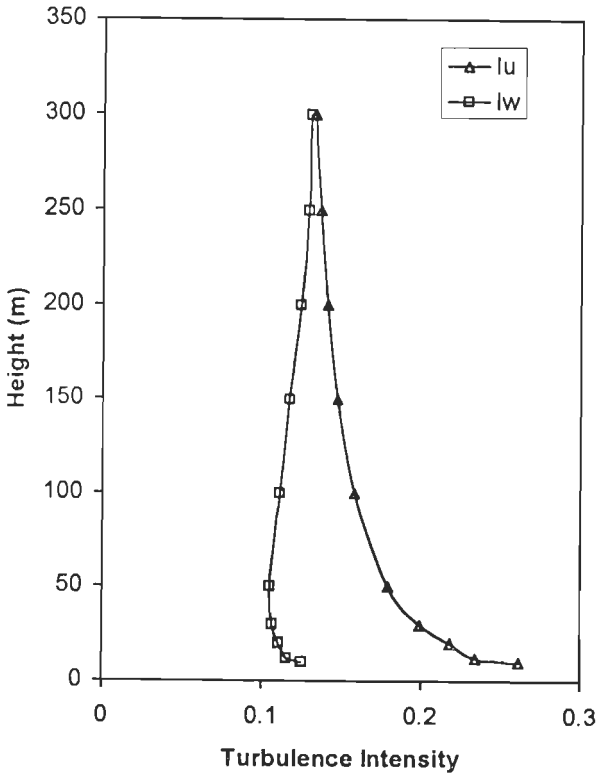

(c) z_o = 0.3m

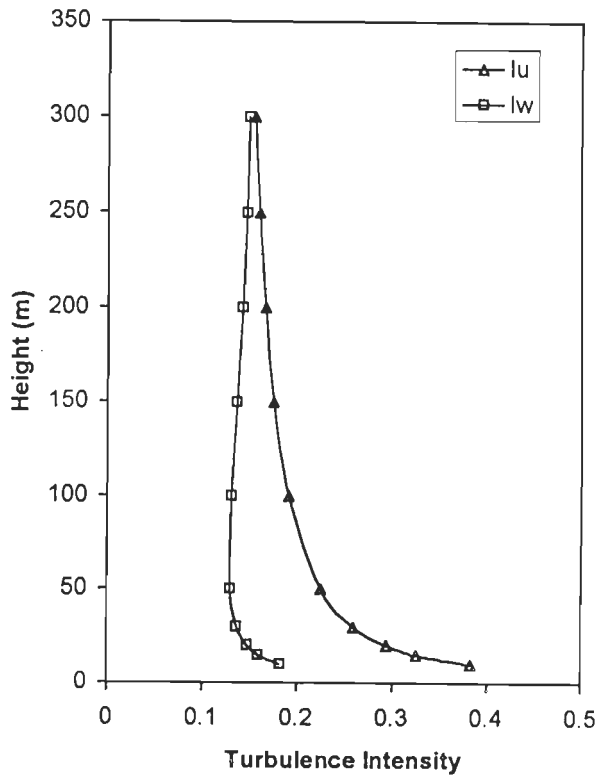

(d) z_o = 1.0m

Fig. 4.3 : Variation of Longitudinal (I_u) and Vertical (I_w) Turbulence Intensities with Height – Effect of Terrain Roughness

spatial or autocorrelation functions over the complete range of the appropriate spatial variable. The longitudinal length scale ${}^{x}L_u$ is important, since it is essential in determining the magnitude of dynamic component of wind loading through the spectral density function S_u and is given by:

$$ {}^{x}L_u = \frac{1}{\bar{u}^2}\int_0^{\infty} R_{u_1u_2}(x)dx \tag{4.12} $$

4.2.2.3 Power spectral density functions

Power spectral density functions provide information on frequency distribution of the kinetic energy of the various fluctuating velocity components. These are useful for estimating response of structures subjected to wind loading, as they provide information on energy-input from different frequency ranges.

For longitudinal fluctuations, Von Karman (1948) expressed the spectra as:

$$ \frac{nS_u(n)}{u_*^2} = \frac{4\beta\dfrac{n^{x}L_u}{U}}{\left[1+70.8\left(\dfrac{n^{x}L_u}{U}\right)^2\right]^{5/6}} \tag{4.13} $$

Davenport (1961) proposed the formulation for spectral density function on the basis of average results of wind velocity measurements obtained at various heights above ground as:

$$ S_u(n) = \frac{4u_*^2 f^2}{n(1+f^2)^{4/3}}; \quad f = \frac{1200n}{U(10)} \tag{4.14} $$

Harris (1968) modified the formulation as proposed by Davenport, and suggested the following expression :

$$ S_u(n) = \frac{4u_*^2 f^2}{n(2+f^2)^{5/6}}; \quad f = \frac{1800n}{U(10)} \tag{4.15} $$

Both the above expressions for spectral density functions depend only on mean wind speed U (10) and the friction velocity u_* which is a function of ground roughness

parameter z_0; they are independent of the height, z. This is contrary to the experimental evidence. Hence, Kaimal (1972) came out with a spectral estimate expression, which considers variation in spectra of longitudinal fluctuations with height (z) and has been widely used in design of civil engineering structures.

In the present study, Kaimal spectrum is used to describe the longitudinal velocity fluctuations and is given by:

$$\frac{nS_u(n)}{u_*^2} = \frac{200f}{(1+50f)^{\frac{5}{3}}}; \qquad f = \frac{nz}{U(z)} \tag{4.16}$$

For the spectra of vertical velocity fluctuations upto about a height of 50m Lumley and Panofsky (1964) proposed the following expression:

$$\frac{nS_w(n)}{u_*^2} = \frac{3.36f}{1+10f^{5/3}}; \qquad f = \frac{nz}{U(z)} \tag{4.17}$$

In the present study, the Panofsky-McCormick spectrum (1959) is used for vertical velocity fluctuations and is defined as:

$$\frac{nS_w(n)}{u_*^2} = \frac{6f}{(1+4f)^2}; \qquad f = \frac{nz}{U(z)} \tag{4.18}$$

in which n is the frequency of fluctuating component in Hz.

4.2.2.4 Cross-spectral density / Coherence

Cross-spectrum of two continuous records is a measure of the degree or extent to which the two records are correlated. Coherence function is used to express the cross-spectrum between records at two different locations.

The coherence function defines the degree of the statistical dependence of two spectral densities vs frequency.

Consider L1 and L2 are two locations with co-ordinates (y_1, z_1) and (y_2, z_2) located in a direction perpendicular to the mean wind direction separated by a distance r. An exponential decay function as suggested by Davenport is given below:

$$Coh(r,n) = e^{-\hat{f}} \tag{4.19}$$

$$\hat{f} = \frac{n\left[C_z^2(z_1 - z_2)^2 + C_y^2(y_1 - y_2)^2\right]^{1/2}}{\frac{1}{2}\left[U(z_1) + U(z_2)\right]} \tag{4.20}$$

C_y and C_z are the exponential decay coefficients, with values in the range of 10 to 16. The values are larger for rough terrains; i.e., more for urban area than open terrains. The values of these coefficients further depend on height above ground, wind speed and length scale of turbulence. The cross- spectrum of longitudinal fluctuations is defined as:

$$S_{u1,u2} = S_{(z_1,n)}^{1/2} S_{(z_2,n)}^{1/2} e^{-\hat{f}} \tag{4.21}$$

The cross-spectrum of vertical fluctuations of two locations M1, M2 at an elevation of z above ground surface is expressed as:

$$S_{w1w2}(\Delta y, n) = S_w(z,n) e^{\frac{-8n\Delta y}{U(z)}} \tag{4.22}$$

The longitudinal coherence of longitudinal fluctuations is of importance in some applications, like a wide deck in a double plane cable stayed bridge deck. Let T1, T2 be two locations with co-ordinates (x_1, y, z) and (x_2, y, z) in the transverse direction, separated by bridge deck width 'B', the longitudinal coherence between fluctuations is expressed as:

$$\hat{f}' = \frac{nC_x(x_1 - x_2)}{U(z)} \tag{4.23}$$

The value of C_x =3 and 6 over water and land respectively.

4.2.2.5 Autocorrelation function

The autocorrelation function of a random process f(t) is defined as the average value of product f(t) and f(t+τ). The random process is sampled at time t and then again at t+τ and the average value of the product $E\langle f(t)f(t+\tau)\rangle$ is evaluated which represents the autocorrelation for the ensemble.

Also, the autocorrelation function $R_f(\tau)$ gives information about the frequencies present in the random process indirectly and is obtained by the inverse Fourier transform of power spectral density $S_f(\omega)$. The Fourier transform of $R_f(\tau)$ gives the spectral density of the random process. The relation between the two is given as follows.

$$S_f(\omega) = (1/2\pi)\int R_f(\tau)e^{-i\omega\tau}d\tau \tag{4.24}$$

$$R_f(\tau) = \int S_f(\omega)e^{i\omega\tau}d\omega \tag{4.25}$$

4.2.2.6 Cross-correlation function

The cross-correlation function of random processes {f(t)}and {g(t)} recorded at two different stations j and k in space, are measures of the degree to which the two records are correlated in amplitude domain. The cross-correlation function is computed as:

$$R_{fg}^{jk}(\tau) = \frac{1}{T}\int_{-\infty}^{\infty}\{f(t)\}_j\{g(t+\tau)\}_k dt \tag{4.26}$$

4.2.2.7 Probability density function and peak factor

Probability distribution describes how the magnitudes of the fluctuating velocity components are distributed. A common assumption, for the calculation of wind loads and response of ground-mounted structures, is that the atmospheric turbulence is a 'normal' or Gaussian process as shown in Fig. 4.4 with a probability density function given by:

$$p_i = \frac{1}{\sigma_i\sqrt{(2\pi)}}exp\left[-i^2/(2\sigma_i^2)\right] \tag{4.27}$$

where i = u, v or w. The integral

$$P_i = \int_{-\infty}^{i_p} p_i\, di \tag{4.27a}$$

The probability (P) that any value i will be less than i_p is given by

$$P = \int_{-\infty}^{i_p} p(i)\, di \qquad (4.27b)$$

i.e., P is the proportion of all values having values not greater than i_p. The quantity (1 – P) is the probability that the value i will be greater than i_p. The probability density function p therefore demonstrates the likelihood of a given amplitude of the signal.

If the integral $\int_{-\infty}^{+\infty} i.p(i)\, di$ is evaluated, it will equal the mean value $\bar{i}$ which is zero. Thus, the first moment of area about the i = 0 axis will be zero. The second moment of area about the i = 0 axis gives the variance (standard deviation squared).

$$\sigma_i^2 = \int_{-\infty}^{\infty} i^2.p(i)\, di \qquad (4.27c)$$

The magnitude of the amplitude of the maximum fluctuations that may occur within a given time interval T of such process is expressed as

$$u(t)_{max} = \bar{\kappa}\sigma_u \qquad (4.28)$$

where peak factor $\bar{\kappa} = \sqrt{(2\ln \upsilon T)} + 0.577/\sqrt{(2\ln \upsilon T)}$ (4.29)

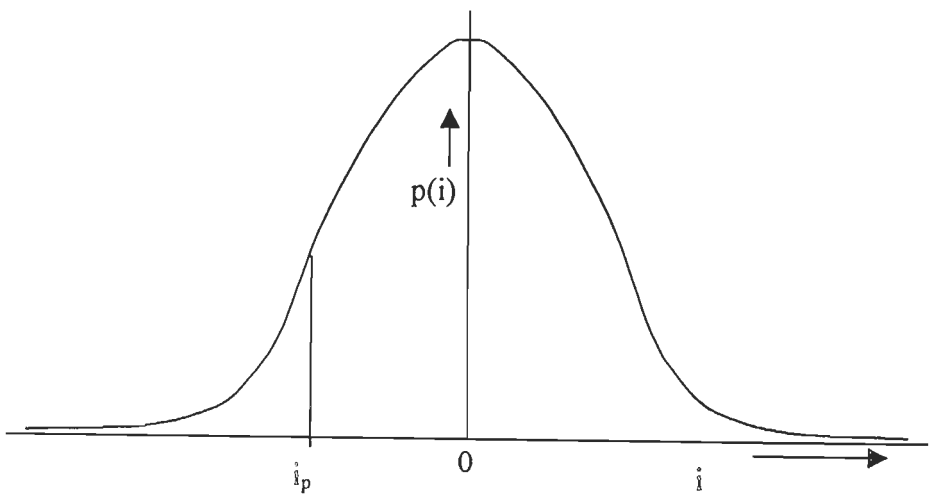

Fig. 4.4 : Probability Density Function

and value of υ is estimated by:

$$\upsilon = \left\{ \int_0^\infty n^2 S_u(n) dn \Big/ \int_0^\infty S_u(n) dn \right\}^{\frac{1}{2}} \tag{4.30}$$

In practice, atmospheric turbulence contains "patches" of a significantly non–Gaussian nature which are found particularly in the lower 30m where larger gusts may occur more frequently. However, as stated in ESDU Item No. 85020, it is generally satisfactory in most civil engineering applications to assume a Gaussian probability density function for atmospheric turbulence.

4.3 SIMULATION OF GAUSSIAN PROCESS – PREVIOUS METHODS

Wind velocity in atmospheric boundary layer exhibits both spatial and temporal randomness. The wind consists of a mean flow component determined by large scale pressure system and superimposed by gust fluctuations due to surface roughness, irregularities, topographical features along the path of wind, mixing of cold air with warm air, etc. The wind velocity thus consists of a mean component U and fluctuating components u, v, and w in X, Y and Z directions respectively. The complete wind velocity field should be treated as a multidimensional, multivariate homogeneous Gaussian Stochastic Process.

The turbulence in atmosphere is generally assumed to be isotropic with nearly uniform directional characteristics. It implies that almost no average rate of momentum transfer occurs across shearing surfaces. The velocity fluctuations in the three orthogonal directions can be considered as random processes with little correlation between them. With this assumption, the wind can be treated as a combination of three independent one-dimensional multivariate stochastic processes.

In the following sections the development of various methods for simulation of Gaussian stochastic process are discussed.

Racicot (1969) modelled wind gust as a filtered Poisson process. In this model,

the wind velocity is represented by the randomly arriving gusts superimposed on mean wind velocity. The gusts are assumed as a Poisson process and are idealized to have rectangular pulse shape as they result from eddies that follow vortex flow within moving air mass.

Shinozuka (1970), Shinozuka and Jan (1972) presented an efficient method for simulating multivariate and multidimensional process with specified cross – spectral density. When the cross – spectral density matrix of a multivariate process is specified, its component processes can be simulated as the sum of cosine functions with random frequencies and random phase angles. Examples of simulation of multi dimensional processes such as horizontal component of wind velocity perpendicular to the axis of a slender structure, the vertical gust velocity field frozen in space, etc., have been illustrated.

Shinozuka and Levy (1977) have described a procedure to generate simulation samples of the two – dimensional fluctuating component of the wind velocity acing on the surface of a paraboloidal antenna.

Lutes and Wang (1991) presented a method for generation of an improved Gaussian time history with time–average moments exactly equal to the expectations for a Gaussian process by a nonlinear transformation of a weakly non - Gaussian time history, and this transformation can be found through a simple iteration procedure.

Ramadan and Novak (1993) described a computationally efficient method for generation of spatially incoherent random ground motions, by means of summation of trigonometric functions. The procedure is simple, but asymptotically accurate, for simulation of stationary random process to fit specified auto spectral density and a specified coherency function. Also introduced another approximate technique that may be sufficient for engineering applications for time histories at discrete stations. These methods can be applied for generating spatially incoherent random processes in ocean and wind engineering also.

Li and Kareem (1993) presented a hybrid DFT and digital filtering technique for generation of long duration time–series. Di Paola (1998) utilized this concept for simulating wind velocity fields.

Deodatis (1996) explained an algorithm based on the extension of spectral representation method for simulation of stationary, multivariate, stochastic process according to its prescribed cross–spectral density matrix. The simulation algorithm generates ergodic sample functions in the sense that the temporal cross-correlation matrix of each and every generated sample function is identical to the corresponding target, when the length of generated sample function is equal to given period. The generated functions are Gaussian in the limit as the number of terms in the frequency discretization of cross-spectral density matrix approaches infinity. An example involving simulation of turbulent wind velocity fluctuations is presented to demonstrate the capabilities and efficiency of the algorithm.

Cao *et al* (2000) presented an improved algorithm for digital simulation of stochastic wind velocity field based on the spectral representation method, on long span bridges, when cross-spectral density matrix is given. The target wind velocity field is assumed to be a one dimensional, multivariate, homogeneous stochastic process. The improvement has been introduced by explicitly expressing the Cholesky decomposition of cross – spectral density matrix in the form of algebraic formulas, then cutting off as many as possible cosine terms, without compromising on the accuracy of the results. Further, the Fast Fourier Transform technique is used to enhance the efficiency of computation. However, they have presented simulation of longitudinal wind velocity fluctuations only, whereas the buffeting response of a long span bridge is greatly influenced by the vertical velocity fluctuations in the wind.

Another approach for stochastic modelling of wind is the time series model, as illustrated by Samaras *et al* (1985), Deodatis and Shinozuka (1988) Li and Kareem (1990), Mignolet and Spanos (1987, 1990,1992a, b) and Faccini (1996). Typically the

models involve autoregressive (AR) and moving average (MA) terms or their combination. The time series model consists of summation of autoregressive terms or a weighted summation of white noise, or their combination. An ARMA model of order 'p' and 'q' is defined as a linear filter that permits simulation of wind velocity u(t) by its past time histories and past and present white noise processes.

$$u(n\Delta t) + \sum_{r=1}^{p} A_r u(n-r)\Delta t = \sum_{r=0}^{q} B_r \varepsilon_{n-r} \tag{4.31}$$

A_r and B_r are the AR and MA coefficient matrices; ε_{n-r} is the vector containing white noise with zero mean and unit variance. The A_r and B_r coefficient matrices are determined from the user specified spectral description of the random field being simulated.

Maeda and Makino (1992) have discussed on the accuracy of gust wind simulation by fitting autoregressive moving average model for Karman's turbulent structure in u and w directions. The autoregressive process is directly estimated using the theoretical autocorrelation function of turbulent structure. The power spectra and the scales of turbulence of auto regressive moving average model are compared with theoretical values of turbulent structure.

Borri *et al* (1995) have compared two different simulation procedures, a parametric and multi-regressive model for generation of stationary and non-stationary stochastic process such as turbulent wind field. The study indicated that, for stationary process, multi-regressive model is faster than the parametric one, with a bit less accurate results. For the generation of non-stationary noise, parametric model proves more useful and flexible than the multi-regressive models.

Smith and Mehta (1995) have shown that autoregressive models of order 3 were found adequate to represent the field measured wind data at WERFL, TTU.

Reed and Scanlan (1983) have used ARIMA time series model in characterizing full-scale wind velocity and wind pressure data collected on two cooling towers.

Jin *et al* (1997) have presented an efficient method for stochastic simulation of time histories of multidimensional, spatially correlated, stationary Gaussian random fields. A key feature of the method is the use of filtering functions in directly expressing the conditional mean value of any component of random field. The general formulation and an updating algorithm for determining the required filtering functions for simulation of any general multidimensional field are established.

Kareem (1999) presented a review on numerical techniques for analysis and modelling of wind effects on structures. He has discussed the spectral techniques, and time series models for simulation of stationary Gaussian process and wavelet transforms for non-stationary Gaussian process. For non–Gaussian processes, correlation distorted based simulation, spectral correction approach, higher order spectral technique and conditional simulation techniques have been discussed.

4.4 PRESENT METHOD

In the present study, the generation of wind turbulent velocity field has been achieved by spectral representation method as described by Shinozuka and Deodatis (1991), Deodatis (1996). This method has been selected because it succeeds in generating ergodic sample functions of a stochastic vector process according to a prescribed target cross-spectral density matrix. Also it is simple, computationally efficient and hence widely used in simulation of stochastic processes. This technique for simulating Gaussian time history, generates the signal by summing up a number of cosine waves with random phase angles.

Kaimal's spectrum and Panofsky-McCormick spectrum as given by Eqs. 4.16 and 4.18 respectively have been used to describe longitudinal and vertical velocity fluctuations.

In digital simulation of wind velocity field, the following assumptions are made:

(i) Turbulent wind velocity is a Gaussian stationary random process.

(ii) u(t), v(t) and w(t) are incoherent in three orthogonal directions.

(iii) The fluctuating component v(t) has negligible effect.

(iv) Spectra for longitudinal and vertical velocity fluctuations along the bridge span remain the same.

4.4.1 Spectral Representation Method –Theoretical Background

Consider one dimensional, multivariate stochastic process $\left\{f^0(t)\right\}$, which has N-components, $f_1^0(t), f_2^0(t), f_3^0(t) \ldots f_N^0(t)$ with mean value zero.

$$E\left\langle f_j^0(t)\right\rangle = 0; j = 1,2,3 \ldots N \tag{4.32}$$

The cross-correlation matrix is given by

$$\left[R^0(\tau)\right] = \begin{bmatrix} R_{11}^0(\tau) & R_{12}^0(\tau) & \ldots & R_{1N}^0(\tau) \\ R_{21}^0(\tau) & R_{22}^0(\tau) & \ldots & R_{2N}^0(\tau) \\ \ldots & \ldots & \ldots & \ldots \\ R_{N1}^0(\tau) & R_{N2}^0(\tau) & \ldots & R_{NN}^0(\tau) \end{bmatrix} \tag{4.33}$$

The cross-spectral density matrix of random fluctuations is given by

$$[S^0(\omega)] = \begin{bmatrix} S_{11}^0(\omega & S_{12}^0(\omega) & \ldots & S_{1N}^0(\omega) \\ S_{21}^0(\omega) & S_{22}^0(\omega) & \ldots & S_{2N}^0(\omega) \\ \ldots & \ldots & \ldots & \ldots \\ S_{N1}^0(\omega) & S_{N2}^0(\omega) & \ldots & S_{NN}^0(\omega) \end{bmatrix} \tag{4.34}$$

In Eq. 4.33, $R_{jj}^0(\tau) : j = 1,2,\ldots,N$, the diagonal terms of cross-correlation matrix represent the autocorrelation functions and the off-diagonal elements, $R_{jm}^0(\tau), j = m = 1,2,\ldots,N : j \neq m$ represent the cross-correlation functions of the stochastic process. Due to the stationary hypothesis, the following relations are valid:

$$R_{jj}^0(\tau) = R_{jj}^0(-\tau), j = 1,2,\ldots,N \tag{4.35}$$

$$R_{jm}^0(\tau) = R_{mj}^0(-\tau), j = m = 1,2,\ldots,N; j \neq m \tag{4.36}$$

The elements of cross-correlation matrix are related to the corresponding elements of the cross-spectral density matrix through Wiener-Khintchine

transformation (τ is the time lag and ω is the frequency)

$$S^0_{jm}(\omega) = \frac{1}{2\pi}\int_{-\infty}^{\infty} R^0_{jm}(\tau)e^{-i\omega\tau}d\tau, j,m = 1,2,\ldots N \tag{4.37}$$

$$R^0_{jm}(\tau) = \int_{-\infty}^{\infty} S^0_{jm}(\omega)\, e^{-i\omega\tau}d\omega, j,m = 1,2,\ldots,N \tag{4.38}$$

In Eq. 4.34, the diagonal elements of the cross-spectral density matrix, $S^0_{jj}(\omega), j = 1,2,\ldots,N$ represent the power spectral density function of the stochastic process and the off-diagonal elements $S^0_{jm}(\omega);\ j,k = 1,2,\ldots,N;\ j \neq k$ correspond to the cross-spectral density functions. The power density function is a real and positive function of ω, the cross-spectral density function is generally complex function of ω. Because of Eqs. 4.35-4.38, the following relations are valid:

$$S^0_{jj}(\omega) = S^0_{jj}(-\omega), j = 1,2.,\ldots,N \tag{4.39}$$

$$S^0_{jm}(\omega) = S^{0*}_{jm}(-\omega), j,m = 1,2,\ldots,N; j \neq m \tag{4.40}$$

$$S^0_{jm}(\omega) = S^{0*}_{mj}(\omega);\ \ j,m = 1,2,\ldots,N;\ \ j \neq m \tag{4.41}$$

where the asterisk denotes the complex conjugate. Equation 4.41 indicates that the cross-spectral density matrix $[S^0(\omega)]$ is Hermitian. As per Shinozuka (1987), $[S^0(\omega)]$ is positive definite also.

To simulate the stationary stochastic process $\left\{f^0_j(t)\right\}$, j=1, 2, ...N, first its cross-spectral density matrix $[S^0(\omega)]$ must be decomposed into the following product:

$$\left[S^0(\omega)\right] = \left[H(\omega)\right]\left[H^{T*}(\omega)\right] \tag{4.42}$$

The decomposition can be performed using Cholesky's method, in which $[H(\omega)]$ is a lower triangular matrix given by:

$$[H(\omega)] = \begin{bmatrix} H_{11}(\omega) & 0 & \dots & 0 \\ H_{21}(\omega) & H_{22}(\omega) & \dots & 0 \\ \dots & \dots & \dots & \dots \\ H_{N1}(\omega) & H_{N2}(\omega) & \dots & H_{NN}(\omega) \end{bmatrix} \tag{4.43}$$

As $[S^0(\omega)]$ is usually a complex matrix, $[H(\omega)]$ is generally a complex matrix whose diagonal elements are real positive functions of ω, while non zero off-diagonal elements are complex function of ω. The following relations are valid for the elements of matrix $[H(\omega)]$:

$$H_{jj}(\omega) = H_{jj}(-\omega), j = 1,2,3,\dots N \tag{4.44}$$

$$H_{jm}(\omega) = H^*_{jm}(-\omega), j = 1,2,\dots,N, m = 1,2,\dots j-1 \tag{4.45}$$

If the off-diagonal elements are written in polar form as:

$$H_{jm} = \left|H_{jm}(\omega)\right| e^{i\theta_{jm}(\omega)}, j = 1,2,\dots,N, m = 1,2,\dots,j-1 \tag{4.46}$$

where θ_{jm} = complex angle of $H_{jm}(\omega)$ and is given by

$$\theta_{jm}(\omega) = \tan^{-1}\left\{\frac{\mathrm{Im}\left[H_{jm}(\omega)\right]}{\mathrm{Re}\left[H_{jm}(\omega)\right]}\right\} \tag{4.47}$$

With Im and Re as the imaginary and real parts respectively of a complex number, Eq. 4.45 is written equivalently as:

$$\left|H_{jm}(\omega)\right| = \left|H_{jm}(-\omega)\right|; j = 1,2,\dots N, m = 1,2,\dots,j-1; j > k \tag{4.48}$$

$$\theta_{jm}(\omega) = -\theta_{jm}(-\omega); j = 1,2,\dots,N, m = 1,2,\dots,j-1; j > k \tag{4.49}$$

According to Shinozuka *et al* (1989), the period of the simulated sample function will be sufficiently large, if we let

$$\omega_{ml} = (l-1)\Delta\omega + \frac{m}{N}\Delta\omega, \quad l = 1,2,\dots,\overline{N} \tag{4.50}$$

Also for sufficiently large values of $\overline{N}$, the simulated random process matches with the target process if the time step satisfies the following condition:

$$\Delta t \leq \frac{2\pi}{2\omega_{up}} \tag{4.51}$$

The period of the simulated process is determined by the formula

$$T_0 = \frac{2\pi N}{\Delta\omega} = \frac{2\pi N\bar{N}}{\omega_{up}} \tag{4.52}$$

Once $[S^0(\omega)]$ is decomposed in accordance with Eqs. 4.42 and 4.43, according to Shinozuka and Jan (1972), the stochastic process $\{f_j^0(t)\}\, j = 1,2,3,\ldots N$ can be simulated by the following series as $\bar{N} \to \infty$.

$$f_j(t) = \sqrt{2(\Delta\omega)}\sum_{m=1}^{j}\sum_{l=1}^{\bar{N}}\left|H_{jm}(\omega_{ml})\cos(\omega_{ml}t - \theta_{jm}(\omega_{ml}) + \varphi_{ml}\right), \text{j=1,2,...N} \tag{4.53}$$

$\bar{N}$ is a sufficiently large number, $\Delta\omega = (\omega_{up}/\bar{N})$ is the frequency increment, ω_{up} = upper cut off frequency, with the condition that when $\omega > \omega_{up}$, the value of $S^0(\omega)$ is too small and can be ignored. $\varphi_{1l}, \varphi_{2l}, \ldots, \varphi_{jl}$ are sequences of independent random phase angles, distributed over the interval 0 to 2π; $H_{jm}(\omega_{ml})$ is a typical element of matrix $[H(\omega)]$, which is defined by Cholesky's decomposition of cross spectral density matrix $[S^0(\omega)]$.

The ergodicity of the results of Eq. 4.53 has been proved by Deodatis (1996).

4.4.2 Application of Explicit Form for Cholesky's Decomposition in Spectral Representation Method

As seen in the previous section, the cross-spectral density matrix $[S^0(\omega)]$ is usually a complex matrix; hence the Cholesky's decomposition is tedious and often turns to recursion formulae. Since $[H(\omega)]$ is a function of ω, it can be seen from the structure of Eq. 4.53 that the Cholesky's decomposition has to be calculated separately for every frequency ω_{ml}. Moreover, it must be calculated once more when another cosine term is added. This involves lot of computation and time taken for generation of

stochastic process is enormous. Hence for long span bridges, Cao *et al* (2000) introduced simplification by expressing the Cholesky's decomposition using several explicit algebraic formulae, so that the time for computation could be reduced considerably. When the turbulent wind velocity field acting on a long–span cable stayed bridge is simulated, the velocity can be treated as a one–dimensional, multivariate Gaussian process. It could be assumed that the spectra of wind velocities are not varying along the span length of the bridge. Then the power spectra of all nodal points on the bridge deck are the same. Further, as the orthogonal spectrum of wind fluctuations is very small in atmosphere, it could be omitted. Hence $S_{ij}^{0}(\omega)$ could be treated as real and $[S^0(\omega)]$ could be treated as a real matrix. Also, the following relationships are valid:

$$S_{11}^{0}(\omega) = S_{22}^{0}(\omega) = \ldots = S_{NN}^{0}(\omega) = S(\omega) \tag{4.54}$$

and $$S_{jm}^{0}(\omega) = \sqrt{S_{jj}^{0}(\omega) S_{mm}^{0}(\omega)}\ Coh(\Delta_{jm,}\omega) = S(\omega) Coh(\Delta_{jm,}\omega)$$

$$j,m=1,2,\ldots,N;\ j\neq m \tag{4.55}$$

Where Δ_{jm} is the horizontal distance from point j to m; and $\mathrm{Coh}(\Delta_{jm,}\omega)$ is the coherence function between the points j and m.

By adopting the model suggested by Davenport (1968), the coherence function can be obtained with the following equation:

$$Coh(\Delta_{jm,}\omega) = \exp\left(\frac{\lambda\omega\Delta_{jm}}{2\pi U(z)}\right) \tag{4.56}$$

Considering there are 'np' equally spaced points on the bridge deck with a distance of Δ between the successive points, then $\Delta_{jm} = \Delta(j-m)$ when j>m, or $\Delta_{jm} = \Delta(m-j)$ when m>j. Thus $\Delta_{jm} = \Delta|j-m|$. It can be shown that

$$Coh(\Delta_{jm,}\omega) = \exp\left(\frac{\lambda\omega\Delta|j-m|}{2\pi U(z)}\right) = \left(\exp\left(\frac{\lambda\omega\Delta}{2\pi U(z)}\right)\right)^{|j-m|} = C^{|j-m|} \tag{4.57}$$

Where λ is taken between 8 and 10; U(z) is the mean wind velocity at bridge deck level 'z' above the ground and C is a function of ω and is computed by the expression :

$$C = \exp\left(\frac{\lambda\omega\Delta}{2\pi U(z)}\right) \tag{4.58}$$

This Equation is analogous to Eq. 4.20 described in Section 4.2.2.4.

Using the Eqs. 4.54 to 4.58, the cross-spectrum matrix can be written as:

$$\left[S^0(\omega)\right] = S(\omega)\begin{bmatrix} 1 & C & C^2 & \dots & C^{N-1} \\ C & 1 & C & \dots & C^{N-2} \\ C^2 & C & 1 & \dots & C^{N-3} \\ \dots & \dots & \dots & \dots & \dots \\ C^{N-1} & C^{N-2} & C^{N-3} & \dots & 1 \end{bmatrix} \tag{4.59}$$

In Eq. 4.59 $\left[S^0(\omega)\right]$ is expressed in the form of an exponentially decayed matrix. It can be proved using mathematical induction that the Cholesky's decomposition of H(ω) of Eq. 4.59 can be expressed using explicit algebraic formulae(Cao *et al*, 2000); thus

$$H(\omega) = \sqrt{S(\omega)}\,\mathrm{G}(\omega) \tag{4.60}$$

where

$$\left[G(\omega)\right] = \begin{bmatrix} 1 & 0 & 0 & 0 & 0 & 0 \\ C & \sqrt{1-C^2} & 0 & 0 & 0 & 0 \\ C^2 & C\sqrt{1-C^2} & \sqrt{1-C^2} & 0 & 0 & 0 \\ C^3 & C^2\sqrt{1-C^2} & C\sqrt{1-C^2} & \sqrt{1-C^2} & 0 & 0 \\ \dots & \dots & \dots & \dots & \dots & \dots \\ C^{N-1} & C^{N-2}\sqrt{1-C^2} & C^{N-3}\sqrt{1-C^2} & C^{N-4}\sqrt{1-C^2} & \dots & \sqrt{1-C^2} \end{bmatrix} \tag{4.61}$$

[G(ω)] can also be expressed in an explicit form with algebraic formulae as:

$$G_{jm}(\omega) = 0 \qquad \text{when } 1 \le j < m \le N \tag{4.62}$$

$$G_{jm}(\omega) = C^{|j-m|} \qquad \text{when } m = 1, m \le j \le N \tag{4.63}$$

$$G_{jm}(\omega) = C^{|j-m|}\sqrt{(1-C^2)} \qquad \text{when } 2 \le m \le j \le N \tag{4.64}$$

The proof of Cholesky's decomposition of cross-spectral density matrix by explicit algebraic expressions using Eqs. 4.61 to 4.64 has been presented using the method of mathematical induction in Appendix –II.

As $0 < C < 1, \sqrt{\left(1 - C^2\right)}$ must be positive real number, H(ω) is a real matrix and it can be proved that

$$H^{T^*}(\omega) = H^T(\omega) \tag{4.65}$$

$$\theta_{jm}(\omega) = 0 \tag{4.66}$$

It is clear that H(ω), can be computed accurately for each ω_{ml}, using Eqs. 4.62 to 4.64 and Eq. 4.53 can be rewritten as follows:

$$f_j(t) = \sqrt{2(\Delta\omega)} \sum_{m=1}^{j} \sum_{l=1}^{\bar{N}} \sqrt{S(\omega_{ml})}\, G_{jm}(\omega_{ml}) \cos(\omega_{ml} t + \varphi_{ml}), j = 1,2,\ldots,N \tag{4.67}$$

The simulation of wind velocity field on the long span bridge is simplified, when we use Eq. 4.67 together with Eqs. 4.58, 4.61 to 4.64.

The step-by–step procedure for simulation of longitudinal and vertical velocity fluctuations are presented in the following section.

4.4.3 Simulation Procedure

In the present study, the following simulation procedure has been adopted for generation of turbulent velocity field along span length of long span cable stayed bridges using spectral representation method.

(i) Input the data related to bridge such as height of bridge deck above mean ground level, number of points along the span where the wind velocity field is to be generated, distance Δ between these points in metres, and data related to wind such as mean wind speed U in m/sec at deck level, surface roughness factor z_0 (Table 4.1) and decay factors for longitudinal and vertical velocity fluctuations λ_u and λ_w respectively.

(ii) Generation of velocity fluctuations u(x, t) and w(x, t) by spectral representation method, which consists of the following steps:

- Estimation of cross-spectral density matrix using Eqs. 4.54 and 4.55.
- Decomposition of cross-spectral density matrix by Cholesky decomposition or explicit algebraic expressions using Eqs. 4.60 to 4.64.
- Generation of 'n' sets of random phase angles in the range of 0 -2π with uniform density function 1/2π. Compute the mean and variance of the random phase angle and see if they match with the stipulated values for uniformly distributed random numbers with density function 1/2π.

The mean, expectation or average value (m_f) and variance (σ_f^2) of N-samples of data sequence $\{f_k\}$ is computed as:

$$m_f = \frac{1}{N}\sum_{k=0}^{N-1} f_k \tag{4.68}$$

$$\sigma_f^2 = \frac{1}{N-1}\left[\sum_{k=0}^{N-1} f_k^2 - N m_f^2\right] \tag{4.69}$$

- Estimation of random wind velocity field by Eq. 4.67.
- Compute the mean and variance of generated wind velocity using Eqs. 4.68 and 4.69. Mean of the velocity fluctuations has to be zero and using the variance the turbulence intensity of the longitudinal/vertical fluctuations for a particular terrain category and height are estimated. The turbulence intensity of generated wind and target wind should match.
- Check the spectral density match between the target and generated wind velocity field. For that, power spectral density of generated wind velocity field has been estimated by average periodogram method, which uses Discrete Fourier Transform (DFT) of each segment using Hamming window given by:

$$w_k = 0.54 - 0.46\cos\frac{2k\pi}{N-1} \tag{4.70}$$

- Compute the peak factor of the velocity fluctuations using Eqs. 4.29 and 4.30. This should be in the range of 3 to 5.
- For the generated wind fluctuations obtain the autocorrelation and cross-correlation estimates. In the present study they have been estimated via direct computation as discussed in Bendat and Piersol (1971) and are given below:

  For N stationary data values of $\{f_k\}$, k=1, 2,..,N, the estimated autocorrelation function at the displacement rh is defined by the formula

$$\hat{R}_r = \hat{R}_f(rh) = \frac{1}{N-r}\sum_{k=1}^{N-r} f_k f_{k+r}, r = 0,1,2,\ldots,m \tag{4.71}$$

  where r is the lag number, m is the maximum lag number, and $\hat{R}_r$ is the estimate of true value of R_r at lag r, corresponding to the displacement rh and h is the sampling interval Δt given by Eq. 4.51.

  The cross-correlation estimates of two stationary random data series $\{f_k\}$ and $\{g_k\}$ are defined as:

$$\hat{R}_{fg}(rh) = \frac{1}{N-r}\sum_{k=1}^{N-r} f_k g_{k+r} \tag{4.72}$$

$$\hat{R}_{gf}(rh) = \frac{1}{N-r}\sum_{k=1}^{N-r} g_k f_{k+r} \tag{4.73}$$

  Check for autocorrelation and cross-correlation function match for the generated and target wind field respectively.

(iii) Generation of time dependent mean wind U(z, t) by adding value of mean wind speed to white noise.

  The generated wind velocity field is given by

$$\overline{U}(z,t) = \sqrt{(U(z,t)+u(x,t))^2 + w(x,t)^2} \tag{4.74}$$

  and the angle of attack by

$$\alpha_w = \frac{w(x,t)}{\overline{U}(z,t)} \tag{4.75}$$

4.5 DETAILS OF SOFTWARE

A program WINGEN has been developed for generation of stochastic wind field on long span cable stayed bridges assuming wind as a Gaussian process. The orgainisation of main program WINGEN along with subroutines WINDIN, MWIND, and KAIGENU and PANGNV is illustrated in Fig. 4.5. Simulation of longitudinal velocity fluctuations are described by Kaimal's spectrum. PANGENV produces simulation of vertical velocity fluctuations using Panofsky–McCormick Spectrum. Besides, other eight routines are based on digital signal processing.

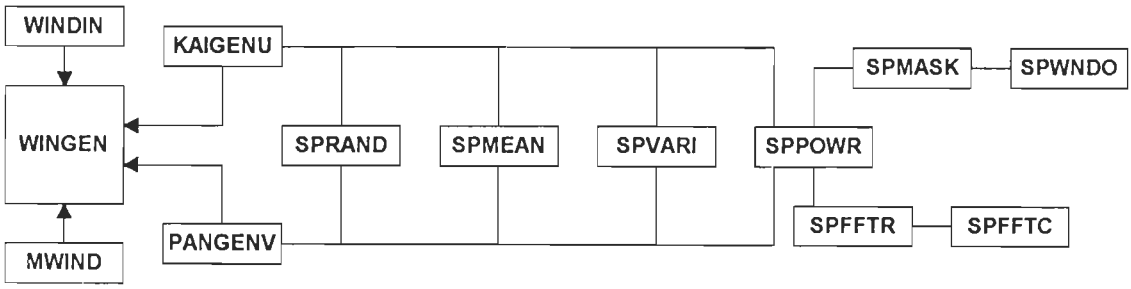

Fig. 4.5 : Schematic Diagram for WINGEN-Digital Simulation of Stochastic Wind Field

WINGEN

The main program generates the wind velocity field along the span of a cable stayed bridge. The input requirement for WINGEN has been discussed in Section 4.4.3, Step (i) and entered through subroutine WINDIN.

It calls the subroutines MWIND, KAIGENU and PANGENV for simulation of time dependent mean wind velocity U(t), and the velocity fluctuations in two directions– longitudinal u(t) and vertical velocity w(t).

The output includes, u(t), w(t), mean, variance, turbulent intensity spectral density, peak factor, autocorrelation and cross-correlation functions of the generated wind field. To check the agreement between the target and generated wind fields, spectral estimate and correlations of the target spectra are also computed.

WINDIN

This routine takes the input data related to bridge and wind for simulation of wind velocity field. Data related to bridge are (i) height (z) of bridge deck about mean ground level, (ii) number of points along the span where the wind velocity field has to be simulated, (iii) distance (Δ) between these simulation points. The data related to wind are (iv) mean wind speed U(z) m/sec at deck level, (v) surface roughness parameter (z_o) indicating the terrain category (Table 4.1), (vi) decay coefficient for longitudinal velocity fluctuations and (vii) decay coefficient for vertical velocity fluctuations.

MWIND

This routine is called to obtain time dependent wind, U(t) by generating white noise and adding the value of mean wind speed.

KAIGENU

It generates the longitudinal velocity fluctuations using the simulation procedure described in Section 4.4.3, Steps (ii) and (iii), with one-sided Kaimal spectrum given by Eq. 4.16 as target spectrum.

PANGENV

It generates the vertical velocity fluctuations using the simulation procedure explained in Section 4.4.3 steps (ii) and (iii). It uses the one-sided Panofsky-McCormick spectrum given by Eq. 4.18 as target spectrum for generation of wind field. Both KAIGENU and PANGENV call SPRAND for obtaining the random phase angles defined in Eq. 4.53 and hence in Eq. 4.67. The routines SPMEAN and SPVARI are used for computing the mean and variance of random phase angles as well as generated turbulent fluctuations. Using the routine SPPOWR, spectral density of generated series is computed by average periodogram method as described by Welch (1967). These

signal-processing routines are based on algorithm described in Stearns and David (1988). Each of these subroutines is described below:

SPRAND

It is a routine that generates uniformly distributed random number between 0 and 1.0, used in generation of random noise sequence. The user initially sets the 'seed' of the random number generator.

It has been used to generate random phase angles in Eq. 4.67 in the range 0-2π, with uniform density function $1/2\pi$.

SPMEAN

The Function SPMEAN is used to estimate the primary statistical parameter namely mean of random data process. Eq. 4.68 describes the function of this routine. The input parameters required for this function are the data vector and number of samples.

It has been used to check the mean of random phase angles generated using SPRAND as well as to estimate the mean of longitudinal and vertical velocity fluctuations.

SPVARI

The function SPVARI is used to estimate variance of $\{x_k\}$, which is the most common measure of squared variation of data vector about its mean value m_x. Eq. 4.69 describes this routine. The standard deviation is the square root of variance. The input requirements for function SPVARI are the data vector and number of samples.

It has been used to check the variance of random phase angles generated using SPRAND as well as to estimate the variance and thereafter the turbulent intensity of the longitudinal and vertical velocity fluctuations given by Eqs. 4.6 and 4.8.

SPPOWR

It is a routine used to estimate power spectra of generated turbulent wind field using average periodogram method as described by Welch (1967).

The average periodogram is obtained by breaking the data sequence into segments of equal length, applying the data window to each segment, then computing the periodogram of windowed segment, and finally averaging the periodograms together. The segment of data may or may not be overlapped. In the present study, the segments are made to overlap, resulting in more segments and periodograms from the same data sequence.

SPPOWR uses a data window on each segment. A data window is a sequence of numbers that is multiplied by data segment before taking the FFT and its purpose is to smooth or shape the periodogram of the data segment. The application of data window is achieved through two data window routines. SPWNDO- a function subprogram that generates a single sample of selected data window and SPMASK – a subroutine that applies a selected data window to a given data vector. The two data window routines are described below.

SPWNDO

This routine is used to apply a single data window. There are six types of data windows included in this routine and are identified with numbers 1 to 6 namely, 1-rectangular, 2-tapered rectangular, 3-triangular, 4-hanning, 5-hamming and 6-Blackman. One of these data windows could be selected on the basis of the nature of random data sequence. For long stationary records, Hamming window is preferred and the same is used in the present study. The input requirement for Function **SPWNDO** is, a number to identify the type of window and number of data samples in a window.

SPMASK

This routine is used to apply a specified data window to a real data vector. The input requirement for **SPMASK** is - a number to indicate the type of data window, size of window and the data vector to be masked by data window.

SPPOWR uses SPFFTR to compute segment periodograms and accumulates the average periodogram by adding segment periodograms. The segment periodogram is defined as the squared magnitude of the Discrete Fourier Transform (DFT) of each segment of the data sequence. For example, given a real data vector $\{x_k\}$, the segment periodogram P_m is given as:

$$P_m = \frac{1}{N}|X_m|^2 \quad \text{m=0, 1, ...N/2} \tag{4.76}$$

where $$X_m = \sum_{k=0}^{N-1} x_k e^{-j(2\pi km/N)} \tag{4.77}$$

The input requirement for SPPOWR includes random data vector, indicator for the type of data window and fraction of each data segment, which is overlapped.

A requirement of this routine is that each data segment length must be a power of 2.

SPFFTR

This routine accomplishes the in-place transformation of a real sequence of length N in half the storage required by SPFFTC using a method given by Brigham (1974). In Brigham's method, the original real data sequence of N points is viewed as a complex sequence of N/2 points, so that,

$$\{x_0, x_1, \ldots, x_{N-1}\} = \{v_0, v_1, \ldots, v_{N/2-1}\} \tag{4.78}$$

In the complex sequence, $\{v_k\}$, the real and imaginary part of v_0 is x_0 and x_1 respectively. The complex routine SPFFTC is then used to take N/2-point transform of $\{v_k\}$, replacing $\{x_k\}$ with:

$$\{V_m\} = \{V_0, V_1, \ldots, V_{N/2-1}\} \tag{4.79}$$

The desired transform $\{X_m\}$ can be obtained from $\{V_m\}$ in accordance with Brigham's expressions as follows:

$$\begin{Bmatrix} X_m \\ X^*_{N/2-m} \end{Bmatrix} = \frac{1}{2}\begin{bmatrix} (1-U_m)(1+U_m) \\ (1+U_m)(1-U_m) \end{bmatrix}\begin{Bmatrix} V_m \\ V^*_{N/2-m} \end{Bmatrix} \tag{4.80}$$

where $U_m = j\,exp(-j2\pi m/N) = sin(2\pi m/N) + j\,cos(2\pi m/N)$ (4.81)

Thus, SPFFTR accomplishes the transformation of $\{x_k\}$ using, Eq. 4.80 and the routine SPFFTC, the details of which are given below.

SPFFTC

This routine performs Fast Fourier Transform of complex data sequence. The algorithm implemented in this routine is the symmetric Cooley-Tukey (1965) algorithm based on time decomposition with input bit reversal. The algorithm is discussed in detail by Bergland (1969), Brigham (1974) and Oppenheim and Schafer (1975).

4.6 VALIDATION OF SOFTWARE

To ensure the accuracy of the wind field generated by WINGEN, several checks have been applied and are discussed below.

As the spectral representation method generates the wind field using random phase angles, sensitivity of wind loads to random numbers has been discussed by Suresh Kumar (2000). However, it was shown that Gaussian wind fields are not sensitive to the random numbers generated. To check this aspect in the present study, the random phase angles of Eq. 4.67 were generated by two methods – first set, using random numbers between 0 and 2π with uniform density function $1/2\pi$ and second set, using random numbers between $-\pi$ and $+\pi$ with uniform density function $1/2\pi$. Again, to generate the first set, uniform random numbers in the range 0 to 1 and for second set, uniform random numbers between $-1/2$ to $+1/2$ were used. The statistical parameters of the longitudinal velocity fluctuations generated with the two different sets of random

phase angles were compared with the target values and good agreement between the values was observed. The first set of random phase angles has been used in the subsequent wind analysis.

The testing of KAIGENU and PANGENV was carried out by changing the height above ground level, mean wind speed and terrain surface roughness parameter. The statistical parameters, such as power spectral density, turbulence intensity and autocorrelation of generated and target wind, showed good agreement. The estimated peak factor of the generated fluctuations was between 3 and 5. From these studies, the accuracy of simulation is ensured.

To validate the spectral representation algorithm discussed earlier, the example illustrated by Cao *et al* (2000) is taken. The problem consists of generation of artificial wind velocity field for Jiangyin Bridge, which is a suspension bridge (Fig. 4.6) with a main span of 1385m across Yangtze River in Jiangsu Province, P.R. China.

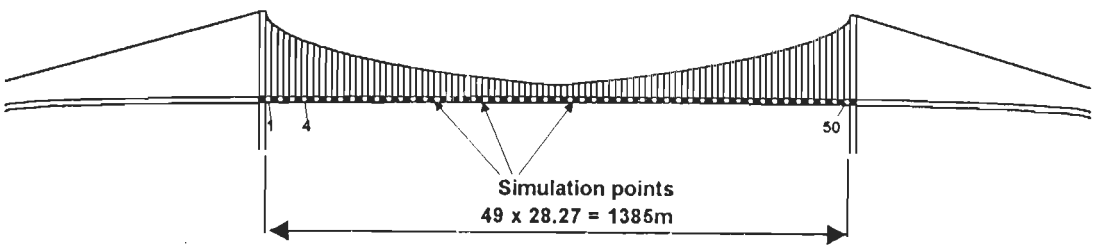

Fig. 4.6 : Jiangyin Bridge with Main Span of 1385 m

The wind velocity field on bridge deck is assumed to be composed of 50 wind velocity waves at 50 different points uniformly distributed along the bridge. The distance between the successive points is 28.27m. The main data of the bridge and of simulating conditions are as follows:

Height of deck above ground (z) = 50m

Surface roughness parameter (z_0) = 0.03m

Average velocity on the deck U(z) = 40m/sec

Number of simulation points	=	50
Interval between the points Δ	=	28.27m
Upper cut off frequency	=	4π rad/sec (2 Hz)
Dividing number of frequency $\overline{N}$	=	1024
Time interval	=	0.25sec
Duration of record T_0	=	512sec

The one-sided target spectrum for longitudinal fluctuations, Kaimal spectrum expressed in terms of circular frequency 'ω', after substituting the relevant parameters pertaining to this example, is written as follows:

$$S_u(\omega) = \frac{185}{(1+9.95\omega)^{5/3}} m^2/(s.rad) \tag{4.82}$$

The one-sided target wind spectrum for vertical velocity fluctuations, Panofsky-McCormick spectrum expressed in terms of 'ω' and using the values of z, z_0, u_*, relevant to this example is written as:

$$S_w(\omega) = \frac{5.552}{(1+0.795\omega)^2} m^2/(s.rad) \tag{4.83}$$

After generating the longitudinal wind fluctuations in wind using WINGEN, it was found that the mean components of the fluctuations are zero and the variance of the longitudinal and vertical fluctuations are 27.64 and 8.32 at point 1. Thus the values of turbulence intensities generated are 13.14% and 7.2% in longitudinal and vertical directions respectively. The friction velocity for target wind is estimated as 2.156m/sec using Eq. 4. 4. From Table 4.2, the value of β corresponding to z_0=0.03m is taken as 6. Using Eqs. 4.9, 4.6 and 4.8, the target longitudinal and vertical turbulence intensities are estimated as 13.2% and 8.15% respectively. Close agreement of turbulence intensities of generated and target wind is observed.

In the present study, the power spectra of the generated wind are calculated by the average periodogram method, whereas Cao *et al* used FFT technique. The spectral match between the target and simulated wind is shown in Fig. 4.7(a) and (b). It can be

observed from the figures that the simulated spectra nearly coincide with the target Spectrum except for very low frequency values. As the low frequency portion of the wind velocity waves exerts very little influence on the buffeting response of the bridge, this simulation result has been considered satisfactory.

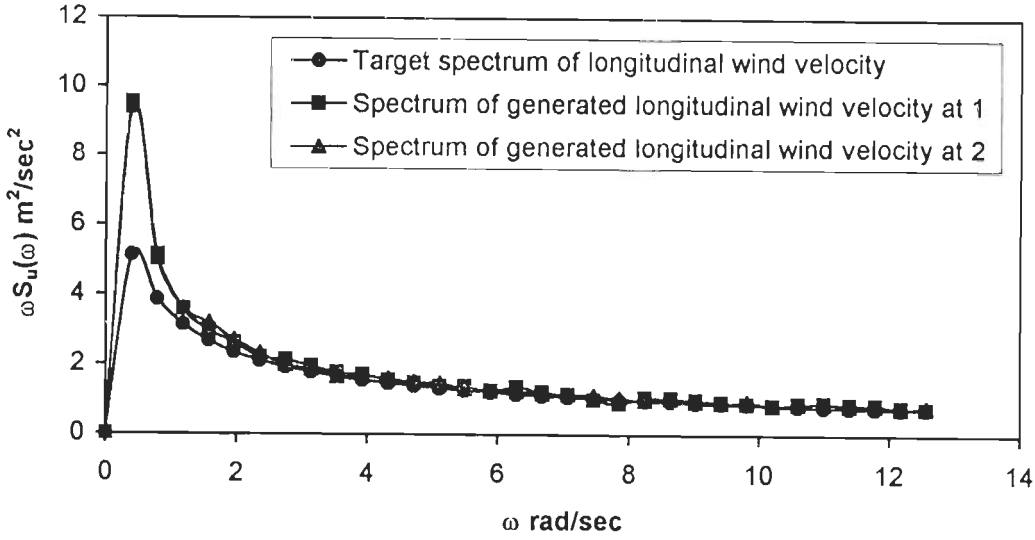

(a) For longitudinal velocity fluctuations

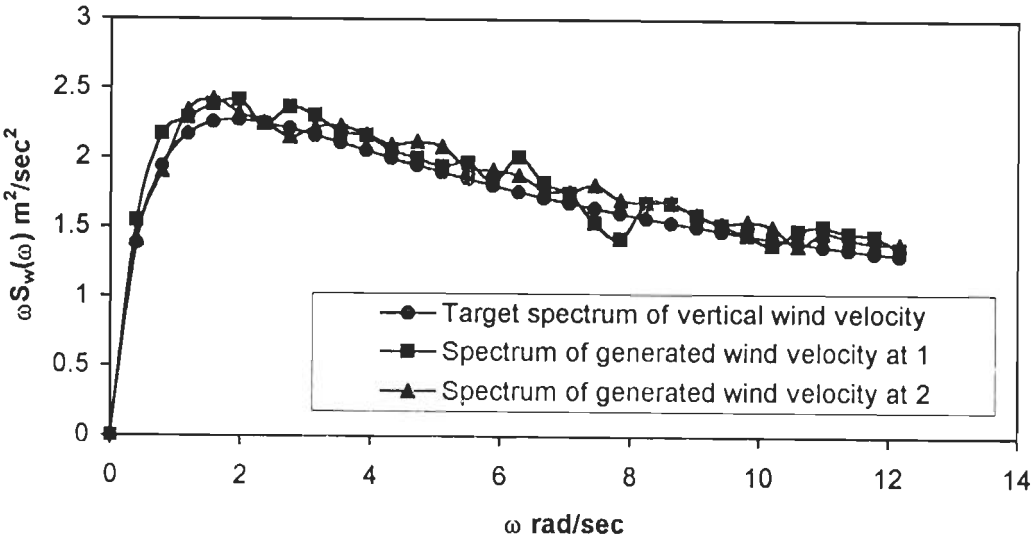

(b) For vertical velocity fluctuations

Fig. 4.7 : Spectral Density Functions for Simulated Wind Field of Jiangyin Bridge

The correlation functions of simulated wind velocities at points 1, 2 are shown in Fig. 4.8. The numerical values of longitudinal velocity spectrum and autocorrelation of generated wind at location 1 match closely with the target wind spectrum given by Eq. 4.82 as well as autocorrelation as discussed by Liu and Wang (2001).

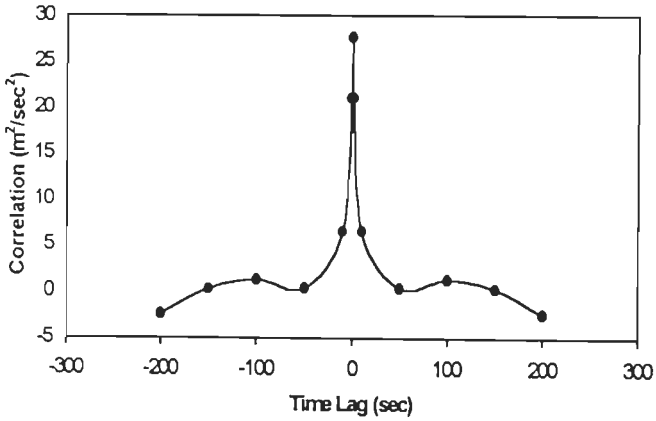

(a) Autocorrelation of u(t) at 1

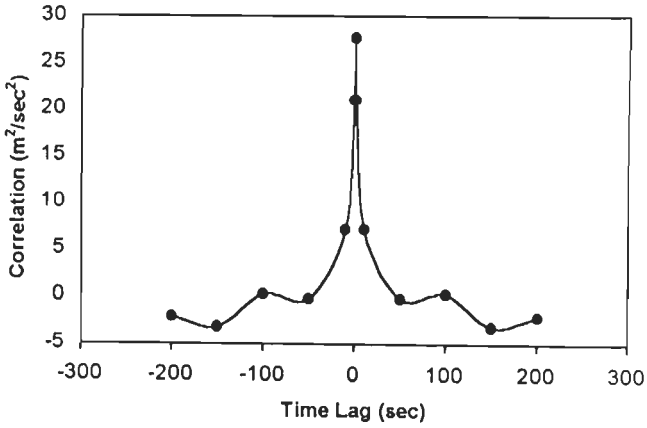

(b) Autocorrelation of u(t) at 2

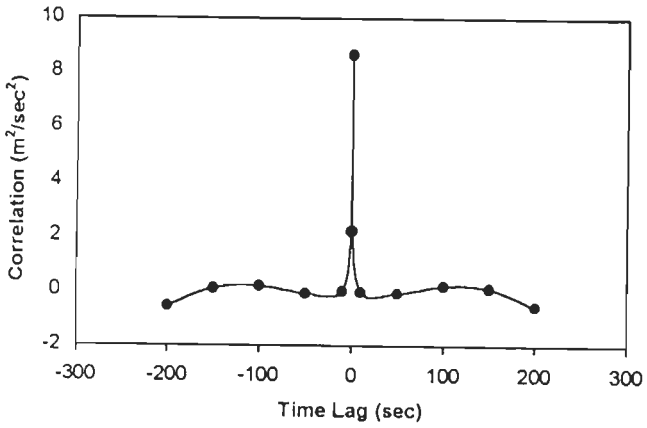

(c) Autocorrelation of w(t) at 1

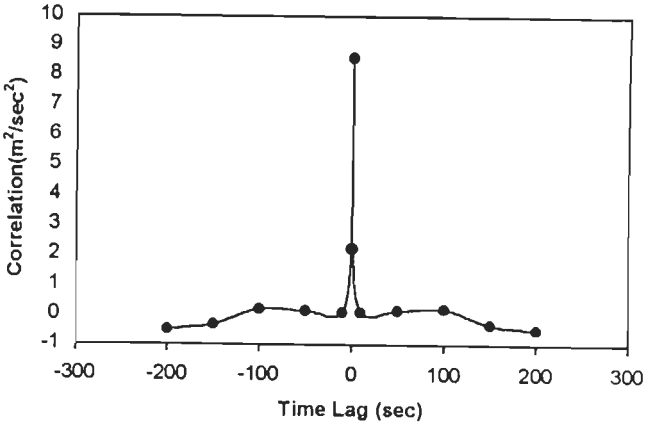

(d) Autocorrelation of u(t) at 2

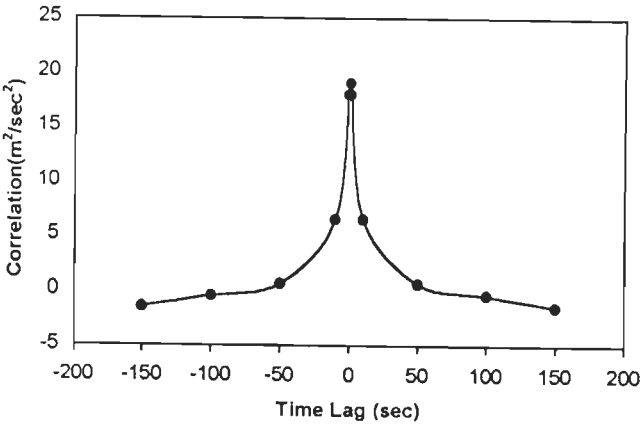

(e) Cross-correlation of longitudinal velocity fluctuations between 1 and 2

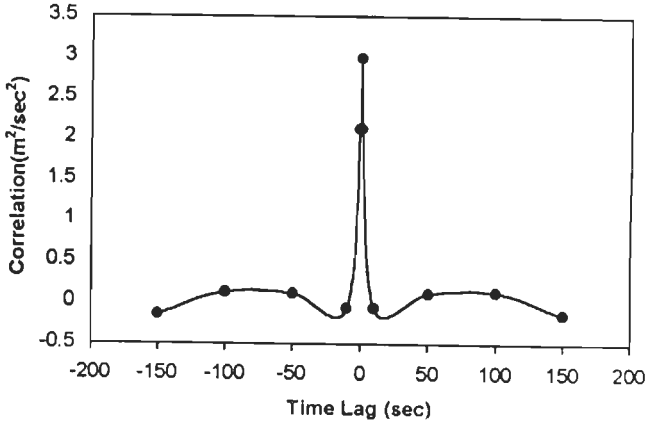

(f) Cross-correlation of vertical velocity fluctuations between 1 and 2

Fig. 4.8 : Correlation Functions for Simulated Wind Field for Jiangyin Bridge

The simulated wind fluctuations in u and v directions at points 1 and 2 obtained by Eq. 4.67. The generated turbulent wind field and angle of attack given by Eqs. 4.74 and 4.75 respectively at points 1 are illustrated in Fig. 4.9. It can be seen that the wind velocities at the points 1 and 2 are strongly correlated, since they are close to each other, while lesser correlation was observed as the distance between the points increases. Further, the peak factor for longitudinal and vertical fluctuations of the generated wind estimated using Eq. 4.29 and 4.30 is 3.979 and 4.060 against the target values of 3.996 and 4.053 respectively.

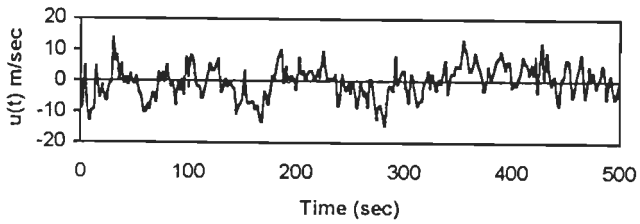

(a) Longitudinal Velocity Fluctuation at 1

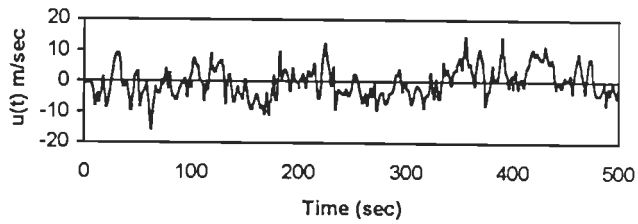

(b) Longitudinal Velocity Fluctuation at 2

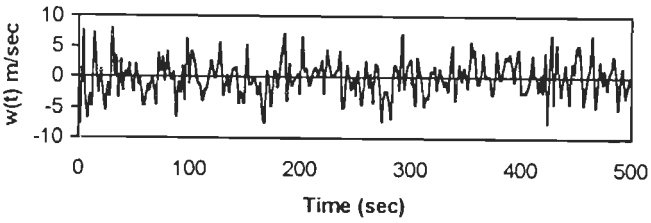

(c) Vertical Velocity Fluctuation at 1

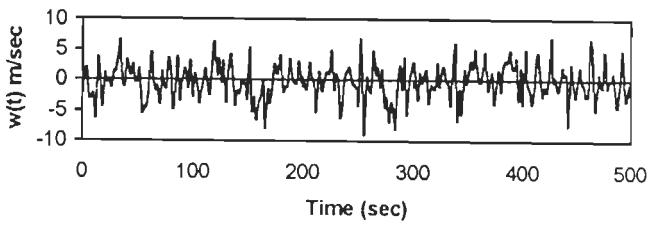

(d) Vertical Velocity Fluctuation at 2

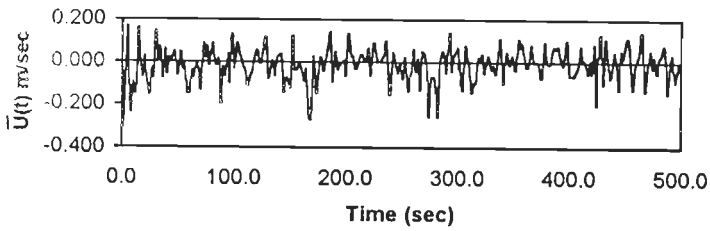

(e) Generated turbulent wind velocity at 1

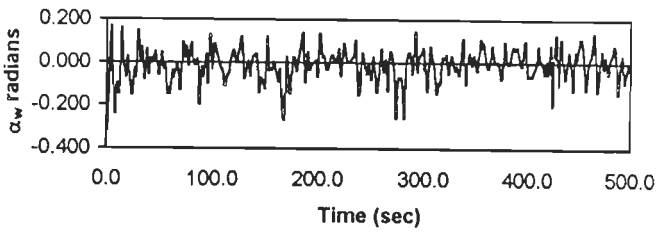

(f) Wind angle of generated turbulent wind velocity

Fig. 4.9 : Digitally Simulated Turbulent Wind Field for Jiangyin Bridge

From the above results the validation of WINGEN, the computer software developed for generation of spatially correlated wind field along the span of a long span bridge, is thus established.

4.7 SUMMARY

This chapter is devoted to digital simulation of stochastic wind field along the span of long span cable stayed bridges. An efficient algorithm for generation of wind velocity field on long span bridges using Kaimal spectrum and Panofsky- McCormick Spectrum as target spectrum for longitudinal and vertical velocity fluctuations respectively is described. The theoretical background of spectral representation method is explained along with the details of software developed. The software has been validated by generating the turbulent wind field for Jiangyin Bridge, China with a main span of 1385m. From the results it is established that the proposed method is accurate and efficient for simulation of turbulent wind fluctuations in atmosphere required for the time domain wind analysis of long span flexible bridges.

The digitally simulated wind velocity field has been used for generation of instantaneous buffeting force along the span of bridge as explained in Chapter 5 and thereafter for time domain buffeting analysis of three span and five span cable stayed bridges in Chapter 6 and 7 respectively.

Chapter 5

TIME DOMAIN BUFFETING ANALYSIS

5.1 INTRODUCTION

This chapter describes the formulations for time domain buffeting analysis of cable stayed bridges subjected to simulated buffeting forces along the span. The advancements in the formulations for buffeting forces and their applications in the present study are discussed. The instantaneous buffeting forces in the along-wind, and across-wind directions and in torsion are computed using a spatially correlated turbulent wind field generated by spectral representation method, as described in the previous chapter. Other important aerodynamic parameters used in computation of buffeting forces such as steady-state force coefficients and aerodynamic admittance functions for bridge decks are also discussed.

Time domain analyses of four cable stayed bridges under digitally simulated buffeting forces have been performed in the present study using modal superposition method. The step-by-step integration of equations of motion is achieved through Wilson-θ method, which has also been discussed. The method used for validating the time domain buffeting analysis has also been explained. Numerical examples illustrating the time domain buffeting analysis for three and five span cable stayed bridges are given in Chapters 6 and 7 respectively.

5.2 AERODYNAMIC FORCES

As seen in the previous chapter, the wind velocity at any one point of the bridge is composed of three components: the mean component U and the fluctuating components u(x, t) and w(x, t) in the along–wind and vertical directions respectively. These three components impose forces namely; drag D, lift L and moment M, as depicted in Fig. 5.1.

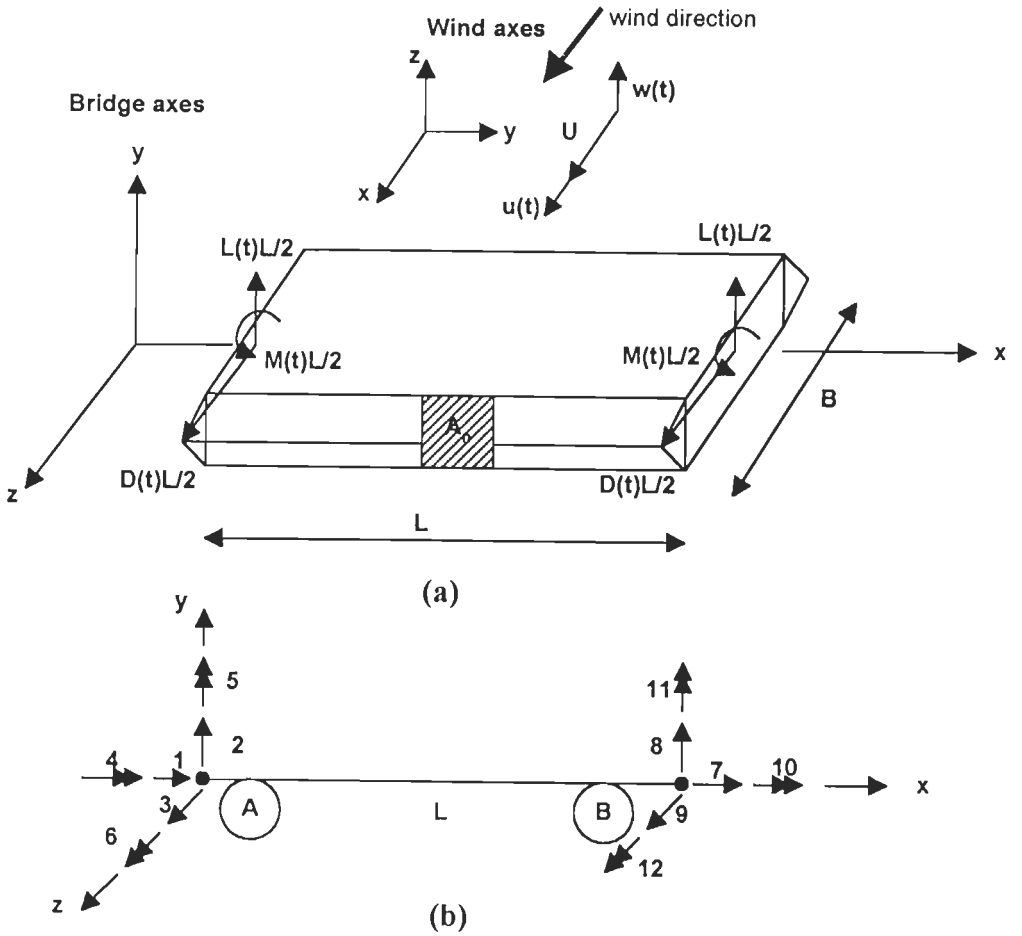

Fig. 5.1: (a) Lumped Aerodynamic Forces; (b) Degrees of Freedom of Beam Element

Generally, these total aerodynamic forces are made up of the steady-state wind forces, the buffeting forces and self-excited or aeroelastic forces. However, the steady-state wind forces are only related to the mean part of the oncoming wind flow and are assumed to act on the bridge deck at all times during the buffeting action. Therefore, these can be regarded as the static loads, which only shift the bridge's equilibrium position to a new position and do not directly affect the buffeting responses. Therefore, in the present study, for the buffeting analysis the effect of steady-state wind forces is not taken into account.

In the study of long span flexible bridges, generally the aerodynamic forces, that is, drag, lift and moment per unit span are expressed as sum of buffeting forces, due to turbulence present in the flow and aeroelastic or self-excited part (Scanlan and Jones, 1991):

$$D = D_b + D_{ae} \tag{5.1}$$

$$L = L_b + L_{ae} \tag{5.2}$$

$$M = M_b + M_{ae} \tag{5.3}$$

in which subscripts *b* and *ae* refer to buffeting and aeroelastic components respectively. The description of buffeting forces is given in the following section.

5.2.1 Buffeting Forces

The buffeting forces are caused by the fluctuating part of wind velocity of which the along wind component *u(x, t)* and vertical component *w(x,t)* are much smaller than the mean wind velocity *U*. By neglecting the u^2, w^2 and *uw*, buffeting loads - drag, lift and moment per unit span - can be expressed according to the quasi-steady theory as follows:

$$D_b = \frac{1}{2}\rho U^2 B\left[2C_D\frac{u(x,t)}{U} + C_D'\frac{w(x,t)}{U}\right] \tag{5.4}$$

$$L_b = \frac{1}{2}\rho U^2 B\left[2C_L\frac{u(x,t)}{U} + (C_L' + C_D)\frac{w(x,t)}{U}\right] \tag{5.5}$$

$$M_b = \frac{1}{2}\rho U^2 B^2\left[2C_M\frac{u(x,t)}{U} + C_M'\frac{w(x,t)}{U}\right] \tag{5.6}$$

where $C_L' = \frac{dC_L}{d\alpha_w}$, $C_D' = \frac{dC_D}{d\alpha_w}$, $C_M' = \frac{dC_M}{d\alpha_w}$ (5.7)

In some cases the above buffeting force descriptions have proven to be adequate, but in others it has been found indispensable for accuracy, to modify them through multiplication by frequency–dependent terms called aerodynamic admittances. This was found necessary because the fixed steady-state force coefficients do not account for the relatively rapidly time varying gust velocities that are agitating the bridge system. The methods of evaluating the aerodynamic admittances have been discussed by Davenport (1962), Holmes (1975), Walshe and Wyatt (1983), Davenport

et al (1992) and Grillaud *et al* (1992) for wind forces acting on bridge decks. The description for buffeting forces, modified using the aerodynamic admittance functions as discussed by Chen *et al* (2000), are given as follows:

$$D_b = \frac{1}{2}\rho U^2 B\left[2C_D\chi_{Dbu}\frac{u(x,t)}{U} + C'_D\chi_{Dbw}\frac{w(x,t)}{U}\right] \tag{5.8}$$

$$L_b = \frac{1}{2}\rho U^2 B\left[2C_L\chi_{Lbu}\frac{u(x,t)}{U} + (C'_L + C_D)\chi_{Lbw}\frac{w(x,t)}{U}\right] \tag{5.9}$$

$$M_b = \frac{1}{2}\rho U^2 B^2\left[2C_M\chi_{Mbu}\frac{u(x,t)}{U} + C'_M\chi_{Mbw}\frac{w(x,t)}{U}\right] \tag{5.10}$$

in which $\chi_{Lbu}, \chi_{Dbu}, \chi_{Mbu}, \chi_{Lbw}, \chi_{Dbw} and \chi_{Mbw}$ are the aerodynamic admittance functions. A detailed discussion on aerodynamic admittance functions is given in Section 5.2.1.2.

Apart from the generated wind velocity field *u(x,t)* and *w(x,t)*using spectral representation method as discussed in Chapter 4, other necessary parameters for evaluation of buffeting forces are the steady-state force coefficients C_D, C_L, C_M and their derivatives with respect to angle of attack of wind (α_w) as well as the aerodynamic admittance functions. These parameters for flexible bridge decks are discussed in the following sections.

5.2.1.1 Steady-state Force Coefficients

The steady-state force coefficients C_D, C_L and C_M for bridge decks are generally obtained by wind tunnel investigations. These force coefficients vary with deck geometrical shape, aspect ratio (B/d), turbulence in the approaching flow, Reynolds number, angle of attack and measuring techniques during wind tunnel studies. This is evident from the results of wind tunnel investigations reported by Wardlaw(1970), Walshe(1981), Walther(1988), Virloguex(1992), Barre and Barnard(1993) and so on. Further, a detailed study to understand the effect of these aspects on steady–state coefficients, based on the available wind tunnel results of bridge decks in literature, is presented by Lakshmy *et al* (1997). The study indicated that the drag coefficient

decreases with increase in *B/d* ratio. The value of drag coefficients is lower for a streamlined deck section in comparison to bluff or truss supported deck section. The steady-state force coefficients are increased by the presence of geometrical features such as handrails, crash barriers, wind fences, etc. on the bridge deck cross section. Reynolds number considerably changes the value of lift C_L and moment C_M coefficients and their derivatives. Underestimating the slope of lift and moment curves leads to underestimation of buffeting response. In the case of bluff bridge cross-sections, the turbulence present in the approaching flow affects these coefficients. Also, during the wind tunnel studies, it is necessary to use appropriate measuring technique to obtain reasonably accurate and reliable values for these coefficients.

The steady-state force coefficients are generally obtained by wind tunnel investigations on sectional models by pressure or force measuring techniques and recently efforts are in progress to evaluate them by computational fluid dynamics techniques. The wind tunnel investigations are time consuming and expensive. Based on literature, a summary of steady-state coefficients and their derivatives for some of the existing cable bridge deck cross-sections are given in Table 5.1. This could provide information on steady-state coefficients, which are used in computation of buffeting forces acting along the span of long span cable stayed bridges.

5.2.1.2 Aerodynamic admittance function

The aerodynamic admittance function is a frequency dependent function expressed as ratio of the fluctuating force in the turbulent wind to the quasi-static force in steady flow. These functions could be evaluated by wind tunnel investigations as reported in the case of Tatara Bridge in Japan by Matsuda *et al* (1999). As it is not easy to measure these aerodynamic admittance functions directly by wind tunnel experiments, Davenport function (1962) is often used to express the aerodynamic admittance for along-wind buffeting, the Sears function as given in Fung (1969) and the

Table 5.1: Steady-state Force Coefficients for Some of the Cable Bridges

Name of Bridge	Description of Cross-section	B/d	C_D	C_L	C_M	$\frac{dC_D}{d\alpha_w}$	$\frac{dC_L}{d\alpha_w}$	$\frac{dC_M}{d\alpha_w}$	Reference
Normandy	Streamlined Box section	7.0	0.448	-0.335	0.0230	0.41	4.66	1.07	Virloguex (1992)
Saint Nazaire	Box section	4.4	0.980	0.055	0.0416	-	3	-	Virloguex (1992)
Oberkassel	Central trapezoidal box	11.1	0.800	-0.40	0.3800	-	5.7	-	Walther (1988)
New Burrard Inlet	Streamlined box		0.9	0.008	0.02	-	-	-	Wardlow (1970)
Oresund Single Level Double Level	Central box with overhang Trapezoidal box	6.14 2.18	1.05 1.18	-0.15 0.21	0.012 0.116	- -	3.3 3.7	0.95 -	Stromnen *et al* (1999)
	Twin Box section	6.00	1.452	-0.17	0.138	-	3.6	0.4	Walshe and Wyatt(1983)
Tatara	Streamlined box	9.37	0.94	-0.02	0.036	-	5.70	1.28	Akiyama (1999)
Yamuna	Deck supported by two edge solid girders	19.0	1.224	-0.0952	-0.0033	0.019	4.66	1.039	Lakshmy *et al* (1998)

Note : The coefficients are based on the plots of steady-state force coefficients given in the references.

Holmes function (1975) are used to express the aerodynamic admittance for vertical and torsional buffeting respectively. These functions are described as follows:

- Davenport function

$$\left|\chi_{Dbu}(\tilde{K})\right|^2 = \frac{2}{(\lambda_u \tilde{K})^2}\left(\lambda_u \tilde{K} - 1 + e^{-\lambda_u \tilde{K}}\right);\ \tilde{K} = nd/U \tag{5.11}$$

where $\left|\chi_{Dbu}(\tilde{K})\right|^2$ is the aerodynamic admittance, λ_u is the decay factor which is assumed to be 7, $\tilde{K} = nd/U$ is the reduced frequency, n is the frequency, d is the deck height and U is the mean wind speed.

- Sears approximate function

$$\left|\chi_{Lbw}(K')\right|^2 = \frac{a + K'}{a + (\pi a + 1)K' + 2\pi K'^2}, \qquad \text{a=0.1811} \tag{5.12}$$

where $\left|\chi_{Lbw}(K')\right|^2$ is the aerodynamic admittance , $K' = (\pi nB/U)$is the reduced frequency and B is the deck width.

- Holmes function

$$\left|\chi_{Lbw}(K)\right|^2 = \frac{1}{4 + K};\ \text{K= nB/U} \tag{5.13}$$

In the above equations $\left|\chi_{Lbw}\right|^2$ represent the aerodynamic admittance function and K=nB/U is the reduced frequency.

5.2.2 Aeroelastic Forces

A common explicit form of describing the sectional aeroelastic forces under sinusoidal motion in lateral (p), vertical (h) and torsional (α) directions as described by Jain *et al* (1996) is given below:

$$D_{ae} = \frac{1}{2}\rho U^2 B\left[KP_1^* \frac{\dot{p}}{U} + KP_2^* \frac{B\dot{\alpha}}{U} + K^2 P_3^* \alpha + K^2 P_4^* \frac{p}{B} + KP_5^* \frac{\dot{h}}{U} + K^2 P_6^* \frac{h}{B}\right] \tag{5.14}$$

$$L_{ae} = \frac{1}{2}\rho U^2 B\left[KH_1^* \frac{\dot{h}}{U} + KH_2^* \frac{B\dot{\alpha}}{U} + K^2 H_3^* \alpha + K^2 H_4^* \frac{h}{B} + KH_5^* \frac{\dot{p}}{U} + K^2 H_6^* \frac{p}{B} \right] \quad (5.15)$$

$$M_{ae} = \frac{1}{2}\rho U^2 B^2\left[KA_1^* \frac{\dot{h}}{U} + KA_2^* \frac{B\dot{\alpha}}{U} + K^2 A_3^* \alpha + K^2 A_4^* \frac{h}{B} + KA_5^* \frac{\dot{p}}{U} + K^2 P_6^* \frac{p}{B} \right] \quad (5.16)$$

where the factors P_i^*, H_i^* and $A_i^* (i = 1,2,\ldots,6)$ are commonly termed as flutter derivatives and are functions of reduced frequency $K = B\omega/U$. These extended forms make advance provision for all likely influences of the possible oscillatory structural motions in the allowable degrees of freedom on drag, lift and moment. More details on flutter derivatives of bridge deck cross-sections are discussed in Chapter 8.

As the aeroelastic forces are functions of reduced frequency, it is necessary to transform these frequency-dependent forces into the time-dependent forces so that they can be applied along with the time dependent buffeting forces in the explicit time domain buffeting analysis. The most common form currently used in aeronautics to transform the aeroelastic force coefficients is a rational function approximation (RFA) as discussed in detail by Roger (1977), and Tiffany and Adams (1988). RFA allows the aeroelastic forces to be cast in a linear time invariant state-space form, which makes time-domain analysis of wind induced response possible in a much simpler and systematic manner.

5.2.3 Rationalised Buffeting Forces

Scanlan (2000) cautioned about the drawbacks of use of static force coefficients rather than the dynamic ones for the computation of buffeting forces. He felt the practice of using static coefficients may result in unrealistic estimates of buffeting response that required correction by invoking empirical frequency–dependent correction factors termed as 'aerodynamic admittance functions'. A step towards formulating a unified and rationalized expression for buffeting force have been presented, which integrates the aerodynamic and aeroelastic forces and implicitly

eliminates the notions of aerodynamic admittance and signature terms from the analysis. The rationalized buffeting forces that encompass both conditions of stability and external and signature turbulence are thus redefined with the following expressions:

$$D_b = \frac{1}{2}\rho U^2 B\left[-KP_5^*(K)\frac{w(x,t)}{U} - KP_1^*(K)\frac{u(x,t)}{U}\right] \tag{5.17}$$

$$L_b = \frac{1}{2}\rho U^2 B\left[-KH_1^*(K)\frac{w(x,t)}{U} - KH_5^*(K)\frac{u(x,t)}{U}\right] \tag{5.18}$$

$$M_b = \frac{1}{2}\rho U^2 B^2\left[-KA_1^*(K)\frac{w(x,t)}{U} - KA_5^*(K)\frac{u(x,t)}{U}\right] \tag{5.19}$$

In the above equations, it is assumed that the flutter derivatives are measured in turbulent flow. By comparing Eqs. 5.17-5.19 with Eqs. 5.4 to 5.6 results in the following expressions for flutter derivatives in terms of the force coefficients of a bridge deck section.

$$C_D' = -KP_5^*(K) \tag{5.20}$$

$$2C_D = -KP_1^*(K) \tag{5.21}$$

$$C_L' + C_D = -KH_1^*(K) \tag{5.22}$$

$$2C_L = -KH_5^*(K) \tag{5.23}$$

$$C_M' = -KA_1^*(K) \tag{5.24}$$

$$2C_M = -KA_5^*(K) \tag{5.25}$$

By comparing Eqs. 5.17-5.19 with Eqs. 5.8-5.10, the following relations for aerodynamic admittance functions can be inferred in terms of flutter derivatives and force coefficients of a bridge deck section.

$$(C_D')^2 \chi_{Dbw}^2 = (KP_5^*)^2 \tag{5.26}$$

$$4C_D^2 \chi_{Dbu}^2 = (KP_1^*)^2 \tag{5.27}$$

$$\left(C_L' + C_D\right)^2 \chi_{Lbw}^2 = \left(KH_1^*\right)^2 \tag{5.28}$$

$$4C_L^2 \chi_{Lbu}^2 = \left(KH_5^*\right)^2 \tag{5.29}$$

$$\left(C_M'\right)^2 \chi_{Mbw}^2 = \left(KA_1^*\right)^2 \tag{5.30}$$

$$4C_M^2 \chi_{Mbu}^2 = \left(KA_5^*\right)^2 \tag{5.31}$$

5.2.4 Refined Model for Aerodynamic Forces

In the formulation of buffeting forces described in Section 5.2.1, the oncoming wind flow is assumed to occur from the direction normal to the bridge span, i.e., the effective angle of attack is zero. However, during the buffeting process, the bridge deck has not only translational displacements but also rotations, which lead to instantaneous change of angle of attack between the bridge deck and wind direction. The change in angle of attack causes a change in wind loads on the bridge deck. For certain cross-sectional shapes of bridge deck, due to their sensitivity to wind direction, the effect of change in the instantaneous angle of attack can be quite significant. Therefore, in some cases, it becomes necessary to include the effect of the changes in angle of attack of wind on the buffeting response of flexible bridges as discussed in their formulations by Miyata *et al* (1995), Xiang *et al* (1995) and Ding *et al* (2000).

In this type of buffeting analysis, the bridge deck is subjected to both mean and fluctuating part of wind loads. Also, the point of application of wind forces, generally assumed as concentrated loads, is not necessarily at the centerline of the bridge deck, but at a point slightly away from the center. The point of application is assumed at 1/4th point of the deck width, B. The relationship between bridge deck motion and wind at time 't' is shown in Fig. 5.2. From this figure, it can be seen that the effective wind angle α_{we} is given by:

$$\alpha_{we} = \psi - \alpha_w \tag{5.32}$$

where $\tan\psi = \dfrac{w - \dot{h} + m_l\dot{\alpha}}{U + u + \dot{p}}$ (5.33)

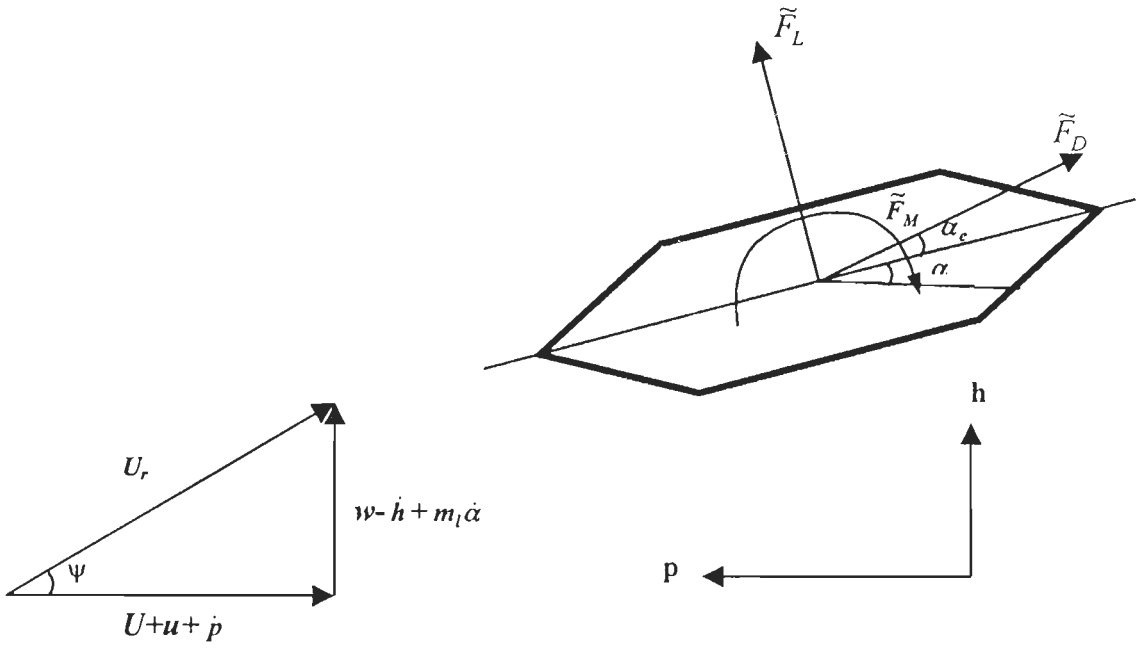

Fig. 5.2 : The Relationship between Relative Velocity U_r and Effective Angle of Attack α_e.

and the relative velocity $U_r(t) = \sqrt{(U+u+\dot{p})^2 + (w-\dot{h}+m_l\dot{\alpha})^2}$ (5.34)

where $\dot{p}, \dot{h}$ and $\dot{\alpha}$ are the velocities of the bridge at time 't' with respect to the transverse, vertical and rotational directions respectively; m_l the distance between point of attack of wind loads and centerline of the bridge deck taken as B/4 in this analysis; and α is the rotation angle of bridge at time 't'.

Equations 5.33 and 5.34 are similar to Eqs. 4.74 and 4.75 except for the fact that the former equations include the relative velocity of bridge due to its movement in transverse, vertical and torsion directions with respect to wind.

Considering the change in wind loads due to instantaneous change in effective attack angle, the wind load including drag, lift and moment at time 't' can be rewritten as:

$$\overline{F}_D(t) = \widetilde{F}_L(t)\sin\psi - \widetilde{F}_D(t)\cos\psi \tag{5.35}$$

$$\overline{F}_L(t) = \widetilde{F}_L(t)\cos\psi + \widetilde{F}_D(t)\sin\psi \tag{5.36}$$

$$\overline{F}_M(t) = \widetilde{F}_M(t) \tag{5.37}$$

where $$\widetilde{F}_D(t) = \frac{1}{2}\rho U_r^2(t) B C_D(\alpha_w) \tag{5.38}$$

$$\widetilde{F}_L(t) = \frac{1}{2}\rho U_r^2(t) B C_L(\alpha_w) \tag{5.39}$$

$$\widetilde{F}_M(t) = \frac{1}{2}\rho U_r^2 B^2 C_M(\alpha_w) \tag{5.40}$$

It should be emphasized that the total drag, lift and moment is a function of effective angle of attack of wind on the bridge deck as the drag, lift and moment coefficients vary with wind angle.

5.2.4 Details of Software

To compute the instantaneous buffeting forces using the digitally simulated spatially correlated time histories of fluctuating wind velocities, a computer routine entitled 'INWINF' has been developed, which calls WINGEN for generation of longitudinal and vertical wind velocity fluctuations.

The input data required for INWINF are grouped into bridge geometrical parameters, data necessary for turbulent wind field description, and bridge deck aerodynamic coefficients. The bridge related factors include- height of bridge deck above ground level (z) in metres, number of uniformly space points along the span at which the buffeting forces are to be estimated, distance between these points in metres and the width of bridge deck (B) in meters. The wind related parameters are mean wind speed U(z) in m/sec, ground surface roughness factor z_0, decay coefficient for longitudinal fluctuations (λ_u), decay coefficient for vertical fluctuations (λ_w) and angle of attack of wind (α_w). Necessary aerodynamic coefficients are, steady-state drag (C_D), lift (C_L) and moment (C_M) coefficients corresponding to specified α_w, the slope of drag, lift and moment curves (C'_D, C'_L and C'_M) and six aerodynamic admittance functions (χ_{Dbu}, χ_{Dbw}, χ_{Lbu}, χ_{Lbw}, χ_{Mbu} and χ_{Mbw}) corresponding to respective U/nB values.

For computation of rationalized buffeting forces, the flutter derivatives ($H_1^*, H_5^*, P_1^*, P_5^*, A_1^*$ and A_5^*) corresponding to the reduced velocity (U/nB) are required, instead of the values of steady-state force coefficients, their derivatives and aerodynamic admittance functions.

The buffeting forces are computed either by the quasi-steady method modified incorporating the aerodynamic admittance functions described by Eqs. 5.8-5.10 or using the rationalized expressions 5.17-5.19 depending on the availability of necessary aerodynamic parameters. The provision to compute the buffeting forces using the buffeting force model that includes the mean wind component is also available in the software.

The output of the software includes the time histories of buffeting drag, lift and moments for a duration of 512 sec, with a time force pair at 0.25 sec interval making 2048 pairs each. These generated time force pairs are used in the time domain buffeting analysis of the cable stayed bridge.

Another important parameter utilized for time domain buffeting response evaluation is the modal damping. The method of evaluating the modal damping is discussed in the following Section.

5.3 MODAL DAMPING

The total modal damping of long span cable stayed bridges under the action of the wind, is the sum of modal structural and aerodynamic dampings and is given by:

$$\xi_T = \xi_s + \xi_{ae} \tag{5.41}$$

Depending on the value of damping, its influence on aerodynamic response can be classified as (i) resonant amplification, (ii) over damped vibration and (iii) instability. These conditions are discussed below :

(i) Resonant amplification: This condition is identified with $0 < (\xi_s + \xi_{ae}) < 1$. This is the normal range of damping and leads to large amplitude of response at

lower damping values and responses of small amplitude at higher damping values, as it approaches unity.

(ii) Over damping: This condition is identified for $(\xi_s + \xi_{ae}) > 1$. This implies no resonant oscillation, and, moreover, some suppression of the quasi-steady background response. Therefore, from the engineering viewpoint this condition is favourable.

(iii) Instability: This condition is identified with $(\xi_s + \xi_{ae}) < 0$. In this condition resonant oscillations grow to large, probably unacceptable amplitudes.

The evaluation of energy based modal structural damping (ξ_s) has been discussed in detail in Section 3.5. Because modal structural damping values are generally small, the aerodynamic damping can exert a strong controlling influence on wind induced oscillatory response of flexible bridges. A general expression for aerodynamic damping is given as

$$\xi_{ae} = (\rho_{air} / \rho_{structure}) C_a(U_R) \tag{5.42}$$

where C_a is the aerodynamic coefficient depending on the reduced velocity U_R, which is given by (U/nB).

In the present study, the method used for estimation of aerodynamic damping is based on the expressions given by Irwin (1977), which predicted values in close agreement with aeroelastic wind tunnel studies for long span cable bridges. The theoretical aerodynamic damping in vertical bending (ξ_{aeh}) and for pure torsion $(\xi_{ae\alpha})$ mode is given by

$$\xi_{aeh} = \frac{1}{8\pi}\left(\frac{\rho B^2}{M}\right) C'_L\left(\frac{U}{n_h B}\right) \tag{5.43}$$

$$\xi_{ae\alpha} = \frac{1}{8\pi} f'\left(\frac{\rho B^4}{I}\right) C'_M\left(\frac{U}{n_\alpha B}\right) \tag{5.44}$$

and $$f' = 0.5 - 0.09\frac{U}{n_\alpha B} \tag{5.45}$$

The aerodynamic damping ratio in the along-wind direction is expressed as:

$$\xi_{aep} = \frac{1}{4\pi}\left(\frac{\rho B^2}{M}\right)\left(\frac{U}{n_p B}\right)C_D \tag{5.46}$$

where M is mass per unit deck length, I is the mass moment of inertia of deck per unit length, n_h, n_α, and n_p are the natural frequencies of bridge in vertical, torsional and lateral directions.

Alternatively, the modal aerodynamic damping can be computed using the following expressions, if flutter derivatives pertaining to the particular bridge deck is available as per Scanlan (1981):

Aerodynamic damping in vertical direction for s^{th}mode is expressed as follows:

$$\xi_{aeh} = \frac{\rho B^2 L J_s}{2M_s} H_1^*\left(\frac{U}{n_s B}\right) \tag{5.47}$$

where, $J_s = \int_0^L \phi^2{}_s(x)dx / L$

$$M_s = \int_0^L M\phi_s^2(x)dx$$

$\phi_s(x)$ represents the modal ordinates of vertical bending mode for s^{th} mode.

$H_1^*\left(\frac{U}{n_s B}\right)$ represents the flutter derivative H_1^* evaluated at $\left(\frac{U}{n_h B}\right)$ for n_h=n_s.

Aerodynamic damping in torsion for the r^{th} mode is computed by the following equation:

$$\xi_{ae\alpha} = \frac{\rho B^4 L}{2I_r} A_2^*\left(\frac{U}{n_r B}\right) G_r \tag{5.48}$$

where $G_r = \int_0^L \phi_r{}^2(x)dx / L$

$$I_r = \int_0^L I\phi_r^2(x)dx$$

$\phi_r(x)$ is the mode shape corresponding to r[th]torsional mode of bridge.

and $A_2^*\left(\frac{U}{n_r B}\right)$ is the value of A_2^* evaluated at $\left(\frac{U}{n_\alpha B}\right)$ for $n_\alpha = n_r$

5.4 TIME DOMAIN ANALYSIS

The time domain analysis is achieved by the solution of equation of motion for the bridge structural system under random wind loads expressed in the conventional matrix notation as:

$$[M]\{\ddot{U}\} + [C]\{\dot{U}\} + [K]\{U\} = [P] \tag{5.49}$$

where [M] is a diagonal matrix containing the mass and mass moment of inertia of all elements lumped at nodes, [C] the damping matrix , [K] the structural stiffness matrix and [P] the buffeting forces alone or wind forces including the mean and fluctuating components. {U} represents the time dependent nodal displacement vector for the bridge structural system. The terms $[M]\{\ddot{U}\}$, $[C]\{\dot{U}\}$ and $[K]\{U\}$ represent the time-dependent inertial, damping and elastic forces present in the system.

There are two methods of solution of equations of motion represented by Eq. 5.49 – the direct integration method and modal superposition method.

In the direct integration method, the individual equation contained in Eq. 5.49 are integrated using a numerical step-by-step-procedure, the term 'direct' meaning that prior to the numerical integration, no transformations of equations into a different form is carried out. The direct numerical integration can be achieved by using two different concepts. First, instead of trying to satisfy the equation of motion represented by Equation 5.49 at any time 't', it is aimed to satisfy them only at discrete time intervals Δt apart. The second concept, on which the direct integration is based, is that a variation

of displacements, velocities and/or accelerations within each time interval Δt is assumed.

The commonly used effective solution techniques are (i) Central difference method, (ii) Houbolt method, (iii) Wilson-θ method, and (iv) Newmark integration method. Details on these methods are presented in Bathe and Wilson (1976).

The above methods, when used in direct integration, require a number of numerical operations directly proportional to the number of time steps used in the analysis. Therefore, direct integration can be expected to be effective only when the response for a relatively short duration, i.e., for a few time steps is required. However, if the integration is to be performed for many time steps, it may be more appropriate to transform Eq. 5.49 into a form in which step-by-step solution is less time consuming and thus cost effective. This is achieved by normal coordinate transformation, in which the nodal displacements are expressed in terms of mode shapes and normal coordinates as described below:

$$\{U\} = [\phi]\{q\} \tag{5.50}$$

where $[\phi]$ is the matrix of undamped mode shapes and {q} is the vector of normal coordinates. On applying this transformation to Eq. 5.49, the transformed equations are expressed as

$$[\overline{M}]\{\ddot{q}\} + [\overline{C}]\{\dot{q}\} + [\overline{K}]\{q\} = \{\overline{P}\} \tag{5.51}$$

where $[\overline{M}] = [\phi]^T [M][\phi]$ (5.52)

$$[\overline{C}] = [\phi]^T [C][\phi] \tag{5.53}$$

$$[\overline{K}] = [\phi]^T [K][\phi] \tag{5.54}$$

$$\{\overline{P}\} = [\phi]^T \{P\} \tag{5.55}$$

The use of mode shapes simply involves a coordinate transformation from finite element displacement coordinates to the modal coordinates. This change of basis is

particularly effective if only a few modal coordinates need to be employed.

In this study, buffeting analysis by time domain approach is performed by solving equations of motion in normal coordinates and superposition of the modal responses.

5.4.1 Application of Wilson-θ Method for Solution of Equations of Motion in Normal Coordinates

In the present study, the numerical integration of equations of motion expressed in normal coordinates is executed utilizing the Wilson-θ method. It is an extension of the linear acceleration method, in which a linear variation of acceleration in assumed between time t and t+θΔt, where θ is taken as 1.40. Solution of equations of motion in normal coordinates using Wilson -θ method is explained.

Using the mass, damping and stiffness matrices of bridge system, equations of dynamic equilibrium at the time t_i are written as

$$[\overline{M}]\{\ddot{q}(t_i)\}+[\overline{C}]\{\dot{q}(t_i)\}+[\overline{K}]\{q(t_i)\}=\{\overline{P}(t_i)\} \tag{5.56}$$

At a time $\tau' = \theta\Delta t$ from a particular time t_i, the equations of dynamic equilibrium are given by:

$$[\overline{M}]\{\ddot{q}(t_i+\tau')\}+[\overline{C}]\{\dot{q}(t_i+\tau')\}+[\overline{K}]\{q(t_i+\tau')\}=\{\overline{P}(t_i+\tau')\} \tag{5.57}$$

By subtracting Eq. 5.56 from Eq. 5.57 results in incremental equations of motion, namely:

$$[\overline{M}]\{\hat{\Delta}\ddot{q}_i\}+[\overline{C}]\{\hat{\Delta}\dot{q}_i\}+[\overline{K}]\{\hat{\Delta}q_i\}=\{\hat{\Delta}\overline{P}_i\} \tag{5.58}$$

In the above equations hat over Δ indicates that the increments are associated with the extended time step τ', thus resulting in following relations:

$$\{\hat{\Delta}\ddot{q}_i\}=\{\ddot{q}(t_i+\tau')\}-\{\ddot{q}(t_i)\} \tag{5.59}$$

$$\{\hat{\Delta}\dot{q}\}=\{\dot{q}(t_i+\tau)\}-\{\dot{q}(t_i)\} \tag{5.60}$$

$$\{\hat{\Delta}q_i\} = \{q(t_i + \tau')\} - \{q(t_i)\} \tag{5.61}$$

$$\{\hat{\Delta}\overline{P}_i\} = \{\overline{P}(t_i + \tau')\} - \{\overline{P}(t_i)\} \tag{5.62}$$

The acceleration may be represented by a linear function during the time step $\tau' = \theta\Delta t$. This yields

$$\{\ddot{q}(t)\} = \{\ddot{q}_i\} + \{\hat{\Delta}\ddot{q}_i\}\frac{(t - t_i)}{\tau'} \tag{5.63}$$

in which $\{\Delta\ddot{q}_i\}$ is given by Eq. 5.59

Integration of Eq. 5.63 twice between the limits t_i and t yields

$$\{\dot{q}(t)\} = \{\dot{q}_i\} + \{\ddot{q}_i\}(t - t_i) + \{\hat{\Delta}q_i\}\frac{(t - t_i)^2}{2\tau'} \tag{5.64}$$

and $$\{q(t)\} = \{q_i\} + \{\dot{q}_i\}(t - t_i) + \{\ddot{q}_i\}\frac{(t - t_i)^2}{2} + \{\hat{\Delta}\ddot{q}_i\}\frac{(t - t_i)^3}{6\tau'} \tag{5.65}$$

Evaluation of Eqs. 5.64 and 5.65 at the end of the extended time interval $t = t_i + \tau'$ results in

$$\{\hat{\Delta}\dot{q}_i\} = \{\ddot{q}_i\}\tau' + \frac{1}{2}\{\hat{\Delta}\ddot{q}_i\}\tau' \tag{5.66}$$

and $$\{\hat{\Delta}q_i\} = \{\dot{q}_i\}\tau' + \frac{1}{2}\{\ddot{q}_i\}\tau'^2 + \frac{1}{6}\{\hat{\Delta}\ddot{q}_i\}\tau'^2 \tag{5.67}$$

Solving Eq. 5.67 for the incremental acceleration $\{\hat{\Delta}\ddot{q}_i\}$ and substituting the same in Eq. 5.66, results in the following:

$$\{\hat{\Delta}\ddot{q}_i\} = \frac{6}{\tau'^2}\{\hat{\Delta}q_i\} - \frac{6}{\tau'}\{\dot{q}_i\} - 3\{\ddot{q}_i\} \tag{5.68}$$

$$\{\hat{\Delta}\dot{q}_i\} = \frac{3}{\tau'}\{\hat{\Delta}q_i\} - 3\{\dot{q}_i\} - \frac{\tau'}{2}\{\ddot{q}_i\} \tag{5.69}$$

By substituting the expressions for incremental acceleration and velocity given by Eqs. 5.68 and 5.69 into Eq. 5.58 gives

$$[\overline{M}]\left[\frac{6}{\tau'^2}\{\hat{\Delta}q_i\} - \frac{6}{\tau'}\{\dot{q}_i\} - 3\{\ddot{q}_i\}\right] + [\overline{C}]\left[\frac{3}{\tau'}\{\hat{\Delta}q_i\} - 3\{\dot{q}_i\} - \frac{\tau'}{2}\{\ddot{q}_i\}\right] + [\overline{K}]\{\hat{\Delta}q_i\} = [\hat{\Delta}\overline{P}_i] \tag{5.70}$$

And can be written as

$$[\overline{K}']\{\hat{\Delta}q_i\} = \{\hat{\Delta}\overline{P}_i\} \tag{5.71}$$

in which the effective stiffness $[\overline{K}'] = [\overline{K}] + \frac{6}{\tau'^2}[\overline{M}] + \frac{3}{\tau'}[\overline{C}]$ (5.72)

and the effective incremental load vector is given by

$$\{\hat{\Delta}\overline{P}_i'\} = \{\hat{\Delta}\overline{P}_i\} + [\overline{M}]\left[\frac{6}{\tau'}\{\dot{q}_i\} + 3\{\ddot{q}_i\}\right] + [C]\left[3\{\dot{q}_i\} + \frac{\tau'}{2}\{\ddot{q}_i\}\right] \tag{5.73}$$

$\{\hat{\Delta}q_i\}$ is obtained by solving Eq. 5.71. Having computed the incremental displacement $\{\hat{\Delta}q_i\}$ at the end of the extended time interval, by using Eq. 5.68, the incremental acceleration $\{\Delta\ddot{q}_i\}$ for the normal time interval Δt is then obtained by simple linear interpolation. Hence

$$\{\Delta\ddot{q}_i\} = \frac{1}{\theta}\{\hat{\Delta}\ddot{q}_i\} \tag{5.74}$$

The incremental velocity $\{\Delta\dot{q}_i\}$ and the incremental displacement $\{\Delta q_i\}$ corresponding to normal time interval Δt, is obtained using Eqs. 5.66 and 5.67 with the extended time interval parameter τ' replaced with Δt, that is

$$\{\Delta\dot{q}_i\} = \{\ddot{q}_i\}\Delta t + \frac{1}{2}\{\Delta\ddot{q}_i\}\Delta t \tag{5.75}$$

$$\{\Delta q_i\} = \{\dot{q}_i\}\Delta t + \frac{1}{2}\{\ddot{q}_i\}(\Delta t)^2 + \frac{1}{6}\{\Delta\ddot{q}_i\}(\Delta t)^2 \tag{5.76}$$

Thus, the displacement, velocity and acceleration at the end of normal time interval, in modal coordinates are obtained, using expressions 5.74-5.76 as:

$$\{q_{i+1}\} = \{q_i\} + \{\Delta q_i\} \tag{5.77}$$

$$\{\dot{q}_{i+1}\} = \{\dot{q}_i\} + \{\Delta\dot{q}_i\} \tag{5.78}$$

$$\{\ddot{q}_{i+1}\} = \{\ddot{q}_i\} + \{\Delta\ddot{q}_i\} \tag{5.79}$$

Since the displacement, velocity and acceleration vectors have been determined

at time t_{i+1}, i.e., $(t_i+\Delta t)$, the above procedure is repeated to calculate these quantities in the next time step $t_{i+2} = t_{i+1}+\Delta t$ and the process is continued to desired time duration or number of time steps.

The values of displacements, velocity and acceleration in system displacement coordinates are obtained by coordinate transformation as given below:

$$\{U_{i+1}\} = [\phi]\{q_{i+1}\} \tag{5.80}$$

$$\{\dot{U}_{i+1}\} = [\phi]\{\dot{q}_{i+1}\} \tag{5.81}$$

$$\{\ddot{U}_{i+1}\} = [\phi]\{\ddot{q}_{i+1}\} \tag{5.82}$$

5.4.2 Time Domain Procedure for Buffeting Response

The overall procedure for time domain buffeting analysis is presented in Fig. 5.3 and the steps are explained below.

Nonlinear static analysis of the cable stayed bridge is performed using the formulation presented in Section 3.3. The modified geometric configuration of bridge is obtained by adding the dead load deformed state to the initial geometry. Free vibration analysis is performed for the dead load deformed configuration using the formulation presented in Section 3.4. After obtaining the frequencies and mode shapes of vibration, the energy based modal structural damping is evaluated using the 'ENDAMP' software developed for the purpose as described in Section 3.5. The number of modes for which the damping values are to be computed is equal to the maximum number of modes to be incorporated in the time domain buffeting analysis.

After deciding the mean wind speed and terrain roughness parameter for which buffeting analysis is to be performed, the spatially correlated time histories of wind are generated using the spectral representation method as described in Section 4.4. Using these time histories, the steady–state force coefficients, and their derivatives for bridge deck cross-section and aerodynamic admittance function, the buffeting forces in the drag, lift and rotational directions are computed using the quasi-steady procedure

described in Section 5.2.1. However, instead of steady–state force coefficients, if the flutter derivatives of bridge deck cross-section extracted by wind tunnel investigations under turbulent flow are available, the rationalized buffeting forces as described in Section 5.2.3 could be computed.

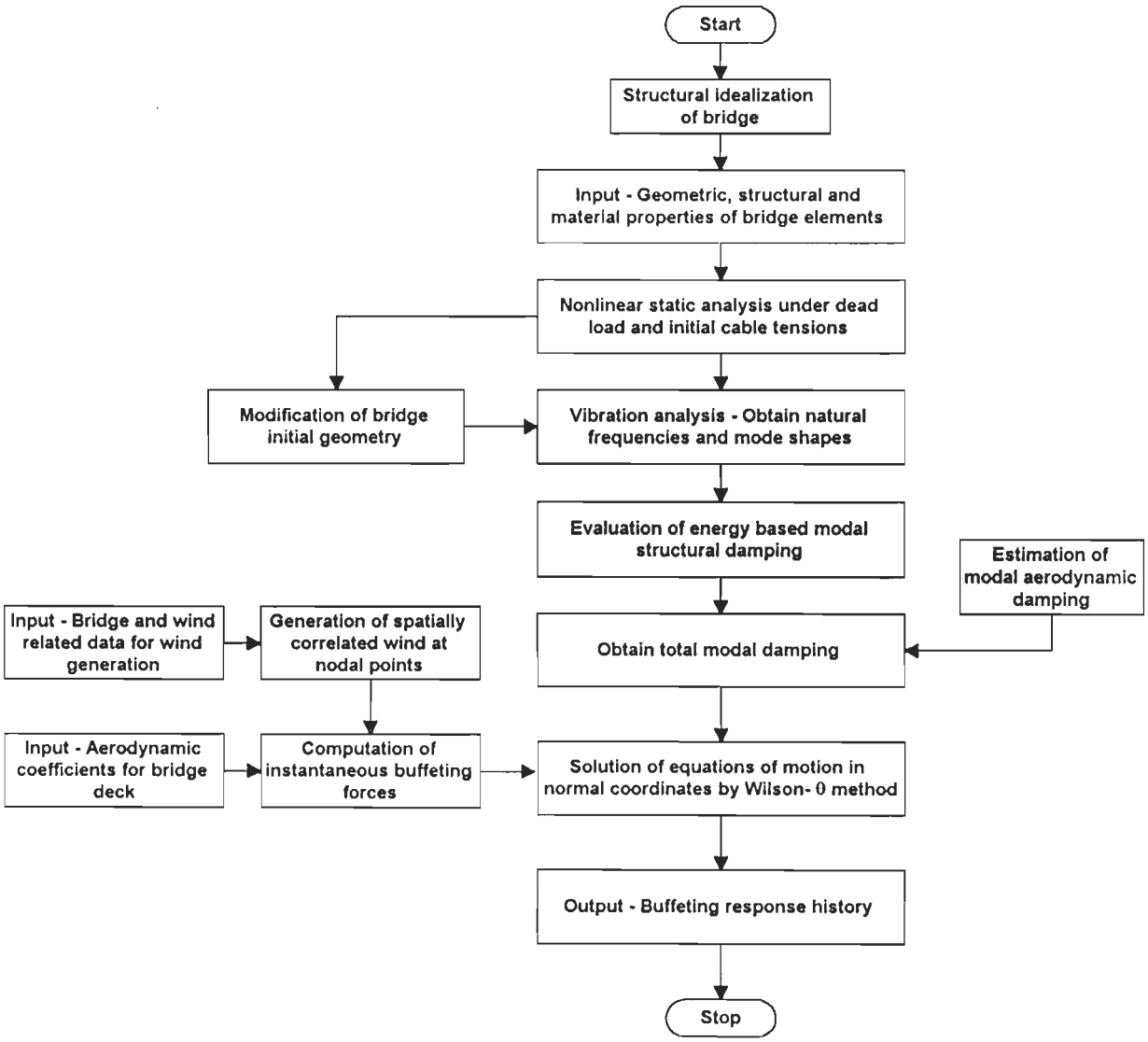

Fig. 5.3 : Schematic Diagram Illustrating the Time Domain Buffeting Analysis

The aerodynamic damping contribution for the desired number of modes is computed using Eqs. 5.43-5.45. Then the total modal damping is obtained by adding the modal structural and aerodynamic damping.

Using the modal superposition method, the equation of motion is solved using the Wilson-θ method to obtain the buffeting response in along-wind and across-wind directions and in torsion. The time histories of the response are used during design for checking the adequacy of bridge deck in buffeting and, if necessary, to incorporate necessary countermeasures to alleviate the buffeting responses.

5.4.3 Validation of Time Domain Analysis

The classical frequency domain analysis has been used in the present study to validate the time domain buffeting analysis. The standard deviation of maximum vertical and torsional buffeting response for a particular mode is estimated using the methodology outlined by Scanlan (1981). Also, the Irwin's theory (1977) on buffeting response, which predicted the responses close to the values obtained in wind tunnel investigations using aeroelastic models, has been utilized for validation. The expressions used to estimate the buffeting responses in frequency domain by these approaches are given in Appendix-III.

The application and validation of time domain buffeting analysis of long span cable stayed bridges is presented in Chapter 6 and 7.

5.5 SUMMARY

The formulations and procedure for time domain buffeting analysis using digitally simulated instantaneous buffeting forces is presented in this Chapter. The methods used for generation of buffeting forces have been discussed in detail. The factors affecting the buffeting response, such as steady–state force coefficients, aerodynamic damping, aerodynamic admittance, etc., have been discussed in detail. The numerical results of time domain buffeting analysis including validation is illustrated in Chapter 6 for three span bridges and in Chapter 7 for five span bridges. In the present study, time domain buffeting analysis is validated through frequency

domain method. Thus, after verification of time domain buffeting analysis, it can be treated as 'numerical wind tunnel test' in evaluating the buffeting response of long span flexible cable bridges. The mathematical formulation seems general enough to be applicable to the superspan cable stayed bridges.

Chapter 6

BUFFETING ANALYSIS OF THREE SPAN CABLE STAYED BRIDGES

6. 1 INTRODUCTION

This chapter is devoted to the buffeting analysis of three span cable stayed bridges namely Bridge #1 and Bridge #2, using the formulations described in Chapter 5.

Analysis of these bridges under buffeting and mean wind forces has been performed to study the effect of variation in (i) mean wind speed, (ii) terrain roughness and (iii) support types for bridge deck at towers and abutments on buffeting response. Before carrying out the analysis using time domain approach, buffeting forces have been generated using the digitally simulated wind velocity fluctuations. The results of the mean wind analysis have been used as reference for comparison and to estimate the dynamic amplification in responses due to buffeting.

6.2 DATA FOR BUFFETING ANALYSIS

The wind data, steady-state force coefficients for various bridge components and modal damping estimates utilized in the analysis of Bridge #1 and Bridge #2 under buffeting forces (to study the influence of mean wind speed, terrain category and support types for bridge deck at towers and abutments on wind induced oscillatory responses) are discussed in the following sections.

6.2.1 Wind Data

To study the effect on buffeting response with increase in mean wind speed, the Bridge #1 is assumed to be located in terrain category TC–1, with terrain roughness

parameter z_0 equal to 0.005m. The mean wind speed at 10 m level has been varied from 30m/sec to 60m/sec in steps of 10m/sec. This indicates the mean wind speed at deck level for this bridge (30m elevation) as 34.3m/sec, 45.8m/sec, 57.2m/sec and 68.6m/sec respectively in terrain category TC-1 corresponding to the range of wind speed selected in this study.

In the case of Bridge#2, it is assumed to be located in terrain category TC-2, with surface roughness parameter equal to 0.03m.The mean wind speed values at deck level, i.e., 45m level are 32.4m/sec, 43.20m/sec, 54.0m/sec and 64.9m/sec corresponding to the four wind speeds at 10m height.

To study the effect of terrain roughness on mean wind response for Bridge#1, mean wind speed at a height of 10m is again taken as 30m/sec corresponding to terrain category TC-1 with z_0 equal to 0.005m. Terrain categories are varied from TC-1 to TC-4 with surface roughness parameter (z_0) equal to 0.005m, 0.03m, 0.3m and 1.0m representing these terrains as described in Section 4.2.2.1. Corresponding to these surface roughness parameters, the turbulent intensity in the longitudinal wind velocity fluctuations (I_u) at bridge deck level is 11.7%, 14.2%, 19.9% and 25.9% respectively. The turbulence intensity in vertical wind velocity fluctuations (I_w) at deck level is 6.0%, 7.75%, 11.7% and 16.20% respectively. The wind speed at an elevation of 30m above mean ground level, that is, the bridge deck level is calculated. The values of mean wind speed are 34.3m/sec, 30.6m/sec, 25.2m/sec and 20.4m/sec corresponding to terrain categories TC-1 to TC-4 respectively. The mean wind speed decreases with increase in terrain roughness.

Similarly, to study the effect of terrain roughness for Bridge#2, the mean wind speed at an elevation of 10m is taken as 40m/sec corresponding to terrain category TC-1 with z_0 equal to 0.005m. For the analysis, it is assumed that the bridge is located in four terrain categories TC-1 to TC-4 with surface roughness parameter (z_0) equal to 0.005m, 0.03m, 0.3m and 1.0m. Corresponding to these surface roughness parameters,

the turbulent intensity in the longitudinal wind velocity fluctuations is 11.4%, 13.4%, 18.2% and 23.1% respectively at deck elevation of 45m above the mean ground level. The turbulence intensity in vertical wind velocity fluctuations at deck level in terrains TC-1 to TC-4 is 6.9%, 8.0%, 10.4% and 13.0% respectively. The values of mean wind speed are 47.9m/sec, 43.2m/sec, 36.6m/sec and 30.4m/sec corresponding to terrain categories TC-1 to TC-4 respectively.

The wind profile along the height of tower for Bridge #1 and Bridge#2 is estimated as per the logarithmic law corresponding to above discussed terrain categories.

6.2.2 Steady-state Force Coefficients

Cross-sectional shape of the bridge deck is worked out to match the bridge deck properties as given in Table 3.1(a) for Bridge #1. The cross-section consists of longitudinal box girders in steel along with transverse beams supporting the orthotropic steel deck slab. To compute the wind loads on Bridge#1, based on data presented in Table 5.1, the steady-state drag, lift and moment coefficients for bridge deck have been taken as C_D = 0.0816, C_L= -0.0952, C_M = -0.0033, C_D' =0.019, C_L' = 4.66 and C_M' =1.039. For tower, the drag coefficient is assumed to vary between 2.2 and 2.5 depending on the aspect ratio of the rectangular leg section and for cables the drag coefficient is taken as 0.70.

Similarly, for Bridge #2, the steady-state drag, lift and moment coefficients of bridge deck at zero angle of attack (normalized with respect to bridge deck width) are taken as C_D = 0.114, C_L= -0.155, C_M = 0.047, C_D' =0.038, C_L' = 4.466 and C_M' =0.546. For tower, the drag coefficient is taken as 1.5 based on the aspect ratio of the rectangular leg section and for cables the drag coefficient is taken as 0.70.

6.2.3 Modal Damping

As discussed in Section 5.3, the net modal damping is the sum of (i) structural and (ii) aerodynamic damping. The theoretically evaluated values of modal structural

damping for Bridge#1 and Bridge #2 are already given in Tables 3.11 and 3.12. The computation of aerodynamic damping is discussed in the following sections.

The aerodynamic damping corresponding to the vertical bending and torsional modes has been computed using the Irwins's method as discussed in Section 5.3. The aerodynamic damping contributed by the first and second vertical symmetric modes (V-S1 and V-S2) for Bridge #1 with type of deck support DST-2 is illustrated in Fig. 6.1. Similarly, the aerodynamic damping contributions by the first and second torsional symmetric modes (T-S1 and T-S2) for Bridge #1 are shown in Fig.6.2.

Similarly, the aerodynamic damping for first and second symmetric modes in vertical bending (V-S1 and V-S2) and torsion (T-S1 and T-S2) are shown in Figs. 6.3 and 6.4 respectively for Bridge #2 with deck support type DST-6.

It is clear from the Figs. 6.1-6.4 that the aerodynamic damping contributed by first vertical symmetric mode (V-S1) is quite substantial in comparison to the modal structural damping of respective modes as given in Table 3.11 and Table 3.12. However, the aerodynamic damping contribution of second vertical symmetric mode (V-S2) is lower than that of the first vertical symmetric mode (V-S1).

From Figs. 6.1 to 6.4, it is clear that the aerodynamic damping in torsional modes is much lower than that of vertical bending modes. In the case of long span bridges, as in the case of Bridge #2, the value of aerodynamic damping contribution of first and second torsional symmetric modes (T-S1 and T-S2) becomes negative with increase in wind speed as illustrated in Fig. 6.4. However, in these bridges, the modal structural damping of torsional mode is higher than that in the vertical bending mode and also the value of net modal damping, even though small, remains positive in the range of wind speed included in this study.

The variation in net modal damping ratio with increase in wind speed, used in the buffeting analysis of the Bridge#1 with deck support type DST-2, is presented in Table 6.1. Similarly, for Bridge #2 with deck support type DST-6, the net modal damping ratio is computed for use in the buffeting analysis.

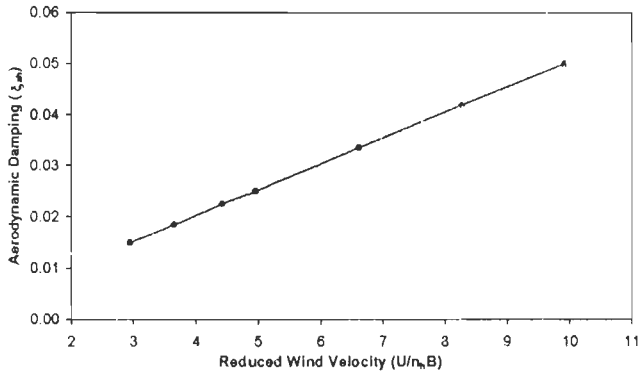

(a) 1st Symmetric Mode

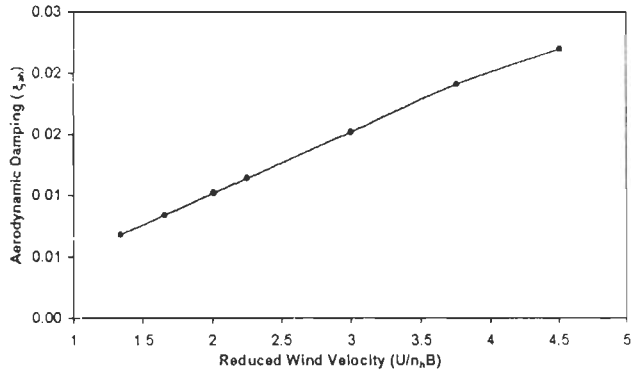

(b) 2nd Symmetric Mode

Fig. 6.1 : Aerodynamic Damping in Vertical Bending Modes for Bridge # 1

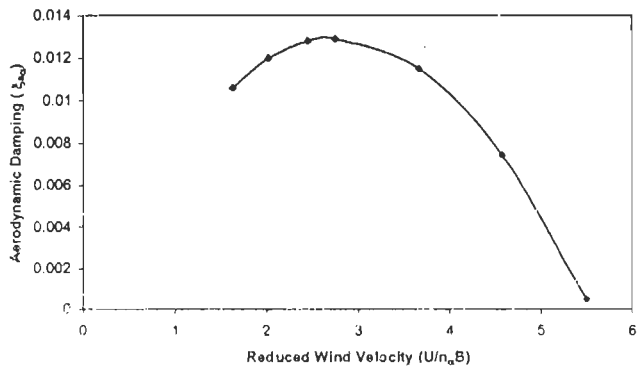

(a) 1st Symmetric Mode

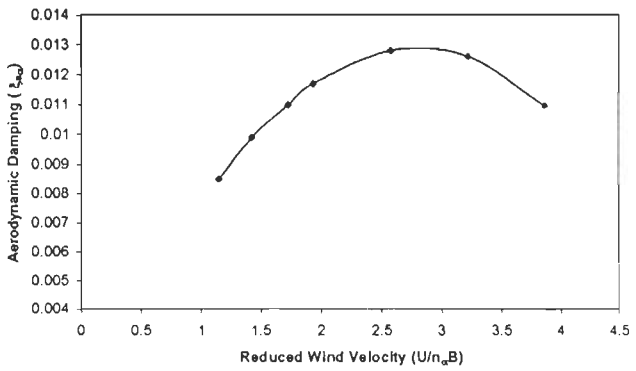

(b) 2nd Symmetric Mode

Fig. 6.2 : Aerodynamic Damping in Torsional Modes for Bridge # 1

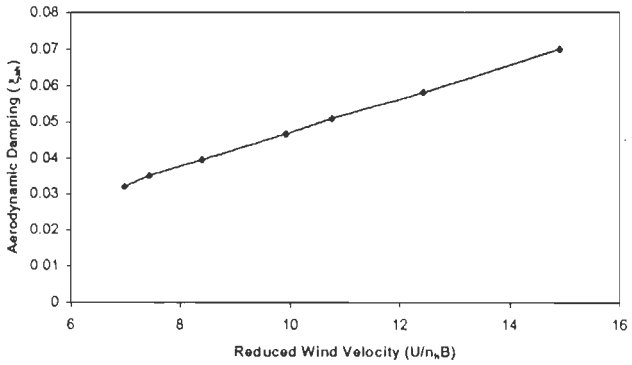

(a) 1st Symmetric Mode

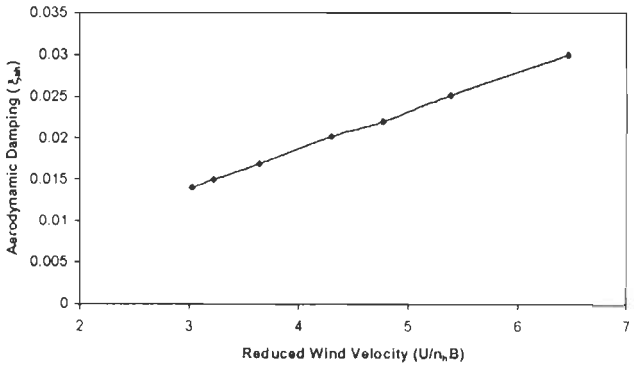

(b) 2nd Symmetric Mode

Fig. 6.3 : Aerodynamic Damping in Vertical Bending Modes for Bridge # 2

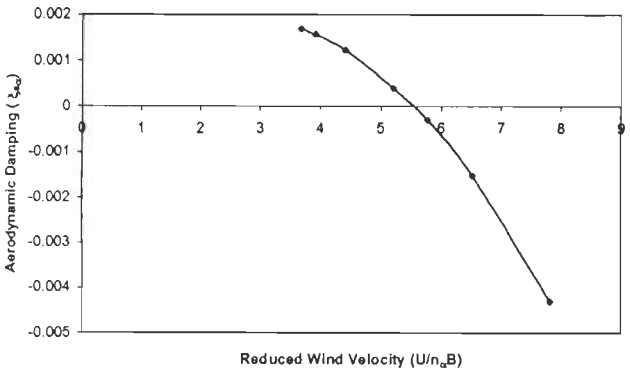

(a) 1st Symmetric Mode

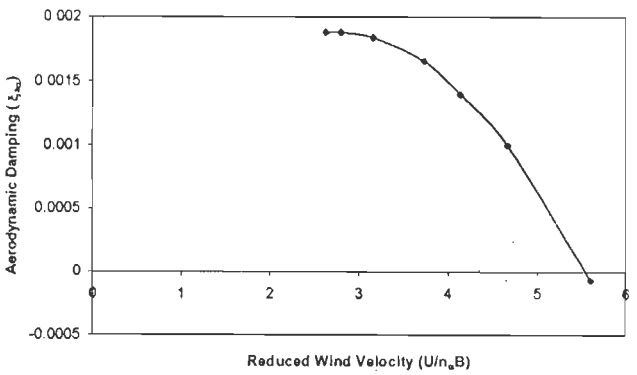

(b) 2nd Symmetric Mode

Fig. 6.4 : Aerodynamic Damping in Torsional Modes for Bridge # 2

Table 6.1 : Net Modal Damping for Bridge #1 –Variation with Mean Wind (Support Type for Bridge Deck - DST-2)

Mode	Frequency (Hz)	Mode Type	Net Damping Ratio for Mean Wind Speed U(10) in m/sec			
			30	40	50	60
1	0.291	V-S1	0.0285	0.0366	0.0451	0.0534
2	0.415	V-AS1	0.0203	0.0260	0.0320	0.0378
3	0.525	T-S1	0.0198	0.0185	0.0144	0.0075
4	0.640	V-S2	0.0133	0.0170	0.0208	0.0245
5	0.692	T-AS1	0.0200	0.0214	0.0207	0.0182
6	0.727	V-AS2	0.0117	0.0149	0.0183	0.0216
7	0.746	T-S2	0.0183	0.0194	0.0192	0.0176
8	0.790	T-AS2	0.0132	0.0146	0.0155	0.0135
9	0.890	V-S3	0.0100	0.0126	0.0155	0.0181
10	0.952	L-S1	0.0029	0.0029	0.0030	0.0031

6.3 MEAN WIND RESPONSES

The responses for Bridge #1 and Bridge #2 under dead load and mean wind forces have been obtained by nonlinear static analysis. Mean wind forces include the drag, lift and wind induced moment acting on bridge deck, and drag forces acting on towers and cables. It is computed using the mean wind speed profile estimated using logarithmic law as well as steady-state coefficients for the cross-sections of bridge components as discussed in Section 6.2.2.

The analyses have been performed for wind description given in Section 6.2.1, to study the effect of increase in mean wind speed, change in terrain category and type of deck supports on responses of these bridges under dead load and mean wind forces. The results are used as reference for comparison with buffeting responses.

From the results, it is observed that the static response in vertical direction of bridge deck reduces with increase in terrain roughness. This is due to decrease in mean wind speed due to increased terrain roughness. Not much variation in cable tension (variation within 1%) due to change in terrain roughness is observed.

To study the effect of type of deck supports, the analysis is also carried out for Bridge #1 at a wind speed of 45.8m/sec at the bridge deck level, with surface roughness equal to 0.005m in terrain category TC-1. The support type for bridge deck is varied from DST-1 to DST-6. The response of this bridge under dead load and mean wind forces is presented in Table.6.2. Also, the variation in cable forces for this bridge under dead load and mean wind forces, with change in support type for bridge deck is given in Table 6.3. From the results, it is clear that outer cable, i.e., cable-1 is subjected to 4% variation in axial force with change in deck support type DST-5 to DST-6.

Table 6.2 : Static Response for Bridge #1 due to Dead Load and Mean Wind Forces - Effect of Support Types for Bridge Deck (Mean Wind Speed U(30)=45.8m/sec for Terrain Category TC-1)

Support Type for Bridge Deck	Mid Span Vertical Response (m)	Maximum Side Span Vertical Response (m)	Left Tower Tip Longitudinal Response (m)
DST-1	0.2442	0.0334	0.0438
DST-2	0.3046	0.0290	0.0466
DST-3	0.3043	0.0208	0.0199
DST-4	0.3049	0.0357	0.0692
DST-5	0.3237	0.0418	0.0714
DST-6	0.3260	0.0125	0.0778

Table 6.3 : Axial Force in Cables of Bridge #1 due to Dead Load and Mean Wind Forces - Effect of Support Types for Bridge Deck (Mean Wind Speed U(30)=45.8m/sec for Terrain Category TC-1)

Cable Number	Cable Force in kN with Different Support Type for Bridge Deck					
	DST-1	DST-2	DST-3	DST-4	DST-5	DST-6
1	8903.0	9003.0	8959.0	8927.0	8781.0	9149.0
2	6034.0	6062.0	6050.0	6041.0	5984.0	6101.0
3	5319.0	5318.0	5319.0	5321.0	5230.0	5313.0
4	4476.0	4466.0	4472.0	4478.0	4223.0	4448.0
5	3480.0	3473.0	3477.0	3481.0	3308.0	3457.0
6	2655.0	2649.0	2647.0	2646.0	4354.0	2668.0
7	9670.0	9677.0	9686.0	9696.0	9627.0	9684.0

For Bridge#2, the nonlinear static analyses have been performed corresponding to wind speed of 43.2m/sec at bridge deck level of 45m, with terrain roughness equal to 0.03m in terrain categoryTC-2. The variation in mean wind response of Bridge #2 with different type of supports for bridge deck at towers and abutments are presented in Table 6.4. Also, the variation in axial force in cables for this bridge with change in type of deck support is given in Table 6.5. It is observed that outer cable (cable-1) is subjected to a maximum variation of 5.7% in axial force with change in deck support type DST-5 to DST-6.

Table 6.4 : Static Response for Bridge #2 due to Dead Load and Mean Wind Forces - Effect of Support Types for Bridge Deck

(Mean Wind Speed U(45)=43.20m/sec for Terrain Category TC-2)

Support Type for Bridge Deck	Mid Span Vertical Response (m)	Maximum Side Span Vertical Response (m)	Left Tower Tip Longitudinal Response (m)
DST-1	0.748	0.125	0.147
DST-2	0.9808	0.105	0.162
DST-3	0.9807	0.095	0.0788
DST-4	0.9821	0.112	0.234
DST-5	1.096	0.166	0.243
DST-6	1.003	0.112	0.246

Table 6.5 : Axial Force in Cables of Bridge #2 due to Dead Load and Mean Wind Forces - Effect of Support Types for Bridge Deck

(Mean Wind Speed U(45)=43.20m/sec for Terrain Category TC-2)

Cable Number	Cable Forces in kN with Different Support Type for Bridge Deck					
	DST-1	DST-2	DST-3	DST-4	DST-5	DST-6
1	20307.0	20599.0	20668.0	20545.0	19960.0	21104.0
2	13766.0	13835.0	13849.0	13821.0	13726.0	13943.0
3	12077.0	12065.0	12058.0	12071.0	12051.0	12028.0
4	9530.0	9511.0	9503.0	9524.0	8956.0	9462.0
5	7648.0	7644.0	7640.0	7652.0	6556.0	7608.0
6	5821.0	5811.0	5812.0	5810.0	9876.0	5815.0
7	22527.0	22767.0	22754.0	22786.0	22935.0	22683.0

6.4 BUFFETING ANALYSIS

As stated earlier, time domain buffeting analysis of the bridges is performed to observe the effect of increase in mean wind speed, terrain roughness and influence of support type for bridge deck at towers and abutments on the buffeting responses. Also a comparison of buffeting response with the mean wind response is made to quantify the dynamic amplification due to buffeting with the help of gust response factor. This factor along the main span of the bridge is computed by dividing the peak buffeting response by mean response. Further, from the results increase in cable force, axial force, shear force and bending moments in the deck and towers, reactions at tower base and forces at deck supports due to buffeting are obtained. The design forces in these components are obtained by adding the mean wind and buffeting induced forces.

Since for time domain analysis, buffeting forces are required; their evaluation is described in the following Section.

6.4.1 Buffeting Forces

The instantaneous buffeting forces in the vertical and lateral directions, and torsional moments acting on Bridge#1 and Bridge#2 have been generated using the computer routine INWINF, which uses the longitudinal and vertical wind velocity fluctuations generated by spectral representation method in which the routine 'WINGEN' has been used as discussed in Section 4.5. The steady-state coefficients as stated in Section 6.2.2 have been used in computation of the buffeting forces. For these bridges, the aerodynamic admittance functions have been assumed to be unity.

For the time domain buffeting analysis, the buffeting drag and lift forces are applied at the centre of bridge deck and moment at a distance B/4 away from the centre. To perform the analysis, the modelling of bridge as described earlier in Section 3.6.2 has been slightly modified with additional node either at the centre or at a distance B/4 away from centre on each cross beam, increasing the total number of nodes to 121 and

total number of elements to196 in the case of bridge with deck support types DST-1 to DST-5.

6.4.2 Buffeting Response

The buffeting responses of the bridges in the vertical and lateral directions and in torsion for the deck have been obtained by time domain approach using the aerodynamic forces computed as described in the preceding section.

The time domain analysis is accomplished by step-by-step integration of equations of motion in modal coordinates by Wilson-θ method as discussed in Section 5.4.1. In the analysis, time integration is performed at a time step of 0.0016 sec.

6.4.2.1 Validation of time domain approach

The validation of buffeting analysis by time domain approach is achieved by comparing results with those obtained by classical frequency domain method given in Scanlan (1981) and Irwin (1977) and briefly discussed in Appendix –III.

To verify the accuracy of the time domain analysis, the Bridge #1 is analysed by both time and frequency domain approaches, using buffeting forces generated for the longitudinal and vertical velocity fluctuations at deck level corresponding to a mean wind speed of 34.7m/sec at deck level for terrain category TC-1. The contributions from first and second vertical symmetric modes (V-S1 and V-S2) are included in the analysis. The peak deflection at centre of main span (mid span) is estimated as 0.4022m by time domain approach, which is in close agreement with the response of 0.4350m obtained by frequency domain approach.

In another study, the peak buffeting response contribution by the first vertical symmetric mode (V-S1) at mid span of the bridge deck for Bridge #1 is computed by time domain as well as frequency domain method by assuming a mean wind speed as 50m/sec at the deck level of 30m with surface roughness parameter z_0 as 0.03m for a net damping of 0.0392. The value of peak-to-peak response at mid span computed by

time domain analysis is 1.08m against the values of 1.17m by Scanlan's method and 1.069m by Irwin's method. Further, the vertical buffeting responses for bridge deck at centre of main span have been computed by varying the net damping values arbitrarily in the range of 0.003 to 0.075. The vertical buffeting responses obtained at the centre of main span by the time domain method as well as by frequency domain method using Scanlan's theory is illustrated in Fig. 6.5. Again, close agreement of the results by time and frequency domain buffeting analyses is observed. Thus the accuracy of time domain buffeting analysis as described in Chapter 5 is established.

After validating the time domain approach for evaluating the buffeting response of cable stayed bridges, sensitivity studies are performed to understand the effect of time duration of buffeting forces, number of modes of vibration and modal damping on the buffeting response. The details and results of sensitivity studies are discussed in the following section.

6.4.2.2 Sensitivity analysis

To make the time domain buffeting analysis computationally efficient for parametric study, it is felt necessary to include the optimum number of modes as well as time duration of the buffeting forces, without compromising on the accuracy of results. Therefore, sensitivity analysis is performed to study understand the effect of time duration of buffeting wind forces, number of modes of vibration and modal damping on the buffeting response.

Analyses have been performed on Bridge #1 at a mean wind speed of 50m/sec taking z_0 as 0.3m by assuming the buffeting forces to act on the bridge for durations of 64, 128, 256 and 512 sec, while including contribution from first four modes for type of deck support DST-3. It is observed that, for this bridge, to make the computation reasonably accurate and efficient, it is sufficient to consider only the first four modes, i.e., including V-S2 (refer Table 6.1 for mode types) and 1024 time-force pairs corresponding to 256 sec in the time domain analysis.

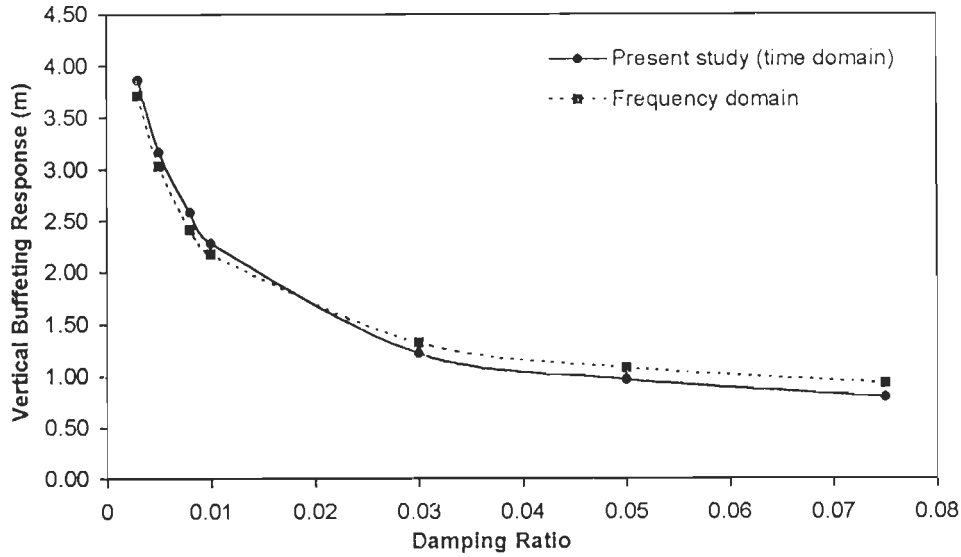

Fig. 6.5 : Comparison of Vertical Buffeting Response at Midspan of Bridge # 1 – Time Domain Vs Frequency Domain Approach

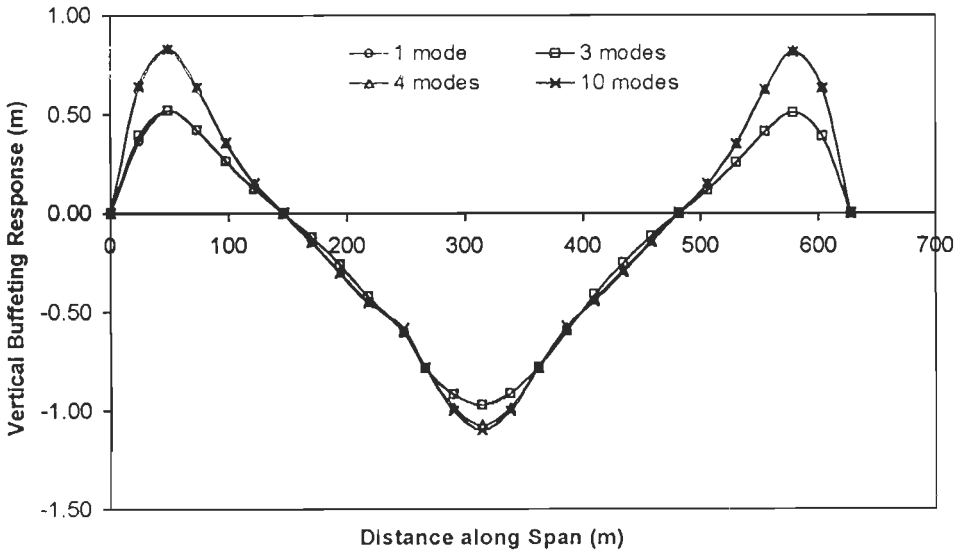

Fig. 6.6 : Peak Vertical Buffeting Response for Bridge # 1 – Variation with Number of Modes

The buffeting analysis for Bridge # 1 is performed at a mean wind speed of 50m/sec taking z_0 as 0.3m and considering the buffeting forces to act on the bridge for 74.75 sec. The number of modes considered in the analysis of this bridge are 1, 2, 3, 4 and 10 (refer Table 6.1 for mode types included in the analysis). The peak mid span and side span response with increase in number of modes considered, taking net modal damping ratio as 0.05, are given in Table 6.6. The profile of peak vertical buffeting response is depicted in Fig. 6.6 with increase in number of modes.

Table 6.6 : Peak Buffeting Response with Number of Modes for Bridge#1

Description	Vertical Response in (m) with Number of Modes				
	1* only V-S1	2* upto V-AS2	3* upto T-S1	4* upto V-S2	10* upto L-S1
Mid Span Vertical Deflection (m)	0.9672	0.9673	0.9673	1.068	1.068
Side Span Maximum Vertical Deflection (m)	0.4236	0.4226	0.4226	0.636	0.636

* Refer Table 6.1 for mode types corresponding to number of modes included in the analysis

From Table 6.6, it is clear that the major contribution to vertical buffeting response at mid span is from mode number 1, i.e., the first vertical symmetric mode (V-S1) to the extent of about 90% and by the second vertical symmetric mode (V-S2) by about 10%, if equal damping is taken in all the modes. A similar study with different modal damping values is conducted and it is found that the contribution of the first vertical symmetric mode (V-S1) is about 83% and the second vertical symmetric mode (V-S2) is 17%. However, in the case of maximum vertical deflection in the side span, it is observed that the contribution of second vertical symmetric mode (V-S2) is 50% of contribution by first vertical symmetric mode (V-S1).

Analyses for Bridge#2 have been carried out by first assuming the same net modal damping in the first and second vertical symmetric modes (V-S1 and V-S2) and then by taking the respective damping values. It is found that in the first case, the contribution to buffeting response by second vertical symmetric mode (VS-2) is about

22% of contribution by first vertical symmetric mode (VS-1). However, in the second case, contribution of V-S2 increases to about 40%. The enhancement in the contribution to response by V-S2 is attributed to relatively lower modal damping for V-S2 (0.0219) in comparison to that for V-S1 (0.05).

These findings are in line with the earlier studies reported on time domain analysis of the longest suspension bridge, Akashi Kaikyo Bridge in Japan, by Miyata *et al* (1995). They reported that the higher mode participation could be clearly identified with time domain analysis and in the case of vertical buffeting response; contribution of both first and second vertical symmetric modes (V-S1 and V-S2) can be seen. The contributions of higher symmetric vertical modes (i.e., beyond second mode) are found to be negligible.

Also, from analyses by changing the type of deck supports, it is concluded that 4 modes are sufficient for Bridge#1 to give reasonably accurate results for this bridge with deck support condition DST-1 to DST-3 and DST-6. For deck supports DST-4 and DST-5, minimum number of modes to be considered is 5 and 7 respectively so that both first and second vertical symmetric modes (V-S1 and V-S2) are included in the analysis. For Bridge #2, it is found necessary to include 5 modes for DST-1 to DST-3, 6modes for DST-4 and DST-6 and 7 modes for DST-5 for reliable results.

After the sensitivity analysis, time domain buffeting analysis of Bridge # 1 and Bridge #2 has been performed to study the effect of (i) increase in mean wind speed, (ii) variation in terrain roughness and (iii) various types of deck supports at towers and abutments on the buffeting response. The details of analysis and results and their interpretation for design are presented in the following Sections.

6.4.3 Effect of Mean Wind Speed

As discussed earlier, to study the effect of mean wind speed on buffeting response, the analysis of the bridges has been conducted by varying the wind speed at

10m height from 30 m/sec to 60m/sec in steps of 10m/sec. The longitudinal and vertical wind velocity fluctuations are generated corresponding to deck level mean wind speed assuming the Bridge#1 and Bridge #2 to be located in terrain categories TC-1 and TC-2 respectively. The vertical buffeting forces are generated using the simulated wind velocity fluctuations. The type of deck support considered for the analysis of Bridge #1 is DST-2 (deck fixed at one of the tower and on rollers at other supports) and for Bridge#2, DST-6 (deck elastically supported at towers and on rollers at other supports).

For Bridge #1, assuming it to be situated in terrain category TC-1, the mean wind speed is increased from 34.3m/sec to 68.6m/sec and time domain analysis is performed. The steps involved in the time domain analysis for estimation of vertical buffeting response such as simulation of longitudinal and vertical wind velocity fluctuations, spectral match for generated longitudinal and vertical velocity fluctuations with their respective target spectrum and time histories of generated vertical buffeting force as well as response at mid span of the deck at a mean wind speed U(30) = 34.3m/sec are illustrated in Fig. 6.7.

The variation in the peak response (buffeting and mean components) for Bridge # 1 at mid span and in side span of the deck as well as the longitudinal movement of the left side tower is illustrated in Fig. 6.8. From this Figure, it is observed that with increase in the mean wind speed U(30) from 34.3m/sec to 68.6m/sec, the mid span and side span vertical buffeting response increased to 2.77 and 3.13 times respectively. The tower longitudinal response increased to 3.12 times. Also, the side span vertical buffeting response is comparable in magnitude to that of the mid span deck response. With increase in wind speed the variation in vertical buffeting response is nonlinear. Also, the analysis for the vertical buffeting response has been performed using four ensembles of the generated vertical buffeting forces and the responses obtained are almost same (within 3% variation), hence consistent.

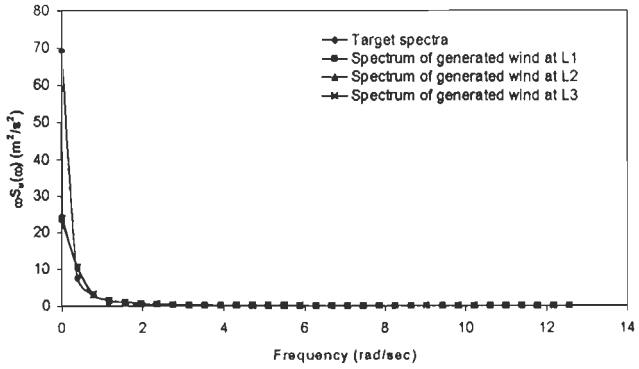

(a) Spectral match for longitudinal velocity fluctuations

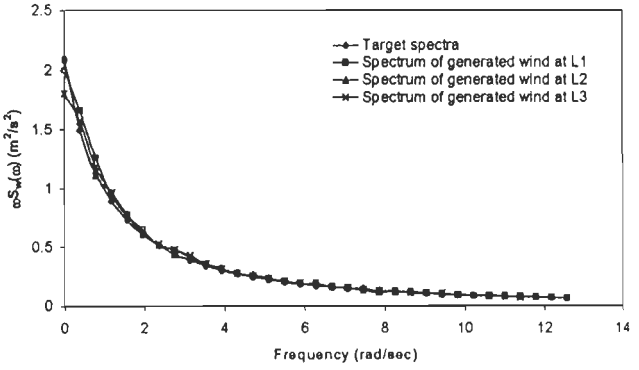

(b) Spectral match for vertical velocity fluctuations

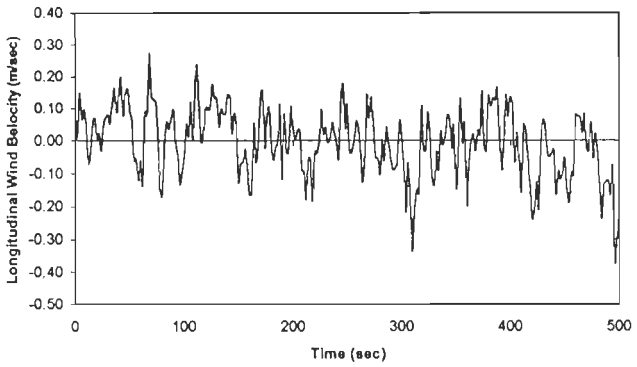

(c) Simulated longitudinal wind velocity fluctuations

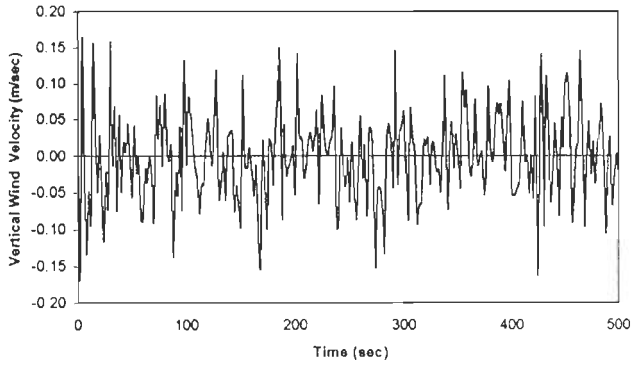

(d) Simulated vertical wind velocity fluctuations

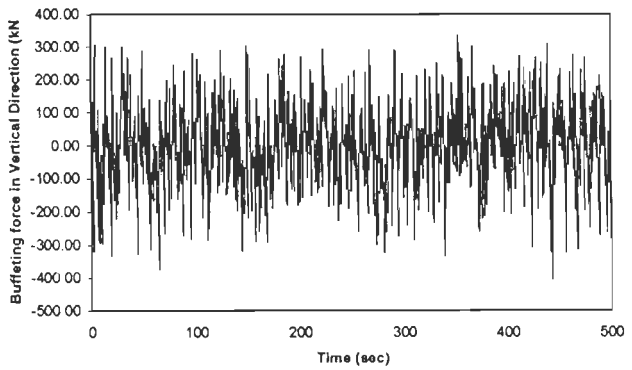

(e) Generated vertical buffeting force

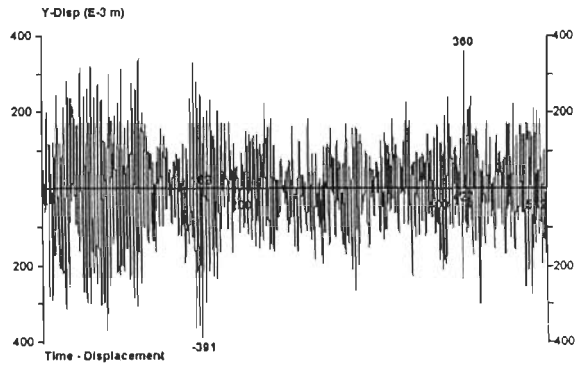

(f) Vertical buffeting response at mid span

Fig. 6.7 : Time Domain Analysis for Vertical Buffeting Response in Bridge # 1 at U(30) = 34.3 m/sec for TC-1

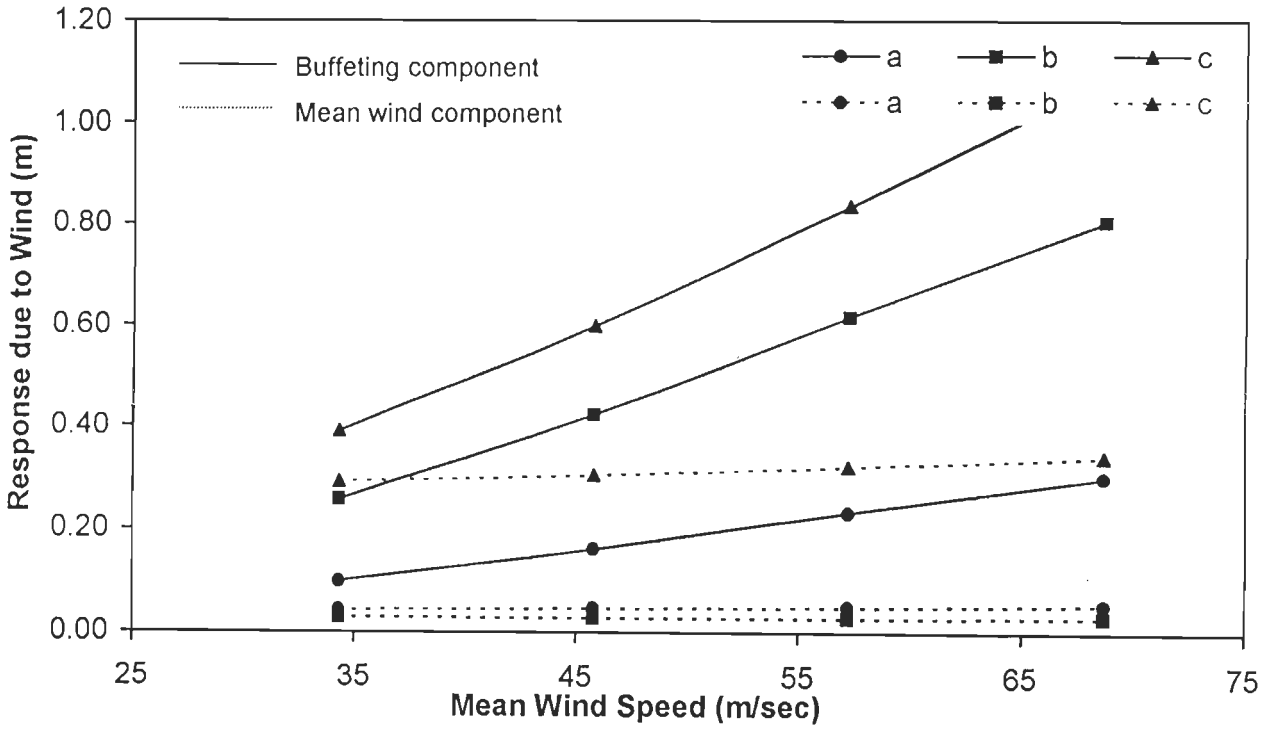

a : Tower tip longitudinal response
b : Maximum side span vertical response
c : Mid span vertical response

Fig. 6.8 : Responses in Bridge # 1 for Terrain Category TC-1 – Variation with Mean Wind Speed

The variation in absolute maximum axial force in cables of Bridge #1 with mean wind speed is presented in Fig. 6.9. It is seen that the outer cables are subjected to higher forces due to buffeting in comparison to the inner cables. Increase in tension in the outer cable (cable-1) is 23% to 70% of the initial cable tension with increase in mean wind speed. The increase in absolute maximum axial force in towers with variation in the mean wind speed is shown in Fig. 6.10. The buffeting induced axial forces in towers increase from 6.7% to 22% of the axial force induced by the dead load and mean wind force. Comparison of absolute maximum axial force in deck due to mean wind and buffeting components is depicted in Fig. 6.11(a) and the variation with increase in buffeting induced axial force in deck with increase in mean wind speed is presented in Fig. 6.11(b). The buffeting forces being random in nature, the induced forces are compressive as well as tensile in nature. Thus, the absolute maximum buffeting induced axial forces in the deck are given in these Figures. The increase in absolute maximum axial force in deck member near tower and vertical reactions at the deck supports at towers and abutments are shown in Fig. 6.12. The axial force in deck, near the tower increases by 12% to 29% of the mean wind component with increase in wind speed. The vertical reaction at deck supports at the abutment increases by 58% to 167% of the mean wind component. Again, it is observed that the variation of the vertical reaction in deck support at abutment is quite high in comparison to the reaction at deck supports at towers. The deck vertical shear force and bending moment diagrams are illustrated in Fig. 6.13 and Fig. 6.14 respectively. It may be noted that due to buffeting, the additional shear force and bending moment acting on the bridge deck are fluctuating in nature, hence reversal in the sign is implied.

The frequency of Bridge#1 in the first lateral mode is 0.952 Hz. As the energy content in wind at this frequency is low, the buffeting response in this direction is too low in comparison to the deck width and is therefore not important in the wind resistant design of this bridge.

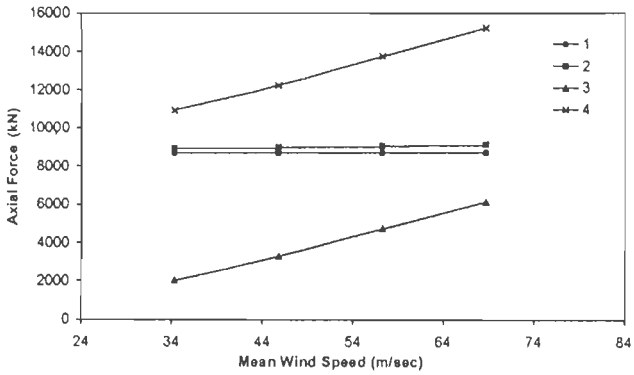

(a) Cable-1

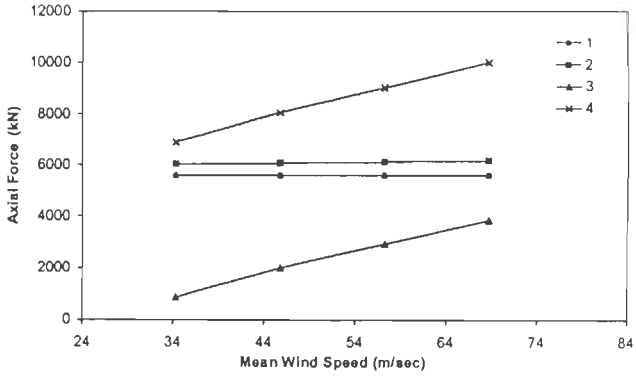

(b) Cable-2

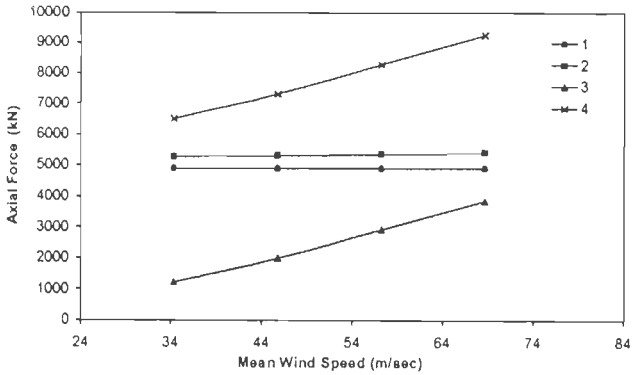

(c) Cable-3

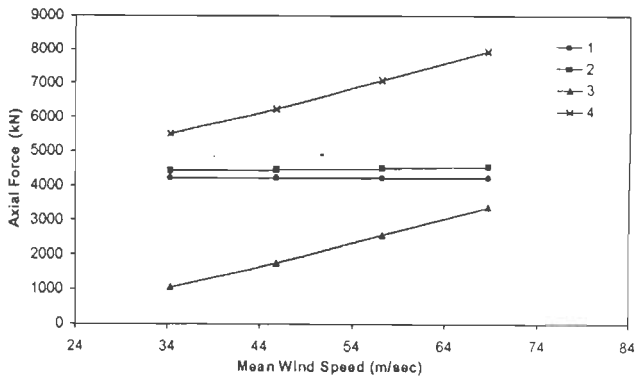

(d) Cable-4

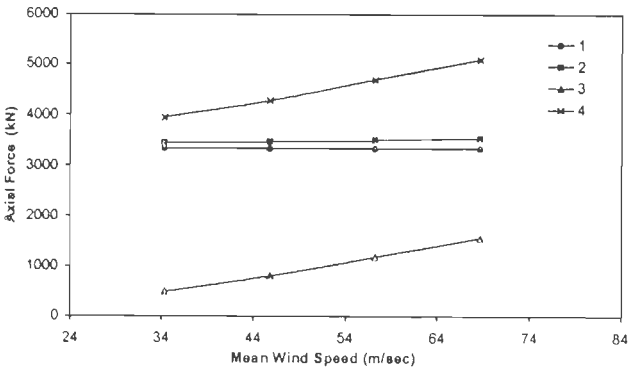

(e) Cable-5

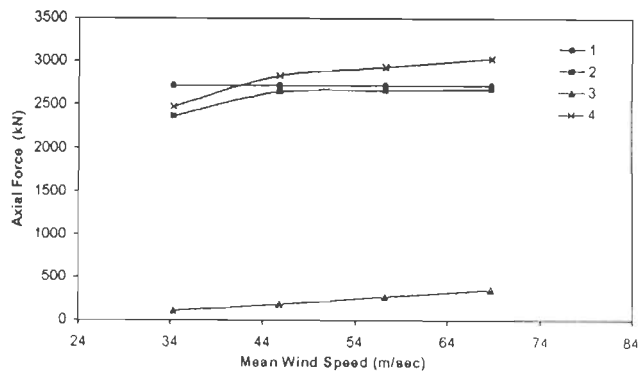

(f) Cable-6

1 : Initial tension 2 : Mean wind component

3 : Buffeting component 4 : Total cable force

Fig. 6.9 : Absolute Maximum Axial Forces in Cables of Bridge # 1 - Variation with Mean Wind Speed

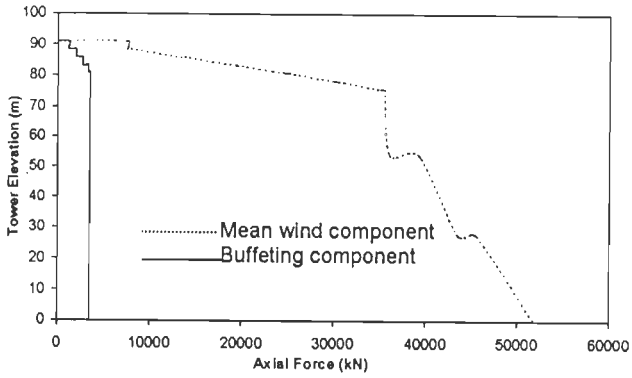

(a) Mean wind speed U(30) = 34.30 m/sec

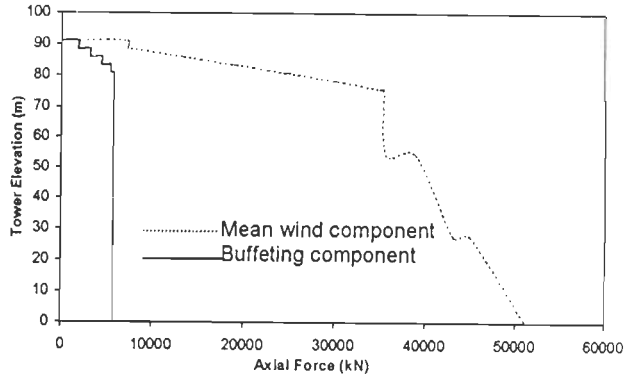

(b) Mean wind speed U(30) = 45.80 m/sec

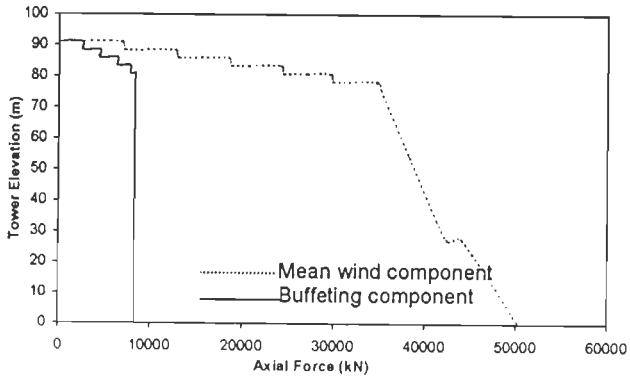

(c) Mean wind speed U(30) = 57.20 m/sec

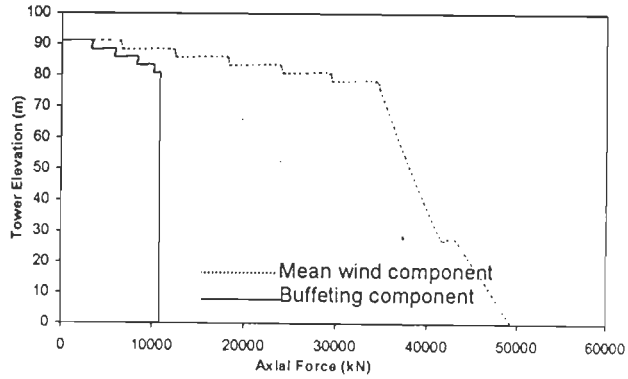

(d) Mean wind speed U(30) = 68.60 m/sec

Fig. 6.10 : Absolute Maximum Axial Force in Towers of Bridge # 1 – Variation with Mean Wind Speed

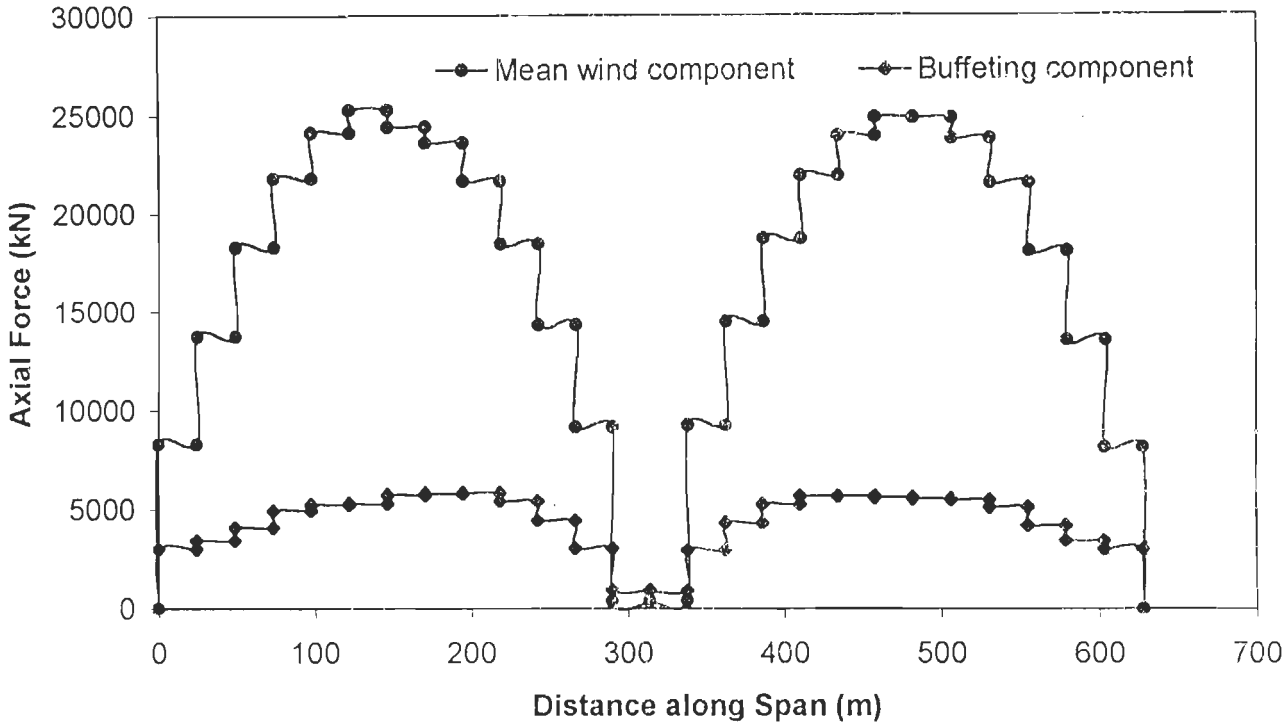

(a) Absolute maximum axial force in deck – Mean wind and buffeting component at U(30) = 34.3 m/sec for TC-1

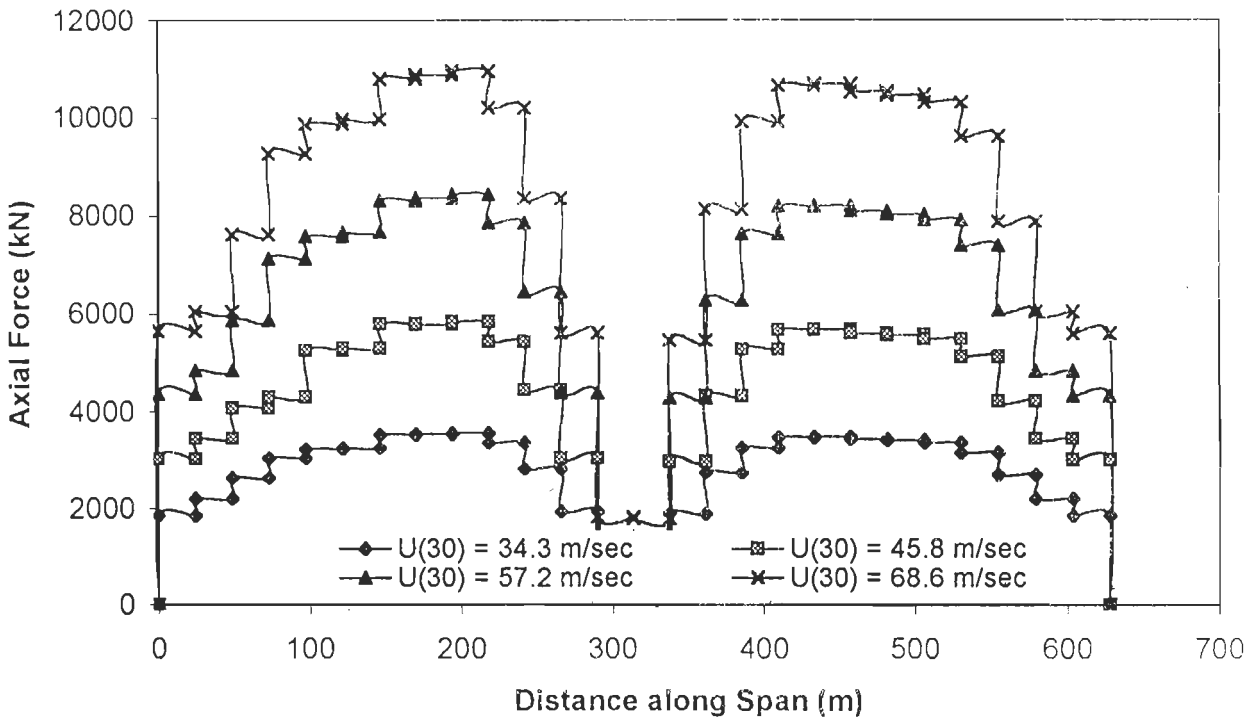

(b) Buffeting induced absolute maximum axial force in deck – Variation with mean wind speed

Fig. 6.11 : Deck Axial Force Diagram for Bridge # 1

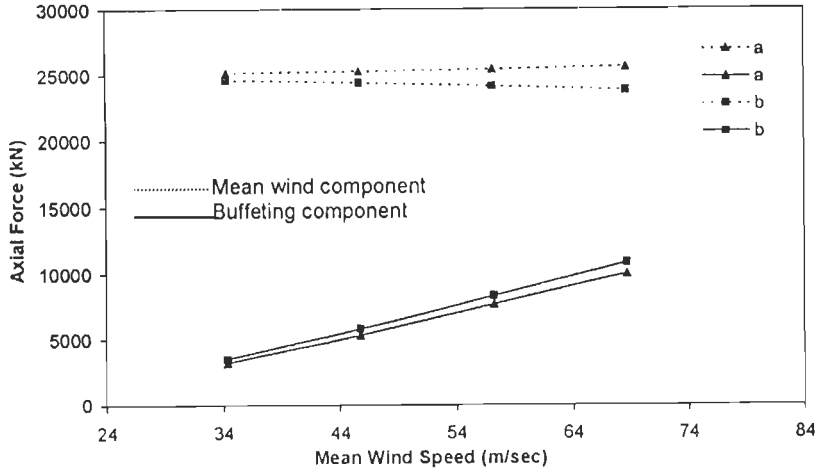

a : Force in member on left side of tower
b : Force in member on right side of tower
(a) Axial force in bridge deck members near left tower support

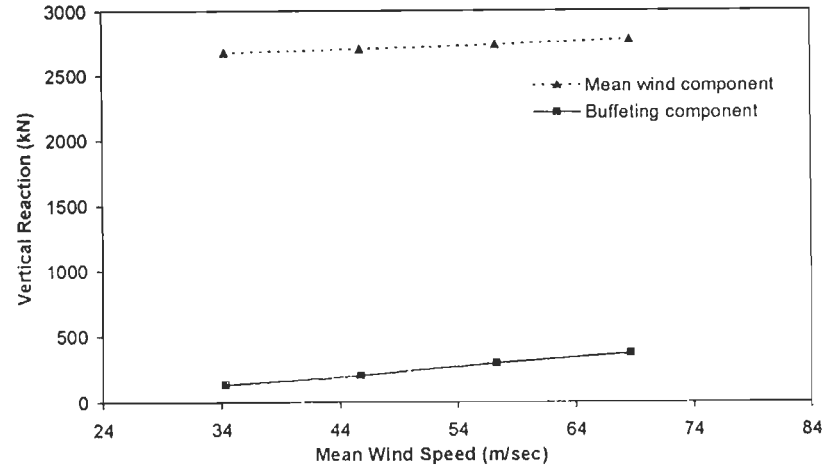

(b) Vertical Reaction in Deck Support at Tower

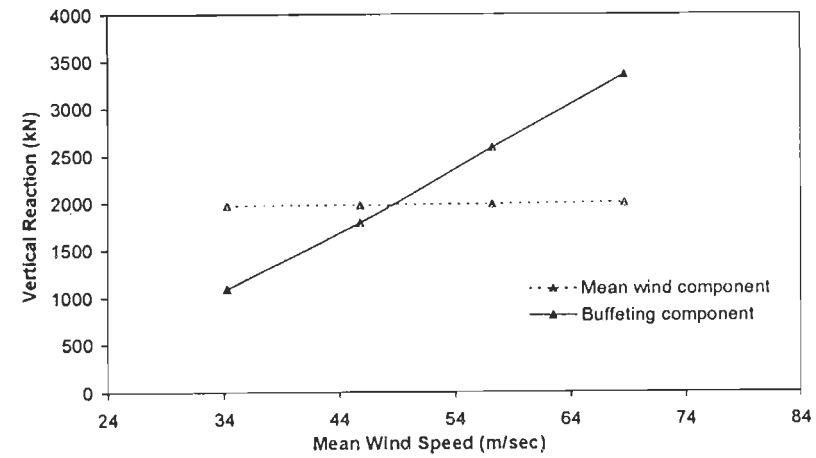

(c) Vertical Reaction in Deck Support at Abutment

Fig. 6.12 : Absolute Maximum Deck Axial Force and Reactions at Deck Supports in Bridge # 1 – Variation with Mean Wind Speed

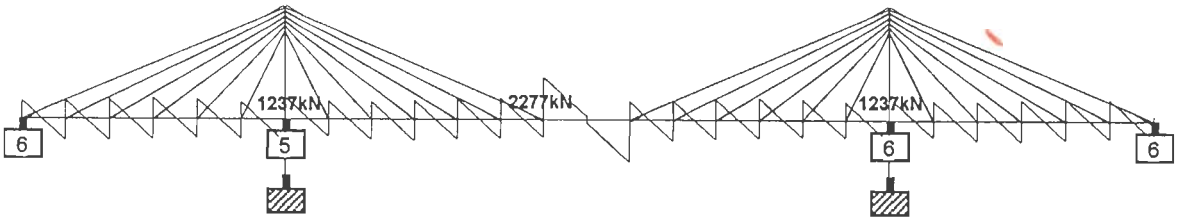

(a) Due to dead load and mean wind forces

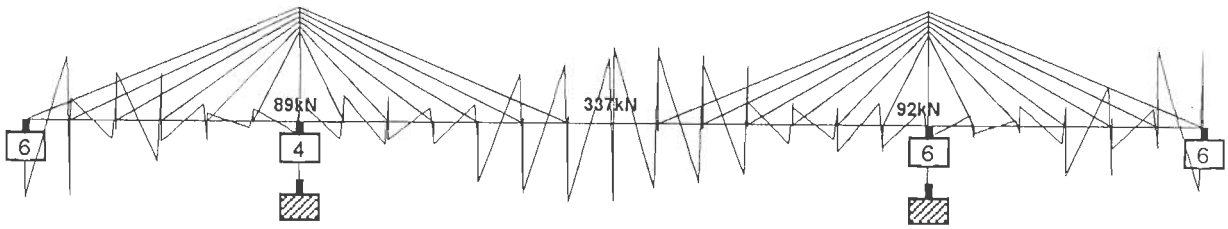

(b) Due to buffeting forces

Fig. 6.13 : Deck Vertical Shear Force Diagram for Bridge # 1 at Wind Speed U(30) = 34.3 m/sec for TC-1

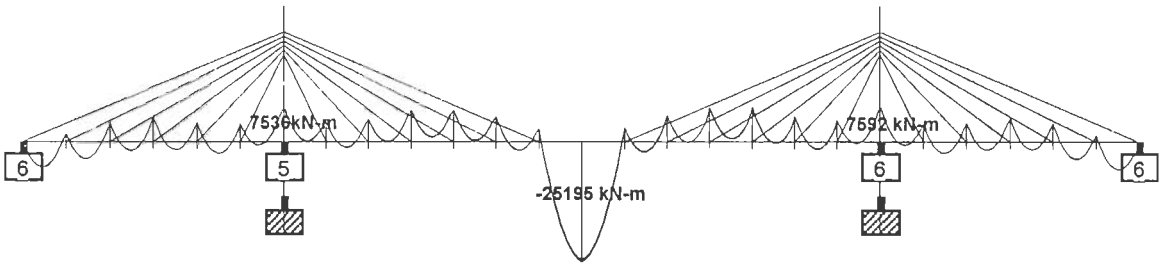

(a) Due to dead load and mean wind forces

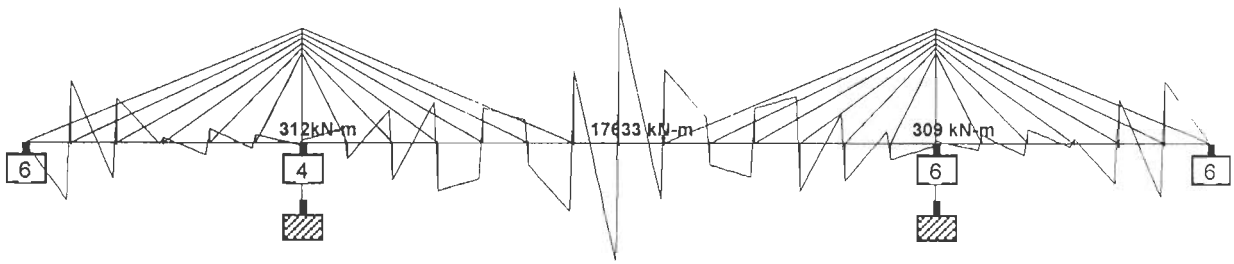

(b) Due to buffeting forces

Fig. 6.14 : Deck Bending Moment Diagram for Bridge # 1 at Wind Speed U(30) = 34.3 m/sec for TC-1

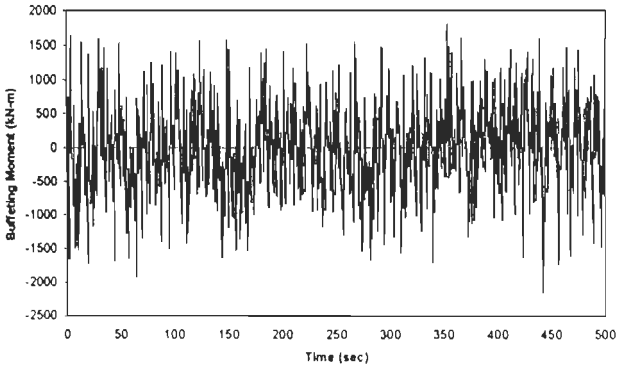

(a) Buffeting moment at U(30) = 34.30 m/sec

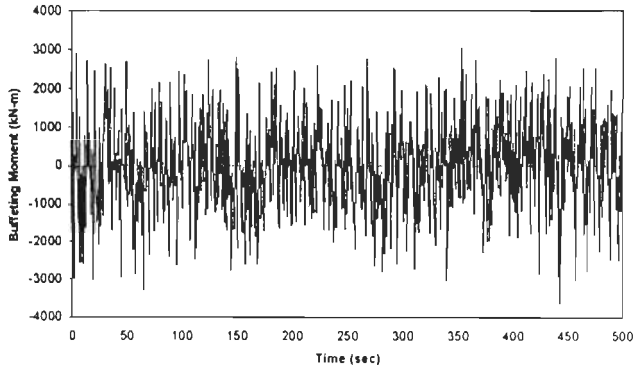

(b) Buffeting moment at U(30) = 45.80 m/sec

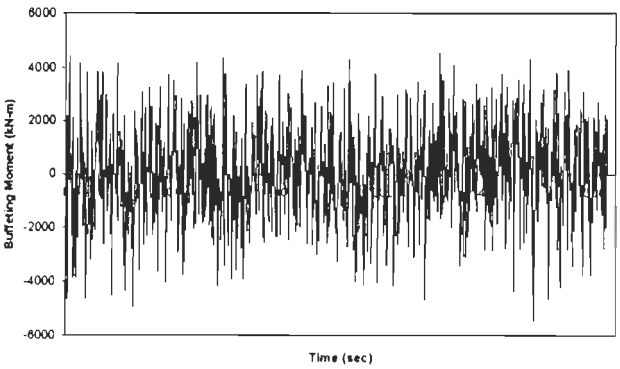

(c) Buffeting moment at U(30) = 57.20 m/sec

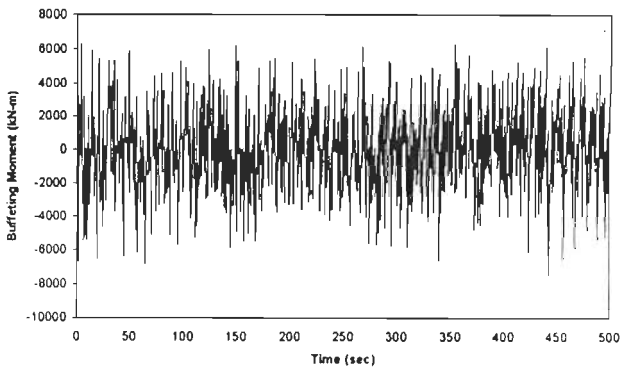

(d) Buffeting moment at U(30) = 68.60 m/sec

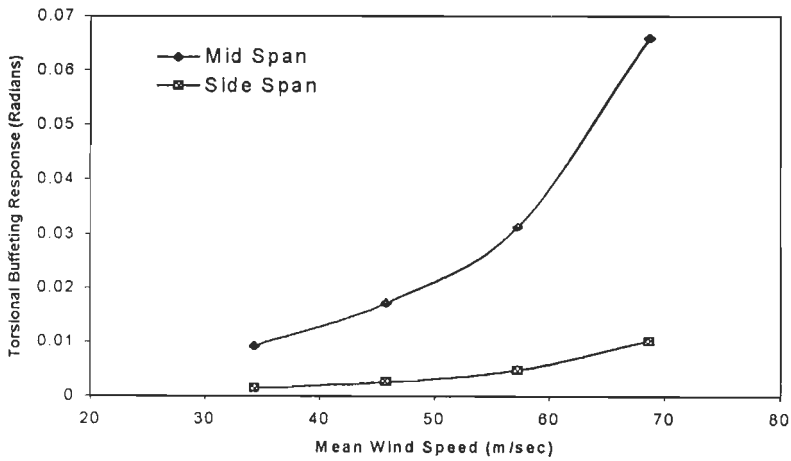

(e) Torsional buffeting response – Variation with mean wind speed

Fig. 6.15 : Time Domain Analysis for Buffeting Response in Torsion for Bridge # 1

Time domain analysis is performed for computing torsional buffeting response of the bridge. The generated buffeting moment at various wind speeds and the variation in torsional buffeting response with increase in mean wind speed are shown in Fig. 6.15. The variation in torsional buffeting response is nonlinear. The side span torsional response is much smaller in comparison to the mid span torsional response.

For Bridge #2, assuming it to be situated in terrain category TC-2, the deck level mean speed U(45) is increased from 32.3m/sec to 64.8m/sec and performed the buffeting analysis. Time domain analysis for the vertical buffeting response at a wind speed of 43.2m/sec for terrain category TC-2 is illustrated in Fig. 6.16

The variation in the peak responses (buffeting and mean wind components) in vertical direction at the mid span and in the side span of the deck as well as the longitudinal movement of left side tower is illustrated in Fig. 6.17. From this Figure, it is observed that with increase in the mean wind speed U(45) from 32.3m/sec to 64.8m/sec, the mid span and side span vertical buffeting response increases to 2.74 and 2.55 times respectively. The tower longitudinal response increases to 2.55 times. Also, the side span vertical buffeting response is comparable in magnitude with that of mid span deck response. With increase in wind speed the variation in vertical buffeting response is nonlinear.

The variation in absolute maximum axial force in cables of Bridge #2 with increase in mean wind speed is presented in Fig. 6.18. It is seen that the outer cables are subjected to more forces due to buffeting in comparison to the inner cables. Increase in tension in outer cable is 20% to 50% of the initial cable tension with increase in the mean wind speed. The increase in absolute maximum axial force in towers with variation in mean wind speed is shown in Fig. 6.19. The buffeting induced axial force in towers increase from 5% to 12% of the axial forces induced by the dead load and mean wind force. Comparison of absolute maximum axial force in deck due to mean wind and buffeting components is shown in Fig. 6.20(a) and the variation in buffeting induced axial force in deck with increase in the mean wind speed is presented in Fig. 6.20(b). The increase in axial force in deck near tower and vertical reaction at deck

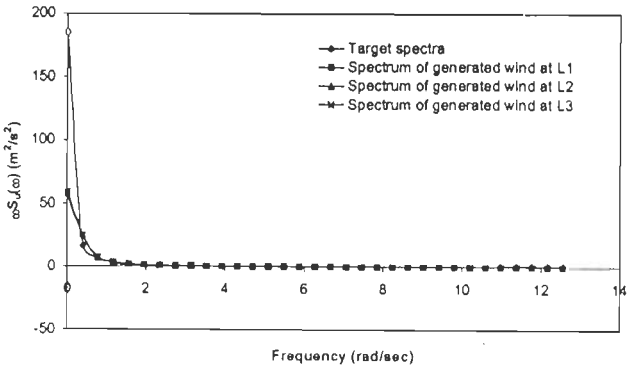

(a) Spectral match for longitudinal velocity fluctuations

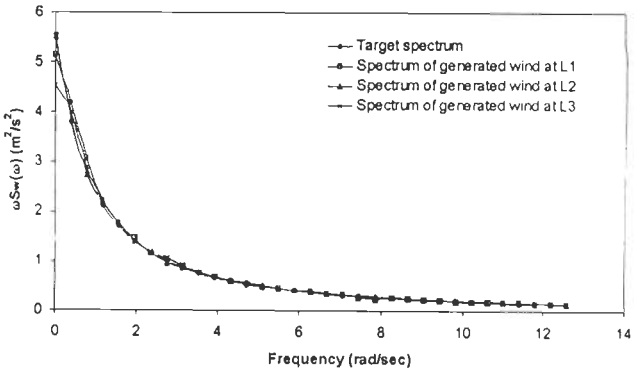

(b) Spectral match for vertical velocity fluctuations

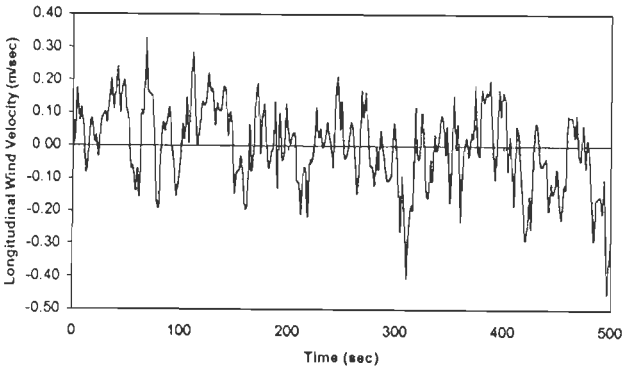

(c) Simulated longitudinal wind velocity fluctuations

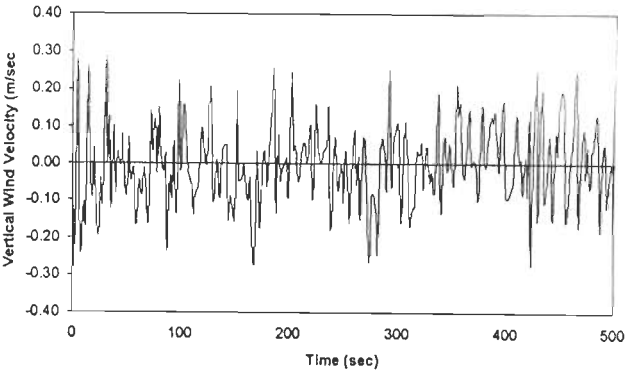

(d) Simulated vertical wind velocity fluctuations

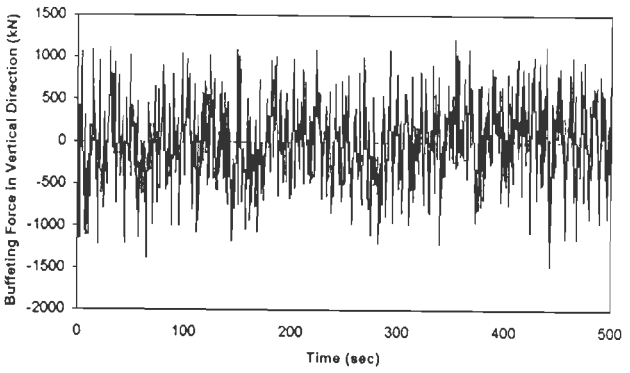

(e) Generated vertical buffeting force

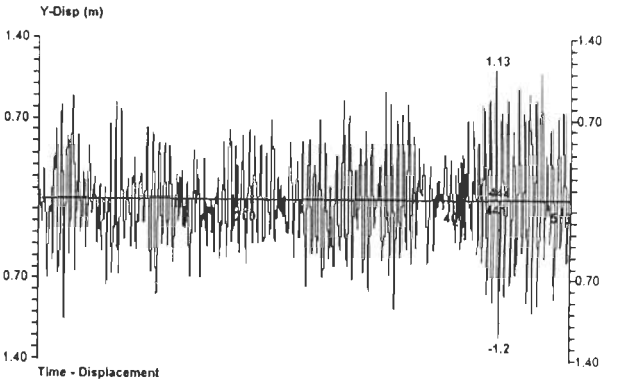

(f) Vertical buffeting response at mid span

Fig. 6.16 : Time Domain Analysis for Vertical Buffeting Response in Bridge # 2 at U(45) = 43.2 m/sec for TC-2

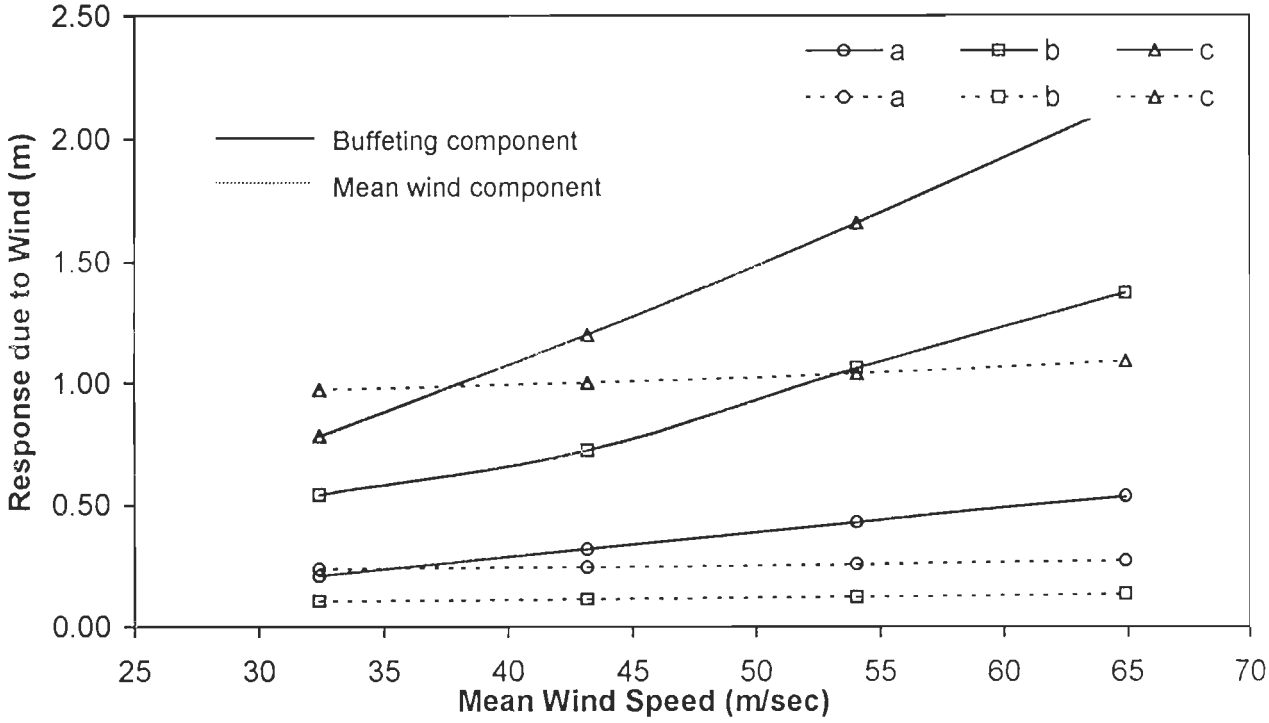

a : Tower tip longitudinal response
b : Maximum side span vertical response
c : Mid span vertical response

Fig. 6.17 : Responses in Bridge # 2 for Terrain Category TC-2 - Variation with Mean Wind Speed

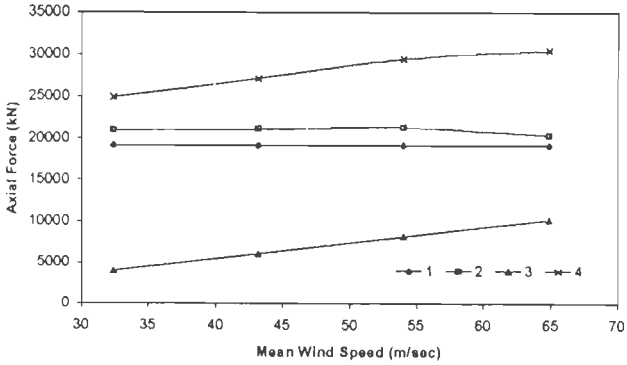

(a) Cable-1

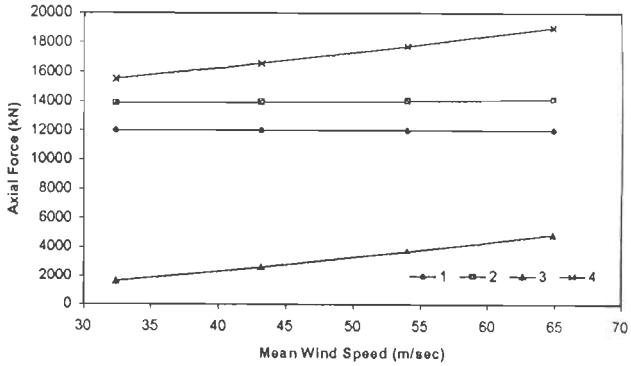

(b) Cable-2

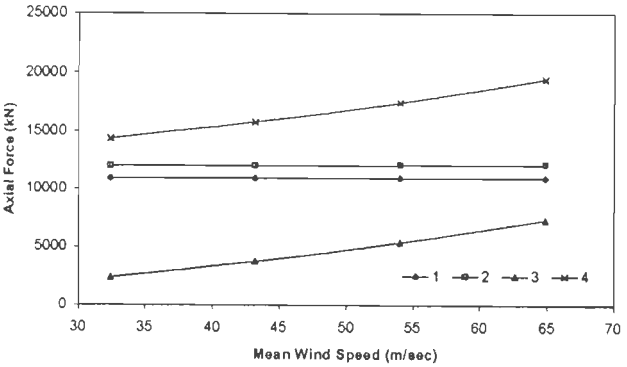

(c) Cable-3

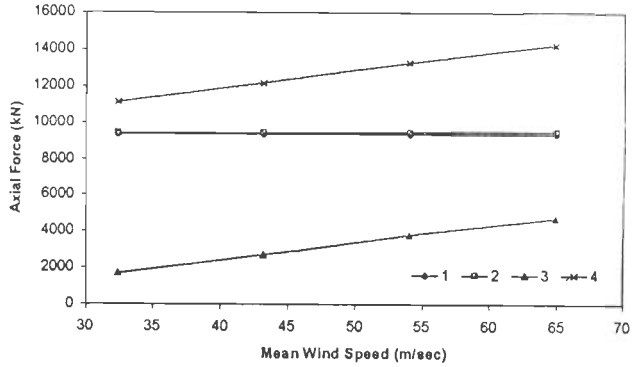

(d) Cable-4

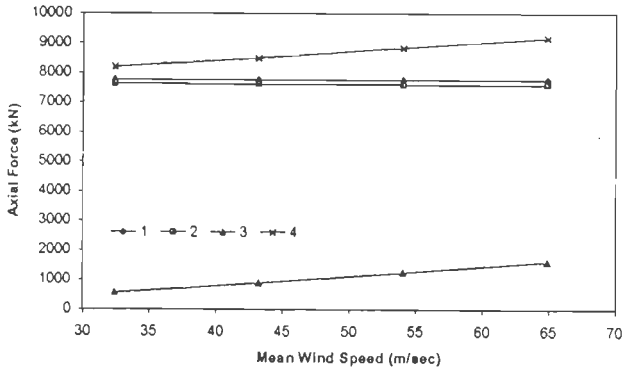

(e) Cable-5

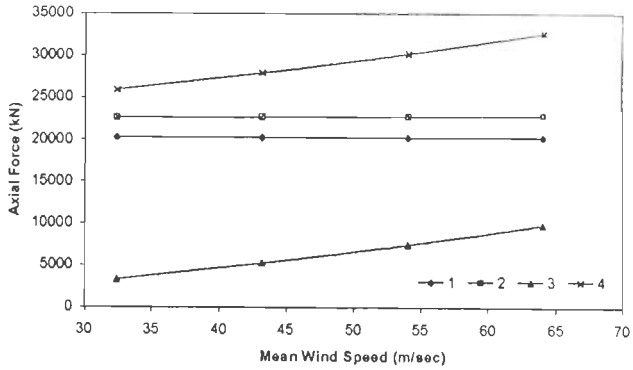

(f) Cable-7

1 : Initial tension
2: Mean wind component
3 : Buffeting component
4 : Total cable force

Fig. 6.18 : Absolute Maximum Axial Forces in Cables of Bridge # 2 – Variation with Mean Wind Speed

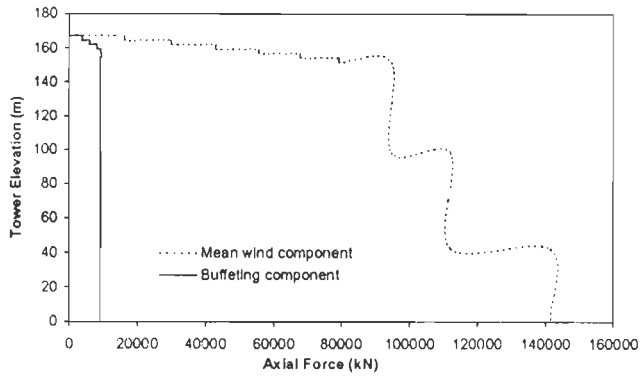

(a) Mean wind speed U(45) = 32.30 m/sec

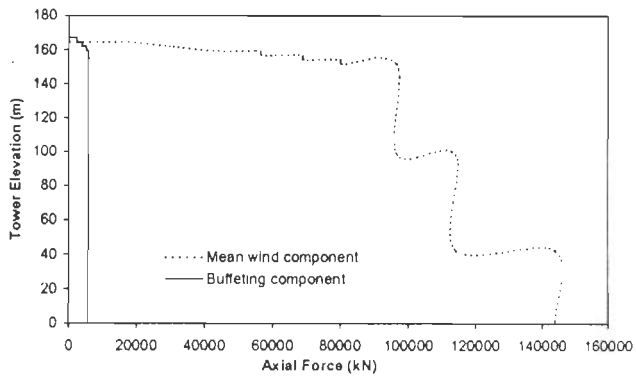

(b) Mean wind speed U(45) = 43.20 m/sec

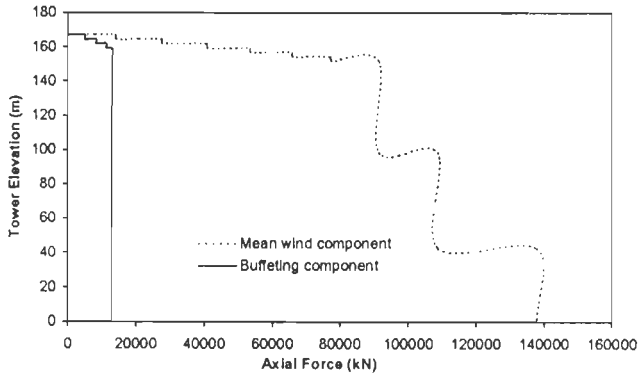

(c) Mean wind speed U(45) = 54.00 m/sec

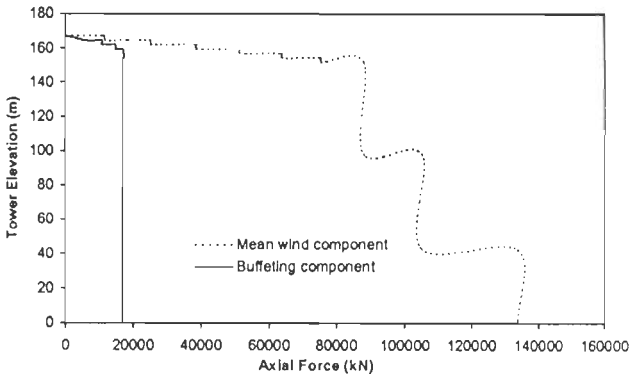

(d) Mean wind speed U(45) = 63.40 m/sec

Fig. 6.19 : Absolute Maximum Axial Force in Towers of Bridge # 2 - Variation with Mean Wind Speed

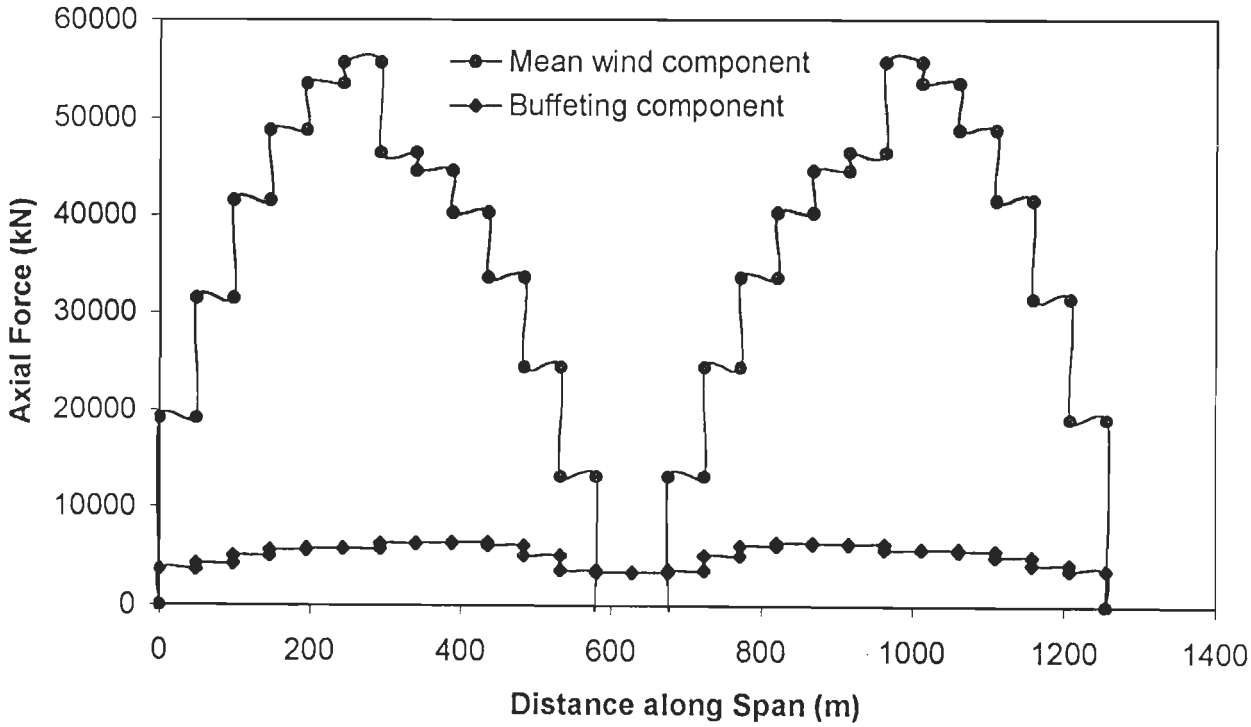

(a) Absolute maximum axial force in deck – Mean and buffeting components at U(45) = 32.30 m/sec for TC-2

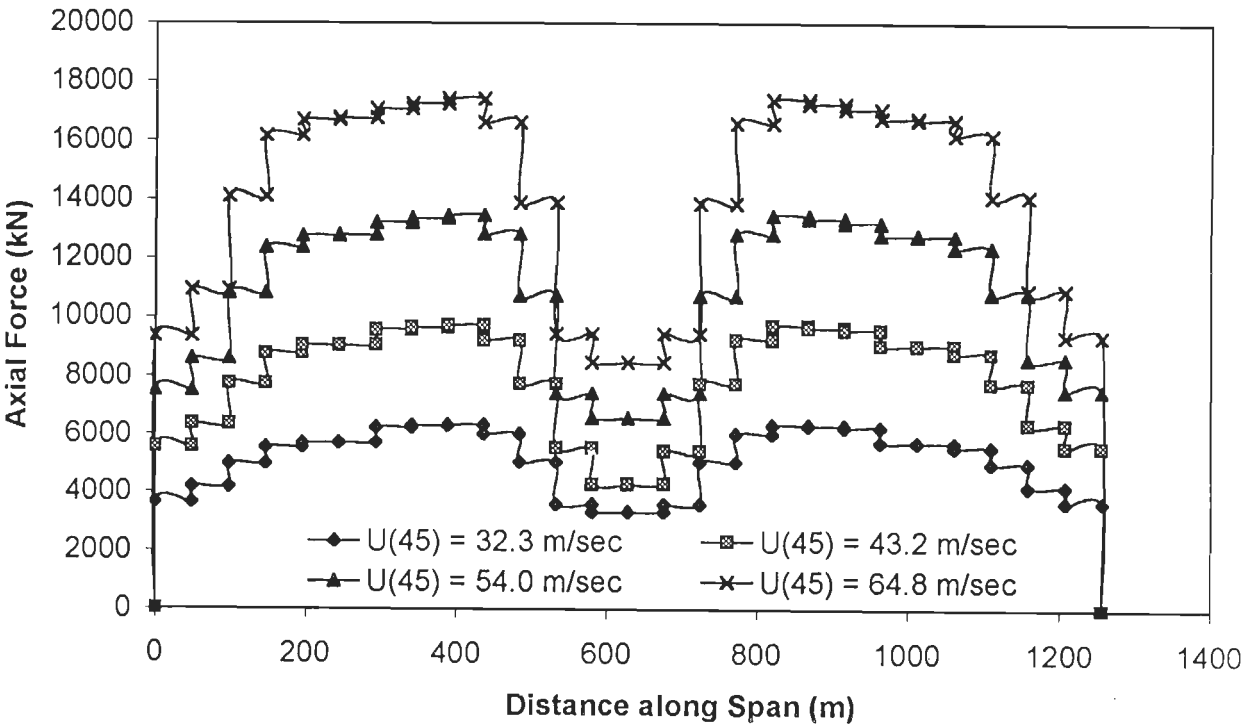

(b) Buffeting induced absolute maximum axial force in deck - Variation with mean wind speed

Fig. 6.20 : Deck Axial Force Diagram for Bridge # 2

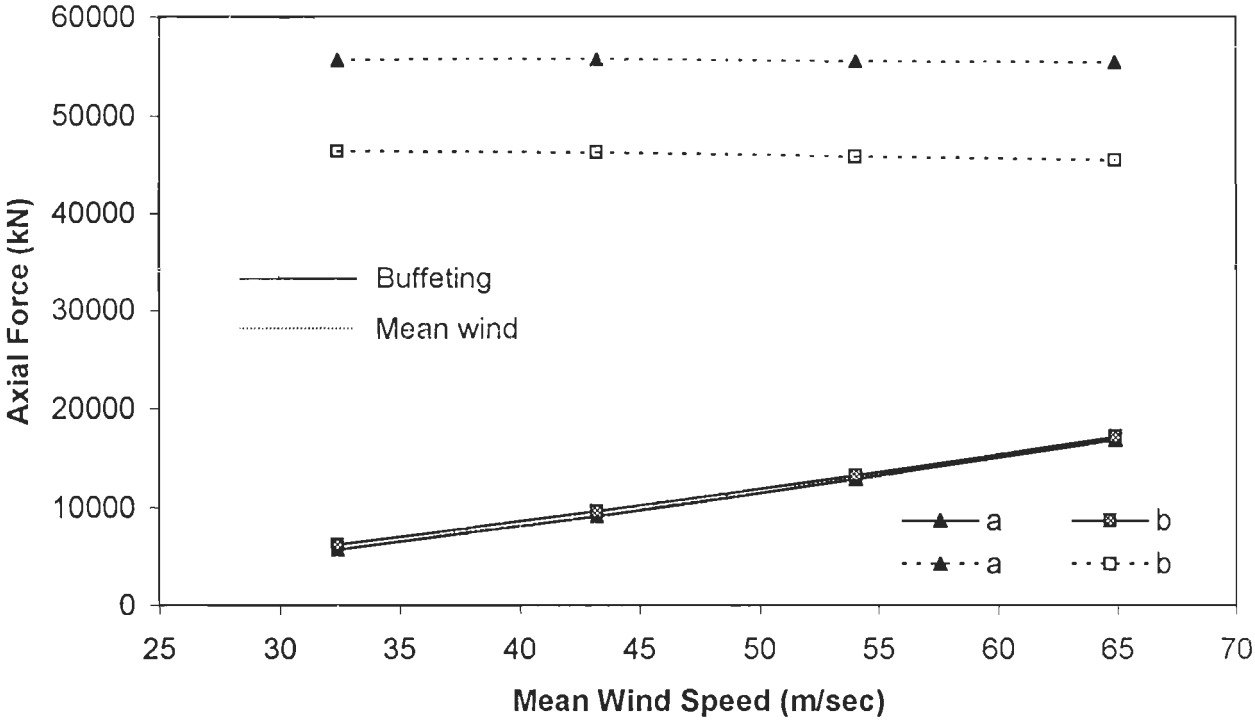

a : Force in member on left side of tower

b : Force in member on right side of tower

(a) Axial force in deck members near left tower support

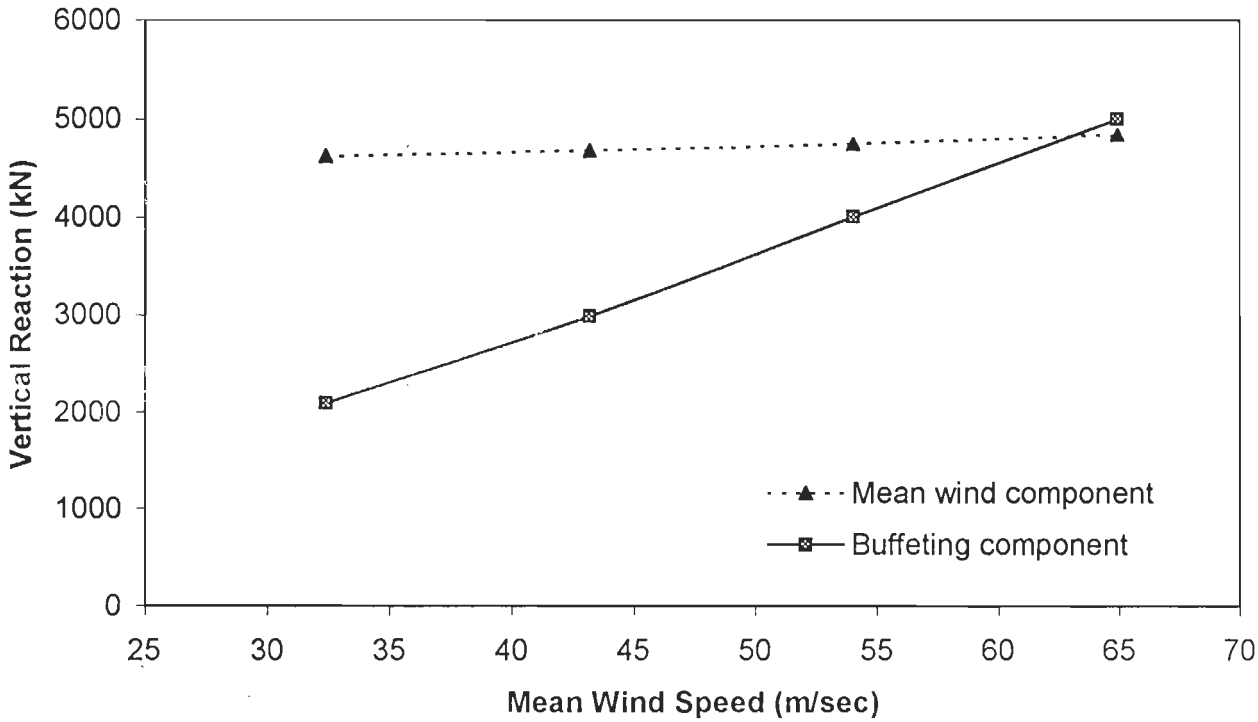

(b) Vertical reaction in deck support at abutment

Fig. 6.21 : Absolute Maximum Axial Force in Deck and Reactions at Deck Supports in Bridge # 2 – Variation with Mean Wind Speed

supports at towers and abutments are shown in Fig. 6.21. The axial force in deck, near the tower increases by 10% to 30% of the mean wind component with increase in wind speed. The vertical reaction at deck supports at the abutments increases by 45% to 103% of the mean wind component. The deck vertical shear force and bending moment diagrams at wind speed U(45) as 43.2m/sec for terrain category TC-2 are illustrated in Figs. 6.22 and 6.23.

The frequency of 1st lateral mode is only 0.303 Hz, and analyses are performed to observe the variation in the lateral buffeting response with increase in wind speed. The lateral buffeting forces generated at different wind speeds are shown in Fig. 6.24(a) to (d). The time history of lateral buffeting response at mid span at mean wind speed U(45) = 54m/sec is shown in Fig 6.24(e). The variation in peak lateral buffeting response at mid span and side span of the deck is illustrated in Fig. 6.24(f). Again, it is observed that the variation in lateral buffeting response is nonlinear with increase in mean wind speed. The maximum response in lateral direction is seen to occur at mid span and is much larger than in the side span.

Further, the analysis for computing the buffeting response of the bridge in torsional direction is performed. The generated buffeting moment at various wind speeds and the variation in torsional buffeting response with increase in mean wind speed are shown in Fig. 6.25. Here also the maximum response at mid span is much larger than in the side span of the deck.

6.4.4 Effect of Terrain Roughness

To study the effect of terrain roughness on buffeting response of Bridge #1, the buffeting forces have been computed using the simulated longitudinal and vertical wind velocity fluctuations at mean speed U(10) of 30m/sec, for different terrain categories TC-1 to TC-4 as discussed in Section 6.2.1. With increase in the terrain roughness the mean wind speed decreases from 34.3m/sec to 20.4m/sec. With change in terrain category from TC-1 to TC-4, the turbulence intensity in longitudinal direction (I_u) varies from 11.7% to 25.9% and in the vertical direction (I_w) from 6% to 16.2%.

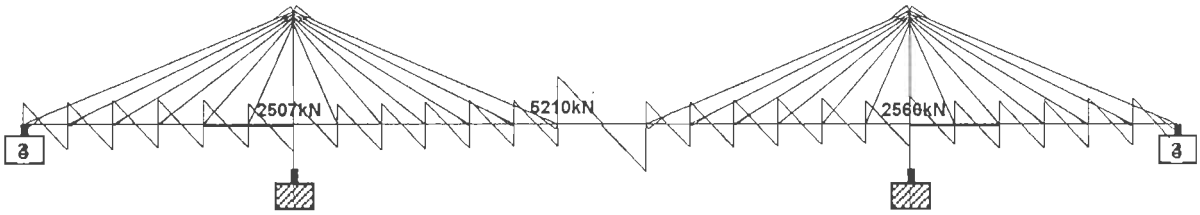

(a) Due to dead load and mean wind forces

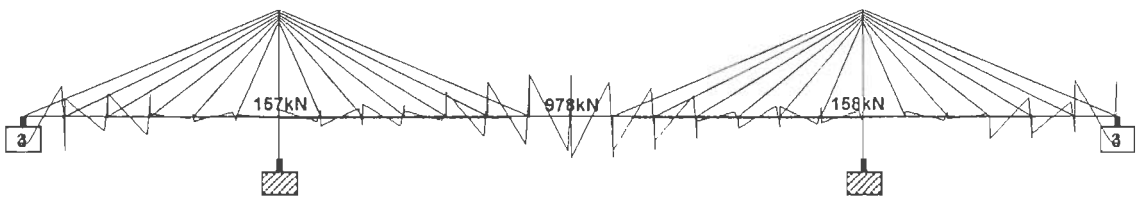

(b) Due to buffeting forces

Fig. 6.22 : Deck Vertical Shear Force Diagram for Bridge # 2 at Wind Speed U(45) = 43.2 m/sec for TC-2

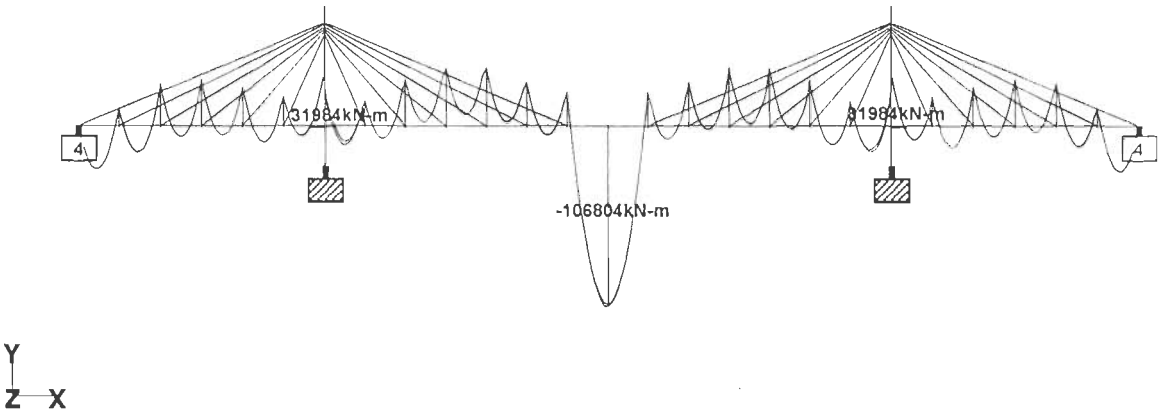

(a) Due to dead load and mean wind forces

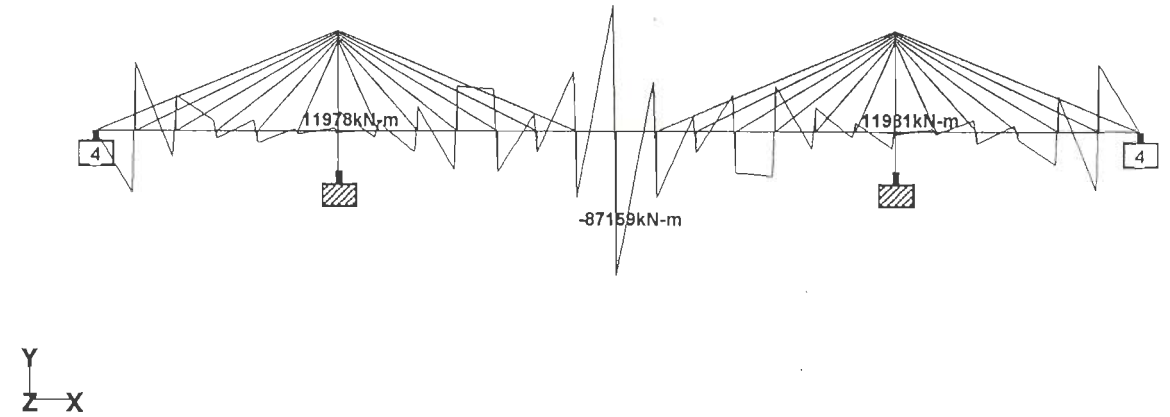

(b) Due to buffeting forces

Fig. 6.23 : Deck Bending Moment Diagram for Bridge # 2 at Wind Speed U(45) = 43.2 m/sec for TC-2

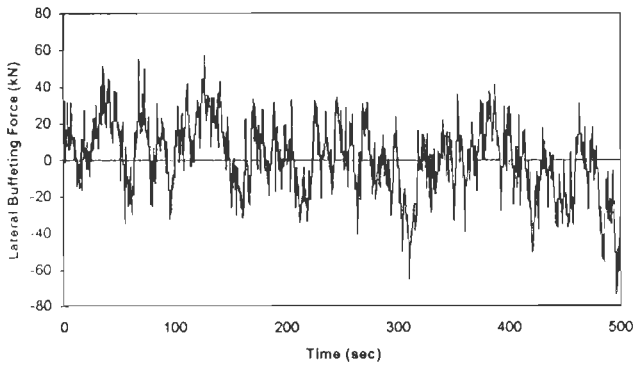

(a) Buffeting force at U(45) = 34.30 m/sec

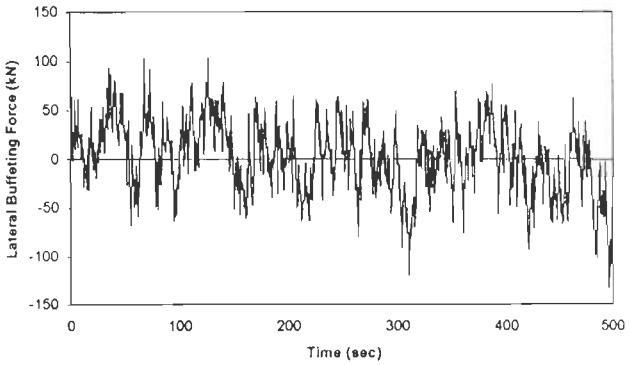

(b) Buffeting force at U(45) = 43.20 m/sec

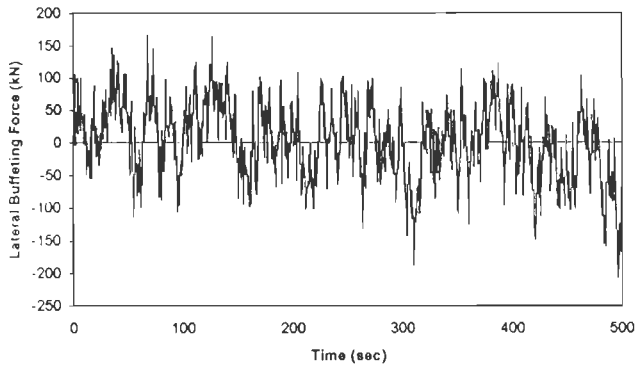

(c) Buffeting force at U(45) = 54.00 m/sec

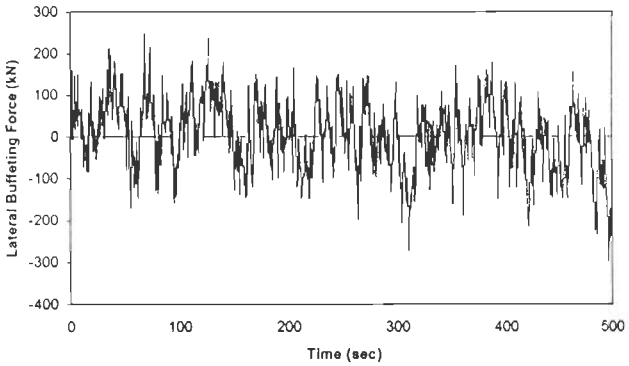

(d) Buffeting force at U(45) = 64.80 m/sec

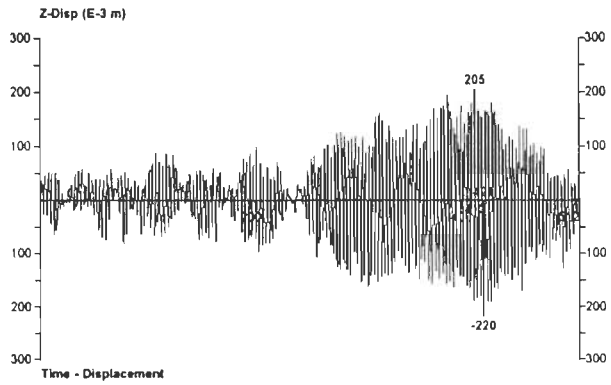

(e) Lateral buffeting response at mid span at U(45) = 54.00 m/sec

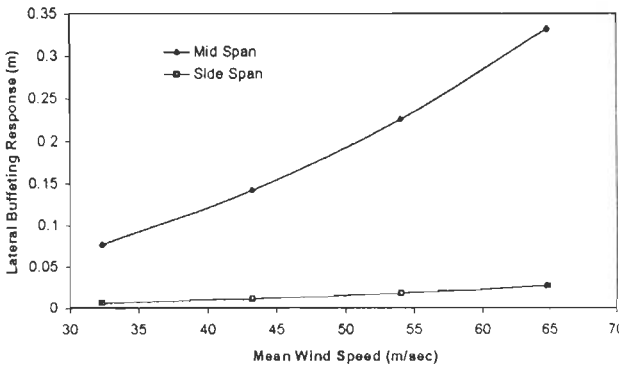

(f) Lateral buffeting response - Variati with mean wind speed

Fig. 6.24 : Time Domain Analysis for Buffeting Response in Lateral Direction for Bridge # 2

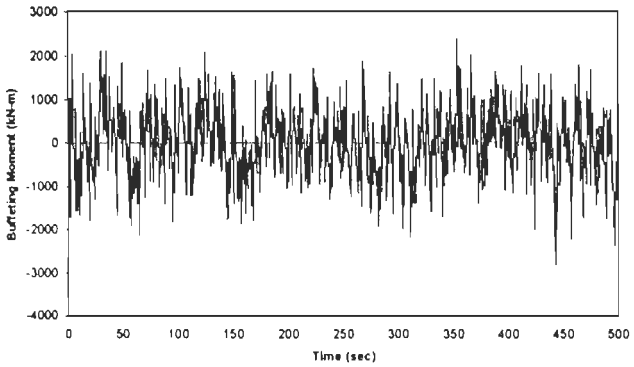

(a) Buffeting moment at U(45) = 34.30 m/sec

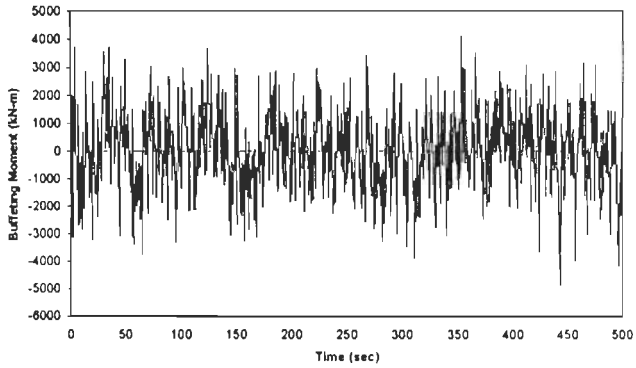

(b) Buffeting moment at U(45) = 43.20 m/sec

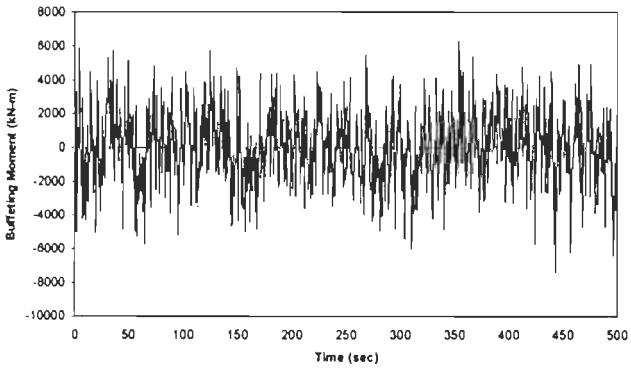

(c) Buffeting moment at U(45) = 54.00 m/sec

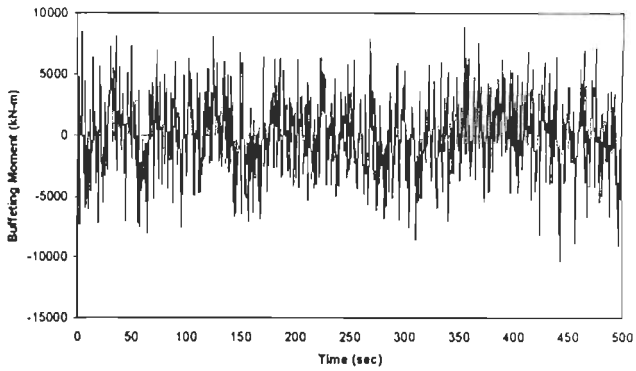

(d) Buffeting moment at U(45) = 64.80 m/sec

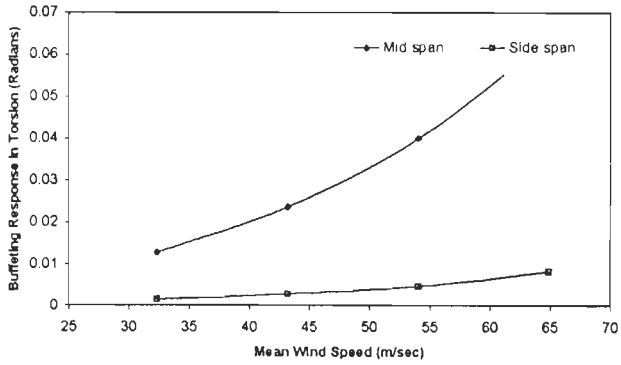

(e) Torsional buffeting response – Variation with mean wind speed

Fig. 6.25 : Time Domain Analysis for Buffeting Response in Torsion for Bridge # 2

The effect of terrain roughness on wind induced response (tower longitudinal response, deck mid span and side span vertical buffeting response) due to mean wind and buffeting forces for Bridge #1 are illustrated in Fig. 6.26. It is clear from the figure that with reduction in mean wind speed, the mean wind response reduces, whereas the buffeting induced response of deck in vertical direction and of tower in longitudinal direction increases nonlinearly with increase in the terrain roughness.

The gust response factor along the span of cable stayed bridges is computed as ratio of peak response to the mean wind response. The variation in gust response factor for Bridge #1 is shown in Fig. 6.27 and a 20% increase in gust response factor is observed with change in terrain category from TC-1 to TC-4.

The effect of terrain roughness on buffeting induced absolute maximum axial force in cables, deck and towers for Bridge#1 is illustrated in Fig. 6.28. With change in terrain category from TC-1 to TC-4, the tension in outer cable increases only slightly from 22.6% to 25.7% of the initial cable tension. Axial force in tower top increases by 16% and in tower base by 4%. Axial force in deck near the tower increases by 5% and the vertical reaction at deck supports at abutments by 7%.

To study the effect of terrain roughness on buffeting response of Bridge #2, at deck level, the terrain roughness in longitudinal direction (I_u) is varied in the range 11% to 24% and in vertical direction (I_w) in the range 7% to 14%. With increase in terrain roughness, the mean wind speed decreases from 47.9m/sec to 30.4m/sec. The buffeting forces have been computed using simulated longitudinal and vertical wind velocity fluctuations at these values of mean wind speed for buffeting analysis.

The effect of terrain roughness on wind induced response (tower longitudinal response, deck mid span and side span vertical buffeting response) due to mean wind and buffeting forces for Bridge #2 is illustrated in Fig. 6.29. It is clear from the Figure that with reduction in mean wind speed, the mean wind response reduces, whereas the buffeting induced response of deck in the vertical direction and of tower in the longitudinal direction increases nonlinearly with increase in terrain roughness.

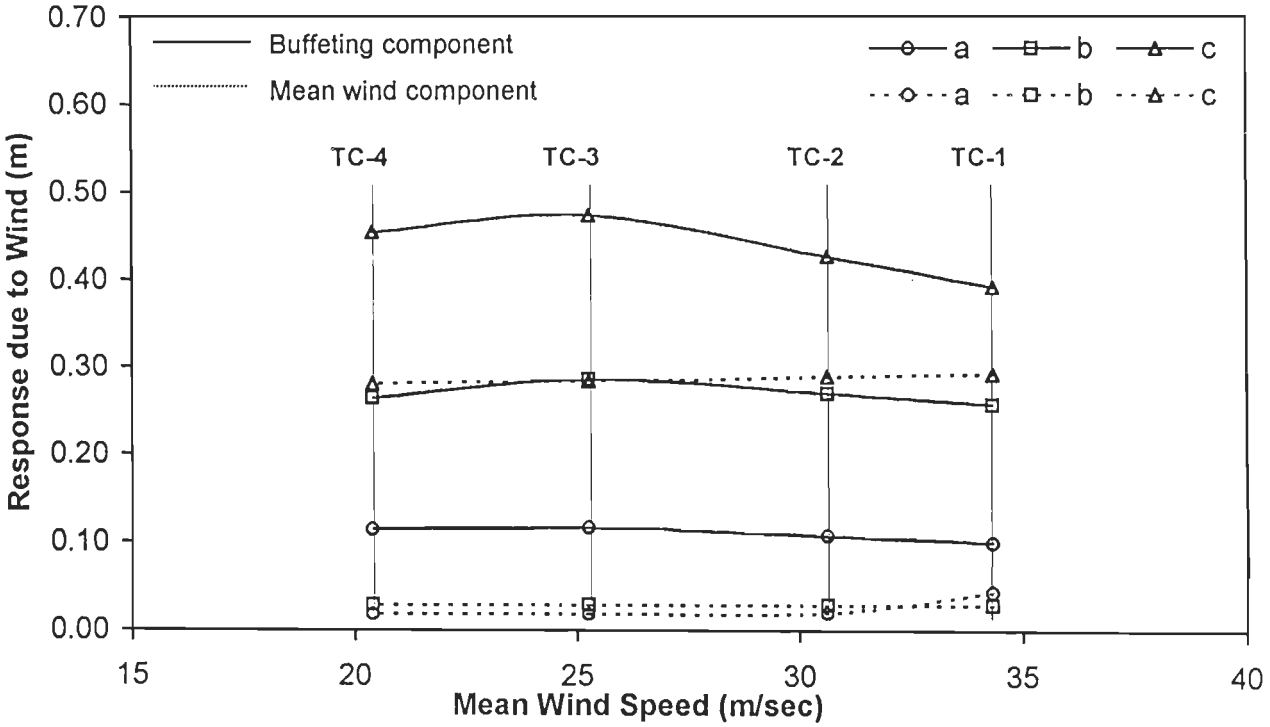

a : Tower tip longitudinal response
b : Maximum side span vertical response
c : Mid span vertical response

Fig. 6.26 : Wind Induced Response of Bridge # 1 – Effect of Terrain Roughness

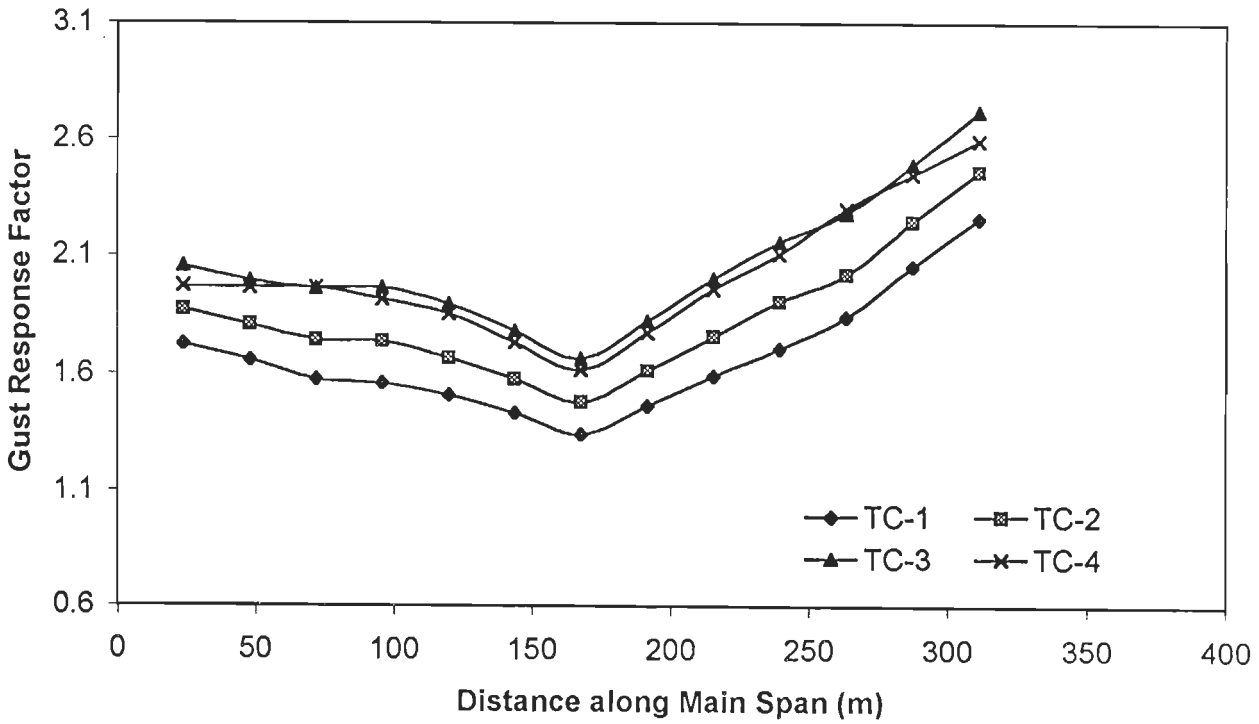

Fig. 6.27 : Spatial Distribution of Gust Response Factor for Bridge # 1 – Effect of Terrain Roughness

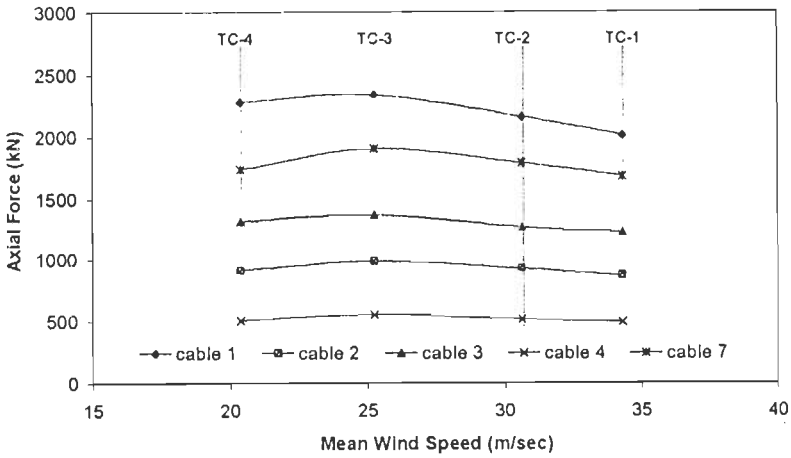

(a) Cable force

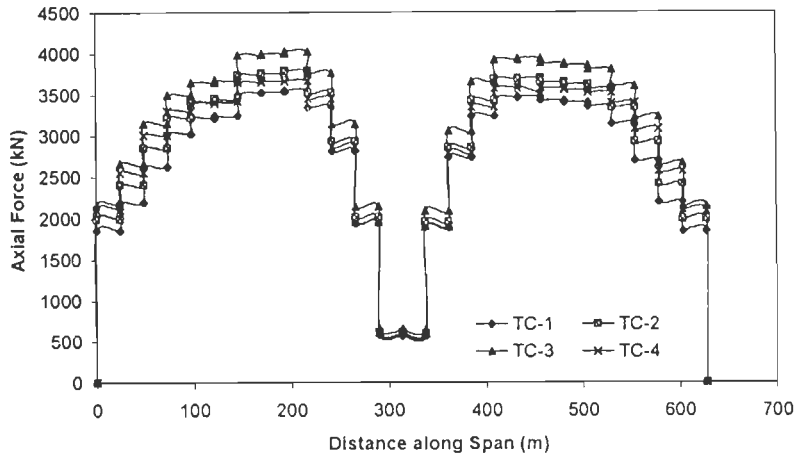

(b) Deck axial force

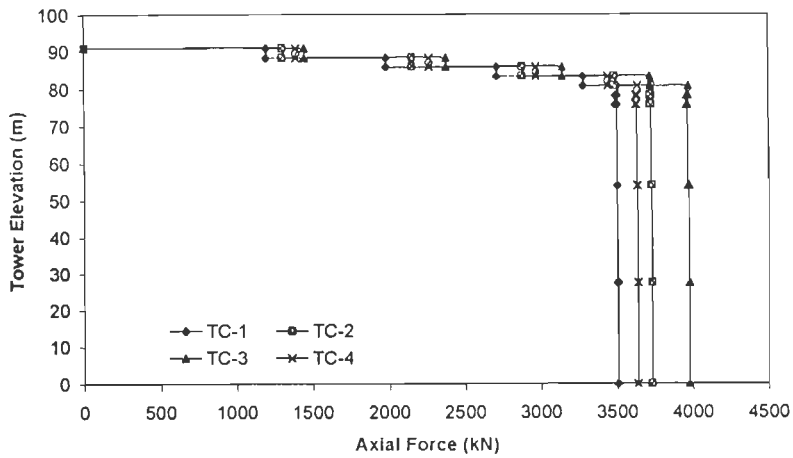

(c) Tower axial force

TC	U(30)m/sec	I_u%	I_w%
TC-1	34.3	11.7	6.00
TC-2	30.6	14.2	7.75
TC-3	25.2	19.9	11.7
TC-4	20.4	25.9	16.2

Fig. 6.28 : Effect of Terrain Roughness on Buffeting Induced Absolute Maximum Axial Force in Components of Bridge # 1

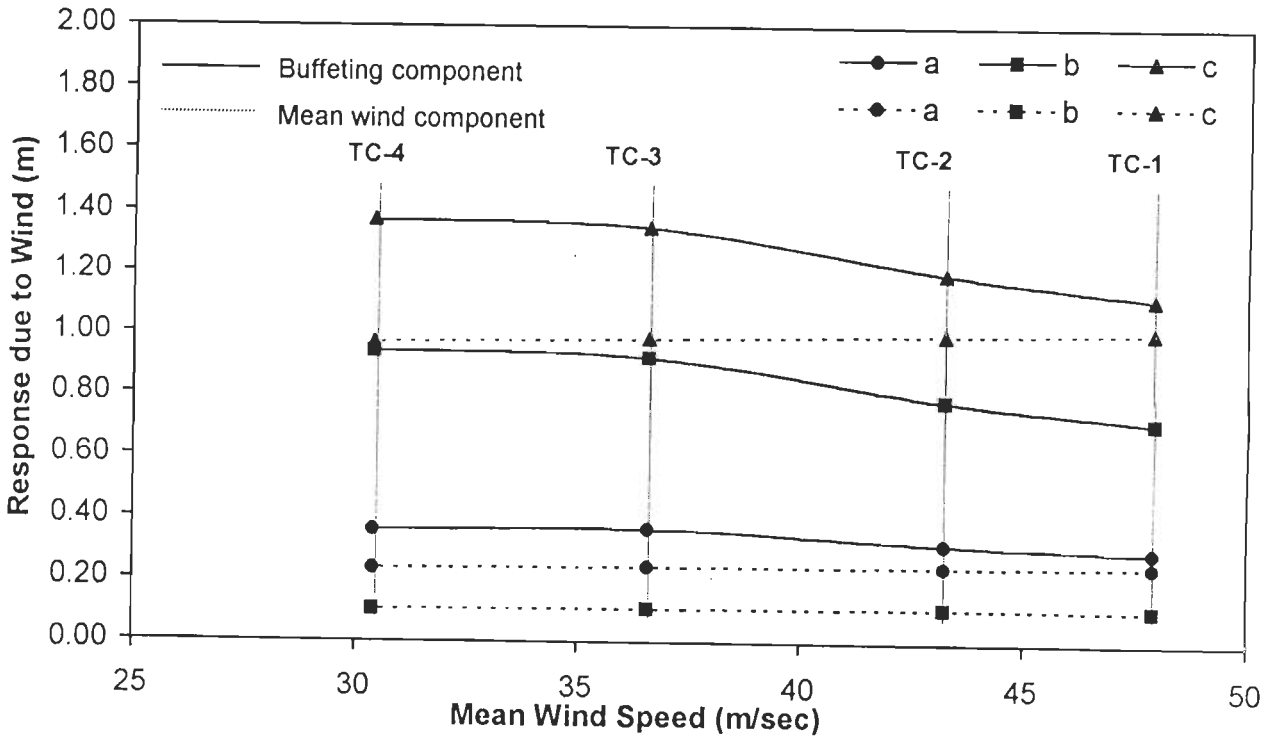

a : Tower tip longitudinal response
b : Maximum side span vertical response
c : Mid span vertical response

Fig. 6.29 : Wind Induced Response of Bridge # 2 – Variation with Terrain Roughness

The variation in gust response factor along the span for Bridge #2 is shown in Fig. 6.30 and a 29% increase in the gust response factor is observed with change in terrain category from TC-1 to TC-4.

The effect of terrain roughness on buffeting induced absolute maximum axial force in cables, deck and towers for Bridge#2 is illustrated in Fig. 6.31. With change in terrain category from TC-1 to TC-4, the tension in outer cable increases from 29% to 36% of the initial cable tension. Axial force at tower top increases by 22% and at its base by 13%. Axial force in deck near the tower increases by 22% and the vertical reaction in deck support at abutment by 32%.

It is observed from the above results that the bridges with longer span lengths are more susceptible to turbulence effects. With longer span length, the bridge becomes more flexible, i.e., its natural frequency reduces whereas the energy in approaching wind is higher at lower frequency. Thus, the wind excites the bridge more vigorously, increasing its response. Also the study indicates that the modelling of turbulence is very important for rational wind analysis.

6.4.5 Effect of Type of Deck Supports

The effect of support type for bridge deck at towers and abutments on buffeting response of Bridge#1 has been studied at a mean wind speed of 40m/sec for terrain category TC-1, by changing the deck support type DST-1 to DST-6. The summary of peak displacements at mid span, side span of deck and longitudinal displacement of tower tip are given in Table 6.7. The change in cable forces due to buffeting in Bridge #1 with deck support types DST-1 to DST-6 is presented in Table 6.8.

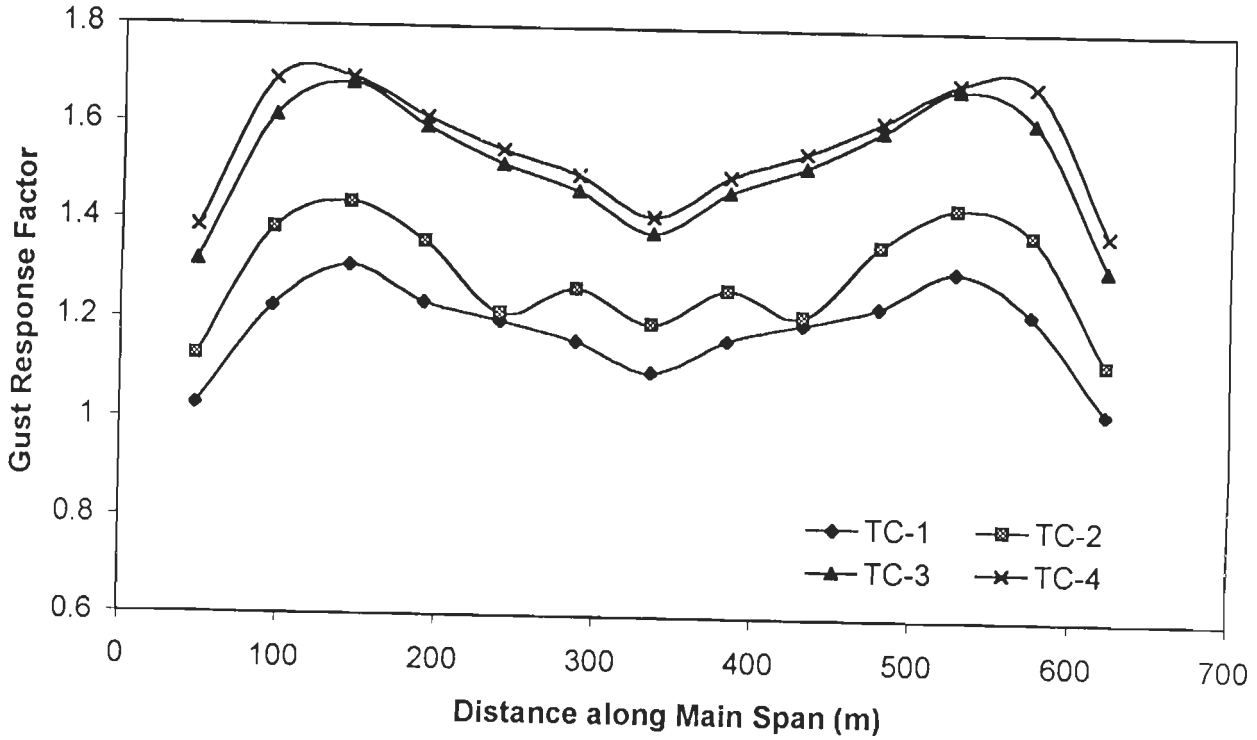

Fig. 6.30 : Spatial Distribution of Gust Response Factor for Bridge # 2 – Effect of Terrain Roughness

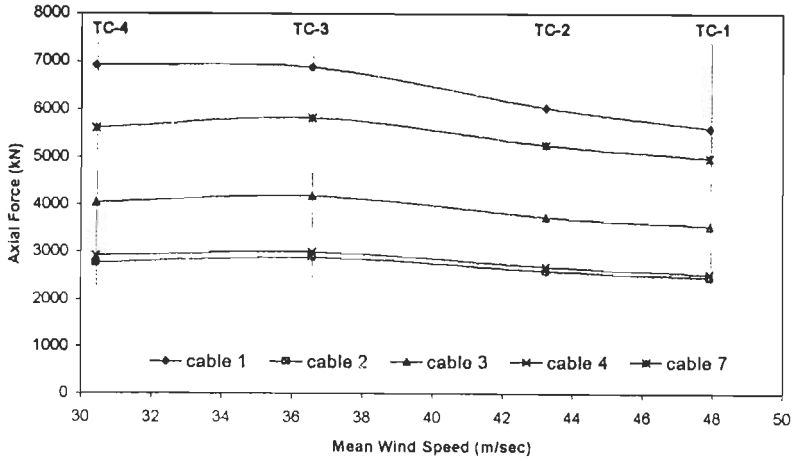

(a) Cable force

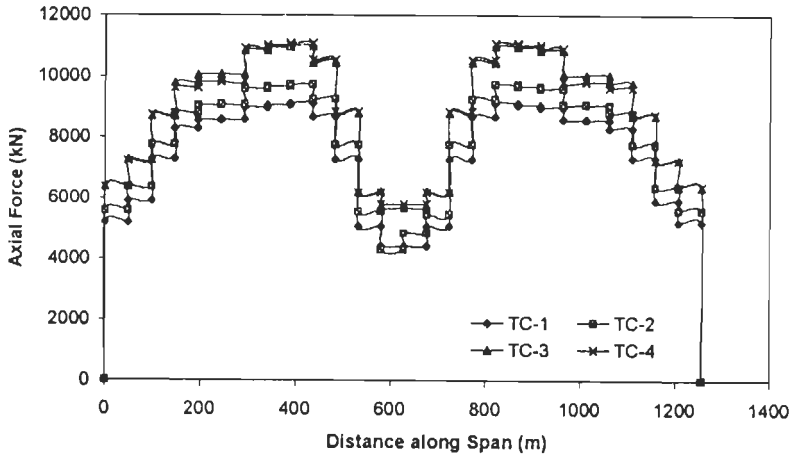

(b) Deck axial force

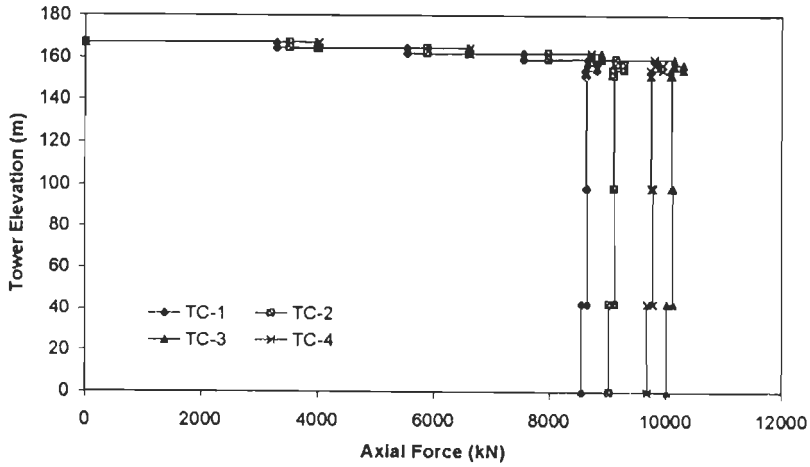

(c) Tower axial force

TC	U(45)m/sec	I_u%	I_w%
TC-1	47.9	11.4	6.90
TC-2	43.2	13.4	8.07
TC-3	36.6	18.2	10.45
TC-4	30.4	23.14	13.05

Fig. 6.31 : Effect of Terrain Roughness on Buffeting Induced Absolute Maximum Axial Force in Components of Bridge # 2

Table 6.7 : Peak Buffeting Response for Bridge # 1 - Effect of Support Types for Bridge Deck

(Mean Wind Speed U(30)=45.8m/sec for Terrain Category TC-1)

Support Type for Bridge Deck	Mid Span Vertical Response (m)	Maximum Side Span Vertical Response (m)	Left Tower Tip Longitudinal Response (m)
DST-1	0.5840	0.4119	0.1594
DST-2	0.5997	0.4236	0.1621
DST-3	0.6343	0.4435	0.1665
DST-4	0.6361	0.4373	0.1670
DST-5	0.6256	0.4305	0.1657
DST-6	0.5636	0.428	0.1704

Table 6.8 : Absolute Maximum Axial Force in Cables of Bridge #1 due to Buffeting – Effect of Support Types for Bridge Deck

Cable Number	Cable Forces in kN with Different Support Type for Bridge Deck					
	DST-1	DST-2	DST-3	DST-4	DST-5	DST-6
1	3224.0	3283.0	3424.0	3387.0	3358.0	3343.0
2	1462.0	1419.0	1464.0	1486.0	1424.0	1476.0
3	2062.0	1992.0	2055.0	2081.0	1970.0	2242.0
4	1803.0	1751.0	1807.0	1830.0	1746.0	1929.0
5	825.0	806.0	828.0	844.0	787.0	839.0
6	187.0	183.0	185.0	193.0	139.0	105.0
7	2838.0	2753.0	2823.0	2871.0	2757.0	2759.0

For Bridge #2, with different type of deck supports, the summary of peak vertical displacement at mid span and side span and peak longitudinal displacement at tower tip are given in Table 6.9. The variation in absolute maximum axial force in cables due to buffeting with change in deck support type DST-1 to DST-6 is presented in Table 6.10.

Table 6.9 : Peak Buffeting Response for Bridge # 2 – Effect of Support Types for Bridge Deck

(Mean Wind Speed U(45) = 43.2 m/sec for Terrain Category TC-2)

Support Type for Bridge Deck	Mid Span Vertical Response (m)	Side Span Vertical Response (m)	Left Tower Tip Longitudinal Response (m)
DST-1	1.1322	0.9378	0.3053
DST-2	1.1066	0.9158	0.3126
DST-3	1.1361	0.9342	0.3143
DST-4	1.1317	0.9317	0.3194
DST-5	1.1254	0.9238	0.3184
DST-6	1.1349	0.9234	0.3305

Table 6.10 : Absolute Maximum Axial Force in Cables of Bridge #2 due to Buffeting - Effect of Support Types for Bridge Deck

(Mean Wind Speed U(45) = 43.2 m/sec for Terrain Category TC-2)

Cable Number	Cable Forces in kN with Different Support Type for Bridge Deck					
	DST-1	DST-2	DST-3	DST-4	DST-5	DST-6
1	6063.0	6258.0	6337.0	6233.0	6218.0	6036.0
2	2681.0	2762.0	2777.0	2780.0	2750.0	2607.0
3	3639.0	3872.0	3991.0	3880.0	3837.0	3749.0
4	2571.0	2736.0	2803.0	2742.0	2722.0	2693.0
5	866.0	919.0	930.40	920.0	916.0	881.0
6	138.0	145.0	132.80	146.0	121.0	66.0
7	5624.0	5769.0	5272.0	5767.0	5707.0	5256.0

The gust response factor along main span length of deck is computed for Bridge #1 and the spatial distribution is presented in Fig. 6.32. The gust response factor is maximum for DST-1 (2.39 at mid span) and minimum for DST-6 (1.729 at mid span), i.e., the gust response factor is 38% more for deck support type DST-1 in comparison to DST-6.

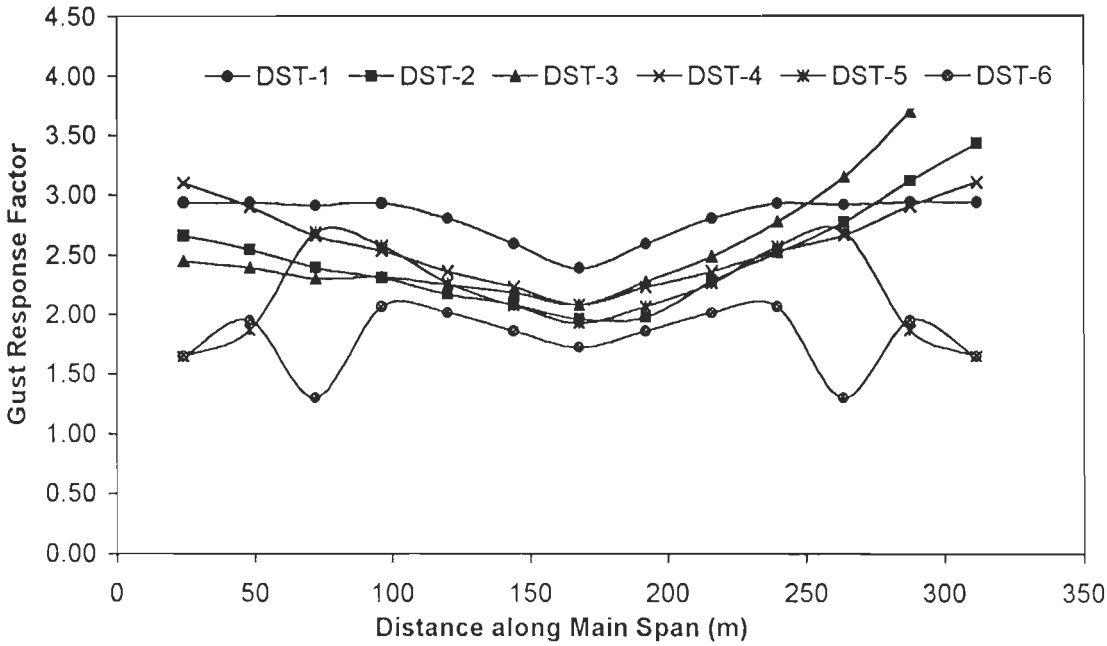

Fig. 6.32 : Spatial Distribution of Gust Response Factor for Bridge # 1 – Variation with Support Types for Bridge Deck

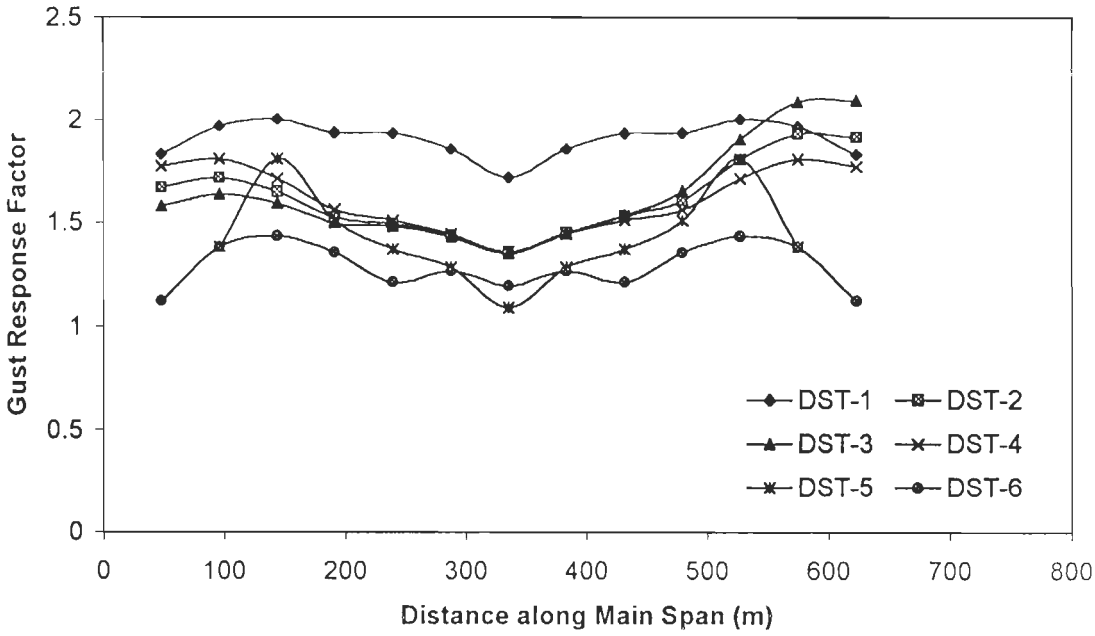

DST-1 : Deck fixed at towers, on rollers at other supports
DST-2 : Deck fixed at one tower, on rollers at other supports
DST-3 : Deck fixed at one end, on rollers at other supports
DST-4 : Deck movable at all supports
DST-5 : Floating Deck
DST-6 : Deck elastically supported at towers, on rollers at other supports

Fig. 6.33 : Spatial Distribution of Gust Response Factor for Bridge # 2 – Variation with Support Types for Bridge Deck

Similarly, the gust response factor along the main span length of deck for Bridge #2 is computed and the spatial distribution is shown in Fig. 6.33. The gust response factor is 57% more for deck support type DST-1 in comparison to DST-5.

With the bridge deck fixed at both the towers, as in DST-1, the bridge becomes more stiff under static loads and therefore the static response is lower than that for a bridge with type of deck support DST-5 or DST-6. However, neither the frequencies nor the damping in vertical bending modes is much affected by type of deck supports. Hence the variation in peak buffeting response with change in type of deck support is not significant. As the gust response factor is the ratio of peak buffeting response to the mean static response, it increases for bridge with DST-1 and reduces for bridge with other types of deck supports. Based on the computed gust response factor, Bridge #1 with deck support type DST-6 as well as Bridge #2 with deck support type DST-5, shall be selected for buffeting based design as they have minimum gust response factor when subjected to dynamic wind loads.

6.5 SUMMARY

The time domain buffeting analysis of three span cable stayed bridges - Bridge #1 (total span 627.8 m) and Bridge# 2 (total span 1255.8 m) - are numerically illustrated in this Chapter. In the present study, effect of buffeting forces on the complete bridge, rather than the deck alone, is evaluated by idealizing the bridge as a three dimensional space structure. The effects of (i) mean wind speed variation, (ii) terrain roughness and (iii) type of bridge deck supports on the buffeting response are studied.

From the results for the two bridges it is clear that, with increase in the mean wind speed, buffeting responses in vertical, lateral and torsional modes increase nonlinearly. The contribution to buffeting response is mainly from 1st and 2nd vertical symmetric modes. The contribution of 2nd vertical symmetric mode (V-S2) substantially

increases with longer span lengths of the bridge on account of the lower natural frequencies, lower damping and larger energy content in turbulent wind at lower frequency of the bridge. In the vertical direction, the buffeting response in side span is about 65% of response in the main span at its centre. However, the lateral and torsional buffeting responses in the side span are only about 8% and 12% of the main span vertical response. The buffeting in lateral modes becomes important with longer spans, like Bridge#2.

The outer cables, deck member near tower and deck supports at abutments in three span cable stayed bridges are subjected to more buffeting induced forces. The forces induced in bridge components, such as, cables, towers, deck as well as deck supports, due to the dead load and mean wind forces, and buffeting forces obtained from the analysis would be useful in the wind resistant design.

The turbulence level in the approaching wind affects the response of bridge as well as the buffeting induced forces considerably. The effect becomes prominent with longer spans and needs to be included in the analysis for a rational wind design.

From the responses of bridges with different type of deck supports, it is observed that elastically supported and floating decks are preferable for buffeting based design of bridges as their behaviour under static and dynamic forces are similar and gust response factor is lower in comparison to bridges with fixed or movable type deck supports.

Chapter 7

BUFFETING ANALYSIS OF FIVE SPAN CABLE STAYED BRIDGES

7.1 INTRODUCTION

This chapter is devoted to the time domain buffeting analysis of five span cable stayed bridges denoted as Bridge #3 and Bridge #4, using the formulations described in Chapter 5.

Analysis of these bridges under buffeting and mean wind forces has been performed to study the effect of (i) mean wind speed and (ii) terrain roughness on buffeting response. For the analysis using time domain approach, the buffeting forces have been generated using the digitally simulated wind velocity fluctuations. The results of the mean wind analysis have been used as reference for comparison and to estimate the dynamic amplification in responses due to buffeting.

7.2 DATA FOR BUFFETING ANALYSIS

The wind data, steady-state force coefficients for various bridge components and modal damping estimates used in the analysis of Bridge #3 and Bridge #4 under buffeting forces (to study the influence of variation in mean wind speed and terrain category on wind induced buffeting responses) are discussed in the following Sections.

7.2.1 Wind Data

To study the effect on buffeting response with variation in mean wind speed, the Bridge #3 is assumed to be located in terrain category TC–3, with terrain roughness parameter z_0 equal to 0.3m. The mean wind speed at 10 m height has been varied from 30m/sec to 60m/sec in steps of 10m/sec. This indicates the mean wind speed at deck

level for this bridge at an elevation of 34m as 25.9m/sec, 34.6m/sec, 43.2m/sec and 51.8m/sec respectively in TC-3 corresponding to the range of wind speed selected in this study. The wind profile along the height of towers for Bridge#3 is also estimated.

In the case of Bridge#4, it is assumed to be located in terrain category TC-1, with surface roughness parameter z_o equal to 0.005m.The mean wind speed values at deck level, i.e., 27m level are calculated as 33.9m/sec, 45.2m/sec, 56.5m/sec and 67.8m/sec corresponding to the four wind speeds at 10m elevation. The wind profile along the height of tower for Bridge #4 is estimated in the same manner as for Bridge # 3.

To study the effect of terrain roughness on the mean wind response for Bridge#3, the mean wind speed at a height of 10m is assumed as 50m/sec. Terrain categories are varied from TC-1 to TC-4 with surface roughness parameter (z_0) equal to 0.005m, 0.03m, 0.3m and 1.0m representing these terrains as discussed in Section 4.2.2.1. Corresponding to these values of surface roughness parameter, the turbulent intensity in the longitudinal wind velocity fluctuations at bridge deck level is obtained as 11.5%, 13.9%, 19.3% and 24.7% respectively. The turbulence intensity in vertical wind velocity fluctuations at deck level is 5.7%, 7.2%, 11.0% and 15.0% respectively. The wind speed in these terrain categories, at an elevation of 34m above the mean ground level is estimated. The mean wind speeds are 58.0m/sec, 51.7m/sec, 43.2m/sec and 35.2m/sec corresponding to TC-1 to TC-4 respectively. Thus, the mean wind speed decreases by a factor of 1.65 with change in terrain category from TC-1 to TC-4 .

Similarly, to study the effect of terrain roughness for Bridge#4, the mean wind speed at an elevation of 10m is taken as 30m/sec. For the analysis, it is assumed that the bridge is located in four terrain categories TC-1 to TC-4 with surface roughness parameter (z_0) equal to 0.005m, 0.03m, 0.3m and 1.0m. Corresponding to these values of surface roughness parameter, the turbulent intensity in the longitudinal wind velocity

fluctuations is obtained as 11.8%, 14.4%, 20.3% and 26.7% respectively at deck elevation of 27m above the mean ground level. The turbulence intensity in vertical wind velocity fluctuations at deck level in terrains TC-1 to TC-4 is obtained as 6.5%, 7.8%, 10.7% and 13.9% respectively. The mean wind speeds are 33.9m/sec, 30.2m/sec, 24.6m/sec and 19.7m/sec corresponding to terrain categories TC-1 to TC-4 respectively.

7.2.2 Steady-state Force Coefficients

The cross-section of deck for Bridge #3 consists of longitudinal trapezoidal box girders in steel along with transverse beams supporting the orthotropic steel deck slab. The width to depth ratio (B/d) for bridge deck is 6.0. To compute the wind loads on Bridge#3, the steady-state drag, lift and moment coefficients for the bridge deck are taken as $C_D = 0.242$, $C_L = -0.17$, $C_M = 0.138$, $C_D' = 0.001$, $C_L' = 3.60$ and $C_M' = 0.40$. These values are based on the wind tunnel studies reported by Walshe (1981) for a twin box girder supported deck section with similar B/d ratio, in turbulent flow with a turbulent intensity I_u of 10.6%. It may be recalled that due to turbulence in the approaching flow, the drag coefficient tends to increase and the slope of lift curve tends to decrease. However, due to non-availability of steady-state coefficients for bridge deck at different turbulence levels included in this study, these coefficients are assumed to be same for the four different terrain categories, TC-1 to TC-4. For tower, the drag coefficient is assumed to vary between 2.2 at top to 1.9 at base depending on the aspect ratio of tower leg cross-section. For cables the drag coefficient is taken as 0.70.

Similarly, for Bridge #4, the steady-state drag, lift and moment coefficients for the bridge deck at zero angle of attack (normalized with respect to bridge deck width) are taken as $C_D = 0.0816$, $C_L = -0.0955$, $C_M = -0.0033$, $C_D' = 0.038$, $C_L' = 4.46$ and $C_M' = 1.039$. These values are obtained by the wind tunnel studies of Yamuna Bridge by Lakshmy *et al* (1997). For tower, the drag coefficient is assumed as 1.5 based on the aspect ratio of the rectangular leg section and for the cables the drag coefficient is taken as 0.70.

7.2.3 Modal Damping

As discussed in Section 5.3, the net modal damping is the sum of (i) structural and (ii) aerodynamic damping. The theoretically evaluated modal structural damping for Bridge#3 and Bridge #4 is given in Tables 3.13 (a) and 3.13(b). The computation of aerodynamic damping is discussed in the following sections.

The aerodynamic damping corresponding to the vertical bending and torsional modes has been computed using the Irwin's method as discussed in Section 5.3. The aerodynamic damping contributed by the first and second vertical symmetric modes (V-S1 and V-S2) for Bridge #3 is illustrated in Fig.7.1. Similarly, the aerodynamic damping contributions by the first and second torsional symmetric modes (T-S1 and T-S2) are shown in Fig.7.2.

For Bridge #4, the aerodynamic damping for first and second symmetric modes in vertical (V-S1 and V-S2) and torsion (T-S1 and T-S2) are shown in Figs. 7.3 and 7.4 respectively.

It is clear from the Figs. 7.1 to 7.4 that the aerodynamic damping contributed by first vertical symmetric mode (V-S1) is quite substantial in comparison to the modal structural damping of the corresponding mode of vibration as given in Tables 3.13(a) and 3.13(b). However, the aerodynamic damping contribution by the second vertical symmetric mode (V-S2) is lower than that contributed by the first vertical symmetric mode (V-S1) of vibration.

The aerodynamic damping in torsional modes is much lower than that in the vertical bending modes of vibration. In the case of long span bridges, as in the case of Bridge #4, the value becomes very low with increase in the wind speed as illustrated in Fig. 7.4.

By comparing the aerodynamic damping of these two bridges, it is found that the values are lower for Bridge#4. This is due to higher mass per unit length of the concrete bridge in comparison to the steel bridge.

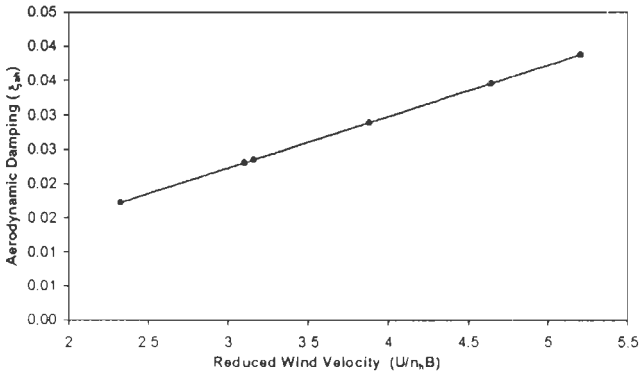

(a) 1st symmetric mode

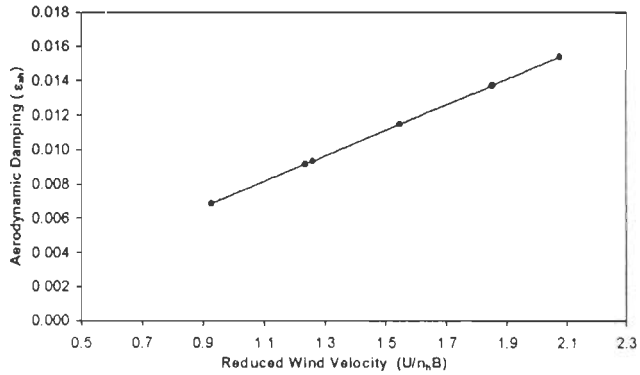

(b) 2nd symmetric mode

Fig. 7.1 : Aerodynamic Damping in Vertical Bending Modes for Bridge # 3

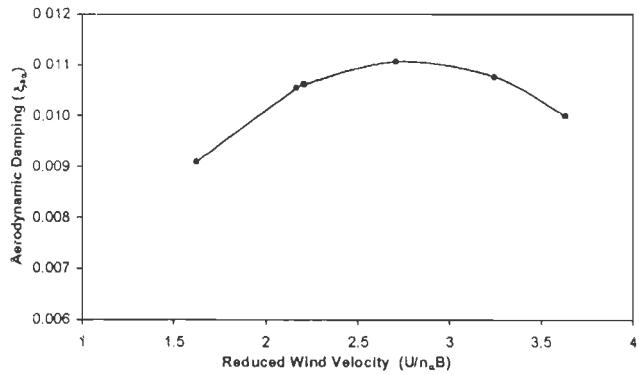

(a) 1st symmetric mode

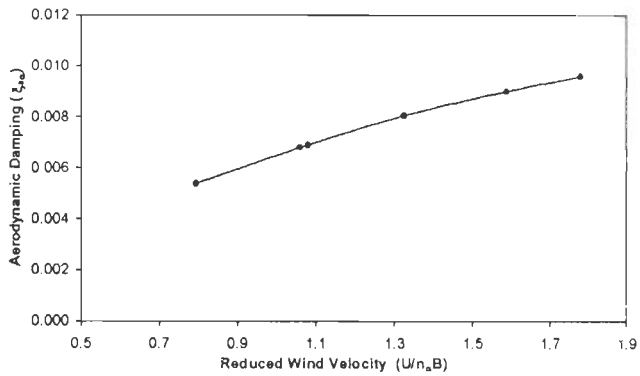

(b) 2nd symmetric mode

Fig. 7.2 : Aerodynamic Damping in Torsional Modes for Bridge # 3

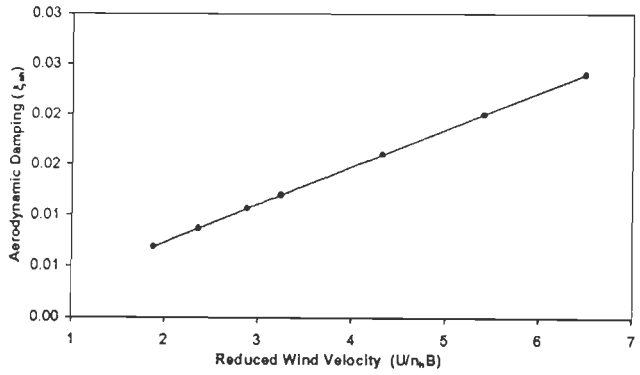

(a) 1st symmetric mode

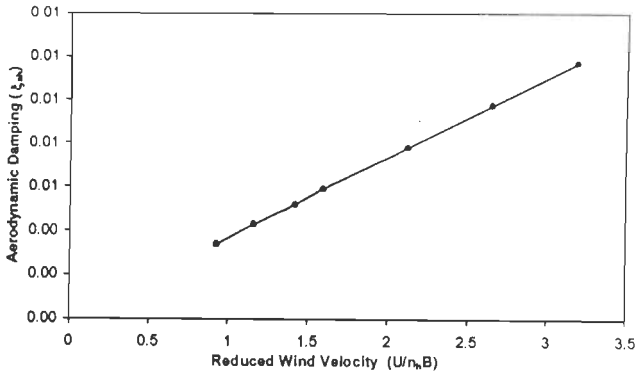

(b) 2nd symmetric mode

Fig. 7.3 : Aerodynamic Damping in Vertical Bending Modes for Bridge # 4

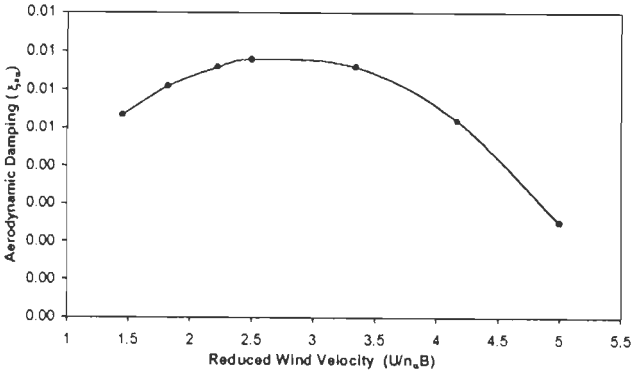

(a) 1st symmetric mode

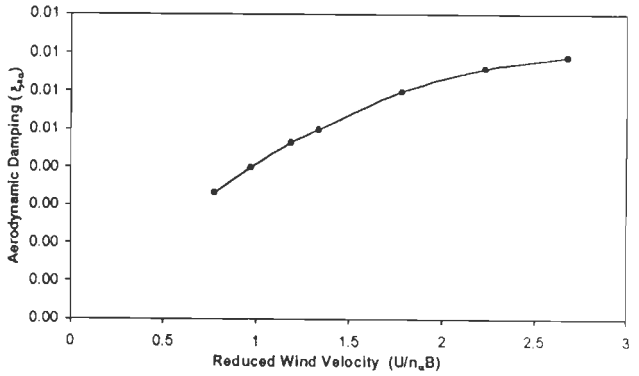

(b) 2nd symmetric mode

Fig. 7.4 : Aerodynamic Damping in Torsional Modes for Bridge # 4

7.3 MEAN WIND RESPONSES

The responses for Bridge #3 and Bridge #4 under dead load and mean wind forces have been obtained by nonlinear static analysis. Mean wind forces include the drag, lift and wind induced moment acting on the bridge deck, and drag forces acting on towers and cables. It is computed using the mean wind speed profile estimated by logarithmic law as well as steady-state coefficients for the cross-sections of bridge components as discussed in Section 7.2.2.

The analyses have been performed for wind description given in Section 7.2.1, to study the effect of variation in mean wind speed and change in terrain category on the responses of these bridges under dead load and mean wind forces. The results are used for comparing the buffeting responses and to estimate gust response factor.

From the results, it is observed that the static response of deck in vertical direction of these bridges reduces with increase in terrain roughness. This is due to decrease in the mean wind speed due to increase in terrain roughness.

7.4 BUFFETING ANALYSIS

As stated earlier, time domain buffeting analyses of the bridges are performed to observe the effect of increase in mean wind speed and terrain roughness on the buffeting responses. Also a comparison of the buffeting response with mean wind response is made to estimate the dynamic amplification due to buffeting with the help of gust response factor. This factor along the main span of the bridge is computed by dividing the peak buffeting response by mean response. Further, the increase in cable force, axial force, shear force and bending moments in deck and towers, reactions at tower base and forces at supports for bridge deck at towers and abutments due to buffeting are obtained. By adding the mean wind and buffeting induced forces, the design forces in these components are obtained.

As for the time domain analysis, buffeting forces are required; their evaluation is described in the following section.

7.4.1 Buffeting Forces

The instantaneous buffeting forces in the lateral and vertical directions and torsional moments acting on Bridge#3 and Bridge#4 have been generated using the computer routine INWINF, which uses the longitudinal and vertical wind velocity fluctuations generated by spectral representation method in which the routine 'WINGEN' has been used as discussed in Section 4.5. The steady-state coefficients as stated in Section 7.2.2 have been used for computation of the buffeting forces. For these bridges, the aerodynamic admittance functions have been assumed to be unity.

For the time domain buffeting analysis, the buffeting drag and lift forces are applied at the centre of bridge deck and the moment at a distance B/4 away from the centre. To perform the analysis, the modelling of bridge as described earlier in Section 3.6.2 has been slightly modified with an additional node defined either at the centre or at a distance B/4 away from centre on each cross beam.

7.4.2 Buffeting Response

The buffeting responses of the bridges in the lateral and vertical directions and in torsion for the deck have been obtained by time domain approach using the aerodynamic forces computed as in the preceding section.

It may be seen from Figs. 3.22 and 3.23, illustrating the vibration modes of Bridge #3 and Bridge #4 respectively, that the frequency of the 1st vertical symmetric mode (V-S1) is 0.398Hz and 0.402Hz respectively. The second vertical symmetric mode (V-S2) in both these bridges is excited as 8th mode with frequency 0.998Hz and 0.819Hz respectively. It appears that with five supports for these bridges along their span, the stiffness is enhanced resulting in higher natural frequencies. In both these bridges, it is observed that the contribution of 2nd vertical symmetric mode (V-S2) to buffeting response is very small on account of much lower energy content of wind at higher frequency. Hence only the 1st vertical symmetric(V-S1) or torsional mode(T-S1) is considered in the present study.

The time domain analysis is achieved by step-by- step integration of equation of motion in modal coordinates by Wilson-θ method as discussed in Section 5.4.1. In the analysis, time integration is performed at a time step of 0.0016 sec.

7.4.3 Effect of Mean Wind Speed

As discussed earlier, to study the effect of mean wind speed on buffeting response the analysis of the bridges has been conducted by varying the wind speed at an elevation of 10m from 30 m/sec to 60m/sec in steps of 10m/sec. The longitudinal and vertical wind velocity fluctuations are generated corresponding to deck level mean wind speed assuming the Bridge#3 and Bridge #4 to be located in terrain category TC-3 and TC-1 respectively. The vertical buffeting forces are generated using the simulated wind velocity fluctuations.

For Bridge #3, the details of time domain analysis for vertical buffeting response at a wind speed of 43.2m/sec for terrain category TC-3 is illustrated in Fig. 7.5. With the increase in wind speed U(34) from 25.9m/sec to 51.8m/sec, the variation in bridge responses and buffeting induced forces for this bridge are discussed.

The variation in the peak response (buffeting and mean wind components) in vertical direction at mid span and side span of the deck as well as longitudinal movement of left side tower is illustrated in Fig. 7.6. From this Figure, it is observed that with increase in mean wind speed from U(34) from 25.9m/sec to 51.8m/sec, the peak mid and side span vertical buffeting responses increase to 3.19 times. The longitudinal response of left tower is also increases to 3.19 times. The side span vertical buffeting response is only 17% of mid span deck response. With increase in wind speed the variation in vertical buffeting response is nonlinear. Also, the analysis for the vertical buffeting response has been performed using four ensembles of the generated vertical buffeting forces and the responses obtained are very close (within 3% variation) and hence consistent.

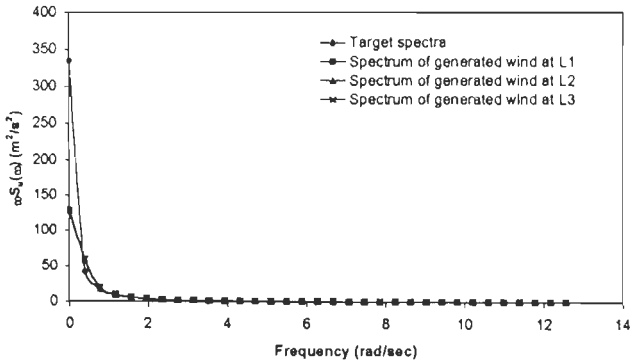

(a) Spectral match for longitudinal velocity fluctuations

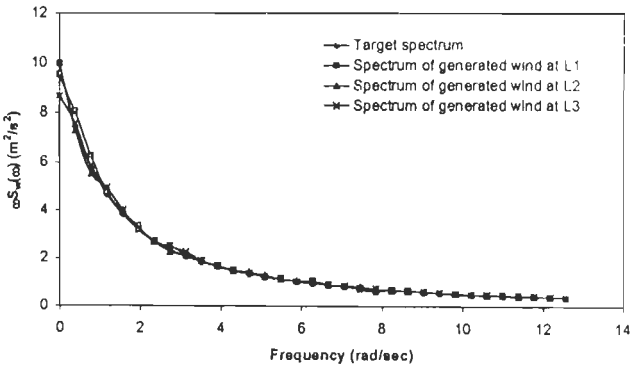

(b) Spectral match for vertical velocity fluctuations

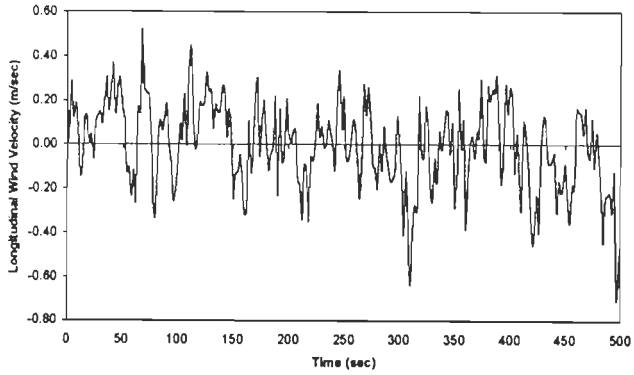

(c) Simulated longitudinal wind velocity fluctuations

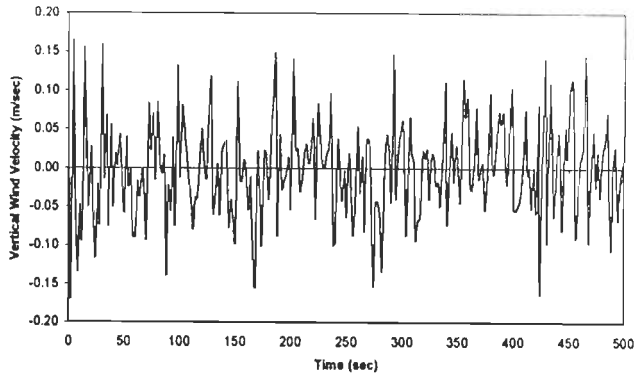

(d) Simulated vertical wind velocity fluctuations

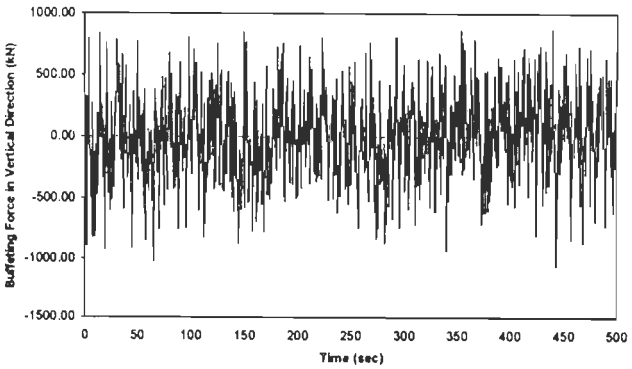

(e) Generated vertical buffeting force

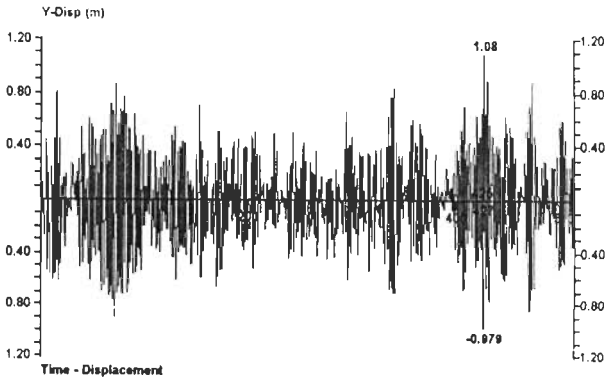

(f) Vertical buffeting response at mid span

Fig. 7.5 : Time Domain Analysis for Vertical Buffeting Response in Bridge # 3 at U(34) = 43.2 m/sec for TC-3

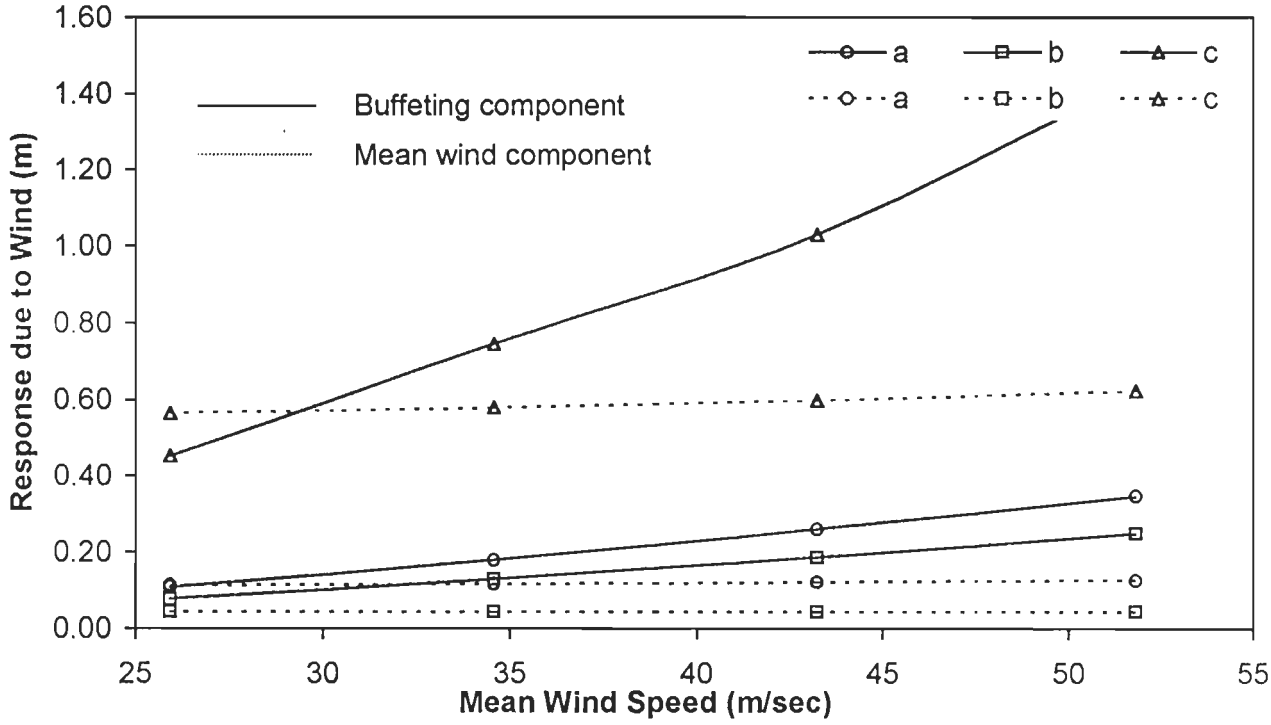

a : Tower tip longitudinal response
b : Maximum side span vertical response
c : Mid span vertical response

Fig. 7.6 : Responses in Bridge # 3 for Terrain Category TC-3 – Variation with Mean Wind Speed

The variation in absolute maximum axial force in cables with increase in mean wind speed is presented in Fig. 7.7. It is seen that the outer cables are subjected to higher force due to buffeting in comparison to inner cables. Increase in tension in outer cable as shown in Fig. 7.7(a) is 31% to 99% of initial cable tension with variation in mean wind speed. The increase in absolute maximum axial force in towers with variation in mean wind speed is shown in Fig.7.8. The buffeting induced axial force in towers increases from 16% to 50% of the axial force induced by the dead load and mean wind forces. Comparison of absolute maximum axial force in deck due to mean wind and buffeting components are depicted in Fig. 7.9(a) and the variation in buffeting induced axial force in deck with increase in mean wind speed is presented in Fig. 7.9(b). It may be noted that the absolute maximum buffeting induced axial force in the deck are presented in these figures. As the buffeting forces are random in nature, the induced forces are also changing from compressive to tensile in nature. The increase in absolute maximum axial force in deck near tower and vertical reactions at the deck supports at towers and abutments is evident from Fig. 7.10. The axial force in deck, near the towers increases by 20% to 61% of the mean wind component, with increase in wind speed from 25.9 to 51.8 m/sec. The vertical reaction at deck supports at abutments (DS-1) increases by 9% to 29% of the mean wind component. However, the buffeting induced vertical reaction at deck supports near outer cable anchorage (DS-2), i.e., at piers is observed to increase drastically with change in the mean wind speed. Again, it is observed that the variation of reaction at deck supports at piers is quite high in comparison to reaction at deck supports at towers. The deck vertical shear force and bending moment diagrams are illustrated in Figs. 7.11 and 7.12. It may be noted that due to buffeting, the additional shear force and bending moment acting on the bridge deck are fluctuating in nature and reversal of sign is implied.

The frequency of 1st lateral symmetrical mode (L-S1) is 0.547Hz, and analyses are performed to find out the variation in lateral buffeting response with increase in

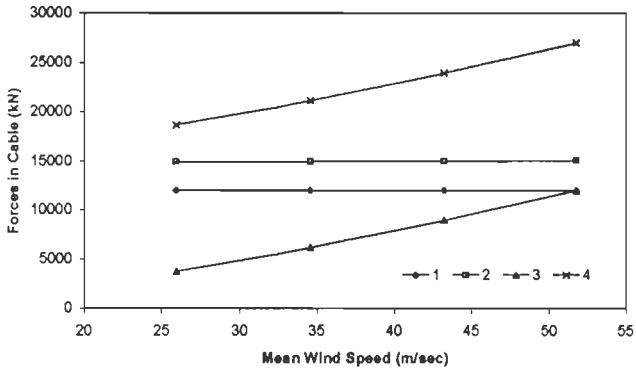

(a) Cable # 1

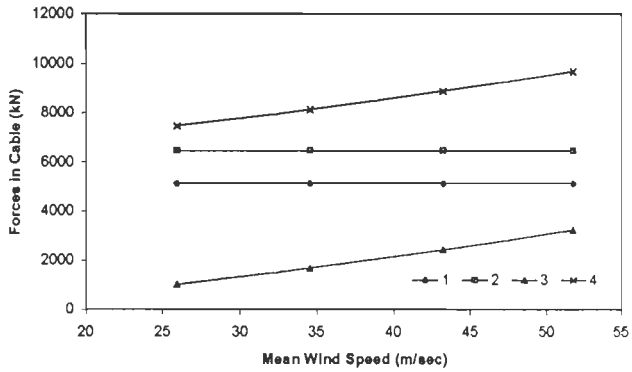

(b) Cable # 2

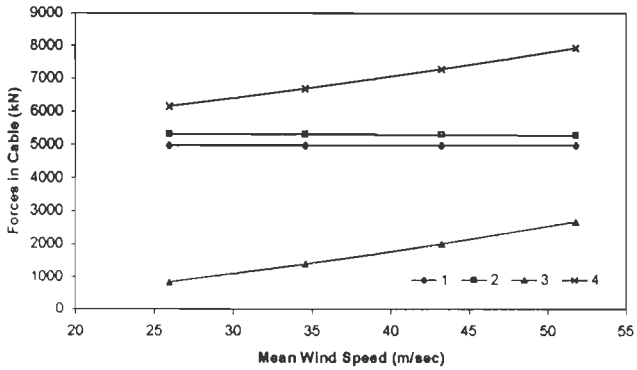

(c) Cable # 4

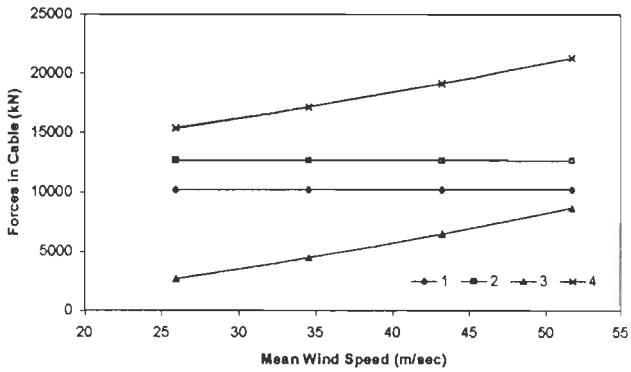

(d) Cable # 5

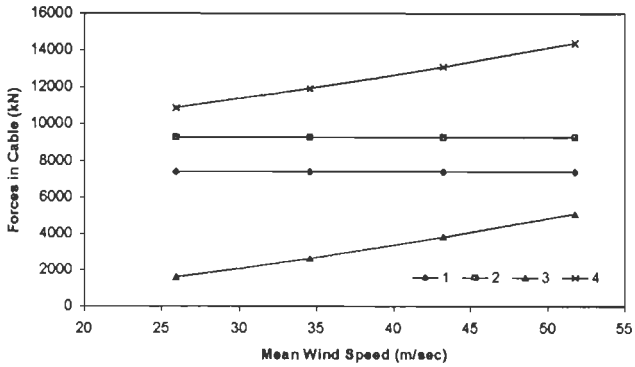

(e) Cable # 6

1 : Initial tension
2 : Mean wind component
3 : Buffeting component
4 : Total cable force

Fig. 7.7 : Forces in Cables of Bridge # 3 – Variation with Mean Wind Speed

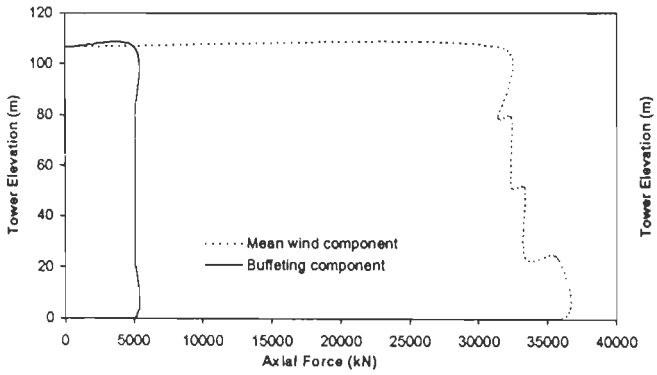

(a) Mean wind speed U(34) = 25.90 m/sec

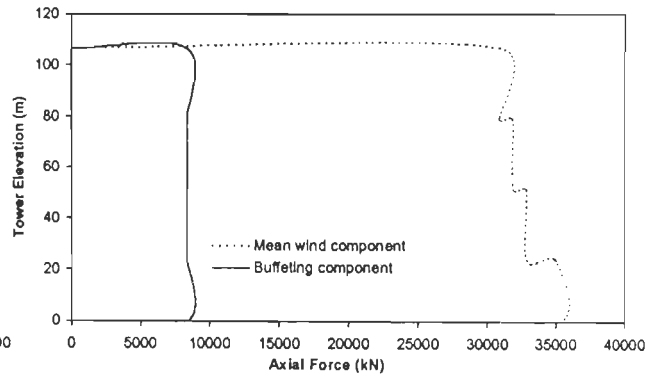

(b) Mean wind speed U(34) = 34.60 m/sec

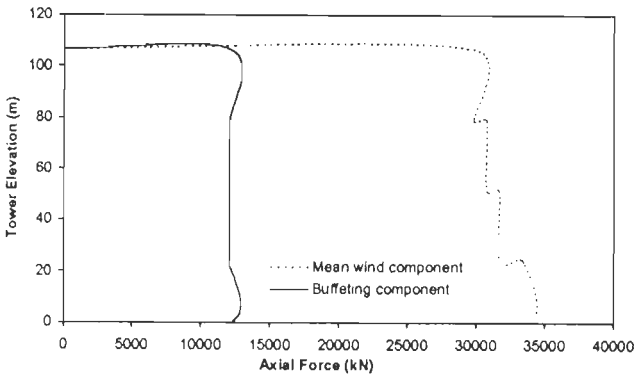

(c) Mean wind speed U(34) = 43.20 m/sec

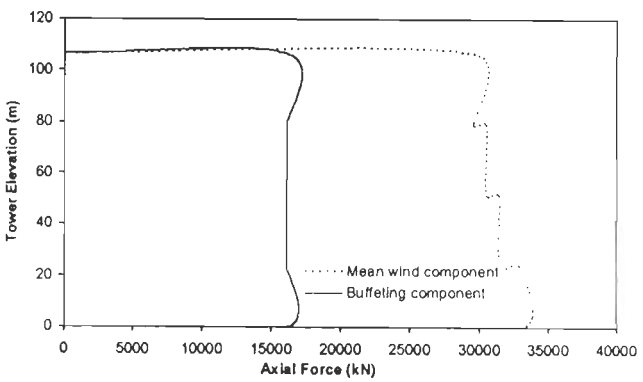

(d) Mean wind speed U(34) = 51.80 m/sec

Fig. 7.8 : Absolute Maximum Axial Force in Towers of Bridge # 3 – Variation with Mean Wind Speed

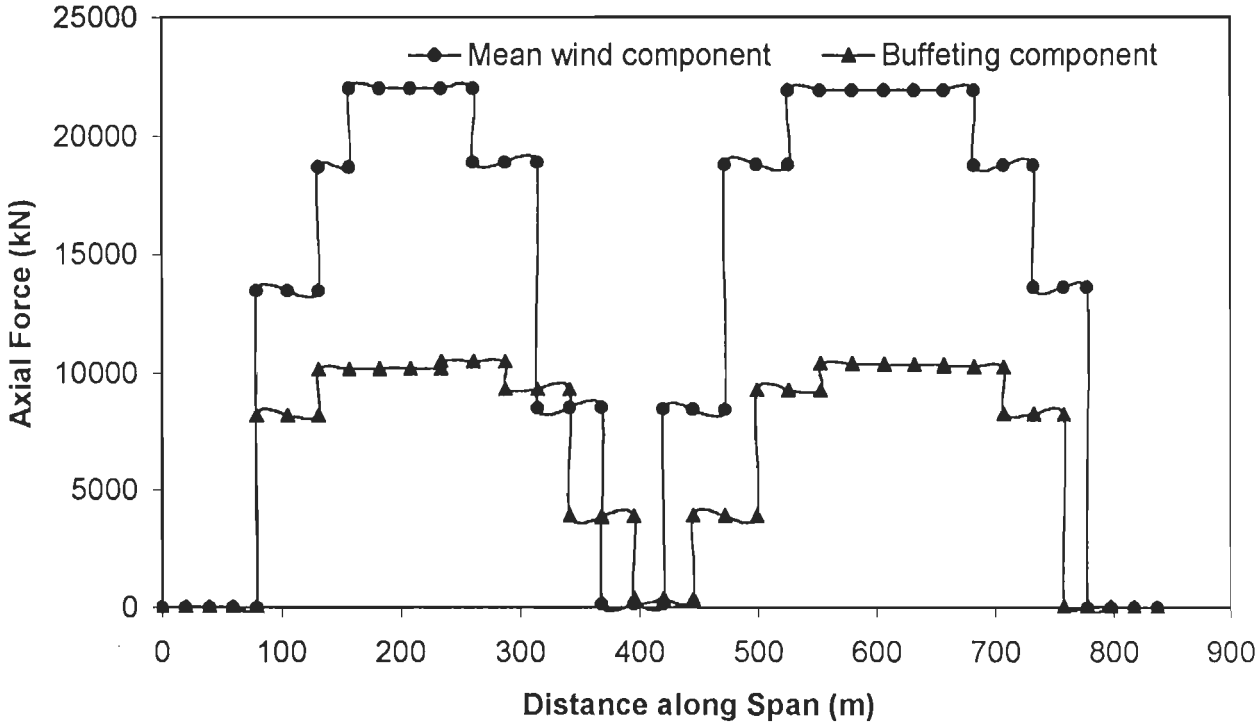

(a) Absolute maximum axial force in deck - Mean wind and buffeting components at U(34) = 43.2 m/sec for TC-3

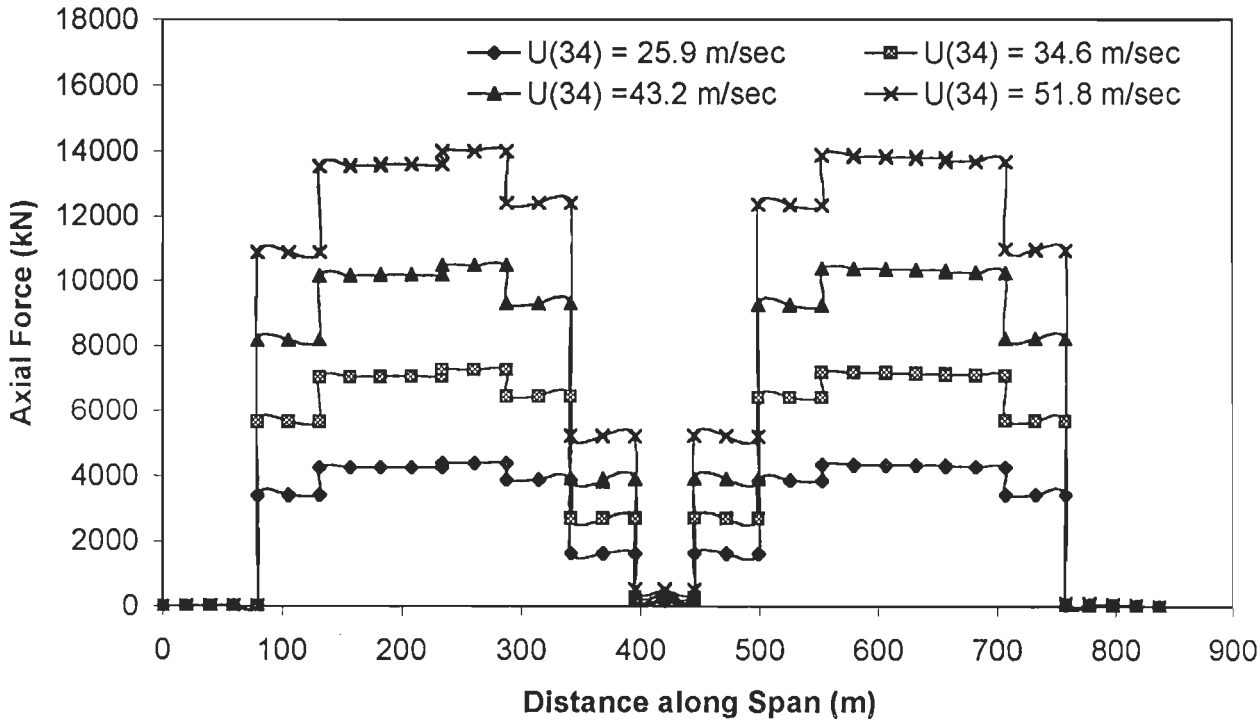

(b) Buffeting induced absolute maximum axial force in deck - Variation with mean wind speed

Fig. 7.9 : Deck Axial Force Diagram for Bridge # 3

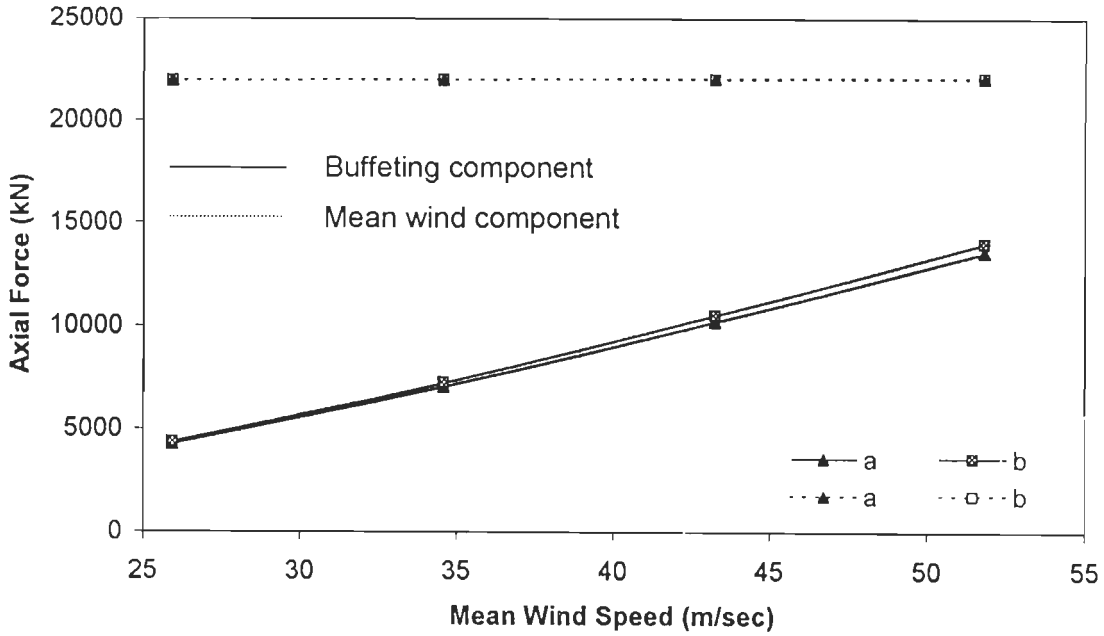

a : Force in member on left side of tower
b : Force in member on right side of tower

(a) Axial force in bridge deck members near left tower support

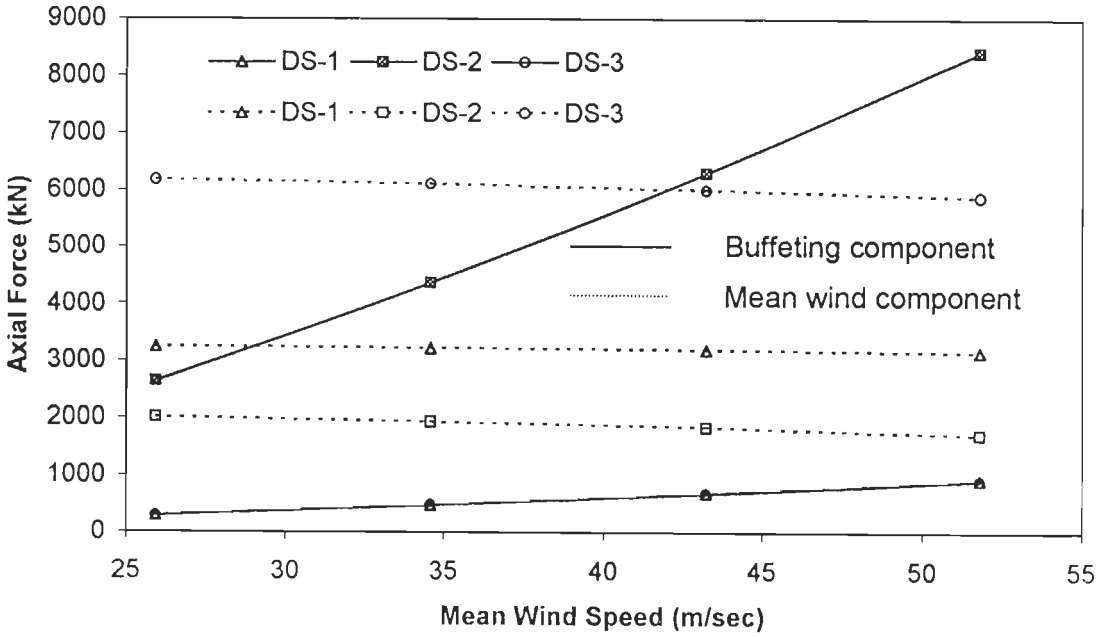

DS-1 : Deck support at abutment
DS-2 : Deck support at pier
DS-3 : Deck support at tower

(b) Vertical reaction at deck supports

Fig. 7.10 : Absolute Maximum Axial Force in Deck and Reactions at Deck Supports in Bridge # 3 – Variation with Mean Wind Speed

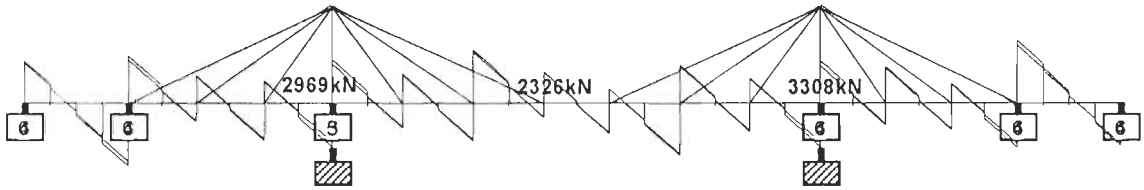

(a) Due to dead load and mean wind forces

(b) Due to buffeting forces

Fig. 7.11 : Deck Vertical Shear Force Diagram for Bridge # 3 at Wind Speed U(34) = 43.2 m/sec for TC-3

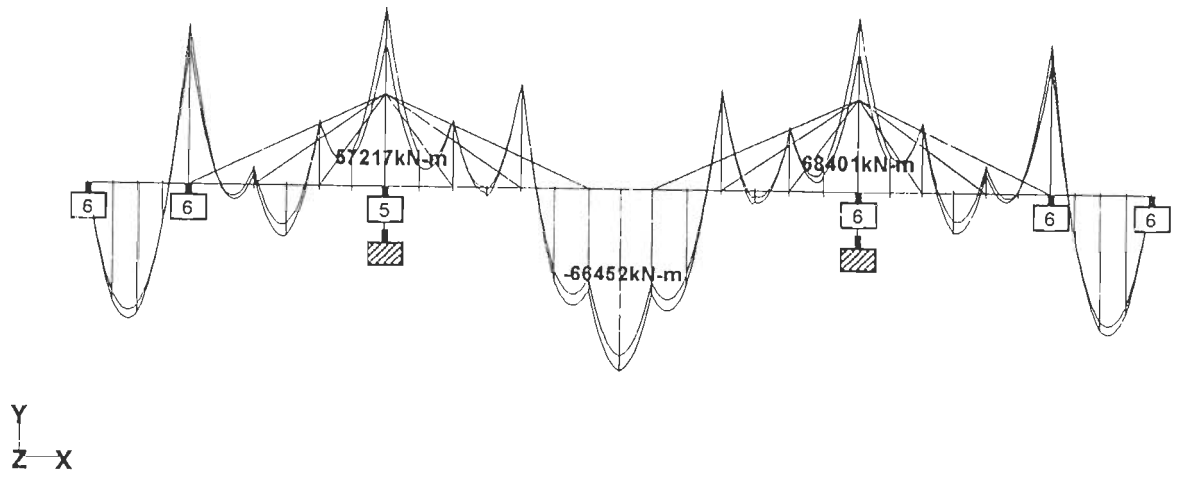

(a) Due to dead load and mean wind forces

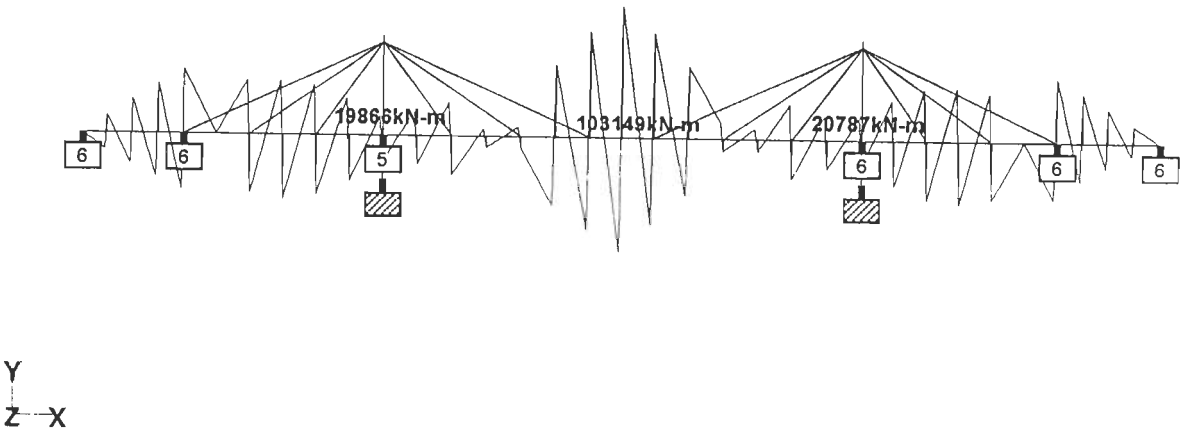

(b) Due to buffeting forces

Fig. 7.12 : Deck Bending Moment Diagram for Bridge # 3 at Wind Speed U(34) = 43.2 m/sec for TC-3

wind speed. The lateral buffeting forces generated at different wind speeds are shown in Fig. 7.13 (a) to (d). The time history of lateral buffeting response at mid span and variation of peak response at mid span and side span are illustrated in Fig. 7.13 (e) and (f). Again it is observed that the variation of response is nonlinear with increase in wind speed. The maximum response in lateral direction is seen to occur at mid span and is much larger than in the side span.

Further, the analysis for computing the torsional buffeting response in Bridge #3 is performed using time domain approach. The generated buffeting moment at various wind speeds and the variation in torsional response with mean wind speed are shown in Fig. 7.14. Here also the maximum response at mid span is much larger than in the side span.

For Bridge #4, assuming it to be situated in terrain category TC-1, the deck level mean speed U(27) has been varied from 33.9m/sec to 67.8m/sec. Time domain analysis for vertical buffeting response for a value of U(27) equal to 45.2m/sec is illustrated in Fig. 7.15.

The variation with mean wind speed of the peak response (buffeting and mean wind components) in the vertical direction at mid span and in the side span of the deck as well as the longitudinal movement of the left side tower is illustrated in Fig. 7.16. From this Figure, it is observed that with increase in the mean wind speed U(27) from 33.9m/sec to 67.8m/sec, the peak mid and side span vertical buffeting response is observed to increase to 3.17 times. The longitudinal response of left tower also increases to 3.17 times. The side span vertical buffeting response is 39% of mid span deck response. With increase in wind speed the variation in vertical buffeting response is nonlinear.

The variation in absolute maximum axial force in selected number of cables due to buffeting is presented in Fig. 7.17. The outer cables are subjected to more force in comparison to inner cables. The tension in outer cable is observed to increase by 24% to

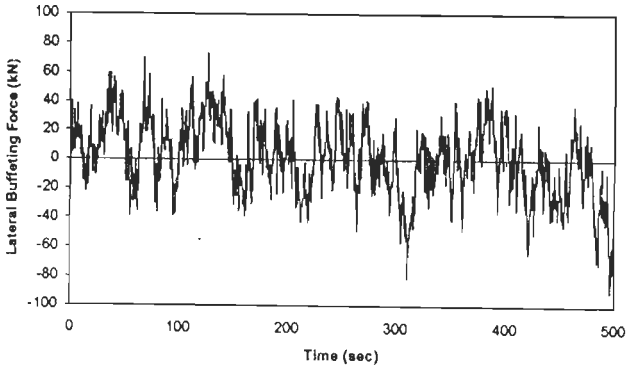

(a) Buffeting force at U(34) = 25.90 m/sec

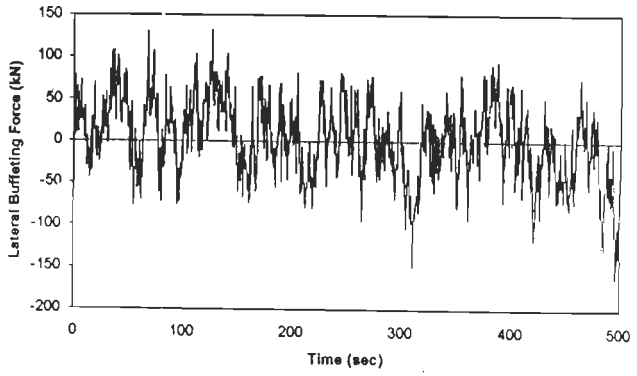

(b) Buffeting force at U(34) = 34.60 m/sec

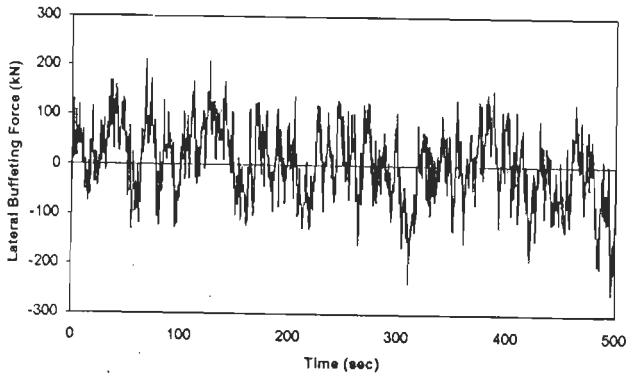

(c) Buffeting force at U(34) = 43.20 m/sec

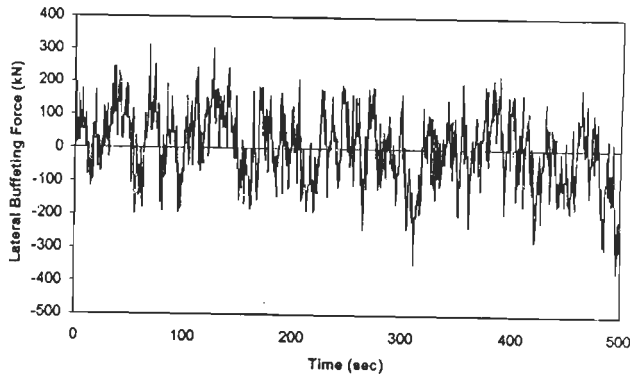

(d) Buffeting force at U(34) = 51.80 m/sec

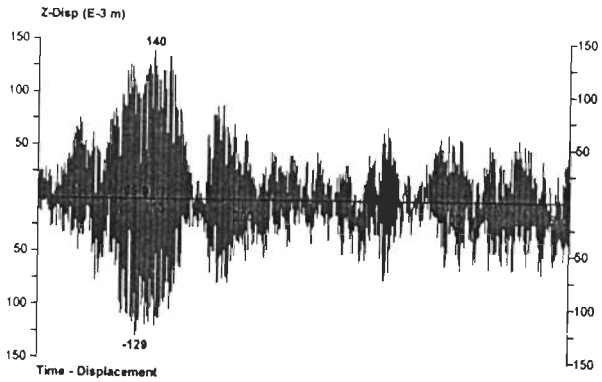

(e) Lateral buffeting response at mid span at U(34) = 43.20 m/sec

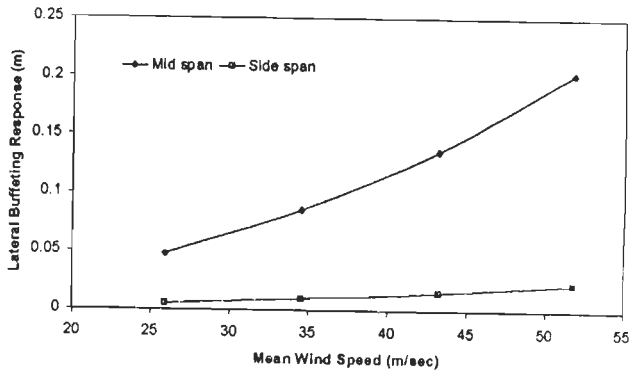

(f) Lateral buffeting response - Variation with mean wind speed

Fig. 7.13 : Time Domain Analysis for Buffeting Response in Lateral Direction for Bridge # 3

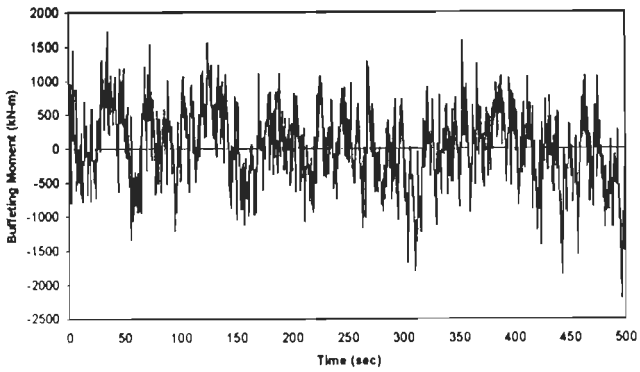

(a) Buffeting moment at U(34) = 25.90 m/sec

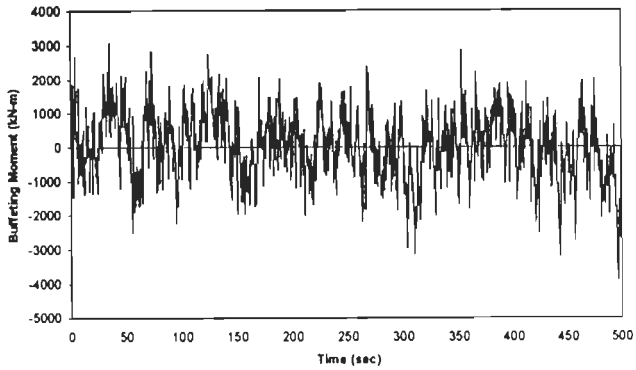

(b) Buffeting moment at U(34) = 34.60 m/sec

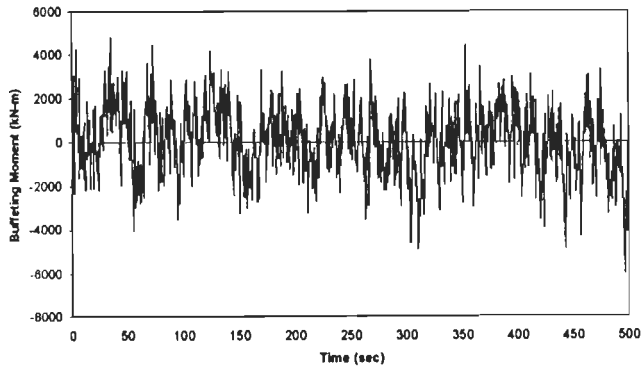

(c) Buffeting moment at U(34) = 43.20 m/sec

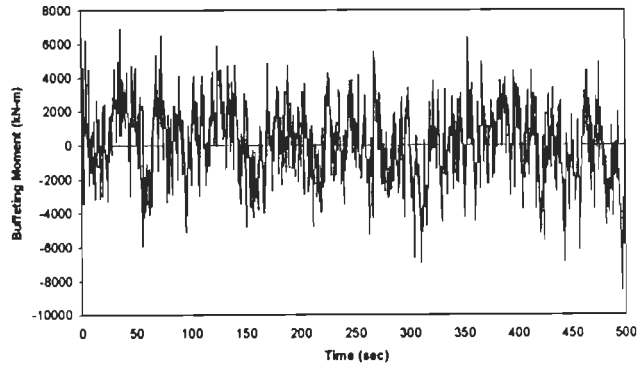

(d) Buffeting moment at U(34) = 51.80 m/sec

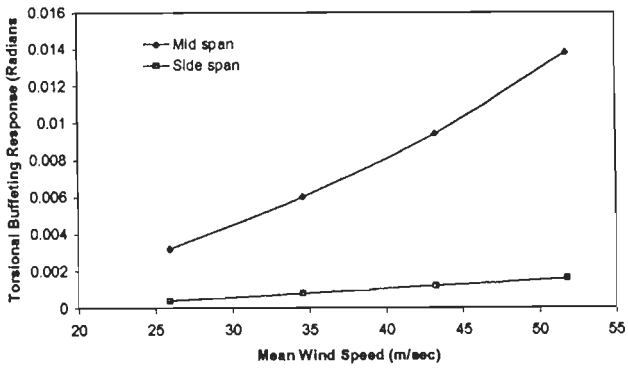

(e) Torsional buffeting response – Variation with mean wind speed

Fig. 7.14 : Time Domain Analysis for Buffeting Response in Torsion for Bridge # 3

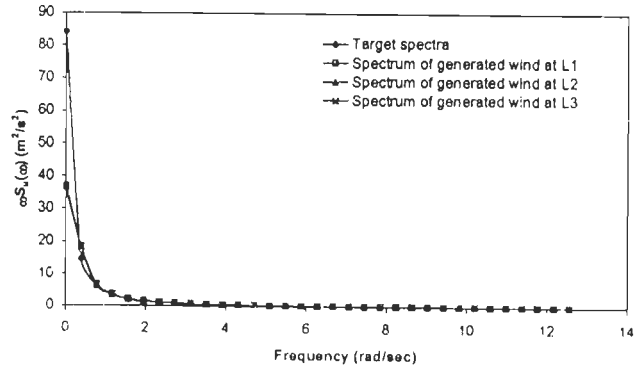

(a) Spectral match for longitudinal wind velocity fluctuations

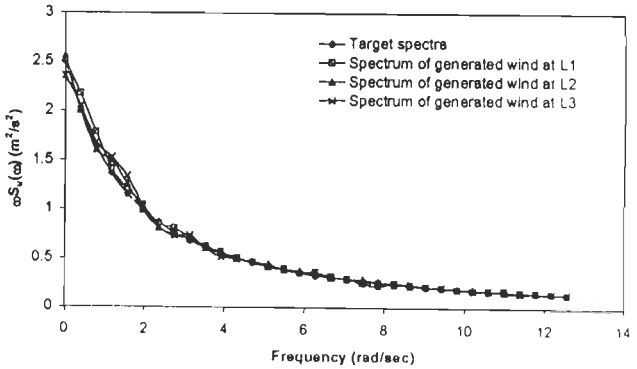

(b) Spectral match for vertical wind velocity fluctuations

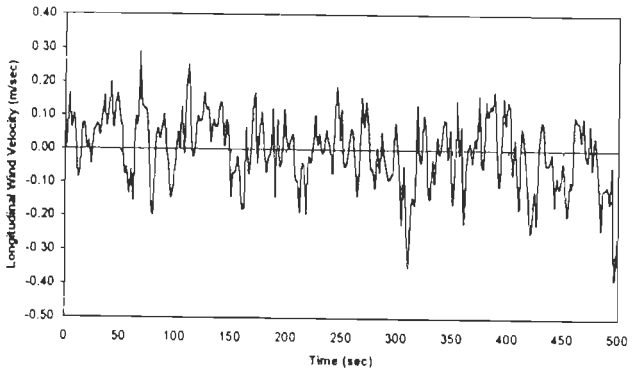

(c) Simulated longitudinal wind velocity fluctuations

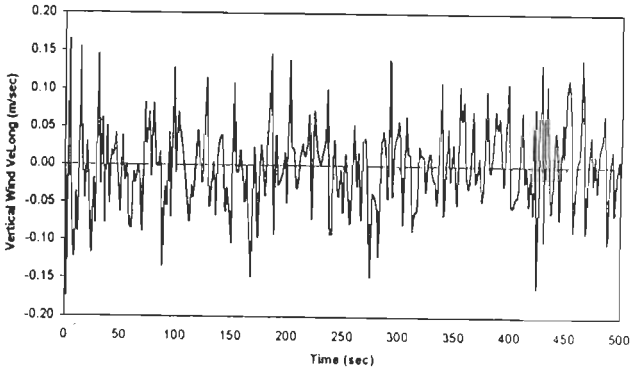

(d) Simulated vertical wind velocity fluctuations

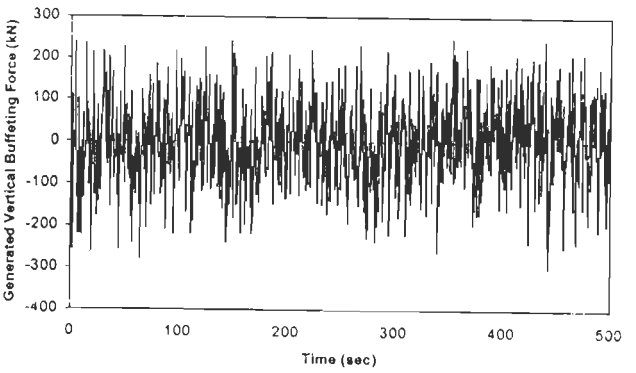

(e) Generated vertical buffeting force

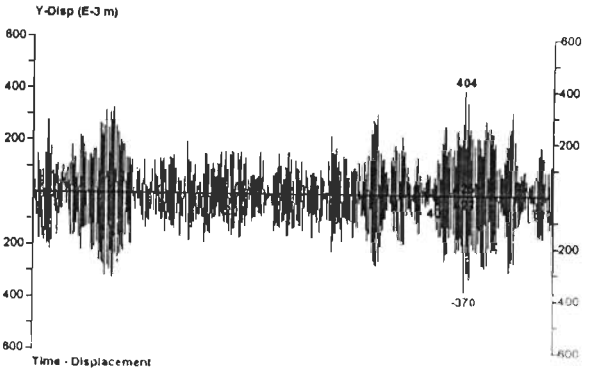

(f) Vertical buffeting response at mid span

Fig. 7.15 : Time Domain Analysis for Vertical Buffeting Response in Bridge # 4 at U(27) = 45.2 m/sec for TC-1

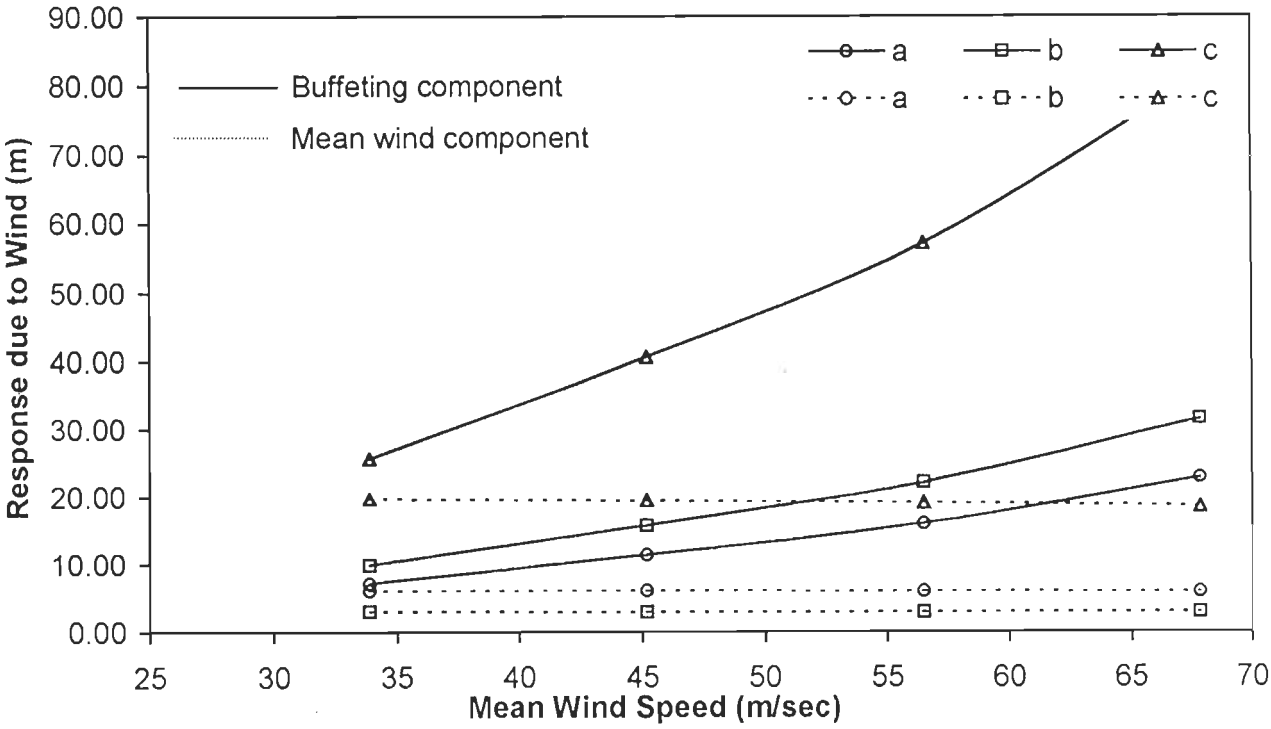

a : Tower tip longitudinal response
b : Maximum side span vertical response
c : Mid span vertical response

Fig. 7.16 : Responses in Bridge # 4 for Terrain Category TC-1 – Variation with Mean Wind Speed

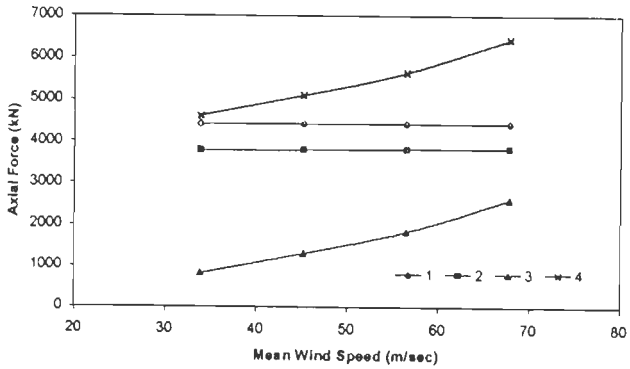

(a) Cable-13L

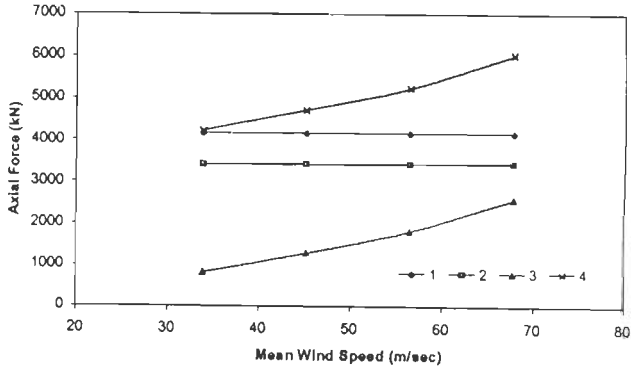

(b) Cable-12L

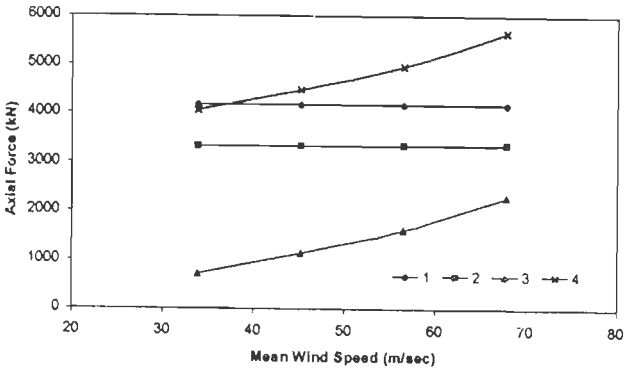

(c) Cable-11L

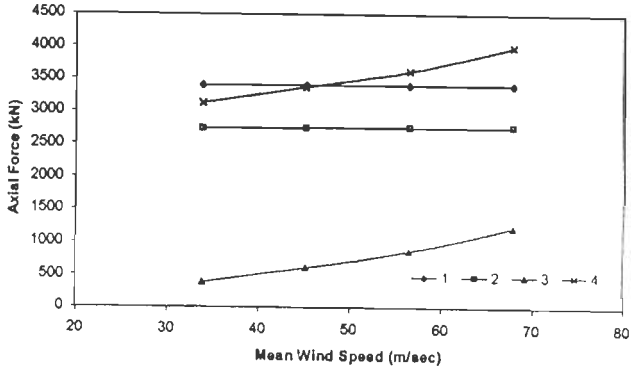

(d) Cable-10L

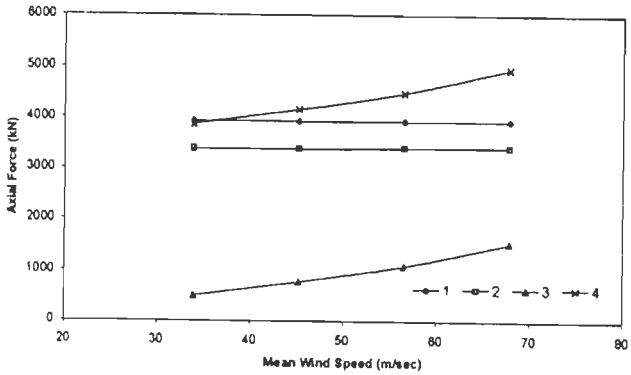

(e) Cable-12R

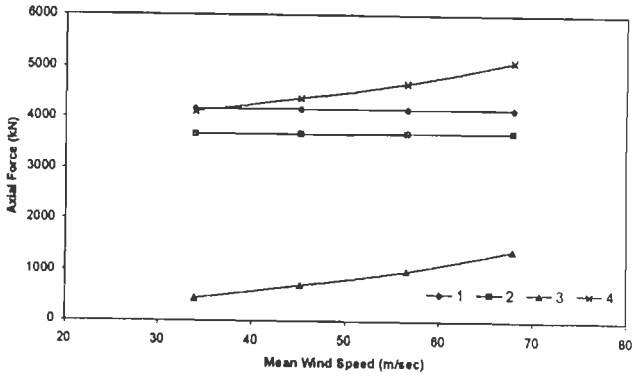

(f) Cable-13R

1 : Initial tension
2 : Mean wind component
3 : Buffeting component
4 : Total cable force

Fig. 7.17 : Absolute Maximum Axial Force in Cables of Bridge # 4 – Variation with Mean Wind Speed

59% of the initial cable tension with increase in mean wind speed. The increase in absolute maximum axial force in towers with variation in mean wind speed is shown in Fig.7.18. The buffeting induced axial force at tower base is seen to increase by 4% to 10% of the axial force induced by dead load and mean wind forces with increase in mean wind speed from 33.9 m/sec to 67.8 m/sec. Comparison of absolute maximum axial force in deck due to mean wind and buffeting forces are depicted in Fig. 7.19(a) and the variation in buffeting induced axial force in deck with increase in mean wind speed is shown in Fig. 7.19(b). The increase in absolute maximum axial force in deck near tower and vertical reaction at deck supports at abutments are shown in Fig. 7.20. The axial force in deck near tower increases by 10 % to 32% of the mean wind component, with increase in wind speed from 33.9 m/sec to 67.8 m/sec. The vertical reaction at deck supports at abutments increases by 11% to 35% of the mean wind component.

By comparison of longitudinal profile of these bridges, it is found that Bridge #4 has 104 cables while Bridge#3 has only 24 cables. It is observed that the variation in buffeting induced forces are lower in Bridge #4. It appears that the higher number of cables in Bridge#4 helps in improving its behavior under random wind forces.

Even though the natural frequency of Bridge#4 in the first lateral mode is 0.585Hz, the buffeting response in this direction is found to be quite low in comparison to the deck width and is not significant enough to be considered in wind resistant design of this bridge.

The analysis for computing the buffeting response of the bridge in torsional direction is performed. The generated buffeting moment at various wind speeds and the variation of torsional buffeting response with mean wind speed is shown in Fig. 7.21. Here also the maximum response at mid span is much higher than in the side span.

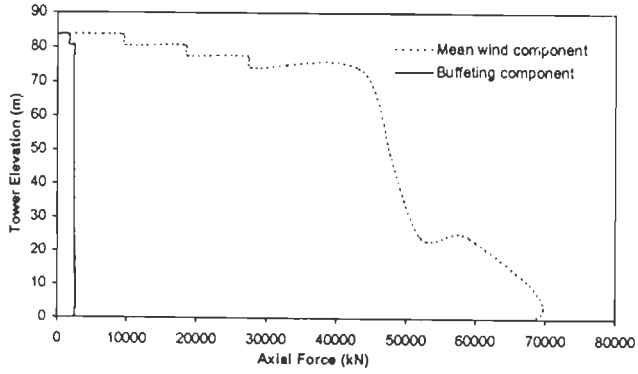

(a) Mean wind speed U(27) = 33.90 m/sec

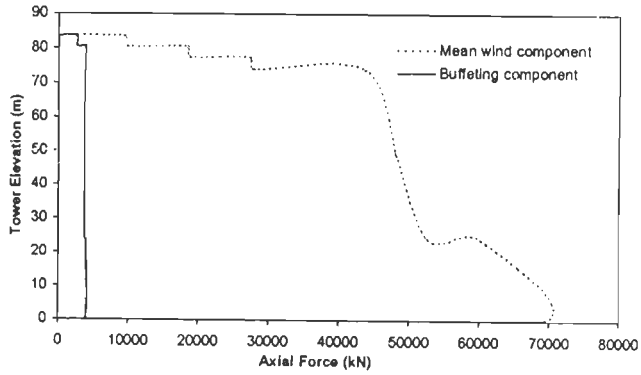

(b) Mean wind speed U(27) = 45.20 m/sec

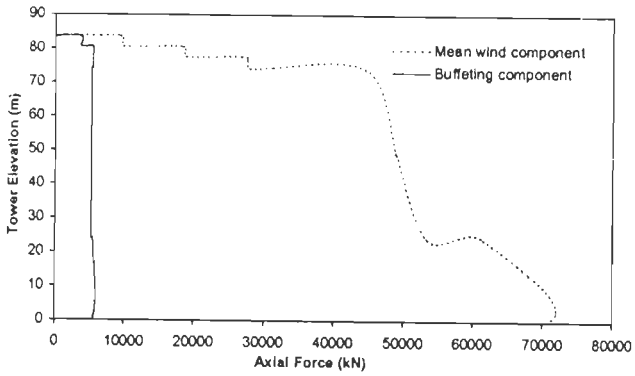

(c) Mean wind speed U(27) = 56.50 m/sec

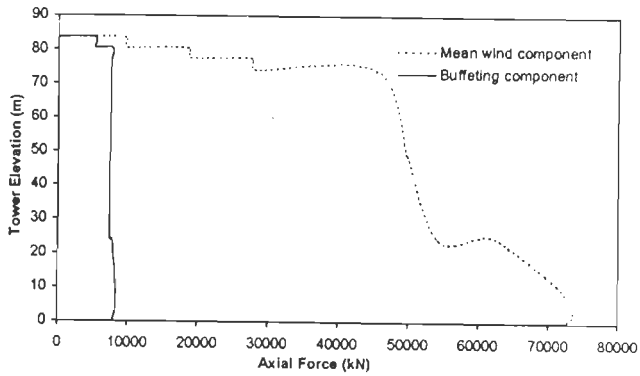

(d) Mean wind speed U(27) = 67.80 m/sec

Fig. 7.18 : Absolute Maximum Axial Force in Towers of Bridge # 4 – Variation with Mean Wind Speed

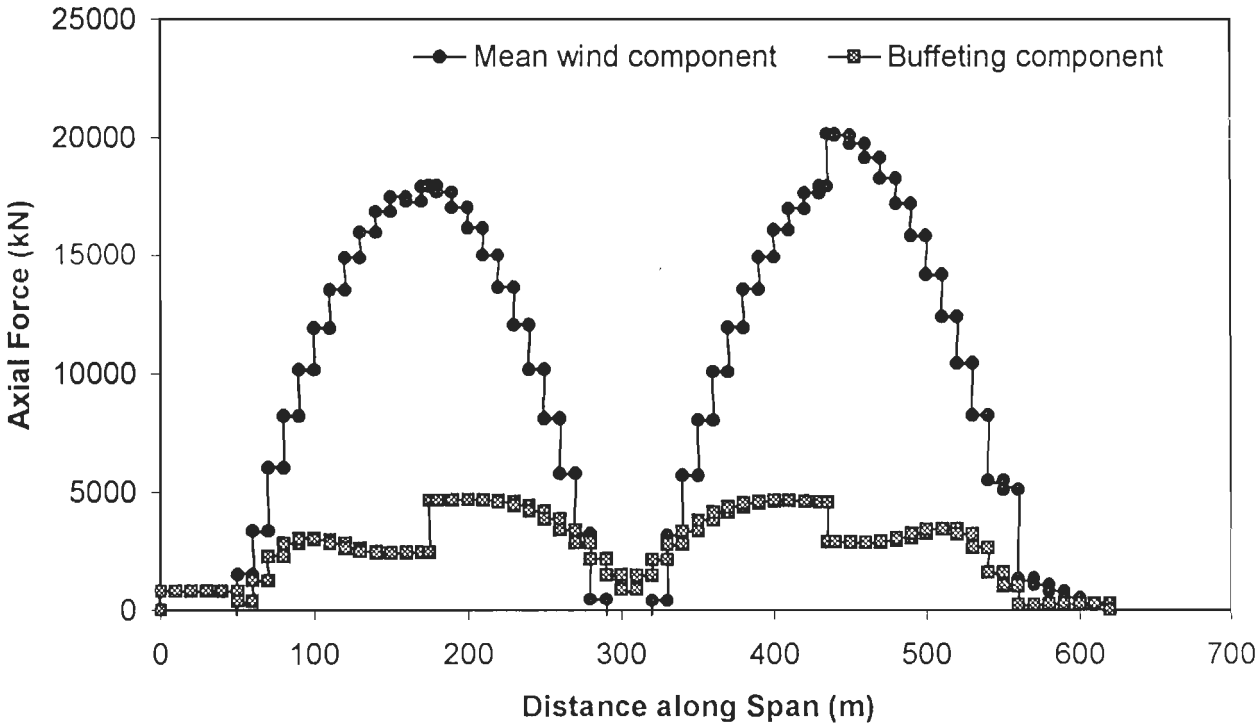

(a) Absolute maximum axial force in deck - Mean wind and buffeting components at U(27) = 45.20 m/sec for TC-1

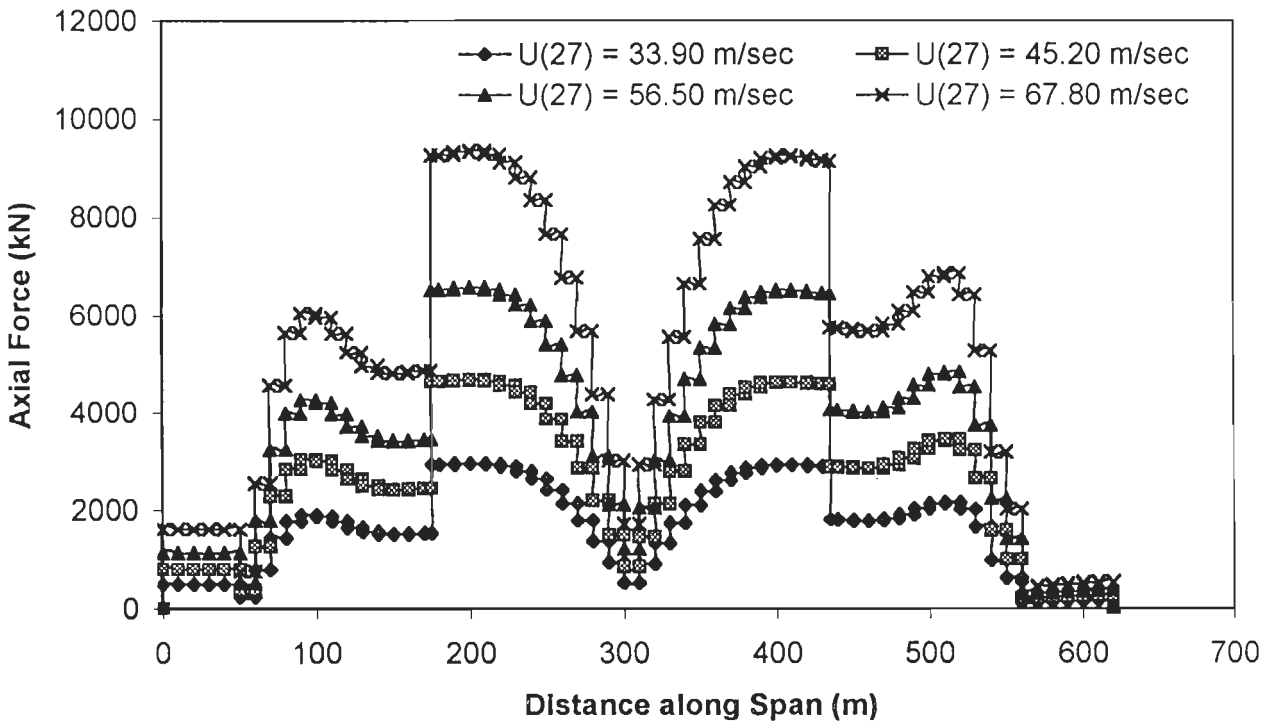

(b) Buffeting induced absolute maximum axial force in deck – Variation with mean wind speed

Fig. 7.19 : Deck Axial Force Diagram for Bridge # 4

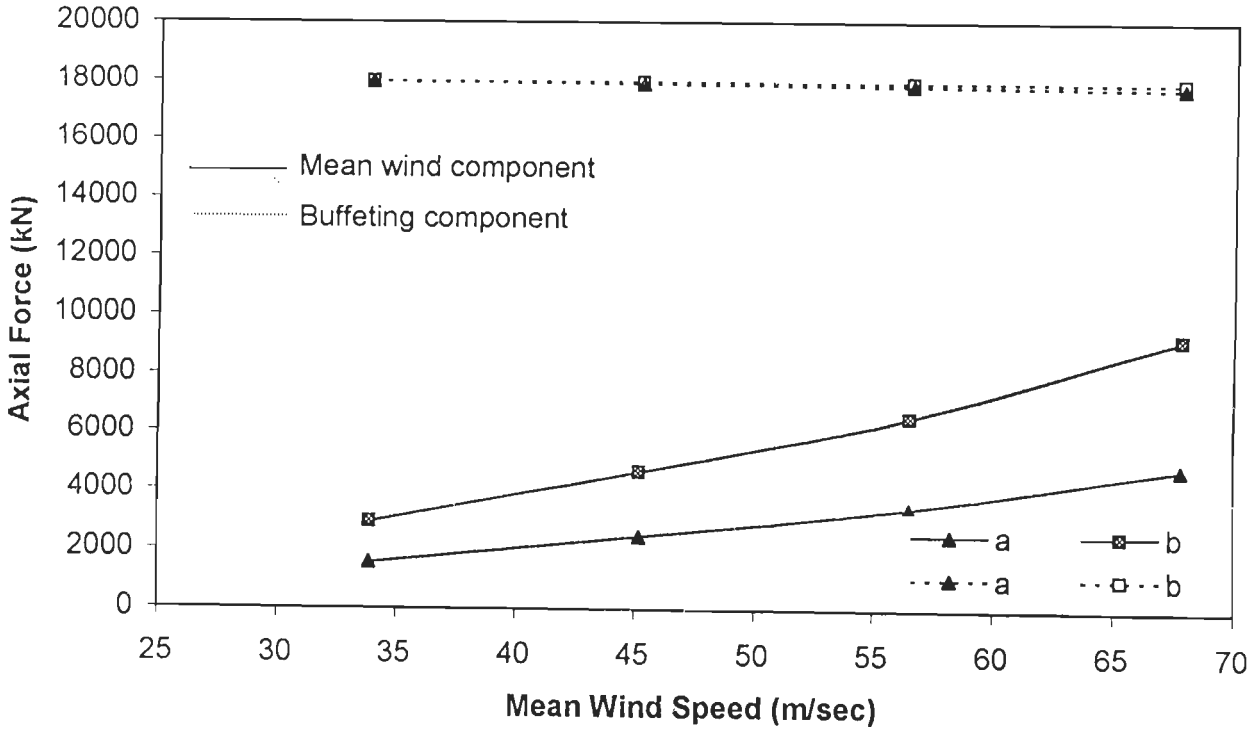

a : Force in member on left side of tower
b : Force in member on right side of tower

(a) Axial force in bridge deck members near left tower support

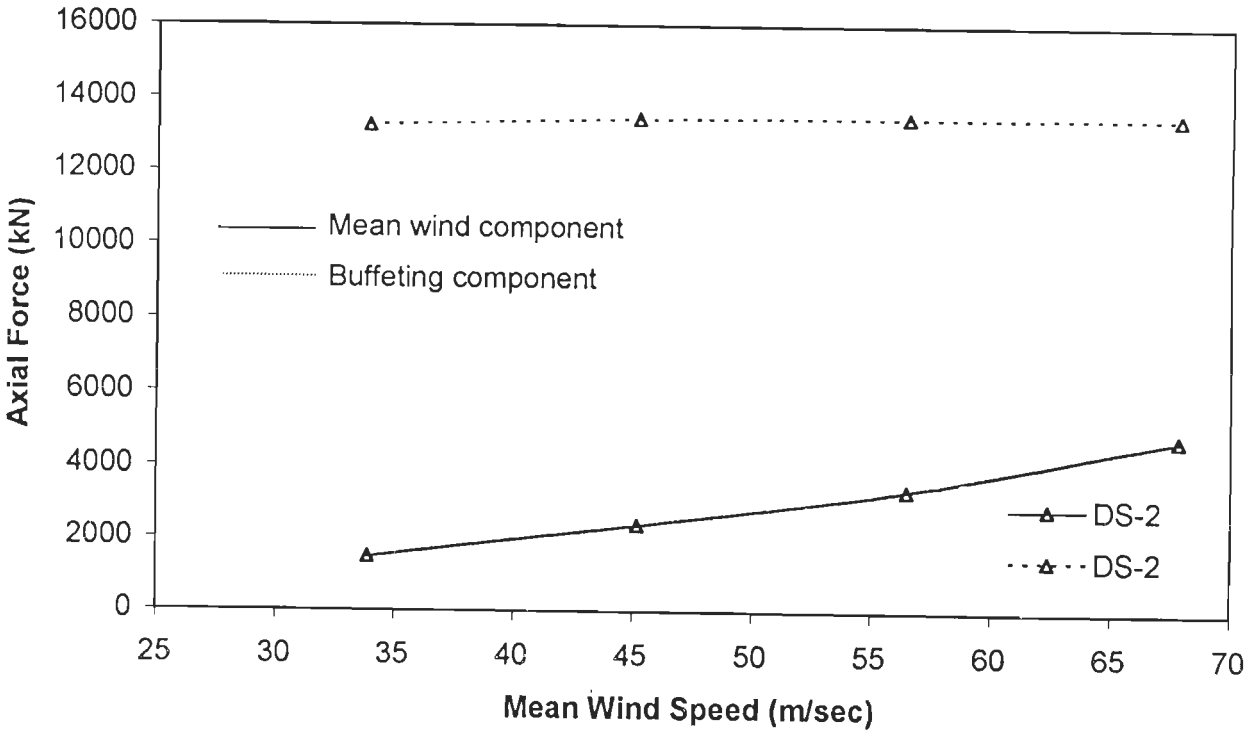

(b) Vertical reaction in deck support at abutment

Fig. 7.20 : Absolute Maximum Axial Force in Deck and Reactions at Deck Supports in Bridge # 4 – Variation with Mean Wind Speed

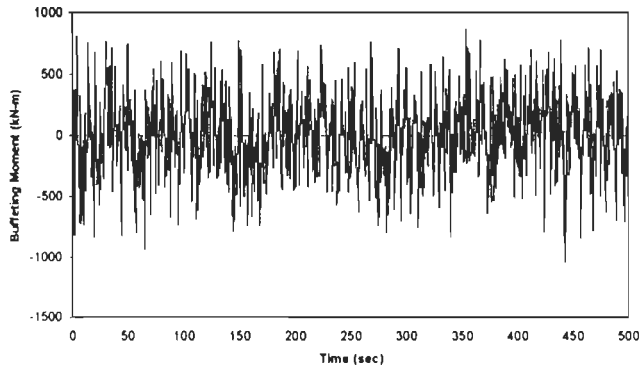

(a) Buffeting moment at U(27) = 33.90 m/sec

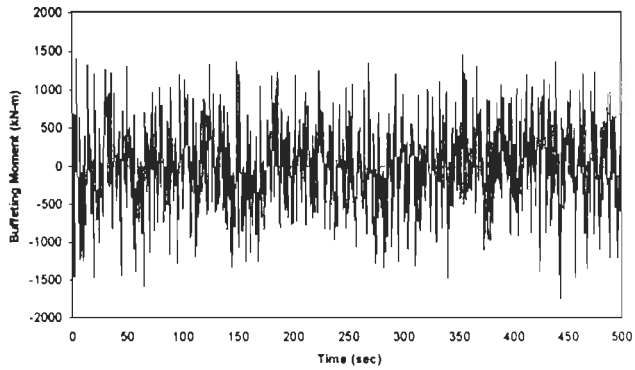

(b) Buffeting moment at U(27) = 45.20 m/sec

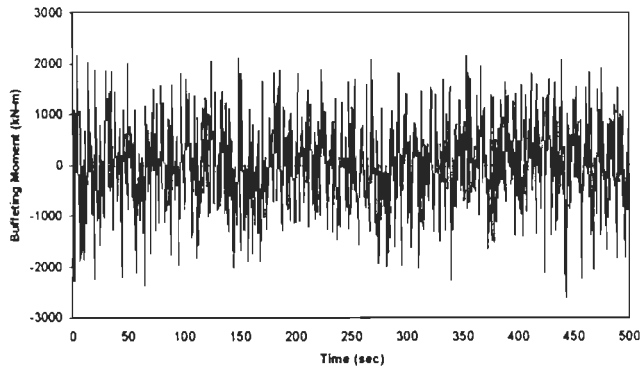

(c) Buffeting moment at U(27) = 56.50 m/sec

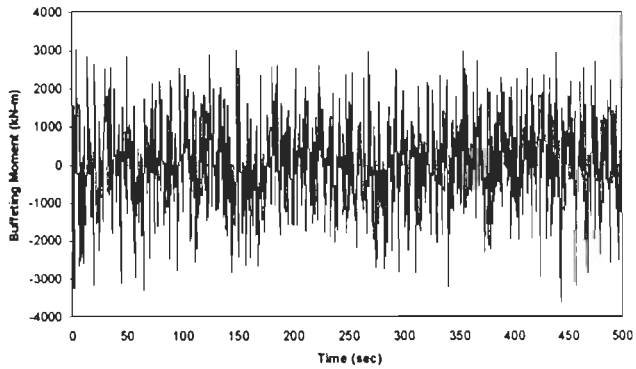

(d) Buffeting moment at U(27) = 67.80 m/sec

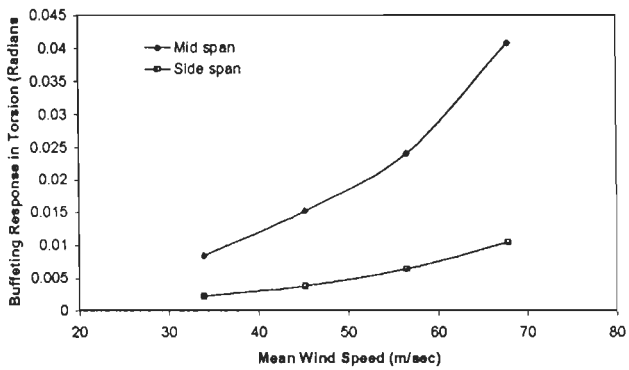

(e) Torsional buffeting response – Variation with mean wind speed

Fig. 7.21 : Time Domain Analysis for Buffeting Response in Torsion for Bridge # 4

7.4.4 Effect of Terrain Roughness

To study the effect of terrain roughness on buffeting response of Bridge #3, the buffeting forces have been computed using the simulated longitudinal and vertical wind velocity fluctuations at a mean speed U(10) of 50m/sec, by varying terrain roughness as discussed in Section 7.2.1, for terrain categories TC-1 to TC-4. With rough terrains the mean wind speed decreases, i.e., from 34.3m/sec to 20.4m/sec. With change in terrain category from TC-1 to TC-4, the turbulence intensity in the longitudinal direction (I_u) varies from 11.5% to 24.7% and in the vertical direction (I_w) from 5.7% to 15.0%.

The effect of terrain roughness on wind induced response – tower longitudinal response, mid span and side span vertical buffeting response due to mean wind and buffeting forces in Bridge #3 is illustrated in Fig. 7.22. It is clear from the Figure that with reduction in mean wind speed, the mean wind response decreases, whereas the buffeting response of deck in the vertical direction and for the tower in longitudinal direction increases nonlinearly with increase in terrain roughness.

The gust response factor along the span of cable stayed bridges is computed as a ratio of the peak buffeting response to mean wind response. The variation in gust response factor for Bridge #3 is shown in Fig. 7.23 and nearly 25% increase in the gust response factor is observed with change in terrain category from TC-1 to TC-4.

The effect of terrain roughness on buffeting induced absolute maximum axial force in cables, deck and towers in Bridge#3 is illustrated in Fig. 7.24. The tension in outer cable has a small increase from 63% to 71.4% of the initial cable tension. However, in cable-2, the axial tension is observed to increase from 40% to 45% of the initial tension with change in terrain roughness. The axial force in tower increases by 11% while the axial force in deck members near the tower increases only by 5%.

To study the effect of terrain roughness on the buffeting response of Bridge #4 at deck level, the terrain roughness in the longitudinal direction (I_u) is varied in the range 11.8% to 26.7% and in the vertical direction (I_w) in the range 6.5% to 13.9%.

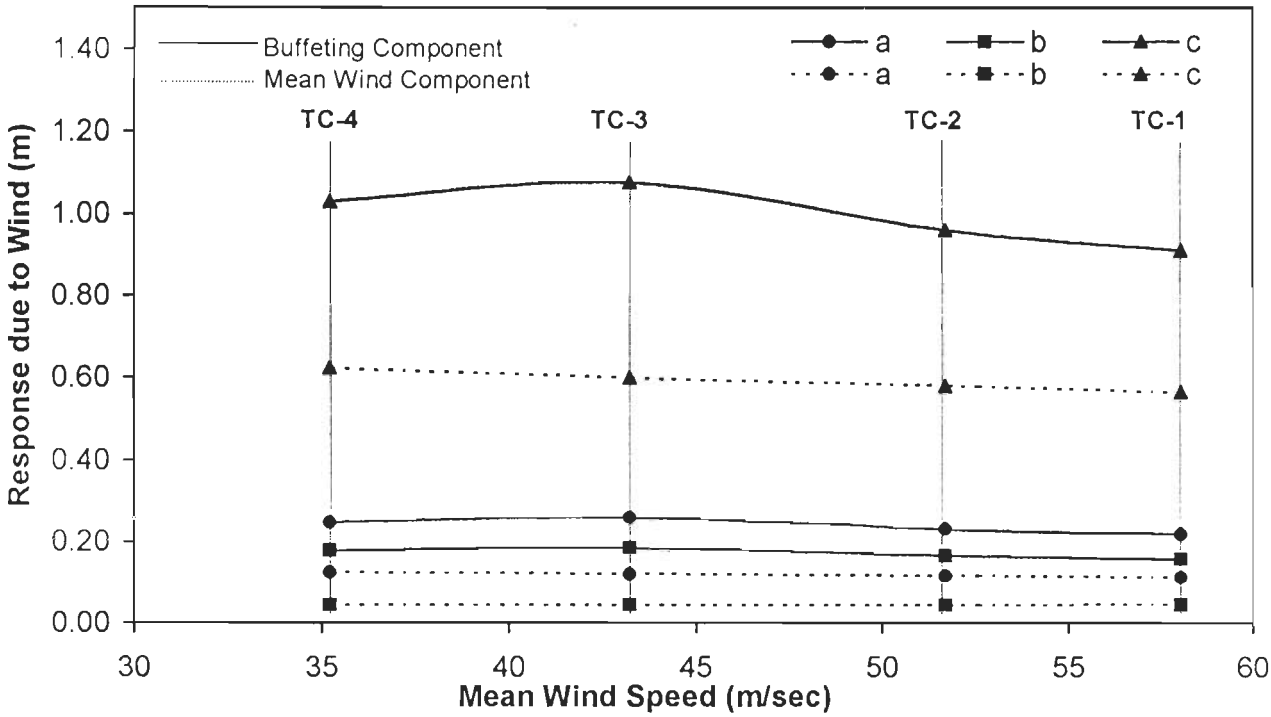

a : Tower tip longitudinal response
b : Maximum side span vertical response
c : Mid span vertical response

Fig. 7.22 : Wind Induced Response of Bridge # 3 - Effect of Terrain Roughness

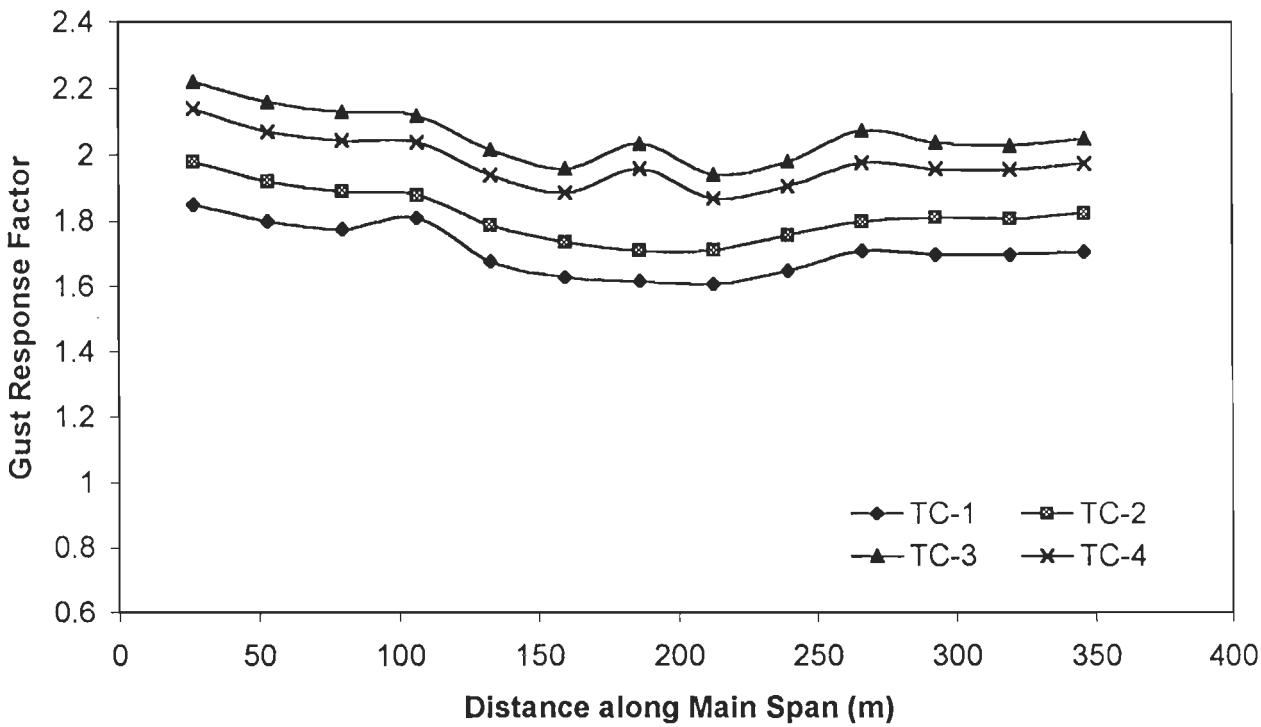

Fig. 7.23 : Spatial Distribution of Gust Response Factor for Bridge # 3 - Effect of Terrain Roughness

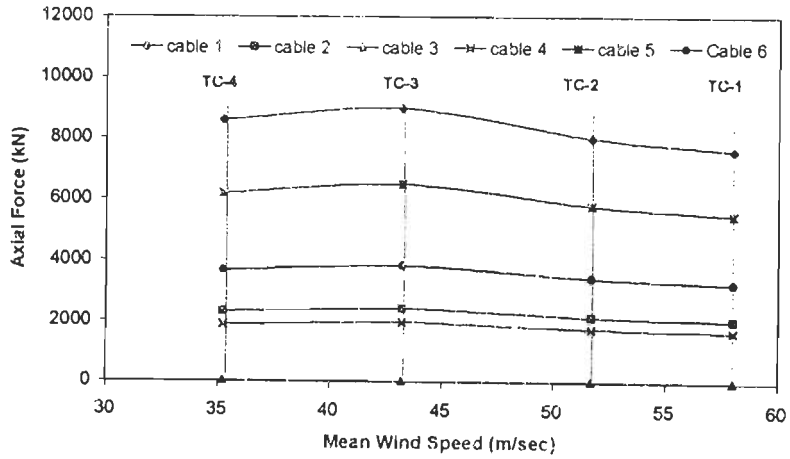

(a) Cable force

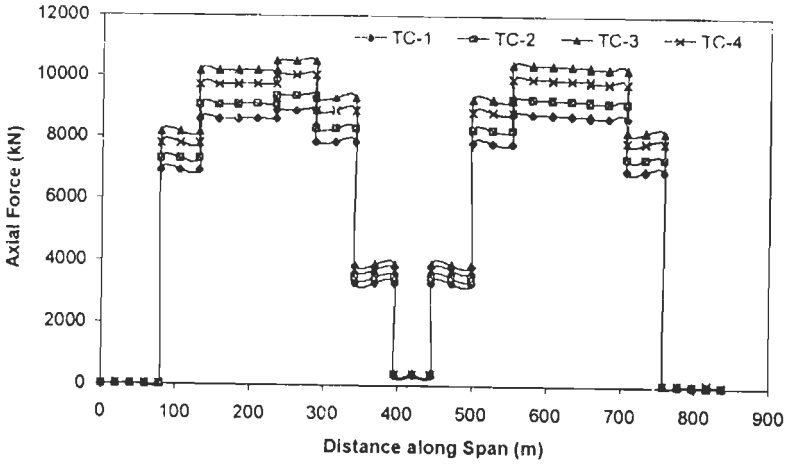

(b) Deck axial force

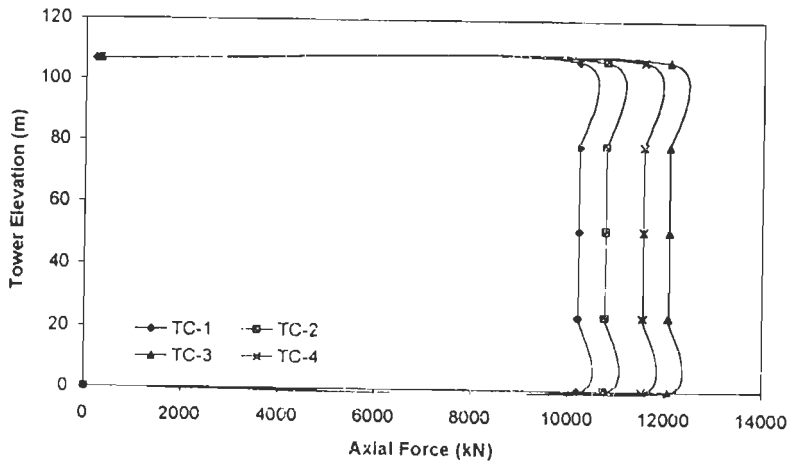

(c) Tower axial force

TC	U(34)m/sec	I_u%	I_w%
TC-1	58.0	11.5	5.7
TC-2	51.7	13.9	7.2
TC-3	43.2	19.3	11.0
TC-4	35.2	24.7	15.0

Fig. 7.24 : Effect of Terrain Roughness on Buffeting Induced Absolute Maximum Axial Force in Components of Bridge # 3

The effect of terrain roughness on wind induced response – tower longitudinal response, mid span and side span vertical buffeting response due to the mean wind and buffeting forces for Bridge #4 is illustrated in Fig. 7.25. It is clear from the figure that with reduction in mean wind speed, the mean wind response reduces, whereas the buffeting response of the deck in vertical direction and for the tower in longitudinal direction increases nonlinearly with increase in terrain roughness.

The variation in gust response factor along the span for Bridge #4 is shown in Fig. 7.26 and a 10% increase in the gust response factor is observed with change in terrain category from TC-1 to TC-4.

The effect of terrain roughness on buffeting induced absolute maximum axial force in cables, deck and towers for Bridge#4 is illustrated in Fig. 7.27. The tension in outer cable increases slightly from 18% to 20% of the initial cable tension and the axial force in tower is observed to increase by 10%.

7.5 SUMMARY

The time domain buffeting analysis of five span cable stayed bridges – Bridge #3 with total span of 836.6m and Bridge# 4 with total span of 610m – are numerically illustrated in this Chapter. In the present study, effect of buffeting forces on the complete bridge, rather than the deck alone, is evaluated by idealizing the bridge as a three dimensional space structure. The effect of (i) mean wind speed variation and (ii) terrain roughness on the buffeting response have been studied.

From the results for the two bridges it is clear that, with increase in the mean wind speed, buffeting responses in vertical, lateral and torsional modes increase nonlinearly. The buffeting response in vertical direction in the side span is below 40% of the response of main span at its centre. However, the lateral and torsional buffeting responses in the side span are only about 12% of the main span vertical response. The buffeting in lateral modes becomes important with longer spans like Bridge#3.

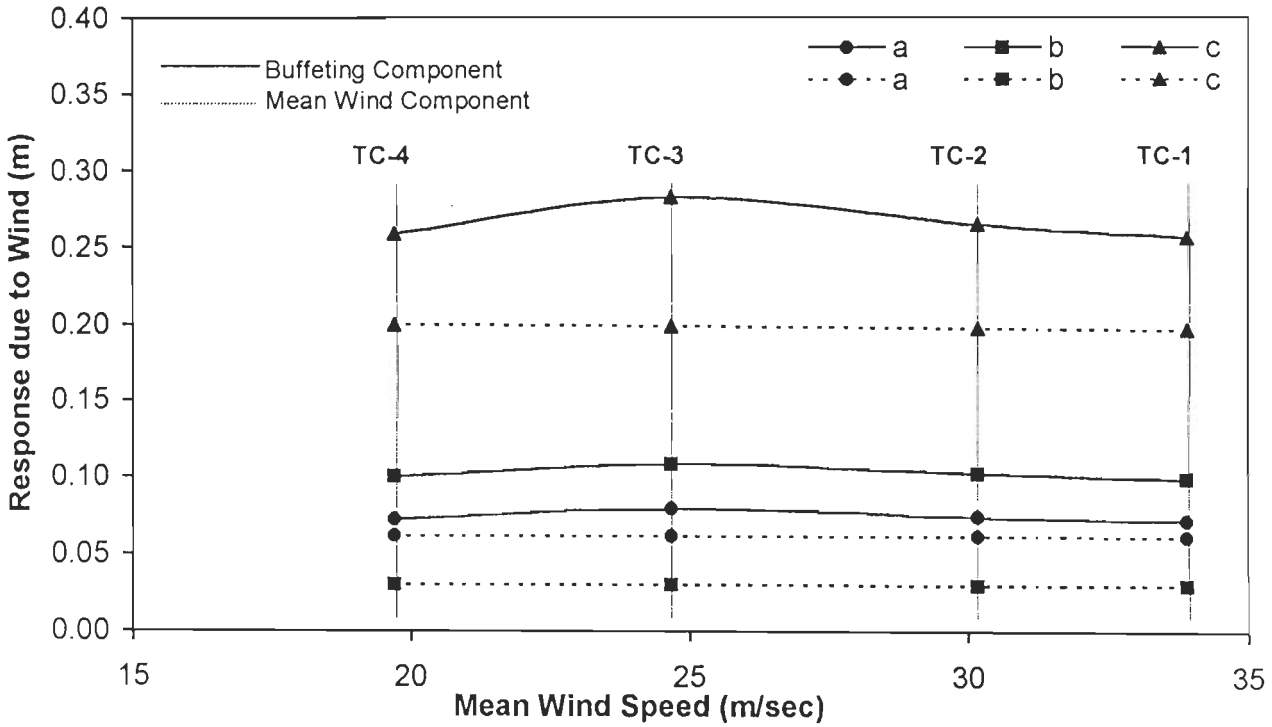

a : Tower tip longitudinal response
b : Maximum side span vertical response
c : Mid span vertical response

Fig. 7.25 : Wind Induced Response of Bridge # 4 – Effect of Terrain Roughness

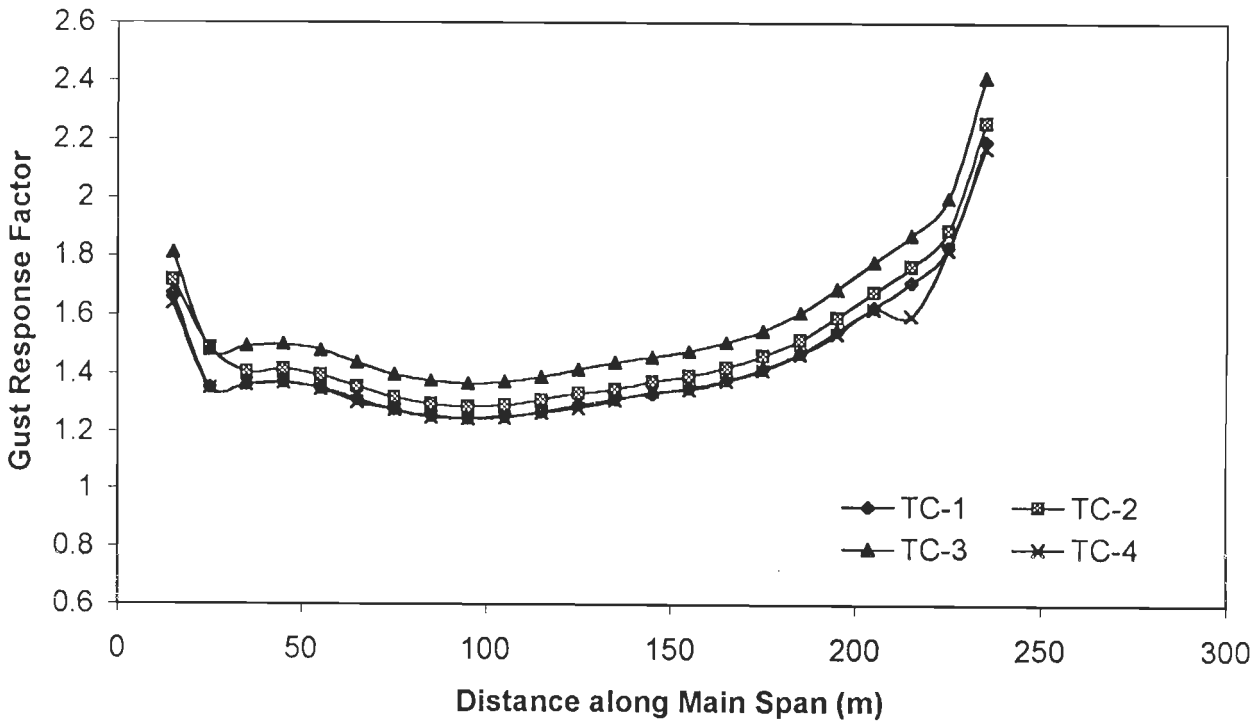

Fig. 7.26 : Spatial Distribution of Gust Response Factor for Bridge # 4 – Effect of Terrain Roughness

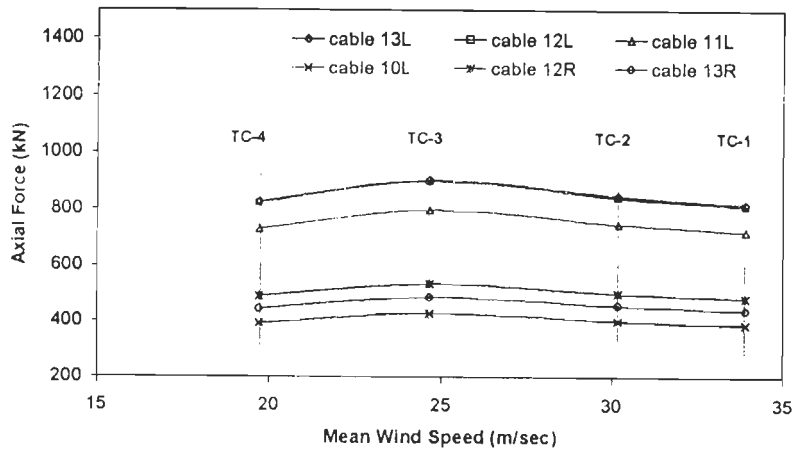

(a) Cable force

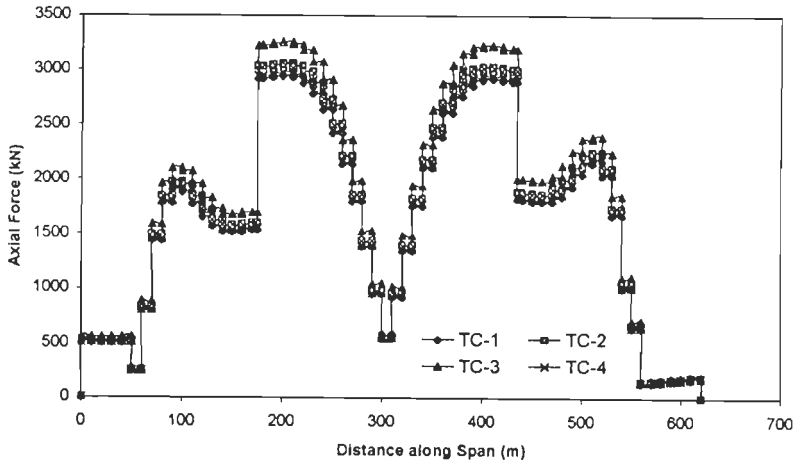

(b) Deck axial force

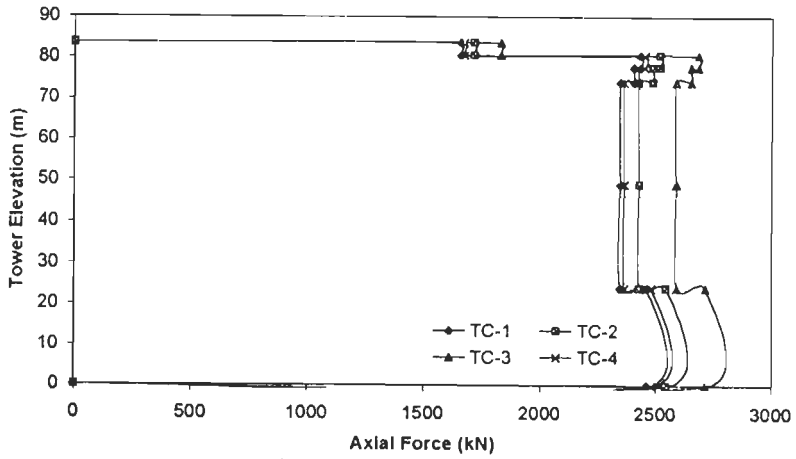

(c) Tower axial force

TC	U(27)m/sec	I_u%	I_w%
TC-1	33.9	11.8	6.5
TC-2	30.2	14.4	7.8
TC-3	24.6	20.3	10.7
TC-4	19.7	26.7	13.9

Fig. 7.27 : Effect of Terrain Roughness on Buffeting Induced Absolute Maximum Axial Force in Components of Bridge # 4

The outer cables, deck members near towers and deck supports at abutments are subjected to higher buffeting induced forces. The forces induced in the bridge components such as cables, towers, deck as well as deck supports due to mean and buffeting forces obtained from the analysis would be useful in wind resistant design.

The turbulence level in the approaching wind is found to affect the response of bridge as well as buffeting induced forces considerably. The effect becomes more prominent for longer spans and needs to be included in the analysis for a rational wind design.

From the study it is observed that five span bridges with larger number of cables are preferable for buffeting based design of bridges as the gust response factor as well as the buffeting induced forces in bridge components tend to be lower.

Chapter 8
FLUTTER ANALYSIS

8.1 INTRODUCTION

This chapter is devoted to theoretical formulations and procedure for two-dimensional and three-dimensional flutter analysis of cable stayed bridges. Also discussed are the flutter derivatives for bridge deck cross-sections typically used in modern cable stayed bridges. Application of flutter derivatives and validation of flutter analysis is also presented with the help of numerical examples.

Flutter analysis of all the four bridges undertaken in this study has been numerically illustrated. Analysis of three span bridges (Bridge #1 and Bridge #2) and five span bridge (Bridge #4) has been performed to study the effect of bridge vibration in higher modes on critical flutter speed. Bridge #3 has been analysed to observe the effect of angle of attack on critical flutter speed. Further, Bridge #2 has been anlaysed to predict the criteria for onset of flutter when the bridge deck is subjected to lateral and torsional motions. Also, the effect of type of deck supports at towers and abutments on flutter tendencies of three span bridges has been examined.

8.2 THEORETICAL FORMULATION FOR FLUTTER

Consider a spring-suspended bridge deck model as shown in Fig. 8.1. The bridge deck system has three degrees of freedom, i.e., it is permitted to displace vertically in h-direction, laterally or sway in p-direction, and rotate through an angle α. The rigidity of the bridge deck section is expressed in terms of stiffness coefficients, K_h, K_p, and K_α, concentrated at the elastic centre. The bridge deck has a mass distribution, m, whose effect is concentrated at the centre of gravity. The governing differential equations of motion of the bridge system can be derived from Lagrange's

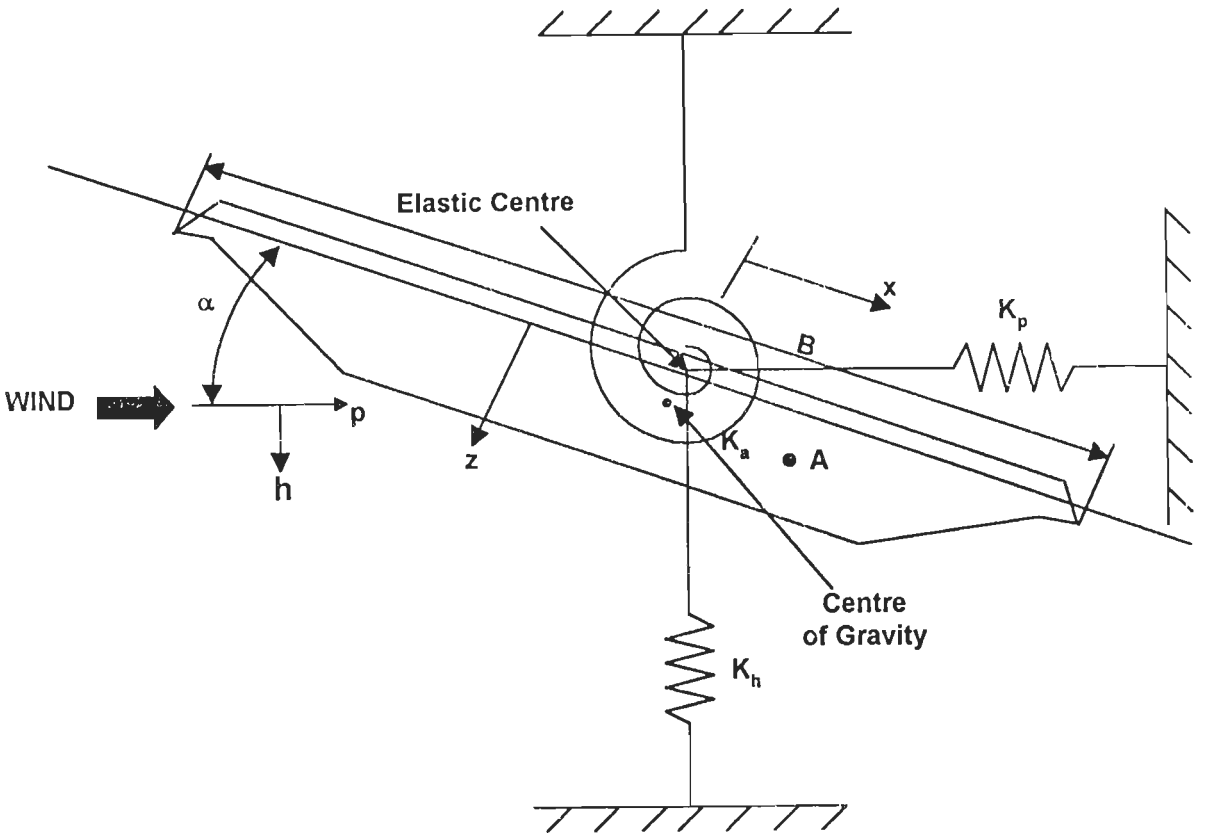

Fig. 8.1 : Spring Suspended Bridge Deck Model with Three Degrees of Freedom

Equation given by,

$$-\frac{d}{dt}\frac{\partial(T-U)}{\partial \dot{q}_i}+\frac{\partial(T-U)}{\partial q_i}+Q_i=0 \tag{8.1}$$

where,

q_i = ith generalized coordinate

$\dot{q}_i$ = ith generalized velocity

Q_i = ith generalized force

T = kinetic energy

U = strain energy

Let the generalized coordinates be q_1=h, q_2= p,q_3 = α. The displacement vector, r, at any point A on the cross-section is,

r = ui + wk

where,

u = horizontal displacement of point A

w = vertical displacement of point A

i,k = unit vectors in horizontal and vertical directions, respectively

From the geometric relationships, it can be shown that,

$$u = p + x(\cos\alpha - 1) - z\sin\alpha \tag{8.2}$$

$$w = h + z(\cos\alpha - 1) + x\sin\alpha \tag{8.3}$$

For small values of rotation, it can be taken as cosα ≅ 1, and sinα =α. Substituting into Eqs. 8.2 and 8.3, results in

$$u = p - z\alpha \tag{8.4}$$

$$w = h + x\alpha \tag{8.5}$$

The kinetic energy, T, is expressed as

$$T = \frac{1}{2}\iint\left[\left(\frac{du}{dt}\right)^2 + \left(\frac{dw}{dt}\right)^2\right]mdxdz$$

$$= \frac{1}{2}M(\dot{p}^2 + \dot{h}^2) + \frac{1}{2}2S_x\dot{h}\dot{\alpha} - \frac{1}{2}2S_z\dot{p}\dot{\alpha} + \frac{1}{2}I\dot{\alpha}^2 \tag{8.6}$$

where,

$$\text{total mass, } M = \iint mdxdz \tag{8.7}$$

Mass moment with respect to x- axis is given as:

$$S_x = \iint xmdxdz \;\; = x_{cg}\mathrm{M} \tag{8.8}$$

Mass moment with respect to z-axis is given as:

$$S_z = \iint zmdxdz \;\; = \mathrm{z_{cg}M}$$

$$\text{Mass moment of inertia, } I = \iint\left(x^2 + z^2\right)mdxdz \tag{8.9}$$

The strain energy, U is given as

$$U = \frac{1}{2}K_h h^2 + \frac{1}{2}K_p p^2 + \frac{1}{2}K_\alpha \alpha^2 \tag{8.10}$$

By substituting Eqs 8.6 and 8.10 in Eq. 8.1, we get the governing equations of bridge motion as:

$$M\ddot{h} + S_x\ddot{\alpha} + K_h h = L_{ae} \tag{8.11}$$

$$M\ddot{p} - S_z\ddot{\alpha} + K_p p = D_{ae} \tag{8.12}$$

$$I\ddot{\alpha} + S_x\ddot{h} - S_z\ddot{p} + K_\alpha \alpha = M_{ae} \tag{8.13}$$

The above equations are coupled through static mass and moment terms. However, bridge decks are symmetrical about centerline, besides the elastic centre and center of gravity are close to each other along the vertical axis. Therefore, the static mass moments S_x and S_z are zero. The uncoupled equations of motion after introducing the terms of structural damping can be written as

$$M\left[\ddot{h} + 2\xi_h\omega_h\dot{h} + \omega_h^2\right] = L_{ae} \tag{8.14}$$

$$M\left[\ddot{p} + 2\xi\omega_p\dot{p} + \omega_p^2\right] = D_{ae} \tag{8.15}$$

$$I\left[\ddot{\alpha} + 2\xi\omega_\alpha\dot{\alpha} + \omega_\alpha^2\right] = M_{ae} \tag{8.16}$$

M, I = mass and mass moment of inertia respectively.

ξ_h, ξ_p, ξ_α = ratio of damping to critical damping for vertical, lateral and torsional degrees of freedom respectively.

$\omega_h, \omega_p, \omega_\alpha$ = circular natural frequencies for vertical, lateral and torsional degrees of freedom respectively

L_{ae}, D_{ae}, M_{ae} = unsteady aerodynamic or self-excited forces in vertical, lateral and torsional degrees of freedom respectively.

As discussed earlier in Section 2.7, the self-excited forces cause flutter and are motion dependent. These may be represented in terms of flutter derivatives as follows (Jain *et al*, 1996):

$$L_{ae} = \frac{1}{2}\rho U^2 B\left[KH_1^*\frac{\dot{h}}{U} + KH_2^*\frac{B\dot{\alpha}}{U} + K^2H_3^*\alpha + K^2H_4^*\frac{h}{B} + KH_5^*\frac{\dot{p}}{U} + K^2H_6^*\frac{p}{B}\right] \tag{8.17}$$

$$D_{ae} = \frac{1}{2}\rho U^2 B\left[KP_1^*\frac{\dot{p}}{U} + KP_2^*\frac{B\dot{\alpha}}{U} + K^2P_3^*\alpha + K^2P_4^*\frac{p}{B} + KP_5^*\frac{\dot{h}}{U} + K^2P_6^*\frac{h}{B}\right] \quad (8.18)$$

$$M_{ae} = \frac{1}{2}\rho U^2 B^2\left[KA_1^*\frac{\dot{h}}{U} + KA_2^*\frac{B\dot{\alpha}}{U} + K^2A_3^*\alpha + K^2A_4^*\frac{h}{B} + KA_5^*\frac{\dot{p}}{B} + K^2A_6^*\frac{p}{B}\right] \quad (8.19)$$

where ρ = air density

U = mean velocity of the oncoming wind(which is turbulent in general)

$K = \frac{B\omega}{U}$ = the reduced frequency

H_i^*, P_i^*, A_i^*, i=1,6 are flutter derivatives and functions of K, determined experimentally or using CFD techniques, for the deck cross-section under investigation.

It may be noted that in Eqs. 8.17-8.19 the entire set of 18 flutter derivatives has been used to express the self-excited or unsteady aerodynamic forces so that the potential coupling amongst different displacement components is fully captured.

8.2.1 Flutter Derivatives

The flutter derivatives H_i^*, P_i^*, A_i^*, i=1,6, indicate the modification in structural damping and structural stiffness of bridge deck in vertical bending, lateral and tosional directions as a result of fluid-structure interaction. Of the 18 flutter derivatives, 6 derivatives $H_1^*, H_4^*, P_1^*, P_4^*, A_2^*, A_3^*$ are direct derivatives and others are cross-flutter derivatives. Direct derivatives are important in single degree of freedom flutter whereas the cross-flutter derivatives play vital role in classical flutter.

As discussed earlier, the vertical and torsional flutter derivatives H_i^* and A_i^* i=1,4 are generally obtained by experimental investigations of bridge deck section. Of late, they are also obtained using CFD techniques. These derivatives are useful in qualitative assessment and quantitative prediction of occurrence of flutter.

Flutter derivatives for bluff and streamlined bridge deck sections, typically

found in modern single plane and double plane long span bridges, obtained by wind tunnel investigations (Scanlan and Tomko, 1971) are shown in Figs. 8.2 and 8.3. These derivatives are functions of geometry of bridge deck cross-section and also change with modification in cross–section details.

The relationships amongst some of the flutter derivatives have also been established on the basis of experimental investigations on different bluff deck sections and flat box girder decks. Matsumato et al (1995) measured the unsteady pressure on the top surface of bluff cross-sections such as rectangular sections with B/d =5, 8,10,12.5,15 and 20, elliptical and rectangular sections with centre-vertical plate, when the models are subjected to forced vibrations and allowed to oscillate in vertical or torsional motion under smooth flow, during wind tunnel studies. By considering the analogy of unsteady pressures between the vertical and torsional motions, the following dependence between the flutter derivatives for bluff sections (like rectangular cross-section with width to depth (B/d) ratio of 10) was established:

$$H_1^* = -kH_3^* \tag{8.20}$$

$$H_4^* = -kH_2^* \tag{8.21}$$

$$A_1^* = kA_3^* \tag{8.22}$$

$$A_4^* = -kA_2^* \tag{8.23}$$

where k= $\frac{b\omega}{U}$ and b is half deck width.

These relations have been confirmed also by Davenport (1992), Reinhold (1992), Virloguex (1992) and Jacobsen (1993) for some flat box bridge girders.

Qualitative assessment of occurrence of flutter is possible with the help of plots of flutter derivatives. The single degree of freedom flutter in vertical bending motion is likely to occur, if H_1^* changes from negative to positive with increase in reduced velocity. The single degree of freedom flutter in torsional motion is likely to occur, if

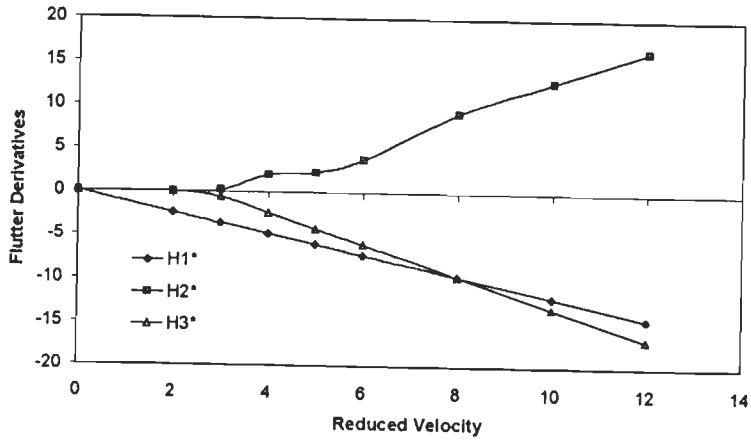

(a) Vertical flutter derivatives

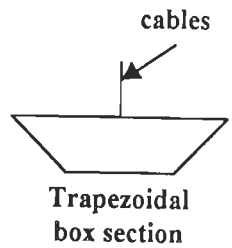

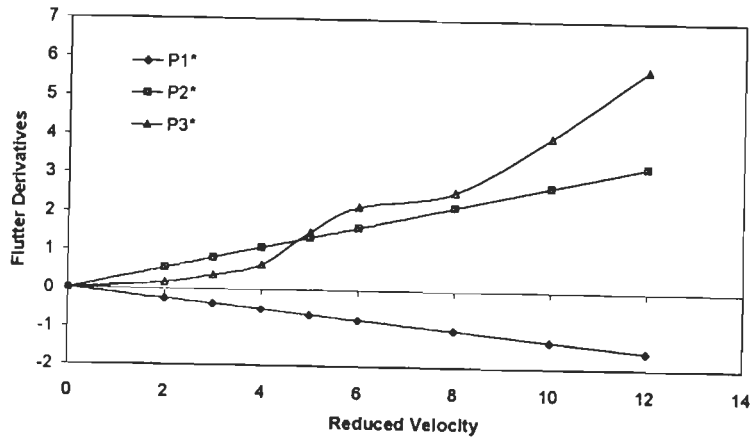

(b) Lateral flutter derivatives

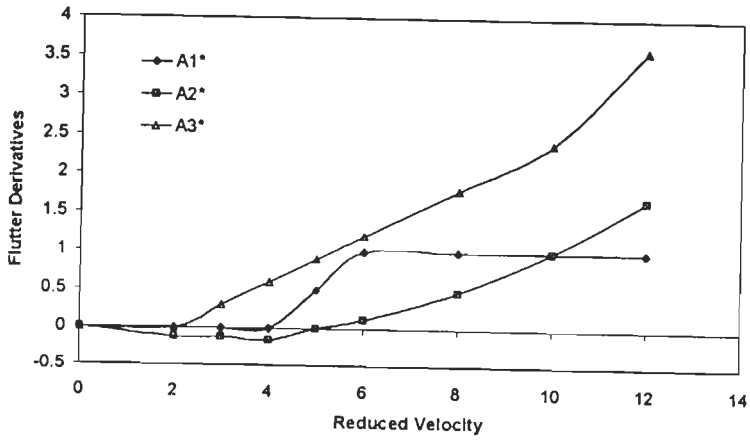

(c) Torsional flutter derivatives

Fig. 8.2 : Flutter Derivatives for a Typical Trapezoidal Box Section

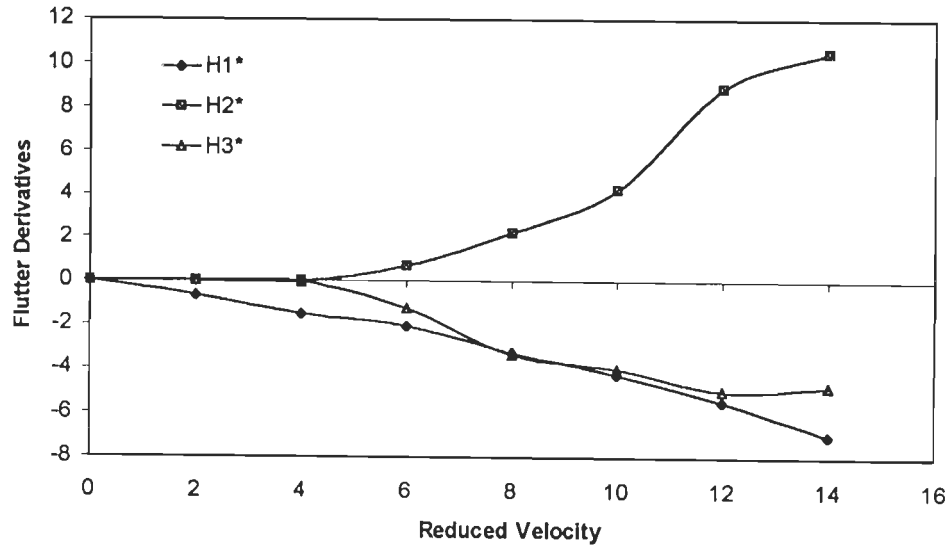

(a) Vertical flutter derivatives

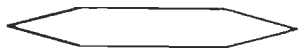

Streamlined box section

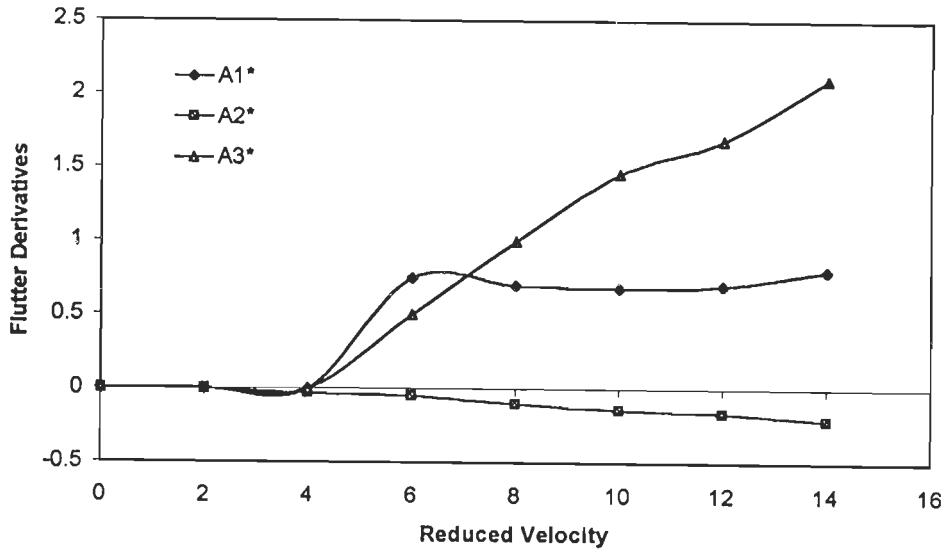

(b) Torsional flutter derivatives

Fig. 8.3 : Flutter Derivatives for a Typical Streamlined Box Section

A_2^* changes from negative to positive, with increase in reduced velocity. The single degree of freedom flutter is likely to occur in a bluff bridge deck cross-section with plots of flutter derivatives as shown in Fig. 8.2. Classical flutter is possible if H_4^*, H_1^*, H_3^* and A_2^* are negative and the other derivatives are positive. Classical flutter is likely to occur in a streamlined bridge deck cross-section with flutter derivatives as shown in Fig. 8.3.

As the experimental investigations to determine these derivatives are expensive and cumbersome, flutter derivatives are available in literature only for deck cross-section of some of the existing bridges.

A close similarity between flat plate derivatives and flutter derivatives of streamlined box girder bridge deck of three existing long span cable bridges (Normandy, Great Belt and Tsurumi Bridge) has been shown by Sarkar (1992). The flat plate derivatives are discussed in the following section.

8.2.1.1 Airfoil and flat plate derivatives

For an oscillating airfoil and flat plate, the flutter derivatives (H_i^*, A_i^*, i=1, 4) can be analytically expressed in terms of Theodorsen's (1935) circulation function $C(K) = F(K) + iG(K)$ as follows :

$$H_1^* = -\frac{2\pi}{K}F(K) \tag{8.24}$$

$$H_2^* = -\frac{\pi}{K}\left[\frac{1+F(K)}{2} + \frac{2G(K)}{K}\right] \tag{8.25}$$

$$H_3^* = -\frac{\pi}{K^2}\left[2F(K) - \frac{KG(K)}{2}\right] \tag{8.26}$$

$$H_4^* = \frac{\pi}{2}\left[1 + \frac{4G(K)}{K}\right] \tag{8.27}$$

$$A_1^* = \frac{\pi}{2K}F(K) \tag{8.28}$$

$$A_2^* = \frac{\pi}{K}\left[\frac{F(K)-1}{8} + \frac{G(K)}{2K}\right] \tag{8.29}$$

$$A_3^* = \frac{\pi}{K^2}\left[\frac{F(K)}{2} - \frac{KG(K)}{8}\right] \tag{8.30}$$

$$A_4^* = -\frac{\pi}{2K}G(K) \tag{8.31}$$

where

$$F(K) = \frac{J_1(K)[J_1(K)+Y_0(K)]+Y_1(K)[Y_1(K)-J_0(K)]}{[J_1(K)+Y_0(K)]^2+[Y_1(K)-J_0(K)]^2} \tag{8.32}$$

$$G(K) = -\frac{Y_1(K)Y_0(K)+J_1(K)J_0(K)}{[J_1(K)+Y_0(K)]^2+[Y_1(K)-J_0(K)]^2} \tag{8.33}$$

in which J_0, J_1, Y_0, Y_1 are Bessel functions of the first and second kind respectively.

The flutter derivatives calculated using Theodorsen's functions are plotted in Fig. 8.4.

In this study, the flat plate derivatives have been used in the flutter analyses of Bridge #1, Bridge #2 and Bridge #4.

8.2.1.2 Experimentally Determined Flutter Derivatives for Bridge #3

For Bridge #3, with deck configurations as shown in Fig. 8.5, the direct flutter derivatives in vertical and torsional directions H_1^*, A_2^* and A_3^* were determined by wind tunnel investigations at different angles of attack (Bosch, 1978). Preliminary investigations into the coupling coefficients revealed that they were negligible, thus reflecting the bridge to be susceptible to only single degree of freedom flutter. The plots of flutter derivatives versus reduced velocity are shown in Figs. 8.6 to 8.8 respectively for section C-2, C-2C and C-1B (refer Table 3.3(a) for structural properties) at angles of attack of -4, -1.75, 0, 2, 4, and 6 degrees.

As seen from Figs. 8.5 to 8.7, the curve of flutter derivative H_1^* for each cross-section, has its value negative or minimally positive throughout the range of the reduced velocity for each angle of attack. Therefore, single degree of freedom flutter in

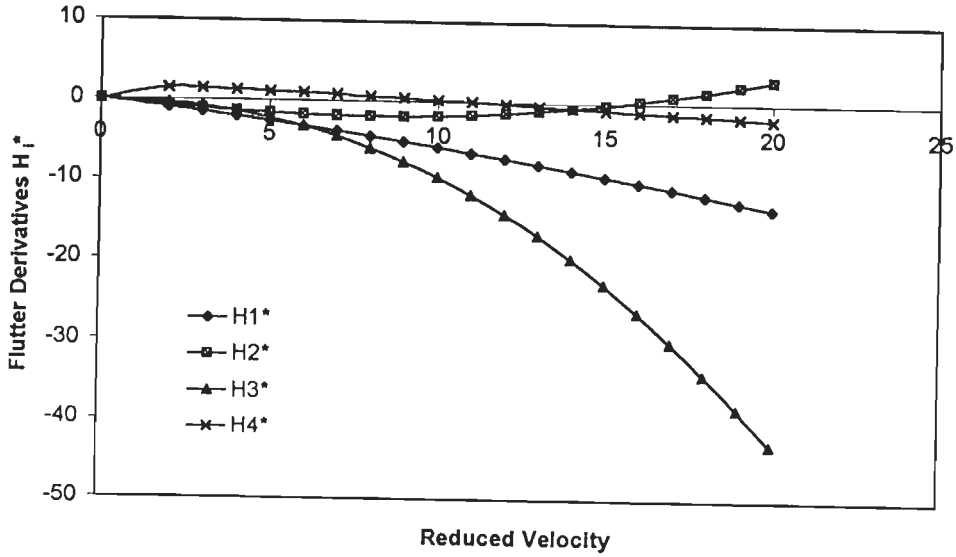

(a) Flutter derivatives H_i^* (i = 1, 4) as a function of reduced velocity

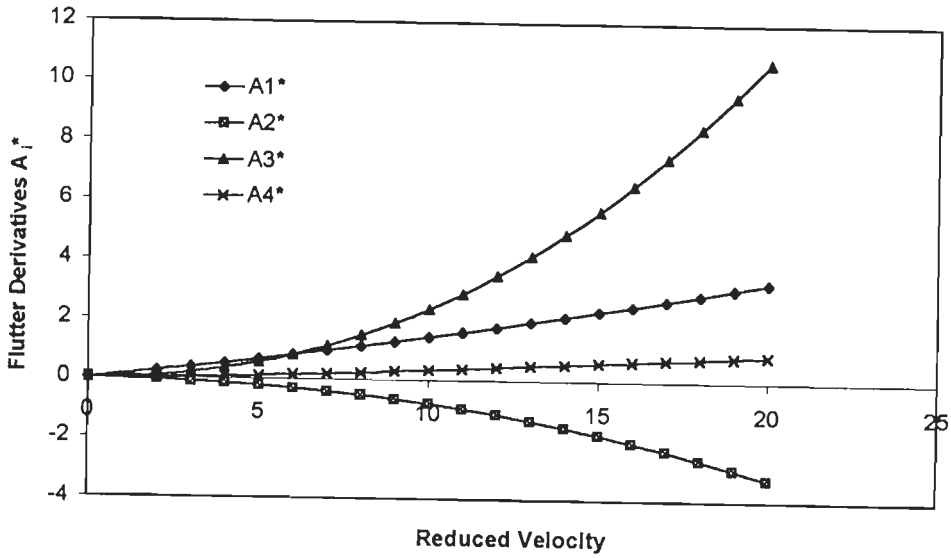

(b) Flutter derivatives A_i^* (i = 1, 4) as a function of reduced velocity

Fig. 8.4 : Flutter Derivatives for Thin Airfoil and Flat Plate

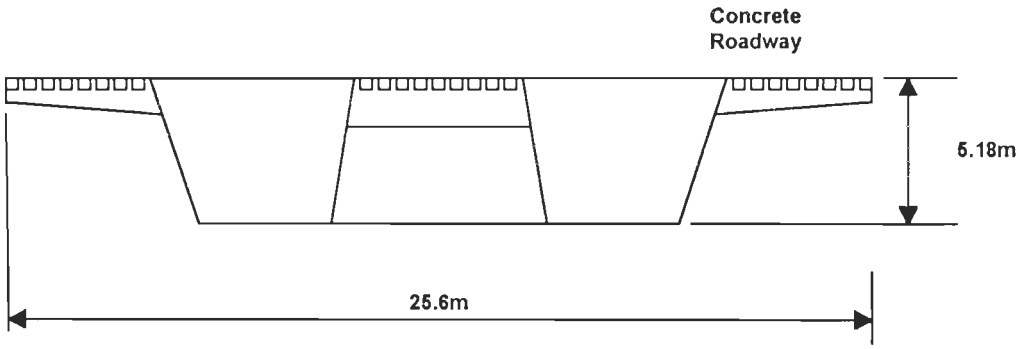

(a) Deck cross-section C-2

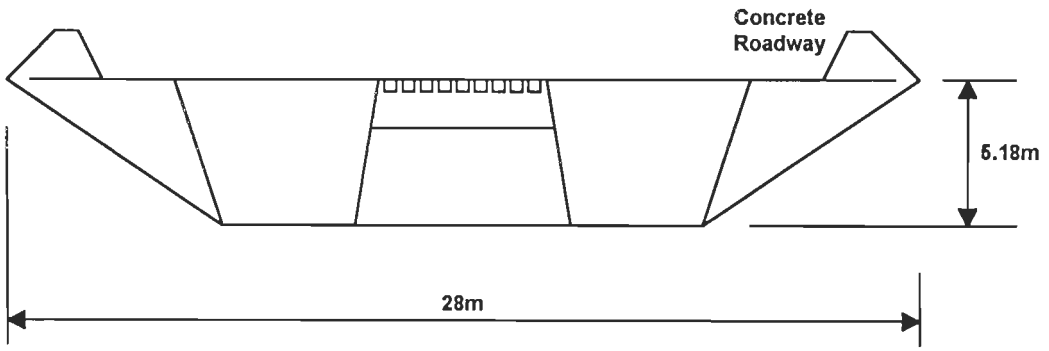

(b) Deck cross-section C-2C

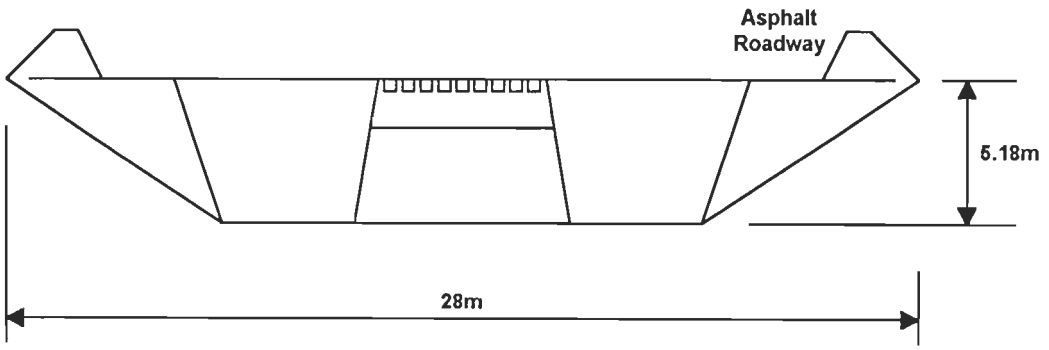

(c) Deck cross-section C-1B

Fig. 8.5 : Comparison of Deck Section Configurations for Bridge #3

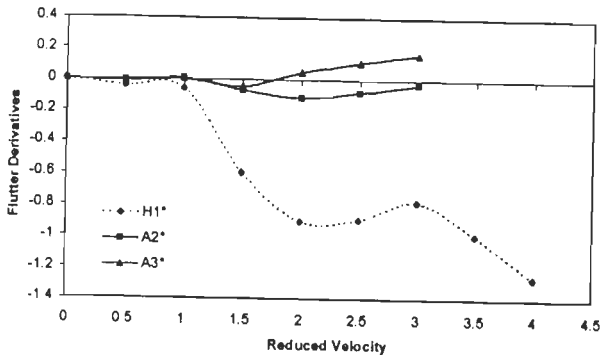

(a) Angle of attack –4°

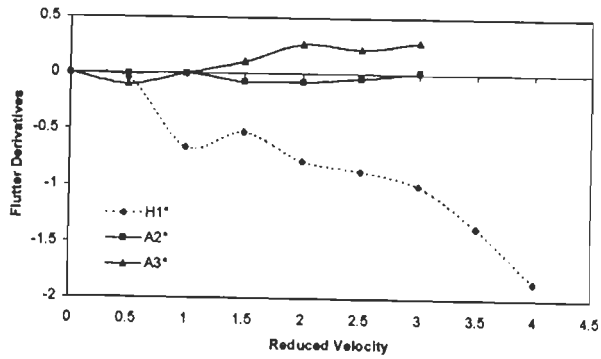

(b) Angle of attack –1.75°

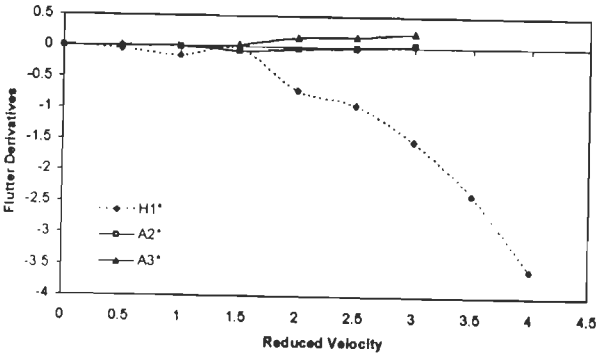

(c) Angle of attack 0°

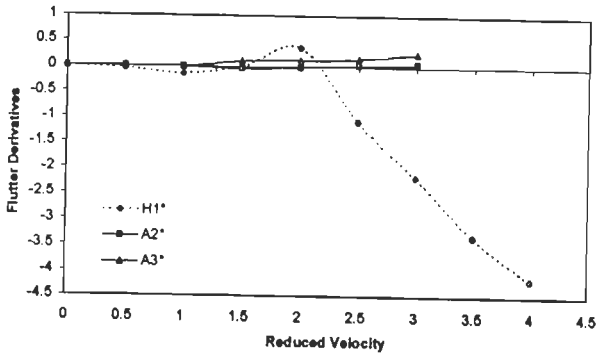

(d) Angle of attack +2°

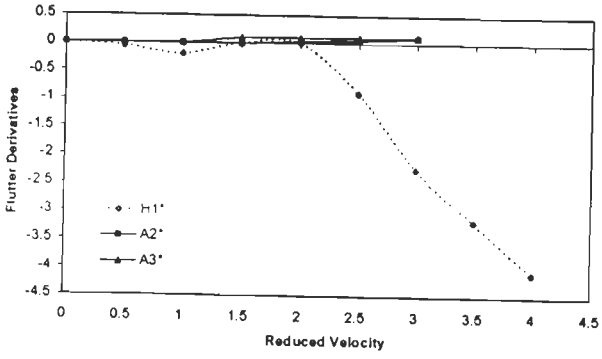

(e) Angle of attack +4°

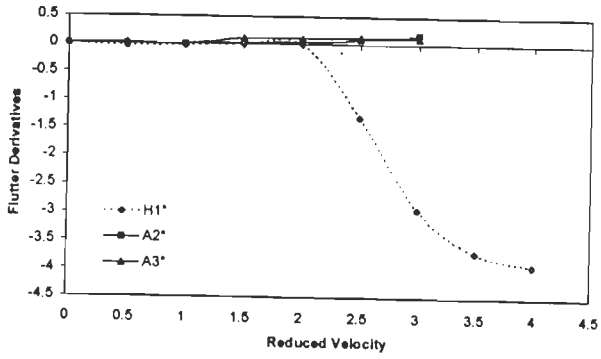

(f) Angle of attack +6°

Fig. 8.6 : Flutter Derivatives for Deck Section C-2 of Bridge #3

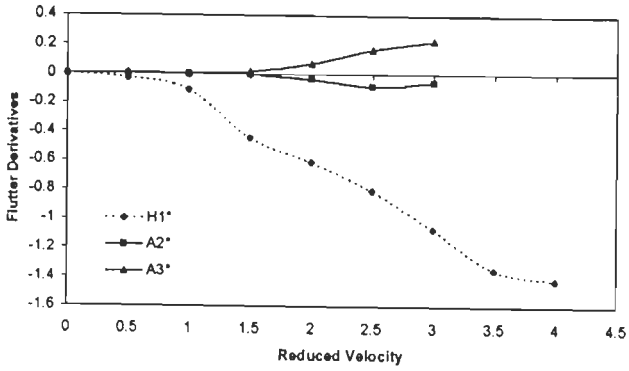

(a) Angle of attack –4°

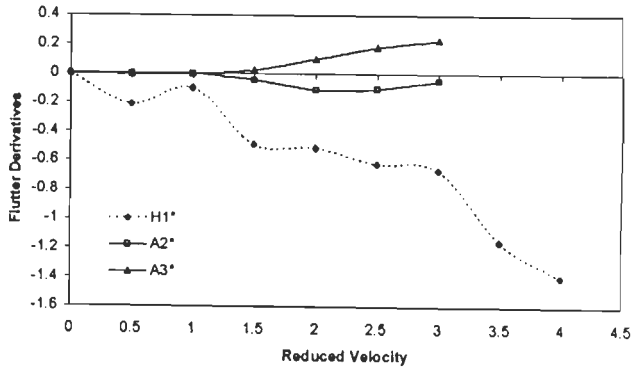

(b) Angle of attack –1.75°

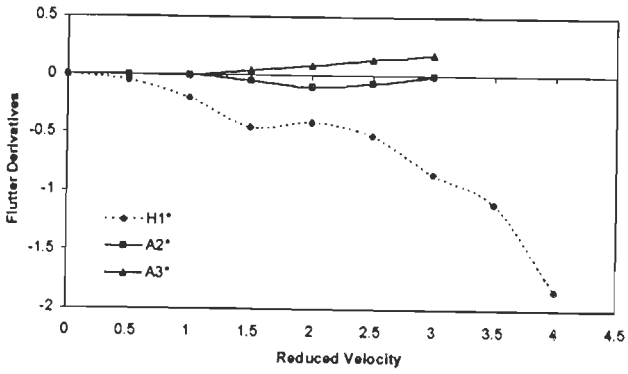

(c) Angle of attack 0°

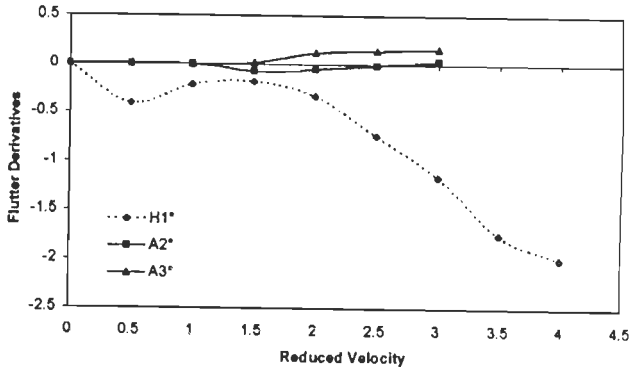

(d) Angle of attack +2°

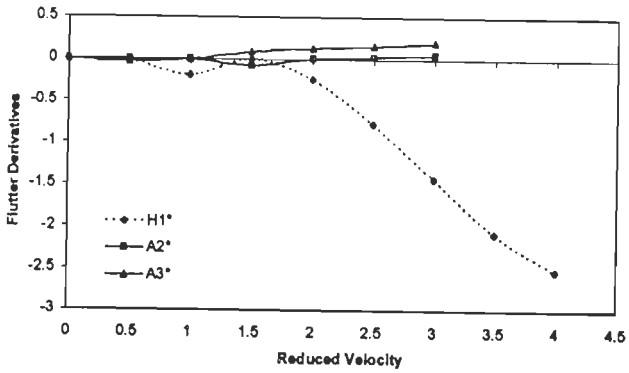

(e) Angle of attack +4°

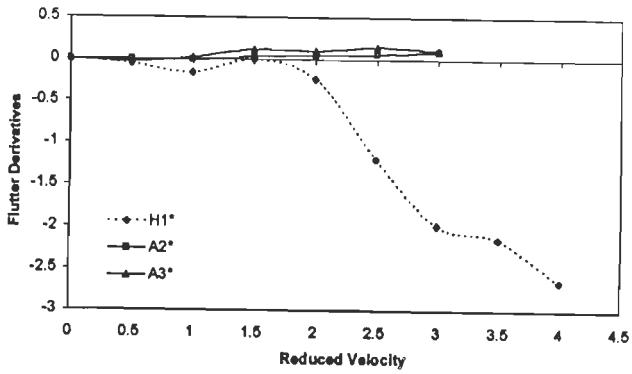

(f) Angle of attack +6°

Fig. 8.7 : Flutter Derivatives for Deck Section C-2C of Bridge #3

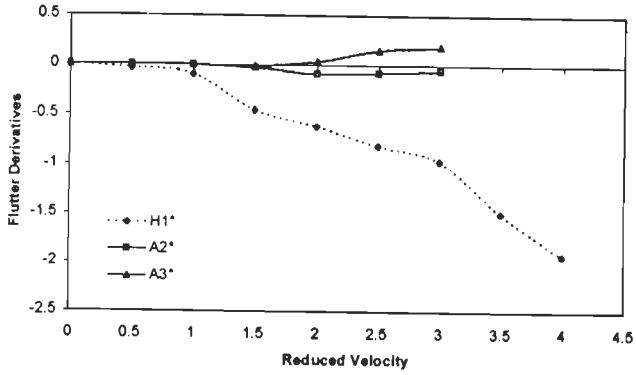

(a) Angle of attack –4°

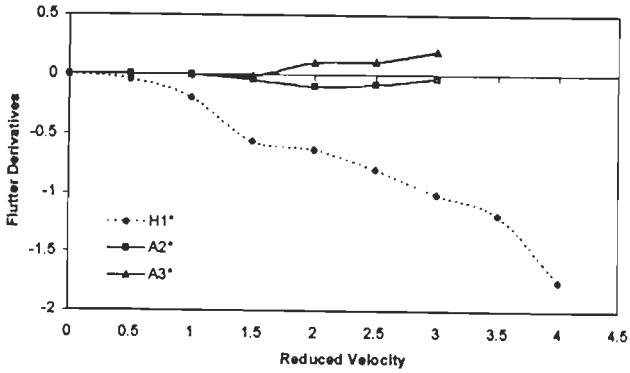

(b) Angle of attack –1.75°

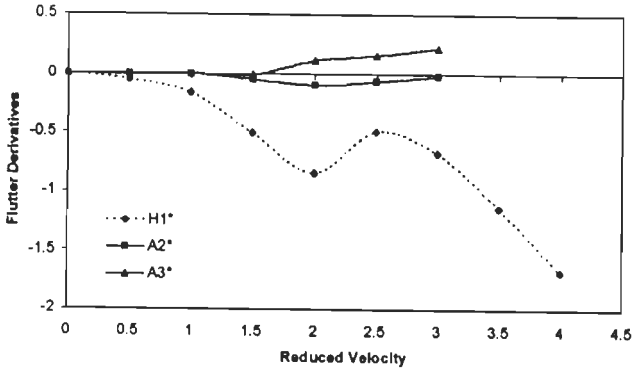

(c) Angle of attack 0°

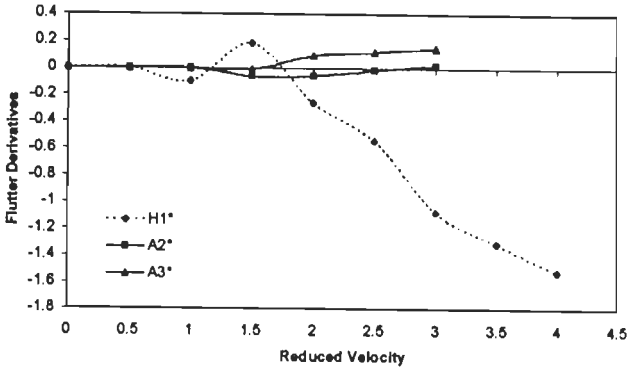

(d) Angle of attack +2°

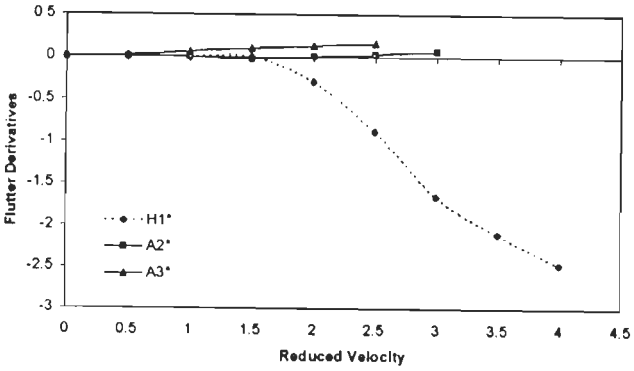

(e) Angle of attack +4°

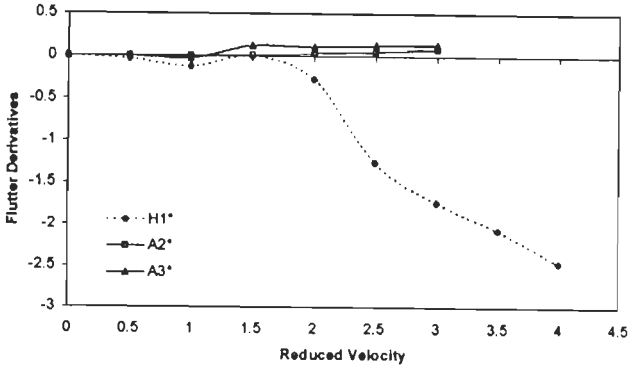

(f) Angle of attack +6°

Fig. 8.8 : Flutter Derivatives for Deck Section C-1B of Bridge #3

vertical bending cannot occur since the aerodynamic lifting force is continually damping the vertical motions. Also, by viewing the plots of flutter derivative A_2^* for each cross-section, its value does change from a negative to positive value over the range of reduced velocities, especially for angles of attack 2, 4 and 6 degrees. This implies that flutter can occur and is single degree of freedom flutter in torsion.

8.2.3 Lateral Flutter Derivatives

As discussed earlier, only in very few cases the lateral derivatives for bridge deck sections such as Tsurumi Bridge and Deer Isle Bridge (Singh *et al*, 1995) have been determined through wind tunnel studies. The lateral flutter derivatives are otherwise obtained from the steady-state force coefficients C_D, C_L and C_M and the slope of drag curve with respect to the angle of attack ($C_D' = \frac{dC_D}{d\alpha_w}$), using quasi-steady theory (Chen *et al*, 2000) as follows:

$$P_1^* = -\frac{2C_D}{K} \tag{8.34}$$

$$P_2^* = \frac{(C_L - C_D')}{2K} \tag{8.35}$$

$$P_3^* = \frac{C_D'}{K^2} \tag{8.36}$$

$$P_4^* = 0 \tag{8.37}$$

$$P_5^* = \frac{(C_D' - C_L)}{K} = -2P_2^* \tag{8.38}$$

$$P_6^* = 0 \tag{8.39}$$

8.3 TWO-DIMENSIONAL FLUTTER ANALYSIS

After extraction of flutter derivatives, either through experimental investigations in wind tunnel or using CFD techniques, the unsteady aerodynamic forces acting on the

bridge are represented using Eqs. 8.17 to 8.19. Once the unsteady aerodynamic forces are established, the critical conditions for the onset of flutter can be calculated. The most traditional way for the analysis is by the application of the 'strip theory', where the interaction between the wind and the bridge system is decided on a two-dimensional section perpendicular to the longitudinal axis of bridge. Consequently, any three-dimensional effects along the longitudinal axis of the structure are assumed to be negligible. The solutions of flutter equations when the bridge deck is subjected to (i) vertical and torsional motions and (ii) lateral and torsional motions are described in the following sections.

8.3.1 Solution of Flutter Equations – Deck Subjected to Vertical and Torsional Motions

The equations of motion when the bridge deck is subjected to simultaneous vertical and torsional motion is represented by Eqs. 8.14 and 8.16. For self-excited forces Eqs. 8.17 and 8.19 are used, with terms corresponding to displacement and velocity in lateral direction p and $\dot{p}$ taken as zero. The equations of motion are rewritten as

$$M\left(\ddot{h}+2\xi_h\omega_h\dot{h}+\omega_h^2 h\right)=\frac{1}{2}\rho U^2 B\left[KH_1^*\frac{\dot{h}}{U}+KH_2^*\frac{B\dot{\alpha}}{U}+K^2H_3^*\alpha+K^2H_4^*\frac{h}{B}\right] \tag{8.40}$$

$$I(\ddot{\alpha}+2\xi_\alpha\omega_\alpha\dot{\alpha}+\omega_\alpha^2\alpha)=\frac{1}{2}\rho U^2 B^2\left[KA_1^*\frac{\dot{h}}{U}+KA_2^*\frac{B\dot{\alpha}}{U}+K^2A_3^*\alpha+K^2A_4^*\frac{h}{B}\right] \tag{8.41}$$

where $K=\dfrac{B\omega}{U}$ is the non-dimensional frequency or reduced frequency.

Solution of differential Eqs. 8.40 and 8.41 is possible, based on the observation that h and α are harmonic in time with common frequency ω at the critical wind speed U_{fc} for onset of flutter. Introduction of time complex harmonic motions, i.e.,

$$h=h_0e^{(i\omega t)} \tag{8.42}$$

$$\alpha = \alpha_0 e^{(i\omega t)} \tag{8.43}$$

in Eqs. 8.40 and 8.41, yields the following set of complex algebraic Equations:

$$\left[-K^2 + i2\xi_h K_h K + K_h^2 - i\left(\frac{\rho B^2}{2M}\right)K^2 H_1^* - \left(\frac{\rho B^2}{2M}\right)K^2 H_4^*\right]\left(\frac{h_0}{B}\right) -$$

$$\left[i\left(\frac{\rho B^2}{2M}\right)K^2 H_2^* + \left(\frac{\rho B^2}{2M}\right)K^2 H_3^*\right]\alpha_0 = 0 \tag{8.44}$$

$$-\left[i\left(\frac{\rho B^4}{2I}\right)K^2 A_1^* + \left(\frac{\rho B^4}{2I}\right)K^2 A_4^*\right]\left(\frac{h_0}{B}\right) +$$

$$\left[-K^2 + i2\xi_\alpha K_\alpha K + K_\alpha^2 - i\left(\frac{\rho B^4}{2I}\right)K^2 A_2^* - \left(\frac{\rho B^4}{2I}\right)K^2 A_3^*\right]\alpha_0 = 0 \tag{8.45}$$

where $K_h = \frac{B\omega_h}{U}$ and $K_\alpha = \frac{B\omega_\alpha}{U}$. Dividing Eqs. 8.44 and 8.45 by K_h and setting the determinant of coefficients of amplitudes 'h' and 'α' to zero results in basic stability condition. This constitutes a complex quartic equation in the unknown flutter frequency ω, which must then be solved. The solution of the above equations will, in general, be of the form $\omega = \omega_1 + i\omega_2$ with $\omega_2 \neq 0$, and will therefore represent a decaying $(\omega_2 > 0)$ or divergent $(\omega_2 < 0)$ oscillation. A new value of K is chosen and the procedure is repeated until $\omega_2 \approx 0$, so that $\omega \approx \omega_1$. To that solution there corresponds to the flutter condition at real frequency ω_1. Let K_C be the value of K for which $\omega \approx \omega_1$. The critical velocity is then computed as

$$U_{fc} = \frac{B\omega_1}{K_C} \tag{8.46}$$

The real and imaginary parts of the complex quartic equation are expressed as follows, in terms of unknown $X = \frac{\omega}{\omega_h}$.

$$X^4\left[1+\left(\frac{\rho B^2}{2M}\right)H_4^*+\left(\frac{\rho B^4}{2I}\right)A_3^*+\left(\frac{\rho B^4}{2I}\right)\left(\frac{\rho B^2}{2M}\right)\left(H_4^*A_3^*+A_1^*H_2^*-H_1^*A_2^*-A_4^*H_3^*\right)\right]+$$

$$X^3\left[\left(\frac{\rho B^4}{2I}\right)2\xi_h A_2^*+\left(\frac{\rho B^2}{2M}\right)2\xi_\alpha\left(\frac{\omega_\alpha}{\omega_h}\right)H_1^*\right]+$$

$$X^2\left[-\left(\frac{\omega_\alpha}{\omega_h}\right)^2-\left(\frac{\rho B^4}{2I}\right)A_3^*-\left(\frac{\rho B^2}{2M}\right)\left(\frac{\omega_\alpha}{\omega_h}\right)^2 H_4^*-4\xi_h\xi_\alpha\left(\frac{\omega_\alpha}{\omega_h}\right)-1\right]+X[0]+\left(\frac{\omega_\alpha}{\omega_h}\right)^2=0 \tag{8.47}$$

$$X^3\left[\left(\frac{\rho B^4}{2I}\right)A_2^*+\left(\frac{\rho B^2}{2M}\right)H_1^*+\left(\frac{\rho B^2}{2M}\right)\left(\frac{\rho B^4}{2I}\right)\left(H_1^*A_3^*+A_2^*H_4^*-A_1^*H_3^*-A_4^*H_2^*\right)\right]+$$

$$X^2\left[-2\xi_h\left(\frac{\omega_\alpha}{\omega_h}\right)-2\xi_h-\left(\frac{\rho B^4}{2I}\right)2\xi_h A_3^*-\left(\frac{\rho B^2}{2M}\right)2\xi_\alpha\left(\frac{\omega_\alpha}{\omega_h}\right)H_4^*\right]+$$

$$X\left[-\left(\frac{\rho B^4}{2I}\right)A_2^*-\left(\frac{\rho B^2}{2M}\right)\left(\frac{\omega_\alpha}{\omega_h}\right)^2 H_1^*\right]+2\xi_h\left(\frac{\omega_\alpha}{\omega_h}\right)^2+2\xi_\alpha\left(\frac{\omega_\alpha}{\omega_h}\right)=0 \tag{8.48}$$

The flutter problem as treated above is seen to be a semi-inverse problem since the aerodynamic coefficients are functions of the solution frequency, and a range of frequency parameters K must therefore be used to survey the solution region. The solution of flutter determinant is possible by plotting the curves corresponding to the roots of the real and imaginary parts given by Eqs. 8.47 and 8.48 as a function of reduced frequency K. The intersection of point (X_C, K_C), where the two plots cross, the flutter condition is identified.

Determination of flutter criteria when the bridge deck is subjected to vertical and torsional motions as described above, has been discussed by Lakshmy (1995).

8.3.2 Solution of Flutter Equations –Deck Subjected to Lateral and Torsional Motions

Similarly, the equations of motion when the bridge deck is subjected to simultaneous lateral and torsional motion are represented by Eqs 8.15 and 8.16. While

representing the self-excited forces using Eqs. 8.18 and 8.19, the terms corresponding to displacement and velocity in vertical direction h and $\dot{h}$ are taken as zero. Thus the equations of motion are written as

$$M\left(\ddot{p}+2\xi_p\omega_p\ \dot{p}+\omega_p^2 p\right)=\frac{1}{2}\rho U^2 B\left[KP_1^*\frac{\dot{p}}{U}+KP_2^*\frac{B\dot{\alpha}}{U}+K^2P_3^*\alpha+K^2P_4^*\frac{p}{B}\right] \tag{8.49}$$

$$I(\ddot{\alpha}+2\xi_\alpha\omega_\alpha\dot{\alpha}+\omega_\alpha^2\alpha)=\frac{1}{2}\rho U^2B^2\left[KA_2^*\frac{B\dot{\alpha}}{U}+K^2A_3^*\alpha++KA_5^*\frac{\dot{p}}{B}+K^2A_6^*\frac{p}{B}\right] \tag{8.50}$$

where $K=\dfrac{B\omega}{U}$ is the non-dimensional frequency or reduced frequency.

Solution of differential Eqs. 8.49 and 8.50 is possible, based on the observation that p and α are harmonic in time with common frequency ω at the critical wind speed U_{fc} for onset of flutter. Introduction of time complex harmonic motions, i.e.,

$$p=p_0e^{(i\omega t)} \tag{8.51}$$

$$\alpha=\alpha_0e^{(i\omega t)} \tag{8.52}$$

in Eqs. 8.49 and 8.50 yields the following set of complex algebraic Equations:

$$\left[-K^2+i2\xi_pK_pK+K_p^2-i\left(\frac{\rho B^2}{2M}\right)K^2P_1^*-\left(\frac{\rho B^2}{2M}\right)K^2P_4^*\right]\left(\frac{p_0}{B}\right)-$$

$$\left[i\left(\frac{\rho B^2}{2M}\right)K^2P_2^*+\left(\frac{\rho B^2}{2M}\right)K^2P_3^*\right]\alpha_0=0 \tag{8.53}$$

$$-\left[i\left(\frac{\rho B^4}{2I}\right)K^2A_5^*+\left(\frac{\rho B^4}{2I}\right)K^2A_6^*\right]\left(\frac{p_0}{B}\right)+$$

$$\left[-K^2+i2\xi_\alpha K_\alpha K+K_\alpha^2-i\left(\frac{\rho B^4}{2I}\right)K^2A_2^*-\left(\frac{\rho B^4}{2I}\right)K^2A_3^*\right]\alpha_0=0 \tag{8.54}$$

where $K_p=\dfrac{B\omega_p}{U}$, $K_\alpha=\dfrac{B\omega_\alpha}{U}$. Dividing Eqs.8.53 and 8.54 by K_p and setting the determinant of coefficients of amplitudes 'p' and 'α' to zero results in basic stability condition. This constitutes a complex quartic equation in the unknown flutter frequency

ω, which must then be solved. The solution of the above equations will, in general, be of the form $\omega = \omega_1 + i\omega_2$ with $\omega_2 \neq 0$, and will therefore represent a decaying $(\omega_2 > 0)$ or divergent $(\omega_2 < 0)$ oscillation. A new value of K is chosen and the procedure is repeated until $\omega_2 \approx 0$, so that $\omega \approx \omega_1$. To that solution there corresponds the flutter condition at real frequency ω_1. Let K_C be the value of K for which $\omega \approx \omega_1$. The critical velocity is then

$$U_{fc} = \frac{B\omega_1}{K_C} \tag{8.55}$$

The real and imaginary parts of the complex quartic equation are expressed as follows,in terms of unknown $X = \frac{\omega}{\omega_p}$.

$$X^4\left[1+\left(\frac{\rho B^2}{2M}\right)P_4^* + \left(\frac{\rho B^4}{2I}\right)A_3^* + \left(\frac{\rho B^4}{2I}\right)\left(\frac{\rho B^2}{2M}\right)\left(P_4^*A_3^* + A_5^*P_2^* - P_1^*A_2^* - A_6^*P_3^*\right)\right] +$$

$$X^3\left[\left(\frac{\rho B^4}{I}\right)\xi_p A_2^* + \left(\frac{\rho B^2}{M}\right)\xi_\alpha\left(\frac{\omega_\alpha}{\omega_p}\right)P_1^*\right] +$$

$$X^2\left[-\left(\frac{\omega_\alpha}{\omega_p}\right)^2 - \left(\frac{\rho B^4}{2I}\right)A_3^* - \left(\frac{\rho B^2}{2M}\right)\left(\frac{\omega_\alpha}{\omega_p}\right)^2 P_4^* - 4\xi_p\xi_\alpha\left(\frac{\omega_\alpha}{\omega_p}\right) - 1\right] + X[0] + \left(\frac{\omega_\alpha}{\omega_p}\right)^2 = 0 \tag{8.56}$$

$$X^3\left[\left(\frac{\rho B^4}{2I}\right)A_2^* + \left(\frac{\rho B^2}{2M}\right)P_1^* + \left(\frac{\rho B^2}{2M}\right)\left(\frac{\rho B^4}{2I}\right)\left(P_1^*A_3^* + A_2^*P_4^* - A_5^*P_3^* - A_6^*P_2^*\right)\right] +$$

$$X^2\left[-2\xi_p\left(\frac{\omega_\alpha}{\omega_p}\right) - 2\xi_p - \left(\frac{\rho B^4}{2I}\right)2\xi_p A_3^* - \left(\frac{\rho B^2}{2M}\right)2\xi_\alpha\left(\frac{\omega_\alpha}{\omega_p}\right)P_4^*\right] +$$

$$X\left[-\left(\frac{\rho B^4}{2I}\right)A_2^* - \left(\frac{\rho B^2}{2M}\right)\left(\frac{\omega_\alpha}{\omega_p}\right)^2 P_1^*\right] + 2\xi_p\left(\frac{\omega_\alpha}{\omega_p}\right)^2 + 2\xi_\alpha\left(\frac{\omega_\alpha}{\omega_p}\right) = 0 \tag{8.57}$$

The flutter problem as treated above is seen to be a semi-inverse problem since the aerodynamic coefficients are functions of the solution frequency, and a range of frequency parameters K must therefore be used to survey the solution region. The solution of flutter determinant is possible by plotting the curves corresponding to the

roots of the real and imaginary parts given by Eqs. 8.56 and 8.57 as a function of reduced frequency K. The intersection of point (X_C, K_C), where the two plots cross, the flutter condition is identified.

In the present study, the methodology for solution of flutter equations when deck is subjected to vertical and torsional motions has been extended to predict the criteria for onset of coupled lateral and torsional flutter.

8.4 THREE-DIMENSIONAL FLUTTER ANALYSIS

The three-dimensional flutter analysis of long span cable stayed bridges can be performed in two different ways; one is to apply the unsteady aerodynamic forces, either in frequency domain or in time domain directly to a three-dimensional finite element model of bridge structure known as direct method, another is to consider the structural response separately in various vibration modes and assemble them termed as mode superposition method. The various methodologies used by researchers for three-dimensional flutter analysis have been briefly outlined in Section 2.7.3.

In the following section, the equations of motion, flutter equation of the bridge system, aerodynamic stiffness and damping matrices and procedure for three-dimensional flutter analysis using modal superposition method (Ge and Tanaka, 2000) are discussed.

8.4.1 Equations of Motion

The equations of motion of a bridge discretized as a n-degree of freedom system can be formulated by expressing the equilibrium of the effective forces, including the inertia force, damping and elastic forces and applied forces associated with each of its degree of freedom. For the entire structure, the equations of motion in the global axes can be written as

$$[M]_g \{\ddot{U}\} + [C_S]_g \{\dot{U}\} + [K_S]_g \{U\} = \{F\}_g \tag{8.58}$$

where $\{F\}_g$ is the externally applied force vector, $\{\ddot{U}\}_g$, $\{\dot{U}\}_g$ and $\{U\}_g$ are the nodal acceleration , velocity and displacement vectors respectively. $[M]_g$ is the mass matrix for structure, $[K_S]_g$ is the structural stiffness matrix, which is formed using elastic stiffness $[K_E]_g$ and geometric stiffness $[K_G]_g$ matrices as discussed in Chapter 3. The structural damping matrix $[C_S]_g$, is usually expressed as a linear combination of $[M]_g$ and stiffness $[K_S]_g$ matrices as follows:

$$[C_S]_g = a_0[M]_g + a_1[K_S]_g \tag{8.59}$$

in which a_0 and a_1 are real constants.

8.4.2 Flutter Equation of the System

For the cable stayed bridge system under the action of wind, the externally applied force to be considered in the flutter analysis is the self-excited force induced by the flow given by

$$\{F\}_g = \{F_d\}_g + \{F_s\}_g = [A_d]_g\{\dot{U}\}_g + [A_s]_g\{U\}_g \tag{8.60}$$

where $\{F_d\}_g$ and $\{F_s\}_g$ are the aerodynamic damping and stiffness forces, respectively, and the corresponding matrices $[A_d]_g$ and $[A_s]_g$ are represented by either theoretically or experimentally determined flutter derivatives.

Substituting Eq.(8.60) into Eq. (8.59) results a new form of structural equations of motion given by

$$[M]_g\{\ddot{U}\}_g + ([C_S]_g - [A_d]_g)\{\dot{U}\}_g + ([K_S]_g - [A_s]_g)\{U\}_g = 0 \tag{8.61}$$

The system flutter equations as expressed by Eq. 8.61 is very similar to equations of bridge subjected to damped free-vibration and is written as :

$$[M]_g\{\ddot{U}\}_g + [C]_g\{\dot{U}\}_g + [K]_g\{U\}_g = 0 \tag{8.62}$$

in which, the system damping matrix $[C]_g = [C_S]_g - [A_S]_g$ and the system stiffness matrix $[K]_g = [K_S]_g - [A_S]_g$

Since both aerodynamic force components $\{F_d\}$ and $\{F_s\}$ are non

conservative, neither the aerodynamic damping matrix $[A_d]_g$ nor the aerodynamic stiffness matrix $[A_S]_g$ need be symmetric. Subsequently, the system stiffness and system damping matrices are both asymmetric. The asymmetric matrices enable the flutter response to be coupled among the modes of vibration of the bridge.

The aerodynamic stiffness and damping matrices for a three-dimensional beam element are described in the following section.

8.4.2.1 Aerodynamic matrices

As discussed in Section 8.2, the self-excited aerodynamic forces per unit span length of deck is given by Eqs. 8.17 to 8.19. To convert these uniformly distributed forces into equivalent concentrated forces acting at element ends, a simple lumping procedure is adopted. To express self-excited forces using Eq. 8.60, the aerodynamic stiffness and damping matrices are used.

For a three-dimensional beam element with 12-degrees of freedom, as discussed in Section. 3.2.1.2, the aerodynamic stiffness $[A_s]$ and aerodynamic damping $[A_d]$ matrices with the order of 12 × 12 can be defined as follows:

$$[A_s]_e = \frac{1}{4}\rho U^2 L K^2 \begin{bmatrix}
0 & 0 & 0 & 0 & 0 & 0 & 0 & 0 & 0 & 0 & 0 & 0 \\
0 & H_4^* & H_6^* & -BH_3^* & 0 & 0 & 0 & 0 & 0 & 0 & 0 & 0 \\
0 & P_6^* & P_4^* & -BP_3^* & 0 & 0 & 0 & 0 & 0 & 0 & 0 & 0 \\
0 & -BA_4^* & BA_6^* & B^2A_3^* & 0 & 0 & 0 & 0 & 0 & 0 & 0 & 0 \\
0 & 0 & 0 & 0 & 0 & 0 & 0 & 0 & 0 & 0 & 0 & 0 \\
0 & 0 & 0 & 0 & 0 & 0 & 0 & 0 & 0 & 0 & 0 & 0 \\
0 & 0 & 0 & 0 & 0 & 0 & 0 & 0 & 0 & 0 & 0 & 0 \\
0 & 0 & 0 & 0 & 0 & 0 & 0 & H_4^* & H_6^* & -BH_3^* & 0 & 0 \\
0 & 0 & 0 & 0 & 0 & 0 & 0 & P_6^* & P_4^* & -BP_3^* & 0 & 0 \\
0 & 0 & 0 & 0 & 0 & 0 & 0 & -BA_4^* & BA_6^* & B^2A_3^* & 0 & 0 \\
0 & 0 & 0 & 0 & 0 & 0 & 0 & 0 & 0 & 0 & 0 & 0 \\
0 & 0 & 0 & 0 & 0 & 0 & 0 & 0 & 0 & 0 & 0 & 0
\end{bmatrix} \tag{8.63}$$

$$[A_d]_k = \frac{1}{4}\rho UBLK \begin{bmatrix} 0 & 0 & 0 & 0 & 0 & 0 & 0 & 0 & 0 & 0 & 0 & 0 \\ 0 & H_1^* & H_5^* & -BH_2^* & 0 & 0 & 0 & 0 & 0 & 0 & 0 & 0 \\ 0 & P_5^* & P_1^* & -BP_2^* & 0 & 0 & 0 & 0 & 0 & 0 & 0 & 0 \\ 0 & -BA_1^* & BA_5^* & B^2A_2^* & 0 & 0 & 0 & 0 & 0 & 0 & 0 & 0 \\ 0 & 0 & 0 & 0 & 0 & 0 & 0 & 0 & 0 & 0 & 0 & 0 \\ 0 & 0 & 0 & 0 & 0 & 0 & 0 & 0 & 0 & 0 & 0 & 0 \\ 0 & 0 & 0 & 0 & 0 & 0 & 0 & 0 & 0 & 0 & 0 & 0 \\ 0 & 0 & 0 & 0 & 0 & 0 & 0 & H_1^* & H_5^* & -BH_2^* & 0 & 0 \\ 0 & 0 & 0 & 0 & 0 & 0 & 0 & P_5^* & P_1^* & -BP_2^* & 0 & 0 \\ 0 & 0 & 0 & 0 & 0 & 0 & 0 & -BA_1^* & BA_5^* & B^2A_2^* & 0 & 0 \\ 0 & 0 & 0 & 0 & 0 & 0 & 0 & 0 & 0 & 0 & 0 & 0 \\ 0 & 0 & 0 & 0 & 0 & 0 & 0 & 0 & 0 & 0 & 0 & 0 \end{bmatrix} \tag{8.64}$$

8.4.3 Quadratic Eigenvalue Problem

Using the following transformation, in which the nodal displacements are expressed in terms of mode shapes and normal coordinates:

$$\{U\} = [\phi]\{q\} \tag{8.65}$$

the flutter equation for bridge structure given by Eq. 8.62 is expressed in terms of normal coordinates as

$$[\overline{M}]_g \{\ddot{q}\} + [\overline{C}]_g \{\dot{q}\} + [\overline{K}]_g \{q\} = 0 \tag{8.66}$$

where $[\phi]$ is the matrix of undamped mode shapes and $[\overline{M}]_g$, $[\overline{C}]_g$ and $[\overline{K}]_g$ are the generalized mass, damping and stiffness matrix defined by:

$$[\overline{M}]_g = [\phi]^T [M]_g [\phi] \tag{8.67}$$

$$[\overline{C}]_g = [\phi]^T ([C_S]_g - [A_d]_g)[\phi] \tag{8.68}$$

$$[\overline{K}]_g = [\phi]^T ([K_S]_g - [A_s]_g)[\phi] \tag{8.69}$$

For solving the flutter equation in normal coordinates as given by Eq. 8.66, it will be assumed that the amplitude of vibration is small at the onset of flutter. The reason for this assumption is that the flutter problem is concerned with the identification of critical stage between the stable and unstable oscillation. Therefore, it is sufficient to analyse vibration with exponential time dependence, since all other motions can be built up by superposition. Thus it is assumed that

$$\{q\} = \{\phi\} e^{\lambda t} \tag{8.70}$$

Substitution for $\{q$ given by Eq. 8.70 and its derivatives in Eq. 8.66 gives

$$\left(\lambda^2 [\overline{M}]_g + \lambda [\overline{C}]_g + [\overline{K}_g]\right)\{\phi\} = \{0\} \tag{8.71}$$

where λ is the eigenvalue of the flutter system and $\{\phi\}$ is the corresponding eigenvector of the system.

Equation 8.71 can have a nontrivial solution for $\{\phi\}$ only, provides that the term with the parantheses on the left-hand side is singular. This equation, in fact, represents a quadratic eigenvalue problem.

It is appropriate to transform the quadratic eigenvalue problem to a linearised form, since it allows for the use of methods applicable to the eigen solution of an undamped case. The steps involved in converting the quadratic eigenvalue problem into linearized form is discussed in the following section.

8.4.4 Linearised Eigenvalue Problem

To obtain the linearized form, the additional equation is written in the following way:

$$[\overline{M}]_g \{\dot{q}\} - [\overline{M}]_g \{\dot{q}\} = \{0\} \tag{8.72}$$

Equations 8.72 and 8.66 can be combined into the following equation :

$$\begin{bmatrix} [0] & [\overline{M}]_g \\ [\overline{M}]_g & [\overline{C}]_g \end{bmatrix} \begin{Bmatrix} \{\ddot{q}\} \\ \{\dot{q}\} \end{Bmatrix} + \begin{bmatrix} -[\overline{M}]_g & [0] \\ [0] & [\overline{K}]_g \end{bmatrix} \begin{Bmatrix} \{\dot{q}\} \\ \{q\} \end{Bmatrix} = \begin{Bmatrix} \{0\} \\ \{0\} \end{Bmatrix} \tag{8.73}$$

Equation 8.73 is known as the reduced form of Eq. 8.71 and can be written as

$$[A]\{\dot{y}\} = [B]\{y\} \tag{8.74}$$

where

$$[A] = \begin{bmatrix} [0] & -[\overline{M}]_g \\ -[\overline{M}]_g & -[\overline{C}]_g \end{bmatrix} \tag{8.75}$$

$$[B] = \begin{bmatrix} -[M] & [0] \\ [0] & [K] \end{bmatrix} \tag{8.76}$$

$$\{y\} = \begin{Bmatrix} \{\dot{q}\} \\ \{q\} \end{Bmatrix} = \begin{Bmatrix} \lambda\{\phi\} \\ \{\phi\} \end{Bmatrix} e^{\lambda t} = \lambda\{y\} \tag{8.77}$$

By defining $\{x\} = \begin{Bmatrix} \lambda\{\phi\} \\ \{\phi\} \end{Bmatrix}$, the generalized eigenvalue equation can be obtained as follows:

$$[B]\{x\} = \lambda[A]\{x\} \tag{8.78}$$

Also, the direct inverse forms of the normalizes eigenvalue equations can be expressed as

$$[D]\{x\} = \lambda\{x\} \tag{8.79}$$

where $[D]$ is the dynamic matrix, is described as

$$[D] = [A]^{-1}[B] = \begin{bmatrix} -[\overline{M}]_g^{-1}[\overline{C}]_g & -[\overline{M}]_g^{-1}[\overline{K}]_g \\ [I] & [0] \end{bmatrix} \tag{8.80}$$

It may be noted that the matrices $[A]$ $[B]$ and $[D]$ are all asymmetric and of order 2n.

8.4.5 Computational Procedure

The critical flutter condition can be identified by solving the aeroelastic eigen problem defined by Eq. 8.79. By examining the elements of dynamic matrix, it is seen that they are functions of air density ρ, the wind speed U, and reduced frequency K, the flutter derivatives H_i^*, P_i^* and $A_1^*(i = 1,2,\ldots 6)$ as well as the deck width B and

element length L. There are two basic variables as characteristic for the flutter oscillation : the critical wind speed U_{fc} and circular flutter frequency ω_{fc}.

To extract the eigenvalues and eigenvectors standard Double QR method may be applied to the upper Hessenberg matrix that results from $A^{-1}B$ by similarity transformation.

8.5 DETAILS OF SOFTWARE

Software VTCFLUT and LTCFLUT are developed for the two-dimensional flutter analysis of the bridges to predict the critical flutter speed for flutter when the deck is subjected to (i) vertical and torsional motions, and (ii) lateral and torsional motions respectively using the soulution techniques for flutter equations described in Sections 8.3.1 and 8.3.2 respectively.

The input parameters for VTCFLUT includes – bridge deck width, frequencies of vibration in vertical and torsional motions, mass per unit length , mass moment of inertia per unit length, number of sets of flutter derivatives available, the reduced velocities and corresponding flutter derivatives in vertical (H_1^*, H_2^*, H_3^* and H_4^*) and torsional (A_1^*, A_2^*, A_3^* and A_4^*) directions.

Similarly, the input parameters for LTCFLUT includes – bridge deck width, frequencies of vibration in lateral and torsional, mass per unit length, mass moment of inertia per unit length, number of sets of flutter derivatives available, the reduced velocities and corresponding flutter derivatives in lateral (P_1^*, P_2^*, P_3^* and P_4^*) and torsional (A_1^*, A_2^*, A_3^* and A_4^*) directions.

The output includes the coefficients of quartic equations corresponding to real part as well as cubic equations corresponding to imaginary part of the complex stability equation as well as the roots of quartic and cubic equations. The equations are solved through subroutines QUARTIC and CUBIC incorporated in the program. It may be

mentioned that depending on the nature of flutter derivatives, the flutter equations sometimes become ill-conditioned and the accuracy of solution of cubic and quartic equations is ensured using routines for finding the roots of equations available in MATLAB.

8.5.1 Validation of Software

To validate the VTCFLUT software developed for two-dimensional flutter analysis, two examples of existing cable suspended bridges; Lions' Gate Bridge and Vasco da Gama Bridge have been chosen. The details of these bridges and results of flutter analysis have been presented.

Lions' Gate Bridge

The Lions' Gate Bridge was constructed to provide fixed link across Burrard Inlet from the City of Vancouver to the north shore. Built and owned by private enterprise initial planning began in 1926 with bridge opening to traffic in 1938. The bridge crosses at the First Narrows of Burrard Inlet, located at the entrance to the natural harbour of Vancouver. The crossing consists of a 847m suspension bridge with a 670m approach viaduct. The suspension span has 472.4 m main span with equal side spans of 187.1m. The bridge carried two 1.3m sidewalks and a 8.8m roadway that originally was divided into two traffic lanes.

In the 1970's design work was completed to widen the existing crossing to provide a 10.7m, 3 lane roadway. The original roadway and sidewalk deck of the North Approach Viaduct was removed and replaced by an orthotropic steel deck that was designed to act compositely with original main girders. At that time a design was also completed for widening the suspended spans, but the project was not advanced to construction stage. During the design of the widened suspended spans several aerodynamic studies were undertaken for various options at the National Research Council of Canada.

Since the 1970's, the bridge has undergone a number of structural modifications to address the changing conditions of the structure, environment and usage.

In 1997, it was decided to renovate the Lions' Gate Bridge with 3.56m wide lanes and 2.6m-sidewalk/cycle path on each side. This configuration produces a bridge deck that is 16.76m wide. The orthotrpic steel deck is supported by 2.5m deep trusses below the deck. The orthotropic deck is fabricated with a 14mm deck plate stiffened by 240mm deep longitudinal troughs at 600mm spacing across the width of deck. Transverse floor beams spaced at 4.9m act compositely with deck and cantilever beyond the stiffening truss. Other elements of the bridge that impart the wind characteristics include: 1400mm high fences at the edge of the deck, 810mm high solid traffic barriers separating the roadway from sidewalks, and 150mm high cable trays hung outboard of the stiffening trusses from the underside of the floor beams.

From the above details, it is clear that compared to the original design the deck width of the modified deck is increased by almost 40%, while the total dead load has remained about the same. To ensure that the modified structure had not become sensitive to the dynamic action of wind, studies were conducted by Queen *et al* (1999) to determine the aerodynamic properties of modified configuration of bridge deck. They simulated the aerodynamic behaviour of renewed Lions' Gate Bridge using CFD technique by computer program DVMFLOW. The aerodynamic derivatives extracted using DVMFLOW simulations follow the original definition proposed by Simiu and Scanlan (1986), but include all 8 coefficients necessary to fully model two degree of freedom self-excited aerodynamic lift and moment. The aerodynamic derivatives thus obtained by DVMFLOW for the truss supported bridge deck section of renewed Lion's Gate Bridge are shown in Fig 8.9. The inertia and frequency parameters for the renewed Lions' Gate Bridge are given in Table 8.1.

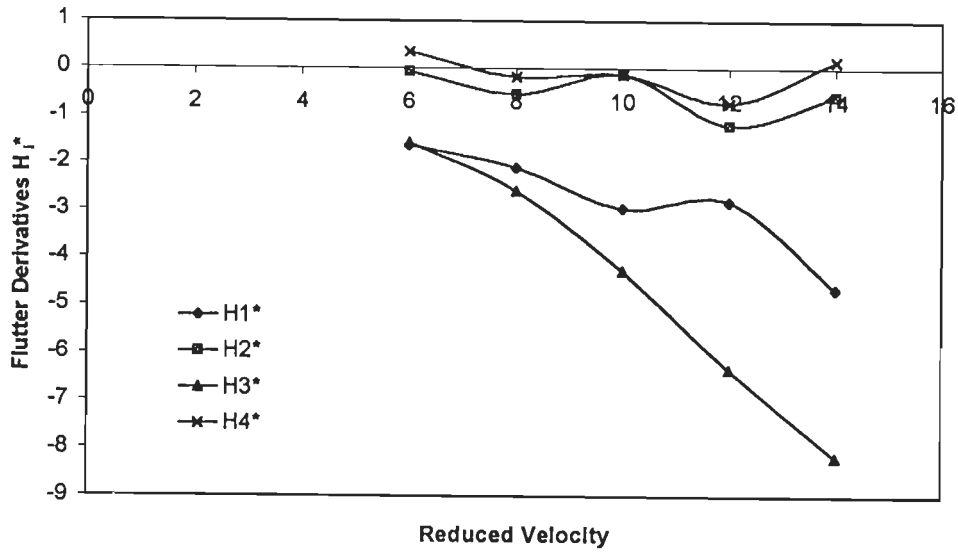

(a) Flutter derivatives H_i^* (i = 1, 4) as a function of reduced velocity

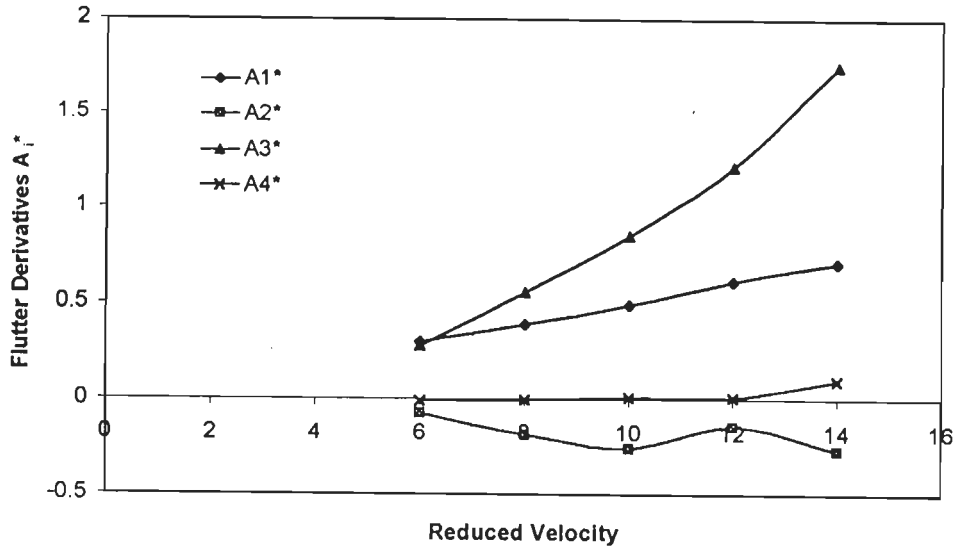

(b) Flutter derivatives A_i^* (i = 1, 4) as a function of reduced velocity

Fig. 8.9 : Flutter Derivatives for Lions' Gate Bridge
(Renovated Deck Cross-Section)

Table 8.1: Inertia and Frequency Parameters for the Renewed Lions' Gate Bridge Deck Section

Mass Kg/m	Mass Moment of Inertia Kg m^2/m	Vertical Frequency (Hz)	Torsional Frequency (Hz)
6.82×10^3	0.1675×10^6	0.173	0.575

A flutter analysis is carried out using structural parameters given in Table 8.1, structural damping in vertical and torsional directions of 0.005 and flutter derivatives given in Fig. 8.9. The determination of critical wind speed for flutter when vertical and torsional motions are coupled is illustrated in Fig. 8.10. The critical wind speed for onset of flutter is estimated as 85.4m/sec using VTCFLUT against the reported value of 86m/sec by Queen *et al* (1999).

They have also reported about wind tunnel investigations conducted to identify the incipient flutter state. Flutter instability was observed during wind tunnel tests at an equivalent full-scale mean wind speed at deck level of 81m/sec, in smooth flow and at a slightly lower wind speed of 79m/sec in turbulent flow, for an angle of attack of zero degree. Thus the critical flutter speed predicted using the flutter derivatives extracted using CFD techniques is in close agreement (within 6%) with the observed flutter speed during wind tunnel investigations.

Vasco da Gama Bridge

Vasco da Gama Bridge (main span 420m) has been discussed in detail by Mendes and Branco (1988). The bridge deck width is 30.6m. The inertia and frequency parameters are shown in Table 8.2.

Table 8.2: Inertia and Frequency Parameters for Vaso da Gama Bridge Deck Section

Mass Kg/m	Mass Moment of Inertia Kg m^2/m	Vertical Frequency (Hz)	Torsional Frequency (Hz)
53.9×10^3	6.8×10^6	0.33	0.672

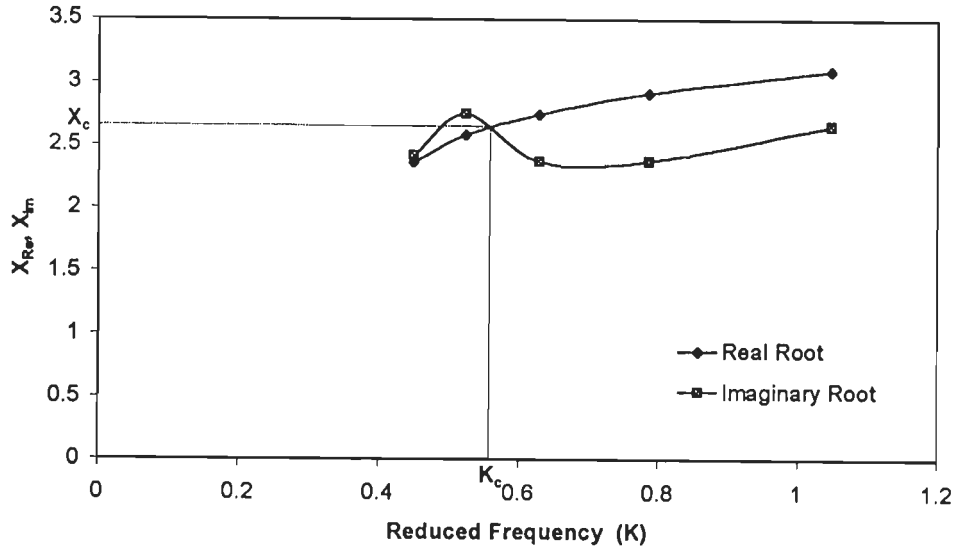

Fig. 8.10 : Determination of Incipient Stage for Flutter for Lions' Gate Bridge

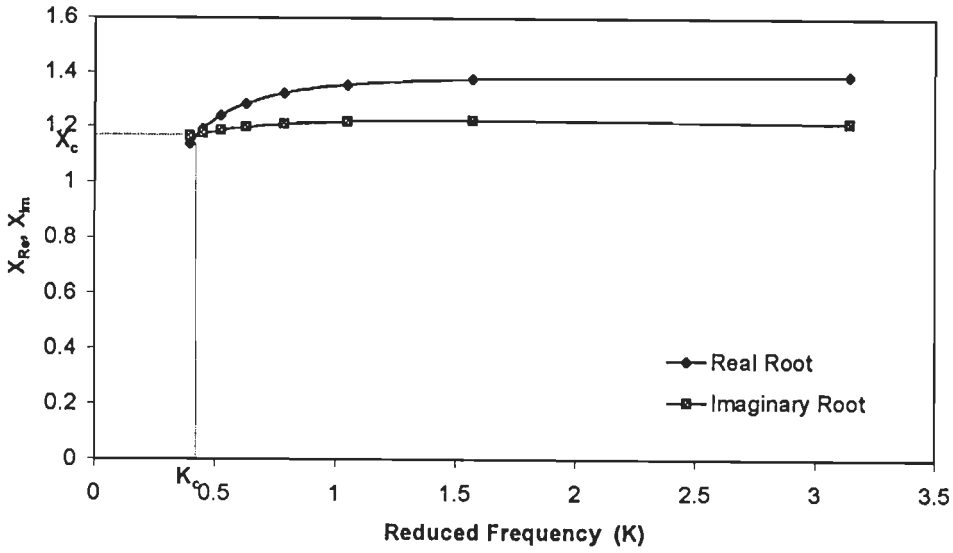

Fig. 8.11 : Determination of Incipient Stage for Flutter for Vasco da Gama Bridge

The deck has been assumed as a thin airfoil, and flutter derivatives as depicted in Fig. 8.4, and the damping ratio is taken as $\xi_s = 0.0063$ for both vertical bending and torsional modes, as suggested in Eurocode 1 for prestressed concrete bridges. In fact the value given in this code is the logarithmic decrement and it is indicated only for the fundamental flexural mode.

Flutter analysis is performed for the above mentioned structural and aerodynamic data for this bridge using VTCFLUT and determination of flutter condition is illustrated in Fig. 8.11. The critical wind speed for flutter is estimated as 178m/sec in the present study and is in close agreement (within 4%) with the critical flutter speed of 171.1m/sec reported by Mendes and Semiao (1999) using three-dimensional flutter analysis.

From the results of the above bridges, it is evident that the software developed using the formulations for flutter analysis described in the present study is accurate enough to predict the critical flutter speed for long span cable bridges.

After validating the flutter analysis, numerical analysis of cable stayed bridges has been performed to study the effect of (i) bridge vibration in higher modes, (ii) variation in angle of attack on flutter criteria. Analysis is performed to identify the flutter condition when the deck is subjected to simultaneous lateral and torsional motions. Also, the effect of type of deck supports at towers and abutments on flutter tendencies of three span bridges has been examined. The details of these analyses are given in the following section.

8.6 NUMERICAL ANALYSIS FOR FLUTTER

In this section the numerical flutter analysis of all the four bridges included in this study are presented. Bridge #1, Bridge #2 and Bridge #4 have been analysed using flat plate flutter derivatives to observe the effect of bridge deck vibration in higher modes on the criteria for onset of flutter when vertical and torsional motions are

coupled. Bridge #3 has been analysed using experimentally obtained flutter derivatives to observe the effect of angle of attack on flutter speed for three different cross-section C-2, C-2C and C –1B. Further, for Bridge #2, analysis has been performed to determine the critical wind speed at which coupled flutter due to lateral and torsional motions is likely to occur. Analysis of three span bridges has also been carried out to study the influence of type of deck supports on flutter tendencies.

8.6.1 Effect of Bridge Vibration in Higher Modes

From the vibration characteristics of Bridge #1 and Bridge #2, presented in Tables 3.9 and 3.10, it is clear that the natural frequencies of cable stayed bridges are closely spaced. The frequency ratios of torsional to vertical frequency for first symmetric, first asymmetric, second symmetric and third symmetric for Bridge #1 with deck support type DST-2 are 1.804, 1.667, 1.165 and 1.11 respectively. The frequency corresponding to these vertical bending modes are 0.291Hz, 0.692 Hz, 0.746Hz and 0.890Hz. Similarly for Bridge #2 with deck support type DST-6, the frequency ratios of torsional to vertical frequency for first symmetric (V-S1), first asymmetric (V-AS1), second symmetric (VS-2) and third symmetric (V-S3) modes are 1.907, 1.824, 1.154 and 1.099. However, for this bridge with total span of 1255.8m, the frequency for these vertical bending modes are 0.183Hz, 0.251Hz, 0.422 Hz and 0.573Hz, much lower frequencies in comparison to Bridge #1 with total span of 627.8m. It is seen that, while the frequency of vibration increases for higher modes, the ratio of frequency in torsional to vertical mode decreases. Therefore, analyses have been performed using flutter derivatives for flat plate given in Fig. 8.4 and theoretically estimated modal structural damping as given in Tables 3.11(a) and 3.12(c) for Bridge #1 and Bridge #2 to observe the effect of bridge vibration in higher modes on the flutter tendencies for these bridges.

For Bridge #1, the flutter analysis has been performed and the determination of incipient stage for flutter is illustrated in Fig. 8.12. The critical flutter speed for coupled bridge oscillations in vertical and torsional modes for first symmetric, first asymmetric, second symmetric and third symmetric modes is 120.5m/sec, 165 m/sec,128.3m/sec,172.2 m/sec respectively.

Similarly, for Bridge #2, the analysis has been performed and influence of bridge vibration in higher modes on flutter tendencies is presented in Fig. 8.13. The critical wind speed for onset of flutter is estimated as 128 m/sec and 113 m/sec respectively for coupling of vertical and torsional modes corresponding to first symmetric and second symmetric modes.

As for Bridge #3, the experimentally determined direct flutter derivatives are only available, as discussed in Section 8.2.1.2. However, to identify the incipient stage for classical flutter, cross flutter derivatives are also needed. Also, by examining the flutter derivatives for three deck configurations (C-2, C-2C and C-1B), it is clear that Bridge #3 is prone to single degree of freedom flutter in torsion, hence not studied for flutter due to coupled vertical and torsional modes.

Again, Bridge #4 has been analysed using flat plate derivatives and the study to identify the flutter condition is presented in Fig. 8.14. The critical wind speed for flutter due to coupling of first symmetric vertical and torsional modes is 177 m/sec.

From the results, it is seen that bridge vibration in higher modes is affecting the flutter criteria in long span bridge (Bridge #2) on account of low structural frequencies and damping values.

The higher critical flutter speeds for Bridge #1, Bridge #2 and Bridge #4 can be attributed to the requirement of higher wind speeds to develop the effective coupling forces affecting modes with low frequency values (1^{st} and 2^{nd} symmetric modes) that are involved in the flutter.

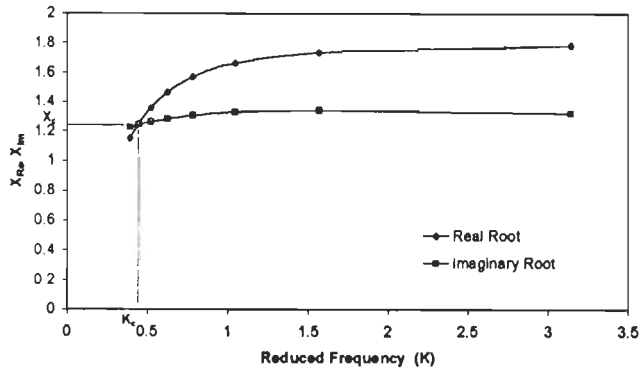

(a) 1st symmetric modes

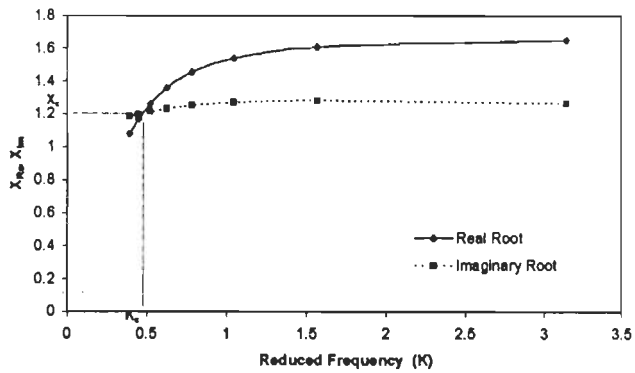

(b) 1st asymmetric modes

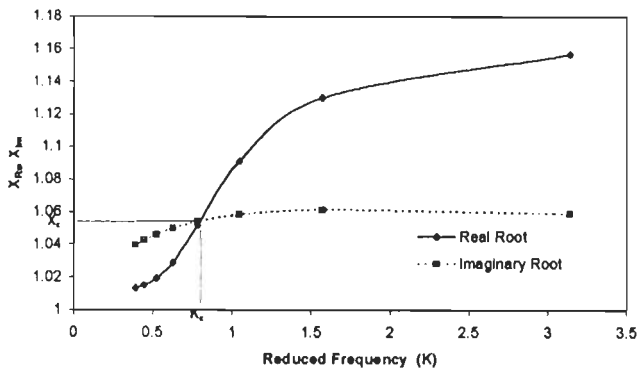

(c) 2nd symmetric modes

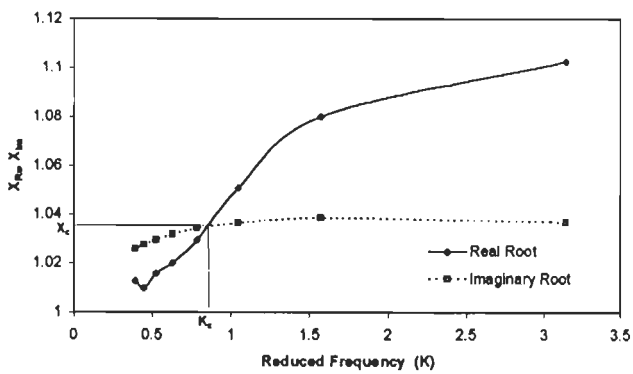

(d) 3rd symmetric modes

Fig. 8.12 : Determination of Incipient Stage for Flutter of Bridge #1 – Effect of Bridge Deck Vibration in Higher Modes

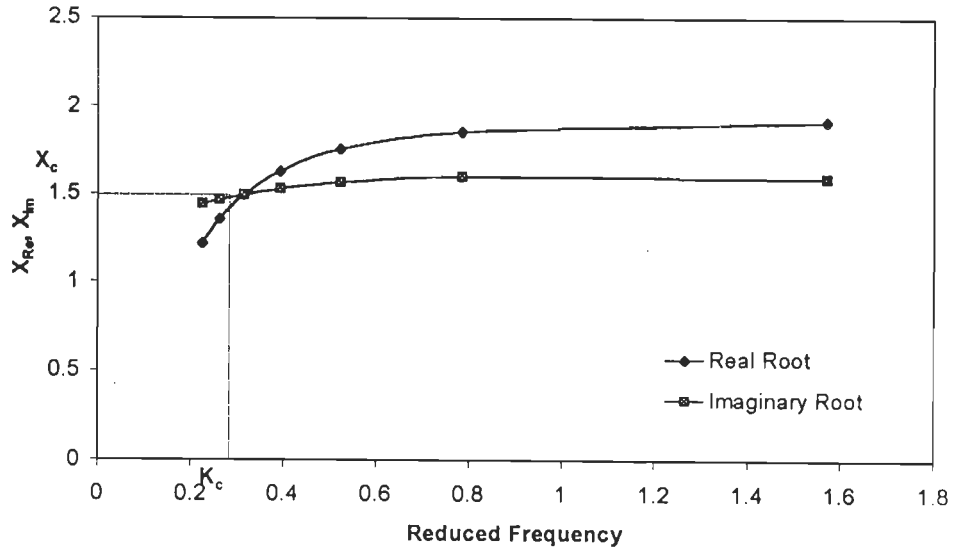

(a) 1st Symmetrical, Vertical and Torsional Modes

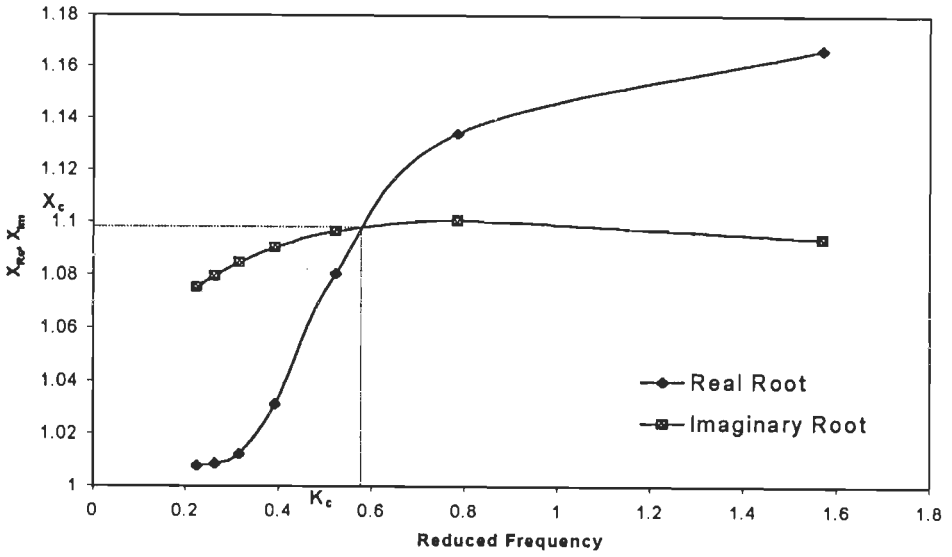

(b) 2nd Symmetrical, Vertical and Torsional Modes

Fig. 8.13 : Determination of Incipient Stage for Flutter of Bridge # 2 – Effect of Bridge Deck Vibration in Higher Modes

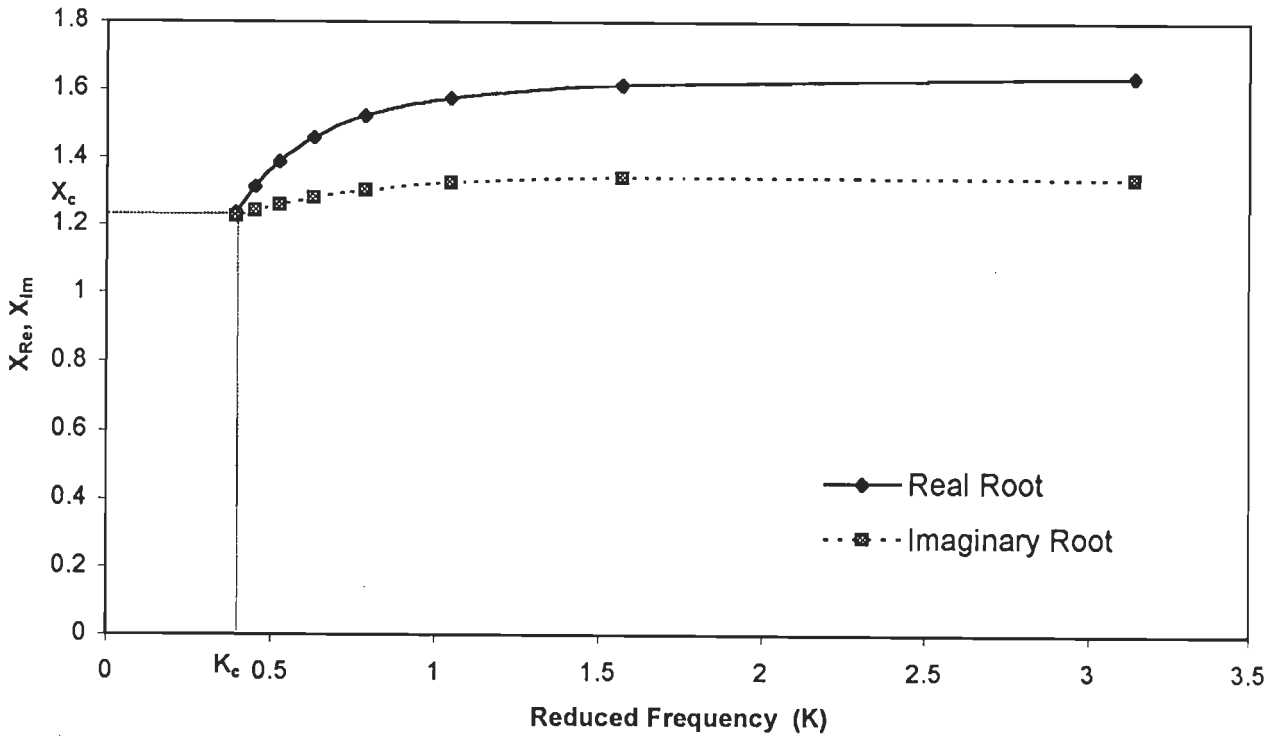

Fig. 8.14 : Determination of Incipient Stage for Flutter of Bridge #4 (1^{st} Symmetric Vertical and Torsional Modes)

8.6.2 Effect of Angle of Attack

Analysis for Bridge #3 with three different deck configurations indicated by C-2, C-2C and C-1B has been carried out using the experimentally determined flutter derivatives given in Figs 8.6 to 8.8 for angles of attack -4, -1.75, 0, +2 and +4 degrees. The flutter analysis has been illustrated in Fig. 8.15 for this bridge with deck configuration C-1B. Similarly, the critical flutter speeds have been estimated for these wind angles for bridge deck cross-sections C-2 and C-2C. The effect of angles of attack on critical flutter speed for Bridge #3 with different deck configurations is presented in Table 8.3.

Table 8.3: Critical Flutter Speed for Bridge #3 with Different Deck Configuration- Effect of Angles of Attack of Approaching Wind

Angle of Attack in Degrees	Critical Flutter Speed in m/sec For Different Deck Cross-section		
	C-2	C-2C	C-1B
-4	118.0	121.5	124
-1.75	95.6	96.3	116
0	92.8	92.9	109
2	71.7	73.8	89
4	37.8	37.7	43.5
6	36.4	36.4	39.4

From Table 8.3, it is clear that the critical flutter speed is dependent on angle of attack and does not occur at an angle of attack of 0 degree. The flutter speed decreases for positive angles of attack. Therefore, it is essential to determine the flutter derivatives at various positive and negative wind angles. Further, flutter analysis has to be performed at these angles of attack to establish rational flutter criteria for wind resistant design of long span cable stayed bridges. Also, the flutter criteria varies with geometric, structural and aerodynamic properties of deck configuration.

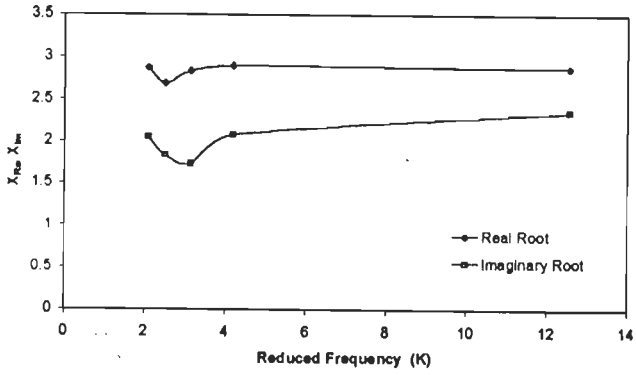

(a) Angle of attack = -4°

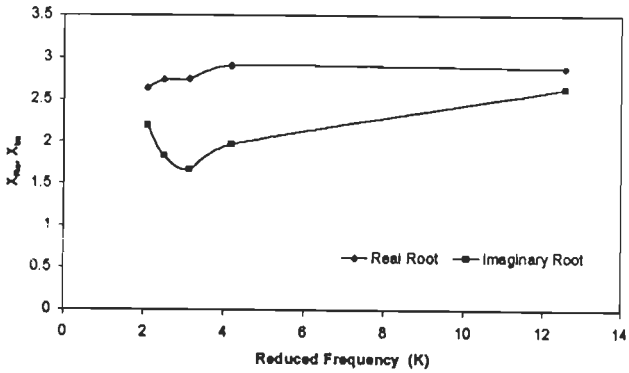

(b) Angle of attack = -1.75°

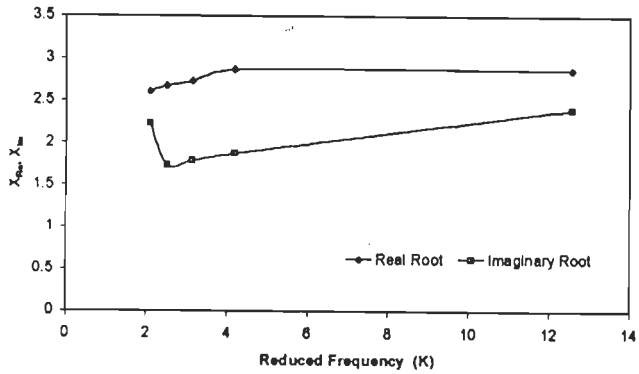

(c) Angle of attack = 0°

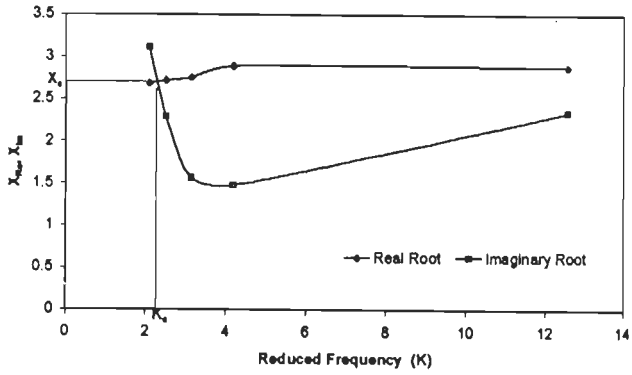

(d) Angle of attack = +1.75°

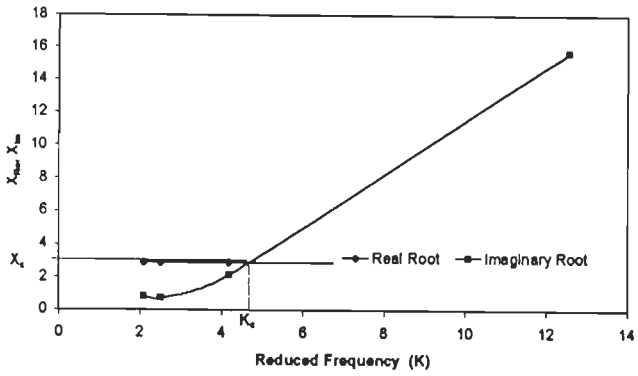

(e) Angle of attack = +4°

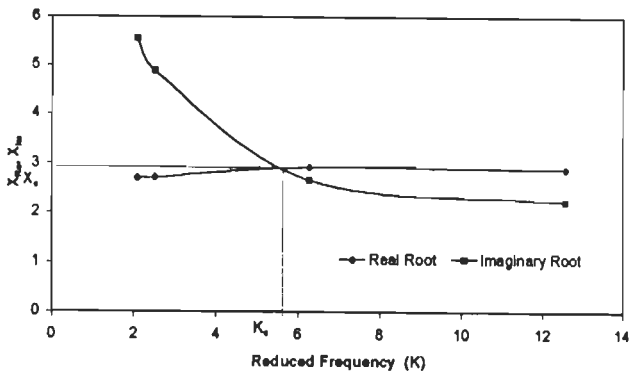

(f) Angle of attack = +6°

Fig. 8.15 : Determination of Incipient Stage for Flutter of Bridge # 3 with Deck Configuration C-1B at Various Angles of Attack

8.6.3 Flutter Criteria for Onset of Coupled Lateral and Torsional Motions

By examining the vibration characteristics of Bridge #2 with deck support type DST-6, it is observed that the frequency in first lateral and torsional symmetric modes is 0.303Hz and 0.349Hz. The frequency ratio is 1.15, which is close to 1.00. Therefore, it is necessary to examine the possibility of occurrence of flutter due to coupled lateral and torsional modes. The lateral derivatives are computed using Eqs. 8.34 to 8.39, using the steady–state force coefficients and slope of drag curve for Bridge #2 as discussed in Section 6.2.2. To establish a flutter criterion for onset of flutter, analysis has been performed using routine LTCFLUT based on formulations given in Section 8.3.2. The plots of real and imaginary roots for determination of incipient flutter stage is shown in Fig. 8.16. From the results of the analysis and plots in Fig. 8.16, it is seen that a flutter condition could not be predicted from the flutter derivatives used in this analysis.

The frequency in the first lateral and torsional symmetric mode is 0.952Hz and 0.525Hz for Bridge #1 with type of deck support DST-2. As the lateral frequency is much higher than the torsional frequency, there is no possibility of coupling of these modes.

8.6.4 Effect of Type of Deck Supports

To observe the effect of type of deck supports on flutter tendencies of three span bridges with different deck supports (DST-1 to DST-6), as a first step the vibration characteristics are studied in detail. The frequency of first vertical and torsional symmetric modes does not vary much with type of deck support (variation in frequency ratios between 1.75 and 1.80 for Bridge #1 and between 1.85 and 1.93 for Bridge #2). Flutter analysis has been performed for Bridge #1 and Bridge #2. Effect of type of deck supports on flutter criteria is presented in Fig. 8.17 and 8.18 for Bridge #1 and Bridge #2 respectively. From the results, it is observed that the critical flutter speed varies within 7% and 4% for Bridge #1 and Bridge #2 respectively with change in type of deck supports at towers and abutments.

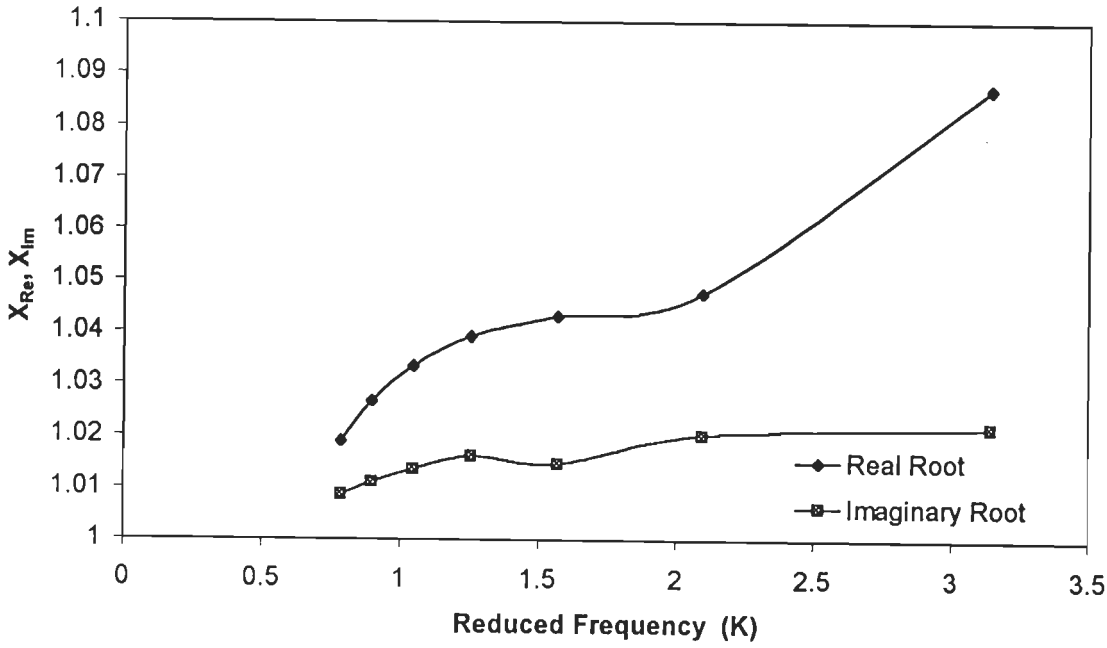

(a) For deck support type DST-4 (1st symmetric lateral and torsional modes)

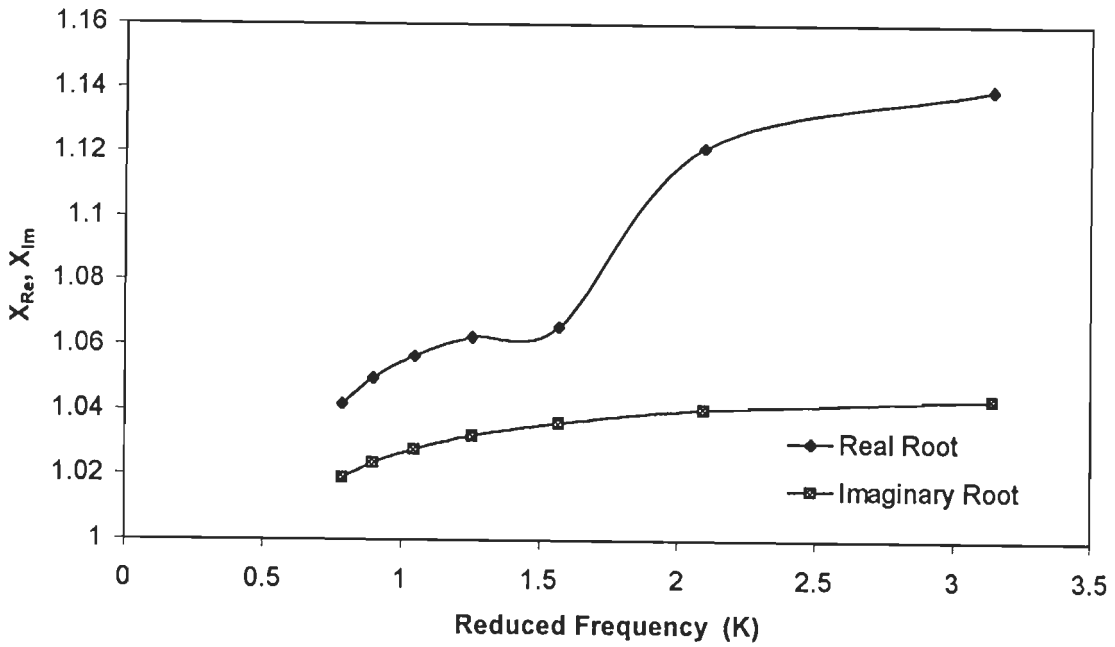

(b) For deck support type DST-6 (1st symmetric lateral and torsional modes)

DST-4 : Deck movable at all supports

DST-6 : Deck elastically supported at towers, on rollers at other supports

Fig. 8.16 : Determination of Incipient Stage for Coupled Lateral and Torsional Flutter of Bridge #2

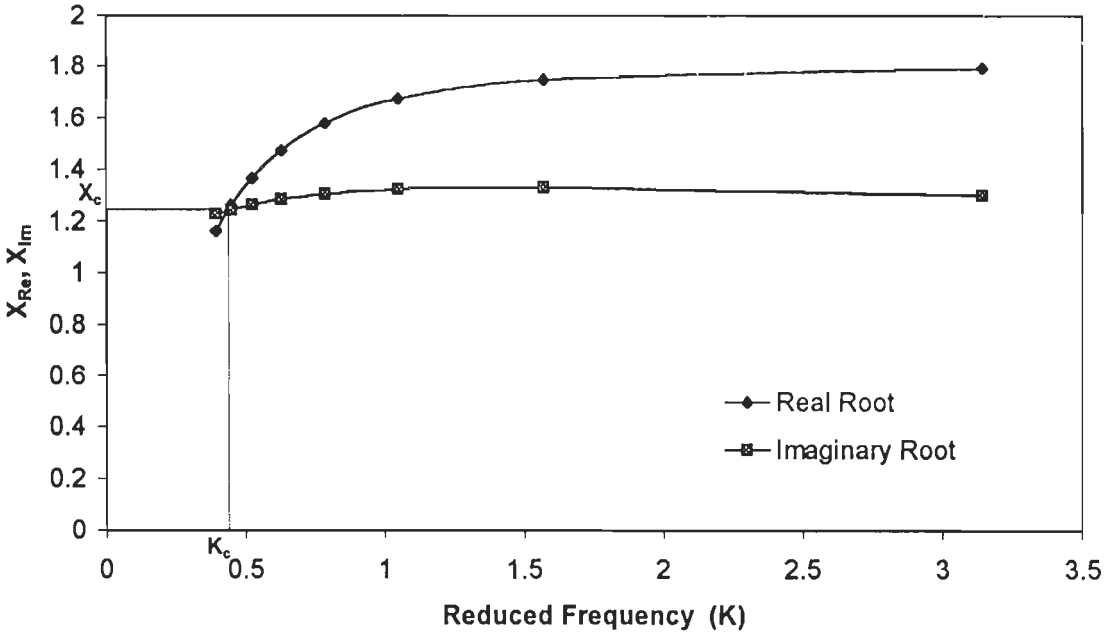

(a) For deck support type DST-5 (1st symmetric vertical and torsional modes)

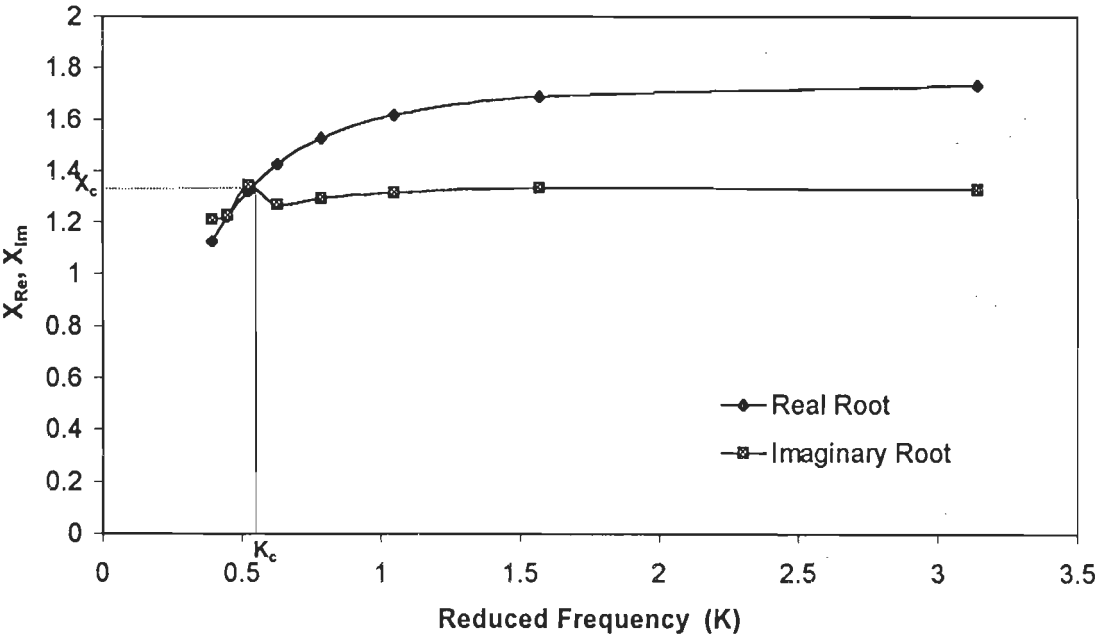

(b) For deck support type DST-6 (1st symmetric vertical and torsional modes)

DST-5 : Floating Deck

DST-6 : Deck elastically supported at towers, on rollers at other supports

Fig. 8.17 : Determination of Incipient Stage for Flutter of Bridge #1 – Effect of Type of Deck Supports

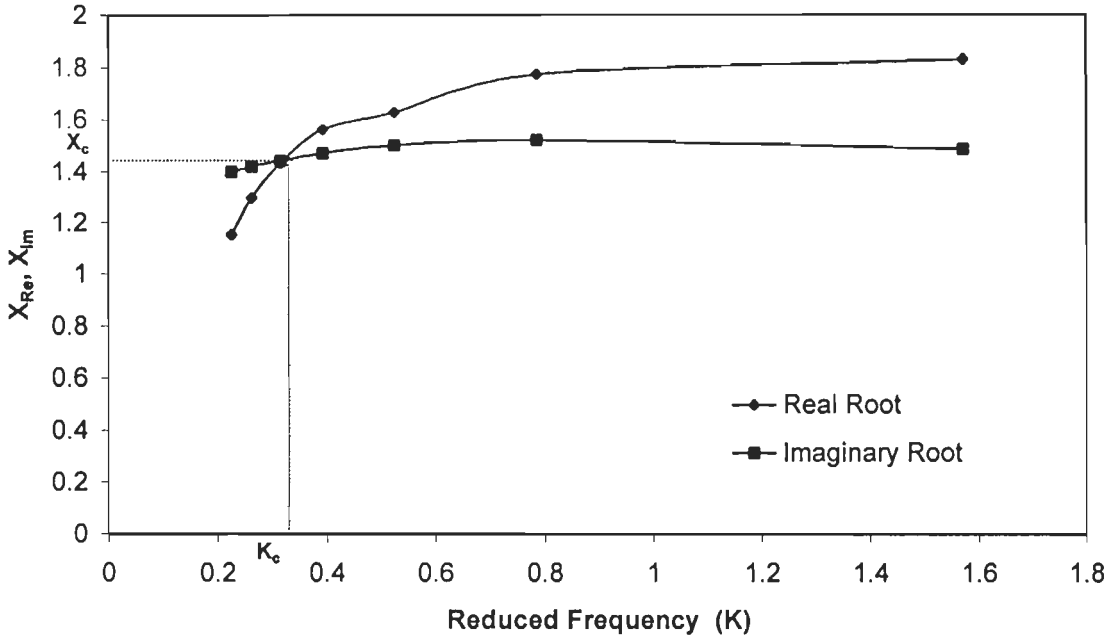

(a) For deck support type DST-2 (1st symmetric vertical and torsional modes)

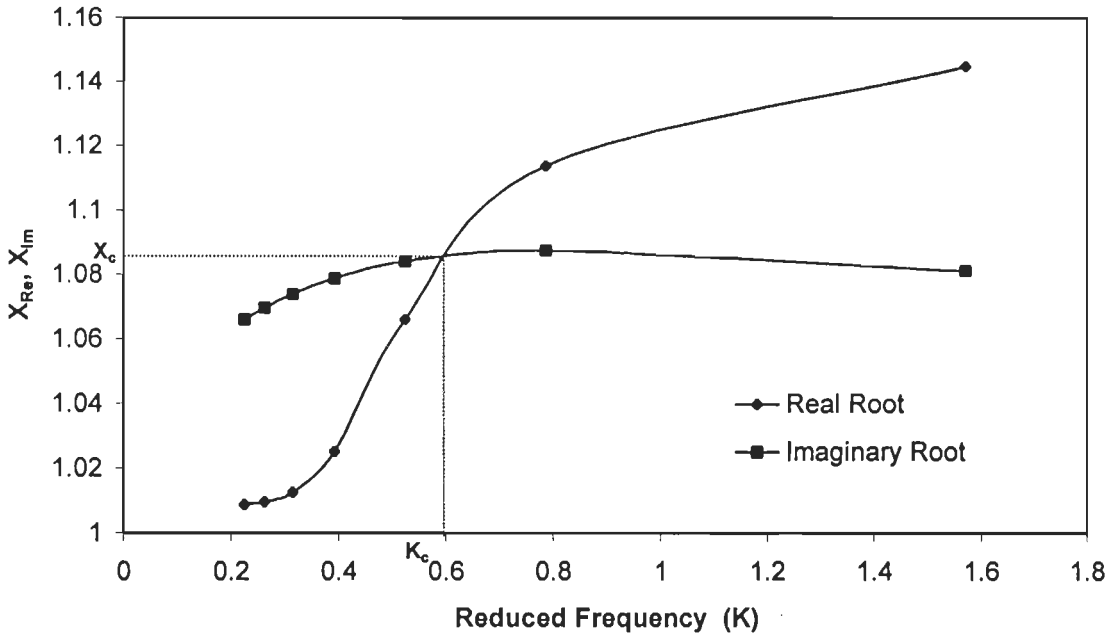

(b) For deck support type DST-1 (2nd symmetric vertical and torsional modes)

DST-1 : Deck fixed at towers, on rollers at other supports

DST-2 : Deck fixed at one tower, on rollers at other supports

Fig. 8.18 : Determination of Incipient Stage for Flutter of Bridge #2 – Effect of Type of Deck Supports

The critical wind speed for occurrence of flutter varies with change in type of deck supports at towers and abutments as the frequency ratios, damping values are also dependent on deck support types.

8.7 SUMMARY

This chapter deals with the formulations, methodology and numerical examples of cable stayed bridges illustrating the flutter analysis. The validation of software developed is illustrated with analysis of Lions' Gate Bridge using theoretically evaluated flutter derivatives obtained by applying CFD techniques and Vasco da Gama Bridge using flat plate derivatives.

Flutter analyses of bridges included in this work have been performed to observe the effect of (i) bridge vibration in higher modes for Bridge #1, Bridge #2 and Bridge #4 (ii) variation of angle of attack and deck configuration in Bridge #3 (iii) type of deck supports at towers and abutments in three span bridges, Bridge #1 and Bridge #2 on the criteria for onset of flutter. Also, the longest bridge included in the study (total span 1255.8 m) has been analysed to estimate the critical flutter speed for coupled flutter due to lateral and torsional vibrations. Based on the results obtained from the analyses, the following conclusions are drawn :

(i) From the flutter analysis of bridge to study the effect of bridge vibration in higher modes on criteria for onset of flutter, it is seen that the bridge deck vibration in higher modes tend to reduce the critical wind speed by 13% in a long span bridge like Bridge #2 (total span 1255.8 m).

(ii) The angle of attack of wind plays an important role in flutter analysis, as the critical flutter speed for occurrence of flutter significantly decreases with increase in the angle of attack (positive). Therefore, it is necessary to determine the flutter derivatives at various wind angles (positive as well as negative) and perform flutter analysis at different angles of attack of wind for a rational wind design.

(iii) The methodology for determination of flutter speed when the bridge deck undergoes oscillations in coupled vertical and torsional directions has been extended to the bridge deck subjected to coupled lateral and torsional oscillations.

(iv) It is observed that the type of deck supports at towers and abutments does not alter much (within 7% variation) the critical flutter speed due to coupling of vertical and torsinal modes. However, by judicious selection of support types for bridge deck at towers and abutments helps in avoiding the possibility of coupling of lateral and torsional modes, and hence increasing the critical wind speed for flutter due to coupled lateral and torsional motions of bridge deck.

Chapter 9
CONCLUSIONS AND SCOPE FOR FUTURE RESEARCH

9.1 OVERVIEW

The present study contains development of complete analysis for buffeting and flutter of long span cable stayed bridges. In this study the comprehensive approach used for analysis of wind induced oscillations of long span cable stayed bridges includes (i) nonlinear static analysis under dead load and initial cable tensions to obtain the deformed state (ii) vibration analysis using the dead load deformed configuration of bridge (ii) theoretical estimation of modal structural damping using energy based approach (iv) digital simulation of turbulent wind velocity field using spectral representation method (v) generation of buffeting forces acting along the span of bridge in vertical and lateral directions as well as torsional moment (vi) buffeting analysis by time domain approach (vii) flutter analysis to identify the incipient flutter state by determining the critical wind speed for flutter when bridge is subjected to coupled vertical and torsional as well as coupled lateral and torsional motions.

For the buffeting analysis using time domain approach, the complete bridge has been modelled as a three-dimensional space system and it gives very useful results on buffeting induced forces in main components of bridge such as deck, cables, towers, deck supports and abutments. To make a quantitative assessment of buffeting induced design wind forces, the response obtained by the nonlinear static analysis of bridges under dead loads and mean wind forces has been used. The total design loads for wind resistant design of deck, cables, towers, deck supports and abutments are obtained by adding the responses due to mean and fluctuating wind components. This information

is extremely useful in the design of bridges and this methodology could be used in the ultimate load design. It may be worth mentioning here that complete information on response of bridge under the action of turbulent wind is obtained only by time domain approach. The details such as buffeting induced forces in components of bridge and the vertical reactions at deck supports can neither be accurately obtained by frequency domain approach nor by the aeroelastic model studies in wind tunnel.

The time domain buffeting analysis has been used to study the effect of (i) variation in mean wind speed, and (ii) change in terrain roughness on buffeting response of three span and five span cable stayed bridges.

To observe the effect of mean wind speed on buffeting response, the mean wind speed was increased from 30m/sec to 60m/sec in steps of 10m/sec at 10m level assigning surface roughness parameter z_0=0.005m for terrain category TC-1.

Also undertaken in the study is the effect of turbulence on buffeting response and buffeting induced forces in various components of long span cable stayed bridges located in four different terrains with surface roughness parameter z_0 as 0.005m, 0.03m, 0.3m and 1.0m.

The procedure described for flutter analysis of cable stayed bridges has been used to study the effect of bridge deck vibration in higher modes on coupled flutter due to vertical and torsional motions for three span and five span cable stayed bridges. Also, the methodology developed for coupled lateral torsional flutter analysis has been used to estimate critical wind speed for flutter in Bridge #2 with total span of 1255.8 m. As the coupling of lateral and torsional modes is likely to occur in long span bridges, the procedure developed would be useful in design of long and super long bridges.

Another important aspect included in this study is the effect of following support types of bridge deck at towers and abutments on static, dynamic and aerodynamic behaviour of three span cable stayed bridges.

DST-1: Deck fixed at both towers, on rollers at other supports

DST-2: Deck fixed at one tower, on rollers at other supports

DST-3: Deck fixed at one end, on rollers at other supports

DST-4: Deck movable at all supports

DST-5: Floating deck

DST-6: Deck elastically supported at towers, on rollers at other supports

Gust response factor has been used as a tool to judge the performance of these deck supports under the action of turbulent wind and to select a suitable type of deck support for wind resistant design.

9.2 CONCLUSIONS

Three span, composite bridges Bridge #1 (total span 627.8m), Bridge #2 (total span 1255.8m) as well as five span bridges- Bridge #3, an existing steel bridge (total span 836.6m) and Bridge# 4, a concrete bridge under construction (total span 610m) have been numerically analysed using the comprehensive procedure, developed in this work for the analysis of wind induced oscillations. Based on the buffeting and flutter analysis of these bridges, important conclusions are drawn which are discussed in the following sections.

9.2.1 Buffeting Response

The time domain approach used in this study to compute buffeting response of cable stayed bridges, serves as an alternate tool to aeroelastic wind tunnel testing which is time consuming and expensive. It is capable of incorporating the nonlinearities in the long span cable stayed bridge system and is therefore also suitable for ultimate load analysis and design.

9.2.1.1 Effect of mean wind speed

With increase in mean wind speed, the vertical, lateral and torsional buffeting responses of three span as well as five span cable stayed bridges increases nonlinearly. In the three span cable stayed bridges, the first and second vertical symmetric bending modes (V-S1 and V-S2) contribute significantly to vertical buffeting response. For the two bridges included in this study, Bridge #3 and Bridge #4, it is observed that only the contribution of the 1st vertical symmetric mode (V-S1) is significant. This is due to the fact that, with five supports along the span of a bridge, the stiffness increases, thereby increasing the natural frequency of second vertical bending mode to about 0.9Hz, and at this frequency the energy content in the wind fluctuations is too small.

Also, it is observed that in the case of three span bridges the side span vertical buffeting response is about 60% of the response at centre of the main span. However, in five span bridges the side span response is only about 40% of response at centre of the main span. The side span buffeting response in lateral direction and in torsion is very small in comparison to the response at centre of the main span.

Buffeting induced forces in outer cables, deck member near tower as well as the vertical reaction at deck supports at abutments or near cable anchorages are significantly high in comparison to forces induced by mean wind.

Further, the study shows that a five span bridge with large number of cables (like Bridge #4) shall be preferred if its design is buffeting based, since the buffeting induced forces in various components of bridge tend to reduce in comparison to the mean wind forces.

9.2.1.2 Effect of terrain roughness

It is observed that with increase in terrain roughness (turbulence intensity of longitudinal velocity fluctuations in the range 10% to 26%, and turbulence intensity of vertical velocity fluctuations in the range 5% to 16%) the gust response factor is

increased by 10% in Bridge #4 – five span bridge (with total span of 610m) and 29% in Bridge #2 – three span bridge (total span of 1255.8m).

9.2.2 Flutter Analysis

For the flutter analysis of long span cable stayed bridges, the necessary software has been developed so that once the geometric, structural properties, vibration characteristics and flutter derivatives are known, the incipient stage for flutter when (i) the bridge is subjected to vertical and torsional motions or (ii) lateral and torsional motions could be predicted accurately. The motions in either case may be independent (for single degree of freedom) flutter or coupled. These routines have been utilised to identify the critical flutter speed for the four bridges included in the study. Based on the results of the present study, the following conclusions are drawn.

9.2.2.1 Effect of bridge deck vibration in higher modes

From flutter analysis of bridge considering participation of higher modes of vibration (2^{nd} symmetric vertical and torsional modes), it is observed that the critical wind speed for onset of flutter in a long span bridge like Bridge #2 is reduced by 13%.

9.2.2.2 Effect of angle of attack

The angle of attack of wind plays an important role in the flutter analysis as the critical wind speed for occurrence of flutter significantly decreases with increase in angle of attack (positive). Therefore, it is necessary to determine the flutter derivative at various wind angles and perform flutter analysis at different angles of attack of wind for a rational wind design of long span cable stayed bridges.

9.2.3 Effect of Support Types for Bridge Deck in Static, Dynamic and Aerodynamic Behaviour of Three Span Bridges

Nonlinear static response of three span cable stayed bridges is dependent on the support types for bridge deck at towers and abutments. The vertical deck deflection is

lowest for a deck fixed at both towers, highest for floating deck, and can be controlled by supporting the deck elastically.

The mode type and the order in which the bridge gets excited, varies with type of deck supports for the three span cable stayed bridges.

The modal strain energy distribution is different in various modes of vibration and this causes mode dependency of structural damping. Also, the modal structural damping varies with change in type of deck support for the bridge. It is seen that in three span bridges, modal damping in torsion is higher than the damping in vertical bending mode, on account of the A-shaped tower with deck level and upper struts as well as cross-beams in deck system.

From the buffeting response of Bridge #1 and Bridge #2, with different types of deck supports at towers and abutments, it is observed that floating deck or elastically supported deck at towers behave in the same fashion under static and dynamic loads and hence the gust response factor seems to be lower in comparison to bridge with other deck support types. Hence, these support types are preferable for buffeting based design of long span cable stayed bridges.

From the flutter analysis to study the effect of deck support types on flutter tendencies of three span cable stayed bridges, it is seen that the type of deck supports at abutments and towers does not alter the critical wind speed much (variation within 7%) due to coupling of vertical and torsional modes. However, a judicious selection of deck support type helps in avoiding the possibility of coupling of lateral and torsional modes, and hence increasing the critical wind speed for occurrence of flutter due to lateral and torsional motions of bridge deck.

9.3 ADVANCEMENTS

Improvement in state-of–the-art has been achieved in analysis of wind induced oscillations in cable stayed bridges by (i) application of theoretically estimated

structural damping for wind analysis rather than the generally assumed damping value, (ii) buffeting analysis of the cable stayed bridge by idealizing it as a three-dimensional space system, under digitally simulated spatially correlated wind, using time domain approach and (iii) examining the possibility of flutter by coupling of lateral and torsional motions. The effect of deck support types on static, dynamic and aerodynamic behaviour is another useful aspect in design of long span cable stayed bridges.

9.4 SCOPE FOR FUTURE RESEARCH

To take full advantage of analytical methods to study the wind induced oscillations in cable stayed bridges, the research needs to be carried out in the following areas:

1. The aerodynamic design parameters for bridge deck, tower and cable cross-sections of a cable stayed bridge should be evaluated by wind tunnel investigations under turbulent flow or using CFD techniques.
2. Research on application of computational fluid dynamics techniques to simulate wind flow around bridge decks would help in quick determination of aerodynamic and aeroelastic parameters as well as for the development of bridge deck sections suitable for super spans.
3. The dynamic and aerodynamic behaviour of long span cable stayed bridges at different construction stages needs to be investigated.

To achieve cable stayed bridges with very long spans research needs to be concentrated on the following aspects:

1. Development of ideal geometric shapes for deck, tower, cables as well as parapets, railings and wind screens, to achieve wind resistant design of super span cable stayed bridges is another challenging area.

2. With very long span bridges, the inclined stay lengths are becoming longer so that cable vibration and its control need to be given due attention.
3. The use of vibration control devices to suppress wind induced oscillations in cable stayed bridges is gaining popularity. Efforts are necessary for developing efficient and economical control devices for long span bridges.
4. Development of ideal geometric shapes for deck, tower, cables as well as parapets, railings and wind screens, to achieve wind resistant design of super span cable stayed bridges is another remaining challenging area.

Appendix-I

STABILITY FUNCTIONS FOR BEAM ELEMENT

Stability functions are used to account for the coupling between axial and flexural stiffness in a beam element as described in Section 3.2.1.2. These functions are multiplication factors used to modify both bending and axial stiffness of elements. These functions are expressed in terms of member axial force P, and member end moments $M1$ and $M2$ at both ends about the member local y and z-axes, as defined in Fig. A-1.1.

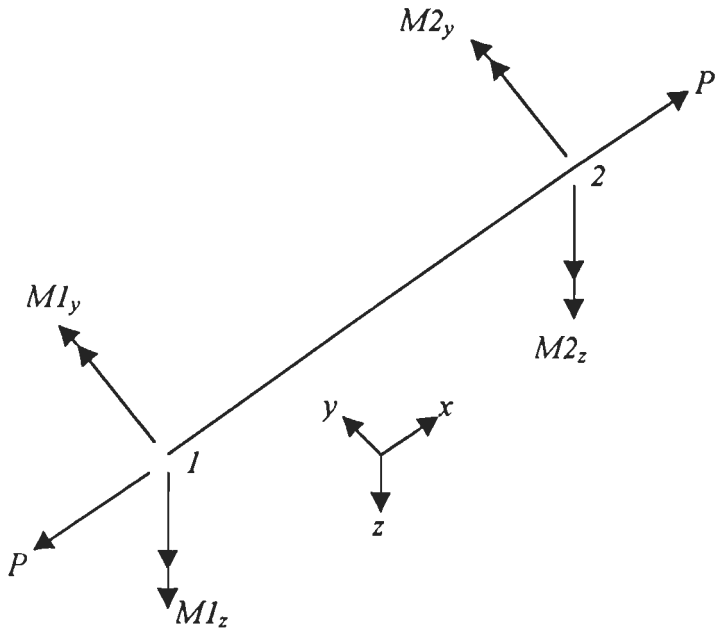

Fig. A-1.1 : Axial Forces and End Moments for a Beam Element

For a tension member (P is positive) the stability functions $S1_z$ through $S4_z$ are defined as;

$$S1_z = \varpi^3 \sinh \varpi / 12R_t \qquad \text{(A-1.1)}$$

$$S2_z = \varpi^2 (\cosh \varpi - 1) / 6R_t \qquad \text{(A-1.2)}$$

$$S3_z = \varpi(\varpi\cosh\varpi - \sinh\varpi)/4R_t \quad \text{(A-1.3)}$$

$$S4_z = \varpi(\sinh\varpi - \varpi)/2R_t \quad \text{(A-1.4)}$$

in which $\varpi = \mu L and \mu^2 = P/EI_z$ (A-1.5)

and $R_t = 2 - 2\cosh\varpi + \varpi\sinh\varpi$ (A-1.6)

For a compression member (P is negative), the stability functions SI_z through $S4_z$ are defined as:

$$SI_z = \varpi^3\sinh\varpi/12R_c \quad \text{(A-1.7)}$$

$$S2_z = \varpi^2(1-\cosh\varpi)/6R_c \quad \text{(A-1.8)}$$

$$S3_z = \varpi(\sin\varpi - \varpi\cos\varpi)/4R_c \quad \text{(A-1.9)}$$

$$S4_z = \varpi(\varpi - \sin\varpi)/2R_c \quad \text{(A-1.10)}$$

in which $\varpi = \mu L and \mu^2 = P/EI_z$ (A-1.11)

$$R_c = 2 - 2\cos\varpi - \varpi\sin\varpi \quad \text{(A-1.12)}$$

The stability functions SI_y through $S4_y$ can be determined in the same way replacing I_z by I_y in the Eqs. A-1.1 to A1.12. The stability function S5 can be obtained for a tension member as follows:

$$S5 = 1/\left[1 - EA(R_{tmy} + R_{tmz})/4P^3L^2\right. \quad \text{(A-1.13)}$$

where $R_{tmy} = \varpi_y\left(M1_y^2 + M2_y^2\right)\left(\coth\varpi_y + \varpi_y\,\mathrm{cosec}h^2\varpi_y\right)$

$$-2(M1_y + M2_y)^2 + (MI_yM2_y)\times\left(1+\varpi_y\coth\varpi_y\right)\left(2\varpi_y\,\mathrm{cosec}h\varpi_y\right) \quad \text{(A-1.14)}$$

in which $\varpi_y = \mu_y L and \mu_y^2 = P/EI_y$ (A-1.15)

and $R_{tmz} = \varpi_z(M1_z^2 + M2_z^2)(\coth\varpi_z + \varpi_z\,\mathrm{cosec}h^2\varpi_z)$

$$-2(M1_z + M2_z)^2 + (M1_zM2_z)$$

$$\times\left(1+\varpi_z\coth\varpi_z\right)\left(2\varpi_z\,\mathrm{cosec}h\varpi_z\right) \quad \text{(A-1.16)}$$

in which $\varpi_z = \mu_z L and \mu_z^2 = P/EI_z$ (A-1.17)

For a compression member (P is negative), $S5$ is given by:

$$S5 = 1/\left[1 - EA(R_{cmy} + R_{cmz})/4P^3L^2\right] \tag{A-1.18}$$

where

$$R_{cmy} = \varpi_y(M1_y^2 + M2_y^2)(\cot\varpi_y + \cos ec^2\varpi_y)$$
$$-2(M1_y + M2_y)^2 + (M1_y M2_y)$$
$$\times(1 + \varpi_y \cot\varpi_y)(2\varpi_y \cos ec\,\varpi_y) \tag{A-1.19}$$

$$\varpi_y = \mu_y Land\mu_y^2 = PI_y \tag{A-1.20}$$

and $$R_{cmz} = \varpi_z(M1_z^2 + M2_z^2)(\cot\varpi_z + \varpi_z \cos ec^2\varpi_z)$$
$$-2(M1_z + M2_z)^2 + (M1_z M2_z)$$
$$\times(1 + \varpi_z \cot\varpi_z)(2\varpi_z \cos ec\,\varpi_z) \tag{A-1.21}$$

in which $$\varpi_z = \mu_z Land\mu_z^2 = P/EI_z \tag{A-1.22}$$

As the effect of axial force in the bending of member is not considered in the present study, all the S's take the value 1.

Appendix-II

CHOLESKY's DECOMPOSITION BY EXPLICIT ALGEBRAIC FORMULAE

The proof for explicit algebraic formulae for Cholesky's Decomposition used in Chapter 4 is given below:

The cross-spectral density matrix is expressed as

$$S^0(\omega) = S(\omega)\begin{bmatrix} 1 & C & C^2 & \dots & C^{N-1} \\ C & 1 & C & \dots & C^{N-2} \\ C^2 & C & 1 & \dots & C^{N-3} \\ \dots & \dots & \dots & \dots & \dots \\ C^{N-1} & C^{N-2} & C^{N-3} & \dots & 1 \end{bmatrix} \quad \text{(A-2.1)}$$

According to the standard formulae of Cholesky's decomposition, G(ω) is computed as

$$G_{11}(\omega) = \sqrt{S_{11}(\omega)};\ G_{i1}(\omega) = \frac{S_{i1}(\omega)}{G_{11}(\omega)};$$

$$G_{kk}(\omega) = \left(S_{kk}(\omega) - \sum_{r=1}^{k-1} G_{kr}^2(\omega) \right)^{\frac{1}{2}};$$

$$G_{ik}(\omega) = \frac{S_{ik}\omega - \sum_{r=1}^{k-1} G_{ir}(\omega) G_{kr}(\omega)}{G_{kk}}; \quad k=1, 2, \dots,N;\ \ i=k+1, k+2, \dots,N \quad \text{(A-2.2)}$$

When N=1 in Eq. A-2.1, the Cholesky's decomposition of $S^0(\omega)$ is

$$S^o(\omega) = 1$$

Obviously, $G(\omega) = 1$.

When N = 2 in Eq. A-2.1, the Cholesky's decomposition of $S^o(\omega)$ can be computed according to Eq. A-2.2. The values of G(ω) are:

$$G_{11}(\omega) = 1;\ G_{21}(\omega) = S_{21}(\omega)/1 = C$$

$$G_{22}(\omega) = \left(S_{22}(\omega) - G_{21}^2(\omega)\right)^{1/2} = \sqrt{1 - C^2} \quad \text{(A-2.3)}$$

It can be seen from Eq. A-2.3 that for N=1 and N=2, the values of G(ω) agree with Eq. 4.61 to 4.64. We can suppose that for N=p-1, the values of G(ω) can be computed according to Eq. A-2.2.

The new value of the first column of G(ω) is

$$G_{p1}(\omega) = \frac{S_{p1}(\omega)}{G_{11}(\omega)} = S_{p1}(\omega) = C^{p-1} \tag{A-2.4}$$

The value of $G_{p1}(\omega)$ agrees with Eqs. 4.61 to 4.64. The new value of the second column of $G(\omega)$ is

$$G_{p2}(\omega) = \frac{S_{p2}(\omega) - G_{p1}(\omega)G_{21}(\omega)}{G_{22}(\omega)} = \frac{C^{p-2} - C^{p-1}C}{\sqrt{1-C^2}} = C^{p-2}\sqrt{1-C^2} \tag{A-2.5}$$

Again the value of $G_{p2}(\omega)$ agrees with Eqs. 4.61 to 4.64.

Suppose the new value of column s-1 (s<p-1) agrees with Eqs. 4.61 to 4.64; then the new value of column s from Eq. A-2.2 is:

$$G_{ps}(\omega) = \frac{S_{ps} - \sum_{r=1}^{s-1} G_{pr}(\omega)G_{sr}(\omega)}{G_{ss}}$$

$$= \frac{C^{p-s} - C^{p-1}C^{s-1} - \sum_{r=2}^{s-1} C^{p-r}\sqrt{1-C^2}.C^{s-r}\sqrt{1-C^2}}{\sqrt{1-C^2}}$$

$$= \frac{C^{p-s} - C^{p+s-2} - (C^{p-s+2} - C^{p+s-2})}{\sqrt{1-C^2}} = C^{p-s}\sqrt{1-C^2} \tag{A-2.6}$$

The new value of column p is

$$G_{pp}(\omega) = \left(S_{pp}(\omega) - \sum_{r=1}^{p-1} G_{pr}^2(\omega) \right)^{1/2}$$

$$= \left(1 - C^{2(p-1)} - (1-C^2)\sum_{r=2}^{p-1} C^{2(p-r)} \right)^{1/2}$$

$$= \left(1 - C^{2p-2} + C^{2p-2} - C^2\right)^{1/2} = \sqrt{1-C^2} \tag{A-2.7}$$

It can be seen from Eq. A-2.6 and Eq. A-2.7 that for N=p, all new values of $G(\omega)$ agree with Eqs. 4.61 to 4.64. So for any arbitrary order of matrix $[S^0(\omega)]$, the Cholesky's decomposition agrees with the explicit algebraic formulae given by Eqs. 4.61 to 4.64.

Appendix-III

EVALUATION OF BUFFETING RESPONSE BY FREQUENCY DOMAIN ANALYSIS

In the buffeting theory, as discussed by Scanlan (1981), the maximum mean square buffeting deflections beyond mean steady deflections as distributed along the bridge span are obtained by a pair of formulae, one for response in bending and other for buffeting in torsion. They are formulated by solving the equation of motion of bridge deck subjected to random buffeting and self excited components in frequency domain. In the present study, these formulae are used to compute the buffeting responses and used in validation of results obtained by time domain buffeting analysis. Therefore, the method of evaluation of buffeting response in frequency domain is explained.

The variance of buffeting response at a location 'x' along the span of bridge, in vertical direction, is expressed using the following equation:

$$(\sigma^2{}_h / B)(x) = \frac{\phi_s^2(x)}{K_s^4}\left[\frac{\rho B^2}{M}\right]^2 \frac{1}{J_s}\left[\frac{2(\tilde{C}-1)}{\tilde{C}^2}\right]\frac{1}{U^2}E(\xi_s, C_{Lu}, C_{Lw}, S_u, S_w) \quad \text{(A-3.1)}$$

where

$\phi_s(x)$ = the modal ordinate in the vertical direction for s^{th} vertical bending mode

$$K_s = \frac{2\pi n_s B}{U}$$

ρ = air density

B = bridge deck width in m

M = mass per unit length of deck section

$$J_s = \int_0^L \phi_s^2(x)\frac{dx}{L} \quad \text{(A-3.2)}$$

$\frac{2(\tilde{C}-1)}{\tilde{C}^2}$ is computed for $\tilde{C} = 7n_sL/U$

U is the mean wind speed at bridge deck level as specified by logarithmic law as discussed in Section 4.2.1

$$E(\xi_s, C_{Lu}, C_{Lw}, S_u, S_w) = C_{Lu}^2\left[\frac{(2\pi n_s)S_u(n_s)}{8\xi_{sT}} + 6u_*^2\right] + C_{Lw}^2\left[\frac{(2\pi n_s)S_w(n_s)}{8\xi_{sT}} + 1.75u_*^2\right] \quad \text{(A-3.3)}$$

ξ_{sT} is the net damping in vertical bending for s^{th} mode and is computed using the formula given below:

$$\xi_{sT} = \xi_s - \frac{\rho B^2 L J_s}{2M_s} H_1^*\left(\frac{U}{n_s B}\right) \quad \text{(A-3.4)}$$

ξ_s is the structural damping of s^{th} vertical bending mode.

It may be noted that, H_1^* may reverse sign for bridge deck cross-section as an indication of vortex induced oscillation.

$C_{Lu} = C_L$; C_L is the lift coefficient at angle of attack $\alpha_w = 0$

$$C_{Lw} = \frac{1}{2}\left[C_L' + \frac{A_n}{B}C_D\right] \quad \text{(A-3.5)}$$

A_n is the projected frontal area of deck per unit span.

C_L, C_D indicate the drag and lift coefficients normalized with respect to the bridge deck width, B.

$6u_*^2; 1.75u_*^2$ are the background spectral terms obtained by integration of spectra of longitudinal and vertical velocity fluctuations respectively as follows:

$$\int_0^\infty S_u(n_s)\,dn = 6u_*^2 \quad \text{(A-3.6)}$$

$$\int_0^\infty S_w(n_s)\,dn = 1.75u_*^2 \quad \text{(A-3.7)}$$

$S_u(n_s)$ and $S_w(n_s)$ indicate the power spectral density function for longitudinal and vertical velocity fluctuations, respectively, at vertical bending frequency n_s. (See Eqs. 4.16 and 4.18)

Similarly, the variance for torsional buffeting response is computed using the following equation:

$$\sigma_\alpha^2 = \frac{\phi_r^2(x)}{K_r^4}\left[\frac{\rho B^4}{I_r}\right]^2 \frac{1}{G_r}\left[\frac{2(\tilde{\tilde{C}}-1)}{\tilde{\tilde{C}}^2}\right]\frac{1}{U^2}F\left(\xi_r, C_M, C'_M, S_u, S_w\right) \qquad \text{(A-3.8)}$$

where

$\phi_r^2(x)$ = square of dimensionless modal ordinate in torsion at x along the span

$$K_r = \frac{2\pi n_\alpha B}{U} \qquad \text{(A-3.9)}$$

$$I_r = \int_0^L I\phi_r^2(x)dx \text{ the generalized inertia} \qquad \text{(A-3.10)}$$

$$G_r = \int_0^L \phi_r^2(x)dx/L \text{ the modal integral for r}^{\text{th}} \text{ mode} \qquad \text{(A-3.11)}$$

$$\frac{2(\tilde{\tilde{C}}-1)}{\tilde{\tilde{C}}^2} \text{ is computed for } \tilde{\tilde{C}} = \frac{7n_r L}{U} \qquad \text{(A-3.12)}$$

Net damping ratio for r$^{\text{th}}$ torsional mode is given by

$$\xi_{rT} = \xi_r - \frac{\rho B^4 L}{2I_r}A_2^*\left(\frac{U}{n_r B}\right)G_r \qquad \text{(A-3.13)}$$

and $$F(\xi_r, C_M, C'_M, S_u, S_w) = C_M^2\left[\frac{(2\pi n_r)S_u(n_r)}{8\xi_r} + 6u_*^2\right] + \frac{C_M'^2}{4}\left[\frac{(2\pi n_r)S_w(n_r)}{8\xi_r}\right] \qquad \text{(A-3.14)}$$

In the Irwin's (1977) theory, the buffeting responses are obtained by solving the equation of motion of bridge subjected to random buffeting forces in frequency domain. Certain assumptions are made in computation of buffeting responses.

They are :

(i) Mean wind is taken normal to the bridge and spanwise velocity fluctuations are assumed to have negligible effect.

(ii) The velocity fluctuations of wind are taken to be of the order 0.1 times the mean velocity.

(iii) Aerodynamic coupling between the vertical and torsional modes are ignored.

(iv) Turbulence length scale is much larger than the cross-sectional dimensions of the bridge deck.

(v) Two dimensional aerodynamic admittance functions are incorporated to account for the non-uniformity of velocity field in the neighbourhood of the deck cross-section.

The variance of buffeting response in vertical bending mode 'r' in terms of generalized coordinate is given as

$$\sigma^2(q_r) = \left[\frac{1}{2} \left(\frac{1}{2\pi} \right)^2 \left(\frac{\rho B^2}{M} \right) \left(\frac{U}{n_r B} \right)^2 \left(\frac{w'}{U} \right) \frac{B}{L} \frac{dC_L}{d\alpha_w} \right]^2 L \bar{S}_w(n_r) C_{IWW}(n_r) \left(\frac{\pi n_r}{4\xi_{rT}} \right) \quad \text{(A-3.15)}$$

To find the total variance due to all vertical modes, the variance of individual modes are summed, i.e.,

$$\sigma^2(h) = \sum_r \sigma^2(q_r) \phi_r^2(x) \quad \text{(A-3.16)}$$

The variance of torsional buffeting response for r^{th} mode in generalized coordinates can be estimated as :

$$\sigma^2(q_r) = \left(\frac{1}{2\pi} \right)^4 \left(\frac{\rho B^4}{I} \right)^2 \left(\frac{U}{n_r B} \right)^4 \frac{1}{L} \left[\frac{1}{4} \left(\frac{dC_M}{d\alpha_w} \right)^2 \left(\frac{w'}{U} \right)^2 \bar{S}_w(n_r) C_{IWW}(n_r) \right] \left(\frac{\pi n_r}{4\xi_{rT}} \right)$$

(A-3.17)

To find the total variance of due to all torsional modes, the variance of individual modes are summed, i.e.,

$$\sigma^2(\alpha) = \sum_r \sigma^2(q_r)\phi_r^2(x) \tag{A-3.18}$$

The variance of lateral generalized buffeting response for r[th] mode is given as:

$$\sigma^2(q_r) = \left(\frac{1}{2\pi}\right)^4 \left(\frac{\rho B^2}{M}\right) \left(\frac{U}{n_r B}\right)^4 \left(\frac{B}{L}\right)^2 LC_D^2 \left(\frac{u'}{U}\right)^2 \bar{S}_u(n_r) C_{IUU}(n_r) \left(\frac{\pi n_r}{4\xi_{rT}}\right) \tag{A-3.19}$$

To find the total variance of due to all lateral modes, the variance of individual modes are summed, i.e.,

$$\sigma^2(p) = \sum_r \sigma^2(q_r)\phi_r^2(x) \tag{A-3.20}$$

where u',v', and w' are the r.m.s. values of fluctuating velocity components u, v, and w respectively; $\bar{S}_u = \frac{S_u}{u'^2}; \bar{S}_w = \frac{S_w}{w'^2}$; C_{IUU}, C_{IWW} are the integrals of normalized cross-spectra and ξ_{rT} is net damping in vertical bending, torsional and lateral modes of vibration. They are obtained by adding the aerodynamic damping computed using Eqs. 5.43, 5.44 and 5.46 and respective modal structural damping in vertical, torsional and lateral directions.

REFERENCES

1. Abdel-Ghaffar and Khalifa, M.A.(1991), "Importance of Cable Vibrations in Dynamics of Cable stayed Bridges", J. Eng. Mech, ASCE, vol.117, No.11, pp.2571-2589.

2. Agar, T.J.A. (1989), "Aerodynamic Flutter Analysis of Suspension Bridges by a Modal Technique", Eng. Struct., Vol. 11 , pp. 75- 82.

3. Agar, T.J.A. (1991), "Dynamic Instability of Suspension Bridges", Comp. and Struct., Vol. 41, No. 6, pp. 1321-1328.

4. Akiyama, H. (1999), "Wind Resistant Design of Tatara Bridge", Long-Span Bridges and Aerodynamics, Miyata, T. et al (Eds.), Springer,, 266-277.

5. Baron, F., and Venkatesan, M.S. (1971), "Non-linear Analysis of Cable and Truss Structures", J. Struct. Div. ASCE, 97, ST2, pp. 679-710.

6. Barre, C., and Barnard, G.(1993), "High Reynolds Number Simulation Techniques and Their Application to Shaped Structure Model Test", Proc. First IAWE European and African Regional Conf. on Wind Eng., pp. 83-94.

7. Bartoli, G., Borri, C. and Gusella, V. (1995), "Aeroelastic Behaviour of Bridge Decks: A Sensitivity Analysis of the Turbulent Nonlinear Response", Proc. 9ICWE, New Delhi, India, pp. 851- 862.

8. Bathe, K.L, and Wilson, E.L. (1976), "*Numerical Methods in Finite Element Analysis*", Prentice Hall, Inc., Englewood Cliffs, New Jersey.

9. Bendat, J.S., and Piersol, A.G. (1971), "*Random Data: Analysis and Measurements Procedures*", Wiley-Interscience, New York.

10. Bergland, G. D. (1969), "A Guided Tour of The Fast Fourier Transform", IEEE Spectrum, Vol. 6: 41.

11. Blevins, R. D. (1990), "*Flow-Induced Vibration*", 2nd Ed. Van Nostrand Reinhold, New York.

12. Borri, C., Crocchini, F., and Spinelli, P. (1995), " Numerical Simulation of Stationary and Non-stationary Stochastic Processes: A Comparative Analysis for Turbulent Wind Fields", Proc. 9ICWE, New Delhi, India, Vol. 1, pp. 47-55.

13. Borri, C., Hoffer, R., and Zahlten, W. (1995), "A Non-linear Approach for Evaluating Simultaneous Buffeting and Aero elastic Effects on Bridge Decks", Proc. 9ICWE, India, pp. 839- 850.

14. Bosch, H.R., (1978), " aerodynamic Investigations of the Luling, Louisiana Cable-Stayed Bridge", Federal Highway Administration, Washington, D.C.

15. Brigham, E.O. (1974), "*The Fast Fourier Transform*", Prentice-Hall Inc., Englewood Cliffs, New Jersey.

16. Bruno, D., and Leonardi, A. (1998), "Natural Periods of Long-Span Cable-Stayed Bridges", J. Bridge Eng., ASCE Vol. 2, No. 3, pp. 105 –115.

17. Bucher, C. G., and Lin, Y.K. (1988), "Stochastic Stability of Bridges Considering Coupled Modes", J. Eng. Mech., ASCE, Vol. 114, No. 12, pp. 2055-2071.

18. Cai, C. S., and Albrecht, P. (2000), "Flutter Derivative Based Random Parametric Excitation Aerodynamic Analysis", Comp. and Struct., Vol. 75, pp. 463-477.

19. Cai, C.S, Albrecht, P., and Bosch. (1999), "Flutter and Buffeting Analysis. I: Finite Element and RPE solution", J. Bridge Eng., ASCE Vol.4, No. 3, pp. 174-188.

20. Cao, Y., Xiang, H., and Zhou, Y. (2000), "Simulation of Stochastic Wind Velocity Field on Long-Span Bridges", J. Eng. Mech., ASCE, Vol. 126, No. 1, pp. 1-6.

21. Chen, W., Gu, M., and Xiang, H. F. (1993), "Study on Buffeting Response Spectrum Method for Long Span Bridges", Proc. 3rd Asia - Pacific Symp. on Wind Eng., Hong Kong, Vol. 1 , pp. 205 – 211.

22. Chen, X., Matsumato, M., and Kareem, A. (2000), "Aerodynamic Coupling Effects on Flutter and Buffeting Response of Bridges", J. Eng. Mech., ASCE, Vol.126, No. 1, pp. 17-26.

23. Chen, X., Matsumoto, M., and Kareem, A. (2000), "Time Domain Flutter and Buffeting Response Analysis of Bridges", J. Eng. Mech., ASCE, Vol.126, No. 1, pp. 7-16.

24. Cheung, Y., K., and Kajita, T. (1973), "Finite Element Analysis of Cable Stayed Bridges", Int. Assoc. of Bridge and Struct. Eng., pp. 101-112.

25. Clough R. W., and Penzien, J. (1993), "*Dynamics of Structures*", 2nd Ed. McGraw-Hill.

26. Cooley, J.W., and Tukey, J.W. (1965), "An Algorithm for Machine Calculations of Complex Fourier Series", Math. Comput., Vol. 19, pp.297.

27. Davenport, A.G. (1961), "The Application of Statistical Concepts to the Wind Loading of Structures", Proc. Inst. of Civil Engrs., London, U. K. Vol. 19, pp. 449-472.

28. Davenport, A.G. (1961), "The Spectrum of Horizontal Gustiness Near the Ground in High Winds", Q.J.R. Met. Soc, Vol.87, pp.194-211.

29. Davenport, A.G. (1962), "Buffeting of a Suspension Bridge by Stormy Winds", J. Struct. Div., Proc. ASCE, Vol. 88(3), pp. 233-268.

30. Davenport, A.G. (1968), "The Dependence of Wind Load upon Meteorological Parameters", Proc. Int. Res. Seminar on Wind Effects on Build. and Struct., University of Toronto Press, Toronto.

31. Davenport, A.G., King. J.P.C., and Larose, G.L., (1992), "Taut Strip Model Tests", Aerodynamics of Large Bridges, A Larsen, Ed., Balkema, Rotterdam, The Netherlands, pp. 113-124.

32. Delaunay, D., Grillaud, G., Bietry, J., and Sacre, C. (1999), "In-situ Validations of Wind Design Studies for Long –Span Bridges", Wind Engg. Into the 21st Century, Larsen et al (eds), Balkema, Rotterdam, pp. 863-869.

33. Deodatis, G., and Shinozuka, M. (1988), " Auto- Regressive Model for Non-stationary Stochastic Processes", J. of Eng. Mech., Vol. 114, No. 11, pp. 1995 – 2012.

34. Deodatis, G. (1996), "Simulation of Ergodic Multivariate Stochastic Processes", J. Eng. Mech., ASCE, Vol. 122, No. 8, pp. 778 –787.

35. Di Paola, M. (1998), " Digital Simulation of Wind Field Velocity", J. Wind Eng. and Ind. Aerodyn., Vol. 74-76, pp. 91-109.

36. Diana, G. et al. (1986), "Wind Effects on the Dynamic Behaviour of a Suspension Bridge", Technical Report, Departimento di Meccanica di Milano.

37. Diana, G., Cheli, F., and Resta, F. (1995), "Time Domain Aeroelastic Force Identification on Bridge decks", Proc. 9ICWE, New Delhi, India, pp. 938-949.

38. Ding, Q., Lee, P.K.K, and Lo, S.H.(2000), "Time Domain Buffeting Analysis of Suspension Bridges Subjected to Turbulent Wind with Effective Angle of Attack", J. of Sound and Vib., Vol. 233(2), pp.311-327.

39. Ehsan, A. (1988), "The Vortex- Induced Response of Long, Suspended-Span Bridges", Doctoral Dissertation, Department of Civil Engineering, Johns Hopkins University, Baltimotre, MD.

40. Endo, T., Iijima, T., Okukawa, A., and Ito, M. (1991), "The Technical Challenge of a Long Cable-stayed Bridge - Tatara Bridge", Cable stayed Bridges-Recent Developments and Their Future, pp. 417-436.

41. Enevoldsen, I., Hansen, S.O, Kvamsdal, T., Pedersen, C., and Thorbek, L.T. (1999), "Computational Wind Simulations For Cable–supported Bridges", Wind Engineering into 21st Century, Larsen, A., et al. Balkema, Rotterdam, Vol. 2 pp. 1265-1270.

42. Ernst, H. J. (1965), "Der E-Modul von Seilen under Beruckseihtigung des Durchanges, Der Bauingenieur 40, 2. (In German)

43. ESDU. (1985), "Characteristics of Atmospheric Turbulence Near the Ground", Item No. 85020, ESDU International, London.

44. Faccini, L. (1996), "The Numerical Simulation of Gaussian Cross – correlated Wind Velocity Fluctuations by Means of a Hybrid Model", J. Wind Eng. and Ind. Aerodyn., Vol. 64, pp. 187 –202.

45. Fleming, J., F. (1979), "Nonlinear Static Analysis of Cable-Stayed Bridge Structures", Comp. and Struct., Vol. 10, 1979, pp. 621- 635.

46. Fleming, J. F., and Egeseli, E. A. (1980), "Dynamic Behaviour of a Cable-Stayed Bridge ", Int. J. Earthquake Eng. and Struct. Dyn., Vol. 8, pp. 1-16.

47. Forsching, H. (1958), "Aero elastic Stability Investigations on Prismatic Beams", Proc. of Symp. on Wind Effects on Buildings ad Structures, Loughborough.

48. Frandsen, J.B., and McRobie, F.A. (1999), "Computational Aeroelastic Modelling to Guide Long-Span Bridge Cross-Section Design", Wind Engineering into 21st Century, Larsen, A., et al. Balkema, Rotterdam, Vol. 2, pp. 1277-1285.

49. Fujino, Y., and Nagai, M. (1994a), " Steel Cable–stayed Bridges with Emphasis on Japanese Bridges", Proc. IABSE/FIP Int. Conf. Cable-Stayed and Suspension Bridges, Deauville, pp –173-184.

50. Fujino, Y. and Nagai, M. (1994b), "Cable-supported Bridges and their Future", J. Steel Const. Engg., Vol. 1 (3): pp. 17-35 (in Japanese).

51. Fujino, Y., Wilde, K., Masukawa, J., and Bhartia, B. (1995), "Rational Function Approximation of Aerodynamic forces on Bridge deck and its Application to Active Control of Flutter", Proc. 9ICWE, New Delhi, India, pp. 994- 1005.

52. Fung, Y.C. (1969), "*An Introduction to the Theory of Aeroelasticity*", Dover, New York.

53. Gade, R. H. (1974), " Status of the Investigation of the Aerodynamic Behaviour of the Sitka Harbor Bridge", Symposium on Full-Scale Measurements of Wind Effects on Tall Buildings and Other Structures, London, Canada.

54. Garevski, M. A., and Severn, R. T. (1993), "Damping and Response Measurement on a Small-Scale Model of a Cable-stayed Bridge", Int. J. Earthquake Eng. and Struct. Dyn., Vol. 22, No. 13, pp. 13-29.

55. Ge, Y. J., and Tanaka, H. (2000), "Aerodynamic Flutter Analysis of Cable-Supported Bridges by Multi-mode and Full-mode Approaches", J. Wind Eng. and Ind. Aerodyn.,Vol.86, pp.123-153.

56. Ghosh, A. (1992), "Bearings for 2nd Hooghly Bridge", paper No. 415, IRC Journal, Vol. 53 (3), pp. 471-497.

57. Gimsing, N. J. (1996). *Cable -Supported Bridges*. 2nd Ed., John Wiley & Sons.

58. Grillaud, G., Chauvin, A., and Betry, J. (1992), " Comportement dynamique d'un pont a haubans dans une turbulence de sillage", J Wind Eng. and Ind. Aerodyn. , Vol.41-44, pp. 1181-1189 (in French).

59. Gu. M., Xiang, H. F., Chen, A. R. (1993), "A Practical Method of Passive TMD for Suppressing Wind-Induced Response Analysis for Suspension Bridge", Proc. 3rd Asia-Pacific Symp. on Wind Engg., Hong Kong, Vol. 1, pp. 223 – 228.

60. Gu, M., Chang, C. C., Wu, W., and Xiang, H. F. (1998). "Increase of Critical Flutter Wind Speed of Long –Span Bridges Using Tuned Mass Dampers." J. Wind Eng. and Ind. Aerodyn., Vol. 73, pp. 111-123.

61. Gu, M., Chen, S.R., and Chang, C.C. (1999), "Buffeting Control of the Yangpu Bridge Using Multiple Tuned Mass Dampers", Wind Engineering into 21st Century, Larsen, A. et al, Balkema, Rotterdam, Vol. 2, pp. 893 –898.

62. Gu, M., Xiang, H., and Lin, Z. (1999), "Flutter and Buffeting–based Selection of Long-span Bridges", J. Wind Engg. and Ind. Aerodyn., Vol. 80, pp.373-382.

63. Harris, R.I. (1968), " On the Spectrum and Auto-Correlation Function of Gustiness in High Winds", ERA Report No.5273.

64. Hikami, Y., and Shirashi, N. (1988), "Rain–wind Induced Vibrations of Cables in Cable Stayed Bridges", J. Wind Engg. and Ind. Aerodynamics, Vol. 29, pp 409-418.

65. Holmes, J.D. (1975), "Prediction of the Response of a Cable-Stayed Bridge to Turbulence", Proc. 4th Int. Conf. on Wind Effects on Build. and Struct. , K.J.Eaton ed., Cambridge University Press, London, pp. 187-197.

66. Humar, J. L. (1990), " *Dynamics of Structures*", Prentice Hall, Englewood Cliffs, New Jersey.

67. Inglis, C.E.(1934), "A Mathematical Treatise on Vibrations in Railway Bridges", Cambridge University Press.

68. Irwin, H.P.A.H. (1977), "Wind Tunnel and Analytical Investigations of the Response of Lion's Gate Bridge in Smooth and Turbulent Flow", Technical Report, LTA–LA-210, National Research Council, Ottawa, Canada.

69. Isyumov, N., and Tschanz, T. (1977), "A study of Wind action for Weirton-Steubenville Cable stayed Bridge", Boundary layer Wind Tunnel Laboratory, University of Western Ontario.

70. Ito, M., and Nakamura, Y. (1982), "Aerodynamic Stability of Structures in Wind", IABSE Surveys, S-20/82, pp. 33-56.

71. Ito, M., Fujino, Y., Miyata, T., and Narita, N. (eds.) (1991), *Cable-Stayed Bridges- Recent Developments and their Future*, Series in Development in Civil Engineering 40, Elsevier.

72. Ito, M. (1991), "Cable stayed Bridges in Japan", Cable stayed Bridges – Recent Developments and their future, pp. 341-356.

73. Ito, M. (1992), "Supporting devices of long span cable-stayed bridge girder", Innovative Large Span Structures, Vol.1, CSCE, pp 255-266.

74. Jacobsen, J., B. and Hjorth-Hansen, E. (1993)," Determination of the Aerodynamic Derivatives by System Identification Method", Wind Engineering: 1st AWE European and African Regional Conference, ed. By Cook, N.J., pp. 367-377, Thomas Telford.

75. Jacobsen, J.B. (1995), "Estimation of Motion Induced Wind Forces by a System Identification Method", Proc. 9ICWE, New Delhi, India, pp. 815-826.

76. Jain, A., Jones, N.P., and Scanlan, R. H. (1995), "Fully-Coupled Buffeting Analysis of Long Span Bridges", Proc. 9ICWE, New Delhi, India, pp. 962-971.

77. Jain, A., Jones, N. P., and Scanlan, R. H. (1996), "Coupled Aero elastic and Aerodynamic Response Analysis of Long -Span Bridges", J. Wind Engg. and Ind. Aerodyn., Vol. 60, pp. 69-80.

78. Jain, A., Jones, N. P., and Scanlan, R. H. (1996), "Coupled Flutter and Buffeting Analysis of Long–Span Bridges", J. Struct. Eng., ASCE, Vol. 122, No. 7, pp. 716-725.

79. Jin, S., Lutes, L. D., and Sarkani, S. (1997), " Efficient Simulation of Multidimensional Random Fields", J. of Eng. Mech., Vol. 123, No. 10, pp. 1082 – 1089.

80. Jones, N. P., and Spartz, C. A. (1990), "Structural Damping Estimation For Long-Span Bridges", J. Eng. Mech., ASCE, Vol. 116, No. 11, pp. 2414-2433.

81. Jones, N.P., Scanlan, R.H., Sarkar, P.P., and Singh, L. (1993), "The Effect of Section Model Details on Aeroelastic Parameters", 3rd Asia- Pacific Symp. on Wind Eng., Hong Kong, pp. 71-76.

82. Jones, N. P., and Scanlan, R. H. (1998), "Advances (and Challenges) in the Prediction of Long–span Bridge Response to Wind", Bridge Aerodynamics, Larsen & Esdahl (eds), Balkema, Rotterdam, pp. 59 –85.

83. Kaimal, J.C. et al (1972), "Spectral Characteristics of Surface-Layer Turbulence", J. Royal Meteorol. Soc., 98, pp. 563-589.

84. Kareem, A. (1999), "Analysis and Modeling of Wind Effects", Wind Engineering into 21st Century, Larsen, A. ed. Balkema, Rotterdam, Vol. 1, pp. 43- 54.

85. Katsuchi, H., and Saeki, S. (1998), "Analytical Assessment in Wind-Resistant Design of Long –Span Bridges in Japan", Bridge aerodynamics, Larsen & Esdahl (eds), Balkema, Rotterdam, pp.87-98.

86. Kawashima, K., and Unjoh, S. (1991), "Seismic Behaviour of Cable Stayed Bridges", Cable –Stayed Bridge, Recent Developments and Their Future, Ito, M. et al (ed.), pp. 193 – 212.

87. Kawashima, K., Unjoh, S., and Tunomoto, M. (1993), "Estimation of Damping Ratio of Cable-Stayed Bridges for Seismic Design", J. Struct. Eng., ASCE, Vol. 119, No. 4, pp. 1015-1031.

88. Kawasumi, H., and Shima. E. (1965), "Some Applications of a Correlator on Earthquake Engineering", Proc., 3rd World Conf. on Earthquake Eng., New Zealand, Vol.2, pp. 298-316.

89. Kimura, K., Ohara, T., Huang, Z.Y., and Tanaka, H. (1999), "Lateral Sway Buffeting of Bridge Decks Due to Yaw Wind", Wind Engineering into 21st Century, Larsen, A., et al. Balkema, Rotterdam, Vol. 2 pp. 919 – 926.

90. Kiviluoma, R. (1998), "Coupled–mode Buffeting And Flutter analysis of Bridges", Comp. and Struct., Vol. 70, pp. 219-228.

91. Kobayashi, H., Hatanaka, A., Manabe, S. and Kawase, A. (1993), "Effects of Turbulence on Torsional Flutter of a Bridge Deck." Proc. 3rd Asia–Pacific Symp. on Wind Eng., Hong Kong, pp. 83 –88.

92. Kobayashi, H., Minami, Y., and Miki, M. (1994), "Prevention of Rain–Wind Induced Vibration of an Inclined Cable by Surface Processing", Proc. 9ICWE, New Delhi, India, Vol. 4, pp. 753-758.

93. Kovacs, I., Svensson, H. S., and Jordet, E. (1992), "Analytical Aerodynamic Investigation of Cable- Stayed Helgeland Bridge", J. Struct. Eng., ASCE, Vol. 118, No. 1, pp. 147- 168.

94. Krishna Swamy T. N., Rao G. N. V., Durvasula S., Jagadish K. S. and Jayaram Naik. (1971), "Investigations of Aerodynamic Stability of the Proposed Cable Stayed Bridge across Ganga", Report No. I.W.T.R. 88, Dept of Aeronautical Engg., IIS Bangalore, India.

95. Kumar, B.G.N., Kumar, K., and Krishna, P. (1995), "Wind Tunnel Investigations on Sectional Model of a Girder Deck Cable Stayed Bridge", Proc. 9ICWE, New Delhi, India, pp. 1018- 1029.

96. Lakshmy, P. (1995), "Prediction of Wind Induced Stability of Cable Stayed Bridges", Int. Conf. on Stability of Structures, India, pp. 1039 -1049.

97. Lakshmy, P., Agarwal, S.K, and Trikha, D.N. (1997), " Aerodynamic Force Coefficients for Box Girder Bridges", Proc. 2nd National Seminar on Wind Effects on Structures, India, pp. 297-317.

98. Lakshmy, P., Trikha, D.N, Sharma, D.C, and Sunil Saraswat. (1998), "Wind Tunnel Testing of Yamuna Bridge at Allahabad", Report No. CP-87/97-98, Structural Engineering Research Centre, Ghaziabad.

99. Larsen, A. (1995), "Prediction of Aeroelastic Stability of Suspension Bridges During Erection", Proc. 9ICWE, New Delhi, India, pp. 917-927.

100. Larsen, A., and Walther, J.H. (1997), "Aeroelastic Analysis of Bridge Girder Sections Based on Discrete Vortex Simulation", J. Wind Eng. and Ind. Aerodyn., Vol. 67 –68, pp. 253 –265.

101. Lazan, B. J., (1968). *"Damping of Materials and Members in Structural Mechanics"*, Pergamon Press, London.

102. Lazar, B. E., and Troitsky, M.S. (1972), "Load Balancing Analysis of Cable-Stayed Bridges", J. Struct. Div., ASCE, Vol. 98, ST 8, pp. 1725-1740.

103. Lazar, B., E. (1972), "Stiffness Analysis of Cable- Stayed Bridges", J. Struct. Div., ASCE, Vol. 98, ST 7, pp. 1605-1612.

104. Lee, D.J. (1986), "*Bridge Bearings and Expansion Joints*", E & FN Spon.

105. Lee, D. J. (1994), "*The Theory and Practice of Bearings and Expansion Joints for Bridges*", Cement and Concrete Association, London.

106. Leonhardht, F., and Zellner, W. (1991), "Past, Present and Future of Cable Stayed Bridges", Cable Stayed Bridges - Recent Developments and Future, pp. 1-33, Elsevier.

107. Li, M., and Dexin, He. D. (1995), "The Statistical Approach to Buffeting of Long- Span Bridges", Proc. 9ICWE, New Delhi, India, pp. 893 – 904.

108. Li, Y., and Kareem, A. (1990), " ARMA representation of Wind Field", J.Wind Eng. and Ind. Aerodyn., Vol. 36, Part 1, pp. 415-428.

109. Li, Y., and Kareem, A. (1993), "Simulation of Multivariate Random Processes: A Hybrid DFT and Digital Filtering Approach", J. Eng. Mech., ASCE, Vol. 119, No. 5, pp.1037-1058.

110. Lin, Y. K., and Yang, J .N. (1983), "Multimode Bridge Response to Wind Excitations", J. Eng. Mech., ASCE, Vol.109, No.2, pp. 586-603.

111. Liu, C., and Wang, L. (2001), " Discussion on Simulation of Stochastic Wind Velocity Field on Long-Span Bridges ", J. Eng. Mech. ASCE, Vol. 127, No.4, pp. 408-409.

112. Loganathan, K., Raman, N., and Rajaraman A. (1980), "Nonlinear Analysis of Cable-Stayed Bridges", Int. Assoc. for Bridge and Struct. Eng., 1980, pp. 205-216.

113. Lumley, J.L., and Panofsky, H.A. (1964), "The Structure of Atmospheric Turbulence", Wiley, New York, 1964.

114. Lutes, L. D., and Wang, J. (1991), "Simulation of Improved Gaussian Time History", J. of Eng. Mech., ASCE, Vol. 117, No. 1, pp. 218 – 224.

115. Maeda, J., and Makino, M. (1992), "Characteristics of Gusty Winds Simulated By an A. R. M. A. Model", J. Wind Eng. and Ind. Aerodyn., Vol. 41-44, pp. 427-436.

116. Maeda, K., Otsuka, A., and Takano, H. (1991), "The Design and Construction of Yokohoma Bay Bridge", Cable stayed Bridges–Recent Developments and their Future, pp. 377-396.

117. Matsuda, K., Hikami, Y., Fujiwara, T., and Moriyama, A.(1999), "Aerodynamic Admittance and 'Strip Theory' for Horizontal Buffeting Forces on a Bridge Deck", J. of Wind Eng. and Ind. Aerodyn., Vol. 83, pp. 337-346.

118. Matsumato, M. (1988), "Observed Behaviour of Prototype Cable Vibrations and its Generation Mechanism", Bridge Aerodynamics, Larsen & Esdahl (eds), Balkema, Rotterdam.

119. Matsumato, M., and Shirashi, N., and Shirato, H. (1992). "Rain–Wind Induced Vibrations of Cables of Cable-Stayed Bridges." J. Wind Engg. and Ind. Aerodynamics, Vol. 41-44, pp. 2011-2022.

120. Matsumato, M., Yamagishi, M., Aoki, J., and Shirashi, N. (1995), "Various Mechanisms of Inclined Cable Aerodynamics", Proc. 9ICWE, New Delhi, India, Vol. 4, pp. 759-770.

121. Matsumato, M., Kobayashi, Y., Shirato, H., and Hamasaki, H. (1995), "Flutter Mechanism and its Stabilization of Bluff Bodies", Proc. 9ICWE, New Delhi, India, pp. 827-838.

122. Matsumato, M., Shirato, H., and Yagi, T. (2000), "Recent topics on Bridge Aerodynamics", Wind and Structures, Vol. 3, No. 4, pp 267 –277.

123. Mendes, P., and Branco, F.(1998), " Numerical Wind Tunnel Studies for the Vasco da Gama Bridge", Structural Engineering Inernational, Vol. 8(2), pp. 124-128.

124. Mendes, P.M., and Semiao, C.V. (1999), "Numerical Analysis of the Aerodynamic Stability of Bridges", Wind Engineering into 21st century, Larsen, A. et al, Balkema, Rotterdam, pp. 987-992.

125. Mignolet, M. .P., and Spanos, P.D. (1987), " Recursive Simulation of Stationary Multivariate Random Processes", J. of App. Mech, ASME, Vol. 109, pp. 674-680.

126. Mignolet, M.P., and Spanos, P.D. (1990), " MA to ARMA modeling of wind", J. Wind Eng. and Ind. Aerodyn., Vol. 36 Part 1, pp. 429-438.

127. Mignolet, M.P., and Spanos, P.D. (1992a), "Simulation Of Homogeneous Two Dimensional Random Field: Part I, AR and ARMA Models", J. of App. Mech, ASCE, 59:260-268.

128. Mignolet, M.P., and Spanos, P.D. (1992b), "Simulation Of Homogeneous Two Dimensional Random Field: Part I, MA and ARMA Models", J. of App. Mech, ASCE, 59:269-277.

129. Milne, M. *et al.* (1981), *Bridge Aerodynamics,* Conference Proceedings, Institute of Civil Engineers, Thomas Telford Limited, London.

130. Miyata, T., and Kubo, Y., Ito, M. (1975), "Analysis of Aero elastic Oscillations of Long–Span Structures by Nonlinear Multi- dimensional Procedures." Proc. Fourth Int. Conf. on Wind Effects on Buildings and Structures, U. K., pp. 215-225.

131. Miyata, T., and Yamada, H. (1990), "Coupled Flutter Estimate of a Suspension Bridge", J. Wind Eng. Ind. Aerodyn., Vol. 33, pp. 341-348.

132. Miyata, T., Yamada, H., Boonyapinyo, V., and Santos, J.C. (1995), "Analytical Investigations on the Response of a Long Suspension Bridge under Gusty Wind." Proc. 9ICWE, New Delhi, India, pp. 1006 – 1017.

133. Miyata, T., Yamada, H., Kazama, K. (1995), "On Application of the Direct FEM Analysis For Long Span Bridges", Proc. 9ICWE, New Delhi, India, pp. 1030- 1041.

134. Morimitsu, Y., Ito, M., and Miyata, T. (1973), "Aeroelastic Oscillations of Structures due to Nonlinear Aerodynamic Forces", Proc. JSCE, Vol. 219, pp. 27-36.

135. Morris, N. F. (1974), "Dynamic Analysis of Cable-stiffened Structures", J. Struct. Div. ASCE, May, pp. 971-981.

136. Muria-Vila, D., Gomez, R., and King, C. (1991), "Dynamic Structural Properties of Cable-Stayed Tampico Bridge", J. Struct. Eng., ASCE, Vol. 117, No. 11, pp. 3396-3416.

137. Nagao, F., Utsunomiya, H., Manabe, S., and Kawase, A. (1993), "Improvements of Aerodynamic Behaviour for Box Girder Bridges with Triangular Fairings", Proc., 3rd Asia-Pacific Symp. on Wind Eng., Hong Kong, pp. 77-82.

138. Nagao, F., Utsunomiya, H., Ujimoto, A., and Kobayashi, H. (1999), " Properties of Vertical and Torsional Vortex-induced Oscillations for a Box-girder Deck Section", Proc. Tenth Int. Conf. Wind Eng. - Wind Engineering into 21st Century, Denmark, Vol. 2, pp 999-1004.

139. Namini, A. (1989), "The Aerodynamic Stability of Cable-stayed Bridges", Doctoral Dissertation, University of Maryland, MD.

140. Namini, A., Albrecht, P., and Bosch, H. (1992), "Finite Element Based Flutter Analysis of Cable-Suspended Bridges", J. Struct. Eng., ASCE, Vol. 118(6), pp. 1509-1526.

141. Narita, N., and Sato, H. (1981), "Measurement and Codification of Buffeting Effects on Long –Span Bridges", Bridge Aerodynamics, TTL, London.

142. Narita, N., and Yokoyama, K. (1991), "A Summarized Account of Damping Capacity and Measures against Wind Action in Cable-Stayed Bridges in Japan", Cable Stayed Bridges – Recent Developments and their Future, Ito, M. et al (ed.), pp. 257 – 278.

143. Nazmy, A. S., and Abdel-Ghaffar, A. M. (1990), "Three-Dimensional Nonlinear Static Analysis of Cable –stayed Bridges", Comp. and Struct., Vol. 34, pp.257-271.

144. Niemann, H. J. and Hoffer, R. (1995), "Non-linear Effects in Buffeting Problem", A State of Art in Wind Engineering, IAWE, pp. 320-341.

145. Oppenheim, A., and Schafer, R.(1975), "*Digital Signal Processing*", Prentice-Hall Inc., Englewood Cliffs, New Jersey.

146. Oran, C. (1973), "Tangent Stiffness in Space Frames", J. Struct. Div. ASCE, 99, pp. 987-1001.

147. Panofsky, H.A., and McCormick, R.A. (1959), "The Spectrum of Vertical Velocity Near the Surface", Inst. Aero. Sci. Rep. 59-6.

148. Parlett, B. N., and Scott, S. N. (1979), "The Lanczos Algorithm with Selective Orthogonalization", Mathematics of Computation, Vol.33, 1979, pp.217-218.

149. Peterson, A., Larsen, A., and Eilzer, W. (1991), "Outline Design and Special Studies for a 1200m Cable-Stayed Bridges", Proc. of Innovation of Cable-Stayed Bridges, Japan, pp. 367-377.

150. Pfeil, M.S., and Batista, R.C. (1995), "Aerodynamic Stability Analysis of Cable Stayed Bridges", J. Struct. Eng., ASCE, Vol. 121, No. 12, pp. 1784-1788.

151. Podolony, W., and Scalzi, J. B. (1976), "*Construction and design of Cable Stayed Bridge*", John Wiley and Sons.

152. Przemieniecki, J. S. (1968), "*Theory of Matrix Structural Analysis*", McGraw-Hill, New York.

153. Qu, W.L., and Xiang, H.F. (1993), "An Analysis Method for Buffeting Response of Flexible Bridge With Aerodynamic Coupling Between Modes", Proc., 3rd Asia-Pacific Symp. on Wind Eng., Hong Kong, Vol. 1 , pp. 181-186.

154. Queen, D.J., Verjum, T., and Larose, G.L.(1999), "Aerodynamic Studies of Lions'Gate Bridge-3 Lane renovation", pp. Wind Engineering into 21st Century, Larsen, A., et al., Balkema, Rotterdam, Vol. 2, 1027-1034.

155. Racicot, R. L. (1969), "Random Vibration Analysis – Application to Wind Loaded Structure", Ph.D. Thesis, Case Western Reserve University, USA.

156. Ramadan, O., and Novak, M. (1993), " Simulation of Spatially Incoherent Random Ground Motions", J. of Eng. Mech., ASCE, Vol. 119, No. 5, pp. 997-1016.

157. Reed, D. A., and Scanlan, R. H. (1983), " Time Series Analysis of Cooling Tower Loading ", J. of Struct. Eng., ASCE, Vol. 109, No. 2, pp. 538-554.

158. Reihold, T., A. , Brinch, M., and Damsgard, A. (1992), "Wind Tunnel Tests for the Great Belt East Bridge", Aerodynamics of Large Bridges, ed. By Larsen, A., pp. 255-268.

159. Roger, K.L. (1977), "Airplane Math Modeling Methods for Active Control Design", AGARD-CP-228.

160. Ruscheweyh, H. P. (1999), "The Mechanism of Rain-Wind-induced Vibration", Wind Engineering into 21st Century, Larsen, A., et al. Balkema, Rotterdam, Vol. 2, pp. 1041-1048.

161. Sabzevari, A., and Scanlan, R. H. (1968), "Aerodynamic Instability of Suspension Bridges", J. Eng. Mech. Div., Proc. ASCE, Vol.94, pp. 489-519.

162. Samaras, E., and Shinozuka, M., and Tsurui, A. (1985), "ARMA Representation of Random Processes", J. Eng. Mech., ASCE Vol. 111, No. 3, pp. 449-462.

163. Santos, J.C., Miyata, T., and Yamada, H. (1993), "Gust Response of a Long Span Bridge by the Time Domain Approach", Proc. 3rd Asia - Pacific Symp. on Wind Eng., Hong Kong, Vol. 1, pp. 211-216.

164. Sarkar, P. P., Jones, N., P., and Scanlan, R. H. (1992), "System Identification for Identification of Flutter Derivatives", J. Wind Engg. and Ind. Aerodynamics, Vol. 41-44, pp. 1243-1254.

165. Sarkar, P., P. (1992), " New Identification Methods Applied to the Response of Flexible Bridges to Wind", Ph.D. Dissertation, Department of Civil Engineering, Johns Hopkins University, Baltimore, MD.

166. Sarkar, P. P., Jones, N. P., and Scanlan, R.H. (1994), "Identification of Aeroelastic Parameters of Flexible Bridges", J. Engg. Mech., ASCE, Vol. 120(8), pp. 1718-1742.

167. Scanlan, R.H., and Sabzevari, A. (1969), "Experimental Aerodynamic Coefficients in the Analytical Study of Suspension Bridge Flutter", J. Mech. Eng. Sci., Vol. 11, No. 3, pp. 234-242.

168. Scanlan, R.H., and Tomko, J.J. (1971), "Airfoil and Bridge Flutter Derivatives", J. Eng. Mech. Div., ASCE, Vol.97, No. EM6, pp. 1717-1737.

169. Scanlan, R. H., Beliveau, J.G, and Budlong, K.S. (1974), "Indicial Aerodynamic Functions for Bridge Decks", J. of Eng. Mech., ASCE, Vol. 100, EM 4, pp. 657-672.

170. Scanlan, R. H. (1975), "Recent Methods in the Application of Test Results to the Wind Design of Long Suspended-Span Bridges", Report No: FHWA-RD-75-115, Federal Highway Administration, Washington, D.C.

171. Scanlan, R.H., and Gade, R. H. (1977), "Motion of Suspended Spans under Gusty Wind", J. Struct. Div., ASCE, Vol. 103, No. ST 9, pp. 1867-1883.

172. Scanlan, R.H., and Lin, W.H. (1978), "Effects of Turbulence on Bridge Flutter Derivatives", J. Eng. Mech. Div., ASCE, 104 (EM4), pp. 719-733.

173. Scanlan, R. H. (1978a), "The Action of Flexible Bridges under Wind. I: Flutter Theory", J. Sound and Vib. , Vol. 60, No. 2, pp. 187-199.

174. Scanlan, R.H. (1978b), "The Action of Flexible Bridge under Wind II: Buffeting Theory", J. Sound and Vib., Vol. 60(2), pp. 201-211.

175. Scanlan, R. H. (1981), "State-of-the-Art Methods for Calculating Flutter, Vortex-Induced and Buffeting Response of Bridge Structures", Report No. FHWA/RD-80/050, Washington D.C.

176. Scanlan, R.H. (1984), "Role of Indicial Functions in Buffeting Analysis of Bridges", J. Struct. Eng., ASCE, Vol. 110, No. 7, pp. 1433-1446.

177. Scanlan, R.H. (1986), "Interpreting Aeroelastic Models of Cable- Stayed Bridges", J. of Eng. Mech., ASCE, Vol.113, No. 4, pp. 35-55.

178. Scanlan, R. H. (1988), "On Bridge response Build-up Beyond the Critical Wind Velocity for Stability", J. Wind Engg. and Ind. Aerodyn., Vol. 29, pp. 333-338.

179. Scanlan, R. H., and Jones, N. P. (1990), "Aeroelastic Analysis of Cable stayed Bridges", J. Struct. Engg. , ASCE, Vol. 116, No: 2, pp. 279-297.

180. Scanlan, R.H., and Jones, N.P. (1991), "Stochastic Aspect of Bridge Deck Aeroelasticity under Turbulent Flow", Probabilistic Engrg. Mech., England, Vol.6 (3,4), pp.129-133.

181. Scanlan, R. H. (1993), "Problematics in Formulation of Wind-Force Models for Bridge Decks", J. of Eng. Mech., ASCE, Vol. 119, No.7, pp. 1353-1375.

182. Scanlan, R. H. (1993), "Bridge Buffeting by Skew Winds in Erection Stages", J. Eng. Mech., ASCE, Vol.119, No.2, pp. 251-269.

183. Scanlan, R. H. (1999), " Estimates of Skew Wind Speeds for Bridge Flutter", J. Bridge Eng., ASCE, Vol. 4, No. 2, pp. 95-98.

184. Scanlan, R.H. (2000), " Bridge Deck Aeroelastic Admittance Revisited", J. Bridge Eng., ASCE, Vol. 5, No. 1, pp.1-7.

185. Schlaich, J. (1991), "On detailing of Cable stayed Bridges", Cable stayed Bridges – Recent Developments and Their Future, pp. 57 – 76.

186. Scott, D.S. (1981), "The Lanczos Algorithm", *Sparse Matrices and Their Uses* (ed. I.S. Duff), Academic Press, London, pp. 139-159.

187. Selvam, R.P., and Bosch, H, R. (1999), "Finite Element modeling of Flow Around Bridges", Wind Engineering into 21st Century, Larsen, A., et al. Balkema, Rotterdam, Vol. 2 pp. 1321-1328.

188. Sethia, M. R., Krishna, P., and Arya, A.S. (1987), "Model Tests of Cable stayed Bridge", Int. Conf. Cable–stayed Bridge, Bangkok, Vol. 2, pp.927-938.

189. Shinozuka, M. (1970), "Simulation of Multivariate and Multidimensional Random Processes", The J. of Acoust. Society of America, Vol. 49, No. 1(Part 2), pp. 357-367.

190. Shinozuka, M., and Jan, C.M. (1972), "Digital Simulation of Random Processes and its Application", J. of Sound and Vib., Vol. 25, No. 1 pp. 11-28.

191. Shinozuka, M., and Levy, R. (1977), " Digital Generation of Along Wind Velocity Field", J. of Eng. Mech. Div., ASCE, Vol. 103, No. EM4, pp. 689-700.

192. Shinozuka, M. (1987), "Stochastic Fields and their Digital Simulation", Stochastic Methods in Structural Dynamics, G.I. Schueller and Shinozuka, M, (eds.), Martinus Nijhoff Publishers, Dorderecht, The Netherlands, pp. 93-133.

193. Shinozuka, M., and Deodatis, G. (1991), "Simulation of Stochastic Processes by Spectral Representation", Applied Mechanics Review, Vol. 44, No. 4, pp. 191-204.

194. Shiu, Y.J. (1983), "The Nonlinear Analysis of Cable Stayed Bridges", Doctoral Dissertation to The University of Maryland, MD.

195. Simiu, E. (1973), "Logarithmic Profiles and Design Wind Speeds", J. Eng. Mech. Div. , ASCE, Vol.99, EM5, pp. 1073-1083.

196. Simiu, E., and Scanlan, R. H. (1986), "*Wind Effects on Structures*", 2nd Ed., John Wiley & Sons, Inc. New York.

197. Simiu, E., and Scanlan, R. H. (1996), "*Wind Effects on Structures*", 3rd Ed., John Wiley & Sons, Inc. New York.

198. Singh, L., Jones, N. P., and Scanlan, R. H., and Lorendeaux, O. (1995), "Simultaneous Identification of 3-D Aeroelastic Parameters", Proc. 9ICWE, New Delhi, India, pp.972-981.

199. Singh, L., Jones, N.P., Scanlan, R. H., and Lorendeaux, O. (1996), "Identification of Lateral Flutter Derivatives of Bridge Decks", J. Wind Eng. Ind. Aero., Vol. 60, pp. 81-89.

200. Smith, B. S. (1968a), "The Single Plane Cable-Stayed Girder Bridges", A Method of Analysis Suitable for Computer Use", Proc. of Inst. For Civil Engrs, Paper No. 7040, London.

201. Smith, B. S. (1968b), "A Linear Method of Analysis for Double-plane Cable–stayed Girder Bridges", Proc. of Inst. for Civil Engrs, Paper 7011, London.

202. Smith, D. A., and Mehta, K.C. (1995), "An Empirical Autoregressive Model for Wind Data", Proc., 9ICWE, New Delhi, India, Vol. 1, pp. 56 – 68.

203. STAAD-PRO (2001), "*Technical Reference Manual*", Research Engineers International, Release 2001, 5.0.

204. Stearns, S.D., and David, R.A. (1988), "*Signal Processing Algorithms*", Prentice Hall Inc., Englewood Cliffs, New Jersey.

205. Steinman, D. B. (1934), "A Generalized Theory for Suspension Bridges", Trans. ASCE.

206. Steinman, D.B. (1947), "Wind Tunnel Tests Yield Aerodynamically Stable Bridge Sections", Civil Engineering, pp. 746-749.

207. Strommen, E., hjorth-Hansen, E., Hanse, S.O, Jacobsen, J.B. (1999), " Aerdynamic Investigations for Tender Design Concepts of the Oresund Cable-Stayed Bridge", J. of Wind Eng. Ind. Aerodyn., Vol ;80, pp. 351-372.

208. Suresh Kumar, K. (2000), "Random Number Sensitivity in Simulation of Wind Loads", Wind and Structures, Vol.3, No.1, pp.1-10.

209. Svensson, H. S., and Kovacs, I. (1992), "Examples of Analytical Investigations of Long – Span Bridges", Aerodynamics of Large Bridges, Larsen, A. (ed.) Balkema, Rotterdam, pp. 171 –182.

210. Takano, H., Ogasawara, M., Ito, N., and Ichikawa, H. (1998), "Wind-Resistant Design of The Tsurumi Tsubasa Bridge", Long-Span Bridges and Aerodynamics, Miyata, T. et al (eds), Springer, pp. 313-326.

211. Tamhankar, M. G. (1976), "Design of Cables and Their Anchorages in Cable Stayed Girder Bridges", Indian Road Congress Journal, Vol. 37, No. 3, pp. 523-550.

212. Tanaka, H., and Ito, M. (1969), "The Characteristics of Aerodynamic Forces in Self-Excited Oscillations of Bluff Sections", Trans. JSCE, Vol. 1, Part 2, pp. 209-226.

213. Tanaka, H., and Davenport, A.G. (1979), "Effect of Turbulence on Aeroelastic Instability of Suspension Bridges", Proc. of Seventh CANCAM, Sherbrooke, pp. 397-398.

214. Tanaka, H., Yamamura, N., and Tatsumi, M. (1992), "Coupled Mode Flutter Analysis Using Flutter Derivatives", J. Wind Eng. and Ind. Aerodyn., Vol. 41-44, pp. 1279-1290.

215. Tanaka, H., Kimura, K., Nakamura, S., and Larose, G.L. (1995), "Effects of Wind Yaw angles on Bridge Response", Proc. 9ICWE, New Delhi, India, pp. 905-916

216. Tang, M. C. (1971), "Analysis of Cable- Stayed Girder Bridges", J. Struct. Div., ASCE, Vol. 97, ST 5, pp. 1481-1496.

217. Tang, M., C. (1972), "Design of Cable–Stayed Girder Bridges", J. Struct. Div., ASCE, Vol. 98, ST 8, pp. 1789-1802.

218. Tang, M.C. (1998), "Balancing Act", Civil Engineering, pp. 42-45.

219. Tau, D. T., Cheung, M.S., and Cheng, S. H. (2000). "3D Flutter Analysis of Bridge by Spline Finite Strip Method", J. Struct. Eng., ASCE, Vol. 126, No. 10, pp. 1246- 1254.

220. Teunissen, H., W. (1980), "Structure of Mean Winds and Turbulence in Planetary Boundary Layer over Rural Terrain Boundary Layer Meteorology", Vol.19, pp.187-221.

221. Theodorsen, T. (1935), "General Theory of Aerodynamic Instability and Mechanism of Flutter", NACA report No: 496, US Advisory Committee for Aeronautics, Langley, VA.

222. Tiffany, S.H. and Adams, W. M. (1988), "Nonlinear Programming Extensions to Rational Function Approximation Methods for Unsteady Aerodynamic Forces", NASA Tech. Paper 2776, NASA, Washington, D.C.

223. Timoshenko, S. (1927), "Vibrations of Bridges", Trans. ASME, Vol.49-50, Part-II, Paper RR-50.9.

224. Troitsky, M., S., and Lazar, B., E. (1972), "Model Analysis and Design of Cable–stayed Bridges", Proc. of Inst. of Civil Engrs, Paper No. 7375, London.

225. Troitsky, M. S. (1988), "*Cable Stayed Bridges*", 2nd Ed., BSP Professional Books, London.

226. Ukeguchi, N., Sakata, H., Nishitani, H. (1966), "An Investigation of Aeroelastic Instability of Suspension Bridges", Proc. Int. Symp. on Suspension Bridges, Lisbon, pp. 273-284.

227. Ulstrup, Carl C, (1992), "*Guidelines for the Design of Cable-Stayed Bridges*", ASCE, Committee on Cable-Stayed Bridges.

228. Veje, E. M., Ali, A., and Najfi, R., (1999), "Yamuna Bridge at Allahabad/ Naini, Uttar Pradesh", Int. Conf. on Suspension, Cable Supported and Cable Stayed Bridges, pp. 204-218.

229. Virlogeux, M. (1991), "Erection of Cable stayed bridges", Cable-stayed Bridges- Recent Developments and Their Future, pp. 77- 105.

230. Virloguex, M. (1992), "Wind Design and Analysis of Normandy Bridge", Proc. First Int. Symp. on Aerodynamics of Large Bridges, Denmark, 1992.

231. Virlogeux, M. (1998), "Cable Vibrations in Cable-Stayed Bridges", Bridge Aerodynamics, Larsen & Esdahl (eds), Balkema, Rotterdam, pp. 213-233.

232. Von Karman, T. (1948), "Progress in the Statistical Theory of Turbulence", Proc. Nat. Acad. Sci., Washington, DC, pp. 530-539.

233. Walshe, D.E. (1981), "Some Effects of Turbulence on Fluctuating Time–Average Wind Forces on Sectional Models of Box Girder Bridges", Bridge Aerodynamics, ICE, London.

234. Walshe, D.E.J., and Wyatt, T.A. (1983), "Measurement and Application of the Aerodynamic Admittance Function for a Box-Girder Bridge", J. Wind Eng. And Ind. Aerodyn. Vol.14, pp.211-222.

235. Walther, R., Houriet, B., Isler, W., Moria, P. (1988), "*Cable Stayed Bridges*", Thomas Telford, London.

236. Wardlaw, R. L., and Goettler, L.L. (1968), "A Wind Tunnel Study of Modifications to Improve the Aerodynamic Stability of the Longs Creek Bridge", LTR-LA-8, National Aeronautical Establishment, Ottawa, Canada.

237. Wardlaw, R.L.(1970), "Static Force Measurements of Six Deck Sections for the Proposed New Burrard Inlet Crossing, Report No. LTR-LA –53, NAE, National Research Council, Ottawa, Canada.

238. Weaver, W., and Gere, J. (1980), "*Matrix Analysis of Framed Structures*", 2nd Ed. Van Nostrand, New York.

239. Wei, H. W. (1993), "A Study of Wind-Resistant Stability of Long-Span Cable-Stayed Steel Bridge", Proc. 3rd Asia-Pacific Symp. on Wind Eng. , Hong Kong, pp. 247-252.

240. Welch, P.D. (1967), "The Use of The Fast Fourier Transform for The Estimation of Power Spectra", IEEE Trans.,AU-15:70.

241. Wilson, J. C., and Gravelle, W. (1991), "Modeling of a Cable Stayed Bridge for Dynamic Analysis", Int. J. of Earthquake Eng. and Struct. Dyn., Vol. 20, pp. 707- 721.

242. Wilson, J.C., and Liu, T. (1991), "Ambient Vibration Measurements on a Cable Stayed Bridge", Int. J. Earthquake Eng. and Struct. Dyn., Vol. 20, pp. 723-747.

243. *Wind Resistant Design Manual for Highway Bridges* (1991), Japan.

244. Wyatt, T. A. (1991), "The Dynamic Behaviour of Cable–stayed Bridges: Fundamental and Parametric Studies", Cable–stayed Bridges, Recent Developments and Their Future, Ito, M. et al (ed.), pp. 151 – 170.

245. Xiang, H.F., Liu, C.H., and Gu., M. (1995), " Time-domain Analysis of Coupled Buffeting Response of a Long Span Bridge", Proc. 9ICWE, New Delhi, India, pp.881-892.

246. Xu, Y. L., Sun, D. K., Ko, J. M., and Lin, J. H. (1998), "Buffeting Analysis of Long Span Bridges", Comp. and Struct., Vol. 68, pp. 303-313.

247. Xu, Y.L. (1999), "Buffeting of Tsing Ma Suspension Bridge: Analysis and Comparison", Wind Engineering into 21st Century, Larsen, A. et al, Balkema, Rotterdam, Vol. 2, pp. 1075 –1080.

248. Yamada, Y. et al (1991), "Earthquake-Resistant and Wind-Resistant Design of the Higashi-Kobe Bridge", Cable-stayed Bridges-Recent Developments and Their Future, pp. 397-416.

249. Yamaguchi, H., and Ito, M. (1995), "Mode–Dependency of Structural Damping in Cable Stayed Bridges", Proc. 9ICWE, New Delhi, India, Vol. II, pp. 928-937.

250. Yamaguchi, H., and Fujino, Y. (1998), "Stayed Cable Dynamics and its Vibration Control", Bridge Aerodynamics, Larsen & Esdahl (eds), Balkema, Rotterdam, pp. 235-253.